Synthesis and Exploration of the Biological Activity of Silver(I) and Rhenium(I) Complexes Containing Derivatised Phenanthroline Ligands

A thesis submitted to Maynooth University in fulfilment of the requirements for the degree of

Doctor of Philosophy

By

Clara Evans, B.Sc.

Department of Chemistry,

Faculty of Science and Engineering,

Maynooth University,

Maynooth,

Co. Kildare,

Ireland

March 2025

Research Supervisors: Prof Denise Rooney and Prof Frances Heaney

Head of Department: Dr Diego Montagner

Table of Contents

Declaration of Authorship……i

Acknowledgements……ii

Abbreviations……iv

Abstract……ix

Chapter 1: Introduction……1

1.1 Metals in Medicine……2

1.2 Phenanthroline……6

1.3 Biological Activity of Phenanthroline and its Derivatives……8

1.4 Metal Complexes of Phenanthroline……12

1.4.1 Copper Complexes of Phenanthroline……14

1.4.2 Manganese Complexes of Phenanthroline……17

1.4.3 Ruthenium Complexes of Phenanthroline……18

1.5 Modes of Action of Metal Phenanthroline Complexes……19

1.6 Biological Effects of Silver……21

1.7 Applications of Rhenium……24

1.8 CO-Releasing Molecules……28

1.9 Thesis Objectives and Structure……30

Chapter 2: Experimental Methods and Characterisation Data……32

2.1 Materials and Instrumentation……33

2.1.1 Chemicals and Materials……33

2.1.2 Instrumentation……33

2.2 Synthesis of Phenanthroline-based ligands……34

2.2.1 Synthesis of 1,10-Phenanthroline-5,6-dione (**2a**)……34

2.2.2 Synthesis of L-Amino Acid Ester Hydrochlorides **1.1 – 1.8**……35

2.2.3 Synthesis of Phenanthroline-oxazine Ligands **2.1 – 2.4**……40

2.2.4 Synthesis of Pyrido-Phenanthrolinone Ligands **2.5 – 2.8**……44

2.3 Metal Complexation……48

2.3.1 Synthesis of Silver(I) Complexes **3.1 – 3.4**……48

2.3.2 Synthesis of Rhenium(I) Tricarbonyl Complexes……51

2.3.3 Synthesis of $Mn(CO)_5Br$ Starting Material……61

2.4 Biological Screening of Ligands **2.1 - 2.8** and their Metal Complexes **3.1 - 3.3** and **4.1 – 4.8**……62

2.4.1 Materials and Instrumentation……62

2.4.2 Preparation of Microbial Cultures……63

2.4.3 Microbial Susceptibility Testing……63

2.4.4 *In vivo* Testing Towards *Galleria mellonella*……64

2.4.5 Determination of Haemocyte Density of Inoculated *G. mellonella* Larvae……64

2.4.6 Anticancer Testing……65

2.4.6.1 Ovarian Cancer Cell Culture and Cell Seeding……65

2.4.6.2 Treating Cells to Measure Cell Viability……65

2.4.6.3 Treating Cells to Measure Apoptosis……66

Chapter 3: Synthesis, Characterisation and Biological Evaluation of Derivatised Phenanthroline Ligands and Silver(I) Phenanthroline Complexes……67

Compound Structures and Codes for Chapter 3……68

3.1 Introduction……71

3.2 Synthesis and Characterisation of Starting Materials and Phenanthroline-based Ligands **2.1 – 2.8**……75

3.2.1 Synthesis of Starting Materials: 1,10-Phenanthroline-5,6-dione (**2a**) and L- Amino Acid Ester Salts **1.1 –1.8**……75

3.2.2 Synthesis and Characterisation of Phenanthroline-derived Ligands **2.1 – 2.8**……78

3.2.2.1 Development of Phenanthroline-oxazine (**2.1 – 2.4**) and Pyrido -phenanthrolinone Ligands (**2.5 – 2.8**)……78

3.2.2.2 Ligand Design Strategy……81

3.2.2.3 Proposed Mechanism for the Formation of Phenanthroline-oxazine Ligands **2.1 – 2.4** and Phenanthroline-pyrido Ligands **2.5 - 2.8**……..83
3.2.2.4 Synthesis and Characterization of Phenanthroline-oxazine Ligands 2**.1 – 2.4**……84
3.2.2.5 Synthesis and Characterisation of Phenanthroline-pyrido Ligands **2.5 – 2.8**……86
3.3 Synthesis, Characterisation and Biological Evaluation of Ag(I) *bis*(phenanthroline-oxazine) Complexes **3.1 – 3.4**……89
3.3.1 Synthesis and Characterisation of Ag(I) *bis*(phenanthroline-oxazine) Complexes **3.1 – 3.4**……89
3.3.2 Determining the Solution Stoichiometry of Ag(I) *bis*(phenanthroline-oxazine) Complexes **3.1 – 3.3**……95
3.3.3 Solution Behaviour and Stability of Ag(I) *bis*(phenanthroline-oxazine) Complexes **3.1 – 3.3**……99
3.3.3.1 Solution Behaviour of Ag(I) *bis*(phenanthroline-oxazine) Complexes **3.1 – 3.3**……99
3.3.3.2 Stability of Ag(I) *bis*(phenanthroline-oxazine) Complexes in Solution……..105
3.3.4 *In vitro* Activity of Phenanthroline-oxazine Ligands **2.1 – 2.4** and Ag(I) Complexes **3.1 – 3.3** Against *Candida albicans*……106
3.3.5 *In vivo* Toxicity Towards *Galleria mellonella*……..116
3.3.6 Survival Rate of *Galleria mellonella* Infected with *C. albicans* Followed by Treatment with PPO (**2.2**) and $[Ag(PPO)_2]ClO_4$ (**3.2**)……118
3.4 Conclusion……121

Chapter 4: Synthesis and Characterisation of Re(I) Tricarbonyl Phenanthroline Complexes 4.1 – 4.8 and their Photochemical and Electrochemical Properties……123

Compound Structures and Codes for Chapter 4……124

4.1 Introduction……126

4.2 Synthesis and Characterisation of Re(I) Tricarbonyl Phenanthroline Complexes **4.1 – 4.8**……128

4.2.1 Synthesis of Bromopentacarbonylrhenium(I) Starting Material……128

4.2.2. Synthesis of Known Re(I) Tricarbonyl Complexes of 1,10-Phenanthroline (**4a**) and 1,10-Phenanthroline-5,6-dione (**4b**)……129

4.2.3 Synthesis and Characterisation of Re(I) Tricarbonyl Phenanthroline-oxazine Complexes **4.1 – 4.4**……131

4.2.4 Synthesis and Characterisation of Re(I) Tricarbonyl Phenanthroline-pyrido Complexes **4.5 – 4.8**……144

4.3 Properties of Re(I) Tricarbonyl Complexes **4a**, **4b** and **4.1 – 4.8**……151

4.3.1 Solution Stability and Solvatochromism Behaviour of Re(I) tricarbonyl complexes **4.1 – 4.8**……151

4.3.2 Photo-Luminescence Studies on Re(I) complexes Tricarbonyl Phenanthroline Complexes **4a**, **4b**, **4.1 - 4.8**……153

4.3.3 Assessment of the Photochemical Stability of Re(I) Tricarbonyl Complexes **4.1 – 4.8** using UV-visible Spectroscopy……156

4.4 Myoglobin Assays of Re(I) Complexes **4.1 – 4.8**……160

4.5 Electrochemical Studies of Re(I) Complexes……164

4.6 Manganese(I) Tricarbonyl Phenanthroline Complexes……171

4.6.1 Synthesis of Bromopentacarbonylmanganese(I) Starting Material……172

4.6.2 Attempted Synthesis of Novel Mn(I) Phenanthroline-oxazine complex……172

4.6.3 Attempted Synthesis of Novel Mn(I) Phenanthroline-pyrido Complex……174

4.7 Conclusion……177

Chapter 5: Antimicrobial and Anticancer Activity of Novel Re(I) Tricarbonyl Phenanthroline Complexes 4.1 – 4.8……179

Compound Structures and Codes for Chapter 5……180

5.1 Introduction……183

5.2 *In vitro* Antimicrobial Testing of Ligands **2.1 – 2.8** and Re(I) Complexes **4.1 – 4.8**……185

5.2.1 Antibacterial Testing of Ligands **2.1 – 2.8** and Complexes **4.1 – 4.8** against *S. aureus*, MRSA and *E. coli*……185

5.2.1.1 *In vitro* Activity of Ligands **2.1 – 2.8** and Re(I) Complexes **4.1 – 4.8** against *S. aureus*……185

5.2.1.2 *In vitro* Activity of Ligands **2.1 – 2.8** and Re(I) Complexes **4.1 – 4.8** against MRSA……190

5.2.1.3 *In vitro* Activity of Ligands **2.1 – 2.8** and Re(I) Complexes **4.1 – 4.8** against *E. coli*……196

5.2.2 *In vitro* Antifungal Activity of Ligands **2.1 – 2.8** and Re(I) Complexes **4.1 – 4.8** against *C. albicans*……197

5.3 *In vivo* Toxicity Towards *Galleria mellonella*……203

5.4 *In vitro* Anticancer Testing against Ovarian Cancer Cell Lines PEO1 and PEO4……205

5.5 Assessing the Apoptotic Ability of PPO (**2.2**), PPP (**2.7**), RePPO (**4.2**) and RePPP

(**4.7**)……213

5.6 Conclusion……221

Chapter 6: Conclusions and Future Work……223

Bibliography……226

Appendix……258

Declaration of Authorship

I have read and understood the Departmental policy on plagiarism. I declare that this thesis is my own work and has not been submitted in any form for another degree or diploma at any university or other institution of tertiary education. Information derived from the published or unpublished work of others has been acknowledged in the text and a list of references is given.

Signed  Date 27/03/2025

Clara Evans

Acknowledgements

I want to thank to my supervisors Prof Denise Rooney and Prof Frances Heaney so much for their continuous support, encouragement and kindness over the last few years. I have learnt an enormous amount over the course of this research and have been very lucky to work with both of them. I was incredibly grateful to be awarded funding through the Irish Research Council (IRC) which allowed me to carry out the research and travel to several national and international conferences. I have also had the opportunity to work with several fantastic collaborators who helped make this project what is it. Firstly, Prof Kevin Kavanagh and the medical mycology lab who were all so welcoming and taught me so much about microbiology and the techniques involved. Even though I murdered far too many galleria, I was always welcomed back. I want to especially thank Aaron (Galleria man) for his friendship, guidance and knowledge over the years. Secondly, I wish to thank Dr Marion Butler and the cell signalling lab in Maynooth who provided space and training for the anticancer testing. In particular, Jamie who was incredibly patient and supportive when training me and his continuous support since. I was also grateful to work with Dr Neil Conlon in DCU to delve deeper into the cancer studies and get some very cool results! I also wish to thank Dr Brendan Twamley in TCD who was so fascinated in our compounds and helped us finally get some nice crystal structures. I am also incredibly grateful to Mr Martin Kitson and Dr Bernie Creaven in TU Dublin for access to their NMR machine when ours was out of action.

Of course, I have to thank my amazing family, Andy, Pauline, Rhys and Michael. My parents Andy and Pauline have been my biggest support system and provided me with so much love, encouragement and dinners. Andy had the huge (unpaid) task of proof-reading the entire thesis which I am so grateful for. Pauline has been a huge inspiration for me as a woman and made sure I never felt anything was impossible. Rhys, my incredibly supportive and encouraging brother who left the country when I told him I wanted to do a PhD (fair enough). And Abbey who gave me all the sisterly pep talks I needed to keep going. To Michael, who (begrudgingly) accepted me as his roommate and made sure I never took this thing too seriously and actually left the house during the writing stage. To my lovely cats, Coco and Daisy who gave me all the

cuddles and emotional support I needed (they are very good listeners). To Jamie, who has just been the best. Thank you for all the chill nights in, big hugs and silliness that got me through everything, especially the ~~insanity~~ writing phase. You have been my rock. Lastly, I have to thank the girls, Emma, Carrie, Lynn and Emma Dev who have been just as amazing and always supportive. The hours-long catch ups, spooky movie nights and puppy play dates are always the best.

Abbreviations

α	Alpha
A	Absorbance
Å	Angstrom
ACN	Acetonitrile
$AgClO_4$	Silver perchlorate
AMR	Antimicrobial Resistance
Ar	Aromatic
ATR	Attenuated Total Reflection
β	Beta
br s	Broad singlet
bipy	Bipyridine
°C	Degrees Celsius
ca	Circa
^{13}C NMR	Carbon NMR
$CDCl_3$	Deuterated chloroform
CD_3CN	Deuterated acetonitrile
$CF_3SO_3^-$	Triflate
CFU	Colony Forming Units
CH_3Cl	Chloroform
CHN%	Percentage of carbon, hydrogen and nitrogen
ClO_4^-	Perchlorate
cm	Centimetre
cm^{-1}	Wavenumber
CO	Carbon monoxide
CO_2	Carbon dioxide
CORM	CO-Releasing Molecule
COSY	Correlated Spectroscopy
CV	Cyclic Voltammetry
d	Doublet
δ	Delta

DCM	Dichloromethane
dd	Doublet of doublets
Δδ	Change in chemical shift
DEPT	Distortionless Enhancement by Polarization Transfer
dH_2O	Deionised water
DMF	Dimethylformamide
DMSO	Dimethyl sulfoxide
DMSO-d6	Deuterated dimethyl sulfoxide
DNA	Deoxyribonucleic acid
ε	Molar extinction coefficient
EDG	Electron donating group
Et	Ethyl
EtOAc	Ethyl acetate
E_p^{ox}	Oxidation potential
E_p^{red}	Reduction potential
ESI	Electron spray ionisation
EtOH	Ethanol
EWG	Electron withdrawing group
FBS	Fetal Bovine Serum
FTIR	Fourier transform infrared
fac	Facial
Fc	Ferrocene
g	Grammes
G	Gauge
GCE	Glassy Carbon Electrode
h	Hour(s)
HCl	Hydrochloric acid
^{1}H NMR	Proton NMR
Hex	Hexyl
HMBC	Heteronuclear Multiple Bond Correlation
HPLC	High-Performance Liquid Chromatography

HRMS	High resolution mass spectrometry
H_2SO_4	Sulfuric acid
HSQC	Heteronuclear Single Quantum Coherence
Hz	Hertz
IC_{50}	Inhibitory Concentration to reduce growth by 50%
IR	Infrared
J	Joules
KBr	Potassium bromide
$KBrO_3$	Potassium bromate
KCl	Potassium chloride
$KOBu^t$	Potassium tert-butoxide
λ	Lambda
LCMS	Liquid Chromatography – Mass Spectrometry
m	Multiplet
Mb	Myoglobin
MDR	Multi-drug resistance
Me	Methyl
MeIm	Methylimidazole
mer	Meridional
M	Mass
MHz	Mega Hertz
MeOH	Methanol
mg	Milligrams
MIC_{50}	Minimum Inhibitory Concentration to reduce microbial growth to 50%
$MgSO_4$	Magnesium sulfate
Min	Minutes
mL	Millilitres
MLCT	Metal to Ligand Charge Transfer
mmol	Millimoles
mM	Millimolar

MM	Minimal Media
mol	Moles
MRI	Magnetic Resonance Imaging
MRSA	Methicillin-resistance *Staphylococcus aureus*
MS	Mass Spectrometry
mV	Millivolts
mV/s	Millivolts per second
m/z	Mass to charge ratio
NaOH	Sodium peroxide
NO_2	Nitro
NO_3	Nitrate
nm	Nanometre
nM	Nanomolar
NMM	N-methylmorpholine
NMR	Nuclear Magnetic Resonance
NP	Nanoparticle
Oct	Octyl
OD	Optical density
OD_{600}	Optical density at 600 nm
OH	Hydroxyl
p	Para
PDT	Photodynamic therapy
P-value	Statistical probability
PBS	Phosphate buffered saline
PET	Positron Emission Tomography
phen	1,10-Phenanthroline
phendione	1,10-Phenanthroline-5,6-dione
PPh_3	Triphenylphosphine
ppm	Parts per million
π	Pi
Pr	Propyl

q	Quaternary
RNA	Ribonucleic acid
ROS	Reactive Oxygen species
RPMI	Roswell Park Memorial Institute (media)
rt	Room temperature
s	Singlet
SCE	Saturated Calomel Electrode
SOD	Superoxide dismutase
SPECT	Single-Photon Emission Computerized Tomography
t	Triplet
TBATFB	Tertbutylammonium tetrafluoroborate
ϕ	Theta (quantum yield)
THF	Tetrahydrofuran
tip	2-Thiophenimidazo[4,5-f][1,10]phenanthroline
TLC	Thin Layer Chromatography
TOF	Time of Flight
µL	Microlitre
µM	Micromolar
UV-vis	UV-visible spectroscopy
v	Frequency
V	Volts
VC	Vehicle Control
v/v	Volume per volume
VRE	Vancomycin-resistant *Enterococcus*
w/v	Weight per volume
X_L	Molar fraction
YEPD	Yeast Extract Peptone Dextrose

Abstract

Antimicrobial resistance (AMR) is a major global health concern that causes millions of deaths each year. There is an urgent need for novel antimicrobial agents with unique modes of action to combat the increasing instances of resistance. 1,10-Phenanthroline continues to be a useful ligand in the design of novel therapeutic agents.

Two families of derivatised 1,10-phenanthroline ligands, the first with a phenanthroline core fused with an oxazine ring (phen-oxazine), and the second with the phenanthroline core fused with a pyridine ring (phen-pyrido) with varying lipophilicity were synthesised and characterised along with their respective Ag(I) and Re(I) tricarbonyl complexes. The Ag(I) complexes were found to exhibit fluxional behaviour in solution. Antifungal testing of the phen-oxazine ligands against *Candida albicans* showed a clear lipophilic effect; the MIC_{50} values decreased from > 60 µM (R=Me), to 43.3 µM (R=Pr), to 14.6 µM (R=Hex). Complexation of phen-oxazine to Ag(I) was shown to greatly enhance the antifungal effects; all complexes held fungal growth below 15% of the negative control experiment at all concentrations tested (60 – 15 µM). The uncoordinated phen-oxazine with a propyl sidechain and its Ag(I) complex were found to be well tolerated *in vivo* by *Galleria mellonella* larvae.

The Re(I) tricarbonyl phen-oxazine complexes were found to form as a pair of diastereomers. Crystal structures were obtained for one diastereomer of the propyl derivative of the Re(I) phen-oxazine complex and of the corresponding Re(I) phen-pyrido complex. Both crystals presented as distorted octahedral *fac*-isomers. Irradiation of the Re(I) complexes with broad band light resulted in gradual changes in their UV-visible spectra consistent with a photochemical reaction, however, myoglobin assays did not provide evidence for CO loss upon irradiation. Cyclic voltammetry revealed that the Re(I) phen-pyrido complexes were more redox active than the corresponding phen-oxazine analogues. Synthesis of analogues Mn(I) tricarbonyl complexes of phen-oxazine and phen-pyrido was attempted but was not successful.

The biological activity of free phen-oxazine and phen-pyrido ligands and their Re(I) tricarbonyl complexes was evaluated against several microbial strains, *G. mellonella* and ovarian cancer cell lines PEO1 and PEO4. Antimicrobial testing was conducted against *Staphylococcus aureus*, methicillin-resistant *Staphylococcus aures* (MRSA), *Escherichia coli* and *C. albicans*. The phen-oxazine ligands showed a clear correlation between lipophilicity and activity against *S. aureus* and MRSA with the most lipophilic octyl analogue having MIC_{50} values of < 3.75 μM. The phen-pyrido ligands were determined to have significant broad-spectrum antimicrobial effects with activity at concentrations as low as 0.11 μM. In general, complexation to Re(I) reduced the antimicrobial effects. A study with *G. mellonella* larvae showed limited *in vivo* toxicity d for the uncoordinated propyl phen-pyrido analogue and its Re(I) complex . Anticancer testing of a representative phen-oxazine and phen-pyrido ligand as well as their corresponding Re(I) complexes against PEO1 and PEO4 revealed that all bar Re(I) propyl phen-oxazine significantly reduced cell viability of both ovarian cancer cell lines and were more active than cisplatin. Apoptosis assays revealed the propyl phen-oxazine induced apoptosis while Re(I) propyl phen-pyrido inhibited proliferation by an alternative mechanism.

Chapter 1

Introduction

1.1 Metals in Medicine

The use of metals in medicine has existed for several centuries. Metals such as silver and copper were historically used in food preservation and agriculture.[1] The first medicinal inorganic compound was discovered in the early 20th century by German physician Paul Ehrlich. He developed arsphenamine, known commercially as Salvarsan (**Figure 1.1a**) which was the first antibiotic to effectively treat syphilis. Ehrlich discovered that Salvarsan would selectively kill pathogenic cells over healthy cells and published this work in 1912.[2]

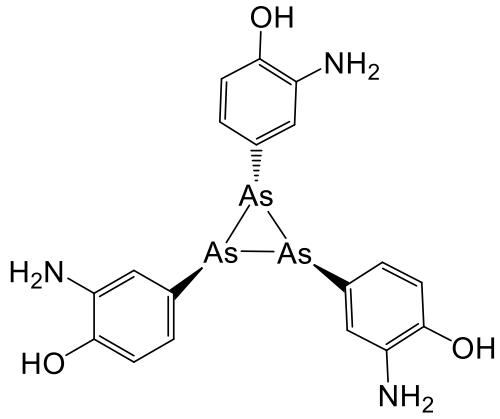

Figure 1.1: Structure of the landmark medicinal inorganic compound Salvarsan.

A major breakthrough for modern medicinal chemistry was the development of diamminedichloroplatinum(II) (*cis*-[$Pt(NH_3)_2(Cl)_2$]), known as cisplatin (**Figure 1.2a**). Although cisplatin was developed in 1845 by Michele Peyrone, it wasn't until 1965 that biophysicist Barnett Rosenburg discovered its ability to inhibit cell division.[3, 4] New generations of cisplatin were soon developed. The first was carboplatin (**Figure 1.2b**) in the 1980's followed by oxaliplatin (**Figure 1.2c**) in the 1990's. These three platinum-based drugs are the amongst the most widely used chemotherapy agents.[5]

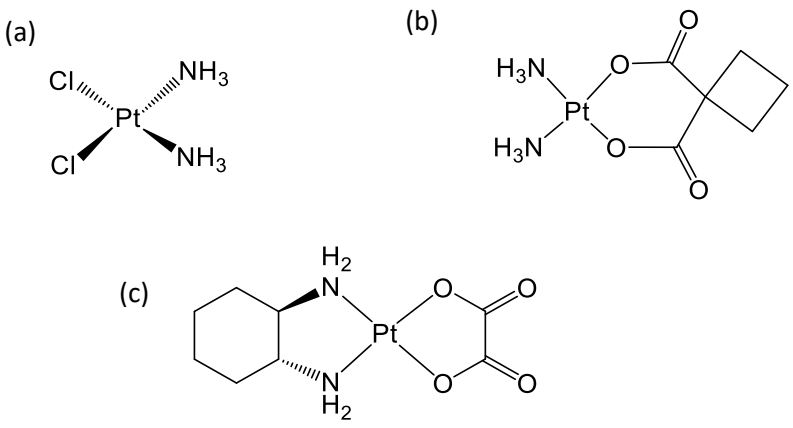

Figure 1.2: Structures of platinum-based chemotherapy agents: cisplatin (a), carboplatin (b) and oxaliplatin (c).

The interest in metals for medicinal purposes stems from the importance of metals for many biological functions. It is estimated that transition metals are required for the function of 25% of human proteins.[6] A key example is iron (Fe), which is a vital component of haemoglobin within red blood cells and plays an essential role in efficient oxygen transport and storage within the body.[7] Iron is also required for processes such as DNA replication, respiration and metabolism.[8] Metal ions of Fe, Mn, Zn and Cu are key components of many proteins that function as metalloenzymes. Metalloenzymes are enzymes which selectively bind a metal ion to carry out their function. Some examples of metalloenzymes and their cofactors include cytochrome c oxidase (Cu(I)/(II)), alcohol dehydrogenase (Zn(II)) ascorbic acid oxidase (Cu(I)/(II)) and glutathione peroxidase (Se(-1)).[9] Another example is cobalt (Co) which is present in vitamin B_{12} (cobalamin), an essential vitamin for neurological function. Vitamin B_{12} has a role to play in the synthesis of nucleic acids and neurotransmitters, formation of red blood cells and in maintaining the integrity of myelin sheaths.[10, 11] Microbial growth and homeostasis is highly dependent on the function of metalloenzymes[12], therefore they are good targets for antimicrobial agents.

The rate of development of novel metal-based compounds as medicinal agents has increased exponentially in the last number of decades. The advantages of metal-based therapeutics include structural diversity and access to multiple oxidation

states. Additionally, complexation of organic ligands can greatly improve solubility, stability and delivery of the drug to the desired cellular target.[13] A plethora of metallodrugs have been developed to treat cancer[14], microbial infections[15] and neurological disorders[16]. Metals such as Ru(III), Au(I), Fe(II), Pd(II), Cu(II) and Ir(III) have all been employed in development of anticancer agents[17]. Metal complexes are also used in the treatment of arthritis (Au), ulcers (Bi), diabetes (V), viral infections (Co, Hg), cardiovascular conditions (Bi, Mn) and psychotherapeutics (Li)[18]. Some examples include auranofin, an Au(III) based compound used for arthritis that has also been re-purposed for use in cancer treatment (**Figure 1.3a**).[19] The vanadium-based compound, *bis*(ethylmaltolato)oxovanadium(IV) (BEOV) is used for the treatment of diabetes and more recently Alzheimer's disease (**Figure 1.3b**).[20] The antimalarial drug chloroquine has been derivatised to from ferroquine (**Figure 1.3c**) which can successfully treat resistant strains of *Plasmodium falciparum*, the parasite that causes malarial infections.[21]

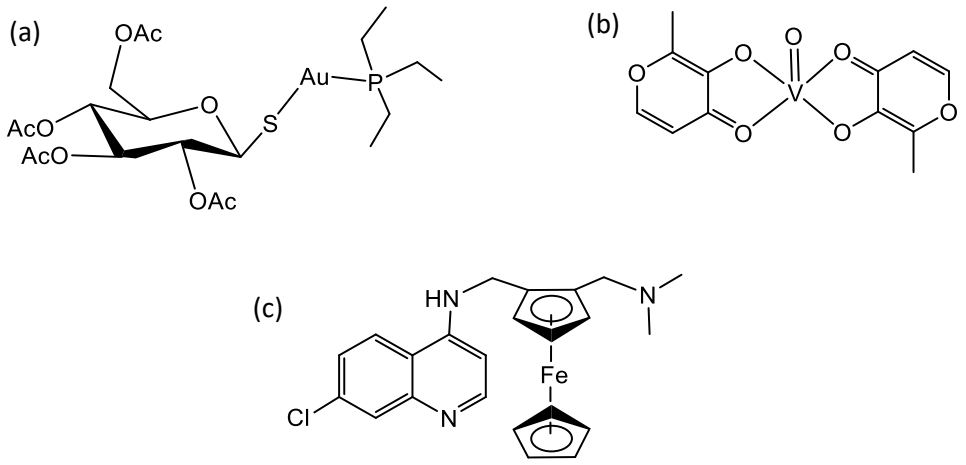

Figure 1.3: Structures of antiarthritic and anticancer agent auranofin (a), diabetes and Alzheimer's treatment *bis*(ethylmaltolato)oxovanadium(IV) (BEOV) (b) and antimalarial drug Ferroquine (c).

Metal complexes have also been developed for use as diagnostics tools. Imaging agents are used for the diagnosis of many medical issues including cancer, infections, cardiovascular abnormalities and neurological disorders.[22] A well-known example is the use of gadolinium (Gd) in magnetic resonance imaging (MRI) contrast agents. Gd(III) is a paramagnetic ion which can enhance nuclear relaxation times for MRI.

Complexes of Gd(III) have been developed that can target particular areas of the body. For example, gadoterate meglumine, known commercially as Dotarem, is used for imaging the brain, spine and associated tissues (**Figure 1.4a**).[23] Technetium is also widely used in radiopharmaceuticals. The radioisotope ^{99m}Tc is used for PET and SPECT scans.[24] Cardiolite is one of the dominant ^{99m}Tc agents used for heart imaging in the US (**Figure 1.4b**).[18]

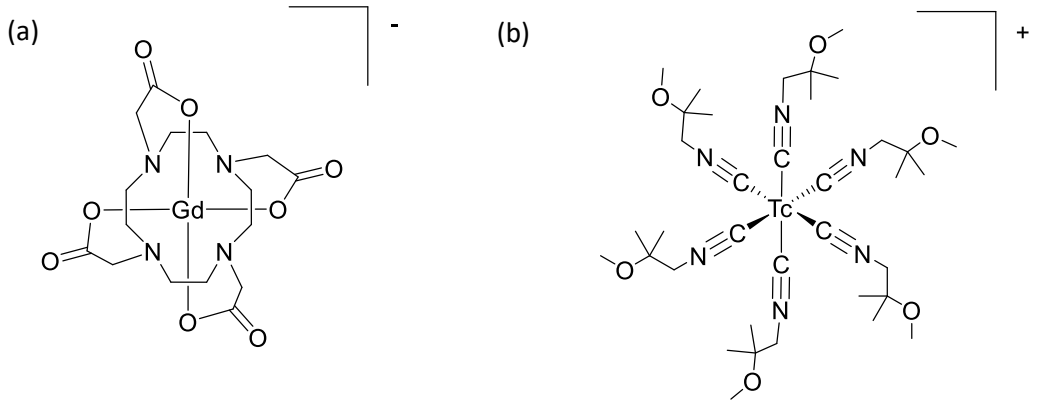

Figure 1.4: Structure of MRI contrast agent Dotarem (a) and heart imaging agent Cardiolite (b).

The activity of novel metal complexes is highly dependent on the nature of the ligands as well as the metal centre. For a complex to be biologically viable, it must be thermodynamically stable. The stability of a complex is greatly influenced by the properties of the coordinating ligands.[13] Additionally, the kinetics of the metal-ligand interaction is also an important factor, particularly when the ligand is required to dissociate from the metal centre to elicit the desired therapeutic effect. Ligands can also exist as chelating pro-drugs that interact with metal targets within the cell. These pro-drug ligands can either inhibit biological functions through coordination, or by formation of an intracellular therapeutic complex *in vivo*. Chelating ligand pro-drugs are used in the treatment of neurodegenerative conditions such as Alzheimer's and Parkinson's disease.[25, 26]

A major advancement in the field of medicinal chemistry was the incorporation of bidentate diimine ligands into metal complexes.[27] Transition metals coordinated to nitrogen containing ligands form very stable complexes. The presence of a nitrogen

atom in fused ring structural moieties such as phenanthrene and 9,10-phenanthrenequinone greatly increases antimicrobial activity compared to non-nitrogen containing compounds.[28] 1,10-Phenanthroline (phen) (**Figure 1.5a**) is a well-established N,N'-chelating ligand with diverse biological effects. Phen has the ability to act as a pro-drug as well as a coordinating ligand in many biologically relevant compounds.[29]

1.2 Phenanthroline

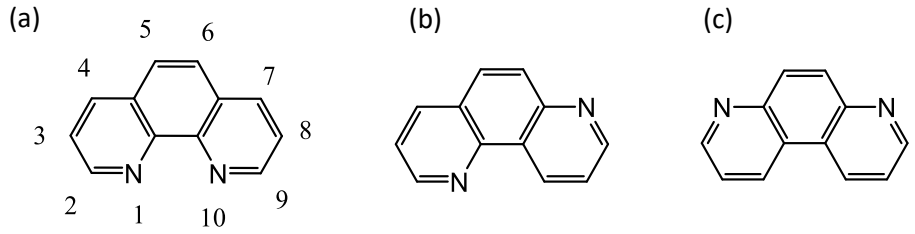

Figure 1.5: Structure of 1,10-phenanthroline (a), 1,7-phenanthroline (b) and 4,7-phenanthroline (c).

Phen is a planar fused heterocyclic system. It is a hydrophobic and electron deficient organic molecule. The basic nitrogen atoms at the 1 and 10 positions are well placed to allow for bidentate chelation to a metal centre.[8] The biological activity of phen is highly dependent on its ability to act as a chelator. In 1952, MacLeod and coworkers examined the activity of 1,7- and 4,7-phenanthroline (**Figure 1.5b,c**). Both isomers were determined to be inactive against lactic acid bacteria while 1,10-phenanthroline had good activity. They concluded that the juxtaposition of the N atoms of phen are essential for its biological effects.[30] Phen is a bidentate chelating ligand which means it can bind to a metal centre through both N atoms. The rigid nature of the N-C-C-N binding site also makes phen a more entropically favoured bidentate ligand compared to a more flexible ligand such as 2,2-bipyridine (bipy). This is supported by the fact that the binding constants for phen with various metal centres is higher than the corresponding bipy analogues of the same ion with the same stoichiometry. For example for the complexes $[MnL_3]^{2+}$, measured in 0.1 M KCl, the logarithm of the association constants are 5.6 (when L = bipy) and 12.7 (when L = phen).[31]

Synthesis of phen was first established in the late 19th century by Blau.[32] The synthesis proceeds by two successive Skraup condensation reactions. The Skraup condensation involves reaction of an aniline with glycerol in the presence of sulfuric acid and an oxidising agent such as arsenic pentoxide. Specifically, for the synthesis of phen, nitroaniline is reacted to produce 8-aminoquinoline. A second Skraup condensation reaction produces 1,10-phenanthroline monohydrate as shown in **Scheme 1.1.**[33]

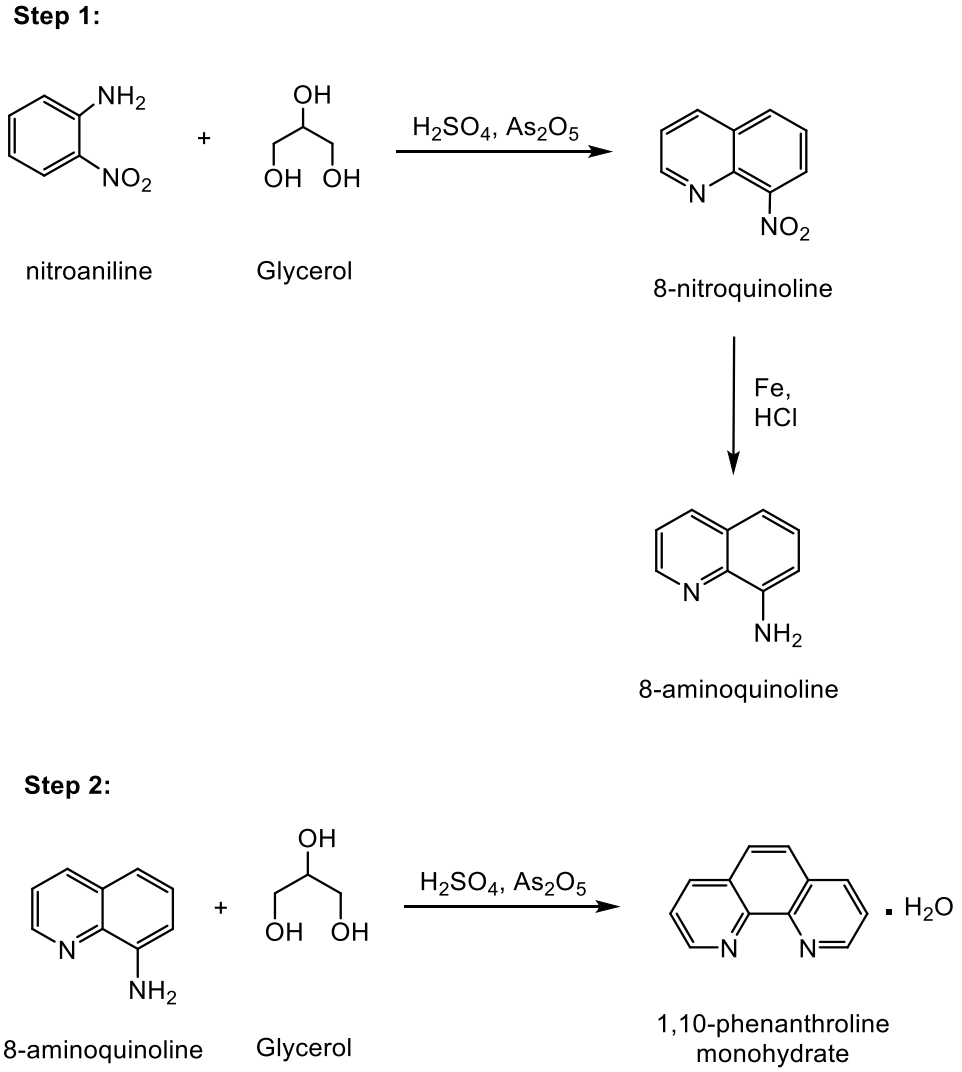

Scheme 1.1: Synthesis of 1,10-phenanthroline *via* double Skraup condensation.

Since this original synthetic approach, other methods have been developed. For example, the Wittig approach which involves reacting 2-bromonicotinaldehyde and the phosphonium salt of 2-bromo-3-bromomethylpyridine leads to phen (**Scheme**

1.2). This has also been used to produce phen derivatives substituted at the 2-, 4-, 8- or 9-positions.[34]

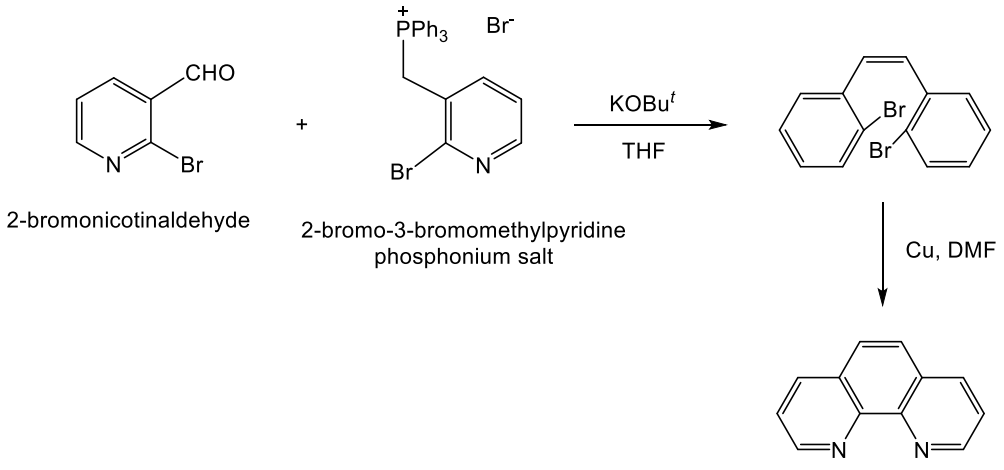

Scheme 1.2: Wittig reaction to form phen.

1.3 Biological Activity of Phenanthroline and its Derivatives

The biological effects of phen were realised in the 1950's. Leiter and coworkers discovered the antineoplastic activity of phen in a mouse model in 1953.[35] Following this, Dwyer and colleagues contributed pioneering research in the late 1960's into the antibacterial effects of phen.[36] Research in the 1970's and 1980's demonstrated the ability of phen to inhibit DNA synthesis at just 5 μM. This activity was attributed to the ability of phen to sequester zinc ions which are essential for DNA synthesis. Additionally, phen was found to inhibit entry into synthesis (S) and gap 2 (G_2) phases of the cell cycle, therefore preventing cell division.[37, 38]

It was Dwyer and coworkers who also discovered the benefits of functionalising phen; their studies revealed that alkylated derivatives had greater biological effects than unsubstituted phen against microbes. They concluded that increasing the lipophilicity of phen strongly correlated with increased potency.[36] Derivatisation of phen has led to an immense library of useful ligands which have been deployed in medicinal inorganic chemistry. The versatility of phen comes from its ability to be substituted at all positions from 2 – 8. Methylation of phen is a common modulation that has been

shown to significantly increase biological activity.[39] Symmetric di-substitution is a common modification with 4,7-dimethyl-phen (**Figure 1.5a**) and 2,9-dimethyl-phen, known as neocuproine, having been prepared (**Figure 1.2b**). The 3,5,6,8-tetramethyl-derivative (**Figure 1.5c**) is known to elicit an antibacterial effect against *Mycobacterium tuberculosis* that is 30 times greater than phen.[36] The position of the substituent(s) is an important consideration. *Ortho*-substitution was found to greatly enhance the activity of phen.[40, 41] The 2,9-disubstituted neocuproine is a highly cytotoxic agent against bacteria. A comparison of the anticancer abilities of phen and its various methylated derivatives is presented in **Table 1.1.** The 2,9-disubstituted neocuproine is significantly more active than its 4,7-analogue. The nature of the substituent can be equally important as the position of the substituent. For example, 2,9-disecbutyl-1,10-phenanthroline (SBP) (**Figure 1.5d**) was found to be far more potent than neocuproine.[27]

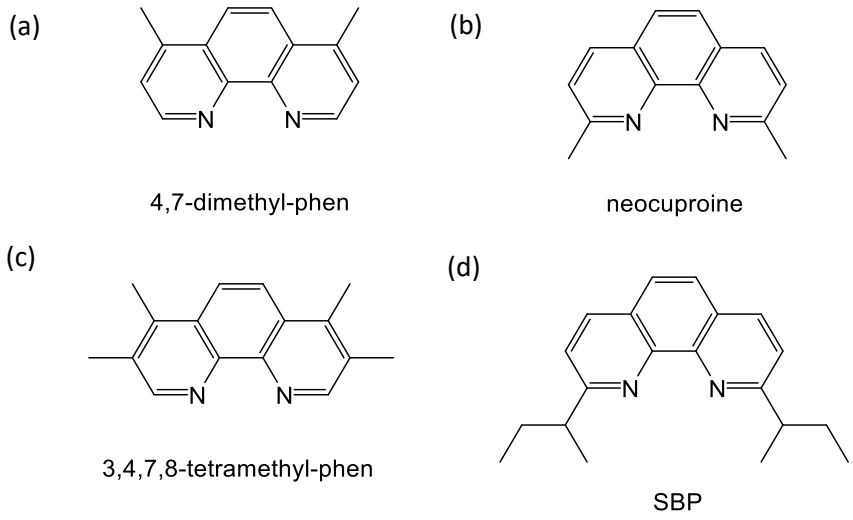

Figure 1.6: Substituted derivatives of phen with biological activity.

Table 1.1: IC_{50} values determined for methylated derivatives of phen[27]

Compound	IC_{50} (μM)*
phen	4.7
4,7-dimethyl-phen	1.9
3,4,7,8-tetramethyl-phen	1.9
2,9-dimethy-phen (neocuproine)	0.07

*tested against HL60 leukaemia cells

The 5-amino substituted phen, (5-NH_2-phen) is another highly active variant. This derivative has applications in catalysis, solar energy conversion and as pH and anions sensors.[42] 5-NH_2-phen has also been shown to possess antioxidant and antitumour abilities which are greatly enhanced by complexation to Pd(II).[43] Halogenation of phen is also possible. For example, 5-bromo-phen and 5,6-dibromo-phen can be synthesised by reacting phen with bromine and H_2SO_4.[44] These brominated phen ligands are used in chemo-sensing, catalysis and photodynamic therapy.

1,10-Phenanthroline-5,6-dione (phendione) is a well-known phen derivative first synthesised in 1947 (**Figure 1.7a**).[45] There are a number of synthetic procedures employed to synthesise phendione. Currently the most used protocol is that established by Goss and Abruna in 1985. This method involves reacting phen with $KbrO_3$ in a mixture of sulfuric and nitric acid for 4 hours.[46] Phendione is an incredibly versatile compound. The O,O'-quinoid functional group provides additional sites for coordination and increases the redox capabilities. Phendione has many uses such as in catalysis and the oxidation of amines.[47] In 2015, Tay and coworkers discovered the antimicrobial activities of phendione. They determined that phendione had the ability to completely disrupt biofilms of *Enterococcus faecalis*. The authors also concluded that the activity of phendione is due to its affinity for metal ions including Zn^{2+}, Ni^{2+}, Fe^{2+}, Cu^{2+} and Co^{2+}. Chelation of phendione to these essential microbial ions, in particular Zn^{2+}, leads to disruption of cellular homeostasis and hence microbial cell death.[48] Phendione was subsequently found to be more active than phen against a number of microbes. MIC_{50} values were determined for phen and phendione against bacteria species *S. aureus*, *E. coli* and *P. aeruginosa*. MIC_{50} values for unsubstituted phen were 278 – 416 μM (*S. aureus*), >555 μM (*E. coli*) and 416 –

555 µM (*P. aeruginosa*) while values for phendione were determined to be 30 – 45 µM (*S. aureus*) and 15 – 22 µM (*E. coli* and *P. aeruginosa*), that is phendione is about an order of magnitude more active than the parent heterocycle.[49] In addition to the significant antibacterial activity, phendione was also found to be a better antifungal agent. MIC_{50} values determined for phen and phendione against *C. albicans* were 13.9 and 2.9 µM respectively.[50] Cu(II) and Ag(I) complexes of phendione have also been reported with significant antitumour properties.[51] In recent years, phendione has been employed in the development of anti-parasitic compounds.[52, 53] The analogous compound 4,7-phenanthroline-5,6-dione, known as phanquinone, is formed through oxidation of 4,7-phenanthroline. Phanquinone is used in the treatment of Alzheimer's disease and has no known side effects.[54]

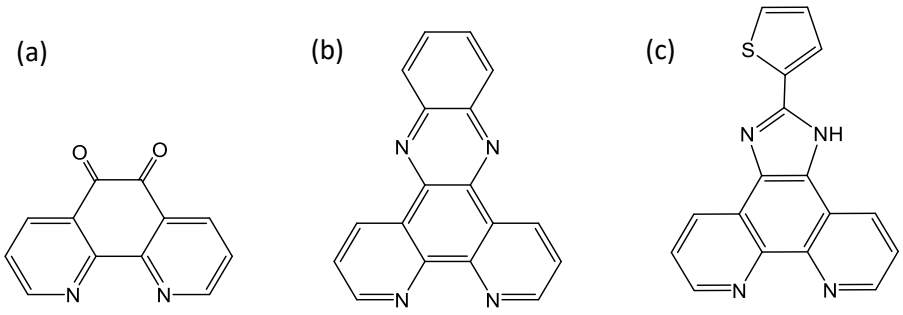

Figure 1.7: Structures of biologically relevant phen derivatives (a) phendione, (b) dppz and (c) tip

Phen derivatives have also been established with extended aromaticity. One such compound is dipyridophenazine (dppz) (**Figure 1.7b**). Dppz can be formed using a Schiff base condensation reaction between phendione and diaminobenzene (**Scheme 1.3**) [55]. 2-Thiophenimidazo[4,5-f][1,10]phenanthroline (tip) is another phen derivative with extended conjugation. Tip-based ligands have been developed for use as sensors, they have also been studied for their environmental and medicinal purposes.[56]

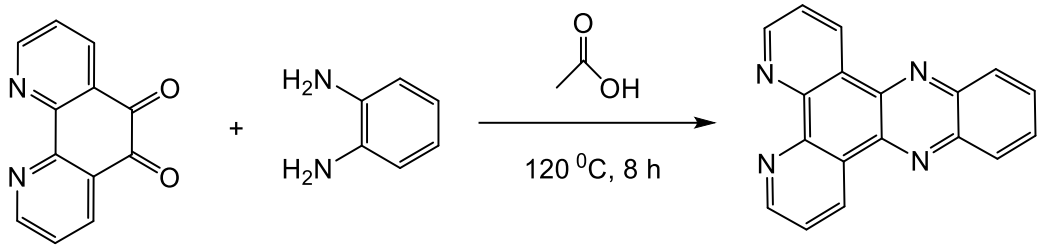

Scheme 1.3: Schiff base condensation reaction to form dipyridophenazine (dppz).

Medicinal Chemistry research has also focussed on incorporation of bioactive compounds into known therapeutic agents. In one example, folic acid was conjugated to the known cytotoxic agent curcumin. The conjugate was found to greatly increase inhibitory effects [57]. Bioconjugates of phen have been developed, examples include the ethynylestradiol and ethisterone derivatives (**Figure 1.8**).[58]

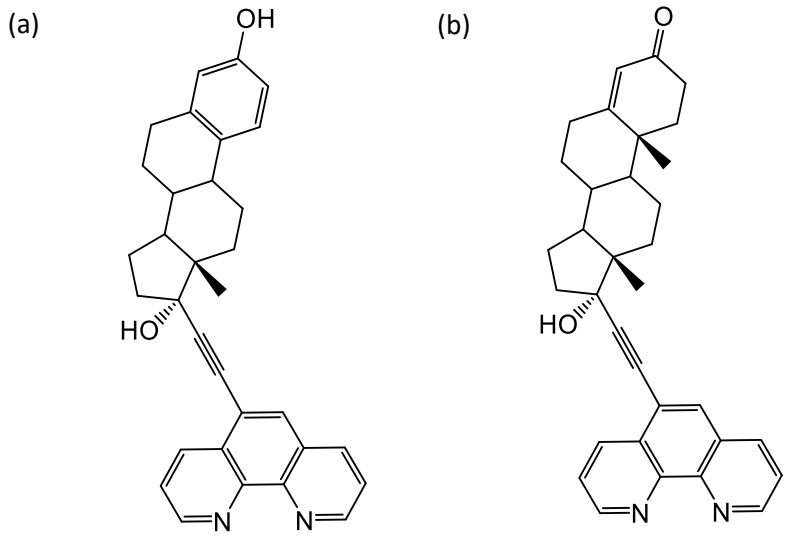

Figure 1.8: Bioconjugates of phen containing (a) ethynylestradiol and (b) ethisterone.

1.4 Metal Complexes of Phenanthroline

Phenanthroline has been a cornerstone to the development of coordination chemistry. Modulation of the core phen structure has been shown to alter the biological, photochemical and physiochemical effects.[8] Phenanthroline and its organic derivatives are of great interest for their diverse biological activities.[31] Phen and its derivatives have the potential to bind to a multitude of transition metal ions,

forming a variety of geometries. This allows for greater versatility and refinement for biological function. The biological activity of phen is primarily associated with this affinity for metal ions. This is in part a result of synergistic activity between the ligand and metal ion.[59]

The comprehensive studies by Dwyer *et al* in 1969 determined that coordination of phen to labile metal centres such as Cd(II), Cu(II), Ni(II), Co(II), Ru(II) Zn(II), and Mn(II), led to greatly improved biological activity.[36] The complexes were substantially more active than free phen against *S. aureus*, *S. pneumonia*, *M. tuberculosis*, *P. Vulgaris* and *E. coli*. The antimicrobial activity was also generally independent of the metal centre. The metal phen complexes had MIC_{50} values as low as 0.032 µM against *M. tuberculosis*, 1.9 µM against *S. aureus* and 4 µM against *S. pyogenes*. These studies also concluded that metal phen complexes were largely inactive active against gram-negative bacteria.[36] A decade after Dwyer's studies Sigman and colleagues identified DNA nuclease activity of $[Cu(phen)_2]^{2+}$ in the presence of a reducing agent. This behaviour was subsequently found to be a marker of anticancer activity.[60] Metal phen complexes have since been extensively reported for their broad spectrum antibacterial[61], antifungal[62] antiviral[63] and antitumour[64] activity.

Phen derived metal complexes have been increasingly useful in tackling microbial infections and antimicrobial resistance (AMR). Studies conducted in the 1970's demonstrated that multiple M^{2+} complexes containing 3,4,7,8-tetramethyl-phen (where M = Ni, Fe, Co, Cu, Zn, Cd, Mn, or Ru) were bactericidal against *Erysipelothrix rhusiopathiae*, a common bacterial infection in pigs. Furthermore, this bacterial species did not have the ability to gain resistance following treatment with these complexes.[65] Similar results were observed when *S. aureus*, *M. tuberculosis*, *E. coli* and *C. albicans* were treated with $[Cu(3,4,7,8\text{-tetramethyl-phen})_2]R_2$ (R = benzoate or acetate). Furthermore, the highly stable Ni(II) complex of the same ligand was found to be just as effective as the standard antiseptic hexachlorophene when used on skin prior to operations, reducing instances of *S. aureus* infections.[66] Complexation of phen continues to attract huge interest in drug design strategies. Recent studies by O'Shaughnessy and coworkers revealed the significant activity of Cu(II), Mn(II) and Ag(I) phen complexes against resistant gram-negative species *P. aeruginosa*.[67] The

authors concluded that the metal phen complexes were much more active than the analogues without phen and the metal-free ligand. Another study demonstrated the ability of Cu(I) and Ag(I) phendione complexes to inhibit *Klebsiella pneumoniae*, a gram-negative bacteria which contributes significantly to antibiotic resistance. The phendione complexes were found to have low MIC_{50} values of 9.88 µM (Cu) and 10.10 µM (Ag).[68]

The antifungal effects of phen complexes are also well documented. McCann *et al* assessed the antifungal activity of metal complexes of phendione. These studies revealed that Cu(II) and Ag(I) complexes of phendione had much lower MIC_{50} values against *C. albicans* than free phendione. In addition, the Cu(II) and Ag(I) phendione complexes were found to have greater activity than the phen analogues.[69] More recent studies by Gandra *et al* present the antifungal effects of phen and phendione based Mn(II), Cu(II) and Ag(I) complexes against eight different *Candida* species including *C. albicans*, *C. dublinesis* and *C. parapsilosis*. The majority of the complexes showed good activity across the range of species with the most active being a dimeric Mn(I) phen complex which had an MIC_{50} of 0.4 – 3.25 µM.[62]

1.4.1 Copper Complexes of Phenanthroline

Copper phen complexes have been extensively reported for their many biological abilities. Cu functions in many essential biological processes. It predominantly exists in Cu(I) and Cu(II) oxidation states. It is a vital component of numerous metalloproteins and has many enzymatic functions.[70] Cu is an excellent candidate for therapeutic agents as it is well tolerated within the body compared to other transition metals. Copper ions can disrupt metalloproteins, membrane integrity and produce reactive oxygen species (ROS). Through these mechanisms, Cu is known to elicit anti-inflammatory, anticancer, antibacterial and antifungal effects. Cu has also found use in superoxide dismutase (SOD) mimetics, nuclease mimetics and in radiopharmaceuticals.[71] Excess Cu can greatly affect pathogenesis of *S. aureus*. Two

ways this is achieved is through reduction of virulence factors produced by *S. aureus* and inhibition of biofilm formation.[72]

Ligands may be used to facilitate uptake of Cu into the cell to reach its desired target such as DNA. Cu requires a lipophilic component to enter the cell.[73] Bioactive ligands can also be incorporated that allow for synergistic effects. Phen is an excellent ligand of choice due to its well established biological effects. Cu and phen are known to work cooperatively in the complex $[Cu(phen)_2]^{2+}$ to elicit their biological effects. The hydrophobicity of phen aids passive diffusion into the nucleus where it can then intercalate DNA. The Cu(II) centre is then responsible for the nuclease activity during which the complex may release Cu ions.[74] Cu(II) phen complexes have recently been developed that substantially reduce growth and biofilm formation of *S. aureus*, *S. epidermidis* and *E. coli* which predominantly cause health-care related infections.[75]

Creaven and colleagues studied the antifungal activity of two coumarin-based complexes, $[Cu(cdoa)(phen)_2].8H_2O$ and $[Cu(4\text{-}Mecdoa)(phen)_2].13H_2O$ (where $cdoaH_2$ = coumarin-6,7-dioxyacetic acid and $4\text{-}MecdoaH_2$ = 4-methylcoumarin-6,7-dioxyacetic acid). These studies revealed the significant antifungal activity of both complexes against *C. albicans*. The complexes were much more active than the free coumarin ligands and the Cu-coumarin complexes without phen.[76]

A number Cu complexes with derivatised phen ligands have improved biological activity. Heteroleptic complexes are commonly formed with phen-based ligands. Steroid-derived phen ligands have been coordinated to Cu(II) (**Figure 1.9**). These complexes with bio-conjugated ligands exhibit significant *in vitro* and *in vivo* activity against gram-positive *S. aureus* and MRSA. MIC_{50} values were found to be 1.5 µM against *S. aureus* and 17.5 µM against MRSA.[58]

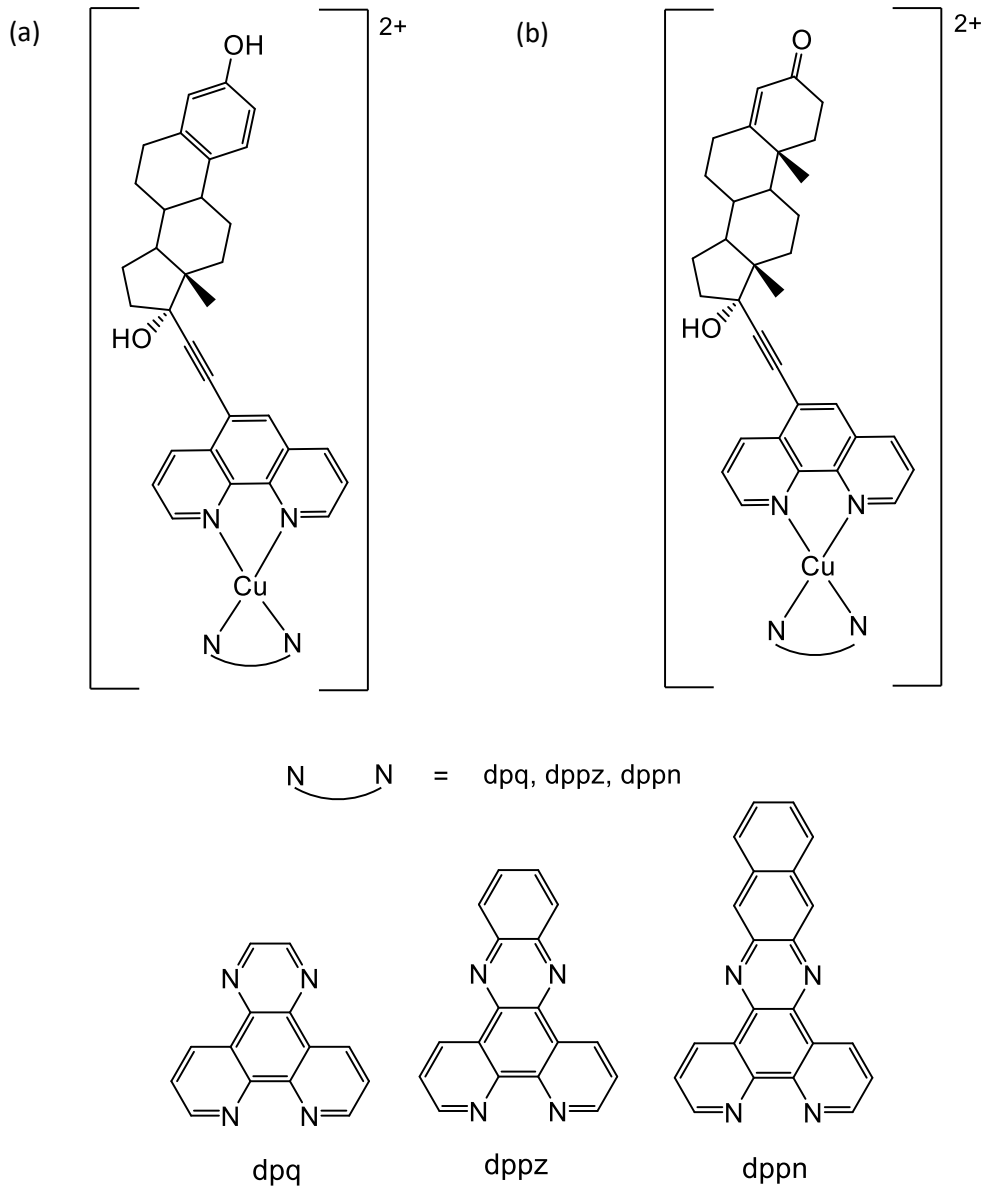

Figure 1.9: Cu(II) complexes containing a phen derivative and steroid-derived phen bioconjugate of ethynylestradiol (a) and ethisterone (b).

As mentioned in the previous section, the incorporation of amino acid moieties within complex structures have often resulted in improved biological activity. Cu(II) phen complexes with amino acids such as methionine, histidine, phenylalanine, leucine and valine have the ability to bind and cleave DNA. This has manifested in significant antibacterial activity against *Bacillus cereus* and *Micrococcus luteus.*[77] Research has also led to the incorporation of known DNA intercalators into Cu(II) phen complexes through binding of an amino acid group to enhance DNA binding capabilities. One such example is incorporation of ferrocene into a Cu(II) phen

complex (**Figure 1.10a**). This complex acts to cleave DNA upon irradiation of light.[78] Another Cu(II) phen complex that has been developed for DNA cleavage is [Cu(lomefloxacin)(NO_3)(phen)] (**Figure 1.10b**). This complex incorporates the clinical antibacterial agent, lomefloxacin which is known to target DNA and enzymes. Coordination to Cu(II) enhances DNA binding abilities and phen ensures physiological stability of the complex.[79]

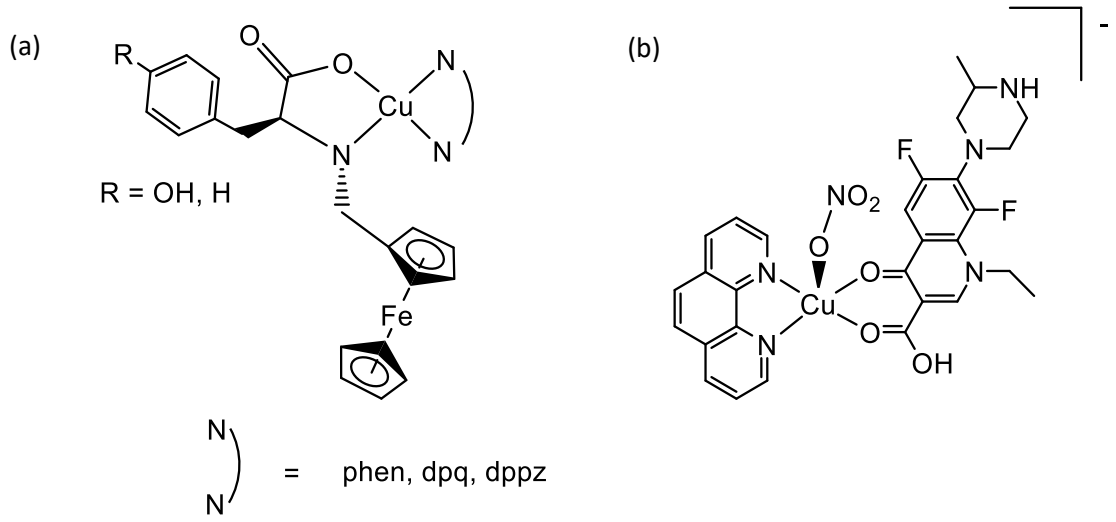

Figure 1.10: Amino acid derived Cu(II) complex (a) and [Cu(lomefloxacin)(NO_3)(phen)] (b).

1.4.2 Manganese Complexes of Phenanthroline

Manganese is another essential metal for life. It is highly versatile given its numerous oxidation states; Mn(II/III/IV).[80] It functions in many redox reactions of enzymes. One example is ribonucleotide reductase which functions to synthesise ribonucleotides for RNA and deoxyribonucleotides for DNA and enzymes including catalase, peroxidase and superoxide dismutase (SOD).[81] Mn has found application in catalysis, flame retardants, MRI contrast agents and many biomedical areas.[71] Mn complexes are well established for their antibacterial activity.[82] Mn(II) complexes have been shown to possess significant activity against gram-negative bacterial strains.[83] Mn(II) complexes have also been found to exhibit much more inhibition than the free ligands or simple Mn salts. Mn(II) have been shown to cleave DNA as a mode of action.[84]

Recent studies showed the complexes [Mn](CO)$_3$(phendione)Br] (**Figure 1.11a**) and [Mn(CO)$_3$(acridine)(phendione)]CF_3SO_3 (**Figure 1.11b**) exhibit significant anticancer activity against ovarian cancer cell line A2780. It was determined that both complexes induce production of ROS that leads to cell death.[85]

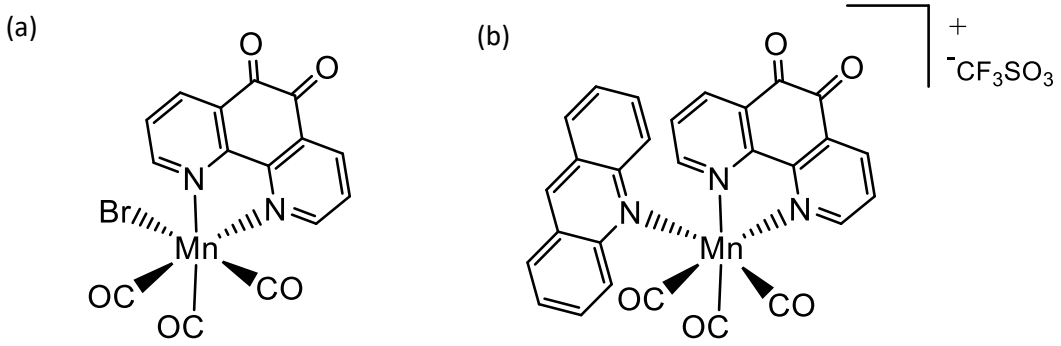

Figure 1.11: Structures of anticancer compounds [Mn(CO)$_3$(phendione)Br] (a) and [Mn(CO)$_3$(acridine)(phendione)]CF_3SO (b)

1.4.3 Ruthenium Complexes of Phenanthroline

Ruthenium complexes are also widely known for their biological effects. Ru(II) ions have been employed to improve antimicrobial activity. The conjugated dppz has been shown to possess little antibacterial activity as a free ligand.[86] However, the[Ru(bb)$_7$(dppz)]$^{2+}$ (**Figure 1.12a**) has greatly increased antibacterial activity when compared to analogous ruthenium complexes containing a phen or neocuproine (2,9-dimethyl-phen) ligand. [Ru(bb)$_7$(dppz)] has the ability to inhibit gram-positive bacterial growth at a concentration of 2 µg/ml and gram-negative growth at 8 µg/ml.[87] Another biologically relevant Ru(II) complex is [Ru(phen)$_2$(tip)]$^{2+}$ (**Figure 1.12b**). This complex possesses tip, a phen-based ligand with extended aromaticity. This complex has been shown to elicit its antibacterial activity through disruption of the bacterial cell wall and through DNA and RNA damage.[88] Ru(II) phen-based complexes have been shown to possess some antibacterial activity but this is greatly enhanced through formation of complexes with higher nuclearity.[89] Di-, tri- and tetra-Ru(II) phen-based complexes have been shown to exhibit greater inhibitory effects. In particular, di-nuclear complexes of general formula [Ru$_2$(phen)$_4$(bb$_n$)] (**Figure**

1.12c) are much more potent than the monomeric Ru(II) analogues against resistant MRSA and VRE.

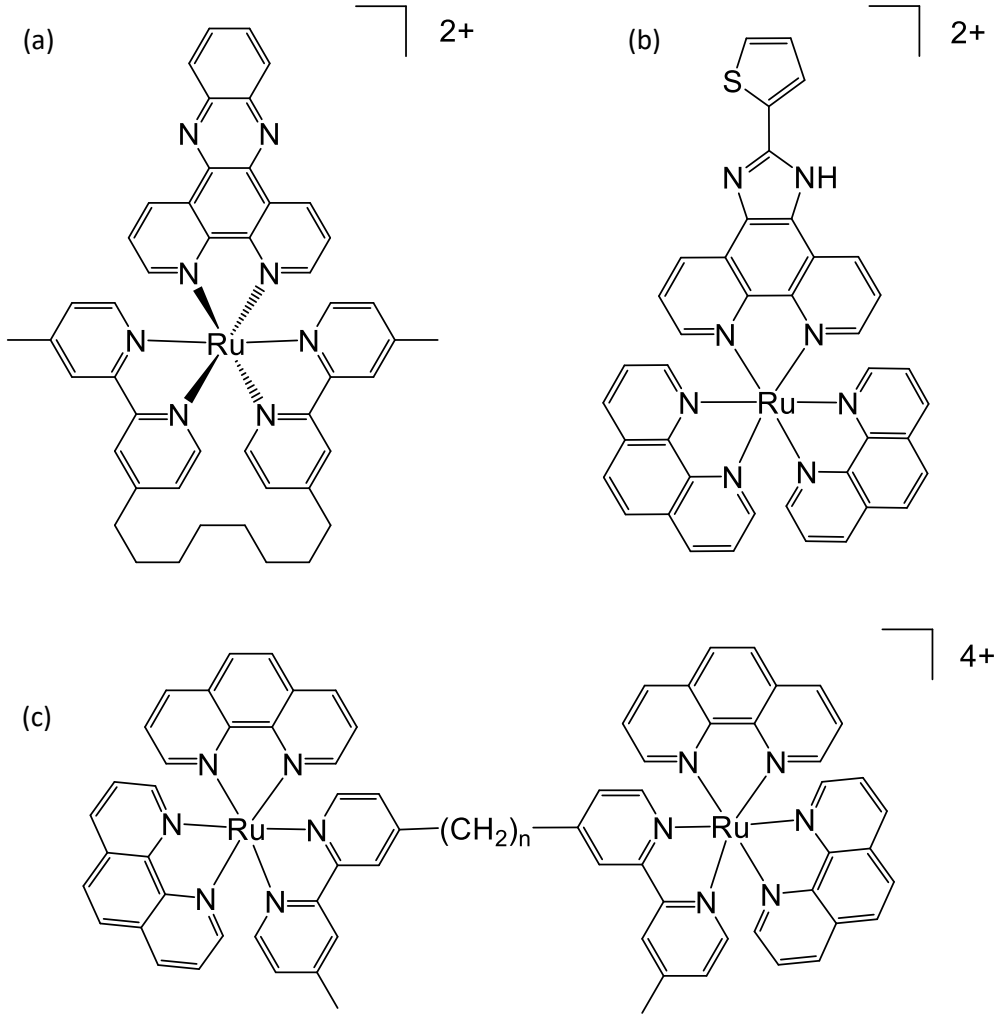

Figure 1.12: Ru(II) phen-based complexes; Ru(II) dppz (a), Ru(II) tip (b) and di-Ru(II) phen (c).

1.5 Modes of Action of Metal Phenanthroline Complexes

Metal-phen complexes exert their activity through a variety of mechanisms. A major mode of action is DNA binding and/or damage. DNA is essential for cellular processes and homeostasis which makes it a desirable target for therapeutic drugs. The planar structure of phen makes it an excellent DNA intercalator. Coordination of phen to a multitude of metal centres allows for enhanced intercalative and cleavage abilities as

well as alternative DNA binding modes.[90] Reaching DNA and other intracellular targets is dependent on the cell permeability of the complex. Phen-based ligands are hydrophobic which allow for efficient transport across the cell's membrane. Phen ligands can facilitate transport of cationic metal complexes that would not normally pass through the membrane. Introduction of a phen ligand reduces the overall polarity of the complex, making it more lipophilic.[91] This reduction in polarity can be an important strategy in drug design as permeability of gram-negative cells such as *E. coli* and *P. aeruginosa* are a particular challenge for researchers.

Some antimicrobial agents also function through cell wall damage. Disruption of the cell wall can lead to cytoplasmic leakage. This can also be coupled with DNA or RNA damage.[88] An example of a copper complex that targets the cell wall is ([Cu(4,7-diphenyl-phen)(R)]$^{2+}$ (where R = (*1S,2S*)- and (1*R*,2*R*)-diaminocyclohexane). This complex was found to severely disrupt the integrity of the cell wall of *S. aureus.*[92]

It has been extensively reported that metal phen complexes induce ROS as their mode of action. Generation of ROS leads to superoxide production and results in release of iron from iron-sulphur proteins. The free iron then catalyses the formation of hydroxyl radicals. These radicals then have the capacity to oxidise macromolecules including lipids, DNA or proteins.[8] Oxidative stress within the cell can also lead to cross-linkage of proteins and DNA, cell wall damage and deactivation of enzymes which ultimately induces cell death.[93]

Uncoordinated phen has a high affinity for metal ions. Phen-based ligands can therefore act to sequester essential metal ions within the cell. This can result in disruption or inactivation of key enzymes. Redox-active metal complexes are known to inhibit enzyme function through generation of ROS.[8] An example of a metal phen complex that inhibit enzymes is [Zn(quinolone)(phen)Cl] (quinolone = flumequine, oxolinic acid or enrofloxacin) reported by Tarushi and coworkers in 2013. This complex targets bacterial DNA gyrase and topoisomerase IV, enzymes essential for DNA replication. This complex was shown to possess significant antibacterial effects against *B. subtilis* and *B. cereus* through this mechanism.[94]

1.6 Biological Effects of Silver

It is estimated that the medicinal use of silver was apparent as early as 300 BC. The antimicrobial effects of silver were realised in the late 1800's with the use of $AgNO_3$ to treat ulcers. However, the introduction of antibiotics resulted in their use as the standard treatment of infections which meant silver-based treatments became redundant.[95] The discovery of penicillin by Scottish physician Alexander Fleming in the 1920's was ground-breaking. The next few decades, known as the 'antibiotic era' saw a surge in the development of new antibiotics. The antibiotic era is also characterised by the subsequent emergence of antibiotic resistance following misuse and overuse of new antibiotics. This led to highly resistant bacterial strains such as methicillin-resistant *Staphylococcus aureus* (MRSA) and vancomycin-resistant *Enterococcus* (VRE).[96] In recent decades, resistance to commonly used antifungals has also become apparent. Resistance to antibiotic and antifungal agents is now known collectively as antimicrobial resistance (AMR). AMR has become one of the biggest health threats, globally.[97] Resistant microbes are characterised as having either multi-drug resistance (MDR) or extensive drug resistance (XDR). MDR species are those which are non-susceptible to three or more groups of antimicrobial agents. XDR strains are those which are non-susceptible to all types of antimicrobials.[98]

The onset of AMR has led to a focus on the development of alternative treatments with new modes of action. As a result, there has been a renewed interest in the biological effects of silver. Silver was found to selectively target microbial cells over mammalian cells in the 19th century.[99] Colloidal silver was approved for wound care by the US Food and Drug Administration (FDA) in the 1920's. There are numerous silver-based treatments that are now commercially available. Solutions containing 0.5% v/v $AgNO_3$ were first used to treat burns in the 1960's. This was later adapted to incorporate the antibiotic sulphonamide to produce silver sulphadiazine, sold under the name Silvadene (**Figure 1.13**). Silvadene is a topical treatment for burns and aids prevention of infections.[95] Dilute solutions of $AgNO_3$ are used to treat conjunctivitis in newborns.[100] Silver has been employed in wound dressing products such as Acticoat and Actisorb. Vascular and catheter devices have also incorporated silver for clinical use.[101] Products have been developed with silver nanoparticles (AgNPs) that

have potent antimicrobial and antiviral effects.[102] AgNPs facilitate delivery and enhanced action of the anticancer treatment paclitaxel. This combination exhibits fewer side effects than paclitaxel alone.[103]

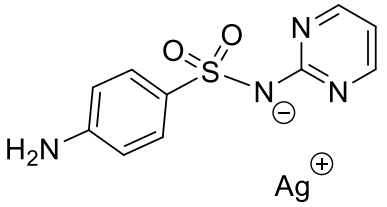

Figure 1.13: Structure of silver(I) sulfadiazine used for burns.

In recent years, as AMR has emerged, it has been noted that silver has remained effective against both sensitive and resistant cells.[104] Evidence of resistance to silver-based compounds is limited. The free Ag^+ ion can target components of the cell wall and disrupt proteins involved in cell wall synthesis.[99] Ag^+ ions have an affinity for O, N, P and S atoms which facilitates binding to amino, disulphide, carbonyl and phosphate groups of cell wall components.[104] Silver complexes are incredibly versatile and can target a broad range of microbes. Development of novel antimicrobial agents that target gram-negative bacteria is a huge challenge for researchers due to issues with cell wall permeability.[105, 106] Novel drugs that target gram-positive species are much more prevalent. One study found that pre-exposure of resistant gram-negative bacteria to Ag^+ ions can improve membrane permeability and restore susceptibility of these species to a broad range antibiotics.[107] Drug-resistant fungal infections have become increasingly prevalent in recent years. Silver is known to exhibit significant antifungal activity; Ag^+ ions can target proteins in the fungal cell wall, leading to rapid efflux of potassium ions. Additionally, Ag^+ ions target intracellular enzymes and mitochondria, disrupting their function.[108]

Ag phen complexes are well established as potent antimicrobial agents. Ag(I) complexes containing phen or phen derivatives are widely reported for their antibacterial effects.[67, 109, 110] Phen-based ligand, phen-INH is derived from the *M. tuberculosis* treatment isoniazid (INH). Complexation of the phen-INH ligand to Ag(I) (**Figure 1.14**) resulted in 5 fold greater activity (2.9 µM) than free phen-INH (15.1 µM)

against *M. tuberculosis*.[111] In other studies, $[Ag(phendione)_2]^+$ had the ability to greatly reduce mature biofilms of gram-negative *P. aeruginosa*. The complex was found to have an IC_{50} of 10.1 µM.[109] Thornton and colleagues have reported a *tris*-phen complex, $[Ag_2(phen)_3(udda)]$ ($uddaH_2$ = undecanedioic acid) with substantial antibacterial activity.[112] This Ag(I) complex had the ability to inhibit gram-positive and gram-negative bacteria. The IC_{50} values were determined to be 14.1 µM against *S. aureus*, 9.5 µM against *E. coli* and 32.4 µM against *P. aeruginosa*.

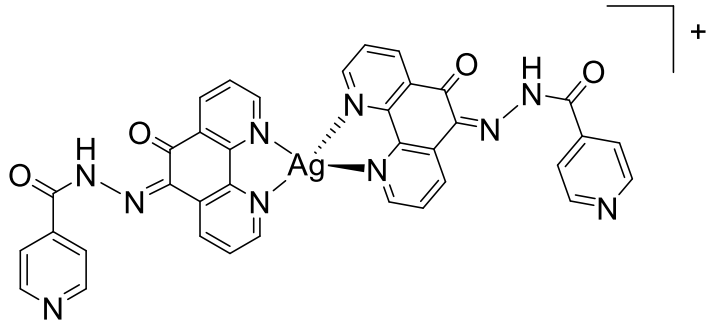

Figure 1.14: Ag(I) complex of phen-based isoniazid ligand.

The antifungal effects of Ag phen-based complexes are also well known and are particularly important since the emergence of antifungal resistance. The *bis*-phen complex $[Ag(phen)_2]ClO_4$ (**Figure 1.15a**) was found to have an MIC_{50} of 8.8 µM against *C. albicans*. The analogous phendione complex $[Ag(phendione)_2]ClO_4$ (**Figure 1.15b**) was found to have more significant antifungal activity, with an MIC_{50} of 0.5 µM.[69] Ag(I) phen complexes have also been reported for their anticancer activity.[112, 113]

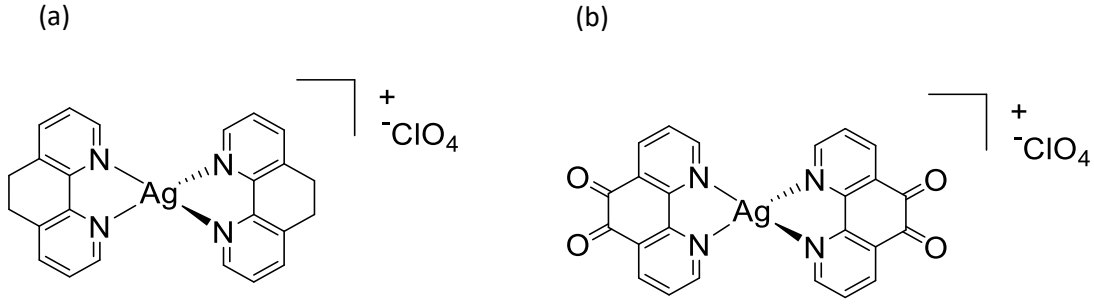

Figure 1.15: Structures of antimicrobial silver compounds $[Ag(phen)_2]ClO_4$ (a) and $[Ag(phendione)_2]ClO_4$ (b).

1.7 Applications of Rhenium

Rhenium is considered one of rarest earth metals. It is the element with the highest boiling point and the third highest melting point.[114] It has many important purposes including its use since the early 2000's to make incredibly strong superalloys for jet engines as it can withstand high temperatures.[115] The non-naturally occurring β-emitting isotopes ^{186}Re and ^{188}Re are analogous to ^{99m}Tc and used in radiopharmaceuticals as medical imaging and diagnostic agents.[116] These isotopes are also employed as biomarkers and chemical sensors.[114] Rhenium tricarbonyl complexes have been investigated for a number of decades due to their diverse photophysical and spectroscopic properties. These include long-lived luminescence, large Stokes shifts, high quantum yields as well as thermal and photochemical stability.[117, 118] Complexes containing the $Re(CO)_3$ core are usually kinetically inert which extends their half-life and hence their ability to reach the desired biological target.[117] Re(I) tricarbonyl compounds have extensive applications in electro- and photocatalysis,[119, 120] solar energy conversion,[121] artificial photosynthetic materials,[122] light-emitting diodes,[123] nuclear medicine,[124] and oncology.[125] The most biologically active Re(I) tricarbonyl complexes are those bound to bidentate N,N'-chelating ligands. It is estimated that 82% of active Re(I) tricarbonyl complexes incorporate phen-based ligands[125] which are of particular interest due to their versatility and tunability.

Re(I) tricarbonyl phen (Re phen) complexes have been extensively reported for their antimicrobial and anticancer effects. Studies by Siegmund *et al* uncovered Re phen complexes with potent antibacterial effects. The complex in **Figure 1.16a** was shown to be the most active against *S. aureus* and *B. subtilis* with MIC_{50} values of 0.7 – 1.3 µM.[126] Sovari and colleagues reported a similar Re phen complex (**Figure 1.16b**) with the ability to limit *S. aureus* growth at concentrations as low as 300 ng/mL. This complex also had the capacity to significantly reduce *C.albicans-S.aureus* and *C. albicans*-MRSA co-infections.[127]

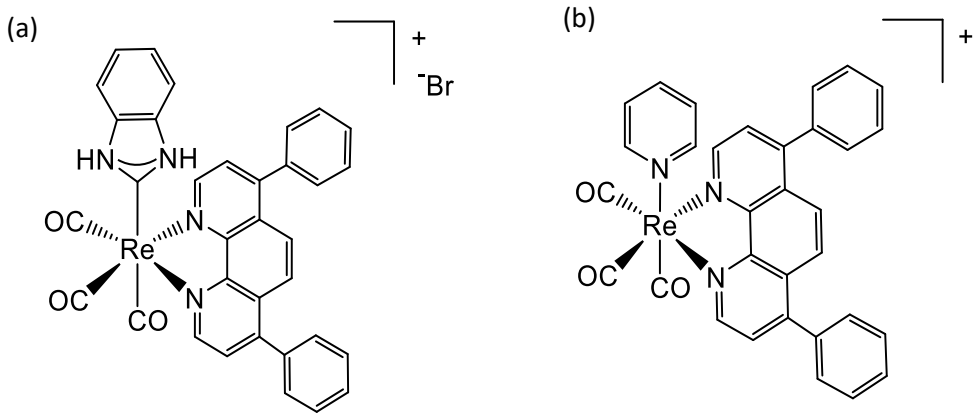

Figure 1.16: Structure of antimicrobial Re(I) tricarbonyl phen-based complexes.

Re phen complexes are most notable for their anticancer effects.[125] A key feature of these complexes is the potential for carbon monoxide release. CO-releasing molecules (CORMs) are designed to deliver controlled amounts of CO to a biological target. CORMs are employed in photodynamic therapy (PDT). This is a form of cancer treatment that involves the photo-induced release of CO into the microenvironment of the tumour.[128] Re phen complexes are widely reported as dual action pro-drugs that can act as a therapeutic complex coupled with the release of CO molecules.[129-131] The diverse luminescent properties of Re(I) tricarbonyl phen complexes has led to the development of biological labelling agents and biological probes for cellular and biomolecule imaging.[117] These compounds serve both therapeutic and diagnostic (theranostic) purposes. They can also provide key information on cellular localisation and mechanism of action using emission spectroscopy. Complexes with multiple mechanisms of action are greatly beneficial as this can reduce instances of ineffectiveness and resistance. Chemo-resistance is a huge obstacle in healthcare. Cisplatin and its analogues, oxaliplatin and carboplatin are the most widely used chemotherapies. In addition to their high toxicity and adverse side effects, instances of resistance are increasingly apparent. This is often seen with aggressive cancers such as brain, breast, prostate, ovarian and stomach.[132] Therefore, development of novel treatments to combat resistance and toxicity are necessary. Re(I) tricarbonyl compounds are of particular interest for their low *in vivo* toxicity and limited side effects.[133, 134]

Chakraborty *et al* reported the anticancer effects of luminescent $[Re(CO)_3(phen)X]$ (where X = Cl^-, $CF_3SO_3^-$, PPh_3, methylimidazole (MeIm)) (**Figure 1.17**) against breast cancer cells through photo-induced CO release. These complexes also had the ability to act as trackable CORMs, providing information on the cellular uptake and localisation. Using fluorescent confocal microscopy, it was observed that all complexes were effectively internalised by the breast cancer cells although, the cationic species (X = PPh_3, MeIm) were shown to be internalised to a greater extent than the others. All complexes were observed within the cytosol but the phosphine complex (X = PPh_3) was also present in the nucleus.[129] Marker and coworkers developed several photo-active Re phen complexes. The complexes of general formula $[Re(CO)_3(phen)(PR_3)]^+$ undergo photo-induced CO release using 365 nm UV light. Irradiation also leads to formation of reactive oxygen in the form of $^1O_2$. The complexes were found to be minimally cytotoxic in the absence of light. Irradiation of the complexes leads to significant anticancer activity against cervical (HeLa) and ovarian (A2780) cancer cell lines. The most active complex (where PR_3 = DAPTA) had an IC_{50} of 6 µM against HeLa cells upon irradiation[131]

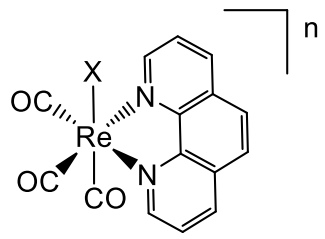

X = Cl, CF_3SO_3 (n = 0)
X = PPh_3, MeIm (n = +)

Figure 1.17: Structure of $[Re(CO)_3(phen)(X)]^n$.

Re(I) tricarbonyl complexes containing substituted and conjugated phen ligands have also been investigated for their anticancer properties. Knopf *et al* demonstrate the biodistribution and anticancer abilities of $[Re(CO)_3(neocuproine)(H_2O)]^+$ (**Figure 1.18a**). The complex had the ability to substantially limit cervical cancer (HeLa) cell viability, with an IC_{50} of 1.2 µM which was much more active than cisplatin (3.0 µM). The intrinsic luminescence of the complex revealed localisation in the cytosol. The complex was found to induce cell death by cytosolic vacuolisation rather than by

more typical pathways such as apoptosis.[130] Konkankit and coworkers demonstrated the *in vivo* anticancer abilities of $[Re(CO)_3(neocuproine)(H_2O)]^+$ against ovarian cancer cell lines A2780 and A2780CP70 . This phen-based complex was found to induce cell death by an alternative mechanism to cisplatin, greatly reducing the likelihood of resistance.[135] Enslin and colleagues studied a family of complexes that incorporated tip-based ligands. The complex shown in **Figure 1.18b** was found to be the most active against prostate (PC3) cancer cells. The complex was extremely potent with an IC_{50} of 50 nM. It was also much more active than cisplatin which had an IC_{50} of 6.9 µM.

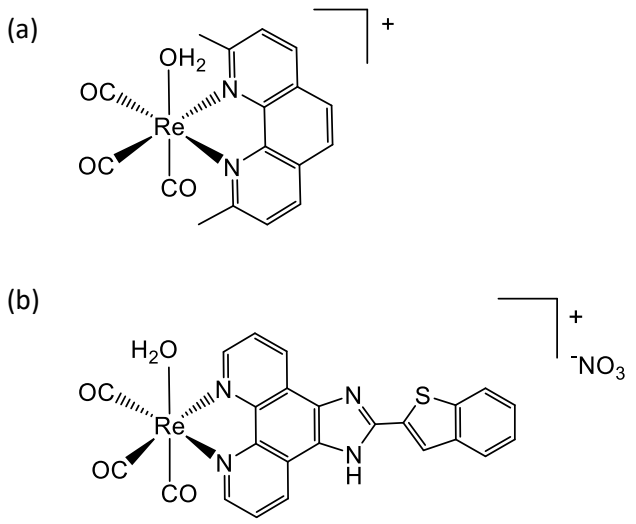

Figure 1.18: Structures of $[Re(CO)_3(neocuproine)(H_2O)]^+$ (a) and Re(I) tricarbonyl tip-based complex (b).

1.8 CO-Releasing Molecules

Carbon monoxide is well known as a colourless, highly toxic gas. CO poisoning occurs when CO molecules replace O_2 molecules in the haemoglobin proteins within red blood cells. In recent years, however, the therapeutic properties of CO have been realised. CO is produced endogenously within the body through the breakdown of heme proteins.[136] Endogenous CO has been found to play an important role in anti-inflammatory and anti-apoptotic pathways[137] as well as in vasodilation which in turns helps regulate blood pressure.[138] CO also been found to regulate the release of neurotransmitters.[128] Given the extensive benefits of CO, it is no surprise that CO-releasing molecules (CORMs) are at the forefront of drug design. CORMs can be triggered to release controlled amounts of CO into the biological environment through enzyme interaction, light stimulus and ligand exchange.[139] Metal carbonyl complexes are particularly desirable due to their stability and biocompatibility. Metal carbonyl bonds are strong due to the formation of both a σ and π bond. The σ bond is formed by donation of electrons from the carbon atom to the metal d-orbital. The π bond is then formed through donation of electrons from the metal d-orbital to an antibonding π* orbital of the CO ligand. This is known as π back-bonding and results in a highly stable metal-carbonyl bond.[140]

Metal carbonyl complexes have been extensively studied for their wide range of therapeutic applications. Metal-based CORMs have been used to provide low doses of CO to treat inflammation associated with colitis[141] and rheumatoid arthritis.[142] They have also been successful in organ preservation following transplantation and in reduction of instances of heart attack as a result of cardiovascular disease.[143] The most well-known application of metal CORMs is in photodynamic therapy to treat cancer. CO has been found to induce apoptosis of cancer cells, reduce new blood vessel formation and prevent tumour growth.[144] CORMs most commonly contain a Fe, Co, Mn or Ru metal centre.[145] The first CORM to be developed was $[Mn_2(CO)_{10}]$, known as CORM-1. This was closely followed by $[Ru(CO)_3Cl_2]_2$ (CORM-2) and $[Ru(CO)_3Cl$-glycinate] (CORM-3) (**Figure 1.19**). CORM-2 has been successful in the treatment of breast, prostate and lung cancers.[144]

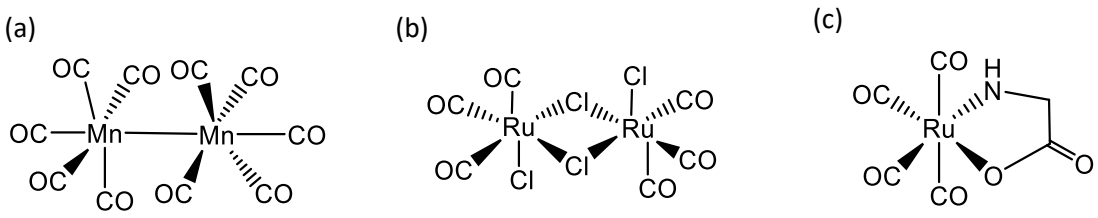

Figure 1.19: Structures of first generation CORMs, CORM-1 (a), CORM-2 (b) and CORM-3 (c)

1.9 Thesis Objectives and Structure:

This thesis focuses on the development of silver(I) and rhenium(I) complexes with the aim of producing novel antimicrobial and anticancer agents to combat drug resistance. The first aim was to synthesise two families of derivatised phen ligands: phenanthroline-oxazine (**2.1 – 2.2**) and pyrido-phenanthrolinone (**2.5 – 2.8**). The lipophilicity of the ligands would be varied through elongation of the alkyl chain of the ester moieties to identify the most biologically active derivatives. Given the biological relevance of silver outlined in this chapter, we aimed to form Ag(I) complexes from a family of phen-oxazines and assess their antifungal activity against the pathogenic yeast, *C. albicans*. The extensive literature precedent for application of Re(I) tricarbonyl complexes as CO releasing molecules also provided us with the goal of producing two novel families of CORMs: Re(I) tricarbonyl phen-oxazine (**4.1 – 4.4)** and Re(I) tricarbonyl phen-pyrido complexes (**4.5 – 4.8**). We aimed to determine the spectroscopic and electrochemical properties of the Re(I) complexes and to screen them for antimicrobial and anticancer activities.

Chapter 1: Introduction and Thesis Objectives

Chapter 2: Synthetic procedures to form starting materials, ligands and metal complexes and the associated characterisation data. Description of materials and methods for biological testing.

Chapter 3: Discussion of the synthesis and characterisation of the amino acid ester hydrochlorides (**1.1 – 1.8**), phen-derivatised ligands (**2.1 – 2.8**) and Ag(I) phen-oxazine complexes (**3.1 – 3.4**). Discussion of the stability, solution behaviour and speciation of the Ag(I) phen-oxazine complexes. Presentation of the antifungal activity of the phen-oxazine ligands (**2.1 – 2.3**) and the Ag(I) phen-oxazine complexes (**3.1 – 3.3**) against *C. albicans*. *In vivo* toxicity of phen-oxazine and Ag(I) phen-oxazine against moth larvae, *Galleria mellonella*.

Chapter 4: Discussion of the synthesis and characterisation of the Re(I) tricarbonyl complexes (**4.1 – 4.8**). Studies of their luminescent properties, CO-releasing potential and electrochemical behaviour.

Chapter 5: Biological evaluation of the ligands (**2.1 – 2.8**) and Re(I) complexes (**4.1 – 4.8**) against a range of microbes: *S. aureus*, MRSA, *E. coli* and *C. albicans* and presentation of the *in vivo* toxicity towards *G. mellonella*. Assessment of the anticancer abilities of lead compounds against ovarian cancer. Presentation of mode of action studies.

Chapter 6: Future Perspectives

Chapter 2

Experimental Methods and Characterisation Data

2.1 Materials and Instrumentation

2.1.1 Chemicals and Materials:

All chemicals, solvents and reagents were purchased from Sigma Aldrich and were used without further purification. 1,10-Phenanthroline (≥99%), potassium bromate (≥99.8%), sulfuric acid, sodium hydroxide (≥97%), L-tyrosine (≥99%), *p*-nitro-L-phenylalanine (≥98%), acetyl chloride (≥99%), *N*-methylmorpholine (≥99%), 1-propanol (≥99.9%), 1-hexanol (≥99%), 1-octanol (≥99%), dimethyl sulfoxide (≥99%), dichloromethane (≥99.8%), methanol (≥99%), ethanol (≥99%), diethyl ether (≥99%), magnesium sulfate (≥99.5%), silver perchlorate (97%), dirhenium decacarbonyl (98%), rhenium pentacarbonyl chloride (98%), DMSO-d6 (99.9%), CD_3CN (99.8%), $CDCl_3$ (99.8%).

2.1.2 Instrumentation:

NMR (Nuclear Magnetic Resonance) spectra were recorded on a Bruker Avance spectrometer operating at 500 MHz for the ^{1}H nucleus and 126 MHz for the ^{13}C nucleus. The probe temperature was maintained at 25 °C. Residual solvent peaks were used at internal standards. Chemical shifts are given in parts per million (ppm) and coupling constants (*J*) are given in Hz. Multiplicity is denoted as: bs (broad singlet), s (singlet), d (doublet), dd (doublet of doublets), m (multiplet). Proton and carbon signals were assigned with the aid of DEPT (45, 90 and 135), COSY, HMBC and HSQC 2D experiments.

FTIR spectra were recorded on a Nicolet iS50 FTIR instrument using ATR or KBr mode.

High Resolution Mass Spectrometry (HRMS) analysis was carried out at the University of Bath on a Bruker MaXis HD ESI-QTOF mass spectrometer.

CHN elemental analysis was carried out at Maynooth University on a FLASH EA 1112 Series Elemental Analyser with Eager 300 operating Software.

UV-visible spectra were recorded in a 1 cm pathlength quartz cuvette on a PerkinElmer Lambda 35 spectrometer.

Cyclic Voltammograms were recorded using a Solartron 1287 potentiostat.

2.2 Synthesis of Phenanthroline-based Ligands

2.2.1 Synthesis of 1,10-Phenanthroline-5,6-dione (2a)

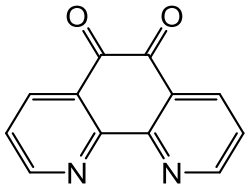

Figure 2.1: Structure of 1,10-phenanthroline-5,6-dione (**2a**)

1, 10-Phenanthroline-5,6-dione (**2a**) was synthesised with modification to a literature procedure.[146] 1,10-Phenanthroline (3.00 g, 16.65 mmol) was dissolved in cold 60% H_2SO_4 (36 mL) sitting on an ice bath. $KBrO_3$ (3.05 g, 18.18 mmol) was carefully added in small portions over 30 minutes while stirring. The reaction mixture was removed from the ice bath and heated at 30 °C overnight. The clear deep red solution was poured over ice (400 g) and neutralised using saturated NaOH solution. The product was separated using DCM, recrystallized from MeOH and washed with MeOH (3 x 20 mL) and dried under vacuum to yield the bright orange solid.

Yield: 2.86 g, 82% (fine orange solid).

^{1}H NMR (DMSO-d6, 500 MHz): **δ** 8.98 (dd, *J* = 4.6, 1.8 Hz, 2H, 2 x *ortho*-**H**), 8.38 (dd, *J* = 7.8, 1.8 Hz, 2H, 2 x *para*-**H**), 7.66 (dd, *J* = 7.8, 4.6 Hz, 2H, 2 x *meta*-**H**) ppm.

^{13}C NMR (DMSO-d6, 126 MHz): **δ** 178.2 (**C**=O), 154.8 (N-**C**H), 152.7 (N=**C**), 136.1 (**C**H), 129.5 (q**C**=C), 125.7 (**C**H) ppm.

FTIR (ATR, cm^{-1}): 3064, 1684 (**C**=O), 1564, 1462, 1414, 1294, 1201, 1113, 1033, 927, 809, 735.

2.2.2 Synthesis of L-Amino Acid Ester Hydrochlorides 1.1 – 1.8

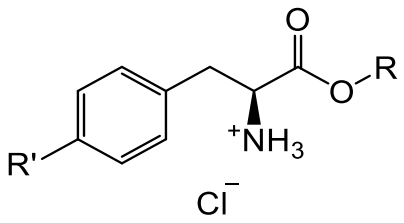

Product	R	R’	Code
1.1	CH_3	-OH	LTME
1.2	C_3H_7	-OH	LTPE
1.3	C_6H_{13}	-OH	LTHE
1.4	C_8H_{17}	-OH	LTOE
1.5	CH_3	$-NO_2$	NPME
1.6	C_2H_5	$-NO_2$	NPEE
1.7	C_3H_7	$-NO_2$	NPPE
1.8	C_6H_{13}	$-NO_2$	NPHE

Figure 2.2: Structure L-amino acid ester hydrochlorides **1.1 - 1.8**.

General Procedure 1 for the synthesis of L-amino acid ester salts 1.1 – 1.8

Synthesis of the L-amino acid ester salts was carried out with modification to a literature method.[147] Acetyl chloride (4.35 mL, 60.9 mmol) was added dropwise to cold alcohol. L-amino acid (11.04 mmol) was added and the solution was heated at reflux for 3 h before cooling to rt. The volume of the reaction solution was reduced in vacuo to ~5 mL before pouring into a beaker of diethyl ether (200 mL). The product precipitated as a white solid and was washed with diethyl ether (3 x 20 mL) and dried under vacuum.

Products **1.1 – 1.8** were synthesised using this protocol and modifications are detailed below.

L-Tyrosine methyl ester hydrochloride (1.1, LTME):

L-Tyrosine (2.00 g) was added to a MeOH solution (56 mL, 1.4 mol) containing acetyl chloride and reacted according to general procedure 1.

Yield: 2.34g, 92% (white solid).

^{1}H NMR (DMSO-d6, 500 MHz): **δ** 9.55 (s, 1H, O**H**), 8.67 (bs, 3H, $^+$N**H**$_3$), 7.01 (d, *J* = 8.5

Hz, 2H, Ar**H**), 6.74 (d, *J* = 8.5 Hz, 2H, Ar**H**), 4.12 – 4.14 (m, 1H, α**H**), 3.65 (s, 3H, -OC**H**$_3$), 3.09 (dd, *J* = 14.1, 5.6 Hz, 1H, β**H**), 3.00 (dd, *J* = 14.1, 7.8 Hz, 1H, β**H**) ppm.

^{13}C NMR (DMSO-d6, 126 MHz): **δ** 170.0 (**C**=O), 157.2 (**C**-OH), 130.8 (Ar**C**), 124.9 (Ar**C**), 115.9 (Ar**C**), 53.9 (α**C**), 52.9 (-O**C**H$_3$), 35.6 (β**C**) ppm.

FTIR (ATR, cm^{-1}): 2874 (OH), 1740 (C=O), 1617, 1588, 1521, 1445, 1451, 1228, 1143, 1108, 1060, 990, 936, 867, 842, 733.

L-Tyrosine propyl ester hydrochloride (1.2, LTPE):

L-tyrosine (2.00 g) was added to a 1-propanol solution (103, 1.4 mol) containing acetyl chloride and was reacted according to general procedure 1.

Yield: 2.54 g, 89% (white solid).

^{1}H NMR (DMSO-d6, 500 MHz): **δ** 9.45 (s, 1H, O**H**), 8.54 (bs, 3H, $^{+}$N**H**$_3$), 7.00 (d, *J* = 8.4 Hz, 2H, Ar**H**), 6.71 (d, *J* = 8.4 Hz, 2H, Ar**H**), 4.13 – 4.16 (m, 1H, α**H**), 4.00 – 4.02 (m, 2H, -OC**H**$_2$), 3.07 (dd, *J* = 14.1, 5.7 Hz, 1H, β**H**), 2.95 (dd, *J* = 14.1, 7.5 Hz, 1H, β**H**), 1.56 - 1.46 (m, 2H, C**H**$_2$), 0.80 (t, *J* = 7.4 Hz, 3H, C**H**$_3$) ppm.

^{13}C NMR (DMSO-d6, 126 MHz): **δ** 169.6 (**C**=O), 157.2 (**C**-OH), 130.8 (Ar**C**), 124.9 (Ar**C**), 115.8 (Ar**C**), 67.4 (-O**C**H$_2$), 53.9 (α**C**), 35.7 (β**C**), 21.7 (**C**H$_2$), 10.6 (**C**H$_3$) ppm.

FTIR (ATR, cm^{-1}): 2874 (OH), 1740 (C=O), 1617, 1596, 1518, 1443, 1411, 1360, 1228, 1209, 1195, 1104, 1057, 838, 729.

L-Tyrosine hexyl ester hydrochloride (1.3, LTHE):

L-tyrosine (2.00 g) was added to a 1-hexanol solution (75 mL, 0.6 mol) containing acetyl chloride. The solution was heated to 100 °C for 3 h and then hot-filtered. The

product was precipitated by pouring into a beaker containing petroleum ether (400 mL), washed with petroleum ether (3 x 50 mL) and dried under vacuum.

Yield: 2.84 g, 85% (white solid).

^{1}H NMR (DMSO-d6, 500 MHz): **δ** 9.44 (s, 1H, O**H**), 8.52 (bs, 3H, $^{+}$N**H**$_3$), 7.00 (d, *J* = 8.5 Hz, 2H, Ar**H**), 6.70 (d, *J* = 8.5 Hz, 2H, Ar**H**), 4.05 – 4.14 (m, 1H, α**H**), 4.07-3.99 (m, 2H, -OC**H**$_2$), 3.06 (dd, *J* = 14.1, 4.3, 1H, β**H**), 2.93 (dd, *J* = 14.1, 7.8 Hz, 1H, β**H**), 1.48 - 1.43 (m, 2H, C**H**$_2$), 1.27 - 1.88 (m, 3x C**H**$_2$), 0.85 (t, *J* = 14.1, 3H, C**H**$_3$) ppm.

^{13}C NMR (DMSO-d6, 126 MHz): **δ** 169.7 (**C**=O), 157.2 (**C**-OH), 130.8 (Ar**C**), 124.9 (Ar**C**), 115.8 (Ar**C**), 65.9 (-O**C**H$_2$), 53.9 (α**C**), 35.7 (β**C**), 31.3 (**C**H$_2$), 28.3 (**C**H$_2$), 25.3 (**C**H$_2$), 22.4 (**C**H$_2$), 14.4 (**C**H$_3$) ppm.

FTIR (ATR, cm^{-1}): 3283, 2864 (OH), 1736 (C=O), 1613, 1586, 1516, 1498, 1470, 1445, 1411, 1355, 1294, 1233, 1103, 1055, 983, 945, 844, 732.

L-Tyrosine octyl ester hydrochloride (1.4, LTOE):

L-Tyrosine (2.00 g) was added to a 1-octanol solution (75 mL, 0.48 mol) containing acetyl chloride. The same procedure for L-Tyrosine hexyl ester (**1.3**) above was followed.

Yield: 2.17 g, 67% (white solid).

^{1}H NMR (DMSO-d6, 500 MHz): **δ** 9.44 (s, 1H, O**H**), 8.58 (bs, 3H, $^{+}$N**H**$_3$), 7.01 (d, *J* = 8.3 Hz, 2H, Ar**H**), 6.72 (d, *J* = 8.4 Hz 2H, Ar**H**), 4.13 – 4.16 (m, 1H, α**H**), 4.03 – 4.06 (m, 2H, -OC**H**$_2$), 3.09 (dd, *J* = 14.1, 5.6 Hz, 1H, β**H**), 2.96 (dd, *J* = 14.1, 7.7 Hz, 1H, β**H**), 1.44 (m, 2H, C**H**$_2$), 1.24 (m, *J* = 8.8, 7.8 Hz, 10H, 5 x **C**H$_2$), 0.87 (t, *J* = 7.0, 3.0 Hz, 3H, C**H**$_3$) ppm.

^{13}C NMR (DMSO-d6, 126 MHz): **δ** 169.6 (**C**=O), 157.2 (**C**-OH), 130.8 (Ar**C**), 124.9 (Ar**C**), 115.8 (Ar**C**), 65.9 (-O**C**H$_2$), 53.9 (α**C**), 35.8 (β**C**), 31.7 (**C**H$_2$), 29.0 (**C**H$_2$), 28.9 (**C**H$_2$), 28.3 (**C**H$_2$), 25.7 (**C**H$_2$), 22.5 (**C**H$_2$), 14.4 (**C**H$_3$) ppm.

FTIR (ATR, cm^{-1}): 3283, 2925 (OH), 1742 (C=O), 1612, 1586, 1520, 1468, 1382, 1359, 1232, 1117, 1059, 947, 843, 731, 621, 506, 431.

4-Nitro-L-phenylalanine methyl ester hydrochloride (1.5, NPME):

p-Nitro-L-phenylalanine (2.32 g) was added to a MeOH solution (56 mL, 1.4 mol) containing acetyl chloride and reacted according to general procedure 1.

Yield: 2.37 g, 87% (white solid).

^{1}H NMR (DMSO-d6, 500 MHz): **δ** 8.87 (bs, 3H, $^+$N**H**$_3$), 8.19 (d, *J* = 8.7 Hz, 2H, Ar**H**), 7.58 (d, *J* = 8.7 Hz, 2H, Ar**H**), 4.36 – 4.39 (m, 1H, α**H**), 3.66 (s, 3H, C**H**$_3$), 3.35 (d, *J* = 5.8 Hz, 1H, β**H**), 3.28 (dd, *J* = 13.9, 7.5 Hz, 1H, β**H**) ppm.

^{13}C NMR (DMSO-d6, 126 MHz): **δ** 169.1 (**C**=O), 146.8 (Ar**C**), 143.2 (Ar**C**), 131.0 (Ar**C**), 123.6 (Ar**C**), 52.78 (-O**C**H$_3$), 52.75 (α**C**), 35.3 (β**C**) ppm.

FTIR (ATR, cm^{-1}): 1740 (C=O), 1605, 1491 (NO_2), 1454, 1342 (NO_2), 1239, 1184, 1153, 1104, 1061, 978, 952, 935, 858, 844, 812, 752, 700, 660, 508, 488.

HRMS: (ESI +): Calcd *m/z* for $C_{10}H_{12}N_2O_4$: $(M+H)^+$ 225.0870; Found $(M+H)^+$ 225.0871. Difference: 0.75 ppm.

4-Nitro-L-phenylalanine ethyl ester hydrochloride (1.6, NPEE):

p-Nitro-L-phenylalanine (2.32 g) was added to an ethanol solution (82 mL, 1.4 mol) containing acetyl chloride and reacted according to general procedure 1.

Yield: 2.68 g, 93% (white solid)

^{1}H NMR (DMSO-d6, 500 MHz): **δ** 8.73 (bs, 3H, $^+$N**H**$_3$), 8.20 (d, *J* = 8.7 Hz, 2H, Ar**H**), 7.58 (d, *J* = 8.7 Hz, 2H, ArH), 4.13 – 4.36 (m, 1H, α**H**), 4.16 - 4.06 (m, 2H, -OC**H**$_2$), 3.24 (dd, *J* = 13.9, 7.8 Hz, 1H, β**H**), 1.10 (t, *J* = 7.1Hz, 3H, C**H**$_3$) ppm.

^{13}C NMR (DMSO-d6, 126 MHz): **δ** 169.1 (**C**=O), 147.5 (Ar**C**), 144.0 (Ar**C**), 131.5 (Ar**C**), 123.8 (Ar**C**), 62.3 (-O**C**H_2), 53.2 (α**C**), 35.9 (β**C**), 14.1 (**C**H_3) ppm.

FTIR (ATR, cm^{-1}): 1734 (C=O), 1604, 1521 (NO_2), 1507, 1450, 1349 (NO_2), 1240, 1215, 1108, 1059, 1013, 855, 810, 746, 703, 646, 482, 436.

4-Nitro-L-phenylalanine propyl ester hydrochloride (1.7, NPPE):

p-Nitro-L-phenylalanine (2.32 g) was added to a 1-propanol solution (103 mL, 1.4 mol) containing acetyl chloride and reacted according to general procedure 1.

Yield: 2.92 g, 95% (white solid)

^{1}H NMR (DMSO-d6, 500 MHz): **δ** 8.73 (bs, 3H, $^{+}$N**H**$_3$), 8.20 (d, *J* = 8.6 Hz, 2H, Ar**H**), 7.58 (d, *J* = 8.8 Hz, 2H, Ar**H**), 4.34 – 4.38 (m, 1H, α**H**), 4.16 – 4.06 (m, 2H, -OC**H**$_2$), 3.24 (dd, *J* = 13.9, 7.8 Hz, 1H, β**H**), 1.444 – 1.53 (m, 2H, C**H**$_2$), 0.75 (t, *J* = 7.1 Hz, 3H, C**H**$_3$) ppm.

^{13}C NMR (DMSO-d6, 126 MHz): **δ** 169.2 (**C**=O), 147.2 (Ar**C**), 143.6 (Ar**C**), 131.4 (Ar**C**), 124.0 (Ar**C**), 67.6 (-O**C**H_2), 53.1 (α**C**), 35.9 (β**C**), 21.6 (**C**H_2), 10.5 (**C**H_3) ppm.

FTIR (ATR, cm^{-1}): 1739 (C=O), 1602, 1513 (NO_2), 1446, 1409, 1348 (NO_2), 1287, 1232, 1211, 1147, 1105, 1055, 925, 898, 877, 856, 744, 701, 657, 625, 531, 492, 455.

HRMS: Calcd *m/z* for $C_{12}H_{16}N_2O_4$: $(M+H)^+$ 253.1183; Found $(M+H)^+$ 253.1183. Difference: 0.19 ppm.

4-Nitro-L-phenylalanine hexyl ester hydrochloride (1.8, NPHE):

p-Nitro-L-phenylalanine (2.32 g) was added to a 1-hexanol solution (75 mL, 0.6 mol) containing acetyl chloride. The product was extracted as described for L-Tyrosine hexyl ester hydrochloride (**1.3**).

Yield: 2.60 g, 82% (white solid).

^{1}H NMR (DMSO-d6, 500 MHz): **δ** 8.77 (bs, 3H, $^{+}$N**H**$_3$), 8.20 (d, *J* = 8.7 Hz, 2H, Ar**H**), 7.58 (d, *J* = 8.7 Hz, 2H, Ar**H**), 4.36 – 4.39 (m, 1H, α**H**), 4.06 – 3.98 (m, 2H, -OC**H**$_2$), 3.20, (dd, *J* = 13.9, 8.6 Hz, 1H, β**H**), 1.45 – 1.34 (m, 2H, C**H**$_2$), 1.20 – 1.00 (m, 6H, 3 x C**H**$_2$), 0.81 (t, *J* = 6.9 Hz, 3H, C**H**$_3$) ppm.

^{13}C NMR (DMSO-d6, 126 MHz): **δ** 169.2 (**C**=O), 147.2 (Ar**C**), 143.7 (Ar**C**), 131.3 (Ar**C**), 124.0 (Ar**C**), 66.1 (-O**C**H$_2$), 53.1 (α**C**), 36.0 (β**C**), 31.2 (**C**H$_2$), 28.2 (**C**H$_2$), 25.3 (**C**H$_2$), 22.3 (**C**H$_2$), 14.3 (**C**H$_3$) ppm.

FTIR (ATR, cm^{-1}): 1736 (C=O), 1608, 1514 (NO_2), 1345 (NO_2), 1288, 1207, 1112, 1085, 1054, 862746, 699, 655, 481.

HRMS: Calcd *m/z* for $C_{15}H_{22}N_2O_4$: $(M+H)^+$ 295.1653; Found $(M+H)^+$ 295.1651. Difference: -0.20 ppm.

2.2.3 Synthesis of Phenanthroline-oxazine Ligands 2.1 – 2.4

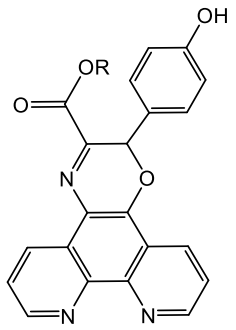

Product	R	Code
2.1	CH_3	MPO
2.2	C_3H_7	PPO
2.3	C_6H_{13}	HPO
2.4	C_8H_{17}	OPO

Figure 2.3: General structure of phenanthroline-oxazine ligands **2.1 - 2.4**.

General Procedure 2 for the synthesis of ligands 2.1 – 2.4

The appropriate L-amino acid ester hydrochloride salt (2.00 mmol) was dissolved in DMSO (35 mL) and to this solution, *N*-methylmorpholine (NMM) (0.242 mL, 2.20 mmol) was added. The solution was heated to 75 °C with stirring and phendione (**2a**) (0.42 g, 2.00 mmol) was added to give a bright yellow solution that was reacted for 24 h. The resulting clear orange solution was mixed with cold DCM (200 mL), washed

with dH_2O (5 x 150 mL) and dried using $MgSO_4$. The resulting DCM solution was evaporated to dryness to give the crude product. Hot MeOH (30 mL) was added to the crude product and this was left to stand overnight. The resulting bright yellow solid was filtered and washed with MeOH (3 x 20 mL) and dried under vacuum.

Methyl-2-(4-hydroxyphenyl)-2*H*-[1,4]oxazino[2,3-*f*][1,10]phenanthroline-3-carboxylate (2.1, MPO):

LTME (**1.1**) (0.46 g) was reacted with phendione (**2a**) according to general procedure 2.

Yield: 326.7 mg, 42% (orange solid).

^{1}H NMR (DMSO-d6, 500 MHz): **δ** 9.69 (bs, 1H, O**H**), 9.12 (dd, *J* = 4.3, 1.7 Hz, 1H, Phen**H**), 9.03 (dd, *J* = 4.3, 1.7 Hz, 1H, Phen**H**), 8.88 (dd, *J* = 8.3, 2.2 Hz, 1H, Phen**H**), 8.63 (dd, *J* = 8.2, 1.7 Hz, 1H, Phen**H**), 7.84 (dd, *J* = 8.2, 4.3 Hz, 1H, Phen**H**), 7.79 (dd, *J* = 8.3, 4.3 Hz, 1H, Phen**H**), 7.19 (d, *J* = 8.6, 2H, Ar**H**), 6.66 (d, *J* = 8.6 Hz, 2H, Ar**H**), 6.58 (s, 1H, oxazine-**H**), 3.89 (s, 3H, C**H**$_3$) ppm.

^{13}C NMR (DMSO-d6, 126 MHz): **δ** 163.1 (**C**=O), 159.2 (**C**-OH), 152.0 (Phen**C**), 150.1 (oxazine**C**=N), 149.1 (Phen**C**), 146.8 (Phen**C**), 142.7 (Phen**C**), 138.8 (Phen**C**-O), 131.4 (Phen**C**), 130.3 (Phen**C**), 129.4 (Ar**C**), 126.4 (Phen**C**-N), 125.2 (Ar**C**), 124.6 (Phen**C**), 124.2 (Phen**C**), 122.2 (Phen**C**), 121.6 (Phen**C**), 116.2 (Ar**C**), 72.4 (oxazine**C**-O), 53.4 (-O**C**H$_3$) ppm.

FTIR (ATR, cm^{-1}): 3280 (OH), 1708 (C=O), 1609, 1589, 1513, 1503, 1436, 1350, 1258, 1173, 1132, 1063, 1020, 970, 920, 806, 739, 678.

Propyl-2-(4-hydroxyphenyl)-2*H*-[1,4]oxazino[2,3-*f*][1,10]phenanthroline-3-carboxylate (2.2, PPO):

LTPE (**1.2**) (0.52 g) was reacted with phendione (**2a**) according to general procedure 2.

Yield: 359.9 mg, 43% (orange solid).

^{1}H NMR (DMSO-d6, 500 MHz): **δ** 9.69 (bs, 1H, O**H**), 9.12 (dd, *J* = 4.3, 1.7 Hz, 1H, Phen**H**), 9.03 (dd, *J* = 4.3, 1.7 Hz, 1H, Phen**H**), 8.88 (dd, *J* = 8.2, 1.7 Hz, 1H, Phen**H**), 8.59 (dd, *J* = 8.2, 1.7 Hz, 1H, Phen**H**), 7.85 (dd, *J* = 8.2, 4.3 Hz, 1H, Phen**H**), 7.79 (dd, *J* = 8.3, 4.3 Hz, 1H, Phen**H**), 7.19 (d, *J* = 8.5 Hz, 2H, Ar**H**), 6.66 (d, *J* = 8.6 Hz, 2H, Ar**H**), 6.5 (s, 1H, oxazine-**H**), 4.29 – 4.20 (m, 2H, -OC**H**$_2$), 1.73 – 1.66 (m, 2H, C**H**$_2$), 0.91 (t, *J* = 7.3, 3H, C**H**$_3$) ppm.

^{13}C NMR (DMSO-d6, 126 MHz): **δ** 162.0 (**C**=O), 158.7 (**C**-OH), 151.6 (Phen**C**), 150.2 (oxazine **C**=N), 148.7 (Phen**C**), 146.1 (Phen**C**), 141.9 (Phen**C**), 138.4 (Phen**C**), 131.1 (Phen**C**), 129.9 (Phen**C**), 128.9 (Ar**C**), 126.0 (Phen**C**-N), 124.9 (Ar**C**), 124.2 (Phen**C**), 123.9 (Phen**C**), 121.6 (Phen**C**), 121.2 (Phen**C**), 115.8, (Ar**C**), 72.2 (oxazine O-**C**H), 67.1 (-O**C**H$_2$), 21.4 (**C**H$_2$), 10.2 (**C**H$_3$) ppm.

FTIR (ATR, cm^{-1}): 2968 (OH), 1733 (C=O), 1611, 1572, 1515, 1499, 1457, 1445m 1380, 1312, 1284, 1253, 1222, 1171, 1096, 1073, 1022, 967, 925, 865, 806, 785, 744, 677.

Hexyl-2-(4-hydroxyphenyl)-2*H*-[1,4]oxazino[2,3-*f*][1,10]phenanthroline-3-carboxylate (2.3, HPO):

LTHE (**1.3**) (0.60 g) was reacted with phendione (**2a**) according to general procedure 2.

Yield: 342 mg, 36% (orange solid).

^{1}H NMR (DMSO-d6, 500 MHz): **δ** 9.72 (bs, 1H, O**H**), 9.12 (dd, *J* = 4.3, 1.7 Hz, 1H, Phen**H**), 9.03 (dd, *J* = 4.3, 1.7 Hz, 1H, Phen**H**), 8.87 (dd, *J* = 8.2, 1.7 Hz, 1H, Phen**H**), 8.58 (dd, *J* = 8.3, 1.7 Hz, 1H, Phen**H**), 7.85 (dd, *J* = 8.2, 4.3 Hz, 1H, Phen**H**), 7.79 (dd, *J* = 8.2, 4.3 Hz, 1H, Phen**H**), 7.18 (d, *J* = 8.6 H, 2H, Ar**H**), 6.65 (d, *J* = 8.7 Hz, 2H, Ar**H**), 6.57 (s, 1H, oxazine-**H**), 4.32 – 4.22 (m, 2H, -OC**H**$_2$), 1.68 – 1.62 (m, 2H, C**H**$_2$), 1.31 – 1.23 (m, 6H, 3 x C**H**$_2$), 0.85 (t, *J* = 3.3, 3H, C**H**$_3$) ppm.

^{13}C NMR (DMSO-d6, 126 MHz): **δ** 162.0 (**C**=O), 158.8 (**C**-OH), 151.5 (Phen**C**), 150.2 (oxazine **C**=N), 148.6 (Phen**C**), 146.4 (Phen**C**), 142.2 (Phen**C**), 138.4 (Phen **C**-O), 130.9

(Phen**C**), 129.8 (Phen**C**), 129.0 (Ar**C**), 126.0 (Phen**C**-N), 124.9 (Ar**C**), 124.1 (Phen**C**), 123.8 (Phen**C**), 121.6 (Phen**C**), 121.2 (Phen**C**), 115.8 (Ar**C**), 72.2 (oxazine O-**C**H), 65.7 (-O**C**H_2), 30.8 (**C**H_2), 27.9 (**C**H_2) 24.9 (**C**H_2), 22.0 (**C**H_2), 13.9 (**C**H_3) ppm.

FTIR (ATR, cm^{-1}): 3088 (OH), 1705 (C=O), 1601, 1583, 1514, 1450, 1434, 1339, 1264, 1239, 1193, 1171, 1131, 1093, 1057, 1021, 956, 840, 817, 740, 684.

Octyl-2-(4-hydroxyphenyl)-2*H*-[1,4]oxazino[2,3-*f*][1,10]phenanthroline-3-carboxylate (2.4 OPO):

LTOE (**1.4**) (0.66 g) was reacted with phendione (**2a**) according to general procedure 2.

Yield: 280 mg, 29% (orange solid).

^{1}H NMR (DMSO-d6, 500 MHz): **δ** 9.77 (s, 1H, OH), 9.20 (dd, *J* = 4.2, 1.6 Hz, 1H, Phen**H**), 9.11 (dd, *J* = 4.2, 1.6 Hz, 1H, Phen**H**), 8.95 (dd, *J* = 8.2, 1.6 Hz, 1H, Phen**H**), 8.67 (dd, *J* = 8.2, 1,6 Hz, 1H, Phen**H**), 7.93 (dd, *J* = 8.2, 4.3 Hz, 1H, Phen**H**), 7.86 (dd, *J* = 8.2, 4.3 Hz, 1H, Phen**H**), 7.26 (d, *J* = 8.6 Hz, 2H, Ar**H**), 6.72 (d, *J* = 8.6 Hz, 2H, Ar**H**), 4.36 (t, 2H, -OC**H**$_2$), 1.73 (m, 2H, C**H**$_2$), 1.35 (m, *J* = 16.9, 7,3 Hz, 10H, C**H**$_2$), 0.91 (t, *J* = 6.9 Hz, 3H, C**H**$_3$) ppm.

^{13}C NMR (DMSO-d6, 126 MHz): **δ** 162.4 (**C**=O), 159.2 (**C**-OH), 152.0 (Phen**C**-H), 150.6 (oxazine **C**=N), 149.1 (Phen**C**-H), 146.8 (Phen**C**), 142.7 (Phen**C**), 138.8 (Phen**C**), 131.4 (Phen**C**-H), 130.2 (Phen**C**-H), 129.4 (Ar**C**), 126.5 (Phen**C**), 125.4 (Ar**C**), 124.5 (Phen**C**-H), 124.2 (Phen**C**-H), 122.1 (Phen**C**), 121.7 (Phen**C**), 116.2 (Ar**C**), 72.7 (oxazine O-**C**H), 66.2 (-O**C**H_2), 31.6 (**C**H_2), 29.0 (**C**H_2), 29.0 (**C**H_2), 28.4 (**C**H_2), 25.7 (**C**H_2), 22.5 (**C**H_2), 14.4 (**C**H_3) ppm.

FTIR (ATR, cm^{-1}): 3213 (OH), 1738 (C=O), 1609, 1894, 1576, 1516, 1465, 1431, 1373, 1312, 1276, 1236, 1222, 1194, 1171, 1139, 1097, 1072, 1024, 945, 839, 817, 793, 743, 677.

2.2.4 Synthesis of Pyrido-Phenanthrolinone Ligands 2.5 – 2.8

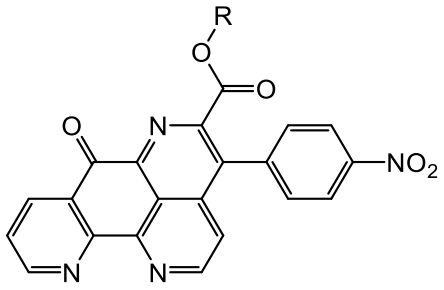

Product	R	Code
2.5	CH_3	MPP
2.6	C_2H_5	EPP
2.7	C_3H_7	PPP
2.8	C_6H_{13}	HPP

Figure 2.4: General structure of pyrido-phenanthrolinone ligands (**2.5 - 2.8**).

General Procedure 3 for the synthesis of ligands 2.5 – 2.8

The appropriate L-amino acid ester hydrochloride salt (2.00 mmol) was dissolved in DMSO (35 mL). The solution was heated to 75 °C with stirring and phendione (**2a**) (0.42 g, 2.00 mmol) was added to give an orange solution and was reacted for 24 h. The resulting clear deep red solution was mixed with cold DCM (200 mL), washed with dH_2O (7 x 150 mL) and dried using $MgSO_4$. The resulting DCM solution was evaporated to dryness to give the crude product. Hot EtOH (30 mL) was added to the crude product, and it was left to stand overnight. The resulting brown solid was filtered and washed with EtOH (3 x 20mL) and dried under vacuum.

Methyl 4-(4-nitrophenyl)-7-oxo-7*H*-pyrido[4,3,2-*de*][1,10]phenanthroline-5-carboxylate (2.5, MPP)

NPME (**1.5**) (0.49 g) reacted with phendione (**2a**) according to general procedure 3.

Yield: 164.3 mg, 20% (brown solid).

^{1}H NMR (DMSO-d6, 500 MHz): **δ** 9.15 (dd, *J* = 1.4, 4.4 Hz, 1H, Phen**H**), 9.07 (d, *J* = 5.8 Hz, 1H, Phen**H**), 8.67 (dd, *J* = 1.2, 7.9 Hz, 1H, Phen**H**), 8.48 (d, *J* = 8.6 Hz, 2H, Ar**H**), 7.86 (dd, *J* = 4.6, 7.6 Hz, 1H, Phen**H**), 7.79 (d, *J* = 8.6 Hz, 2H, Ar**H**), 7.60 (d, *J* = 5.8, 1H, Phen**H**), 3.5 (s, 3H, C**H**$_3$) ppm.

^{13}C NMR (DMSO-d6, 126 MHz): **δ** 180.5 (**C**=O), 165.6 (ester **C**=O), 154.9 (Phen**C**), 151.2 (Phen**C**), 150.3 (Phen**C**), 148.8 (Phen**C**), 147.8 (Ar**C**), 146.7 (pyrido **C**-N), 145.7

(Phen**C**=N) 140.5 (Ar**C**), 138.1 (Phen**C**), 135.6 (Phen**C**), 134.0 (pyrido N-**C**), 131.2 (Ar**C**), 129.0 (Phen**C**), 126.2 (Phen**C**), 123.7 (Ar**C**), 120.3 (Phen**C**), 119.2 (Phen**C**), 52.87 (**C**H_3) ppm.

FTIR (ATR, cm^{-1}): 1732 (C=O), 1677 (C=O), 1597, 1579, 1504 (NO_2), 1343 (NO_2), 1285, 1210, 1104, 858, 711, 608.

HRMS (**ESI +):** Calcd *m/z* for $C_{22}H_{12}N_4O_5$: $(M+Na)^+$ 435.0711; Found $(M+Na)^+$ 435.0707. Difference: 2.68 ppm.

UV-vis: ε = 10,843 M^{-1} cm^{-1} (DMSO, λ_{max} = 378 nm).

Ethyl 4-(4-nitrophenyl)-7-oxo-7*H*-pyrido[4,3,2-*de*][1,10]phenanthroline-5-carboxylate (2.6, EPP)

NPEE (**1.6**) (0.52 g) reacted with phendione (**2a**) according to general procedure 3.

Yield: 136 mg, 16% (brown solid).

^{1}H NMR (DMSO-d6, 500 MHz): **δ** 9.15 (dd, *J* = 1.7, 4.5, 1H, Phen**H**), 9.07 (d, *J* = 5.6 Hz, 1H, Phen**H**), 8.67 (dd, *J* = 1.7, 7.9 Hz, 1H, Phen**H**), 8.48 (d, *J* = 8.7, 2H, Ar**H**), 7.85 (dd, *J* = 4.6, 7.9 Hz, 1H, Phen**H**), 7.79 (d, *J* = 8.7 Hz, 2H, Ar**H**), 7.61 (d, *J* = 5.9 Hz, 1H, Phen**H**), 4.18 (dd, *J* = 7.1, 14.2 Hz, 2H, OC$\mathbf{H}_2$), 1.02 (t, *J* = 7.2 Hz, 3H, C$\mathbf{H}_3$) ppm.

^{13}C NMR (DMSO-d6, 126 MHz): **δ** 180.5 (**C**=O), 165.1 (ester **C**=O), 154.9 (Phen**C**), 151.2 (Phen**C**), 150.3 (Phen**C**), 148.8 (Phen**C**), 147.9 (Ar**C**), 146.7 (pyrido **C**-N), 146.2 (Phen**C**=N), 140.5 (Ar**C**), 138.0 (Phen**C**), 135.6 (Phen**C**), 133.6 (pyrido N-**C**), 131.3 (Ar**C**), 129.0 (Phen**C**), 126.2 (Phen**C**), 123.7 (Ar**C**), 120.2 (Phen**C**), 119.2 (Phen**C**), 61.8 (-O**C**H_2), 13.5 (**C**H_3) ppm.

FTIR (ATR, cm^{-1}): 1723 (C=O), 1678 (C=O), 1598, 1581, 1508 (NO_2), 1341 (NO_2), 1284, 1206, 1104, 866, 709, 606.

HRMS (ESI +): Calcd *m/z* for $C_{23}H_{14}N_4O_5$: $(M+Na)^+$ 449.0866; Found $(M+Na)^+$ 449.0865. Difference: 3.04 ppm.

CHN (%): Calculated $C_{23}H_{14}N_4O_5$: C, 64.79; H, 3.31; N, 13.14. Found: C, 64.55; H, 3.09; N, 13.25.

UV-vis: ε = 10,010 M^{-1} cm^{-1} (DMSO, λ_{max} = 376 nm).

Propyl 4-(4-nitrophenyl)-7-oxo-7*H*-pyrido[4,3,2-*de*][1,10]phenanthroline-5-carboxylate (2.7, PPP)

NPPE (**1.7**) (0.55 g) reacted with phendione (**2a**) according to general procedure 3.

Yield: 172.8 mg, 19% (brown solid).

^{1}H NMR (DMSO-d6, 500 MHz): **δ** 9.14 (dd, *J* = 1.8, 4.6 Hz, 1H, Phen**H**), 9.06 (d, *J* = 5.9 Hz, 1H, Phen**H**), 8.66 (dd, *J* = 1.8, 7.95 Hz, 1H, Phen**H**), 8.48 (d, *J* = 8.8 Hz, 2H, Ar**H**), 7.85 (dd, *J* = 4.6, 7.9 Hz, 1H, Phen**H**), 7.81 (d, *J* = 8.8 Hz, 2H, Ar**H**), 7.61 (d, *J* = 5.4 Hz, 1H, Phen**H**), 4.11 – 4.08 (m, 2H, -OC**H**$_2$), 1.45 – 1.41 (m, 2H, C**H**$_2$), 0.76 (t, *J* = 7.4 Hz, 3H, C**H**$_3$) ppm.

^{13}C NMR (DMSO-d6, 126 MHz): **δ** 180.5 (**C**=O), 165.3 (ester **C**=O), 154.9 (Phen**C**), 151.1 (Phen**C**), 150.3 (Phen**C**), 148.8 (Phen**C**), 147.9 (Ar**C**), 146.7 (pyrido **C**-N), 146.4 (Phen**C**=N), 140.4 (Ar**C**), 138.0 (Phen**C**), 135.6 (Phen**C**), 133.4 (pyrido **C**-N), 131.3 (Ar**C**), 129.0 (Phen**C**), 126.2 (Phen**C**), 123.7 (Ar**C**), 120.2 (Phen**C**), 119.2 (Phen**C**), 67.3 (-O**C**H$_2$), 21.1 (**C**H$_2$), 10.0 (**C**H$_3$) ppm.

FTIR (ATR, cm^{-1}): 1727 (C=O), 1676 (C=O), 1600, 1581, 1518 (NO_2), 1345 (NO_2), 1281, 1232, 1203, 1177, 1127, 1106, 999, 938, 862, 818, 769, 746, 699, 661, 611, 507, 423.

HRMS (ESI +): Calcd *m/z* for $C_{24}H_{16}N_4O_5$: $(M+Na)^+$ 463.1013; Found $(M+Na)^+$ 463.1016. Difference: 2.52 ppm.

CHN (%): Calculated $C_{24}H_{16}N_4O_5.H_2O$: C, 62.88; H, 3.96; N, 12.22. Found: C, 63.06; H, 3.85; N, 12.25.

UV-vis: 8,154.3 M^{-1} cm^{-1} (DMSO, λ_{max} = 377 nm).

Hexyl 4-(4-nitrophenyl)-7-oxo-7*H*-pyrido[4,3,2-*de*][1,10]phenanthroline-5-carboxylate (2.8, HPP)

NPHE (**1.8**) (0.62 g) reacted with phendione (**2a**) according to general procedure 3.

Yield: 153 mg, 15% (red solid).

^{1}H NMR (DMSO-d6, 500 MHz): **δ** 9.12 (dd, *J* = 1.8, 4.6 Hz, 1H, Phen**H**), 9.04 (d, *J* = 5.9 Hz, 1H Phen**H**), 8.65 (dd, *J* = 1.8, 8.0 Hz, 1H, Phen**H**), 8.47 (d, *J* = 8.7 Hz, 2H, Ar**H**), 7.84 (dd, *J* = 4.6, 7.9 Hz, 1H, Phen**H**), 7.79 (d, *J* = 8.8 Hz, 2H, Ar**H**), 7.60 (d, *J* = 5.9 Hz, 1H, Phen**H**), 4.10 (t, *J* = 6.4 Hz, 2H, -OC**H**$_2$), 1.33 - 1.28 (m, 2H, C**H**$_2$), 1.18 - 1.04 (m, 6H, 3 x C**H**$_2$), 0.80 (t, *J* = 7.1 Hz, 3H, C**H**$_3$) ppm.

^{13}C NMR (DMSO-d6, 126 MHz): **δ** 181.1 (C=O), 165.8 (ester C=O), 155.4 (PhenC) 151.6 (PhenC), 150.7 (PhenC), 149.3 (PhenC), 148.3 (ArC), 147.3 (pyridoC=N), 146.9 (PhenC=N), 141.0 (ArC), 138.5 (PhenC), 136.1 (PhenC), 133.8 (pyridoC), 131.9 (ArC-H), 129.5 (PhenC), 126.8 (PhenC), 124.3 (ArC-H), 120.7 (PhenC), 119..7 (PhenC), 66.4 (-OCH$_2$), 31.3 (CH$_2$), 28.1 (CH$_2$), 25.3 (CH$_2$), 22.3 (CH$_2$), 14.3 (CH$_3$) ppm.

FTIR (ATR, cm^{-1}): 1733 (C=O), 1680 (C=O), 1598, 1581, 1509 (NO$_2$), 1343 (NO$_2$), 1284, 1284, 1235, 1207, 1104, 1018, 863, 815, 770, 744. 711, 607.

HRMS (ESI +): Calcd *m/z* for $C_{27}H_{22}N_4O_5$: $(M+Na)^+$ 505.1482; Found $(M+Na)^+$ 505.1488. Difference: 2.26 ppm.

UV-vis: 9,433 M^{-1} cm^{-1} (DMSO, λ_{max} = 376 nm).

2.3 Metal Complexation

2.3.1 Synthesis of Silver(I) Complexes 3.1 – 3.4

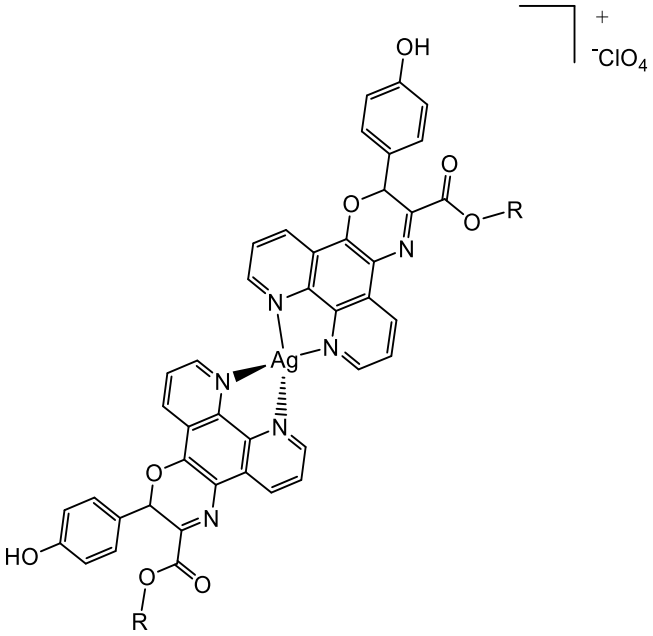

Product	R	Code
3.1	CH_3	$[Ag(MPO)_2]ClO_4$
3.2	C_3H_7	$[Ag(PPO)_2]ClO_4$
3.3	C_6H_{13}	$[Ag(HPO)_2]ClO_4$
3.4	C_8H_{17}	$[Ag(OPO)_2]ClO_4$

Figure 2.5: Proposed structure of silver(I) complex of phenanthroline-oxazine ligands (**3.1 – 3.4**).

General procedure 4 for the synthesis of complexes 3.1 – 3.4

$AgClO_4$ (54 mg, 0.25 mmol) was added to heated ACN (100 mL) containing ligand (0.52 mmol). The reaction mixture was heated at reflux for 2 h in the absence of light. The resulting yellow solution was cooled to rt and was reduced *in vacuo* to ~5 mL. The product was precipitated by addition to a beaker of cold diethyl ether (400 mL). The product was retrieved from the mixture via vacuum filtration, washed with cold diethyl ether (3 x 50 mL) and dried under vacuum.

$[Ag(MPO)_2]ClO_4$ (3.1)

MPO (**2.1**) (208 mg) was reacted according to general procedure 4.

Yield: 191 mg, 75% (orange solid).

^{1}H NMR (DMSO-d6, 500 MHz): **δ** 9.75 (bs, 1H, O**H**), 9.12 (d, *J* = 4.3 Hz, 1H, Phen**H**), 9.04 – 9.01 (m, 2H, Phen**H**), 8.76 (d, *J* = 8.1 Hz, 1H, Phen**H**), 8.01 - 7.95 (m, 2H, Phen**H**), 7.23 (d, *J* = 8.7 Hz, 2H, Ar**H**), 6.68 (d, *J* = 8.6 Hz, 2H, Ar**H**), 6.65 (s, 1H, oxazineC**H**), 3.91 (s, 3H, C**H**$_3$) ppm.

^{13}C NMR (DMSO-d6, 126 MHz): **δ** 162.5 (**C**=O), 158.9 (Ar**C**-OH), 152.6 (Phen**C**-H), 150.6 (oxazine-**C**=N), 149.9 (Phen**C**-H), 142.9 (Phen**C**), 138.7 (Phen**C**), 133.0 (Phen**C**-H), 131.9 (Phen**C**-H), 129.2 (Ar**C**), 126.7 (oxazine-**C**N), 125.7 (Phen**C**-H), 125.4 Phen**C**-H), 124.6 (Phen**C**), 122.0 (Phen**C**), 121.8 (Phen**C**), 115.9 (Ar**C**), 72.4 (oxazine-**C**O), 53.1 (-O**C**H$_3$) ppm.

FTIR (KBr, cm^{-1}): 3415, 1714 (C=O), 1611, 1588, 1577, 1513, 1436, 1382, 1349, 1260, 1228, 1174, 1099, 1032, 810, 736, 623.

UV-vis: 13,172 M^{-1} cm^{-1} (DMSO, λ_{max} = 389 nm).

[Ag(PPO)$_2$]ClO$_4$ (3.2):

PPO (**2.2**) (214 mg) was reacted according to general procedure 4.

Yield: 0.191 g, 75% (yellow solid).

^{1}H NMR (DMSO-d6, 500 MHz): **δ** 9.78 (bs, 1H, O**H**), 9.12 (d, *J* = 3.1 Hz, 1H, Phen**H**), 9.05 (d, *J* = 3.2 Hz, 1H Phen**H**), 9.02 (d, *J* = 8.2 Hz, 1H, Phen**H**), 8.75 (d, *J* = 7.9 Hz, 1H, Phen**H**), 8.01 (dd, *J* = 4.4, 7.9 Hz, 1H, Phen**H**), 7.96 (dd, *J* = 4.4, 8.0 Hz, 1H, Phen**H**), 7.24 (d, *J* = 8.4 Hz, 2H, Ar**H**), 6.70 (d, *J* = 8.5 Hz, 2H, Ar**H**), 6.64 (s, 1H, oxazineC-**H**), 4.33 – 4.24 (m, 2H, -OC**H$_2$**), 1.74 – 1.70 (m, 2H, C**H$_2$**), 0.93 (t, *J* = 7.3 Hz, 3H, C**H$_3$**) ppm.

^{13}C NMR (DMSO-d6, 126 MHz): **δ** 161.9 (**C**=O), 158.9 (**C**-OH), 152.6 (Phen**C**-H), 151.1 (oxazine**C**=N), 149.9 (Phen**C**-H), 142.8 (Phen**C**), 138.7 (oxazine-**C**O), 138.7 (Ar**C**), 133.0 (Phen**C**-H), 131.9 (Phen**C**-H), 129.2 (Ar**C**-H), 126.8 (oxazine-**C**N), 125.7 (Phen**C**-H), 125.4 (Phen**C**-H), 124.8 (Phen**C**), 122.0 (Phen**C**), 121.7 (Phen**C**), 115.9 (Ar**C**-H), 72.6 (oxazine**C**-H), 67.4 (O**C**H$_2$), 21.5 (**C**H$_2$), 10.2 (**C**H$_3$) ppm.

FTIR (KBr, cm^{-1}): 3395, 1740 (C=O), 1717, 1617, 1511, 1436, 1388, 1328, 1262, 1098, 815, 735, 623.

CHN(%): Calculated $[Ag(C_{24}H_{19}N_3O_4)_2](ClO_4)$.DCM: C 52.59, H 3.60, N 7.50; Found: C 52.15, H 3.64, N 7.39.

UV-vis: 15,629 M^{-1} cm^{-1} (DMSO, λ_{max} = 390 nm).

$[Ag(HPO)_2]ClO_4$ (3.3):

HPO (**2.3**) (236 mg) was reacted according to general procedure 4.

Yield: 0.148 g, 63% (yellow solid).

^{1}H NMR (DMSO-d6, 500 MHz): **δ** 9.73 (s, 1H, O**H**), 9.13 (dd, *J* = 1.6, 4.5 Hz, 1H, Phen**H**), 9.05 (dd, *J* = 1.5, 4.4 Hz, 1H, Phen**H**), 9.0 (dd, *J* = 1.6, 8.3 Hz 1H, Phen**H**), 8.76 (dd, *J* = 1.6, 8.3 Hz, 1H, Phen**H**), 8.02 (dd, *J* = 4.5, 8.3 Hz, 1H, Phen**H**), 7.95 (dd, *J* = 4.5, 8.3 Hz, 1H, Phen**H**), 7.23 (d, *J* = 8.7 Hz 2H, Ar**H**), 6.68 (d, *J* = 8.7 Hz, 2H, Ar**H**), 6.63 (s, 1H, oxazine-C**H**), 4.35 – 4.25 (m, 2H, -OC**H**$_2$), 1.68 – 1.64 (m, 2H, C**H**$_2$), 1.29 – 1.27 (m, 6H, 3 x C**H**$_2$), 0.86 (t, *J* = 6.8 Hz 3H, C**H**$_3$) ppm.

^{13}C NMR (DMSO-d6, 126 MHz): **δ** 161.8 (**C**=O), 158.9 (**C**-OH), 152.5 (Phen**C**-H), 151.1 (oxazine-**C**=N), 149.9 (Phen**C**-H), 142.7 (Phen**C**), 138.7 (oxazine-**C**O), 138.3 (Ar**C**), 133.0 (Phen**C**-H), 131.9 (Phen**C**-H), 129.1 (Ar**C**-H), 126.8 (oxazine-**C**N), 125.7 (Phen**C**-H), 125.3 (Phen**C**-H), 124.7 (Phen**C**), 121.9 (Phen**C**), 121.6 (Phen**C**), 115.8 (Ar**C**-H), 72.7 (oxazine-**C**H**),** 65.9 (O**C**H$_2$), 30.8 (OCH$_2$**C**H$_2$), 27.9 (**C**H$_2$), 24.9 (**C**H$_2$), 22.0 (**C**H$_2$), 13.9 (**C**H$_3$) ppm.

FTIR (KBr, cm^{-1}): 3395, 1740 (C=O), 1741, 1614, 1511, 1439, 1253, 1107, 1101, 809, 735, 623.

CHN (%): Calculated for $[Ag(C_{27}H_{25}N_3O_4)2](ClO_4)$.DCM: C 54.90, H 4.36, N 6.98; Found: C 54.54, H 4.19, N 6.45

UV-vis: 15,877 M^{-1} cm^{-1} (DMSO, λ_{max} = 391 nm).

$[Ag(OPO)_2]ClO_4$ (3.4):

OPO (**2.4**) (125 mg) was reacted with $AgClO_4$ (27 mg) according to general procedure 4.

Yield: 106.7 mg, 34% (orange solid).

^{1}H NMR (DMSO-d6, 500 MHz): **δ** 9.77 (s, 1H, O**H**), 9.11 (d, *J* = 3.3 Hz, 1H, Phen**H**), 9.04 (d, *J* = 3.3 Hz, 1H, Phen**H**), 9.00 (d, *J* = 8.1 Hz, 1H, Phen**H**), 8.74 (d, *J* = 7.9 Hz, 1H, Phen**H**), 8.00 (dd, *J* = 4.4, 8.1 Hz, 1H, Phen**H**), 7.95 (dd, *J* = 4.5, 8.1 Hz, 1H, Phen**H**), 7.22 (d, *J* = 8.5 Hz, 2H, Ar**H**), 6.67 (d, *J* = 8.5 Hz, 2H, Ar**H**), 6.62 (s, 1H, oxazine-C**H**), 4.35 - 4.24 (m, 2H, -OC**H**$_2$), 1.67 – 1.65 (m, 2H, C**H**$_2$), 1.26 – 1.22 (m, 10H, 5 x C**H**$_2$), 0.84 (t, *J* = 6.6 Hz, 3H, C**H**$_3$) ppm.

^{13}C NMR (DMSO-d6, 126 MHz): **δ** 162.2 (**C**=O), 159.4 (Ar**C**-OH), 153.0 (Phen**C**H), 151.5 (oxazine-**C**=N), 150.3 (Phen**C**-H), 143.3 (Phen**C**), 139.2 (Phen**C**), 139.1 (Phen**C**), 133.4 (Phen**C**-H), 132.3 (Phen**C**-H), 129.6 (Ar**C**), 127.2 (Phen**C**), 126.1 (Phen**C**-H), 125.8 (Phen**C**-H), 125.1 (Ar**C**), 122.4 (Phen**C**), 122.1 (Phen**C**), 116.3 (Ar**C**-H), 73.1 (oxazine-**C**H), 66.3 (O-**C**H$_2$), 31.6 (**C**H$_2$), 29.06 (**C**H$_2$), 29.03 (**C**H$_2$), 28.4 (**C**H$_2$), 25.7 (**C**H$_2$), 22.5 (**C**H$_2$), 14.4 (**C**H$_3$) ppm.

FTIR (KBr, cm^{-1}): 3387, 2926, 1737 (C=O), 1714, 1611, 1517, 1442, 1382, 1325, 1262, 1104, 815, 735, 623.

HRMS (ESI +): Calcd *m/z* for $C_{58}H_{58}AgN6O8$: $(M+H)^+$ 1075.3425; Found $(M+H)^+$ 1075.3371. Difference: -5.00 ppm.

UV-vis: 15,656 M^{-1} cm^{-1} (DMSO, λ_{max} = 390 nm).

2.3.2 Synthesis of Rhenium(I) Tricarbonyl Complexes

Starting material $Re(CO)_3Br$ was synthesised according to the literature[148] where $Re_2(CO)_{10}$ (0.50 g) was dissolved in DCM (20 mL) by stirring at rt to give a clear colourless solution. Bromine (3-4 drops) was slowly added dropwise until a slight

orange colour remained. The reaction mixture was left to stir for a further 5 minutes. A white precipitate formed that was filtered and washed with DCM (3 x 10 mL) and dried under vacuum. IR spectrum agreed with that of the literature.

Yield: 364.9 mg, 88% (white solid).

FTIR (ATR, cm^{-1}): *ν*(C≡O) 2052, 2021, 1987, 1954.

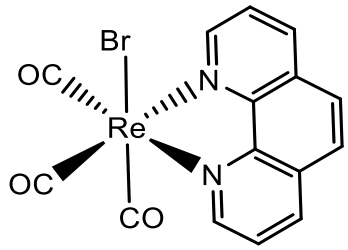

Figure 2.6: Re(I) tricarbonyl phenanthroline complex (**4a**).

[$ReBr(CO)_3$(phen)] (4a):

(1,10-phenanthroline)$Re(CO)_3Br$ was synthesised with slight modification to literature procedures.[149] $Re(CO)_3Br$ (0.45 g, 0.85 mmol) and 1,10-phenanthroline (0.2 g, 0.85 mmol) were dissolved in toluene (50 mL) and heated at reflux for 24 h with vigorous stirring. The desired product precipitated from solution. The reaction was cooled to rt before filtering and washing with petroleum ether (3 x 20 mL) and drying under vacuum to yield the bright yellow product.

Yield: 0.475 g, 80% (yellow solid)

^{1}H-NMR: (DMSO-d6, 500 MHz) **δ** = 9.46 (dd, *J* = 1.4, 3.8 Hz, 2H, 2 x *ortho*-**H**), 8.97 (dd, *J* = 1.4, 6.9 Hz, 2H, 2 x meta-**H**), 8.33 (s, 2H, 2 x C**H**), 8.11 (dd, *J* = 5.1, 3.1 Hz, 2H, 2 x *para*-**H**) ppm.

^{13}C-NMR: (DMSO-d6, 126 MHz) **δ** 192.6 (**C**≡O), 189.8 (**C**≡O), 154.1 (PhenN=**C**), 146.3 (PhenN-**C**), 139.8 (*meta*-Phen**C**H), 131.0 (q-Phen**C**), 128.2 (q-Phen**C**), 127.0 (Phen**C**-H) ppm.

FTIR (ATR, cm^{-1}): *ν*(C≡O) 2014, 1925, 1886 cm^{-1}.

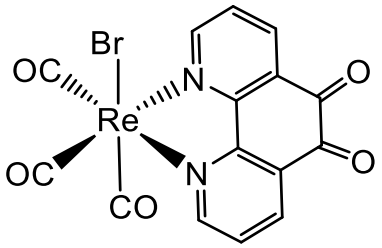

Figure 2.7: Re(I) tricarbonyl phendione complex (**4b**).

[ReBr(CO)$_3$(phendione)] (4b)

The product was synthesised with minor modification to literature procedures.[150, 151] Briefly, Re(CO)$_5$(Br) (0.3 g, 0.738 mmol) and 1,10-phenanthroline-5,6-dione (0.155 g, 0.738 mmol) were dissolved in toluene (50 mL) and heated at reflux for 24 h. The deep red product precipitated from solution and was filtered and washed with petroleum ether (3 x 20 mL) and dried under vacuum.

Yield: 306 mg, 74% (red solid).

^{1}H-NMR: (CD_3CN, 500MHz) **δ** 9.25 (dd, *J* = 1.4, 4.1 Hz, 2 x *ortho*-**H**), 8.67 (dd, J = 1.4, 6.6 Hz, 2 x *meta*-**H**), 7.85 (dd, J = 2.5, 5.5 Hz, 2 x *para*-**H**) ppm.

^{13}C NMR: (CD_3CN, 126 MHz) **δ** 197.2 (**C**≡O), 188.7 (**C**≡O), 175.5 (**C**=O), 158.9 (N-**C**H), 155.3 (N=**C**), 139.0 (**C**H), 131.0 (q**C**=C). 129.4 (**C**H) ppm.

FTIR (ATR, cm^{-1}): *ν*(C≡O) 2023, 1938, 1878.

General procedure 5 for the synthesis of complexes 4.1 – 4.8

Re(CO)$_5$Br (100 mg, 0.25 mmol) and ligand of choice (0.25 mmol) were dissolved in 30 mL of dried distilled toluene. The reaction mixture was degassed with nitrogen for 30 minutes. The reaction was heated at reflux and stirred vigorously overnight. The reaction mixture was cooled to rt and the volume of the flask was reduced to dryness. The purple solid that remained was washed with diethyl ether (3 x 20 mL) and collected by vacuum filtration.

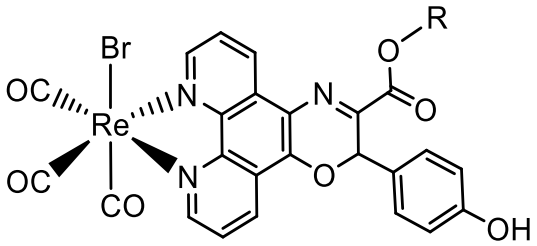

Product	R	Code
4.1	CH_3	ReMPO
4.2	C_3H_7	RePPO
4.3	C_6H_{13}	ReHPO
4.4	C_8H_{17}	ReOPO

Figure 2.8: Rhenium(I) tricarbonyl complex of phenanthroline-oxazine ligand (**4.1 - 4.4**).

N.B. NMR data revealed the presence of diastereomeric products from the reactions to form **4.1 – 4.4**. Where signals are duplicated in the ^{1}H or ^{13}C NMR spectra, they are denoted as A and B to represent different isomers. The details of the assignments for these complexes will be discussed in Chapter 4.

[ReBr(CO)$_3$(2.1)] (4.1, ReMPO):

MPO (**2.1**) (96 mg) was reacted according to general procedure 5.

Yield: 128 mg, 70% (orange solid).

^{1}H-NMR: (DMSO-d6, 500 MHz) **δ** 9.79 (m, 1H, O**H**), 9.45 (d, *J* = 4.9 Hz, 1H, Phen**H**), 9.37 (d, *J* = 5.0 Hz, 1H, Phen**H**), 9.18 – 9.16 (m, 1H, Phen**H**), 8.94 – 8.92 (m, 1H, Phen**H**), 8.13 (dd, 5.1, 8.3 1H, Phen**H**), 8.06 (dd, *J* = 5.2, 8.4 Hz, 1H, Phen**H**), 7.26 (m, 2H, Ar**H**), 6.71 – 6.68 (m, 3H, Ar**H**, oxazine**H**), 3.89 (s, 3H, C**H**$_3$, A), 3.88 (s, 3H, C**H**$_3$, B) ppm.

^{13}C NMR: (DMSO-d6, 126 MHz) **δ** 197.0 (**C**≡O) 196.9 (**C**≡O), 189.0 (**C**≡O), 162.22 (**C**=O, A), 162.18 (**C**=O, B), 159.15 (**C**-OH, A), 159.09 (**C**-OH, B), 154.8 (Phen**C**H), 152.1 (Phen**C**-O), 151.47 (oxazine**C**=N, A), 151.28 (oxazine**C**=N, B), 146.67 (Phen**C**, A), 146.60 (Phen**C**, B), 142.47 (Phen**C**, A), 142.41 (Phen**C**), 139.49 (Phen**C**-N, A), 139.49 (Phen**C**-N, B), 134.1 (Phen**C**H), 133.30 (Phen**C**H, A), 133.17 (Phen**C**H, B), 129.4 (Ar**C**), 128.21 (Phen**C**, A), 128.14 (Phen**C**, B). 127.33 (Phen**C**H, A), 127.27 (Phen**C**H, B), 126.92 (Phen**C**H, A), 126.90 (Phen**C**H, B) 124.7 (Ar**C**), 124.2 (Phen**C**), 123.36 (Phen**C**, A), 123.29 (Phen**C**, B), 122.04, 116.05 (Ar**C**, A), 115.95 (Ar**C**, B), 73.17 (oxazine-O**C**H, A), 72.99 (oxazine-O**C**H, B), 53.14 (-O**C**H$_3$, A), 53.11 (-O**C**H$_3$, B) ppm.

FTIR (ATR, cm^{-1}): 2018 (C≡O), 1884 (C≡O), 1717 (C=O), 1608, 1514, 1433, 1354, 1260, 1172, 1139, 1089, 1043, 810, 727.

HRMS (ESI +): Calculated *m/z* for [Re($C_{25}H_{15}N_3O_7$)Br]; $(M+Na)^+$ 757.8651; Found: $(M+Na)^+$ 757.951. Difference = -1.09 ppm.

UV-vis (DMSO) ε = 8,362.2 M^{-1} cm^{-1} (λ_{max} = 388 nm).

[ReBr(CO)$_3$(2.2)] (4.2, RePPO):

PPO (**2.2**) (103 mg) was reacted according to general procedure 5.

Yield: 146 mg, 82% (orange solid).

^{1}H NMR: (DMSO-d6, 500 MHz) **δ** 9.80 (bs 1H, O**H**), 9.46 (d, *J* = 4.7 Hz, 1H, Phen**H**) 9.38 (dd, *J* = 1.3, 5.1 Hz, 1H, Phen**H**), 9.18 – 9.16 (m, 1H, Phen**H**), 8.93 (dd, *J* = 8.4, 1.3 1H, Phen**H**), 8.15 (dd, *J* = 8.5, 5.2 Hz, 1H, Phen**H**), 8.06 (dd, *J* = 8.4, 5.2 Hz, 1H, Phen**H**), 7.28 – 7.25 (m, 2H, Ar**H**), 6.71 – 6.68 (m, 3H, 2 x Ar**H**, oxazine**H**), 4.28 – 4.19 (m, 2H, -OC**H**$_2$), 1.71 – 1.64 (m, 2H, C**H**$_2$), 0.90 – 0.87 (m, 3H, C**H**$_3$) ppm.

^{13}C NMR: (DMSO-d6, 126 MHz) **δ** 197.0 (**C**≡O), 196.9 (**C**≡O), 189.1 (**C**≡O), 161.62 (**C**=O, A), 161.58 (**C**=O, B), 159.13 (**C**-OH, A), 159.07 (**C**-OH, B), 154.8 (Phen**C**), 152.1 (Phen**C**-O), 151.89 (Phen**C**-H, A), 151.71 (Phen**C**-H, B), 146.65 (Phen**C**, A), 146.57 (Phen**C**, B), 142.46 (Phen**C**, A), 142.38 (Phen**C**, B), 139.62 (oxazine**C**=N, A), 139.45 (oxazine**C**=N, B), 134.1 (Phen**C**-H), 133.24 (Phen**C**-H, A), 133.13 (Phen**C**-H, B), 129.47 (Ar**C**-H, A), 129.45 (Ar**C**-H, B), 128.1 (Phen**C**), 127.34 (Phen**C**-H, A), 127.30 (Phen**C**-H, B), 126.91 (Phen**C**-H, A), 126.88 (Phen**C**-H, B), 124.92 (Ar**C**, A), 124.44 (Ar**C**, B), 123.35 (Phen**C**, A), 123.35 (Phen**C**, B), 121.95 (Phen**C**, A), 121.76 (Phen**C**, B), 116.05 (Ar**C**-H, A), 115.95 (Ar**C**-H, B), 73.41 (oxazineO**C**-H, A), 73.24 (oxazineO**C**-H, B), 67.40 (O**C**H$_2$, A), 67.37 (O**C**H$_2$, B), 21.4 (**C**H$_2$), 10.71 (**C**H$_3$, A), 10.16 (**C**H$_3$, B) ppm.

FTIR (ATR, cm^{-1}): 2019 (C≡O), 1886 (C≡O), 1712 (C=O), 1609, 1513, 1436, 1259, 1231, 1171, 1139, 1090, 1044, 810, 724.

HRMS (ESI +): Calculated *m/z* for [Re($C_{27}H_{19}N_3O_7$)Br]; $(M+Na)^+$ 785.8964; Found $(M+Na)^+$ 785.9834. Difference -1.37 ppm.

UV-vis (DMSO) ε = 9,629.4 M^{-1} cm^{-1} (λ_{max} = 387 nm).

CHN (%): Calculated $C_{27}H_{19}BrN_3O_7Re$: C 42.47, H 2.51, N 5.50; Found: C 42.01, H 2.29, N 5.34.

[ReBr(CO)$_3$(2.3)] (4.3, ReHPO):

HPO (**2.3**) (113 mg) was reacted according to general procedure 5.

Yield: 109 mg, 54% (orange solid).

^{1}H NMR: (DMSO-d6, 500 MHz) **δ** 9.85 (bs, 1H, O**H**), 9.47 (d, *J* = 4.9 Hz, 1H, Phen**H**), 9.38 (d, *J* = 4.7 Hz 1H, Phen**H**), 9.18 – 9.16 (m, 1H, Phen**H**), 8.93 (d, *J* = 8.3 Hz, 1H, Phen**H**), 8.93 – 8.90 (m, 1H, Phen**H**), 8.1 (dd, *J* = 5.1, 8.4 Hz, 1H, Phen**H**), 8.06 (dd, *J* = 5.4, 8.4 Hz, 1H, Phen**H**), 7.27 - 7.24 (m, 2H, Ar**H**), 6.71 – 6.6 (m, 3H, 2 x Ar**H**, oxazine**H**), 4.34 – 4.22 (m, 2H, -OC**H**$_2$), 1.65 – 1.61 (m, 2H, C**H**$_2$), 1.27 – 1.24 (m, 6H, 3 x C**H**$_2$), 0.86 – 0.83 (m, 3H, C**H**$_3$) ppm.

^{13}C NMR: (DMSO-d6, 126 MHz) **δ** 197.9 (**C**≡O), 197.4 (**C**≡O), 189.5 (**C**≡O), 162.01 (**C**=O, A), 161.97 (**C**=O, B), 159.64 (**C**-OH, A), 159.58 (**C**-OH, B), 155.3 (Phen**C**-H), 152.6 (Phen**C**-O), 152.40 (Phen**C**-H, A), 152.22 (Phen**C**H, B), 147.11 (Phen**C**, A), 147.04 (Phen**C**, B), 142.91 (Phen**C**, A), 142.84 (Phen**C**, B), 140.08 (oxazine**C**=N, A), 139.90 (oxazine**C**=N, B), 134.6 (Phen**C**H), 133.5 (Phen**C**H), 129.9 (Ar**C**H). 128.6 (Phen**C**), 127.77 (Phen**C**H, A), 127.73 (Phen**C**H, B), 127.37 (Phen**C**H, A), 127.35 (Phen**C**H, B), 125.3 (Ar**C**), 123.7 (Phen**C**), 122.37 (Phen**C**, A), 122.19 (Phen**C**, B), 116.48 (Ar**C**-H, A), 116.37 (Ar**C**-H, B), 73.93 (oxazineO**C**-H, A), 73.77 (oxazine**C**-H, B), 66.41 (-O**C**H$_2$, A), 66.38 (-O**C**H$_2$, B), 31.2 (**C**H$_2$), 28.3 (**C**H$_2$), 25.3 (**C**H$_2$), 22.42 (**C**H$_2$), 14.3 (**C**H$_3$) ppm.

FTIR (ATR cm^{-1}): 2019 (C≡O), 1878 (C≡O), 1717 (C=O), 1607, 1517, 1437, 1359, 1226, 1172, 1144, 1092, 1046, 989, 951, 816, 797, 727, 689.

HRMS (ESI +): Calcd [Re($C_{30}H_{25}N_3O_7$)Br]: (M) 827.9448 Found $(M+Na)^+$ 828.0298. Difference = -1.31 ppm.

UV-vis (DMSO) ε = 10,259 M^{-1} cm^{-1} (λ_{max} = 386 nm).

CHN (%): Calculated $C_{30}H25_{25}BrN_3O_7Re$: C 44.73, H 3.13, N 5.22; Found C 43.49, H 2.85, N 4.92.

[ReBr(CO)$_3$(2.4)] (4.4, ReOPO):

OPO (**2.4**) (120 mg) was reacted according to general procedure 5.

Yield: 89.9 mg, 43% (orange solid).

^{1}H NMR: (DMSO-d6, 500 MHz) **δ** 9.76 (bs, 1H, O**H**), 9.47 – 9.45 (m, 1H, Phen**H**), 9.37 (dd, *J* = 1.2, 5.0 Hz, 1H, Phen**H**), 9.18 – 9.15 (m, 1H, Phen**H**), 8.92 (dd, *J* = 1.2, 8.3 Hz, 1H, Phen**H**), 8.15 – 8.12 (m, 1H, Phen**H**), 8.06 (dd, *J* = 5.1, 8.5 Hz, 1H, Phen**H**), 7.26 – 7.23 (m, 2H, Ar**H**), 6.70 – 6.67 (m, 3H, Ar**H**, oxazineH), 4.33 – 4.21 (m, 2H, OC**H**$_2$), 1.65 – 1.62 (m, 2H, C**H**$_2$), 1.27 – 1.22 (m, 10H, 5 x C**H**$_2$), 0.84 (t, *J* = x Hz, 3H, C**H**$_3$) ppm.

^{13}C NMR: (DMSO-d6, 126 MHz) **δ** 197.5 (**C**≡O), 197.4 (**C**≡O), 189.5 (**C**≡O), 162.01 (**C**=O, A), 161.97 (**C**=O, B), 159.64 (**C**-OH, A), 159.58 (**C**-OH, B), 155.3 (Phen**C**-H), 152.6 (Phen**C**-O), 152.37 (Phen**C**-H, A), 152.01 (Phen**C**-H, B), 147.11 (Phen**C**, A), 147.02 (Phen**C**, B), 142.92 (Phen**C**, A), 142.84 (Phen**C**, B), 140.07 (oxazine**C**=N, A), 139.90 (oxazine**C**=N, B), 134.6 (Phen**C**-H), 133.64 (Phen**C**-H, A), 133.53 (Phen**C**-H, B), 129.91 (Ar**C**-H, A), 129.89 (Ar**C**-H, B), 128.65 (Phen**C**, A), 128.64 (Phen**C**, B), 127.74 (Phen**C**-H, A), 127.71 (Phen**C**-H, B), 127.37 (Phen**C**-H, A), 127.33 (Phen**C**-H, B), 125.7 (Ar**C**), 124.8 (Phen**C**), 123.80 (Phen**C**, A), 123.75 (Phen**C**, B), 122.38 (Phen**C**, A), 122.21 (Phen**C**, B), 116.48 (Ar**C**-H, A), 116.38 (Ar**C**-H, B), 73.92 (oxazineO**C**-H, A), 73.75 (oxazineO**C**-H, B), 66.44 (-O**C**H$_2$, A), 66.40 (-O**C**H$_2$, B), 31.5 (**C**H$_2$), 29.03 (**C**H$_2$, A), 29.01 (**C**H$_2$, B), 28.3 (**C**H$_2$), 25.7 (**C**H$_2$), 22.5 (**C**H$_2$), 14.4 (**C**H$_3$) ppm.

FTIR (ATR cm^{-1}): 2019 (C≡O), 1883 (C≡O), 1724 (C=O), 1612. 1516, 1462, 1318, 1281, 1175, 973. 817, 727.

HRMS (ESI +): Calcd [Re($C_{32}H_{29}N_3O_7$)Br]: $(M+Na)^+$ 855.9747; Found $(M+Na)^+$ 856.0611. Difference = -1.06 ppm.

UV-vis (DMSO) ε = 11,198 M^{-1} cm^{-1} (λ_{max} = 387 nm).

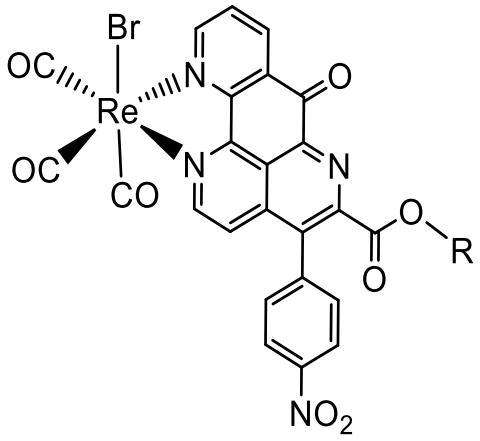

Product	R	Code
4.5	CH_3	ReMPP
4.6	C_2H_5	ReEPP
4.7	C_3H_7	RePPP
4.8	C_6H_{13}	ReHPP

Figure 2.9: Rhenium(I) tricarbonyl complex of pyrido-phenanthrolinone ligand (**4.5 – 4.8**)

[ReBr(CO)$_3$(2.5)] (4.5, ReMPP):

MPP (**2.5**) (103 mg) was reacted according to general procedure 5.

Yield: 96.6 mg, 52% (purple solid).

^{1}H NMR: ($CDCl_3$, 500 MHz) **δ** 9.37 (dd, J = 1.5, 5.4 Hz, 1H, Phen**H**), 9.12 (d, J = 6.5 Hz, 1H, Phen**H**), 9.00 (dd, J = 1.4, 8.0 Hz, 1H, Phen**H**), 8.51 – 8.49 (m, 2H, Ar**H**), 7.97 (dd, J = 5.5, 8.1 Hz, 1H, Phen**H**), 7.67 – 7.60 (m, 3H, ArH, Phen**H**), 3.88 (s, 3H, C**H**$_3$) ppm.

^{13}C NMR: ($CDCl_3$, 126 MHz) **δ** 176.1 (ester **C**=O), 163.5 (**C**=O), 156.3 (Phen**C**-H), 153.2 (Phen**C**), 152.2 (Phen**C**), 149.5 (Phen**C**-H), 147.8 (Ar**C**), 137.0 (Phen**C**), 128.4 (Ar**C**-H), 123.3 (Phen**C**-H), 123.1 (Ar**C**-H), 122.2 (Phen**C**-H), 120.1 (Phen**C**), 53.8 (-OCH_3) ppm.

FTIR (ATR cm^{-1}): 2024 (C≡O), 1895 (C≡O), 1736 (C=O), 1689 (C=O), 1519, 1421, 1344, 1276, 1229, 853, 815, 643, 487.

HRMS (ESI +): Calcd m/z for $C_{25}H_{12}BrN_4O_8Re$: (M+Na)+ 784.9278; Found (M+Na)+ 784.9278 Difference = 0.30 ppm**.**

CHN (%): Calculated $C_{25}H_{12}BrN_4O_8Re.CHCl_3$: C, 35.43; H, 1.49; N, 6.36. Found: C, 35.06; H, 1.36; N, 6.69.

UV-vis (DMSO): ε1 = 12,266 $M^{-1}\,cm^{-1}$ (λ_{max1} = 375 nm), ε2 = 3071.3 $M^{-1}\,cm^{-1}$ (λ_{max2} = 493 nm)

[ReBr(CO)$_3$(2.6)] (4.6, ReEPP):

EPP (**2.6**) (107 mg) was reacted according to general procedure 5.

Yield: 166.8 mg, 87% (purple solid).

FTIR (ATR, cm^{-1}): 2024 (C≡O), 1898 (C≡O), 1729 (C=O), 1690 (C=O), 1521, 1343, 1227, 999, 855, 696, 485.

^{1}H NMR ($CDCl_3$, 500 MHz): **δ** 9.36 – 9.35 (m, 1H, Phen**H**), 9.10 (d, *J* = 6.5 Hz, 1H, Phen**H**), 9.00 – 8.98 (m, 1H, Phen**H**), 8.51 – 8.48 (m, 2H, Ar**H**), 7.97 (dd, *J* = 5.5, 8.0 Hz, 1H, Phen**H**), 7.71 (d, *J* = 5.5 Hz, 1H, Phen**H**), 7.68 – 7.63 (m, 2H, Ar**H**), 4.29 (q, *J* = 7.1 Hz, 2H, -OC**H**$_2$), 1.82 (t, *J* = 6.6 Hz, 3H, C**H**$_3$) ppm.

^{13}C NMR ($CDCl_3$, 126 MHz): **δ** 195.7 (**C**≡O), 195.4 (**C**≡O), 186.0 (**C**≡O), 177.3 (ester **C**=O), 164.3 (**C**=O), 157.4 (Phen**C**-H), 154.3 (Phen**C**), 153.35 (Phen**C**), 150.6 (Phen**C**-H), 149.9 (Phen**C**), 148.9 (Ar**C**), 145.1 (pyrido**C**=N), 138.7 (Ar**C**), 138.3 (Phen**C**-H), 138.2 (Phen**C**), 134.5 (Phen**C**), 131.3 (Phen**C**), 131.0 (Phen**C**), 130.7 (Ar**C**-H), 129.5 (Phen**C**-H), 124.4 (Ar**C**-H), 124.3 (Ar**C**-H), 123.3 (Phen**C**-H), 121.2 (Phen**C**), 63.2 (-O**C**H$_2$), 13.9 (**C**H$_3$) ppm.

HRMS: Calcd *m/z* for $C_{26}H_{14}BrN_4O_8Re$: $(M+Na)^+$ 784.9293; Found $(M+Na)^+$ 784.9278. Difference = 0.30 ppm.

UV-vis (DMSO): ε1 = 14,907 $M^{-1}\,cm^{-1}$ (λ_{max1} = 374 nm), ε2 = 3426.7 $M^{-1}\,cm^{-1}$ (λ_{max2} = 495 nm)

[ReBr(CO)$_3$(2.7)] (4.7, RePPP):

PPP (**2.7**) (110 mg) was reacted according to general procedure 5.

Yield: 141.5 mg, 72% (purple solid)

FTIR (ATR, cm^{-1}): 2020 (C≡O), 1883 (C≡O), 1732 (C=O), 1686 (C=O), 1515, 1423, 1346, 1273, 1221, 1199, 1000, 850, 694, 642, 482,

^{1}H NMR ($CDCl_3$, 400 MHz): **δ** 9.37 (d, *J* = 5.2 Hz, 1H, Phen**H**), 9.11 (d, *J* = 6.5 Hz, 1H, Phen**H**), 9.00 - 8.98 (m, 1H, Phen**H**), 8.51 – 8.48 (m, 2H, Ar**H**), 7.98 – 7.95 (dd, *J* = 1H, Phen**H**), 7.70 (d, *J* = 6.5 Hz, 1H, Phen**H**), 7.66 (dd, *J* = 8.1, 13.3 Hz, 2H, Ar**H**), 4.20 – 4.17 (m, 2H, -OC**H**$_2$), 0.83 (t, *J* = 7.3 Hz, 3H, C**H**$_3$) ppm.

^{13}C NMR ($CDCl_3$, 126 MHz): **δ** 195.3 (**C**≡O), 177.1 (**C**=O), 164.3 (**C**=O), 157.3 (Phen**C**-H), 154.2 (Phen**C**), 153.2 (Phen**C**), 150.5 (Phen**C**-H), 149.9 (Phen**C**), 148.8 (Ar**C**), 144.9 (pyrido**C**=N), 138.6 (Ar**C**), 138.1 (Phen**C**-H), 138.0 (Phen**C**), 134.2 (Phen**C**), 131.1 (Phen**C**), 130.9 (Phen**C**), 130.6 (Ar**C**-H), 129.4 (Phen**C**-H), 124.2 (Ar**C**-H), 123.1 (Phen**C**-H), 121.1 (Phen**C**), 68.6 (-O**C**H$_2$), 21.6 (**C**H$_2$), 10.1 (**C**H$_3$) ppm.

HRMS: Calcd *m/z* for $C_{27}H_{16}BrN_4O_8Re$: $(M+H)^+$ 790.9782; Found $(M+H)^+$ 790.9774. Difference = 0.56 ppm.

CHN (%): Calculated $C_{27}H_{16}BrN_4O_8Re$.2DCM: C, 36.27; H, 2.10; N, 5.84. Found: C, 36.04; H, 1.70; N, 6.09.

UV-vis (DMSO): ε1 = 11,712 M^{-1} cm^{-1} (λ_{max1} = 372 nm), ε2 = 3066.5 M^{-1} cm^{-1} (λ_{max2} = 490 nm)

[ReBr(CO)$_3$(2.8)] (4.8, ReHPP):

HPP (**2.8**) (121 mg) was reacted according to general procedure 5.

Yield: 172.8 mg, 85% (purple solid).

FTIR (ATR, cm^{-1}): 2020 (C≡O), 1889 (C≡O), 1732 (C=O), 1686 (C=O), 1521, 1426, 1349, 1276, 1230, 1181, 997, 853, 807, 697, 645, 479.

^{1}H NMR ($CDCl_3$, 500 MHz): **δ** 9.36 (dd, *J* = 1.4, 5.4 Hz, 1H, Phen**H**), 9.10 (d, *J* = 6.6 Hz, 1H, Phen**H**), 8.99 (dd, *J* = 1.3, 8.0 Hz, 1H, Phen**H**), 8.51 – 8.48 (m, 2H, Ar**H**), 7.96 (dd, *J* = 5.4, 8.0 Hz, 1H, Phen**H**), 7.70 (d, *J* = 6.5 Hz, 1H, Phen**H**), 7.69 – 7.64 (m 2H, Ar**H**), 4.21 (t, *J* = 6.7 Hz, 2H, -OC**H**$_2$), 1.52 – 1.47 (m, 2H, C**H**$_2$), 1.27 – 1.16 (m, 8H, 4 x C**H**$_2$), 0.86 (t, *J* = 6.9 Hz, 3H, C**H**$_3$) ppm.

^{13}C NMR ($CDCl_3$, 126 MHz): **δ** 195.7 (**C**≡O), 195.4 (**C**≡O), 186.0 (**C**≡O), 177.2 (ester **C**=O), 164.5 (**C**=O), 157.4 (Phen**C**-H), 154.3 (Phen**C**), 153.3 (Phen**C**), 150.6 (Phen**C**-H), 150.1 (Phen**C**), 148.9 (Ar**C**), 145.1 (pyrido**C**=N), 138.7 (Ar**C**), 138.3 (Phen**C**-H), 138.2 (Phen**C**), 134.3 (Phen**C**), 131.3 (Phen**C**), 131.0 (Phen**C**), 130.8 (Ar**C**-H), 129.5 (Phen**C**-H), 124.3 (Ar**C**-H), 123.3 (Phen**C**-H), 121.2 (Phen**C**), 67.4 (-O**C**H_2), 31.3 (**C**H_2), 28.3 (**C**H_2), 25.4 (**C**H_2), 22.5 (**C**H_2), 14.0 (**C**H_3) ppm.

HRMS: Calcd *m/z* for $C_{30}H_{22}BrN_4O_8Re$: $(M+Na)^+$ 855.0076; Found $(M+Na)^+$ 855.0063. Difference 0.35 ppm.

CHN (%): Calculated $C_{30}H_{22}BrN_4O_8Re$.DCM: C, 40.58; H, 2.64; N, 6.11. Found: C, 40.45; H, 2.29; N, 6.46.

UV-vis (DMSO): ε1 = 12,612 M^{-1} cm^{-1} (λ_{max} = 371 nm), ε2 = 3250 M^{-1} cm^{-1} (λ_{max2} = 490 nm)

2.3.3 Synthesis of $Mn(CO)_5Br$ Starting Material

$Mn(CO)_5Br$ was synthesised similarly to $Re(CO)_5Br$ detailed above. Commercially available dimanganese decacarbonyl (300 mg, 0.76 mmol) was added to DCM (5 mL) and allowed to stir at rt. Once fully dissolved, 4-5 drops of bromine were added slowly while the solution stirred. Once a deep orange colour persisted, the reaction was stirred for a further 5 minutes. An orange precipitate formed and was collected *via*

vacuum filtration. The product was washed with diethyl ether (3 x 20 mL) and dried under vacuum.

Yield: 179.4 mg, 85% (orange solid).

FTIR (ATR, cm^{-1}): 2141, 2080, 2036, 1982.

The IR spectrum agrees with that present in the literature [152].

2.4 Biological Screening of Ligands 2.1 - 2.8 and their Metal Complexes 3.1 - 3.3 and 4.1 – 4.8

2.4.1 Materials and Instrumentation

All growth media, Phosphate Buffered Saline (PBS), pipette tips and Eppendorf tubes used for antimicrobial testing were sterilised in an autoclave (Dixons ST2228) at 120°C for 15 minutes. All worktop benches and laminar flow cabinets were sterilised with 70% (v/v) EtOH in deionised water (dH_2O) prior to use.

Nutrient broth and PBS were obtained from Sigma-Aldrich and prepared according to the manufacturer's instructions. Minimal Growth Media (MM) was made by dissolving 2% (w/v) D-glucose, 0.17% (w/v) Yeast Nitrogen Base and 0.5% (w/v) ammonium sulfate in dH_2O. Yeast Extract Peptone Dextrose (YEPD) media was made similarly by dissolving 2% (w/v) D-glucose, 2% (w/v) bacteriological peptone and 1% (w/v) yeast extract in dH_2O.

Cultures of *C. albicans*, *S. aureus*, MRSA and *E. coli* were prepared by inoculating 50 mL of the media of choice with a single plate colony and allowed to incubate at 37 °C overnight in an orbital shaker. *C. albicans* was obtained from a clinical MEN (serotype B, wild type originally isolated from ocular infection).

Fungal density was measured using a Neubauer haemocytometer under a light microscope. Bacterial density was determined using an Eppendorf BioPhotometer 6131 Spectrophotometer at 600 nm. The growth of the microbes in 96-well plates

was measured using the Synergy HT Bio-Tek plate reader by reading the Optical Density (OD) at 600 nm.

Sixth instar larvae of *G. mellonella* were obtained from Livefoods Sheffield, England and stored in the dark at 15 °C. Larvae weighing between 200 – 300 mg were used. Inoculation was carried out using a 26G 1 mL syringe from Terumo.

Cancer cell viability measurements were determined by reading the luminescent output on a BMG Clariostar multi-mode microplate reader.

2.4.2 Preparation of Microbial Cultures

C. albicans cultures were prepared by adding a single plate colony to a 50 mL conical flask containing minimal media or YEPD media (for nutrient rich experiments). The fungal density was counted on a haemocytometer. The appropriate dilution was then made to produce a 1 x 10^6 cells/ml working culture.

Nutrient Broth media was prepared by adding 13 g per 1 litre of dH_2O. Bacterial strains *S. aureus*, *E. coli* and MRSA were prepared in the same manner as *C. albicans*. A single plate colony was added to 50 mL of Nutrient broth media. The OD at 600 nm (OD_{600}) of the bacterial culture was measured and the culture was diluted with nutrient broth to produce a bacterial suspension with OD_{600} of 0.1.

2.4.3 Microbial Susceptibility Testing

All compounds were water insoluble, so test compounds were first dissolved in neat DMSO to produce 20 X* stock solutions. A 20% (v/v) DMSO in media solution was then prepared by making a 1:5 dilution with growth media to produce a 4 X solution. 100 µL of test solution was added to one lane of a 96-well plate containing 100 µL of media. From this lane the compound was serially diluted on the plate according to the broth microdilution susceptibility protocol.[153] A working culture of the appropriate microbe was prepared and 100 µL was added to each well. The first lane now contains a 1 X concentration of the test compound, the second lane contained 0.5 X, the third lane 0.25 X and so on down to the lowest concentration. The plate was then incubated overnight at 37 °C. The optical density (OD) was read at 600 nm.

For experiments with *C. albicans* carried out in nutrient rich media, YEPD media was used to grow the cultures and prepare the test solutions. Dilutions were carried out the same as stated above.

* X = the desired top concentration on the 96 well plate.

2.4.4 *In vivo* Testing Towards *Galleria mellonella*

Sixth Instar *G. mellonella* larvae were used for this testing. Five larvae of a similar weight (200 – 300 mg) were placed in a clean petri dish. Three replicates were prepared for each test compound (3 x 5 larvae). A 5% (v/v) DMSO in PBS solution was prepared for each compound at a final concentration of 60, 30 and 15 µM. Each larva was injected with 20 µL of test solution just below the last left pro-leg. All larvae were then incubated at 37 °C and monitored every 24 h for up to 7 days for indications of melanisation. The ability of the larvae to develop into pupae was also noted over this period.

A similar method was employed to determine the ability of test compounds to reduce *in vivo C. albicans* infection. Five larvae were placed in a clean petri dish. Two replicates were prepared per test condition (2 x 5 larvae). Four test groups were prepared. The first was a control group that received an inoculation of 20 µL of 5% (v/v) DMSO in PBS. The second was a control infection group that received 10 µL of a 1 x 10^5 cells/mL dose of *C. albicans*. The third and fourth group also received 10 µL of a 1 x 10^5 cells/mL dose of *C. albicans*. All larvae were placed in an incubator at 37 °C. Larvae that received an infection were removed from the incubator after 1 h. The control infection group were injected with a further 10 µL of 5% (v/v) DMSO in PBS. Groups three and four received a 10 µL dose of 60 µM test compound. All larvae were replaced in the incubator and monitored every 24 hours for 3 days.

2.4.5 Determination of Haemocyte Density of Inoculated *G. mellonella* Larvae

Stock solutions of each test compound were prepared in DMSO to give a concentration of 1200 µM. Test solutions were prepared by diluting the stock solutions in fresh PBS to give a 5% (v/v) DMSO solution of 60 µM. Five larvae per test

compound were injected with 20 µL of the test solution. The larvae were incubated for 3 h at 37°C. Each larva was bled by making a small incision by the trachea and gently massaged to remove the lymph, ensuring only clear lymph was collected in an Eppendorf tube. The lymph was then diluted 1:5 in fresh PBS.

A sample of 100 µL of the diluted lymph solution was added to one side of a haemocytometer and was viewed under a microscope. The number of haemocyte cells were counted. Only cells in the outer corners and middle grid were counted. This number was then multiplied by 5 to account for the dilution of the lymph in PBS and then by 50,000 (each square of the grid contains $1/10{,}000^{th}$ of a mL) to give the number of haemocyte cells/mL.

2.4.6 Anticancer Testing

2.4.6.1 Ovarian Cancer Cell Culture and Cell Seeding

Complete media, consisting of RPMI glutamax media containing 10% (v/v) Fetal Bovine Serum (FBS), was used for all experiments. The vehicle control (VC) used for all experiments consisted of media containing 1% (v/v) DMSO. Patient derived ovarian cancer cell lines PEO1 and PEO4 were cultured in complete media at 37 °C with 5% CO_2. Cells were split and a cell suspension of 5 x 10^4 cells/mL was prepared per cell line. The cell suspension (90 µL) was added to each well of a standard flat bottom 96-well plate. The plate was incubated overnight at 37 °C to allow the cells to adhere to the surface.

2.4.6.2 Treating Cells to Measure Cell Viability

Following incubation of the cells for 24 h as described above, media was removed completely. The appropriate treatments (100 µL), including the controls were added to each well before returning to the incubator for a further 72 h at 37 °C. The plate was removed from the incubator and 2D CellTitre Glo 2.0 reagent (50 µL) was added to each well. Percentage cell viability was determined by measuring ATP using 2D CellTitre Glo 2.0 reagent according to the manufacturer's guidelines.[154] The CellTitre Glo reagent binds extracellular ATP (indicating cell lysis) and produces luminescence.

The plate was covered with foil and allowed to gently mix at 150 RPM on a plate shaker for 5 minutes. The plate was incubated at room temperature for 5-10 minutes before reading the luminescence output on the Clariostar. The luminescent values were analysed using excel and to determine the percentage of cell viability compared to the VC. GraphPad Prism software was used to determine statistical significance. CalcuSyn software was used to determine IC_{50} values.

2.4.6.3 Treating Cells to Measure Apoptosis

Cells were seeded as described above. Following 24 h, the media was removed. Stock complete media used to dilute test compounds was prepared and contained 0.05% (v/v) of Incucyte Caspase-3/7 green dye. Stock solutions of each test compound at each desired concentration (including VCs) were prepared and added to the wells. The plate was placed in an Incucyte cell imaging machine. The incucyte imaging machine analysed the plate every 4 h for five consecutive days. Fluorescent output was monitored and provided a measurement of caspase 3/7 cleavage as a readout of apoptosis. Graphpad prism was used to generate graphs for apoptosis and confluency.

Chapter 3

Synthesis, Characterisation and Biological Evaluation of Derivatised Phenanthroline Ligands and Ag(I) Phenanthroline Complexes

Compound Structures and Codes for Chapter 3

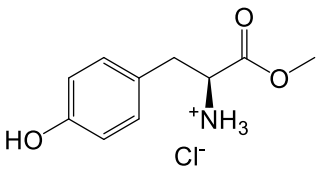

LTME (**1.1**)

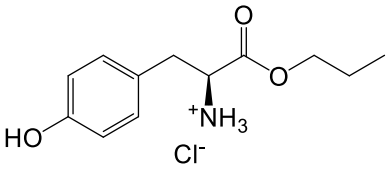

LTPE (**1.2**)

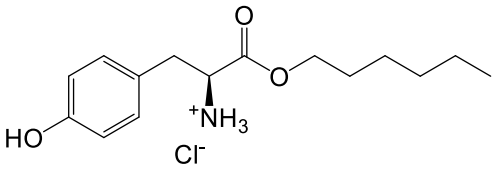

LTHE (**1.3**)

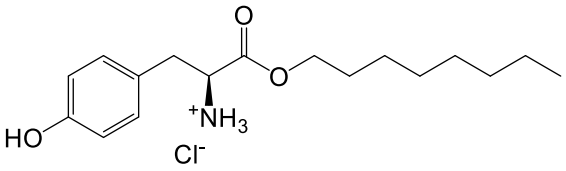

LTOE (**1.4**)

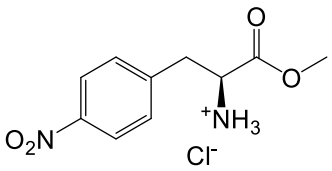

NPME (**1.5**)

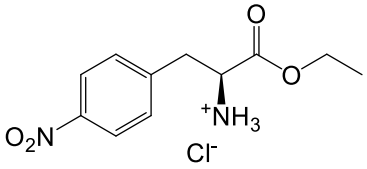

NPEE (**1.6**)

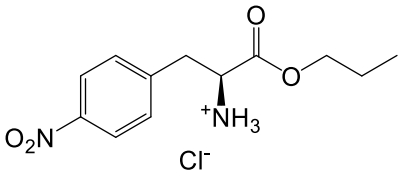

NPPE (**1.7**)

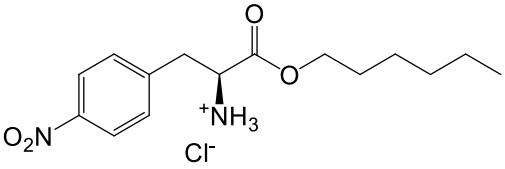

NPHE (**1.5**)

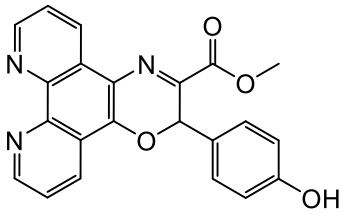

MPO (**2.1**)

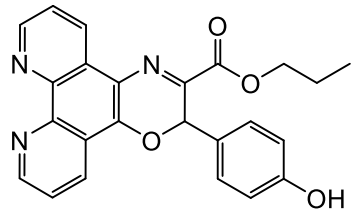

PPO (**2.2**)

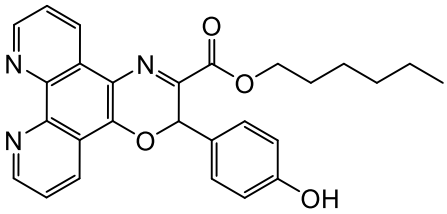

HPO (**2.3**)

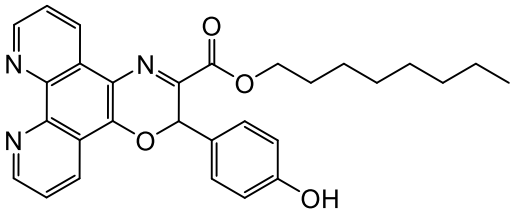

OPO (**2.4**)

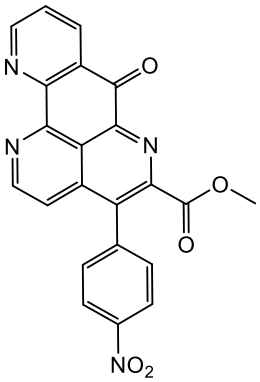

MPP (**2.5**)

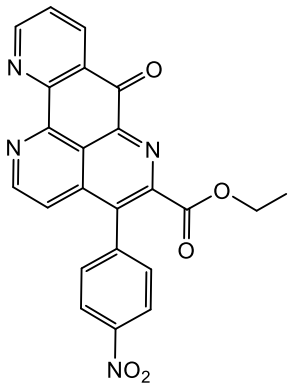

EPP (**2.6**)

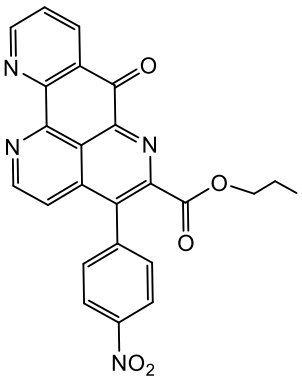

PPP (**2.7**)

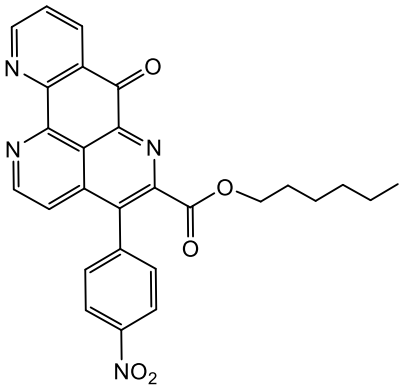

HPP (**2.8**)

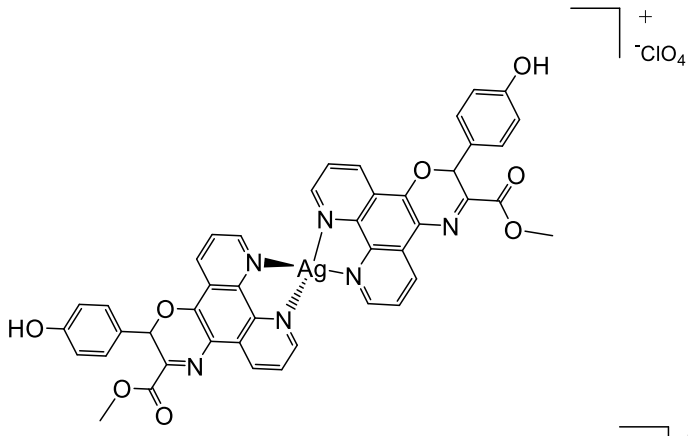

$[Ag(MPO)_2]ClO_4$ (**3.1**)

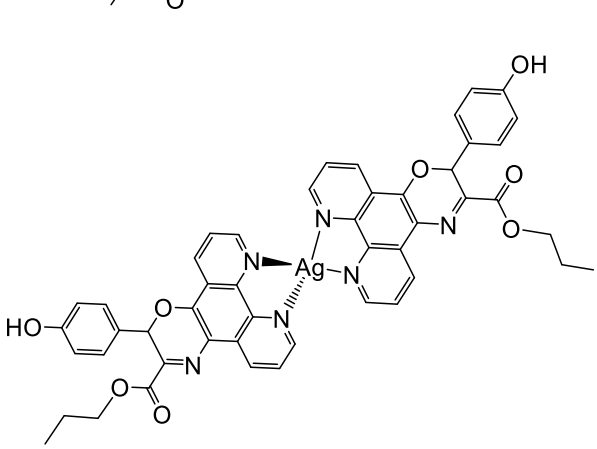

$[Ag(PPO)_2]ClO_4$ (**3.2**)

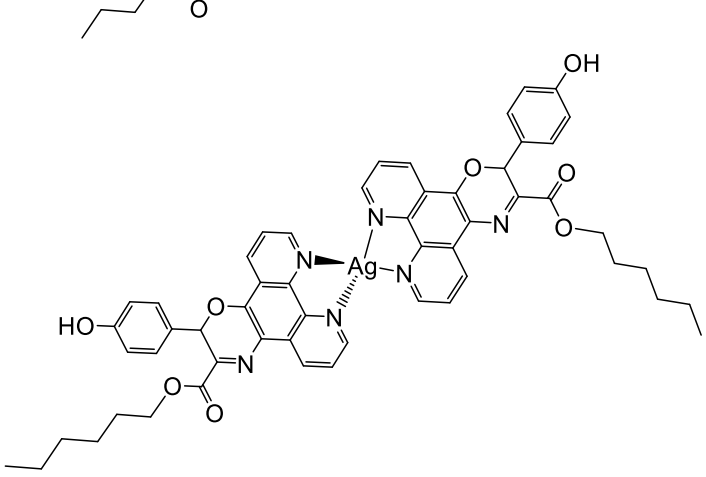

$[Ag(HPO)_2]ClO_4$ (**3.3**)

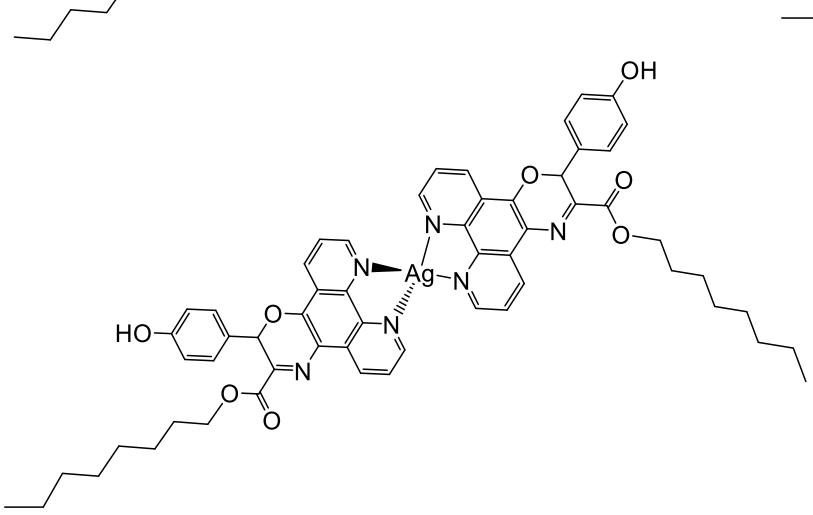

$[Ag(OPO)_2]ClO_4$ (**3.4**)

3.1 Introduction

Antimicrobial resistance (AMR) has become one of the top threats facing human health according to the World Health Organisation (WHO). AMR occurs when bacterial, fungal, viral or parasitic pathogens no longer respond to treatments. This leads to drug resistance and therefore more serious or even fatal infections. AMR is caused by incorrect or excessive use of antimicrobial treatments. The efficacy of standard first line treatments is significantly reduced, emphasizing the need for new treatments which unique modes of action. AMR can have significant consequences for patients undergoing routine surgeries or immunocompromised individuals and people receiving cancer chemotherapy.[97] Antibiotic resistant bacterial infections have been widely recognised as a major challenge in healthcare which has directly led to 1.27 million fatalities globally in 2019 and contributed to 4.95 million deaths.[155] A group of microbes known as the ESKAPEE pathogens are multidrug-resistant bacteria that have advanced mechanisms of resistance and are key targets for novel antibiotics. This group includes *E. coli* and *S. aureus* which cause common, treatable infections but in gaining resistance can lead to major health problems.[156] *E. coli* is a gram-negative bacterial strain that can cause common urinary and gastrointestinal infections. In recent years, it has become one of the top contributors to antibiotic resistance. Moreover, *S. aureus*, known to be a cause of throat infections and acne, is also of major concern for drug resistance. *S. aureus* and its highly resistant strain, MRSA are prevalent in hospital settings and can lead to pneumonia and sepsis. A survey conducted by the WHO in 2022 highlighted that third generation *E. coli* and MRSA infections developed a 42% and 35% rate of resistance, respectively.[157]

While antibiotic resistant infections are rampant, much less attention has been given to drug resistant fungal infections. The emergence of resistant fungal species has seen a sharp rise in the morbidity and mortality caused by these infections. More than 150 million people worldwide suffer serious fungal infection with 1.7 million deaths annually.[158] The WHO has created the first Fungal Priority Pathogens List (FPPL) which is a list of nineteen high risk fungal species including *Candida* and *Aspergillus* species (spp). *Candida* is a yeast that commonly causes thrush and skin infections. *Candida* are one of the leading causes of hospital-associated bloodstream infections and

contributes to a 30 - 40% mortality rate.[159] There is a clear need to develop new antimicrobial therapeutics with unique modes of action.

The antimicrobial activity of silver is well established. Ag(0) and Ag(I) complexes have shown to have low toxicity towards humans.[104, 160] The commercial topical cream Silvadene is an Ag(I) sulfadiazine complex used on burns.[161] $AgNO_3$ as a dilute aqueous solution has also been used to treat infants with bacterial conjunctivitis.[100] Additionally, Ag(0) and Ag(I) complexes have been incorporated into wound dressings.[162] The effectiveness of silver(I) based antimicrobial compounds comes from their ability to dissociate within the cell which allows the release of Ag(I) ions. The free Ag(I) ions can bind to the fungal cell wall proteins and disrupt potassium ion channels and can cause changes to mitochondrial morphology.[108, 163] Additionally, these ions can interrupt the function of intracellular enzymes, inducing cell death.[164] Complexes containing Ag(I) are therefore of great interest as novel antimicrobial agents.

Phen is a fused heterocyclic ring system, and its planar structure makes it a good DNA intercalator. The well positioned *N*-atoms allow bidentate coordination to a metal centre. Ag(I) complexes containing phen or derivatives have been reported as antibacterial[8, 110, 111], antifungal[165] and anticancer[112, 166] agents. This project therefore sought to synthesis a family of novel phen-based Ag(I) complexes and assess their antifungal activity.

This chapter will discuss the synthesis and characterisation of a family of phenanthroline-oxazine (phen-oxazine) ligands **2.1** – **2.4**, pyrido-phenanthrolinone (phen-pyrido) ligands **2.5** - **2.8** and Ag(I) *bis*(phenanthroline-oxazine) complexes **3.1** – **3.4** (**Scheme 3.1**). The synthetic approach employed in this chapter involves first synthesising a family of amino acid ester hydrochloride salts **1.1 - 1.8** with a range of *para* substituents on the aromatic ring and varying alkyl chain lengths to optimise lipophilicity. This chapter will discuss the reaction between the amino acid ester salts **1.1 - 1.8** and phendione (**2a**) to produce the phen-based compounds **2.1 – 2.8**. The reaction parameters will be discussed including the reaction conditions that will favour one ligand over the other. The complexation of phen-oxazine ligands **2.1 – 2.4**

to Ag(I) will be described. Various characteristics of the Ag(I) phen-oxazine complexes will be described including their solution behaviour, stability and antifungal activity. The determination of the solution phase stoichiometry by means of the Job's plot method will be discussed. The antifungal screening of ligands **2.1** – **2.3** and Ag(I) complexes **3.1** – **3.3** against *C. albicans* will be presented.

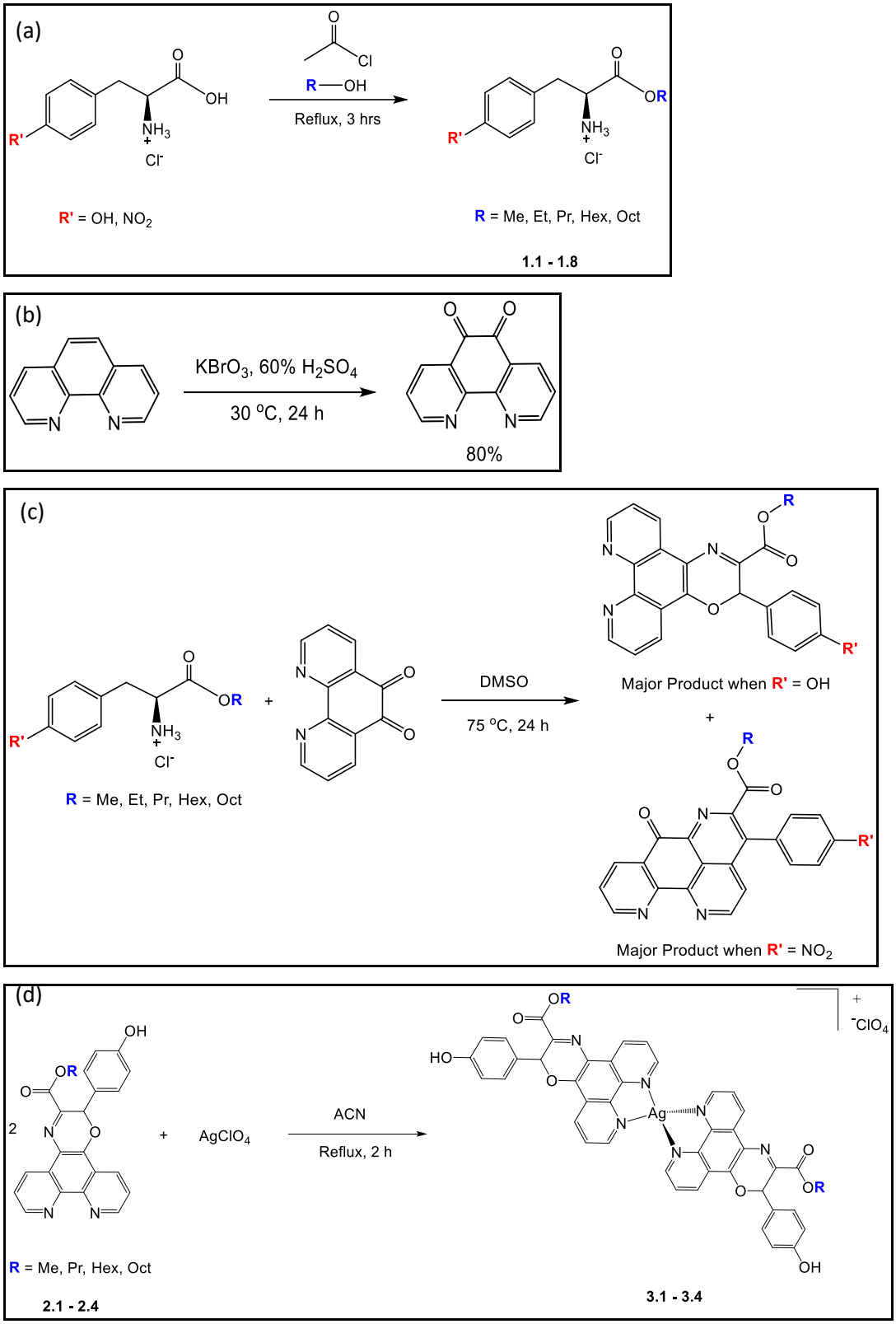

Scheme 3.1: Overview of synthetic procedures to produce amino acid ester salts **1.1 – 1.8** (a), phendione (**2a**) (b), phen-oxazine ligands **2.1 – 2.4** and phen-pyrido ligands **2.5 – 2.8** (b) and Ag(I) *bis*(phen-oxazine) complexes **3.1 – 3.4** (c)

3.2 Synthesis and Characterisation of Starting Materials and Phenanthroline-based Ligands 2.1 – 2.8

3.2.1 Synthesis of Starting Materials: 1,10-Phenanthroline-5,6-dione (2a) and Amino Acid Esters 1.1 - 1.8

1,10-Phenathroline-5,6-dione (**2a**) is a functionalised derivative of 1,10-phenanthroline containing two carbonyl substituents. It is widely used as a reactant to further derivatise the phen framework.[167, 168] Phendione (**2a**) was synthesised with slight modification to literature procedures.[146] 1,10-Phenantroline was reacted with $KBrO_3$ in the presence of 60% (v/v) H_2SO_4 (**Scheme 3.2**). Yields upwards of 80% were consistently achieved with good purity. Characterisation involved NMR and IR spectroscopy and the obtained data agreed with the literature: the proton NMR spectrum in DMSO-d6 shows three distinct peaks at 8.98 (*ortho*-phenH), 8.38 (*para*-phenH) and 7.66 ppm (*meta*-phenH).[169]

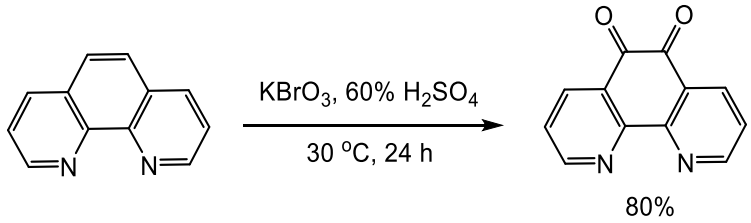

Scheme 3.2: Reaction of 1,10-phenanthroline to produce 1,10-phenanthroline-5,6-dione starting material.

The esterification of amino acids is well established.[170, 171] Amino acid ester hydrochloride salts **1.1 - 1.8** were synthesised with modification to these procedures (**Scheme 3.3**). Good to excellent yields were achieved. Acetyl chloride reacts with water in the alcohol and provides a source of HCl which enables this acid catalysed reaction to proceed. A set of amino acid ester hydrochloride salts was easily achieved by varying the choice of amino acid and alcohol. The electron density of the aromatic group of the amino acid ester can vary depending on the functional group R' of the starting amino acid. L-Tyrosine (R'= OH) was used to synthesise amino acid ester salts **1.1 – 1.4** containing a hydroxy group at the R' position, allowing for an electron donating moiety at the *para* position of the phenyl ring. Amino acid ester salts **1.5 –**

1.8 were synthesised from 4-nitro-L-phenylalanine (R'= NO_2) which provides an electron withdrawing nitro group at the R' position.

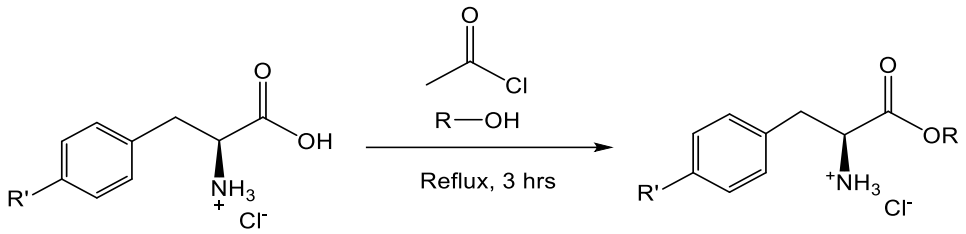

1.1 - 1.8

Product	R'	R	Code	Yield
1.1	-OH	CH_3	LTME	92%
1.2	-OH	C_3H_7	LTPE	89%
1.3	-OH	C_6H_{13}	LTHE	85%
1.4	-OH	C_8H_{17}	LTOE	67%
1.5	-NO_2	CH_3	NPME	87%
1.6	-NO_2	C_2H_5	NPEE	93%
1.7	-NO_2	C_3H_7	NPPE	95%
1.8	-NO_2	C_6H_{13}	NPHE	82%

Scheme 3.3: Esterification reaction of L-amino acid in the presence of acetyl chloride to produce amino acid hydrochloride salts **1.1 – 1.8** in good yields.

The family of amino acid ester salts **1.1 – 1.8** were characterised using NMR and IR spectroscopy and HRMS analysis. Data of published amino acid ester salts **1.1 – 1.6** were in agreement with those presented in the literature.[71, 172]

In the ^{1}H NMR spectra of amino acid ester salts **1.1 - 1.8**, the most distinct difference from the spectra of the starting amino acids is the emergence of the alkyl-associated peaks. The distinct singlet with a relative integral of 3 associated with the methoxy (OCH_3) of **1.1** and **1.5** is observed at 3.65 and 3.66 ppm respectively. Similarly, the amino acid ester salts **1.2 – 1.4** and **1.6 – 1.8** all show a characteristic triplet signal with a relative integral of 2 for the OCH_2 group at approximately 4.0 ppm. This is consistent with the alkylation of the carboxylic acid group (COOH) of L-tyrosine and 4-nitro-L-phenylalanine.[173] Additionally, the broad OH singlet at ~9.5 ppm (DMSO-d6) that is present in the ^{1}H NMR spectrum of 4-nitrophenylalanine is no longer observed in the spectra of amino acid ester salts **1.5 – 1.8**. This further suggests successful

alkylation of the carboxylic acid. Another distinct feature in the NMR spectra for compounds **1.1 – 1.8** is the broad singlet at ~4.5 ppm with a relative integral of 3 that represents the NH_3^+ group. There are also two separate signals observed for Ha and Hb (**Figure 3.1**) at ~3.0 ppm that is consistent with diasterotopic protons. Moreover, the ^{13}C NMR spectra have a peak at ~170 ppm that is associated with the C=O group of the ester. The signal at about 52 ppm for **1.1** and **1.5** and at about 65 ppm for **1.2 – 1.4** and **1.6 – 1.8** is characteristic of the C atom directly bonded to the O atom in alkoxy groups.[173]

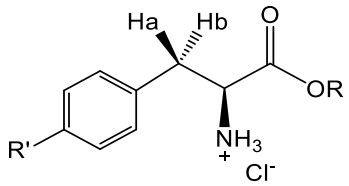

Figure 3.1: General structure of L-amino acid ester salt indicating diasterotopic protons, Ha and Hb.

In the IR spectra, a distinct stretch is observed at ~1740 cm^{-1} which is consistent with what is expected for a carbonyl ν(CO) stretching mode of a carbonyl (C=O) ester functional group.[174] This band is not present in the starting amino acids. The broad band which arises from the ν(OH) stretching mode of the carboxylic acid band that exists between 2600 – 3200 cm^{-1} in the starting material is no longer present in the spectra of the amino acid ester salt products.

HRMS analysis for novel 4-nitro-L-phenylalanine ester salts **1.5**, **1.7** and **1.8** detected a protonated species $(M+H)^+$ (where M is the neutral amino acid ester) that matched the theoretical ionised product (**Table 3.1**).

Table 3.1: Theoretical and observed mass to charge ratios of amino acid esters **1.5**, **1.7** and **1.8**

Compound	Formula	Theoretical $(M+H)^+$ (Da)	Observed $(M+H)^+$ (Da)	Mass error (ppm)
NPME (1.5)	$C_{10}H_{12}N_2O_4$	225.0870	225.0871	0.75
NPPE (1.7)	$C_{12}H_{16}N_2O_4$	253.1183	253.1183	0.19
NPHE (1.8)	$C_{15}H_{22}N_2O_4$	295.1653	295.1651	-0.20

3.2.2 Synthesis and Characterisation of Phenanthroline-derived Ligands 2.1 – 2.8

3.2.2.1 Development of Phenanthroline-oxazine (2.1 – 2.4) and Pyrido-phenanthrolinone Ligands (2.5 – 2.8)

The reaction of L-tyrosine methyl ester salt (**1.1**) and phendione (**2a**) led to the novel synthesis of methyl phenanthroline-oxazine (phen-oxazine) (**2.1**) in 2013 reported by McCann *et al.*[175] Following this, ligands with extended alkyl chains (R) were produced (**2.2 – 2.4**).[176] A study by Ahmed *et al.* in 2019 showed that the product of the reaction between the amino acid ester salts and phendione (**2a**) was dependent on the electron withdrawing or donating properties of the functional group on the *para* position (R') of the phenyl ring of the amino acid ester salt (**Figure 3.2**).

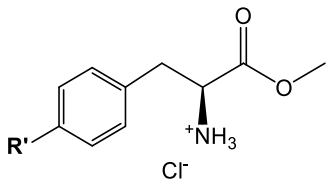

R' = NO_2, CF_3, H, OMe, OH

Figure 3.2: General structure of L-amino acid methyl ester hydrochloride salt.

A series of functional groups at the *para* position of the aromatic group of the amino acid were assessed (**Table 3.2**). A strongly Electron Donating Group (EDG) such as OH or OMe was found to push the reaction in favour of the phen-oxazine ligand (**Scheme**

3.3). Conversely, it was demonstrated that a strongly Electron Withdrawing Group (EWG), NO_2 at the *para* position, an alternative phen-pyrido ligand was synthesised. Reacting the L-tyrosine methyl ester salt with phendione (**2a**) produces nine times more phen-oxazine than phen-pyrido ligand whereas the reaction of the 4-nitro-L-phenylalanine analogue with phendione (**2a**) produces one hundred times more phen-pyrido ligand than phen-oxazine ligand. The electron withdrawing or donating abilities of the functional group at the *para* position of the aromatic ring of the amino acid ester is clearly an important parameter in the selectivity of the reaction.

Table 3.2: Product ratio from the reaction between phendione (**2a**) and *para* substituted L-phenylalanine methyl ester hydrochloride salts (**Figure 3.1**)[172]

Amino acid ester salt	R' group	Phen-pyrido : phen-oxazine ratio*
4-Nitro-L-phenylalanine methyl ester hydrochloride	NO_2	1 : 0.01
4-Trifluoromethyl-L-phenylalanine methyl ester hydrochloride	CF_3	1 : 0.05
L-Phenylalanine methyl ester hydrochloride	H	1 : 1.8
4-Methoxy-L-phenylalanine methyl ester	OMe	1 : 9
L-Tyrosine methyl ester hydrochloride	OH	1 : 9

*Ratio of phen-pyrido : phen-oxazine products is determined by LC-MS analysis of the crude reaction mixtures.

Another variable that was found to control the route of the reaction is temperature.[172] A study was conducted that assessed the impact of temperature on the reaction between phendione (**2a**) and L-phenylalanine methyl ester (**Table 3.3**). It was found that lower reaction temperatures of 50 °C produced ten times more phen-oxazine than phen-pyrido ligands, at 60 °C, there was five times more phen-oxazine than phen-pyrido. At 75 °C there was close to a 1 : 2 ratio of phen-pyrido : phen-oxazine. While at a higher reaction temperature of 85 °C, nine times more phen-pyrido than phen-oxazine was produced. It is evident that lower reaction temperatures favour the production of phen-oxazine as the major product while

much higher temperatures favour the phen-pyrido ligand as the major product. The reaction temperature therefore is a useful parameter for altering the selectivity.

Table 3.3: Ratio of phen-pyrido and phen-oxazine product from the reaction between phendione (**2a**) and L-phenylalanine methyl ester hydrochloride at a range of temperatures.

Reaction temperature (°C)	Ratio of phen-pyrido : phen-oxazine products*
50	1 : 10
60	1 : 5.3
75	1 : 1.8
90	1 : 0.6

*Ratio of phen-pyrido : phen-oxazine products was determined by LC-MS analysis of crude reaction mixture

The experiments outlined in **Tables 3.2 – 3.3** highlight that the electronic properties of the substituent on aromatic group of the amino acid ester (R') and the reaction temperature are important parameters in producing one major product over the other. It was determined that the most ideal parameters for producing the ligands were to maintain the reaction temperature at 75°C and alter the electronic properties to tune the reaction in favour of each product. To produce phen-oxazine as the major product, an electron-donating group at the R' position was incorporated by means of reacting L-tyrosine ester salts with phendione (**Scheme 3.4**). Alternatively, incorporation of an electron withdrawing group by reacting 4-nitrophenylalanine salts with phendione results in phen-pyrido as the major product.

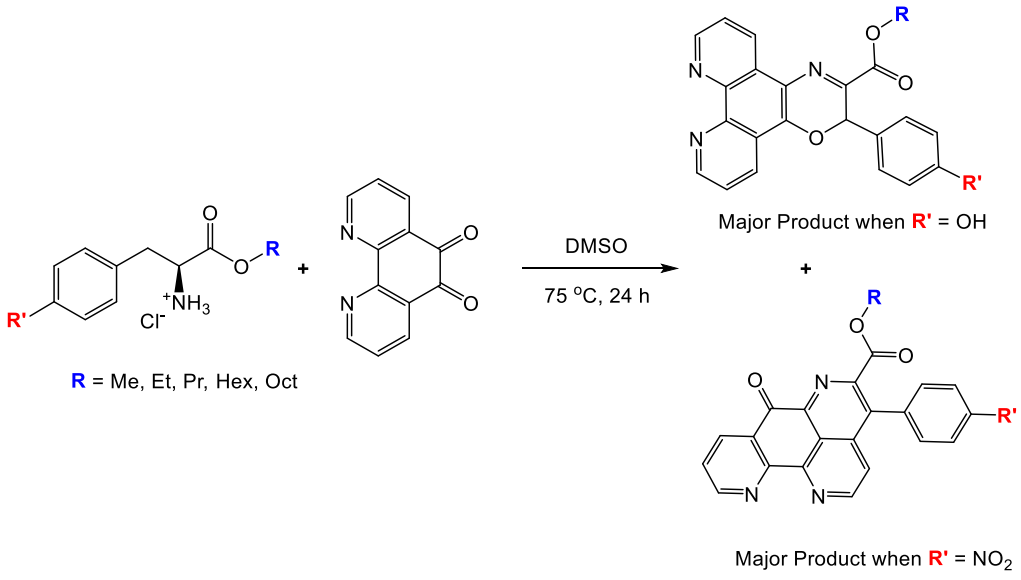

Scheme 3.4: Reaction between L-amino acid ester hydrochloride salts and phendione (**2a**) to produce phen-oxazine ligands (**2.1 – 2.4)** and phen-pyrido ligands (**2.5 – 2.8)**

3.2.2.2 Ligand Design Strategy

Lipophilicity is a key parameter in drug design as it can determine the drugs absorption, distribution and permeability in a biological system. Lipophilicity contributes to the successful uptake of a drug into a cell and therefore its ability to reach its target e.g. DNA.[177] Lipophilicity is measured as the logP of a compound. The LogP value is determined by calculating log10(Partition Coefficient) where the Partition Coefficient is the concentration of the solute in the organic phase divided by the concentration of the solute in the aqueous phase. Specifically, LogP is measured using the partition coefficient between octanol and water.[178] Octanol is used as a standard as it is a good mimic of cell wall lipids due to it's hydrophlilic OH tail and hydrophobic alkyl chain. LogP values can be calculated instead of being determined by experimental measurement.

The lipophilicity of the phen-oxazine and phen-pyrido ligands was altered by the choice of alcohol in the amino acid ester reaction (**Scheme 3.3**). A series of ligands was synthesised in which the alkyl group R (**Scheme 3.4)** altered from R = methyl, propyl, hexyl or octyl for the phen-oxazine ligands and R = methyl, ethyl, propyl or hexyl for phen-pyrido ligands. A previous study in our research group was conducted to analyse the lipophilicity and to compare the clogP of ligands **2.1 – 2.4** and an additional member of this family where R = dodecyl (DPO).[71] This experiment was conducted using reverse phase HPLC where the stationary phase is non-polar and the mobile phase is polar. Gradient elution was employed using H_2O and ACN that gradually changed from a high ratio of H_2O (protic solvent) to a high ratio of ACN (aprotic solvent). This allows for a gradual increase in elution strength of the mobile phase.[179] It was determined that the lipophilicity of the phen-oxazine ligands did increase as the alkyl chain length increased (**Table 3.4**). In the case of the values presented in **Table 3.4**, the clogP was determined using ChemDraw Ultra. A higher clogP value is generally an indicator of better affinity for lipids and organic materials. The premise of altering the alkyl chain length was to determine the optimum chain length for biological activity. This will be discussed later in the chapter.

Table 3.4: Retention time and theoretical LogP values of a series of phen-oxazine ligands

Compound	R	Retention time (min)	Calculated LogP
MPO (2.1)	CH_3	21.7	2.8
PPO (2.2)	C_3H_7	22.5	3.6
HPO (2.3)	C_6H_{13}	27.8	4.9
OPO (2.4)	C_8H_{17}	30.7	5.7
DPO[#]	$C_{10}H_{21}$	35.4	7.4

[#]Dodecyl phenanthroline-oxazine ligand

3.2.2.3 Proposed Mechanism for the Formation of Phenanthroline-oxazine Ligands 2.1 – 2.4 and Phenanthroline-pyrido Ligands 2.5 - 2.8

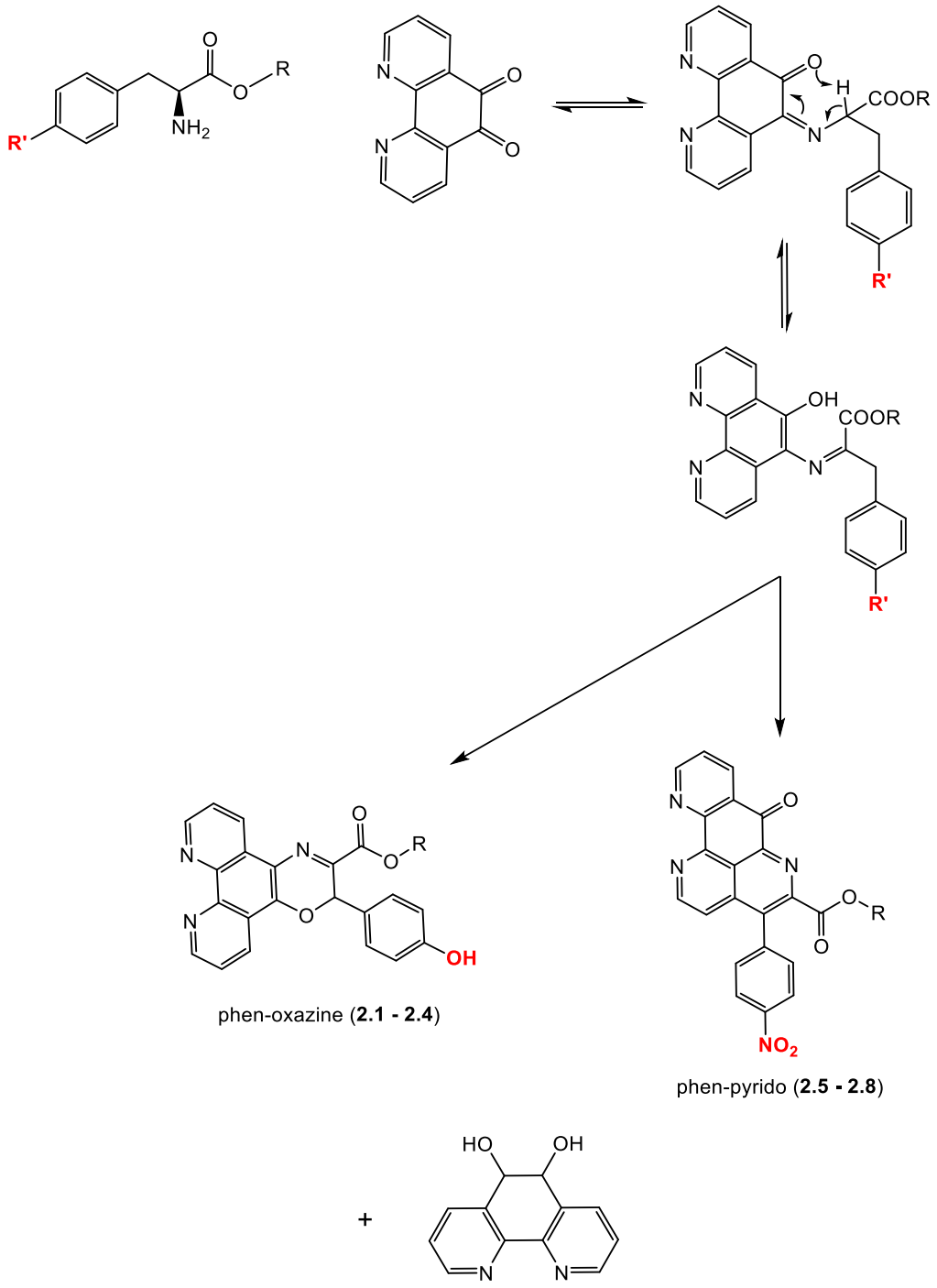

Scheme 3.5: Reported proposed formation of the Schiff-base intermediate into the keto-imine then enol-imine forms[172]

Ligands **2.1 – 2.8** are proposed to be formed by concerted cyclisation reactions and multiple proton transfer steps (**Scheme 3.5**). This reaction to produce both phen-

oxazine and phen-pyrido ligands is initiated by a Schiff base condensation which is widely utilised to derivatise phen using primary amines.[168] Our proposed mechanism is that the reaction between the amino acid ester and the carbonyl positions of phendione produces a keto-imine followed by an enol-imine intermediate. A second phendione molecule then acts as a dehydrogenating agent to form the new C-O bond and therefore cyclisation to the final product.[172] It was found that the dehydrogenation by phendione forms a significant amount of the reduced byproduct phenanthroline-5,6-diol (phen-diol) which limits the potential yield of this reaction.

3.2.2.4 Synthesis and Characterization of Phenanthroline-oxazine Ligands 2.1 – 2.4

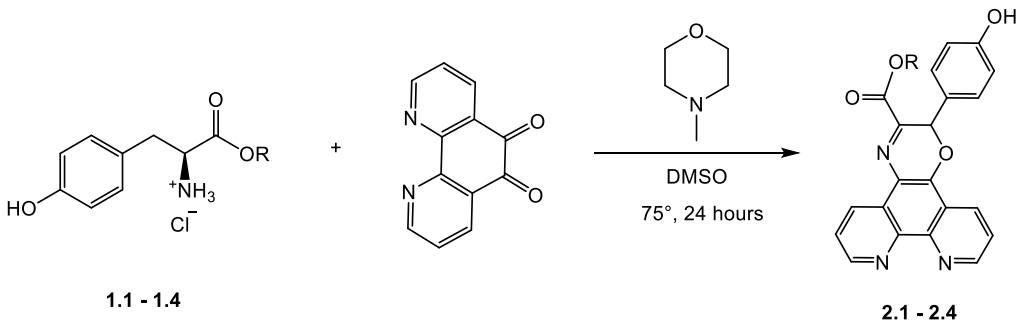

Product	R	Code	Yield
2.1	CH_3	MPO	42%
2.2	C_3H_7	PPO	43%
2.3	C_6H_{13}	HPO	36%
2.4	C_8H_{17}	OPO	29%

Scheme 3.6: Reaction of L-tyrosine ester salts with phendione (**2a**) to produce phen-oxazine ligands **2.1 – 2.4** and their isolated yields.

The series of phen-oxazine ligands **2.1 – 2.4** were synthesised according to previously established procedures in our research group.[172, 175] Optically active L-Tyrosine ester hydrochloride salts (1 mmol) **1.1 – 1.4** were reacted with phendione (**2a**) (1 mmol) in the presence of a base (*N*-methylmorpholine) to form a racemic mixture of phen-oxazine ligand (**Scheme 3.6**). It was found that the reaction could be scaled up by a factor of two (2 mmol) from the established procedure[176] without effecting the efficiency of the reaction. The family of phen-oxazine ligands **2.1 – 2.4** were successfully synthesised and characterisation data agreed with those in the

literature.[175, 176] Yields of isolated phen-oxazine product were less than 43%, with the longer alkyl chains having marginally lower yields (**Scheme 3.6**).

A key feature of the ^{1}H NMR spectrum in DMSO-d6 is the presence of six non-equivalent phen signals between 9.15 – 7.50 ppm, each with a relative integration of one. This is consistent with a loss of symmetry compared to the phendione (**2a**) starting material. The NH_3 signal present in the L-tyrosine ester NMR spectra is no longer observed, suggesting the cyclisation reaction has occurred. Additionally, the α-H signal at about 4.1 ppm and β-H signals at about 3.1 and 2.9 ppm of the amino acid are no longer observed. Instead, there is the presence of a new oxazine-H signal at around 6.5 ppm. The ^{13}C NMR spectra of ligands **2.1 – 2.4** agree with this proposed structure. The NMR spectra for the phen-oxazine ligands **2.1 – 2.4** are all consistent with those presented in the literature.[176]

The IR spectra of phen-oxazine ligands **2.1 – 2.4** show some distinct differences from those of the amino acid ester salts. The band associated with the ν(C=O) stretching mode of the L-tyrosine ester salts observed at 1740 cm^{-1} shifts to ~1700 cm^{-1} in the phen-oxazine spectra. This is consistent with the extended conjunction of this region leading to a shift in the ester signal.[174] The N-H stretch that appears at 614 cm^{-1} in the IR spectra of the amino acid ester salts is no longer present in the IR spectra of the phen-oxazine ligands, again suggesting an alternative structure. Once again, these spectra agree with those published in the literature.[176]

3.2.2.5 Synthesis and Characterisation of Phenanthroline-pyrido Ligands 2.5 – 2.8

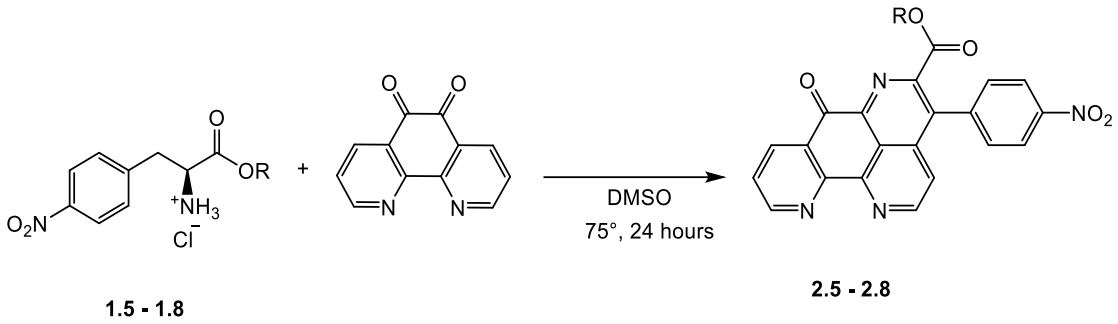

Product	R	Code	Yield
2.5	CH_3	MPP	20%
2.6	C_2H_5	EPP	16%
2.7	C_3H_7	PPP	19%
2.8	C_6H_{13}	HPP	15%

Scheme 3.7: Reaction of 4-nitro-L-phenylalanine ester hydrochloride salts with phendione (**2a**) to produce phen-pyrido ligands **2.5 – 2.8** and their isolated yields.

Phen-pyrido ligands MPP (**2.1**) and EPP (**2.2**) were synthesised and purified according to established procedures.[71, 172] Novel phen-pyrido ligands PPP (**2.3**) and HPP (**2.4**) were additionally synthesised following the same procedure with the appropriate modifications (**Scheme 3.7**). Isolated yields of less than 20% were obtained.

Characterisation was carried out using NMR, IR and HRMS. The ^{1}H NMR spectra for the phen-pyrido ligands show five peaks that represent the non-equivalent phen hydrogen atoms (**Figure 3.3b**). The presence of five rather than six phen signals is consistent with the production of the phen-pyrido ligand rather than the phen-oxazine ligand. The phen-oxazine-H signal present at about 6.5 ppm of the phen-oxazine ^{1}H NMR spectrum (**Figure 3.3a**) is no longer observed in the proton NMR spectrum of the phen-pyrido ligand (**Figure 3.3b**). This suggests the successful synthesis of the alternative cyclised product from the Schiff base-initiated reaction (**Scheme 3.5**). From the ^{1}H NMR spectra of phen-oxazine and phen-pyrido ligands (**Figure 3.3**) it is evident that a pure sample of one ligand over the other can be achieved following the appropriate choice of amino acid ester salt and purification.

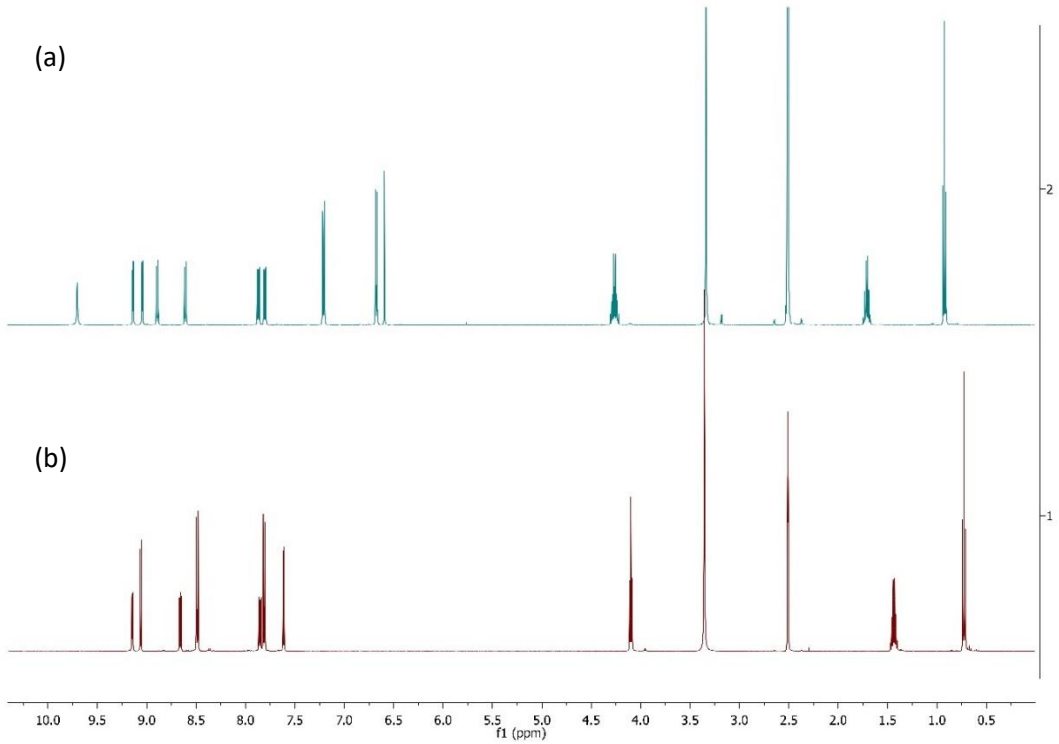

Figure 3.3: ^{1}H NMR spectrum of PPO (**2.2**) (a) and PPP (**2.7**) (b) in DMSO-d6.

The IR spectra obtained for the phen-pyrido ligands have some distinct features. There is the presence of two C=O stretching modes at 1732 and 1725 cm^{-1} due to the additional ester group on the phen moiety of the phen-pyrido ligand. This is different from the IR spectra of the phen-oxazine ligands where only one ester C=O stretching band is observed at ~1732 cm^{-1}.

HRMS analysis also successfully detected the presence of an $(M+Na)^{+}$ ion for novel phen-pyrido ligands **2.5**, **2.7** and **2.8** (**Table 3.5**). The isotopic patterns also matched the simulated ones for these species.

The characterisation data of the phen-pyrido ligands **2.5 – 2.8** are consistent with those presented in the literature.[71, 172]

Table 3.5: Theoretical and observed mass to charge ratio for phen-pyrido ligands **2.5**, **2.7** and **2.8**

Compound	Formula	Theoretical *m/z* (Da)	Observed *m/z* (Da)	Mass error (ppm)
MPP (2.5)	$C_{22}H_{12}N_4O_5$	435.0711	435.0707	2.68
PPP (2.7)	$C_{24}H_{16}N_4O_5$	463.1013	463.1016	2.52
HPP (2.8)	$C_{27}H_{22}N_4O_5$	505.1482	505.1488	2.26

3.3 Synthesis, Characterisation and Biological Evaluation of Silver(I) Phenanthroline-oxazine Complexes 3.1 – 3.4

3.3.1 Synthesis and Characterisation of Silver(I) *bis*(phenanthroline-oxazine) Complexes 3.1 – 3.4

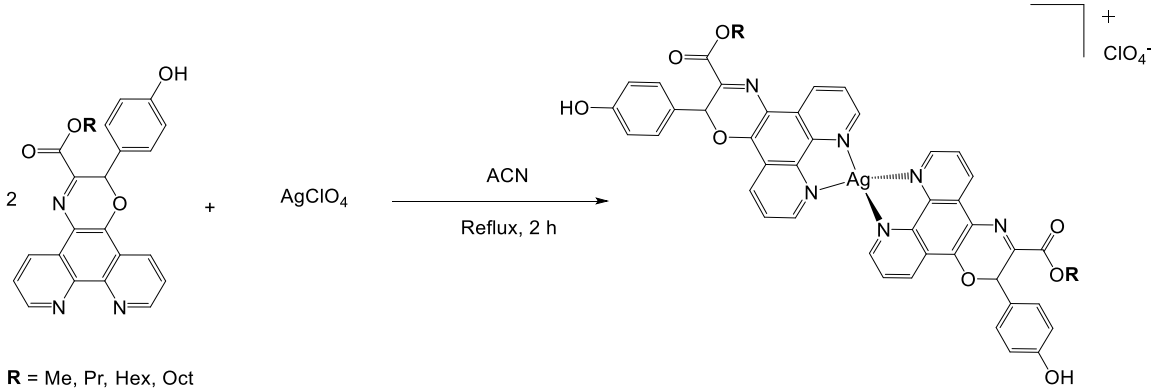

R = Me, Pr, Hex, Oct

2.1 - 2.4

3.1 - 3.4

Product	R	Code	Yield
3.1	CH_3	$[Ag(MPO)_2]ClO_4$	75%
3.2	C_3H_7	$[Ag(PPO)_2]ClO_4$	75%
3.3	C_6H_{13}	$[Ag(HPO)_2]ClO_4$	63%
3.4	C_8H_{17}	$[Ag(OPO)_2]ClO_4$	34%

Scheme 3.8: Reaction of phen-oxazine ligands **2.1 – 2.4** with silver perchlorate to produce silver(I) *bis*(phen-oxazine) complexes **3.1 – 3.4**.

Silver(I) *bis*(phen-oxazine) complex (**3.1**) was synthesised according to a previously determined procedure in our group.[176] Ag(I) complexes **3.2 – 3.4** were additionally synthesised with the intention of increasing the lipophilicity of the Ag(I) complex. The reaction involves heating silver perchlorate with the desired ligand in a 1:2 molar ratio at reflux in ACN for 2 h (**Scheme 3.8**). Isolated product yields of 34 – 75% were obtained. The Ag(I) *bis*(phen-oxazine) product is extracted by precipitation with diethyl ether. It is proposed that complexes **3.1 – 3.4** adopt a distorted tetrahedral structure where each *N*-atom of the phen-oxazine ligands forms a bond with the Ag(I) centre. The crystal structures of $[Ag(phen)_2](NO_3)$ and $[Ag(phendione)_2](ClO_4)$ show this pseudo-tetrahedral formation.[69, 180]

The Ag(I) complexes **3.1 – 3.4** were fully characterised using NMR and IR spectroscopy and HRMS and elemental analysis. Data was consistent with that presented in the literature for known Ag(I) *bis*(phen-oxazine) complex **3.1** ($[Ag(MPO)_2]ClO_4$).[71, 176]

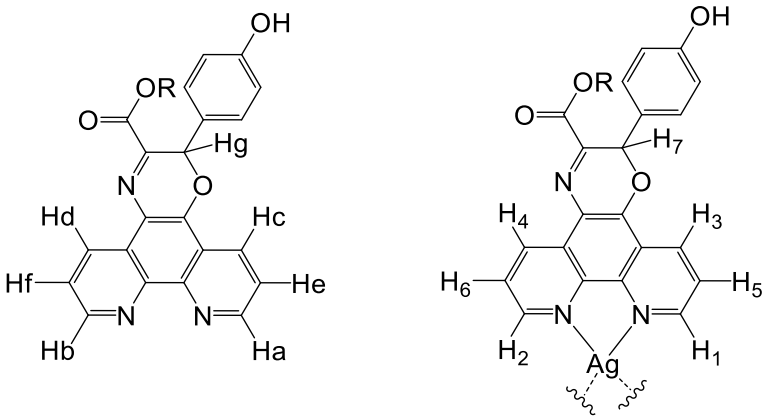

	PPO (2.2)		$[Ag(PPO)_2]ClO_4$ (3.2)		
Signal	Label	δ (ppm)	Label	δ (ppm)	Δδ (ppm)
OH	OH	9.69	OH	9.78	0.09
***ortho*-phenH**	Ha	9.12	H_1	9.12	0.00
***ortho*-phenH**	Hb	9.03	H_2	9.05	0.02
***Para*-phenH**	Hc	8.88	H_3	9.02	0.14
***Para*-phenH**	Hd	8.59	H_4	8.75	0.16
***Meta*-phenH**	He	7.85	H_5	8.01	0.16
***Meta*-phenH**	Hf	7.79	H_6	7.96	0.11
oxazine-H	Hg	6.50	H_7	6.64	0.14

Figure 3.4: ^{1}H NMR signals in DMSO-d6 of free ligand PPO (**2.2**) and Ag(I) complex $[Ag(PPO)_2]ClO_4$ (**3.2**).

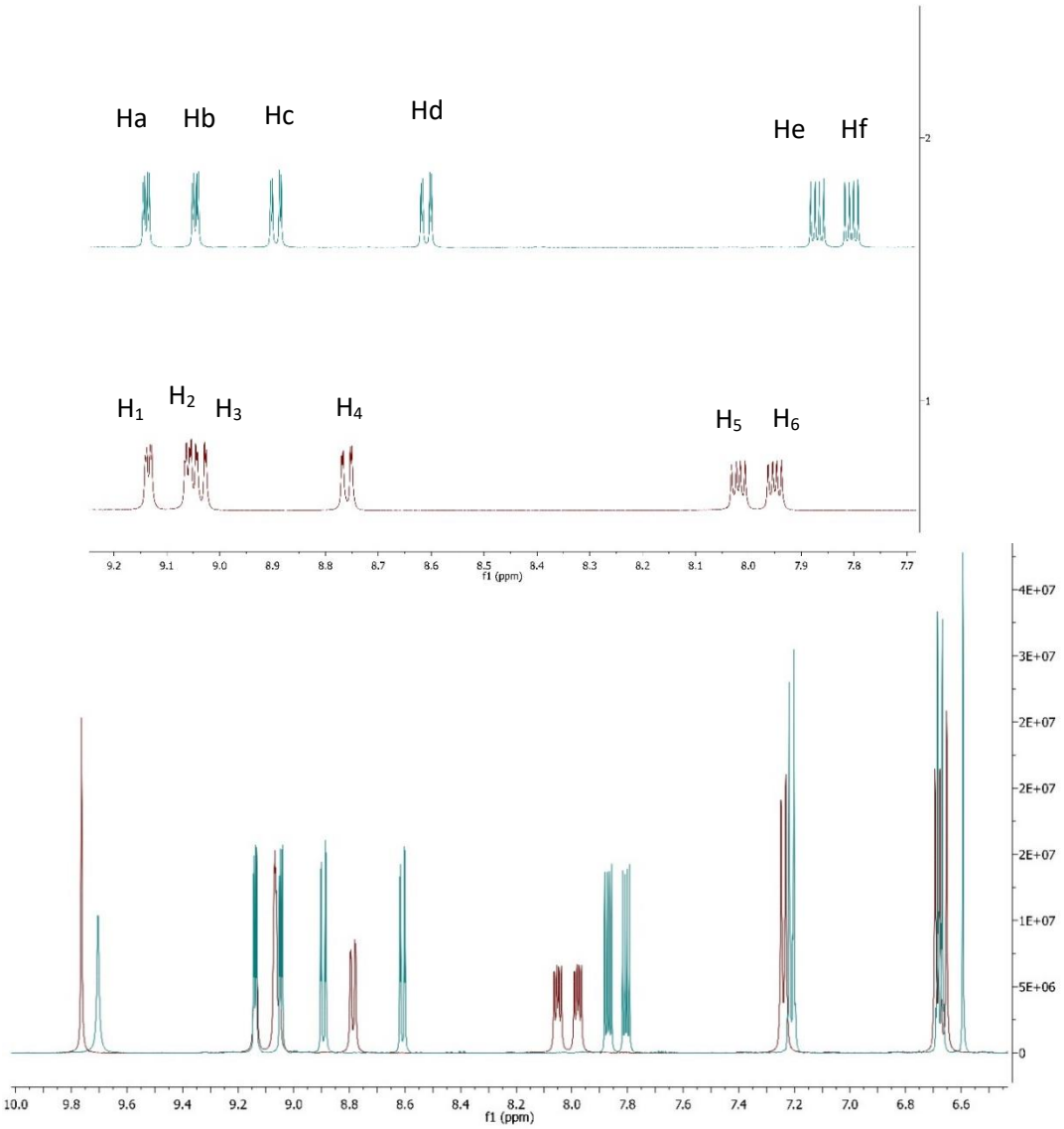

Figure 3.5: Comparison of ^{1}H NMR spectra of PPO (**2.2**) (blue) and $[Ag(PPO)_2]ClO_4$ (**3.2**) (red) in DMSO-d6. Inset shows phen protons in the region 7.7 – 9.2 ppm.

The ^{1}H NMR spectra of the family of Ag(I) *bis*(phen-oxazine) complexes in DMSO-d6 look almost identical to those of the free ligands **2.1 - 2.4**. In keeping with literature precedent for silver(I) complexes, the phen protons are slightly deshielded upon complexation to silver.[181, 182] There is shift of Ag(I) phen-oxazine complex signals of between 0.02 - 0.16 ppm downfield compared to those of the free ligand (**Figure 3.4 – 3.5**). There is a reasonable shift of 0.09 ppm of the OH signal from 9.69 ppm for the free PPO ligand (**2.2**) to 9.78 ppm for the $[Ag(PPO)_2]ClO_4$ (**3.2**) complex. This downfield shift is particularly notable for the phen signals *meta* and *para* to the phen *N*-atoms. *Para*-phen signals shift from 8.88 and 8.59 ppm for the free ligand to 9.02

and 8.75 ppm upon complexation. Similarly, the *meta*-phen signals of the free ligand shift from 7.85 and 7.79 ppm to 8.01 and 7.96 ppm once complexed to Ag(I). There is very little to no shift observed for the *ortho* signals. The more deshielded signals of the protons further from the *N*-atoms is consistent with the bidentate coordination of the phen-oxazine ligands at the *N* positions. The same deshielding effect of coordination to the Ag(I) centre is observed in the ^{13}C NMR spectra of complexes **3.1 – 3.4**. The limited effect of silver complexation on the chemical shifts of **2.1 – 2.4** is compatible with fast ligand exchange for **3.1 – 3.4** in solution on the NMR time scale.[181] The NMR spectra of $[Ag(MPO)_2]ClO_4$ (**3.1**) are in agreement with the reported spectra in DMSO-d6.[71, 176] Spectra of **3.2 – 3.4** are consistent with that of **3.1**.

The IR spectra of complexes **3.1 – 3.4** show some key differences compared to those of the free ligands that are characteristic of metal complexation. A set of intense perchlorate absorptions are observed between ~1150-1000 cm^{-1} and another band at 620 cm^{-1} (**Figure 3.6**) which are indicative of the free perchlorate ions.[183, 184] The aromatic ring stretches that appear between 1600-1500 cm^{-1} shift to higher wavenumbers upon complexation to the Ag(I) metal centre. Free ligand bands at 1609, 1571 and 1500 cm^{-1} move to 1611, 1579 and 1508 cm^{-1} when complexed as expected.[184] Additionally, there is a subtle shift from ~740 cm^{-1} to ~735 cm^{-1} associated with the out of plane bending of the phenC-H bonds upon complexation (**Figure 3.7**).[185]

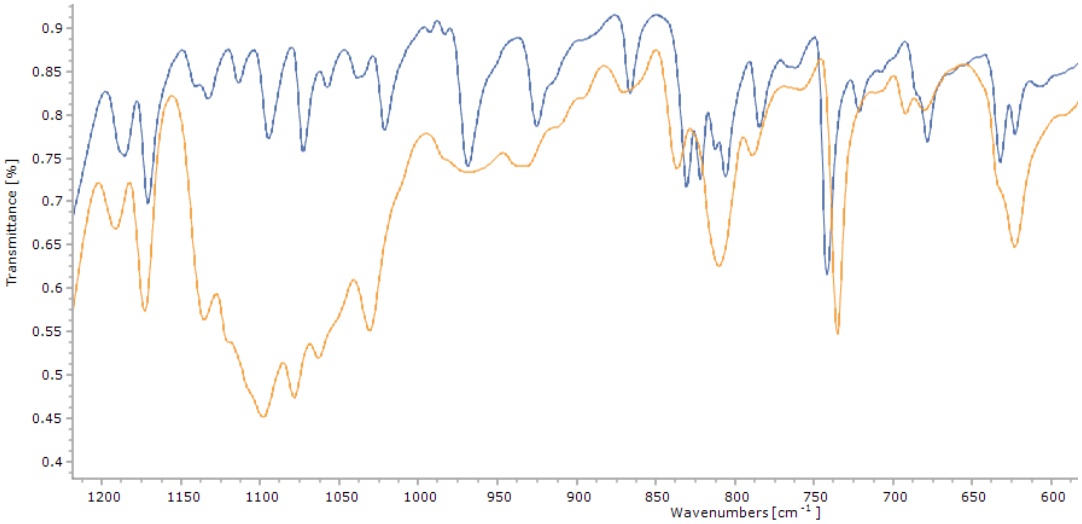

Figure 3.6: IR spectra of PPO (**2.2**) (blue) and $[Ag(PPO)_2]ClO_4$ (**3.2**) (orange) showing the intense perchlorate bands between 1150 – 1000 cm^{-1} and at 620 cm^{-1}.

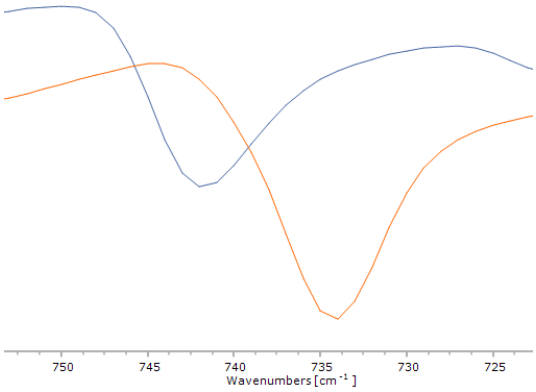

Figure 3.7: IR spectra of PPO (**2.2**) (blue) and $[Ag(PPO)_2]ClO_4$ (**3.2**) (orange) showing the shift of ligand band from 742 to 734 cm^{-1} upon complexation to Ag(I).

HRMS analysis confirmed the presence of $[Ag(MPO)_2]^+$, $[Ag(PPO)_2]^+$, $[Ag(HPO)_2]^+$ (**Table 3.6**) with the simulated isotopic match pattern expected for these species corresponding to the actual isotopic pattern. Elemental analysis confirmed complexes $[Ag(PPO)_2](ClO_4)$.DCM (**3.2**) and $[Ag(HPO)_2](ClO_4)$.DCM (**3.3**). Both HRMS and elemental analysis results support the proposed 1:2 Ag(I):ligand formulation.

Table 3.6: Theoretical and observed mass to charge ratios of Ag(I) complexes **3.1 – 3.4**

Compound	Formula	Theoretical *m/z* (Da)	Observed *m/z* (Da)	Mass error (ppm)
$[Ag(MPO)_2]ClO_4$ (3.1)	$[Ag(C_{22}H_{15}N_3O_4)_2]^+$	877.1171	877.1198	3.08
$[Ag(PPO)_2]ClO_4$ (3.2)	$[Ag(C_{24}H_{19}N_3O_4)_2]^+$	933.1797	933.1868	7.79
$[Ag(HPO)_2]ClO_4$ (3.3)	$[Ag(C_{27}H_{25}N_3O_4)_2]^+$	1017.2736	1017.3406	6.13
$[Ag(OPO)_2]ClO_4$ (3.4)	$[Ag(C_{28}H_{28}N_3O_4)_2]^+$	1075.3425	1075.3371	-5.00

UV-vis spectroscopic studies were also conducted on complexes **3.1 – 3.4** in DMSO. The spectra show an intense band between 300 – 450 nm with a λ_{max} at ~390 nm. This is the lowest energy transition which is proposed to be the $\pi \rightarrow \pi^*$ transition within the ligands which aligns with similar systems in the literature.[186] The extinction coefficient for this band is approximately double that of the phen-oxazine ligands which correlates with the 1:2 Ag(I):ligand ratio (**Table 3.7**).

Table 3.7: Wavelengths of absorption maxima (λ_{max}) and extinction coefficient (ε) values for phen-oxazine ligands **2.1 – 2.3** and silver(I) *bis*(phen-oxazine) complexes **3.1 – 3.3** in DMSO.

Compound	Ligand			Ag(I) complex		
	MPO (**2.1**)	PPO (**2.2**)	HPO (**2.3**)	$[Ag(MPO)_2]ClO_4$ (**3.1**)	$[Ag(PPO)_2]ClO_4$ (**3.2**)	$[Ag(HPO)_2]ClO_4$ (**3.3**)
λ_{max} (nm)	389	390	390	389	390	391
ε (M^{-1} cm^{-1})	7,646	7,717	7,464	13,172	15,629	15,877

3.3.2 Determining the Solution Stoichiometry of Ag(I) *bis*(phenanthroline-oxazine) Complexes 3.1 – 3.3

The characterisation data presented in **section 3.2.1** support the proposal of a solid state 1:2 Ag(I):ligand formulation. The limited effect of metal complexation of the chemical shifts of the phen-oxazine ligands as evident by their NMR spectra suggests fast ligand exchange in solution.[181] The solution stoichiometry of Ag(I) complexes **3.1 – 3.3** was therefore investigated using the continuous variation Job's plot method using NMR spectroscopy.[187] This experiment involved making solutions with varying ratios of $AgClO_4$ to phen-oxazine ligand (**2.1 – 2.3**) with a fixed total concentration of 40 mM in DMSO-d6 at rt. The ^{1}H NMR spectrum for each solution was compared to that of free ligand. The signals at 8.60 (signal **A**), 7.85 (signal **B**) and 7.79 (signal **C**) ppm for the free MPO (**2.1**) ligand were tracked across each NMR spectrum for the varying ratios (**Figure 3.8a**). A clear variation of the chemical shifts of protons in the phen region (7.7 – 8.7 ppm) are observed were multiplied by the mole fraction of ligand and plotted against mole fraction of the ligand to produce a Job's plot (**Figure 3.8b**). Plotting these values produces a bell-shaped curve with a clear maximum at ~0.67 which indicates the formation of a 1:2 complex.[187]

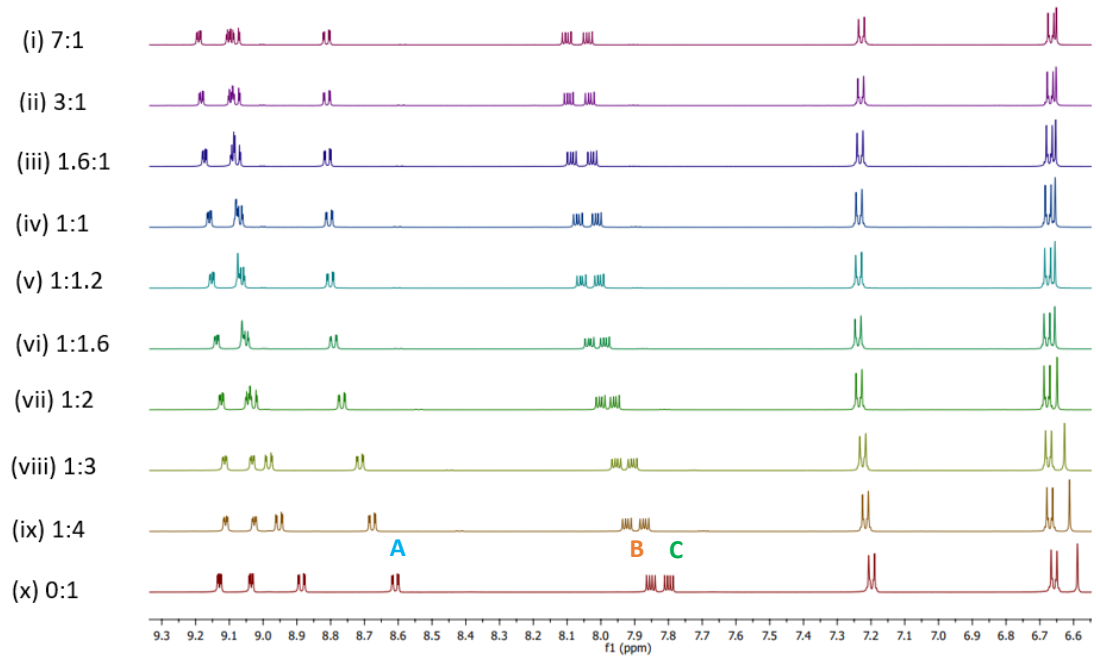

Figure 3.8a: ^{1}H NMR spectra of solutions of $AgClO_4$ and MPO (**2.1**) with a fixed total concentration of 40 mM in DMSO-d6 at 25 °C, with relative ratios varying from (i) 7:1 ($AgClO_4$:MPO) to (x) 0:1 ($AgClO_4$:MPO).

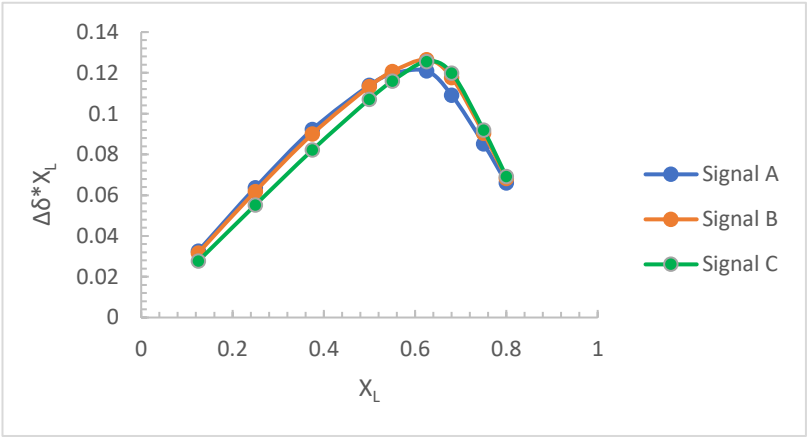

Figure 3.8b: Job's Plot created from data given in **Figure 3.8a** of various $AgClO_4$:MPO solutions, with a fixed total concentration of 40 mM in DMSO-d6 at 25 °C, where X_L is the mole fraction of ligand MPO (**2.1**), $\Delta\delta^*X_L$ is the difference in chemical shift (with reference to free ligand (x)) multiplied by the mole fraction of the ligand.

Similarly, when the same experiment was carried out with the PPO (**2.2**) ligand the same outcome is observed (**Figure 3.9a**). The free ligand signals at 8.60 (signal **A**), 7.86 (signal **B**) and 7.79 (signal **C**) ppm shift downfield upon addition of $AgClO_4$ in

increasing ratios. When this data are graphed to produce a Job's plot, the plot maximum again appears at ~0.67 (**Figure 3.9b**).

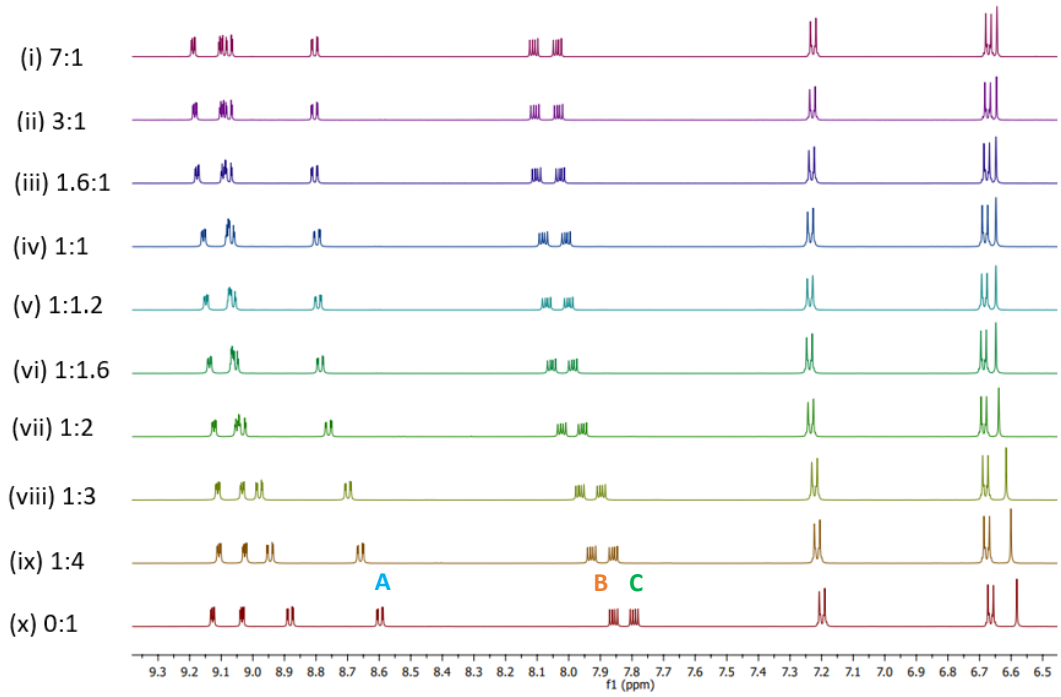

Figure 3.9a: ^{1}H NMR spectra of solutions of $AgClO_4$ and PPO (**2.2**) with a fixed total concentration of 40 mM in DMSO-d6 at 25 °C, with relative ratios varying from (i) 7:1 ($AgClO_4$:PPO) to (x) 0:1 ($AgClO_4$:PPO).

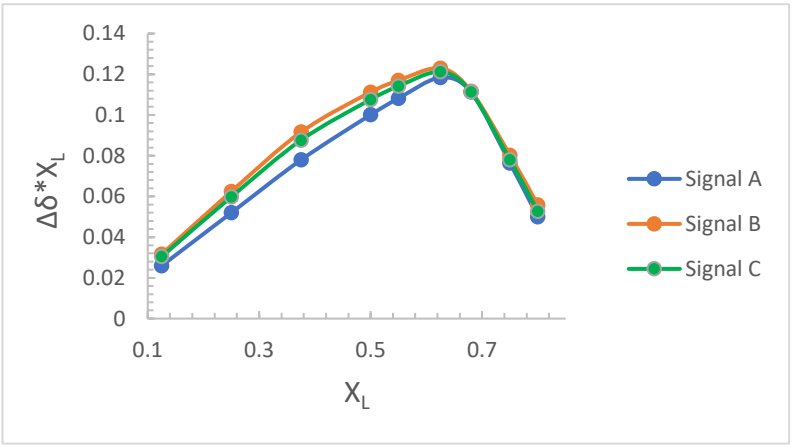

Figure 3.9b: Job's Plot created from data given in **Figure 3.9a** of various $AgClO_4$:PPO solutions, with a fixed total concentration of 40 mM in DMSO-d6 at 25 °C, where X_L is the mole fraction of ligand PPO (**2.2**), $\Delta\delta*X_L$ is the difference in chemical shift (with reference to free ligand (x)) multiplied by the mole fraction of the ligand.

This trend is similarly observed in the case of the HPO (**2.3**) when signals at 8.58 (signal **A**), 7.84 (signal **B**) and 7.78 (signal **C**) ppm are tracked upon addition of $AgClO_4$ (**Figure 3.10a**). The same outcome of a plot maxima at ~0.67 is apparent when a Job's plot is produced (**Figure 3.10b**). This experiment confirms that the most stable equilibrium exists when there are two ligands coordinated to the Ag(I) centre and agrees with what has been previously reported for similar compounds.[69, 180]

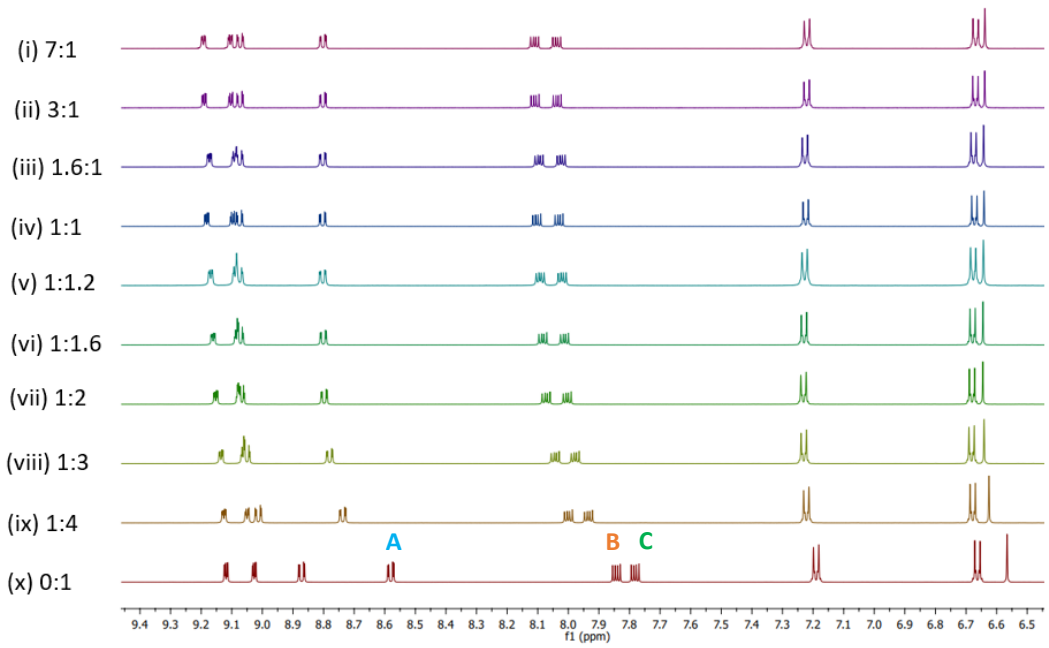

Figure 3.10a: ^1H NMR spectra of solutions of $AgClO_4$ and HPO (**2.3**) with a fixed total concentration of 40 mM in DMSO-d6 at 25 °C, with relative ratios varying from (i) 7:1 ($AgClO_4$:HPO) to (x) 0:1 ($AgClO_4$:HPO).

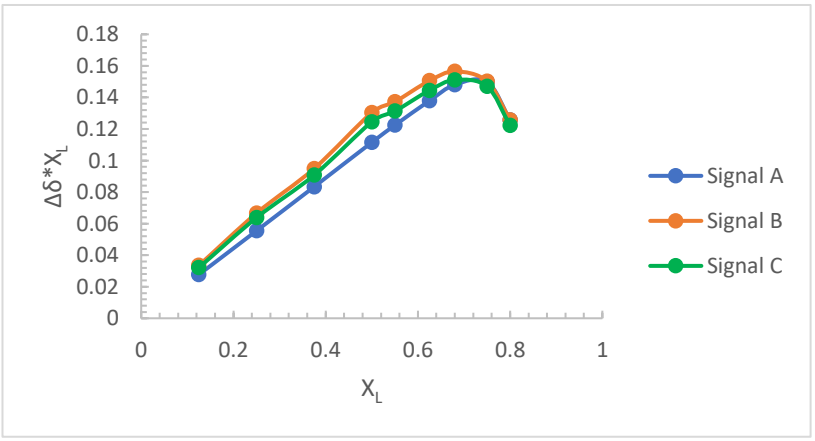

Figure 3.10b: Job's Plot created from data given in **Figure 3.10a** of various $AgClO_4$:HPO solutions, with a fixed total concentration of 40 mM in DMSO-d6 at 25

°C, where X_L is the mole fraction of ligand HPO (**2.3**), $\Delta\delta*X_L$ is the difference in chemical shift (with reference to free ligand (x)) multiplied by the mole fraction of the ligand.

3.3.3 Solution Behaviour and Stability of Ag(I) *bis*(phenanthroline-oxazine) Complexes 3.1 – 3.3

3.3.3.1 Solution behaviour of Ag(I) *bis*(phenanthroline-oxazine) Complexes 3.1 – 3.3

Ag(I) complexes containing phenanthroline ligands are known to have a labile Ag-N bond which means dynamic behaviour in solution is common [188]. Ag(I) is also a d^{10} metal which means its ligand field stabilisation energy is zero, therefore the Ag(I) centre will form weak bonds with ligands.[189] It was noted that while carrying out the Job's plot assays in the previous section that one set of signals was consistently observed for each $AgClO_4$:ligand ratio. This can be attributed to ligand exchange in solution that is faster than the NMR timescale leading to an average of signals.[181] This fluxional behaviour of the Ag(I) complexes was assessed using ^{1}H NMR spectroscopy. ^{1}H NMR spectra were recorded for each Ag(I) phen-oxazine complex **3.1 – 3.3** with the addition of excess ligand in 1:1 and 1:2 ratios and compared to the spectra of ligand only and complex only (**Figures 3.11 - 3.13**). This was achieved by addition of the appropriate volumes of 10 mM solutions of each sample in DMSO-d6. It is observed, as discussed previously in section 3.3.2, that the protons on the phen moiety of the phen-oxazine ligands shift downfield upon complexation to the Ag(I) centre. In **Figure 3.11** it is seen that the doublet signal at 8.60 ppm of MPO (**2.1**) (c) shifts to 8.75 ppm for $[Ag(MPO)_2]ClO_4$ (**3.1**) (a) while the associated signal in the 1:1 Ag(I):L solution is present at 8.70 (b). The doublet of doublets signal at 7.85 ppm for MPO (2.1) shifts to 8.01 ppm upon complexation and the chemical shift of this signal is present at 7.94 ppm for the spectrum of the 1:1 ratio of Ag(I):ligand. The second doublet of doublets signal observed at 7.79 ppm for MPO (2.1) is similarly shifted to 7.96 ppm for $[Ag(MPO)_2]ClO_4$ (**3.1**). Again, the relative signal for this phen proton is

present in between these chemical shifts at 7.88 ppm when the ligand and complex are in a 1:1 molar ratio.

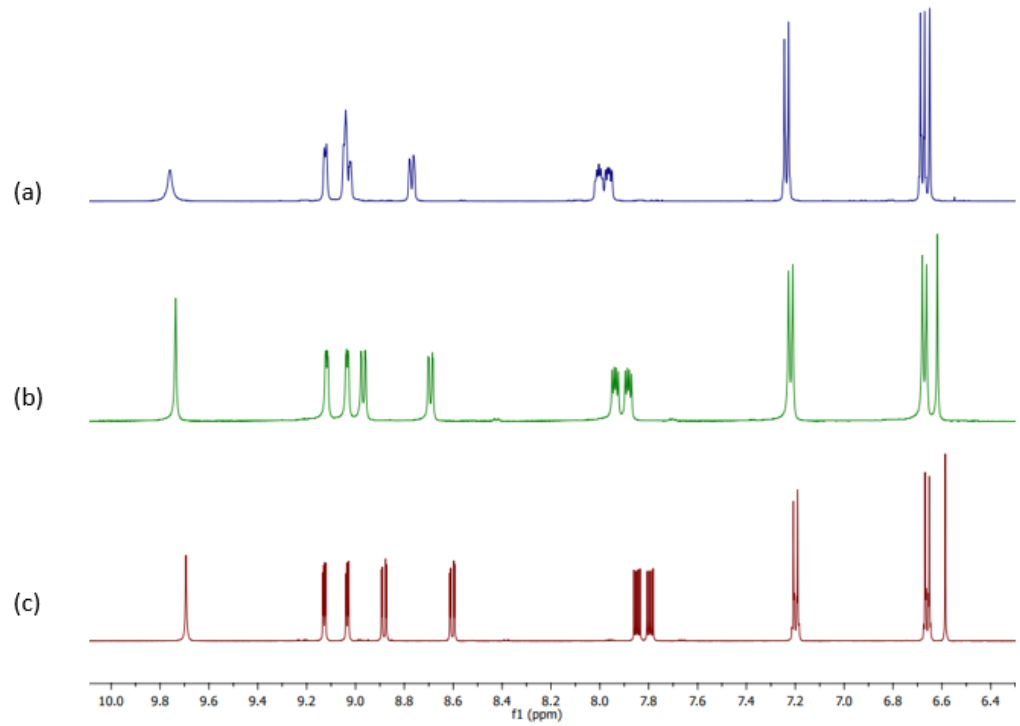

Figure 3.11: ^{1}H NMR spectra with a fixed total concentration 10 mM of (a) $[Ag(MPO)_2]ClO_4$ (**3.1**) (b) MPO (**2.1**) and $[Ag(MPO)_2]ClO_4$ (**3.1**) in a 1:1 ratio (c) PPO (**2.2**) MPO (**2.1**) in DMSO-d6 at 25 °C

The same experiment was conducted with phen-oxazine ligand PPO (**2.2**) and $[Ag(PPO)_2]ClO_4$ (**3.2**). The spectra presented in **Figure 3.12** shows the $[Ag(PPO)_2]ClO_4$ (**3.2**) only spectrum (a), a spectrum of a 1:1 ratio of PPO (**2.1**) : $[Ag(PPO)_2]ClO_4$ (**3.2**), (c) a spectrum of a 2:1 ratio of PPO:$[Ag(PPO)_2]ClO_4$ and (d) PPO (**2.2**) ligand only spectrum. In keeping with the chemical shifts of the phen backbone upon complexation, the signals at 8.59, 7.85 and 7.79 ppm for PPO (**2.2**) (**Figure 3.10d**) shift to 8.75, 8.01 and 7.96 respectively. While these signals in the spectra of the 1:1 and 2:1 ratios of Ligand:Ag(I) show an average of signals, lying at chemical shifts in between the values seen for ligand only and complex only.

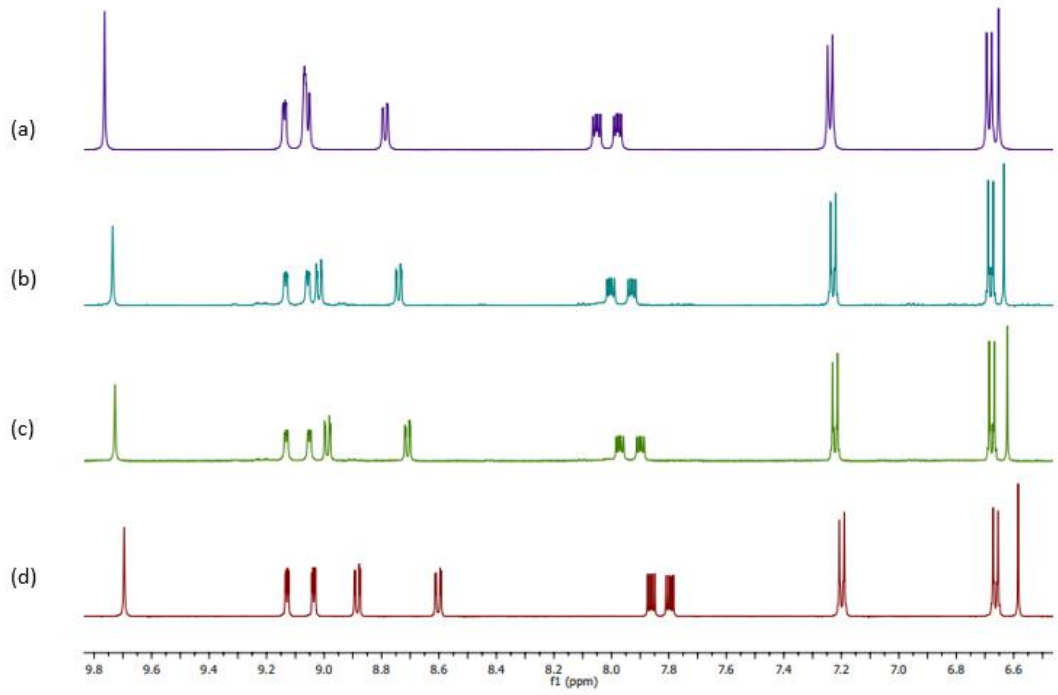

Figure 3.12: ^{1}H NMR spectra with a fixed total concentration 10 mM of (a) $[Ag(PPO)_2]ClO_4$ (**3.2**) (b) PPO (**2.2**) and $[Ag(PPO)_2]ClO_4$ (**3.2**) in a 1:1 ratio (c) PPO (**2.2**) and $[Ag(PPO)_2]ClO_4$ (**3.2**) in a 2:1 ratio (d) PPO (**2.2**) in DMSO-d6 at 25 °C

The dynamic behaviour of $[Ag(HPO)_2]ClO_4$ (**3.3**) was also assessed by the same method (**Figure 3.13**). The resulting spectra were similar to those seen for both $[Ag(MPO)_2]ClO_4$ (**3.1**) and $[Ag(PPO)_2]ClO_4$ (**3.2**) The ligand signals for HPO (**3.3**) show the same chemical shift trend when complexed to Ag(I) to form $[Ag(HPO)_2]ClO_4$ (**3.3**). The doublet of doublets signals present at 8.60, 7.86 and 7.80 ppm that correspond to the phen protons, shift to 8.76, 8.02 and 7.95 ppm respectively. The signals present in the 1:1 HPO (**3.3**) : $[Ag(HPO)_2]ClO_4$ (**3.3**) spectrum (**Figure 3.13b**) associated with these particular phen protons lie at chemical shifts between those observed for ligand only and complex only spectra, reflecting the 1:1 ligand:Ag(I) ratio. One set of signals is consistently observed for spectra of Ag(I) complex with added ligand. This is rationalised to be due to the phen-oxazine ligands dissociating and reassociating to the Ag(I) centre as is expected from literature precedent.[188, 190]

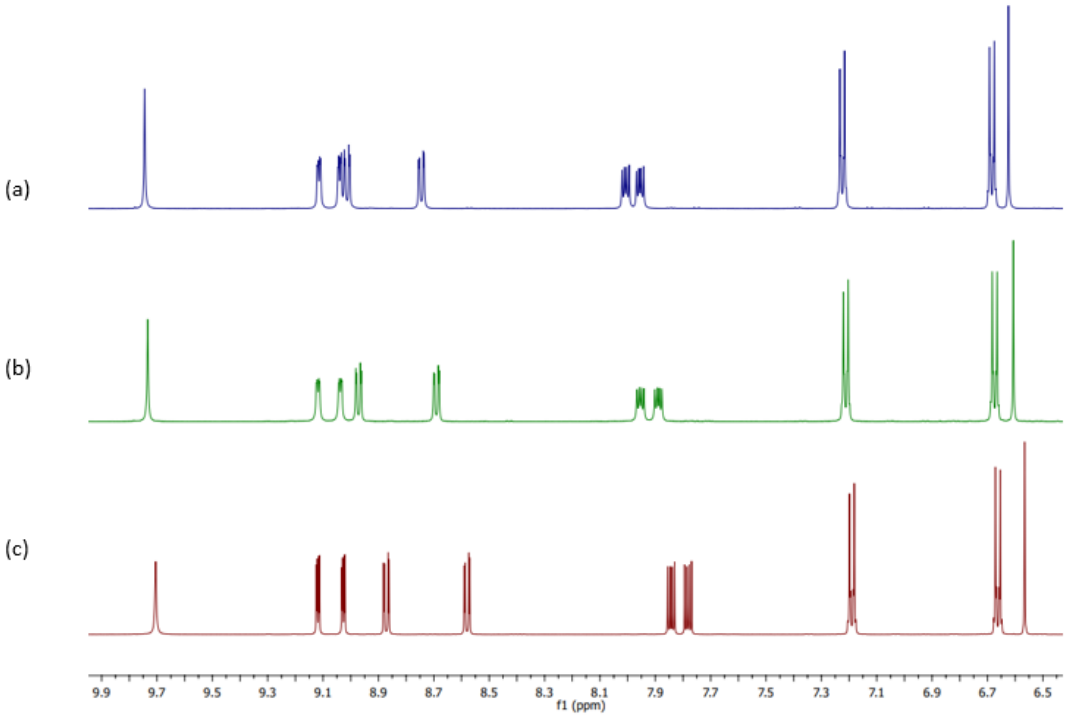

Figure 3.13: ^{1}H NMR spectra with a fixed total concentration 10 mM of (a) $[Ag(HPO)_2]ClO_4$ (**3.3**) (b) HPO (**2.3**) and $[Ag(HPO)_2]ClO_4$ (**3.3**) in a 1:1 ratio (c) HPO (**2.3**) in DMSO-d6 at 25 °C

A similar experiment was conducted in which a bidentate competitor (phen) was added to a solution of Ag(I) phen-oxazine complex in a 1:2 and 1:2 ratio (**Figure 3.14**). This experiment again showed an overall average of signals which can be rationalised as the dissociation and reassociation of the phen-oxazine ligand to the Ag(I) centre at a rate which is faster than the NMR timescale of 0.1 to 10 seconds meaning an average set of signals is observed.[191]

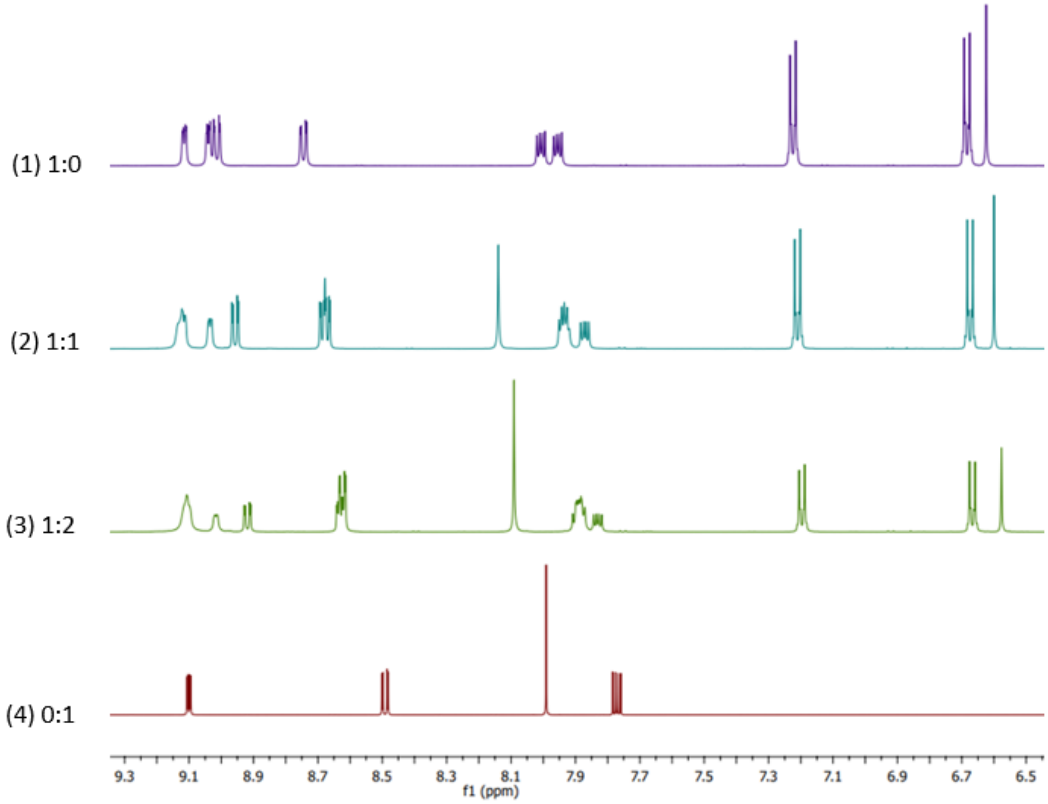

Figure 3.14: ^{1}H NMR spectra at a fixed total concentration 10 mM of (a) complex $[Ag(HPO)_2]ClO_4$ (**3.3**), (b) phen and $[Ag(HPO)_2]ClO_4$ (**3.3**) in a 1:1 ratio, (c) phen and $[Ag(HPO)_2]ClO_4$ (**3.3**) in a 2:1 ratio, (d) phen in DMSO-d6 at 25 °C.

An additional experiment was conducted where pyridine, a monodentate ligand, was added to a solution of Ag(I) complex. It appeared that pyridine is unable to compete with the bidentate phen-oxazine ligands and as a result signals for both $[Ag(HPO)_2]ClO_4$ (**3.3**) and pyridine are present in the spectra (**Figure 3.15**). This is also evident by the lack of shifts on the pyridine and Ag(I) associated peak in the mixture in comparison to complex only and pyridine only spectra. This observation is consistent with the chelate effect where the monodentate pyridine is unable to compete with bidentate phen-oxazine. The chelate effect is a coordination behaviour where ligands with more donor atoms such as phen which has two *N*-donor sites, have a greater affinity for the metal centre than monodentate ligands like pyridine that only have one coordination site.[192]

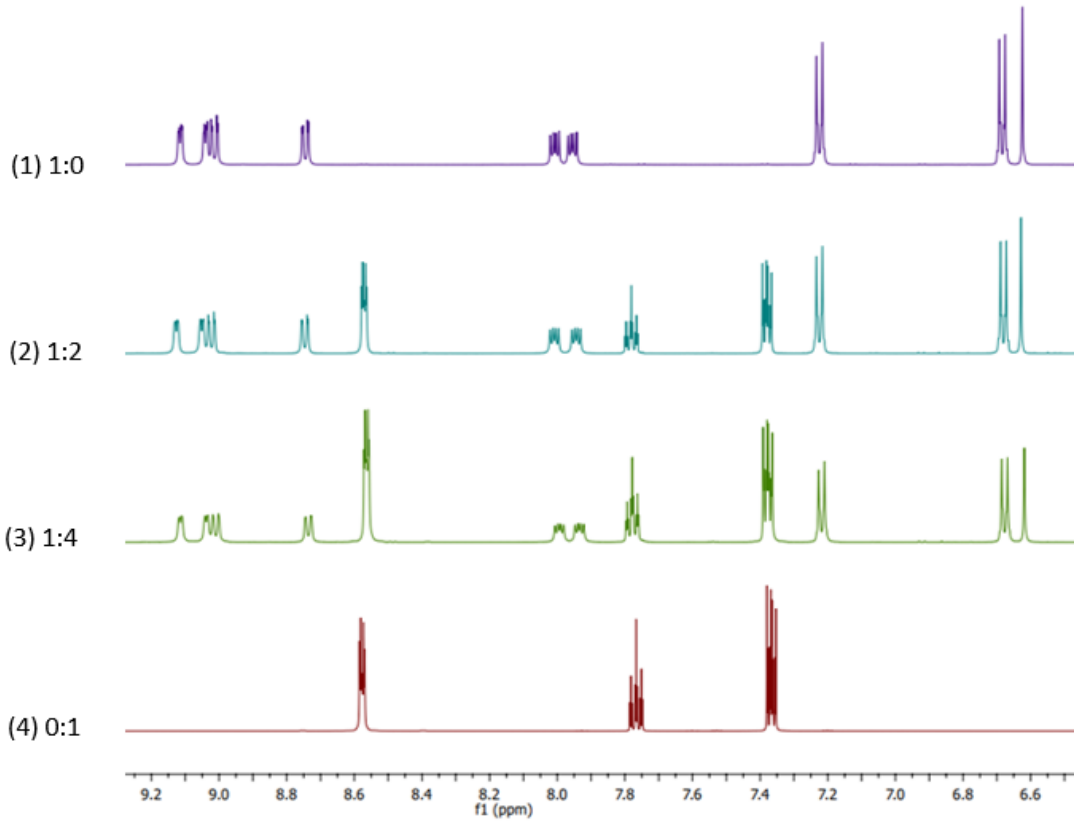

Figure 3.15: ^{1}H NMR spectra at a fixed total concentration 10 mM of (a) $[Ag(HPO)_2]ClO_4$ (**3.3**), (b) pyridine and $[Ag(HPO)_2]ClO_4$ (**3.3**) in a 1:2 ratio, (c) pyridine and $[Ag(HPO)_2]ClO_4$ (**3.3**) in a 4:1 ratio, (d) pyridine in DMSO-d6 at 25 °C.

The fluxional behaviour of the Ag(I) phen-oxazine complexes in solution may have implications for biological activity as it is well known that this can alter the nuclearity of the complex in solution.[188] This effect was observed previously in our group when an Ag(I) *bis*(phenanthroline-isoniazid) complex formed a polymeric crystalline material after slow diffusion of DCM in a solution of the isoniazid complex in DMSO.[111] The speciation of a metal complex in solution is an important factor for understanding the mode of action. Ag(I) ions may bind to compounds found in biological media such as proteins, water or halide anions rendering the complex inactive.[190]

3.3.3.2 Stability of Ag(I) *bis*(phenanthroline-oxazine) Complexes in Solution

The stability of the Ag(I) complexes **3.1 – 3.3** in biological growth media was assessed. Solutions of 5% (v/v) DMSO in minimal media (60 μM) which was used for biological testing were prepared. The samples were then recorded using UV-vis spectroscopy over a 72 h period (**Figure 3.16**). Complexes $[Ag(MPO)_2]ClO_4$ (**3.1**) and $[Ag(PPO)_2]ClO_4$ (**3.2**) had small changes over the time-period whereas $[Ag(HPO)_2]ClO_4$ (**3.3**) had more apparent changes. The band at 392 nm (λ_{max}) for the $[Ag(HPO)_2]ClO_4$ (**3.3**) complex decreases after 6 h and begins to shift to a longer wavelength where λ_{max} moves to 401 nm after 24 h. This complex contains ligands with the longest alkyl chain length and this change in the UV-vis band is indicative of aggregation of the complex in the polar growth media which is observed for similar compounds in the literature.[193]

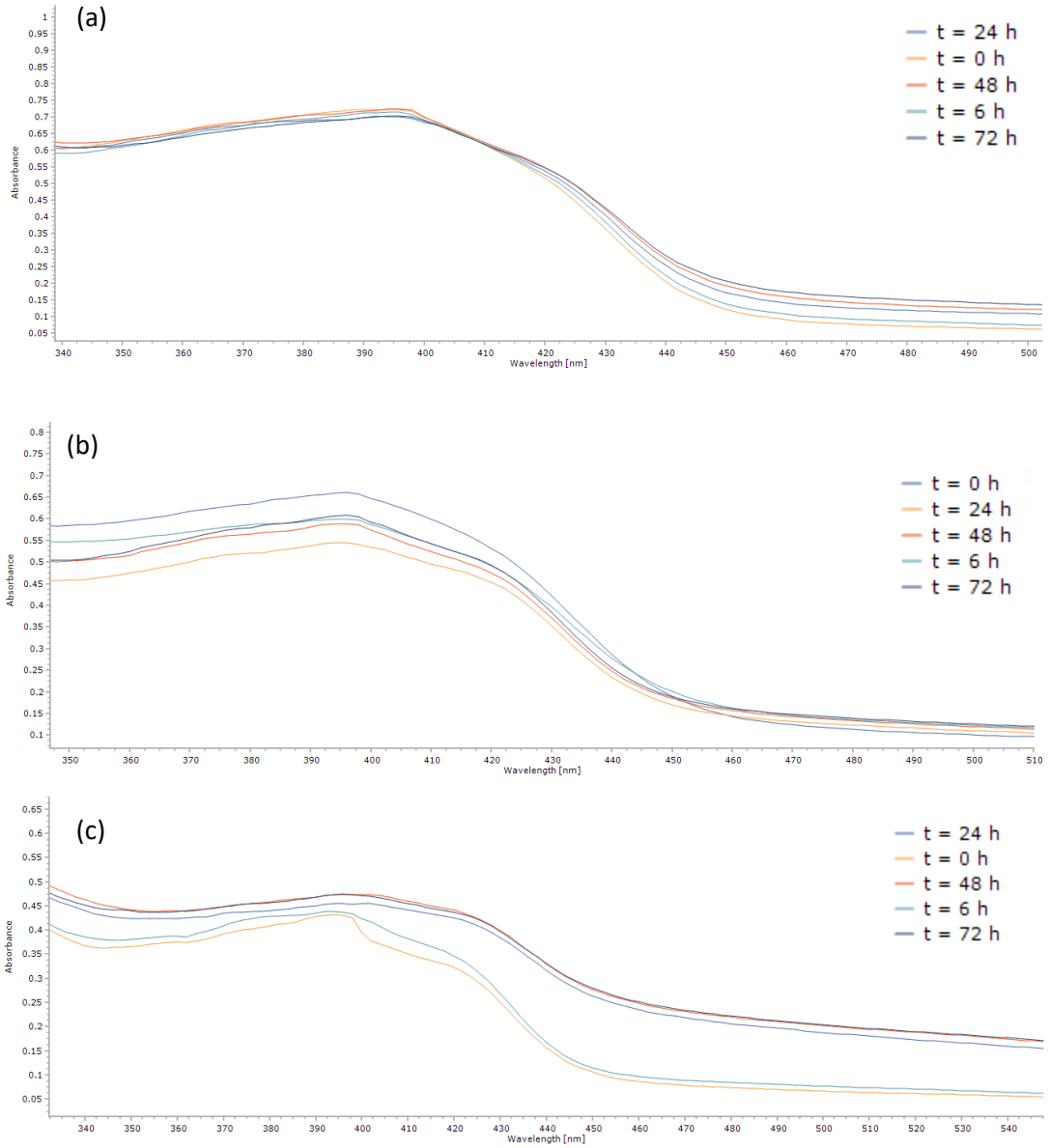

Figure 3.16: UV-visible spectra of a 60 µM solution in 5% (v/v) DMSO in minimal media monitored from 0 - 72 h on standing at ambient temperature in the dark of (a) $[Ag(MPO)_2]ClO_4$ (**3.1**), (b) $[Ag(PPO)_2]ClO_4$ (**3.2**), (c) $[Ag(HPO)_2]ClO_4$ (**3.3**)

3.3.4 *In vitro* Activity of Phenanthroline-oxazine Ligands 2.1 – 2.4 and Ag(I) Complexes 3.1 – 3.3 against *Candida albicans*

The antifungal activity of phen-oxazine ligands MPO (**2.1**), PPO (**2.2**), HPO (**2.3**) and complexes $[Ag(MPO)_2]ClO_4$ (**3.1**), $[Ag(PPO)_2]ClO_4$ (**3.2**) and $[Ag(HPO)_2]ClO_4$ (**3.3**) was assessed against the pathogenic yeast *Candida albicans.* The activity of the free

ligands was compared to that of the ligands coordinated to the Ag(I) centre. All compounds were also compared to silver perchlorate. Standard antifungal testing protocols were used as detailed in section 2.4. This involved incubating the test compounds with *C. albicans* in a 96-well plate for 24 h at 37°C. The OD at 600 nm was measured using a plate reader. The effectiveness of the compounds was determined as the percentage of OD measured with respect to that of the control, where the control was *C. albicans* grown in minimal media. The control was taken to be 100% growth (no inhibition) while 0% would be complete inhibition of growth. The standard protocol to assess antifungal activity involved testing 60 - 15 µM concentrations of each test compound in minimal media. The potential influence of the organic solvent DMSO was also assessed by testing 2.5% (v/v) DMSO in minimal media, the highest concentration in any well. The percentage growth was held above 96% compared to that of the control so was determined to have little impact on fungal growth.

Table 3.8: *In vitro* inhibitory effects of test samples determined as their ability after 24 h incubation to limit the growth of *C. albicans* in minimal media

Test sample and dosage				**Test sample and dosage**			
Ligand	60 µM	30 µM	15 µM	**Silver Salt**	60 µM	30 µM	15 µM
	Percentage Growth*				Percentage Growth*		
MPO (2.1)	67%	99%	100%	**$[Ag(MPO)_2]ClO_4$ (3.1)**	15%	12%	11%
PPO (2.2)	17%	80%	100%	**$[Ag(PPO)_2]ClO_4$ (3.2)**	12%	10%	9%
HPO (2.3)	18%	27%	57%	**$[Ag(HPO)_2]ClO_4$ (3.3)**	11%	12%	14%
				$AgClO_4$	9%	10%	12%

*Percentage growth is determined relative to a control sample where 100% growth = no inhibition, 0% = complete inhibition of growth

All compounds had some ability to limit *C. albicans* growth (**Table 3.8**). MPO (**2.1**) had minimal effectiveness with only the highest concentration of 60 µM having an impact (67% growth). The MIC_{50} (Minimum Concentration to inhibit 50% of growth) was not determined as it was too inactive in the concentration range tested. PPO (**2.2**) was

more effective, having some activity at 30 µM (80% growth). Finally, HPO (**3.3**) clearly demonstrated significant inhibition of *C. albicans* with activity at the lowest concentration of 15 µM where fungal growth was at 57%. MIC_{50} values for PPO (**2.2**) and HPO (**2.3**) were determined to be 43.32 µM and 14.63 µM respectively.

There is a clear correlation between the lipophilicity of the ligands and the activity, with the most lipophilic ligand HPO (**2.3**) ligand having the best antifungal activity against *C. albicans*. Statistical evidence supports this as the effectiveness of HPO (**2.3**) compared to (i) MPO (**2.1**) and (ii) PPO (**2.2**) both give high statistical significance of $P<0.0001$.

When statistically analysing a result, a hypothesis must first be established. In these experiments we create the hypothesis 'The anti-*C. albicans* activity of compound A is similar to if not the same as compound B'. The *P*-value is the probability of the hypothesis being true and will lie between 0 and 1. For example, in the case of comparing the growth inhibition of HPO (**2.3**) to MPO (**2.1**), the P-value is <0.0001. A *P*-value of less than 0.0001 means there is high statistical significance which implies the hypothesis is not correct while little statistical significance would give a *P*-value of >0.05 and hence the statement is very likely to be true.[194] The high statistical significance of P<0.0001 when the antifungal activity of HPO (**2.3**) is compared to (i) MPO (**2.1**) and (ii) PPO (**2.2**) at each concentration confirms that the more lipophilic ligand is more biologically active against *C. albicans* at the concentrations tested. This could be down to the better penetration of the biological membrane by the longer alkyl chain. The lipophilic effect of the phen-oxazine ligands was also evident in previous studies where the longer hexyl and octyl chains demonstrated increased antibacterial activity against *S. aureus* (**Table 3.9**).[176]

Table 3.9: Minimum Inhibitory Concentration (MIC) values of phen-oxazine ligand **2.1 – 2.4** against *S. aureus*

Compound	Calculated log*P*	S. aureus MIC (μM)	
		MIC_{50}	MIC_{80}
MPO (2.1)	2.8	ND	ND
PPO (2.2)	3.6	8	9
HPO (2.3)	4.9	2	4
OPO (2.4)	5.7	2	3

ND = not determined

The antifungal activities of the silver(I) complexes **3.1 – 3.3** and silver perchlorate were far superior to the ligands **2.1 – 2.3**. Treatment with all complexes and $AgClO_4$ resulted in percentage growth of *C. albicans* of less than 15% across the range of concentrations tested (60 – 15 μM). The Ag(I) complexes are therefore much more active than the free ligands and hold activity down to 15 μM. The coordination to Ag(I) undoubtedly enhances antifungal activity. This is backed up by the high statistical significance of $P<0.0001$ at 15 and 30 μM between each ligand and complex pair. The complexes and $AgClO_4$ were too active in the concentration range tested to determine MIC_{50} values. MIC_{80} values would be less than 15 μM for all complexes. From this data it is also apparent that the Ag(I) phen-oxazine complexes are just as active as $AgClO_4$, where $P>0.05$ between each complex and silver perchlorate. Although a lipophilic effect is seen amongst the free ligands, this is not true for the Ag(I) salts. Clearly showing that the complexation to Ag(I) is a more significant factor than the lipophilicity of the ligands for the experiments conducted in the concentration range of 60 – 15 μM. This outcome was also observed in McCann's 2004 study into the anti-*Candida albicans* activity of $[Ag(phen)_2]$ and $[Ag(phendione)_2]$ compared to the free phen or phendione (**2a**) ligands.[69] This enhanced activity upon complexation to a metal centre was evident in previous studies where Ag(I) and Cu(II) *bis* complexes of MPO (**2.1**) show higher DNA binding affinity than phenanthroline analogues.[175] The authors also found that there is increased DNA binding compared to the minor grove binding drugs pentamidine and netropsin. It is proposed that this is due to the extended conjugation of the phen-oxazine ligand that provides a secondary binding sites as the binding constant for

$[Ag(MPO)_2]ClO_4$ (**3.1**) was found to be three times larger than the binding constant for $Ag(phen)_2$.

With cognisance to the dynamic behaviour of the Ag(I) complexes in solution and potential aggregation of the $[Ag(HPO)_2]ClO_4$ (**3.3**) in biological media that is observed using UV-vis spectroscopy (**Figure 3.16c**), the effect of incubating the compounds in minimal media for 0 – 72 h prior to antifungal testing was assessed. The antifungal activity of a compound is greatly influenced by the choice of biological media.[195-197] Minimal media contains glucose, inorganic components such as nitrogen and sulphur and essential amino acids. These components may interact with the Ag^+ ions in solution and impact the activity. The growth, adhesion and formation of biofilms of *Candida* species can also be greatly impacted by the choice of media.[198]

To investigate the impact of the choice of media, test solutions of ligands **2.1 – 2.3**, $AgClO_4$ and Ag(I) complexes **3.1 – 3.3** were freshly prepared at 120 µM in 5% (v/v) DMSO in minimal media and allowed to stand in the dark at rt for 0, 3, 6, 24, 48 and 72 h. Following the specified time, the 120 µM test solutions were inoculated as described above and the plate was read after 24 h. The length of time that the compounds were left in the media prior to use did not have an impact on the antifungal activity against *C. albicans* for any compound at any time standing in media prior to use (**Tables 3.10 - 3.11**). As expected, the activity of the free ligands **2.1 – 2.3** were not affected by prior incubation in media. The 60 µM test solution of PPO (**2.2**) lead to a percentage growth of 17% when left for 0 h, 13% when left for 6 h and 18% when left to stand for 72 h before use (**Table 3.10**). Similarly, a 60 µM test solution of $[Ag(PPO)_2]ClO_4$ (**3.2**) produces inhibition of 12, 9 and 10% following 0, 6 and 72 h standing of media prior to testing (**Table 3.11**). When the values for each time point of each compound are compared against one another, $P>0.05$ is calculated, supporting the conclusion that standing in media for any time period prior to use has no impact on the biological activity against *C. albicans* under the conditions tested. The inhibition observed using the standard protocol matched very closely to all activity observed at the varying time points for all compounds tested at each concentration. This experiment highlights that under the conditions tested, the impact of the dynamic behaviour of the silver complexes is negligible.

Table 3.10: *In vitro* inhibitory effects of ligands **2.1 – 2.3** as determined as their ability after 24 h incubation to limit the growth of *C. albicans*, following prior standing of test solution in minimal media for time periods between 0-72 h.

	Test compound		
Time standing in minimal media (h)	**MPO (2.1)**	**PPO (2.2)**	**HPO (2.3)**
	Percentage Growth* at 60 µM, 30 µM and 15 µM dosage levels		
0 h	67, 99, 100%	17, 80, 100%	18, 27, 59%
3 h	55, 95, 100%	16, 72, 100%	24, 36, 65%
6 h	53, 93, 97%	13, 73, 97%	19, 17, 31%
24 h	80, 100, 100%	20, 99, 100%	20, 61, 94%
48 h	59, 95, 99%	14, 76, 96%	21, 39, 88%
72 h	69, 100, 100%	18, 90, 98%	15, 37, 69%

*Percentage growth is determined relative to a control sample where 100% growth = no inhibition, 0% = complete inhibition of growth

Table 3.11: *In vitro* inhibitory effects of complexes **3.1 – 3.3** and $AgClO_4$ as determined as their ability after 24 h incubation to limit the growth of *C. albicans*, following prior standing of test solution in minimal media for time periods between 0-72 h.

	Test Compound			
Time standing in minimal media (h)	**$[Ag(MPO)_2]ClO_4$ (3.1)**	**$[Ag(PPO)_2]ClO_4$ (3.2)**	**$[Ag(HPO)_2]ClO_4$ (3.3)**	**$AgClO_4$**
	Percentage Growth* at 60 µM, 30 µM and 15 µM dosage levels			
0 h	15, 12, 11%	12, 10, 9%	11, 12, 14%	17, 80, 100%
3 h	13, 13, 12%	10, 9 ,8%	13, 11, 13%	16, 72, 100%
6 h	11, 11, 12%	9, 8, 8%	11, 9, 9%	13, 73, 97%
24 h	13, 13, 13%	12, 11, 10%	14, 12, 19%	20, 99, 100%
48 h	15, 17, 18%	11, 10, 9%	25, 20, 19%	14, 76, 96%
72 h	12, 12, 14%	10, 8, 7%	12, 10, 13%	18, 90, 98%

*Percentage growth is determined relative to a control sample where 100% growth = no inhibition, 0% = complete inhibition of growth

It is known that the incubation time may influence the behaviour of antifungal agents.[199] Therefore, to further probe the biological activity of the compounds in solution, the initiation and duration of activity in minimal media was analysed. This analysis was achieved by reading the OD of the plates at 3, 6, 24 and 48 h following inoculation (**Tables 3.12 – 3.13**). The activity of ligands **2.1 – 2.3** was less than 10% after 3 h incubation. Activity for all compounds became apparent between 3 and 6 h. From 24 h onwards, key differences were observed. All free ligands **2.1 – 2.3** showed their highest activity after 24 h with their potency decreasing at this point. The

activity of the MPO (**2.1**) and PPO (**2.2**) ligands significantly dropped at this point with PPO (**2.2**) decreasing from 17% growth (60 µM, 24 h) to 64% growth (60 µM, 48 h) which gave a statistical significance of P<0.0001. HPO (**2.3**) had better ability to hold some activity, with its inhibition only decreasing from 18% to 24% at the highest dose of 60 µM from 24 h to 48 h. At the lower dose of 30 µM, the activity of HPO (**2.3**) decreased from 27% to 45%.

Table 3.12: *In vitro* inhibitory effects of phen-oxazine ligands **2.1 – 2.3** as determined as their ability after 3 - 48 h incubation to limit the growth of *C. albicans* in minimal media.

	Test Sample		
	Ligands		
Incubation Time	**MPO (2.1)**	**PPO (2.2)**	**HPO (2.3)**
	Percentage Growth* at 60 µM, 30 µM and 15 µM dosage levels		
3 h	90, 93,95%	93, 93, 94%	100, 100, 100%
6 h	75, 83, 91%	75, 78, 84%	100, 92, 87%
24 h	68, 99, 100%	17, 80, 100%	18, 27, 57%
48 h	100, 100, 100%	64, 100, 100%	24, 45, 95%

*Percentage growth is determined relative to a control sample where 100% growth = no inhibition, 0% = complete inhibition of growth

Table 3.13: *In vitro* inhibitory effects of Ag(I) complexes **3.1 – 3.3** and $AgClO_4$ as determined as their ability after 3 - 48 h incubation to limit the growth of *C. albicans* in minimal media.

	Test Compound			
Incubation Time	**$[Ag(MPO)_2]ClO_4$ (3.1)**	**$[Ag(PPO)_2]ClO_4$ (3.2)**	**$[Ag(HPO)_2]ClO_4$ (3.3)**	**$AgClO_4$**
	Percentage Growth* at 60 µM, 30 µM and 15 µM dosage levels			
3 h	100, 100, 97%	100, 100, 100%	100, 100, 100%	100, 90, 93%
6 h	84, 75, 74%	95, 81, 75%	87, 79, 79%	100, 77, 79%
24 h	15, 12, 11%	12, 10, 9%	11, 12, 14%	9, 10, 12%
48 h	19, 19, 17%	13, 10, 9%	15, 17, 21%	11, 91, 100%

*Percentage growth is determined relative to a control sample where 100% growth = no inhibition, 0% = complete inhibition of growth

The most interesting result was that of the complexes. There was a clear difference in effectiveness and duration of activity for the silver(I) phen-oxazine complexes compared to the metal free ligands. There was no significant difference ($P>0.05$) for complexes **3.1 – 3.3** from 24 h to 48 h at all doses (60 – 15 µM). In contrast, silver perchlorate only held activity at the highest dose of 60 µM after 48 h where growth remained at 11%. The activity of $AgClO_4$ after 24 h decreased from 10% to 91% growth at 30 µM and from 12% to 100% growth at 15 µM. The activity of complexes **3.1 – 3.3** was significantly better ($P<0.0001$) compared to silver perchlorate at 48 h.

The dynamic behaviour of Ag(I) complexes **3.1 – 3.3** did not impact the antifungal activity when the susceptibility assays were conducted in nutrient poor minimal media. The impact of the solution behaviour of complexes **3.1 – 3.3** was probed further by conducting similar experiments using nutrient rich, YEPD media. The media composition is an important parameter when conducting antifungal testing and can greatly affect the biological activity.[195, 196, 198] YEPD media is a much more nutrient rich media as it contains peptones and yeast extracts that provide peptides, amino acids, inorganic salts and lipids.[200] The standard 24 h susceptibility assay was conducted for ligands **2.1 – 2.3**, complexes **3.1 – 3.3** and $AgClO_4$ at concentrations of

60 – 15 µM in YEPD against *C. albicans* (**Table 3.14, row A**). There was no fungal inhibition observed at any concentration for any compound. The influence of standing the compounds in YEPD media for varying time points prior to use was also assessed (**Table 3.14, rows B-F**). No fungal inhibition was observed for any compound standing in YEPD media for any time point prior to inoculation. This outcome is consistent with similar experiments where the antifungal growth noticeably varied from media to media. A study by Hoeprich and Huston assessed the zones of inhibition of *C. albicans* using the commercial antifungal drug amphotericin B. Brain-Heart Infusion (BHI) media gave a zone of inhibition of 17.2 mm while Yeast Nitrogen Base (YNB) media gave a larger zone of inhibition of 19.6 mm.[197] A similar study showed that the choice of media can alter the MIC_{50} value of the antifungal agent.[196]

Table 3.14: *In vitro* inhibitory effects of test samples determined as their ability after 24 h incubation to limit the growth of *C. albicans* in YEPD media following standing of test compounds in solution for time periods between 0-72 h

	Time standing in media (h) prior to testing	Percentage Growth* 60 µM dose	Percentage Growth* 30 µM dose	Percentage Growth* 15 µM dose
A	0	100	100	100
B	3	100	100	100
C	6	100	100	100
D	24	100	100	100
E	48	100	100	100
F	72	100	100	100

*Percentage growth is determined relative to a control sample where 100% growth = no inhibition, 0% = complete inhibition of growth.

The antifungal activity of phen-oxazine ligands **2.1 – 2.3** is much less than the activity of phen and phendione against *C. albicans* presented in the literature.[69] HPO (**2.3**) has a similar antifungal effect to phen (**Table 3.15**). The Ag(I) phen-oxazine complexes (**3.1 – 3.3**) appear more effective than unsubstituted phen. They are also predicted to have similar inhibitory effects as phendione, $[Ag(phen)_2]ClO_4$ and $[Ag(phendione)_2]ClO_4$. The Ag(I) phen-oxazine complexes are much more active than the free phen-oxazine ligands and silver salt $AgNO_3$. The standard treatment for *C. albicans* infections is amphotericin B which has an extremely low MIC_{50} of 0.54 µM.[201]

With this in mind, it is clear that the phen-oxazine ligands and Ag(I) complexes are far less potent than the standard treatment.

Table 3.15: Comparison of minimum inhibitory concentrations (MIC) of phen-oxazines, Ag(I) phen-oxazines and reported Ag(I) phen complexes[69]

Ligand	MIC_{50} (µM)	Complex	MIC_{50} (µM)
phen	14	$[Ag(phen)_2]ClO_4$	8.8
phendione	3	$[Ag(phendione)_2]ClO_4$	0.5
MPO (2.1)	> 60	$[Ag(MPO)_2]ClO_4$ (**3.1**)	< 15
PPO (2.2)	43	$[Ag(PPO)_2]ClO_4$ (**3.2**)	< 15
HPO (2.3)	14	$[Ag(HPO)_2]ClO_4$ (**3.3**)	< 15
		$AgNO_3$	30
		$AgClO_4$	< 15

3.3.5 *In vivo* Toxicity Towards *Galleria mellonella*

Galleria mellonella (greater wax moth) is a widely used insect model to indicate toxicity of a compound and to study the pathogenesis of an infection.[202, 203] Larvae of *G. mellonella* have a similar innate immune response to mammals which affords them a valuable model to study *in vivo* toxicity and virulence of infections. The larvae are inexpensive, straightforward to inoculate, have no ethical restrictions and the results are collected within a few days.[204, 205] *G. mellonella* larvae were used to assess the *in vivo* toxicity of a phen-oxazine ligand and an Ag(I) phen-oxazine complex. Test solutions of PPO (**2.2**) and $[Ag(PPO)_2]ClO_4$ (**3.2**) were prepared at 60 µM and 30 µM in 5% (v/v) DMSO in PBS. A control solution of 5% (v/v) DMSO in PBS was also prepared. Five larvae weighing between 200 – 300 mg were placed in a clean petri dish per replicate. Three replicates per test solution were conducted. Each larva was inoculated with 20 µL of test solution beside the last left proleg using a 1 mL insulin syringe. The larvae were placed in an incubator at 37 °C and monitored every 24 h up to 72 h for indications of melanisation or death. Healthy larvae appeared white in colour and had good mobility. They were gently flipped on their back and their ability

to right themselves was noted. All larvae tested survived and appeared healthy after 72 h (**Table 3.16**).

Table 3.16: Percentage survival of larvae after 24, 48 and 72 h incubation following a 20 µL inoculation of test compounds PPO (**2.2**), $[Ag(PPO)_2]ClO_4$ (**3.2**) or control (5% v/v DMSO in PBS).

		% Survival		
Test compound	**Concentration (µM)**	**24 h**	**48 h**	**72 h**
5% (v/v) DMSO in PBS		100	100	100
PPO (2.2)	60	100	100	100
	30	100	100	100
$[Ag(PPO)_2]ClO_4$ (3.2)	60	100	100	100
	30	100	100	100

Another assessment of the *in vivo* toxicity of PPO (**2.1**) and $[Ag(PPO)_2]ClO_4$ (**3.2**) was conducted to determine whether there was an increase in inflammation in the larval bloodstreams following inoculation.[206] Fresh test solutions of 60 µM were prepared as before. Five larvae per test condition were injected with 20 µL of test solution. Following 3 h of incubation at 37 °C, the larvae were collected. A single larva was treated as one replicate, with 3 larvae evaluated per test condition. The lymph of the larvae was collected in a clean Eppendorf. The lymph was diluted by a factor of 5 in fresh PBS. A sample was then pipetted onto a haemocytometer and the number of cells were counted under a microscope. The control number of haemocytes was determined to be 1.23×10^7 cells/ml. For the test group inoculated with 60 µM of PPO (**2.2**), 1.25×10^7 cells/ml were calculated. Similarly, the 60 µM inoculation of $[Ag(PPO)_2]ClO_4$ (**3.2**) was determined to be 9.82×10^6 (**Table 3.17**). Given the haemocyte numbers of PPO (**2.1**) and $[Ag(PPO)_2]ClO_4$ (**3.2**) were similar to that of the PBS control with no significant increases, it was determined that no inflammatory response was induced.

Table 3.17: Haemocyte densities calculated following inoculation of 60 µM test solutions of PPO (**2.2**) and $[Ag(PPO)_2]ClO_4$ (**3.2**)

Test Compound	Concentration (µM)	Haemocyte count (cells/mL)
5% v/v DMSO in PBS	-	1.23×10^7
PPO (**2.2**)	60	1.25×10^7
$[Ag(PPO)_2]ClO_4$ (**3.2**)	60	9.82×10^6

3.3.6 Survival Rate of *Galleria mellonella* Infected with *C. albicans* Followed by Treatment with PPO (2.2) and $[Ag(PPO)_2]ClO_4$ (3.2).

The *G. mellonella* model is a good insect infection model to indicate *in vivo* efficacy of antimicrobial agents as the larvae can be maintained at 37 °C, the temperature human pathogens proliferate at.[203] *G. mellonella* has been widely used as a model to assess treatment of *Candida* infections.[203, 205] The efficacy of antifungal compounds PPO (**2.2**) and $[Ag(PPO)_2]ClO_4$ (**3.2**) was evaluated using *G. mellonella*. From protocols in the literature, a lethal dose of *C. albicans* is administered to the larvae at a range of concentrations of between $1 \times 10^5 – 5 \times 10^5$ CFU/larva.[203, 205, 207] The highest *C. albicans* dose of 5×10^5 CFU/larvae administered to larvae of 0.33 mg weight resulted in a 50% death rate after 48 h.[203] The volume of inoculum used was either 5 or 10 µL.[207, 208] Vertyporokh and coworkers used a lethal 5 µL dose of 2×10^5 CFU/larva to conduct their experiments.[207]

Given the broad range of protocols in the literature, it was decided to first assess the higher *C. albicans* concentration of 5×10^5 CFU/larva against *G. mellonella*. A *C. albicans* culture was grown overnight in YEPD media in an orbital shaker. A working culture of 5×10^7 cells/mL in PBS was prepared. A control solution of 5% (v/v) DMSO in PBS was also prepared. Five larvae per test condition were placed in a clean petri dish. Larvae weighing between 200 – 300 mg were used. Two replicates were conducted per test condition. A control group received a 20 µL dose of 5% (v/v) DMSO in PBS and were placed in an incubator at 37 °C. Three groups of 10 larvae were inoculated with 10 µL of the 1×10^7 cells/mL working culture of *C. albican*s. The infected larvae were placed in the incubator at 37 °C for 1 h. After this time the larvae were taken out of the incubator and given a second inoculation as follows; one group

were injected with a 10 µL dose of 5% (v/v) DMSO in PBS, one group were treated with a 10 µL dose of the 60 µM solution of PPO (**2.2**) ligand and the final group were treated with a 10 µL dose of 60 µM of complex $[Ag(PPO)_2]ClO_4$ (**3.2**). All larvae were placed in the incubator once again and were monitored for survival, melanisation and changes in mobility. After 24 h no larvae infected with *C. albicans* survived. The control group that received the PBS inoculum all survived. The infected larvae had clear patches of dark melanisation which suggested a very high fungal load that spread very quickly.

A second experiment was conducted similar to the first but with the use of a *C. albicans* solution of 1 x 10^5 cells/mL which was administered in a volume of 10 µL. The larvae were again monitored for survival, melanisation and changes in mobility for up to 72 h. This experiment yielded more promising results. The survival rate of the larvae was noted and are presented in **Table 3.18**. After incubation for 24 h, all control larvae were alive, had no melanisation and were fully mobile. The test group infected with *C. albicans* and left untreated showed clear signs of sickness following 24 h. This group showed clear melanisation and were lethargic with a limited ability to right themselves when turned over. Groups infected and followed with treatment of PPO (**2.2**) had minor melanisation after 24 h and appeared quite mobile. The test group treated with $[Ag(PPO)_2]ClO_4$ (**3.2**) appeared similar to those treated with free ligand PPO (**2.2**) but had slightly more melanisation. Upon inspection after 48 h there were obvious differences. Only 60% of infection only larvae were alive while those treated with PPO (**2.2**) and $[Ag(PPO)_2]ClO_4$ (**3.2**) had a survival rate of 90 and 80% respectively at 48 h. It appeared that the free ligand had slightly better antifungal activity at this point. Following 72 h of infection and treatment differences became apparent. As expected, the negative control group infected with *C. albicans* and left untreated had the lowest survival of 60% after 72 h. Interestingly, the survival of the larvae treated with PPO (**2.2**) decreased to 70% while those treated with $[Ag(PPO)_2]ClO_4$ (**3.2**) only decreased to 80%. The ability of the Ag(I) phen-oxazine complex to hold activity for longer agrees with the results presented earlier in **Table 3.11**. There is clear evidence that both PPO (**2.2**) and $[Ag(PPO)_2]ClO_4$ (**3.2**) have *in vivo*

antifungal activity given the survival rates for the larvae treated with these compounds were higher than that of the infection only larvae group.

Table 3.18: Percentage of survival of larvae infected with *C. albicans* and followed by (i) no treatment, (ii) treatment of PPO (**2.2**), (iii) treatment of $[Ag(PPO)_2]ClO_4$ (**3.2**)

			% Survival		
Test condition	**First inoculation**	**Second inoculation**	**24 h**	**48 h**	**72 h**
Control	5% v/v DMSO in PBS (20 µL)	-	100	100	100
i	*C. albicans* (10 µL)	5% v/v DMSO in PBS (10 µL)	90	60	60
ii	*C. albicans* (10 µL)	60 µM PPO (**2.2**) (10 µL)	90	90	70
iii	*C. albicans* (10 µL)	60 µM $[Ag(PPO)_2]ClO_4$ (**3.2**) (10 µL)	80	80	80

3.4 Conclusion

The work in this chapter has described the synthesis and characterisation of starting materials phendione (**2a**) and L-amino acid ester salts **1.1 – 1.8**. The reaction between phendione (**2a**) and L-tyrosine ester hydrochlorides (**1.1 – 1.4**) produces phen-oxazine ligands **2.1 – 2.4** as the major product while reacting phendione (**2a**) with 4-nitro-L-phenylalanine ester hydrochlorides (**1.5 – 1.8**) results in the phen-pyrido ligands **2.4 – 2.8** as the major product. The tuneable nature of the ligand reaction to yield one major product can be attributed to the electron withdrawing or donating ability of the *para* substituent on the phenyl ring of the amino acid. Synthesis and characterisation of phenanthroline-based ligands phen-oxazine (**2.1 – 2.4**) and phen-pyrido (**2.4 – 2.8**) ligands has been presented. The ligands were synthesised with increasing lipophilicity by increasing the alkyl chain length at the ester position. There is precedent that the longer alkyl chain length affords increased *in vitro* biological activity. It is proposed that the mechanism of formation of both ligands is initiated by a Schiff-base condensation reaction that forms a keto-imine intermediate. Following multiple H^+ transfers an enol-imine intermediate if formed which undergoes intramolecular cyclisation to form the phen-oxazine or phen-pyrido ligand. Phen-oxazine ligands **2.1 – 2.3** were complexed to Ag(I) to form complexes **3.1 - 3.3**. Key differences were observed using NMR and IR spectroscopy which suggested successful complexation. The solution stoichiometry of Ag(I) phen-oxazine complexes **3.1 – 3.3** was determined using the Job's Plot method to be 1:2 Ag(I):phen-oxazine. Complexes **3.1 – 3.3** all demonstrated fluxional behaviour in solution. Fast competitive exchange of ligands was apparent in DMSO-d6. Bidentate phen ligands can compete with bidentate phen-oxazine ligands in solution while monodentate pyridine is unable to compete with phen-oxazine which is consistent with the chelate effect. UV-visible spectroscopy of **3.1** and **3.2** in 5% (v/v) DMSO in minimal media suggests solution stability, however, the most lipophilic derivative $[Ag(HPO)_2]ClO_4$ (**3.3**) appears to aggregate after 72 h. Biological evaluation of phen-oxazine ligands **2.1 – 2.3** and Ag(I) complexes **3.1 – 3.3** and $AgClO_4$ against *C. albicans* yielded interesting results. There was a clear lipophilic effect between the ligands, with the antifungal activity increasing as the alkyl chain length and lipophilicity increased. This

result supports the importance of lipophilicity in ligand design. While the Ag(I) phen-oxazine complexes did not appear to have this lipophilic effect, there was clear evidence that complexation to Ag(I) greatly enhanced the anti-*C. albicans* activity of the ligands *in vitro*. All compounds tested had activity in minimal media, but no activity was observed when the same experiments were conducted in YEPD media. There were no significant differences observed between freshly prepared and pre-prepared test solutions of all compounds. Incubating complexes **3.1 - 3.3** for the standard 24 h period suggested they were just as active as $AgClO_4$ but upon extending the study to 48 h, the Ag(I) phen-oxazine complexes held their activity while $AgClO_4$ became inactive. These results highlight the importance of the choice of biological media, sample preparation and incubation time. The extension of the biological studies to the *G. mellonella* model suggested PPO (**2.2**) and $[Ag(PPO)_2]ClO_4$ (**3.2**) were well tolerated *in vivo*. Inoculation of the test compounds did not impact the mobility, cause melanisation or induce an immune response in the larvae. Test compounds PPO (**2.2**) and $[Ag(PPO)_2]ClO_4$ (**3.2**) also had some ability to recover the larvae from *C. albicans* infection after 72 h.

Chapter 4

Synthesis and Characterisation of Re(I) Tricarbonyl Phenanthroline Complexes 4.1 – 4.8 their Photochemical and Electrochemical Properties

Compound Structures and Codes for Chapter 4

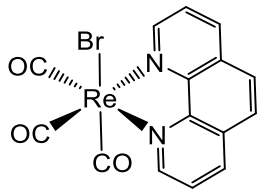

[$ReBr(CO)_3$(phen)] (**4a**)

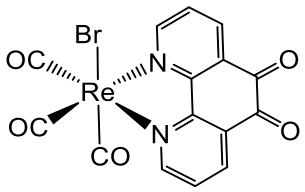

[$ReBr(CO)_3$(phendione)] (**4b**)

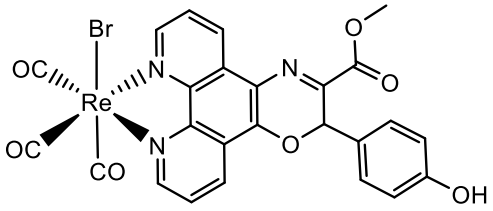

ReMPO (**4.1**)

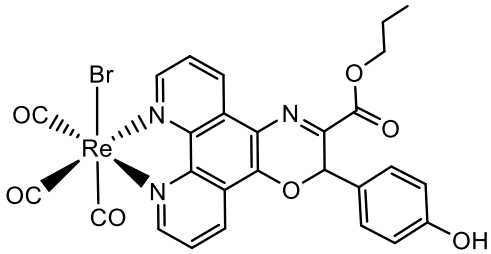

RePPO (**4.2**)

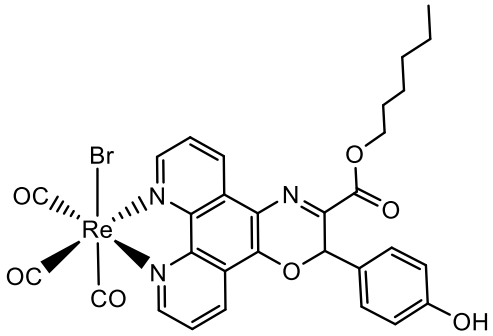

ReHPO (**4.3**)

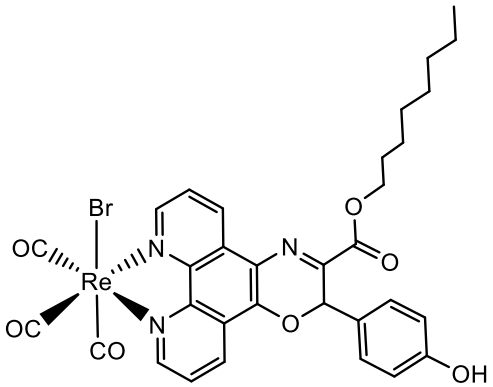

ReOPO (**4.4**)

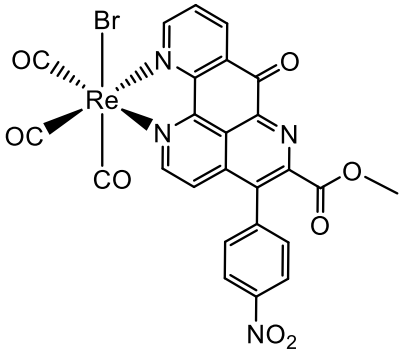

ReMPP (**4.5**)

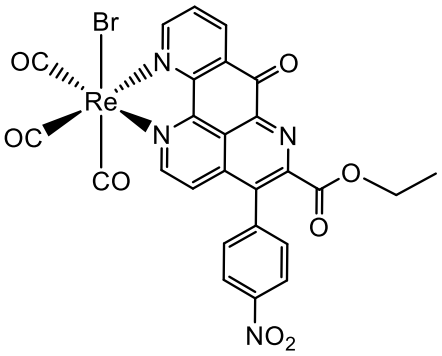

ReEPP (**4.6**)

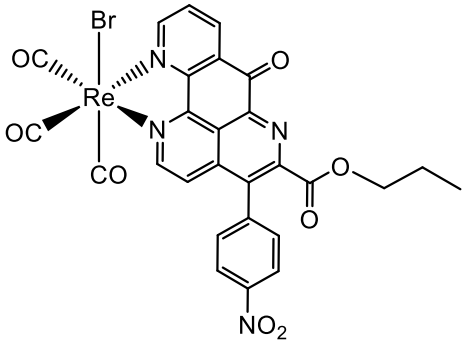

RePPP (**4.7**)

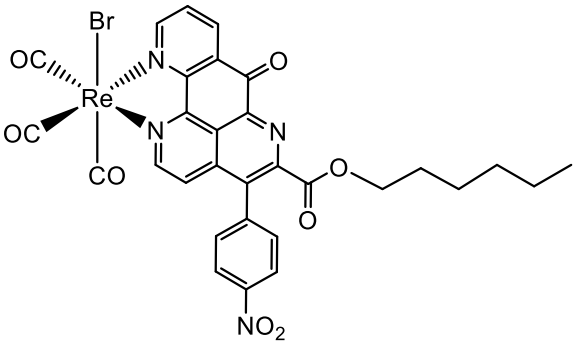

ReHPP (**4.8**)

4.1 Introduction

Rhenium tricarbonyl compounds have been studied extensively due to their diverse spectroscopic and physical properties.[117, 209, 210] Re(I) tricarbonyl complexes have found applications as catalysts in the photoreduction of CO_2[211], cellular imaging agents[129, 209, 212] and photodynamic therapy (PDT) agents to treat cancer[129, 209, 213, 214]. The wide variety of applications of Re(I) tricarbonyl complexes is attributed to their luminescence.[210] Luminescence is the emission of light from a substance due to electronic transition from higher energy molecular orbitals.[215] Re(I) tricarbonyl luminescence arises from the intense emission as a result of the triplet state metal-to-ligand charge transfer (MLCT).[210] Re(I) tricarbonyl phenanthroline compounds are of particular interest as they possess unique luminescent properties such as long emission lifetimes, high photostability and large Stokes shifts.[117, 129, 216] Emission from such complexes can be easily tuned through derivatisation of the phen ligand as the ligand π* orbital dictates the intensity and wavelength of the MLCT.[131, 210] Phen-based Re(I) complexes also provide attractive redox activity. Oxidation of Re(I) to Re(II) has been exploited for photocatalysis[211], artificial photosynthetic materials[122], ion sensors[216] and in solar energy conversion cells.[217]

There are also multiple examples of therapeutic and diagnostic (theranostic) Re(I) agents (**Figure 4.1a,b**) that harness the MLCT luminescence to create anticancer agents that are trackable by fluorescent microscopy to identify cellular localisation.[129, 130] Another key feature of this class of Re(I) complexes is the incorporation of carbon monoxide (CO) ligands. Re(I) diimine complexes containing CO ligands provide wide scope for dual purpose, trackable, targeted therapies in the treatment and diagnosis of cancer.[129-131] Molecules that are designed to release CO molecules into the microenvironment in response to stimuli are known as CO Releasing Molecules (CORMs). PhotoCORMs are molecules that release CO in response to UV or visible light.[218] The ability to stimulate intracellular CO release from Re(I) tricarbonyl phen complexes have provided many examples of potent dual purpose anticancer agents to treat breast (**Figure 4.1b**), cervical and ovarian cancers (**Figure 4.1b,c**).[129, 131]

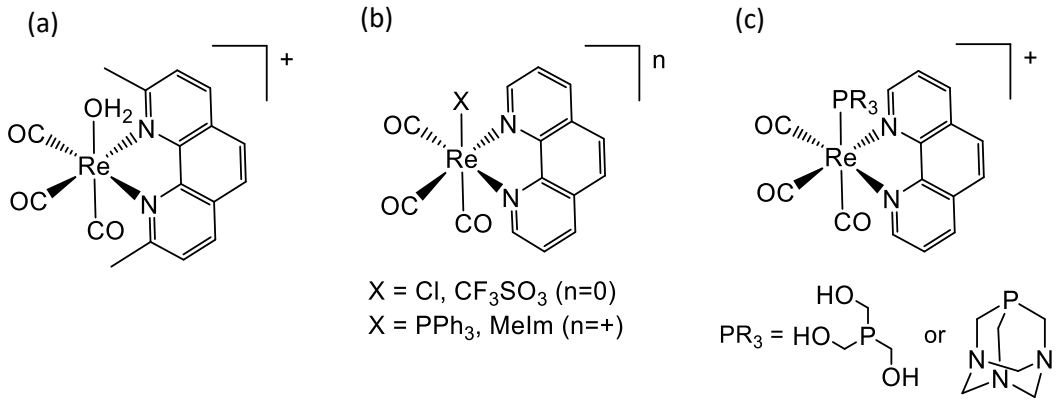

Figure 4.1: Reported Re(I) tricarbonyl phen complexes with dual action photochemical and biological activity (MeIm = methylimidazole).[129-131]

We therefore sought to synthesise a family of novel Re(I) tricarbonyl phenanthroline-based complexes **4.1 – 4.8** (**Figure 4.2**) to explore their biological activity. Photochemical, electrochemical studies and biological screening of complexes **4.1 – 4.8** will be discussed across Chapters 4 and 5. As outlined in Chapter 2, the phen-oxazine ligands **2.1 – 2.4** have shown good biological activity as antibacterial[176] and antifungal[219] agents. The phen-pyrido ligands **2.5 – 2.8** are anticipated to have promising biological activity. The phen-pyrido ligands are analogous to a naturally occurring alkaloid, ascididemin which has exhibited potent anticancer activity.[220] Complexation of a phen-oxazine or phen-pyrido ligand to Re(I) is proposed to provide a structure with potential as a dual action, CO-releasing photoactivated pro-drug. This dual action is proposed to arise from the biological activity of the organic ligand and the photo-induced release of CO into the microenvironment of the cellular target.

This chapter will discuss the synthesis of starting material $Re(CO)_5Br$ and known complexes $[Re(CO)_3Br(phen)]$ (**4a**) and $[Re(CO)_3Br(phendione)]$ (**4b**). Synthesis and characterisation of novel Re(I) tricarbonyl phen-oxazine complexes **4.1 – 4.4** and Re(I) tricarbonyl phen-pyrido complexes **4.5 – 4.8** will be described. The photochemistry of complexes **4.1 – 4.8** will be investigated. Electrochemical analysis to assess redox potential of complexes **4.1 – 4.8** using cyclic voltammetry will be presented.

(a)

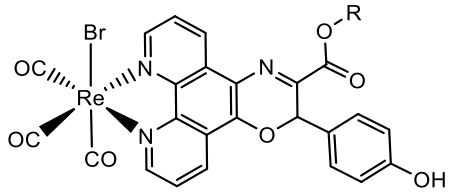

4.1 - 4.4

(b)

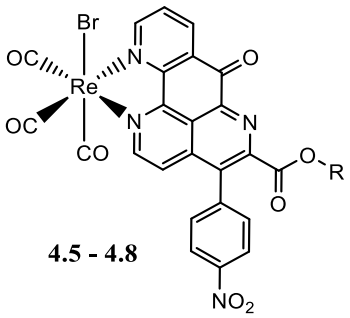

4.5 - 4.8

Figure 4.2: General structures of (a) Re(I) phen-oxazine complexes **4.1 – 4.8** (R = Me, Pr, Hex, Oct) and (b) Re(I) phen-pyrido complexes of **4.5 – 4.8** (R = Me, Et, Pr, Hex).

4.2 Synthesis and Characterisation of Re(I) Tricarbonyl Phenanthroline Complexes 4.1 – 4.8

4.2.1 Synthesis of Bromopentacarbonylrhenium(I) Starting Material

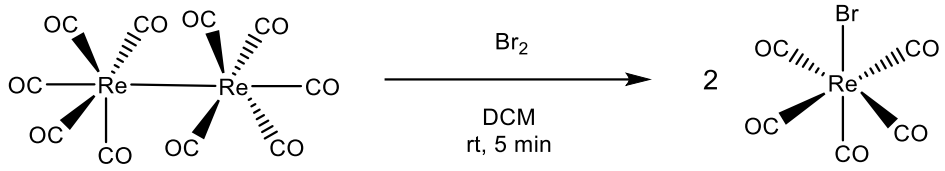

Scheme 4.1: Reaction of dirhenium decacarbonyl in the presence of bromine to produce $Re(CO)_5Br$ starting material

The reaction to produce $Re(CO)_5Br$ involves breaking the metal-to-metal bond of commercially available dirhenium decacarbonyl which is replaced by a bromide ligand to produce the monomeric $Re(CO)_5Br$ starting material (**Scheme 4.1**). This reaction produces up to 88% yield. The IR spectrum of $Re(CO)_5Br$ obtained is consistent with that found in the literature.[148] Re_2CO_{10} has a characteristically intense band at 1920 cm^{-1} that corresponds to a ν(CO) stretch. This shifts to 1946 cm^{-1} and decreases in intensity which is consistent with the production of $Re(CO)_5Br$.

4.2.2. Synthesis of Known Re(I) Tricarbonyl Complexes of 1,10-Phenanthroline (4a) and 1,10-Phenanthroline-5,6-dione (4b)

The known Re(I) tricarbonyl complexes containing phenanthroline (**Scheme 4.2**) and phendione (**2a**) (**Scheme 4.3**) were synthesised as per literature methods.[149-151] Briefly, the ligand of choice (phen or phendione (**2a**)) was reacted in a 1:1 ratio with $Re(CO)_3Br$ and the reaction mixture was heated at reflux in toluene overnight. The resulting suspension was reduced to dryness. The product was re-suspended in diethyl ether, washed with several portions of diethyl ether and dried using vacuum filtration. Good yields of more than 75% were achieved. The structures of $[Re(CO)_3Br(phen)]$ (**4a**) and $[Re(CO)_3Br(phendione)]$ (**4b**) were confirmed using NMR and IR spectroscopy and data obtained agreed with characterisation in the literature.[149, 151]

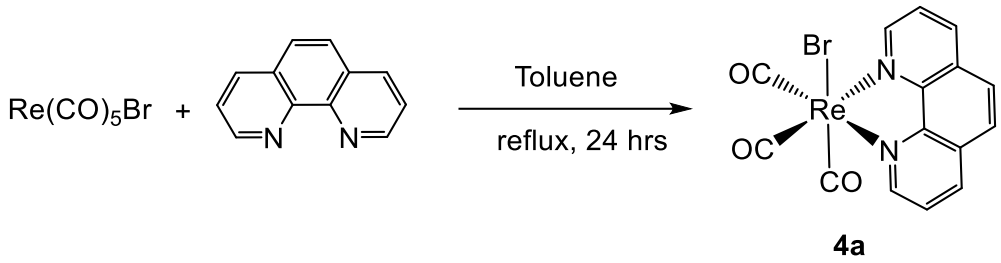

4a

Scheme 4.2: Reaction of phen with $Re(CO)_5Br$ to form $[Re(CO)_3Br(phen)]$ (**4a**)

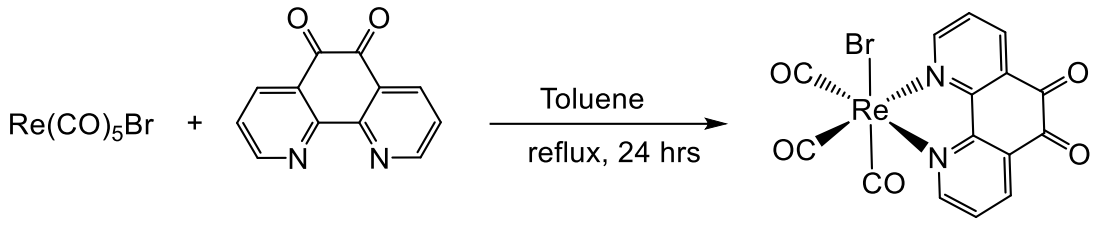

4b

Scheme 4.3: Reaction of phendione (**2a**) with $Re(CO)_5Br$ to form $[Re(CO)_3Br(phendione)]$ (**4b**).

^{1}H NMR spectra recorded for Re(I) complexes **4a** and **4b** appeared almost identical to spectra of the free ligands. All signals present in the DMSO-d6 ^{1}H NMR spectrum of **4a** shift downfield by between 0.35 – 0.49 ppm compared to the proton resonance positions of free phen ligand. For example, the phen signal associated with the protons at the position *ortho* to the N-atoms shifts by 0.49 ppm while the signal of the protons at the position *para* to the N-atoms have a lesser downfield shift of 0.35 ppm. This accords with the reported downfield shift of the protons of **4a** relative to those of the free phen ligand in $CDCl_3$ of between 0.14 – 0.76 ppm reported in the literature.[210]

Similarly, all proton signals of the phendione complex (**4b**) shift downfield by between 0.26 – 0.34 ppm in DMSO-d6 compared to free phendione (**2a**). These downfield changes in chemical shift position of free ligand resonances compared to Re(I) complex are observed for many phen-based Re(I) complexes.[130, 172, 210]

Comparison of ^{13}C NMR spectra recorded for **4a** and **4b** and their respective free ligands shows the appearance of new signals at high chemical shifts associated with the carbon atoms of the carbonyl ligands and shifts of the order of 1 - 2 ppm for other ArC signals. Signals for the carbon nuclei of the carbonyl ligands in **4a** are present at 192.6 and 189.8 ppm. The spectrum recorded for **4b** shows two carbonyl ligand carbon signals at 197.2 and 188.7 ppm. These new carbonyl signals are consistent with the production of the Re(I) complexes.[172, 213]

IR spectra recorded for the reaction products are consistent with the formation of the Re(I) tricarbonyl complexes **4a** and **4b**. The spectra of complex **4a** have three distinct ν(CO) stretching bands at 2014, 1925 and 1886 cm^{-1}. Complex **4b** has similar bands present at 2023, 1938 and 1878 cm^{-1}. These Re-CO stretching bands appear at slightly higher wavenumbers for Re(I) phendione complex **4b**, due to the functionalisation of the phen ring which makes the ligand less electron donating. These three IR stretching modes present in both spectra of complexes **4a** and **4b** are consistent with the formation of *fac*-Re(I) tricarbonyl complexes.[130, 131, 221]

4.2.3 Synthesis and Characterisation of Re(I) Tricarbonyl Phenanthroline-oxazine Complexes 4.1 – 4.4

Synthesis of novel Re(I) complexes containing phen-oxazine ligands (**4.1 – 4.4**) was carried out using similar conditions employed for complexes **4a** and **4b**. The reaction involved heating the ligand of choice (0.25 mmol) in a 1:1 ratio with the $Re(CO)_5Br$ starting material (**Scheme 4.4**) at reflux in toluene overnight as described in **section 2.3.2**. Yields of 43 – 82% were obtained.

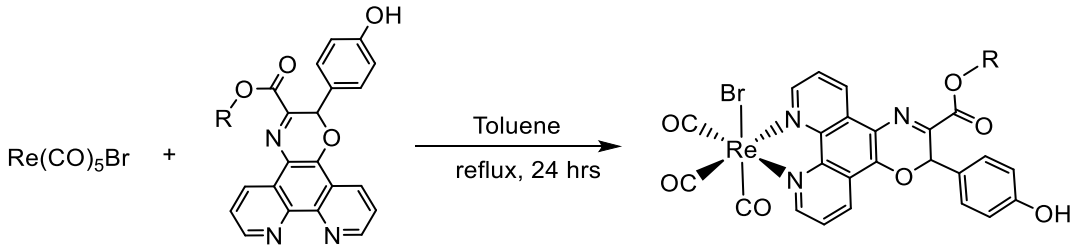

R = Me, Pr, Hex, Oct

2.1 - 2.4

4.1 - 4.4

Product	R	Code	Yield
4.1	CH_3	ReMPO	70%
4.2	C_3H_7	RePPO	82%
4.3	C_6H_{13}	ReHPO	54%
4.4	C_8H_{17}	ReOPO	43%

Scheme 4.4: Reaction between $Re(CO)_5Br$ and phen-oxazine ligands (**2.1 – 2.4**) to form Re(I) tricarbonyl phen-oxazine complexes **4.1 – 4.4**.

Characterisation of the Re(I) phen-oxazine family **4.1 – 4.4** was carried out using NMR, IR and UV/vis spectroscopy, mass spectrometry and x-ray crystallography. The ^1H NMR spectral data of Re(I) phen-oxazine complexes (**4.1 – 4.4**), especially in the 'oxazine' region were more complex than anticipated. Signals for a number of protons appeared to present in duplicate. This observation is suggestive of the presence of a pair of diastereomers. Herrick and co-workers have previously shown that their Re(I) complexes of general formula $[Re(CO)_3Cl(pyca\text{-}R'\text{-}OR)]$ (**Figure 4.3**) formed as a diastereomeric mixture with diastereomer ratios varying from 55:45 to 90:10 depending on the nature of the substituents R and R'.[222] In these complexes Herrick

describes the metal centre as stereogenic, with pseudo-tetrahedral geometry assuming the three facial carbonyls as a single unit. The chiral ligand moiety presents a second stereocentre. The structure shown below is designated as a *S*,*S*-stereoisomer.

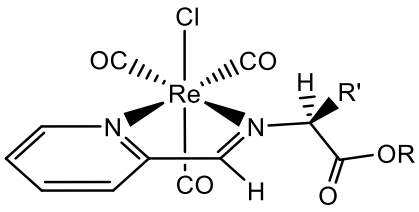

Figure 4.3: General structure of *S*,*S*-[Re(CO)$_3$Cl(pyca-R'-OR)].

Suárez-Ortiz and colleagues also present a Re(I) tricarbonyl complex that formed as a mixture of diastereomers and their respective enantiomers (**Figure 4.4**). The complex was formed from a racemic sample of the bidentate iminopyridine ligand (L$_{(R/S)}$). Taken together with the new Re stereocentre, which is generated in the complexation reaction, four stereoisomers are possible.[223] The configuration of one diastereomeric pair is illustrated below. Again, the CO ligands are grouped as one ligand to give a pseudo-tetrahedral structure around the Re centre as described above. Therefore, the order of significance of the ligands would be: (1) Br, (2) N-ring, (3) N=C. This gives an *S* assignment for the Re centre of structure (a) and an *R* assignment for structure (b). The second stereocentre on the ligand follows the significance (1) N=C, (2) Ph-R, (3) CH$_3$. This gives an *R* assignment for both structures as they are diastereomers.

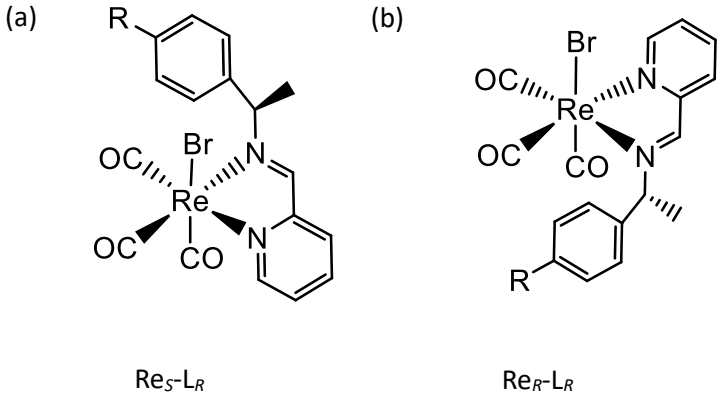

Re$_S$-L$_R$ Re$_R$-L$_R$

Figure 4.4: General structure of one pair diastereomers of *fac*-[Br(CO)$_3$Re$_{(R/S)}$L$_{(R/S)}$].[223]

The Re(I) phen-oxazine adducts **4.1 – 4.4** also potentially present as four stereoisomers: a pair of diastereomers with enantiomers of each. As described above in **section 3.2.2.4,** synthesis of the phen-oxazine ligands began with an optically active amino acid ester, however, the ligand is shown to form as a racemic mixture. Complex formation results in a product with two stereocentres. Starting from the *R*-enantiomer of the ligand, structures **A** and **B** (**Figure 4.5**) are possible diastereomeric products. Structures **C** and **D** can arise from reaction with the *S*-enantiomer of the ligand. The stereoisomers are assigned following the same method as above for the structures in **Figures 4.3 – 4.4**. The CO ligands are grouped as one unit, giving a pseudo-tetrahedral structure as illustrated in **Figure 4.6**. The ligands around the Re centre are then assigned in order of significance. The coordinating N ligands of phen-oxazine are ordered based on the next significant atom. Therefore, the N and O atoms labelled in red are more significant than the N and N atoms labelled in blue. So, the order of significant to assign the stereochemistry around the Re centre follows: (1) Br, (2) N → O (3) N → N.

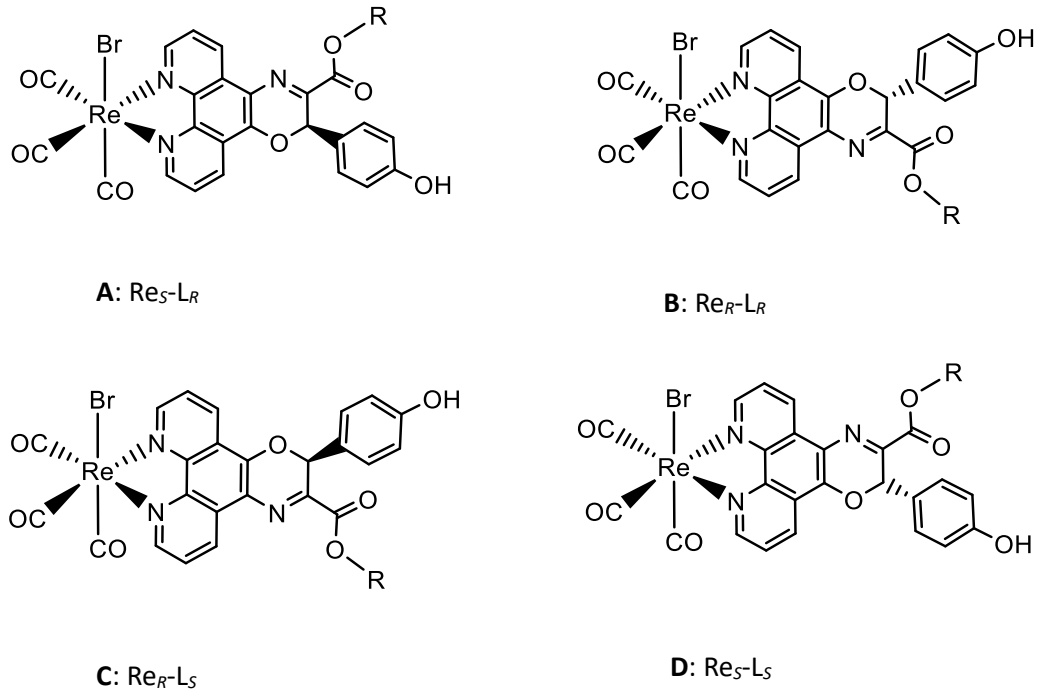

Figure 4.5: Predicted stereoisomeric structures of Re(I) phen-oxazine complexes **4.1 – 4.4**.

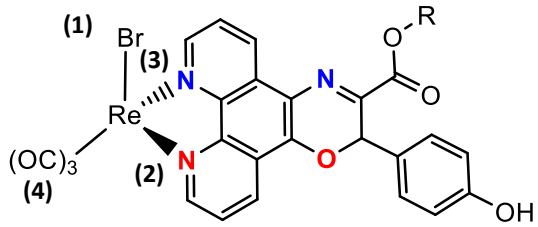

Figure 4.6: Assigning the configuration at the Re centre: *S*-enantiomer

Examination of the ^{13}C data for the family **4.1 – 4.4** showed many more signals than would have been expected for the number of unique carbon atoms, if the reaction produced only one diastereomer. The duplication of the majority of the carbon signals is in keeping with the suggestion of a mixture of diastereomers.[222] Signals at or near 197, 196 and 189 ppm were observed for the family which is consistent with the formation of closely related Re(I) tricarbonyl complexes.[172] It was difficult to unambiguously assign the carbon resonances of the phen region. However, signals can be readily assigned for the carbon nuclei associated with the oxazine moiety and its ester substituent. ^{1}H NMR data show limited evidence for duplication of the phen resonances while two sets of signals are evident for protons in the oxazine region. It was difficult to definitively assign signals as being associated with one diastereomer over the other so duplicate signals are denoted as being associated with diastereomer A or B in **Tables 4.1 – 4.2** showing key signals in the ^{1}H and ^{13}C NMR spectra.

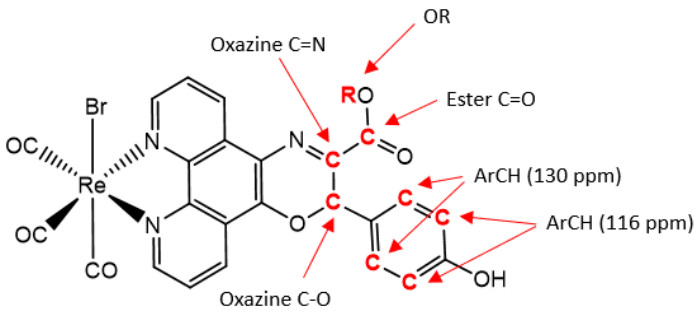

Figure 4.7: General structure of Re(I) phen-oxazine complex identifying carbon atoms for which two resonances appear in the ^{13}C NMR spectra.

After careful examination of ^{1}H, ^{13}C, HSQC and HMBC NMR data for Re(I) complexes **4.1 – 4.4**, key signals for the nuclei associated with the oxazine moiety and its substituents were assigned for each diastereomer based on the characterisation methods employed by Herrick and co-workers.[222] The key signals for the proton and carbon resonances of each diastereomers are presented in **Tables 4.1 - 4.2**. Typically, the carbon nuclei resonances differ by ~0.2 ppm for related signals in the diastereomeric pairs. The ^{13}C resonances were not integrated but the relative heights of corresponding pairs of signals allows a tentative suggestion of an approximately 1:1 ratio of diastereomers.

Table 4.1: Key ^{13}C NMR data for Re(I) phen-oxazine complexes **4.1 – 4.4** in support of the presentation as a pair of diastereomers

Solvent	Diastereomer	Ar<u>C</u>H	Ar<u>C</u>H	Oxazine C-O	Oxazine C=N	Ester C=O	Ester OR
ReMPO (4.1)	A	129.46	115.95	73.16	151.46	162.18	53.13 (OCH_3)
	B		116.05	72.99	151.28	162.21	53.10 (OCH_3)
RePPO (4.2)	A	130.19	116.44	74.10	#	162.58	68.36 (OCH_2), 22.19 (CH_2),
	B	130.17	116.38	73.97		162.53	68.35 (OCH_2), 22.18 (CH_2)
ReHPO (4.3)	A	129.93	116.48	73.93	152.40	162.01	66.43 (OCH_2), 25.35 (CH_2)
	B	129.91	116.37	73.78	152.22	161.97	66.40 (OCH_2), 25.34 (CH_2)
ReOPO (4.4)	A	129.90	116.47	73.90	152.37	162.01	66.43 (OCH_2), 29.02 (CH_2)
	B	129.88	116.37	73.75	152.20	161.96	66.39 (OCH_2), 29.01 (CH_2),
RePPO (4.2)*	A	130.60	116.87	74.53	152.88	163.00	68.75 (OCH_2), 22.61 (CH_2)
	B	130.58	116.81	74.40	152.81	162.96	68.78 (OCH_2), 22.60 (CH_2)

*recorded in CD_3CN; # ^{1}H NMR data correlates to four separate carbon signals at very similar chemical shift positions so the specific signals for the oxazine C=N could not be assigned.

Careful analysis of 2D data helped assign key ^{1}H NMR signals of each diastereomer. For example, the more deshielded aromatic proton resonance of RePPO (**4.2**), at 7.27 ppm, correlated to two carbon signals at 130.19 and 130.17 ppm. The second Ar-H

signal resonates within a 3H multiplet at 6.71 ppm which also represents the oxazine-H This signal correlates with four separate carbon signals; two in the ArCH region, 116.44 and 116.38 ppm, and two in the region where the oxazine C-O is expected, 74.10 and 73.97 ppm.

Signals attributed to the nuclei of the ester functional group, CO_2R, also show some clear duplication in both the ^{1}H and ^{13}C spectra. For example, the methyl protons of ReMPO (**4.1**) presents two singlet signals at 3.88 and 3.89 ppm. These correlate to a pair of carbon resonances at 53.13 and 53.10 ppm. Many of the alkyl proton and carbon signals from other members of the family also appear as duplicate resonances; two ester C=O signals are observed at ~162 ppm in the ^{13}C spectra for all complexes. Key ^{13}C NMR data is summarised in **Table 4.1**.

As stated above there was limited evidence for signal duplication in the ^{1}H NMR spectra in the region where the phen protons resonate. ^{1}H NMR data for complexes **4.1 – 4.4** do show a shift upon complexation. For example, the phen signals of PPO (**2.2**) are deshielded by between 0.25 – 0.33 ppm upon formation of **4.2** (**Figures 4.8 – 4.9**). The most significant shift of 0.33 pm is from 9.05 ppm (Hb) to 9.38 ppm (H_2) for the most deshielded phen signals that are at the position *ortho* to the N-atom of the phen region of the phen-oxazine ligand (**Figure 4.9**). There is a small downfield shift of 0.02 and 0.06 ppm observed for the aromatic proton signals *ortho* and *meta* to the phenolic group of the oxazine ring. These aromatic proton signals shift from 6.68 to 6.70 ppm and 7.21 to 7.27 pm respectively when PPO (**2.2**) is complexed to form RePPO (**4.2**). The magnitude of the chemical shift change is most apparent for the protons closest to the N-atoms of the *phen* moiety similar to what is observed for complexes **4a** and **4b**. On some occasions the signal appeared more complex than expected. For example, in RePPO (**4.2**) the multiplet signal at ~8.15 representing H_5 could be considered as a pair of overlapping dd signals in keeping with formation of the product as a diastereomeric mixture (**Figure 4.10**).

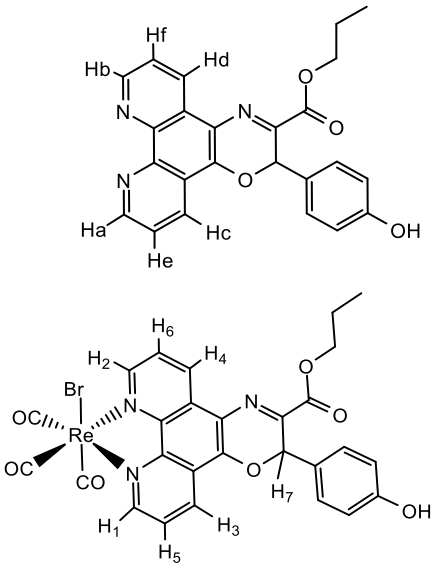

PPO (2.2)		RePPO (4.2)		Δδ (ppm)
Proton	Chemical shift (ppm)	**Proton**	Chemical shift (ppm)	
Ha	9.46	**H_1**	9.14	0.32
Hb	9.38	**H_2**	9.05	0.33
Hc	9.18	**H_3**	8.89	0.29
Hd	8.93	**H_4**	8.61	0.32
He	8.15	**H_5**	7.87	0.28
Hf	8.06	**H_6**	7.87	0.25

Figure 4.8: Chemical shift changes observed for the protons of the phenanthroline core of PPO (**2.2**) upon complexation to Re(I) to form RePPO (**4.2**).

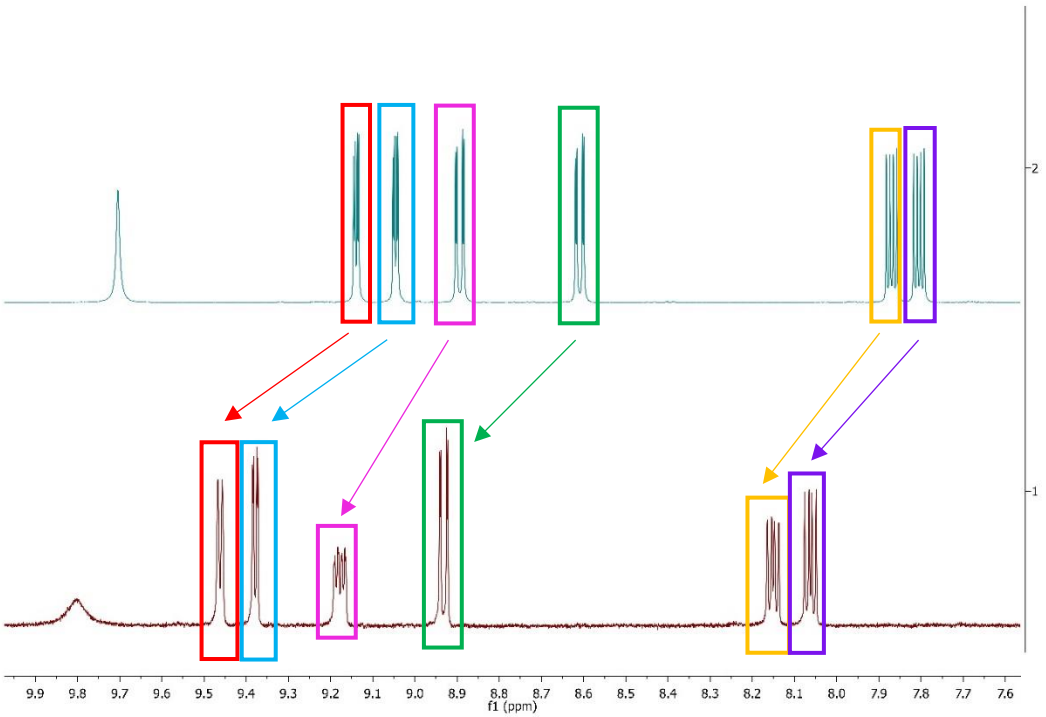

Figure 4.9: ^{1}H NMR spectra of free ligand PPO (**2.2**) (top) and complex RePPO (**4.2**) (bottom) showing the chemical shift changes of the phen signals in DMSO-d6.

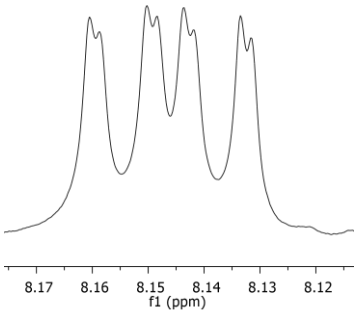

Figure 4.10: Portion of ^{1}H spectrum of RePPO (**4.2**) showing the appearance of the H_5 phen proton as a pair of overlapping dd signals

Similar to the ^{13}C data, the ^{1}H NMR spectra for the complexes **4.1 - 4.4** showed multiple signals for some but not all protons. Signals arising from the oxazine ring, the OH group and those associated with the ester substituent appear in duplicate. Key proton signals for **4.1 – 4.4**, are presented in **Table 4.2**. For example, the methyl protons of ReMPO (**4.1**), resonate as a pair of signals at 3.89 and 3.88 ppm with a relative intensity of 1:1. This is supported by their correlation to duplicate signals in the ^{13}C NMR as discussed above. In almost all cases two resonances were observed for the OH proton which generally appear in an almost 1:1 ratio.

For complexes **4.2 – 4.4** there is no obvious duplication, although the signals appear more complex for protons of the alkyl chain. The alkyl proton signals correlate to two signals in the ^{13}C NMR spectra. For example, for RePPO (**4.2**), the signal at 4.25 ppm correlates to carbon signals at 68.36 and 68.35 ppm. Similarly, the signal at 1.68 ppm correlates to ^{13}C resonances at 22.19 and 22.18 ppm. Generally, the CH_3 signals appear as skewed triplets across the family of **4.1 – 4.4**. Spectra were recorded in DMSO-d6.

Table 4.2: ^{1}H NMR data for Re(I) phen-oxazine complexes **4.1 – 4.4** in support of their presentation as a pair of diastereomers

Complex	Diastereomer	-OH	ArH	ArH	Oxazine-H	CO_2R
ReMPO (4.1)	A	9.80	7.26	6.69		3.89 (OCH_3)
	B	9.78				3.88 (OCH_3)
RePPO (4.2)	A	9.81	7.27	6.71		More complex[#]
	B	9.80				
ReHPO (4.3)	A	9.78	7.26	6.69		More complex[#]
	B	9.76				
ReOPO (4.4)	A	9.81	7.26	6.70		More complex[#]
	B	9.79				
RePPO (4.2)*	A	^	7.29	6.72	6.65	0.96 (CH_3)
	B	^			6.63	0.95 (CH_3)

*recorded in CD_3CN; [#]signals have more complex multiplicities; ^no signal observed

NMR data for complex RePPO (**4.2**) was also recorded in CD_3CN. In this solvent, the signals for the ArH and oxazine-H protons no longer overlap. The oxazine-H proton is now represented by two signals, 6.65 and 6.63 ppm. In this solvent there is an emergence of two triplet signals for the CH_3 group of the ester chain at 0.96 and 0.95 ppm.

In conclusion, there is strong NMR evidence that the Re(I) phen-oxazine complexes for as a pair of diastereomers in keeping with literature reports for related Re complexes.[222, 223]

Suárez-Ortiz and colleagues successfully separated the Re diastereomers using column chromatography over silica gel using a mixture of DCM/EtOAc/hexane.[223] Chromatographic separation of the diastereomers of Re phen-oxazine adducts **4.1 – 4.4** was attempted. A range of standard solvents with varying polarity were used: from very polar solvents such as MeOH, EtOH to ACN, DCM, CH_3Cl, EtOAc and non-polar solvents such as hexane. Different ratios of solvents were also trialled. Both

silica and alumina plates were used. The Re phen-oxazine compounds consistently remained at the baseline with all combinations of mobile and stationary phases. It was noted that Herrick and coworkers did not successfully separate their diastereomers by chromatography or fractional crystallisation.[222]

Attempts to separate the Re phen-oxazine diastereomers were unsuccessful by TLC, however HPLC conditions were found to separate the diastereomers. Samples of complexes **4.1 – 4.4** were prepared by dissolving ~1 mg of complex in 1 mL ACN. The analytes were eluted using reversed-phase chromatography with a mobile phase of 0.01 % (v/v) formic acid in H_2O. **Figure 4.11** shows two analytes with similar intensities elute between 37 and 41 minutes. HPLC analysis conducted on ReMPO (**4.1**), ReHPO (**4.3**) and ReOPO (**4.4**) presented similar chromatograms to that obtained for RePPO (**4.2**) The relative intensity of the two analytes observed by HPLC correlates with the presence of two species in the NMR data.

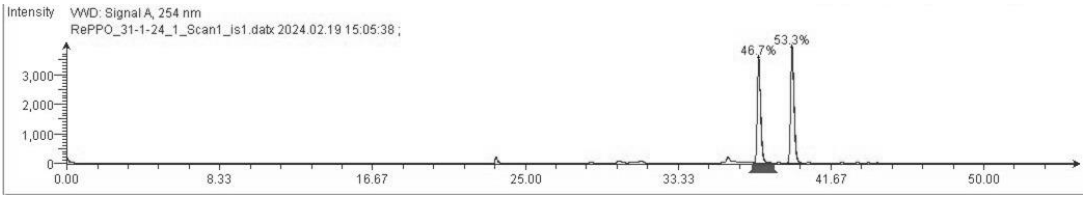

Figure 4.11: HPLC chromatogram of RePPO (**4.2**) showing two analytes with similar retention times

Further characterisation of complexes **4.1 – 4.4** involved IR and UV/vis spectroscopy, mass spectrometry and x-ray crystallography. The IR spectra obtained for Re(I) complexes show some unique signals compared to the free ligands. The key difference is the presence of two intense bands between 2020 - 1800 cm^{-1}. **Figure 4.12** shows the carbonyl stretching region of the IR spectrum of ReMPO (**4.1**). The second band at ~1880 cm^{-1} appears very broad with a consistent shoulder at ~1915 cm^{-1} across the family of Re(I) phen-oxazine complexes **4.1 – 4.4**. The presence of three stretching modes in the metal carbonyl region are characteristic of a facial (*fac*) arrangement of the CO ligands around the Re(I) centre.[221] Although the IR data is consistent with the formation of the *fac* isomer it cannot be confirmed. The ester

ν(C=O) band present in the free phen-oxazine ligands at 1732 cm^{-1} shifts to a lower wavenumber of 1714 cm^{-1} upon complexation to Re(I).

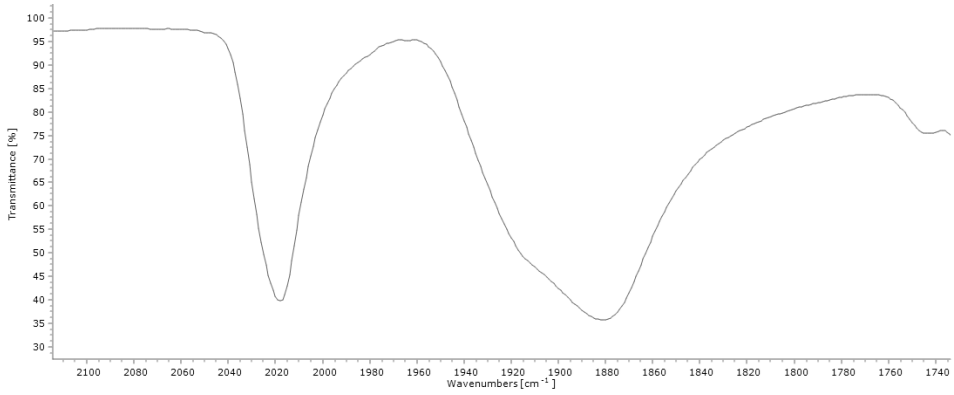

Figure 4.12: Portion of the IR spectrum of ReMPO (**4.1**) showing the Re-CO stretching modes

High resolution mass spectrometry was conducted on the family of novel Re(I) phen-oxazine complexes **4.1 – 4.4.** An $(M+Na)^+$ ion was detected for each complex. The isotope match score was above 97% for all compounds which supports the proposed molecular formulae (**Table 4.3**).

Table 4.3: Theoretical and observed masses of Re(I) complexes **4.1 – 4.4**

Compound	Formula	Theoretical neutral mass (Da)	Observed neutral mass (Da)	Observed mass ($+Na^+$) (m/z)	Mass error (ppm)
ReMPO (4.1)	$[Re(C_{25}H_{15}N_3O_7)Br]$	757.8651	732.9615	757.9519	-1.09
RePPO (4.2)	$[Re(C_{27}H_{19}N_3O_7)Br]$	760.9926	760.9926	785.9834	-1.37
ReHPO (4.3)	$[Re(C_{30}H_{25}N_3O_7)Br]$	803.0405	803.0395	828.0298	-1.31
ReOPO (4.4)	$[Re(C_{32}H_{29}N_3O_7)Br]$	831.0718	831.0710	856.0611	-1.06

X-ray crystallography data were obtained for RePPO (**4.2**) from a clear yellow plate-shaped crystal grown by slow evaporation of solvent from an ACN solution of the complex (**Figure 4.13**). The bond angles around the Re centre range from 75.48 – 99.08° for those expected to be approximately 90°, while those expected to be approximately 180° range from 170.80 – 176.86°. This confirms a distorted octahedral structure. The complex is also confirmed to exist as the *fac* isomer as predicted. The three Re-C bond distances were determined to between 1.91 – 1.95 Å. The two Re-N bonds were 2.17 Å long. The Re-Br bond distance was determined to be 2.61 Å. It is noteworthy that the structure is obtained for *R*,*S*-stereoisomer of RePPO (**4.2**). It is predicted that crystallisation in ACN may selectively crystallise this diastereomer from the ~1:1 isomeric mixture of Re(I) phen-oxazines *fac*-[$Br(CO)_3Re_{(R/S)}L_{(R/S)}$].

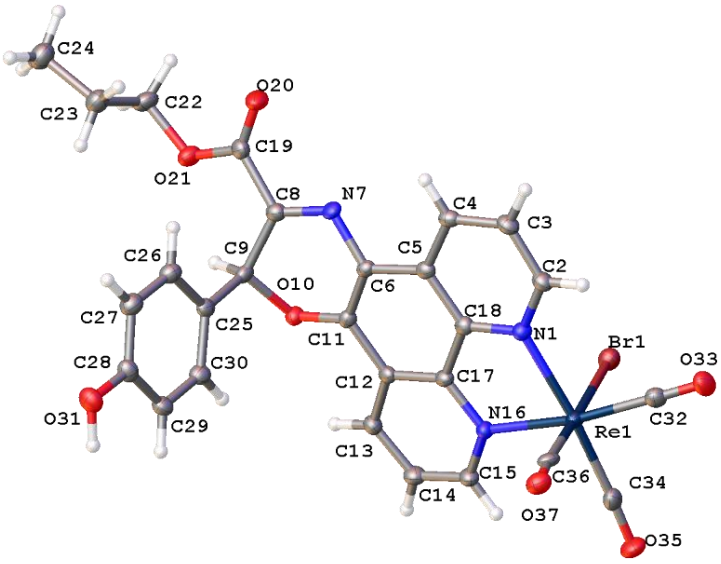

Figure 4.13: Molecular structure of RePPO (**4.2**) with atomic displacement shown at 50% probability.

UV-visible spectroscopy was used to determine the extinction coefficient, ε of the Re(I) complexes **4.1 – 4.4**. A stock solution was prepared for each complex by dissolving 20 mg into DMSO (50 mL). The stock solution was diluted until a sample with an absorbance of 1 was obtained. This sample was serially diluted (**Figure 4.14**). The concentration for each solution was calculated based on the dilution factor. The λ_{max} was identified as the point of highest absorbance for each band. The absorbance at λ_{max} was noted for each solution. The absorbance at λ_{max} was plotted against

concentration for each test solution to produce a standard curve graph. The extinction coefficient was determined to be the slope of the graph. The extinction coefficients for complexes **4.1 – 4.4** are presented in **Table 4.4** and range from 8362 – 11102 $M^{-1}\,cm^{-1}$. The UV/vis spectra for the Re(I) phen-oxazine complexes show an intense band between 350 - 390 nm with a λ_{max} at ~390 nm. This absorption band is consistent with a metal to ligand charge transfer (MLCT) [d(Re(I) → π*(phen-oxazine)] as seen in similar Re(I) tricarbonyl complexes containing a phen-based bidentate ligand.[117, 210, 224, 225] MLCT bands generally have an ε of between 3000 – 4000 $M^{-1}\,cm^{-1}$.[224] The magnitude of the extinction coefficient, ε for complexes **4.1 – 4.4** is much higher than anticipated. The free phen-oxazine ligands **2.1 – 2.4** also absorb at approximately 390 nm; therefore, it is predicted that the complex band is an overlapping intraligand and MLCT band. This overlap of bands has been observed for Re(I) tricarbonyl bipy complexes.[226]

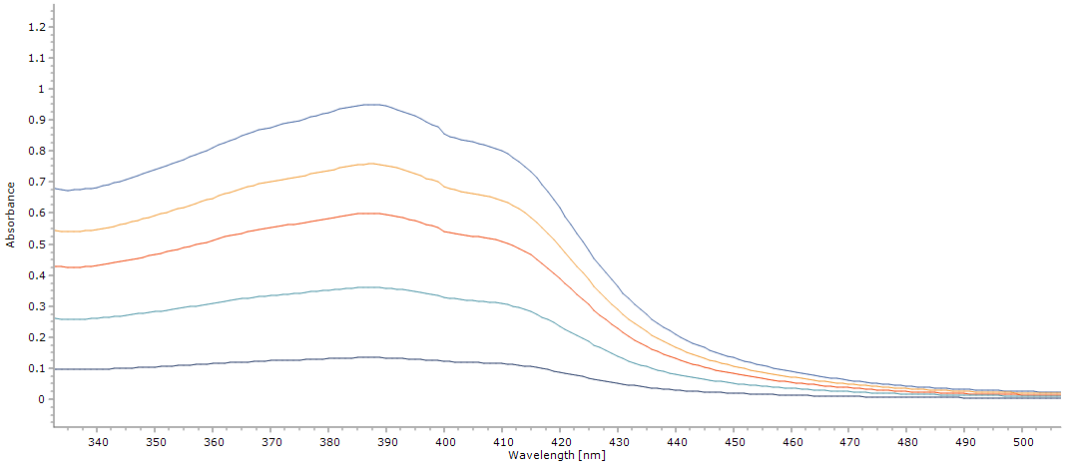

Figure 4.14: UV-visible spectra of RePPO (**4.2**) at concentrations 9.82 x 10^{-5} - 1.35 x 10^{-5} M in DMSO used to determine the extinction coefficient (ε).

Table 4.4: Wavelengths of absorption maxima (λ_{max}) and extinction coefficient (ε) values for Re (I) phen-oxazine complexes **4.1 – 4.4** in DMSO.

Compound	λ_{max} (nm)	ε (M^{-1} cm^{-1})
ReMPO (4.1)	388	8362
RePPO (4.2)	387	9629
ReHPO (4.3)	386	10259
ReOPO (4.4)	387	11102

Novel Re(I) tricarbonyl phen-oxazine complexes **4.1 – 4.4** were successfully synthesised and characterised using NMR, IR and UV-visible spectroscopy, HRMS, HPLC analysis and x-ray crystallography. The family of four phen-oxazine containing Re(I) complexes exhibited duplicate signals in both the ^{1}H and ^{13}C NMR data for all compounds which was due to the presence of diastereomers which is supported by HPLC data. Both the NMR and IR data supported the formation of the series of tricarbonyl Re(I) species. The UV/vis data indicates that the compounds will undergo a MLCT transition upon absorption of visible light (~386 nm). Accurate mass analysis agreed with the predicted molecular formulae of all compounds. X-ray crystallography of RePPO (**4.2**) revealed that the complexes exist in the *fac* isomer and form a distorted octahedral geometry.

4.2.4 Synthesis and Characterisation of Re(I) Tricarbonyl Phenanthroline-pyrido Complexes 4.5 – 4.8

Synthesis of Re(I) phen-pyrido complexes **4.5 – 4.8** was carried out using the same protocol employed for the Re(I) phen-oxazine complexes **4.1 – 4.4**. The phen-pyrido ligand of choice (**2.5 – 2.8**) was heated at reflux in a 1:1 ratio (0.25 mmol) with $Re(CO)_5Br$ in toluene overnight. The resulting suspension was reduced to dryness and the deep purple product was re-suspended in diethyl ether, washed with several

portions of diethyl ether and dried via vacuum filtration. All compounds were obtained in good yield and purity (**Scheme 4.5**).

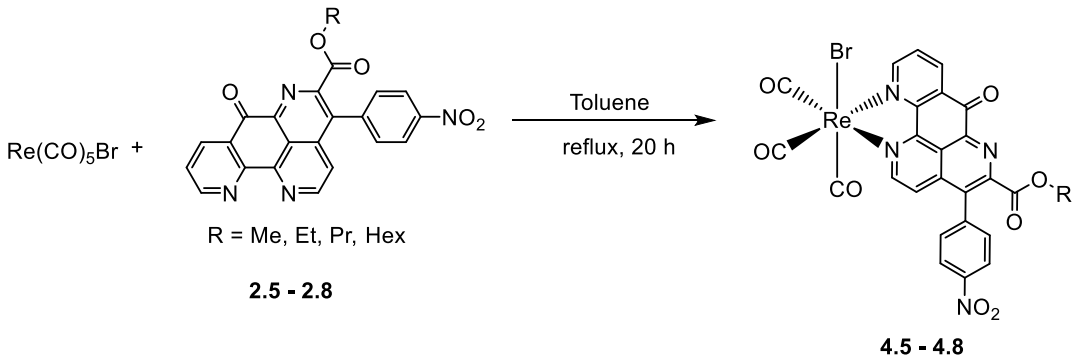

R = Me, Et, Pr, Hex

2.5 - 2.8

4.5 - 4.8

Product	R	Code	Yield
4.5	CH_3	ReMPP	52%
4.6	C_2H_5	ReEPP	87%
4.7	C_3H_7	RePPP	72%
4.8	C_6H_{13}	ReHPP	85%

Scheme 4.5: Reaction between phen-pyrido ligands (**2.5 – 2.8**) and $Re(CO)_5Br$ to from Re(I) phen-pyrido complexes **4.5 – 4.8**.

Characterisation of novel Re(I) phen-pyrido complexes **4.5 – 4.8** was carried out using NMR, IR and UV-visible spectroscopy, mass spectrometry and x-ray crystallography.

^{1}H NMR data obtained for the Re(I) phen-pyrido complexes **4.5 – 4.8** shows a similar pattern to that of the corresponding free phen-pyrido ligands **2.5 – 2.8**. As was expected based on Re(I) complexes **4a**, **4b** and **4.1 – 4.4**, there is a downfield shift for the phen protons upon complexation to Re(I). The phen proton signals of the free ligand shift by between 0.01 – 0.31 ppm when complexed. **Figure 4.16** shows the chemical shift changes of ReMPP (**4.5**) that appear in the ^{1}H NMR spectrum in **Figure 4.17**. The largest changes in chemical shift occur for the phen protons closest to the C=O on the phen moiety. The doublet signals that appear at 9.15 ppm (Ha) and 8.67 ppm (Hc) ppm shift to 9.42 ppm (H_1) and 8.98 ppm (H_3) ppm respectively upon complexation to Re(I). Similarly, the dd signal at 7.86 ppm (He) shifts to 8.13 ppm (H_5).

Another observation is that the aromatic signals of the free ligand that appear at 7.79 and 7.60 ppm become one multiplet at 7.86 ppm that has a relative integration of 4 for the complex. Similar to complexes **4.1 – 4.4**, the Re(I) phen-pyrido complexes **4.5 - 4.8** have a stereogenic centre around the metal. There is however no additional chiral centre within the ligand therefore the phen-pyrido complexes form as a pair of enantiomers (**Figure 4.15**).

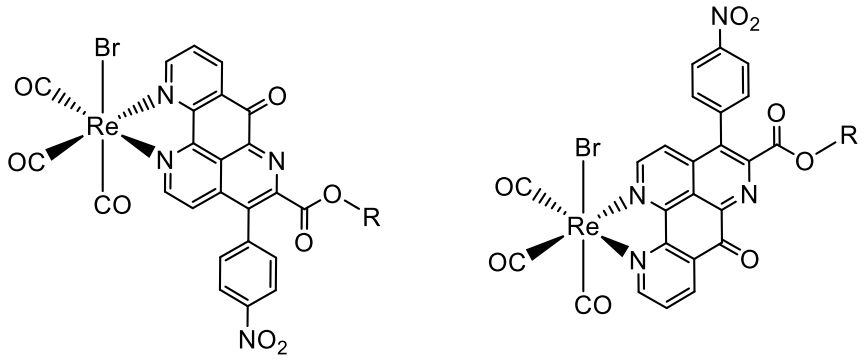

Re_R Re_S

Figure 4.15: Enantiomers of Re phen-pyrido complexes **4.5 – 4.8** formed by the reaction between $Re(CO)_5Br$ and phen-pyrido ligands **2.5 – 2.8**.

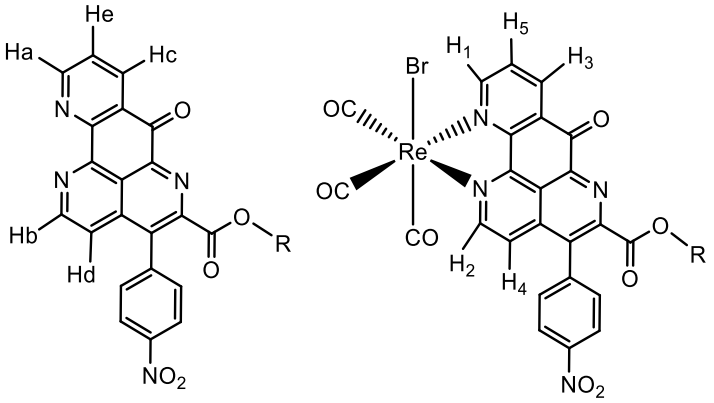

MPP (2.5)		ReMPP (4.5)		Δδ (ppm)
Proton	Chemical shift (ppm)	**Proton**	Chemical shift (ppm)	
Ha	9.15	**H_1**	9.42	0.27
Hb	9.06	**H_2**	9.13	0.07
Hc	8.67	**H_3**	8.98	0.31
Hd	8.48	**H_4**	8.49	0.01
He	7.86	**H_5**	8.13	0.27

Figure 4.16: Chemical shift changes observed for the protons on the phenanthroline core of MPP (**2.5**) upon complexation to Re(I) to form ReMPP (**4.5**)

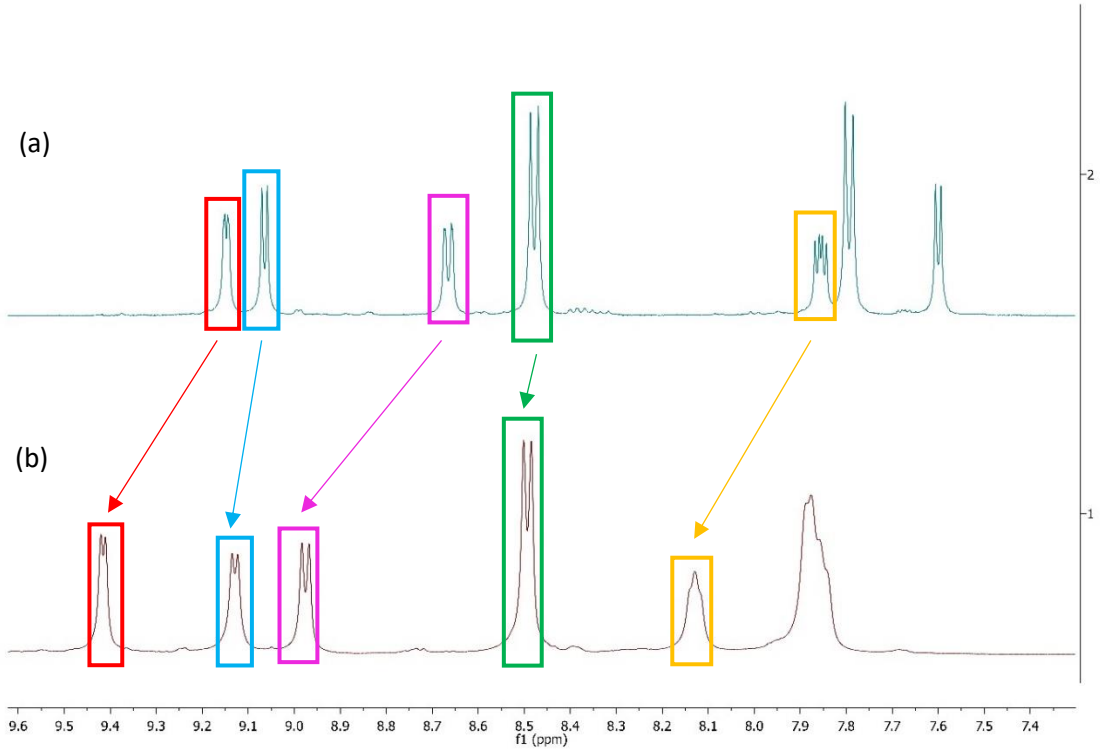

Figure 4.17: ^{1}H NMR spectra of (a) phen-pyrido ligand, MPP (**2.5**) and (b) Re(I) phen-pyrido complex, ReMPP (**4.5**) showing the changes in chemical shift position of the phen protons upon complexation to Re(I) in DMSO-d6.

The ^{13}C NMR spectra obtained for complexes **4.6 – 4.8** supported the synthesis of the Re(I) tricarbonyl structures by the presence of three quaternary carbon signals between 195 – 185 ppm arising from the three Re-CO ligands **Figure 4.17** shows the associated region of the ^{13}C NMR spectrum of ReHPP (**4.9**). It was noted that these carbon signals were not observed for the methyl analogue, ReMPP (**4.5**).

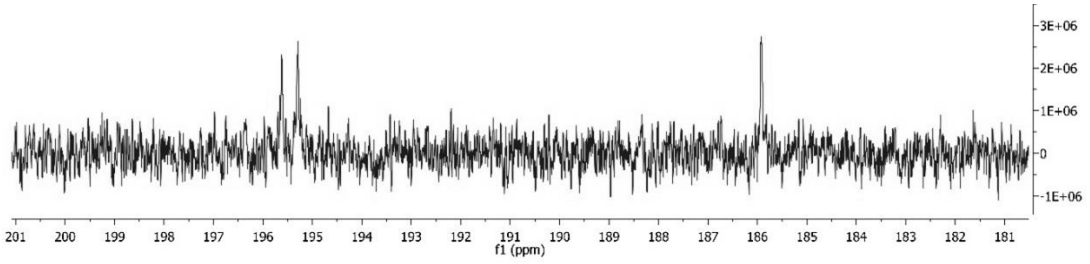

Figure 4.18: Portion of the ^{13}C NMR spectrum of ReHPP (**4.9**) showing the Re-CO signals present at 195.5, 195.3 and 185.8 ppm in DMSO-d6.

The IR data obtained for all Re(I) phen-pyrido complexes **4.5 – 4.8** show two *ν*(CO) stretching bands between 2010 - 1880 cm^{-1}. In all cases the band at 1880 cm^{-1} has a shoulder at ~1920 cm^{-1} The IR spectrum of ReMPP showing this region is given in **Figure 4.19**.

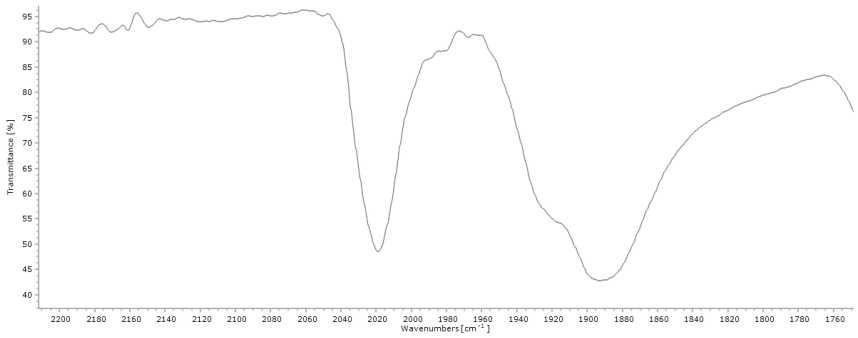

Figure 4.19: IR spectrum of ReMPP (**4.5**) showing the Re-CO stretching modes.

High resolution mass spectrometry was conducted on the family of novel Re(I) phen-pyrido complexes **4.5 – 4.8.** An $(M+H)^+$ ion was detected for ReEPP (**4.6**); $(M+Na)^+$ ions were detected for ReMPP (**4.5**), RePPP (**4.7**) and ReHPP (**4.8**). In each case the isotope match score was above 96% in all cases supporting the predicted molecular formulae (**Table 4.5**)

Table 4.5: Theoretical and observed mass to charge ratios of Re(I) complexes **4.5 – 4.8**

Compound	Formula	Theoretical neutral mass (Da)	Observed neutral mass (Da)	Observed mass ($+Na^+$) (*m/z*)	Mass error (ppm)
ReMPP (4.5)	$[Re(C_{25}H_{12}N_4O_8)Br]$	759.9368	759.9370	784.9278	0.30
ReEPP (4.6)	$[Re(C_{26}H_{14}N_4O_8)Br]$	773.9525	773.9525	776.9619*	0.73
RePPP (4.7)	$[Re(C_{27}H_{18}N_4O_8)Br]$	787.9681	987.686	812.9593	0.56
ReHPP (4.8)	$[Re(C_{30}H_{22}N_4O_8)Br]$	830.0151	830.0153	855.0063	0.35

*Observed mass ($+H^+$)

X-ray crystallography data were obtained for RePPP (**4.7**) from a red, plate-shaped crystal grown by slow evaporation of solvent from a MeOH solution of the complex (**Figure 4.20**). The crystal structure obtained support the formation of the *fac* isomer in a distorted octahedral geometry. Bonds lengths were determined to be 2.6 Å for Re-Br, 2.1 Å for both Re-N bonds are between 1.8 – 1.9 Å for the three Re-CO bonds.

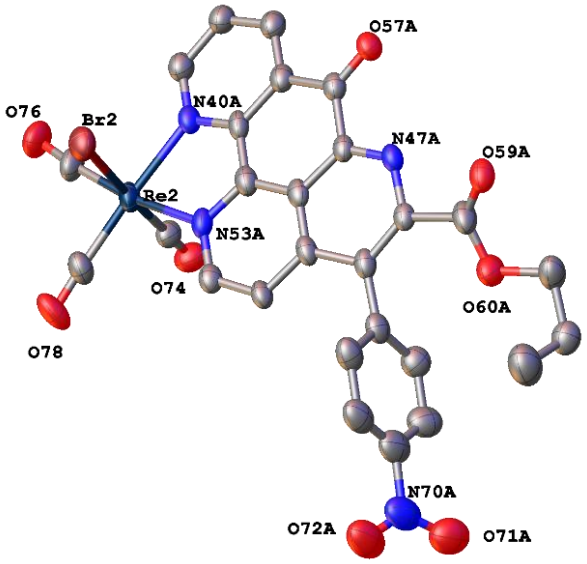

Figure 4.20: RePPP (**4.7**) modelled with disorder shown at a 50% probability.

UV-visible spectroscopy was conducted on complexes **4.5 – 4.8** in DMSO to determine their extinction coefficients, ε. The spectra for the Re(I) phen-pyrido complexes show an intense band between 350 - 390 nm with a λ_{max} at ~375 nm (**Figure 4.21**). The free ligands also absorb at this wavelength. It is predicted that this absorption band consists of an intraligand and a MLCT absorption band ([dπ(Re) -> π*(phen-pyrido)]) similar to the Re(I) phen-oxazine complexes. The extinction coefficients for λ_{max1} (~375 nm) range from 11712 – 14907 M^{-1} cm^{-1} for the family **4.5 – 4.8** and are presented in **Table 4.6**. The magnitude of the extinction coefficient, ε1 associated with λ_{max1} is consistent with the presence of an intraligand and MLCT absorption.[226] A second, less intense band is observed between 440 – 660 nm, assigned as λ_{max2}. The extinction coefficients (ε2) of this second band were calculated to be between 3066 – 3426 M^{-1} cm^{-1}. This band is tentatively assigned as another MLCT band as it is not present in the free ligand. The magnitude of ε2 is consistent with that of an MLCT band for Re(I) complexes.[224] This band also exhibits solvatochromism which is a

common behaviour of MLCT absorption bands. This will be discussed later in the chapter.

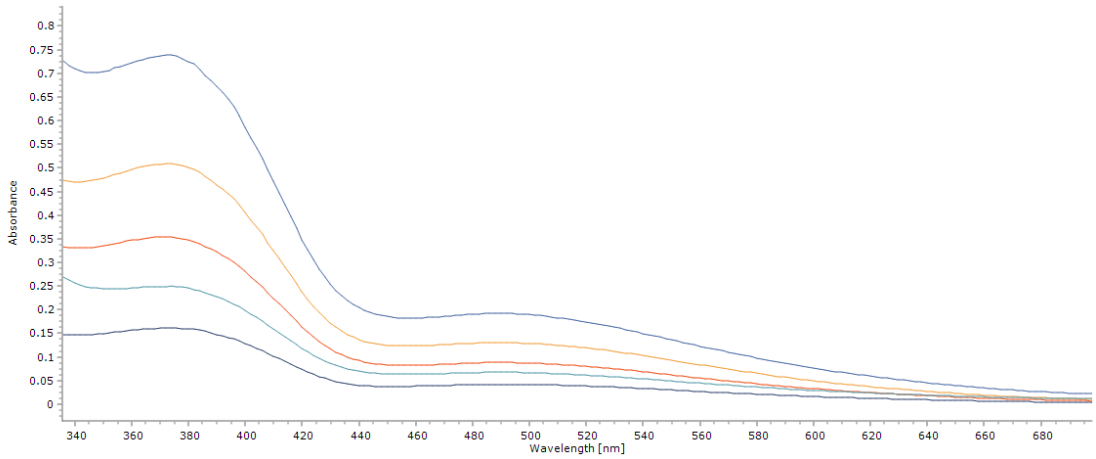

Figure 4.21: UV/vis spectra for ReHPP (**4.8**) at concentrations between 1.39 x 10^{-5} – 5.80 x 10^{-5} M in DMSO used to determine the extinction coefficients (ε1 and ε2).

Table 4.6: Wavelengths of absorption maxima (λ_{max}) and extinction coefficient (ε) values for Re (I) phen-pyrido complexes **4.5 – 4.8** in DMSO.

Compound	λ_{max1} (nm)	ε1 ($M^{-1}\,cm^{-1}$)	λ_{max2} (nm)	ε2 ($M^{-1}\,cm^{-1}$)
ReMPP (4.5)	375	12266	493	3071
ReEPP (4.6)	374	14907	495	3427
RePPP (4.7)	372	11712	490	3066
ReHPP (4.8)	371	12612	490	3250

4.3 Properties of Re(I) Tricarbonyl Complexes 4a, 4b and 4.1 – 4.8

4.3.1 Solution Stability and Solvatochromism Behaviour of Re(I) Tricarbonyl Complexes 4.1 – 4.8

Solution stability, speciation and behaviour are important considerations when assessing biological activity.[219] The solution stability of novel Re(I) complexes **4.1 – 4.8** was first established in DMSO by preparing a 50 µM sample of each compound and standing it in the dark for several days. The data obtained for RePPO (**4.2**) are presented in **Figure 4.22**. Over a 72 h period no changes were observed for any Re(I)

complex using UV-vis spectroscopy. It was determined that complexes **4.1 – 4.8** were highly stable in DMSO in the dark over a 72 h period.

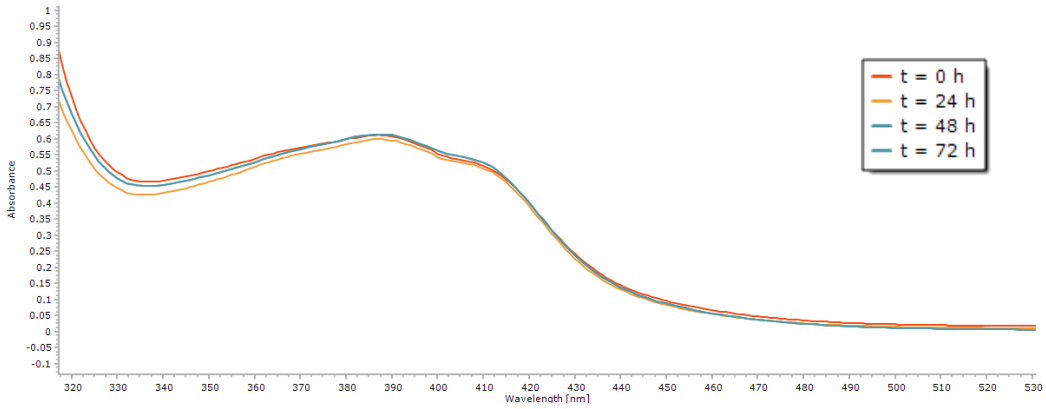

Figure 4.22: UV/vis spectra for a 50 µM DMSO solution of RePPO (**4.2**) left to stand in the dark at rt for 72 h.

Re(I) complexes **4.1 – 4.8** were assessed for solvatochromism. This is a phenomenon where molecules absorb light at different wavelengths depending on the choice of solvent.[227] It is a consequence of differing solvation energy of the ground and excited states when solvent molecules interact with the compound in solution.[228] Solvatochromism is typical of MLCT absorption bands.[229] Solutions of Re(I) phen-oxazine complexes RePPO (**4.2**) and ReHPO (**4.3**) were prepared in both DMSO and ACN. Likewise, solutions of Re(I) phen-pyrido complexes ReMPP (**4.5**) and ReEPP (**4.6**) were prepared in both DMSO and DCM. The choice of solvent was based on the best solubility for each family. UV-vis data were obtained for the complexes in the different solvents. The data show a subtle change of 2 - 3 nm in the λ_{max1} position from one solvent to another for all compounds tested which suggests, as expected for intraligand transitions, the compounds do not exhibit significant solvatochromism at this wavelength. A more evident change is observed for λ_{max2} of phen-pyrido complexes ReMPP (**4.5**) and ReEPP (**4.6**). The λ_{max2} band is present at 491 nm for ReMPP (**4.5**) when dissolved in DMSO but shifts to 558 nm when dissolved in DCM. Similarly, a DMSO solution of ReEPP (**4.6**) shows λ_{max2} at 489 nm while the band shifts to 557 nm when dissolved in DCM. This behaviour is indicative of a MLCT band. The red shift observed for the species when dissolved in DCM suggest the excited state is stabilised by lower polarity solvents and therefore has a small dipole moment.

4.3.2 Photo-Luminescence Studies on Re(I) complexes Tricarbonyl Phenanthroline complexes (4a,b, 4.1-4.8)

Photo-irradiation of rhenium tricarbonyl diimine complexes leading to luminescence has been extensively reported.[123] The photoluminescence occurs through emission from the MLCT triplet state (**Scheme 4.6**).

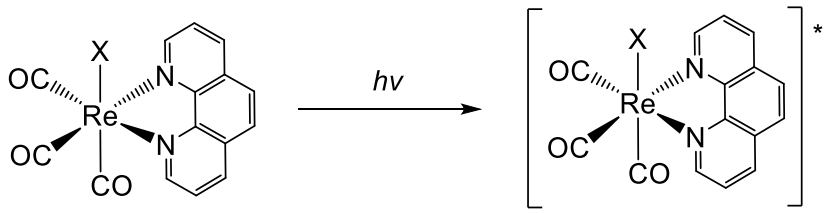

Scheme 4.6: Photoluminescence of rhenium(I) tricarbonyl complexes complex of general formula *fac*-$[Re(CO)_3(phen)X]$

The attractive photophysical properties of Re tricarbonyl phen complexes include the intense near UV/visible absorbance, long emission lifetimes and large Stokes shifts. The electronic properties can be easily tuned through derivatisation of the coordinated phen ligand. The strong emission of Re tricarbonyl phen complexes has found applications as intracellular imaging agents (**Figure 4.23a,b**)[129, 130] and as pH sensors (**Figure 4.23c**).[216]

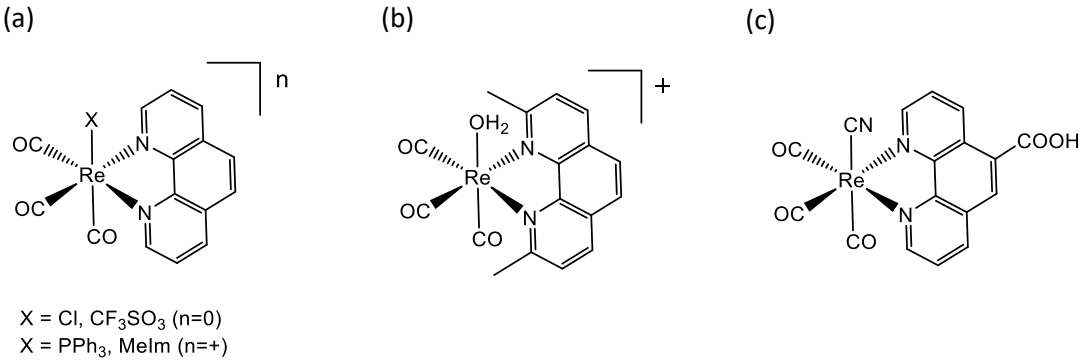

Figure 4.23: Re(I) tricarbonyl phen complexes that function as intracellular imaging agents (a,b) and pH sensors (c).

Standard protocols to assess the luminescence of Re tricarbonyl complexes involves excitation at λ_{max1} of a 2 – 5 x 10^{-5} M solution.[129, 131, 230] Chakraborty and coworkers assessed the luminescence of [$Re(CO)_3$(phen)Cl]. In their study they excited a 4.5 x 10^{-5} M ACN solution at 370 nm. The sample produced an emission band centred at 605 nm. In the present study, the analogous bromide complex [$Re(CO)_3$(phen)Br] (**4a**) was first assessed using a similar protocol. A 2 x 10^{-4} M solution of **4a** was prepared in ACN. Luminescence was visible by eye under a UV lamp operating at 365 nm. The sample was placed in a fluorometer and excited at 385 nm and emission was monitored between 450 -750 nm. A broad band emission was observed at 592 nm with a relative intensity of 220 a.u. (**Figure 4.24**).

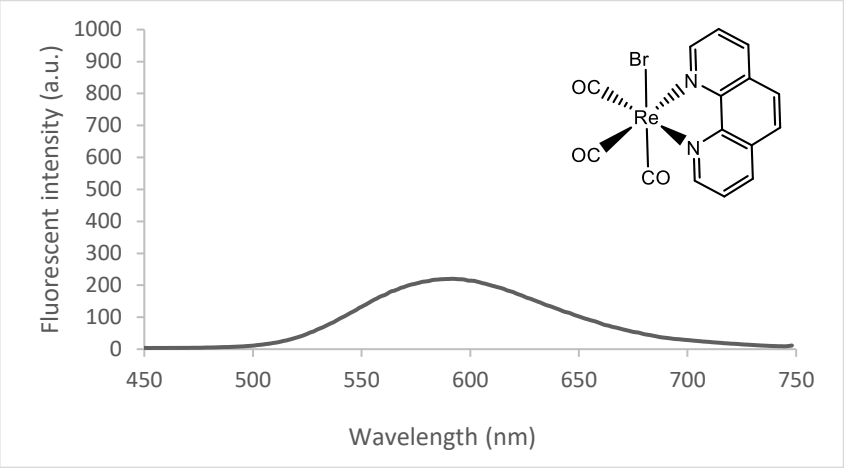

Figure 4.24: Luminescence emission spectrum recorded for **4a** (2 x 10^{-4} M) following excitation at 385 nm in ACN at rt.

The luminescence properties of [$Re(CO)_3$(phendione)Br] (**4b**) were investigated. A 2.2 x 10^{-4} M solution of **4b i**n ACN was prepared. Interestingly, the solution did not appear to be luminescent by eye when exposed to a UV lamp (365 nm). The sample was excited in the fluorometer at a wavelength of 377 nm but no emission band was observed. This is proposed to be a result of functionalisation of the phen ring. There is literature precedent to suggest that substitution of the phen ligand can greatly alter the photophysical properties of the $Re(CO)_3$ complexes.[231-233] The introduction of electron withdrawing groups such as C=O, COOH and NO_2 into the phen ligand can shorten emission lifetimes and reduce emission efficiency.[234] A study by Komreddy and coworkers demonstrated that functionalisation of the phen ligand of

[Re(phen)$(CO)_3$Cl], lowers the emission compared to the unsubstituted analogue. An epoxy ring or a carboxylic acid (COOH) group have the greatest effect on lowering the emission intensity and quantum yields (ϕ) as presented in **Table 4.7**.[210] From these data, it is predicted that the 5,6-disubstituted phendione ligand may quench the emission of **4b**.

Table 4.7: Quantum yields of Re(I) tricarbonyl complexes containing substituted phen ligands[210]

Compound	Substituent	$\phi_{em}{}^{a}$
Re(phen)$(CO)_3$Cl	H	0.032
Re(5-CN-phen)$(CO)_3$Cl	CN	0.015
Re(5-NH_2CO-phen)$(CO)_3$Cl	NH_2CO	0.010
Re(5,6-epoxy-phen)$(CO)_3$Cl	epoxy	0.008
Re(5-COOH-phen)$(CO)_3$Cl	COOH	0.005

[a] ϕ is expressed as a value between 0 and 1

Based on the literature precedent described above, it was predicted that the derivatised phen-oxazine and phen-pyrido ligands may result in little or no emission of the Re(I) complexes. There is evidence in the literature that suggests population of non-emission excited states may result in fluorescent quenching[235] and from our UV-vis studies on the phen-oxazine and phen-pyrido complexes discussed above it would appear the intraligand $\pi \rightarrow \pi^*$ and the MLCT band is overlapping.

Re(I) complexes (**4.1 - 4.8**) were investigated in a similar manner to complexes **4a** and **4b**. A 20 µM ACN solution of each complex **4.1 – 4.8** were prepared. Using a UV lamp, no visual luminescence was observed for any Re(I) phen-oxazine complex. The samples of RePPO (**4.2**) and ReHPO (**4.3**) were assessed using the fluorometer. Each sample was excited at 391 nm. As expected, no luminescence was observed for either phen-oxazine complex. The ACN solutions of RePPP (**4.7**) and ReHPP (**4.8**) were also analysed. The samples were excited at 373 nm. No luminescent output was observed for either phen-pyrido complex.

4.3.3 Assessment of the Photochemical Stability of Re(I) Tricarbonyl Complexes 4.1 – 4.8 using UV-visible Spectroscopy

Rhenium tricarbonyl diimine complexes can undergo a variety of photochemical reactions following irradiation. These include CO release, *fac*/*mer* isomerisation and loss of the ancillary halide (**Scheme 4.7**). CO substitution and *fac*/*mer* isomerisation have previously been observed for *fac*-[Re(bipy)$(CO)_3$Cl] following irradiation.[236] While Chakraborty and co-workers have observed photo-induced CO loss from (Phen)Re$(CO)_3$Cl in both ACN and PBS solutions. They prepared a 4.5 x 10^{-4} M solution in PBS and irradiated at 302 nm at regular intervals. UV/vis data was obtained at each time interval. The resulting spectra showed a clear time-dependent decrease in the intensity of the absorbance band with λmax at 370mn with loss of CO molecules. A key application of these complexes is in photodynamic therapy in the treatment of cancer. Many Re(I) tricarbonyl phen complexes have been identified as potent CO-releasing chemotherapeutic agents.[129, 131, 233, 237]

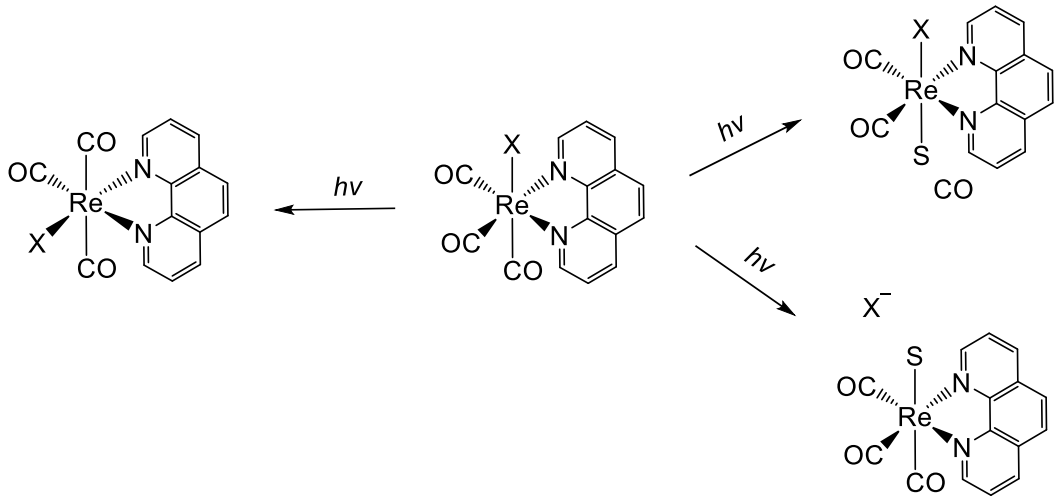

Scheme 4.7: Possible photochemical reactions resulting from irradiation of complex of general formula *fac*-[Re$(CO)_3$(phen)X] (S = solvent molecule, X = halide).

Photochemical stability studies were carried out on complexes **4a**, **4b** and **4.1 – 4.8**. The solutions were prepared by dissolving the desired compound in ACN at a concentration of between 1 – 2 x 10^{-5} M. The test solution, which was left under aerobic conditions in order to reflect a biological system, was added to a quartz cuvette and placed 30 cm from the light source. A broad band xenon lamp that emits

between 240 – 2400 nm was used for all experiments. UV-vis spectra were obtained at regular time intervals to monitor changes following exposure to UV light.

A solution of 1.44 x 10^{-4} M (A = 0.45) of **4a** was prepared in ACN. The sample was irradiated at intervals of 5 – 10 minutes and absorption spectra were obtained at each time point (**Figure 4.25**). Irradiation for a total of 40 minutes reveals a clear time-dependent decrease in the band at λ_{max} while a new band appears centred at a wavelength of 520 nm. A similar experiment conducted using a solution of $[Re(CO)_3(phen)Cl]$ by Chakraborty and co-workers results in the same time-dependent decrease of the complex absorption band following irradiation.[129] Two isosbestic points are present at 350 nm and 416 nm suggesting one photoproduct as is seen in the literature.[213]

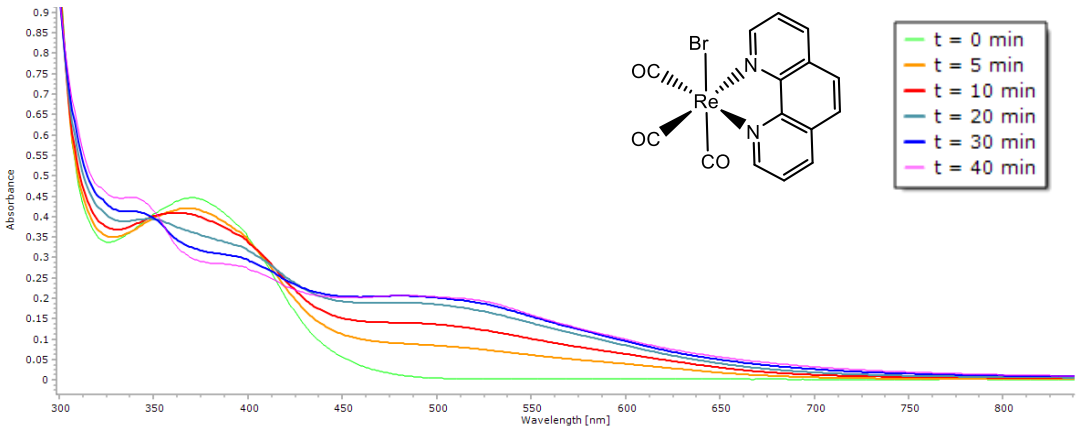

Figure 4.25: UV-visible spectra of **4a** (1.44 x 10^{-4} M) following irradiation by broad band light from 0 – 40 minutes in ACN.

A 2.11 x 10^{-4} M (A = 1) solution of complex **4b** in ACN was prepared. The same experimental set up was used as for the irradiation of **4a**. UV-vis spectra of **4b** following irradiation at 5/10 minute intervals were obtained (**Figure 4.26**) over a time period of 40 minutes. Similarly to **4a**, there is a time-dependent decrease in the absorption band of the starting material at 373 nm. After 30 minutes there is also an apparent shift of λ_{max} from 373 nm to 364 nm. A time-dependent appearance of a new absorption band, centred at ~520 nm which continued increase in intensity is also observed. One isosbestic point is observed at 402 nm.

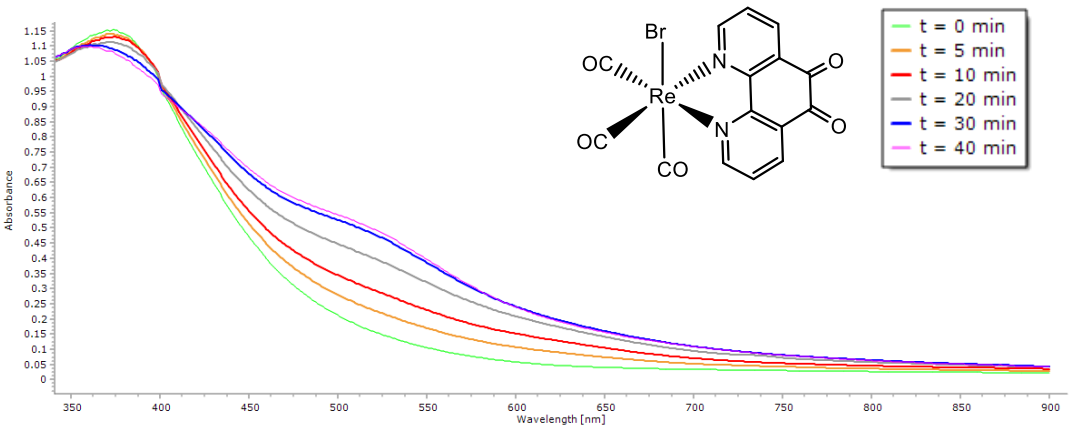

Figure 4.26: UV-visible spectra of **4b** (2.11 x 10^{-4} M) following irradiation by broad band light from 0 – 40 minutes in ACN.

Photo-irradiation of Re(I) phen-oxazine complexes **4.2** and **4.3** was conducted following the same protocol as above. A 9.8 x 10^{-5} M solution of RePPO (**4.2**) in ACN was prepared. The sample was irradiated for a total of 40 minutes and UV-vis spectra were obtained at each time interval (**Figure 4.27**). There is an obvious decrease in the absorbance band λ_{max1} 383 nm. This decrease in absorbance intensity correlates to a decrease in the concentration of the RePPO (**4.2**) starting material. The emergence of a new absorption band centred at 520 nm is indicative of the production of a new photochemical product. A clear isosbestic point is present at 430 nm. The resulting spectra of irradiated RePPO (**4.2**) are suggestive of a similar photo-induced behaviour to that observed for complexes **4a** and **4b**.

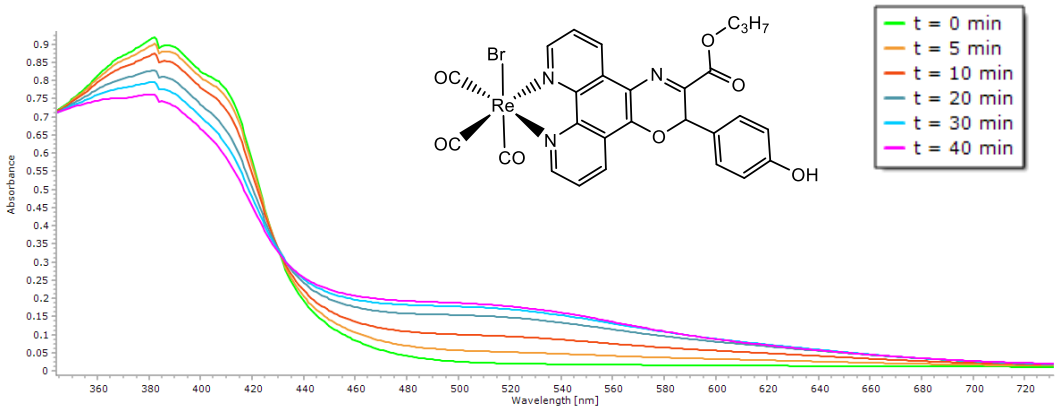

Figure 4.27: UV-visible spectra of RePPO (**4.2**) following irradiation by broad band light from 0 – 40 minutes.

Another member of the Re(I) phen-oxazine family, ReHPO (**4.3**) was assessed in the same manner. A solution of 9.3 x 10^{-5} M was prepared in ACN. A clear time-dependent decrease in the intensity of the band associated with the starting material was observed at λ_{max} and emergence of a new absorption band at 520 nm (**Figure 4.28**). A single isosbestic point appears at 430 nm. The profiles of the UV-vis absorption spectra of RePPO (**4.2**) and ReHPO (**4.3**) following irradiation are almost identical.

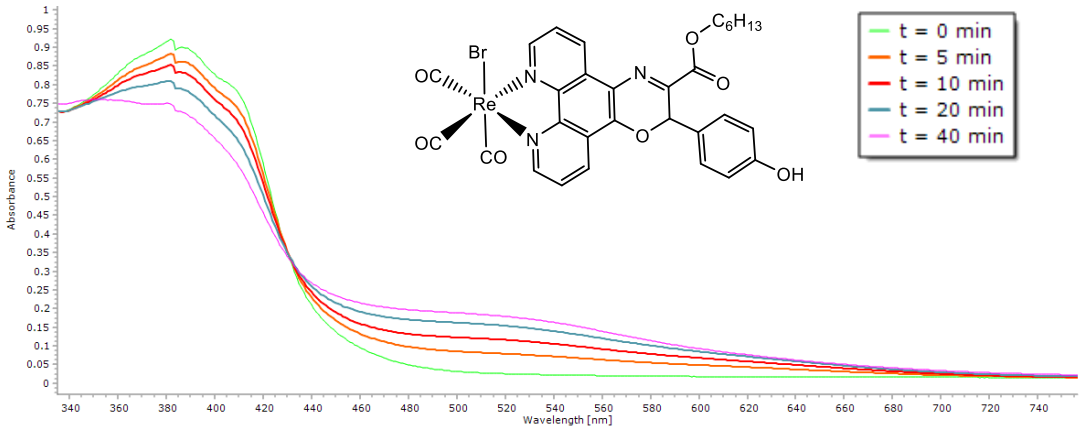

Figure 4.28: UV-visible spectra of ReHPO (**4.3**) following irradiation by broad band light from 0 – 40 minutes.

A member of the Re(I) phen-pyrido complex family was investigated in a similar manner. ReMPP (**4.5**) was dissolved in ACN to give a 6.8 x 10^{-5} M solution. The solution was irradiated at 10 minute intervals for a total of 60 minutes. The Re(I) phen-pyrido complexes possess two absorption bands with λ_{max} ~375 and ~555 nm that both decrease in intensity upon irradiation with a broad band UV lamp (**Figure 4.29**). A small new absorption band emerges at ~830 nm. Irradiation of this solution induces a gradual colour change from purple to brown over the 60 minute period.

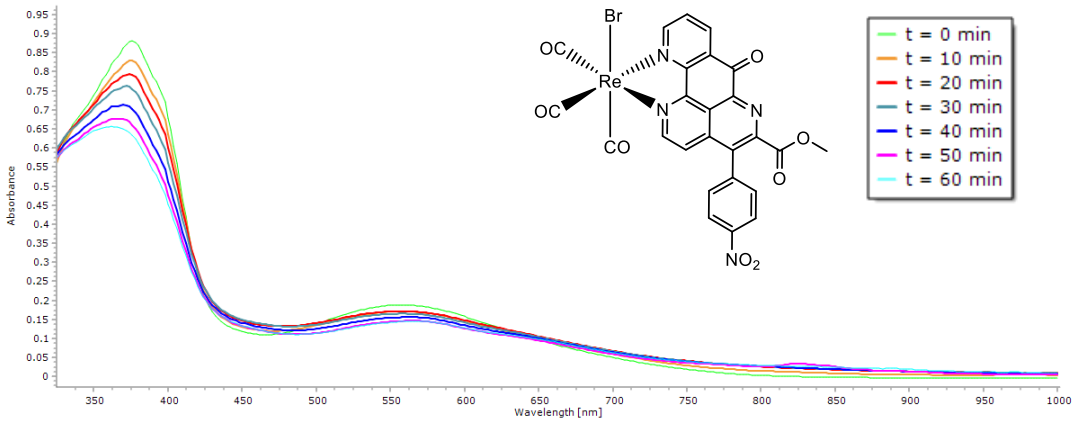

Figure 4.29: UV-visible spectra of ReMPP (**4.5**) following irradiation by broad band light from 0 – 60 minutes.

4.4 Myoglobin Assays of Re(I) Complexes 4.1 – 4.8

There is evidence from the UV-vis studies to suggest the Re(I) complexes are photochemically active (**Figures 4.25 – 4.29**). As the behaviour of the complexes was similar to that reported for UV-vis studies associated with photoactivated CO loss of similar complexes.[129, 213] Studies were carried out on complexes **4b**, **4.2**, **4.3** and **4.7** using a myoglobin assay to assess if there was any evidence of CO loss. Myoglobin (Mb) is a protein primarily present in muscle that reversibly binds oxygen through a Fe(II) centre bound to a heme group.[238] Myoglobin also readily binds CO and can be used to analyse the photo-activated release of CO from CORMs.[239] UV-vis spectra for oxy-myoglobin, carboxy-myoglobin and deoxy-myoglobin were obtained from the literature (**Figure 4.30**).[240] There are two key regions in the spectra: for all species, the most intense band is present in the Soret region between about 350 – 460 nm, one or more bands are also seen in the Q-band region at the longer wavelength of 450 – 700 nm. The most noticeable difference between the three species is observed in the Soret band region. Uncoordinated deoxy-Mb (purple) has an absorption band at 433 nm in the Soret band region and a single band centred at 555 nm in the Q-band region. The Soret band of carboxy-Mb (blue) is seen at 423 nm while the Q-band region for this species has two separate bands at about 545 and 575 nm. The Soret

band of Oxy-Mb (red) is at 417 nm while the Q-band region has two bands at 547 and 581 nm. The wavelengths are summarised in **Figure 4.30**.[240]

Wavelength (nm)		Species
433	555	deoxy-Mb (purple)
417	547, 581	oxy-Mb (red)
423	545, 575	carboxy-Mb (blue)

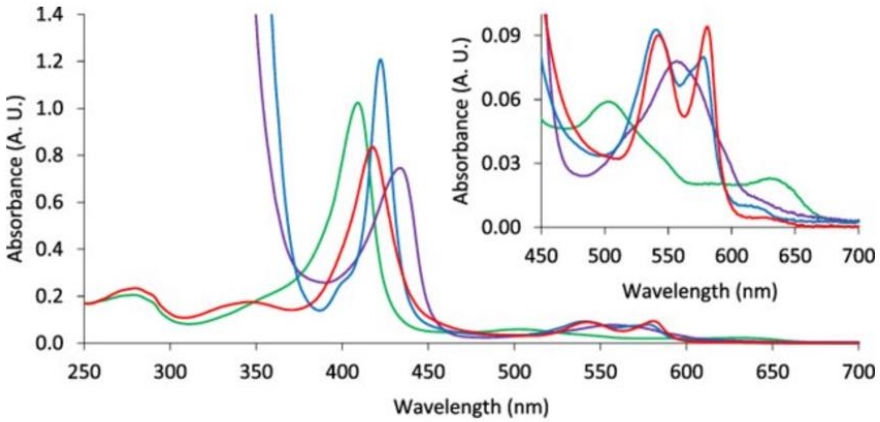

Figure 4.30: UV/vis spectra of oxy-Mb (red), carboxy-Mb (blue) and deoxy-Mb (purple). Inset shows the Q-band region from 450 – 700 nm[240]

Myoglobin assays were conducted on a sample group of Re(I) complexes to assess whether photo-activated CO loss is occurring. A 0.08 mM solution of deoxy-Mb was prepared in fresh PBS. A solution containing 0.09 M sodium hydrosulphite in PBS was also prepared. The role of the sodium hydrosulphite is to maintain an oxygen free solution. Re(I) test compounds were prepared at a concentration of 0.2 mM in ACN. A test solution containing a total volume of 2 mL was prepared, as per **Table 4.8**, in a quartz cuvette and the sample was covered in a small layer of mineral oil.

Table 4.8: Myoglobin assay test solution preparation components

Solution	Stock Concentration	Amount used	Final concentration	Total Volume
Myoglobin	0.08 mM	0.5 mL	0.02 mM	2 mL
Sodium Hydrosulphite	0.09 M	0.5 mL	0.023 mM	
Test compound in ACN	0.2 mM	0.1 mL	0.01 mM	
PBS		0.9 mL		
Mineral oil		A few drops		

RePPO (**4.7**) was prepared according to **Table 4.8**. This involved making a 2 mL solution containing 0.5 mL of the 0.08 mM deoxy-Mb stock solution, 0.5 mL of the 0.09 mM sodium thiosulfate stock solution, 0.1 mL of a 0.02 mM ACN solution of RePPO (4.7), 0.9 mL of PBS and a few drops of mineral oil. The test solution was irradiated with broad band light for a total of 60 minutes and any changes were monitored using UV-vis spectroscopy (**Figure 4.31**). The Soret band is characteristic of deoxy-Mb with a wavelength of maximum intensity at 433 nm. Similarly, the Q-band presents a characteristic single band centred at 555nm. There is a clear decrease in the intensity of both bands. This could suggest a decrease in the concentration of deoxy-Mb but there no evidence for formation of oxy-Mb or carboxy-Mb therefore evidence for CO loss from the complex is limited.

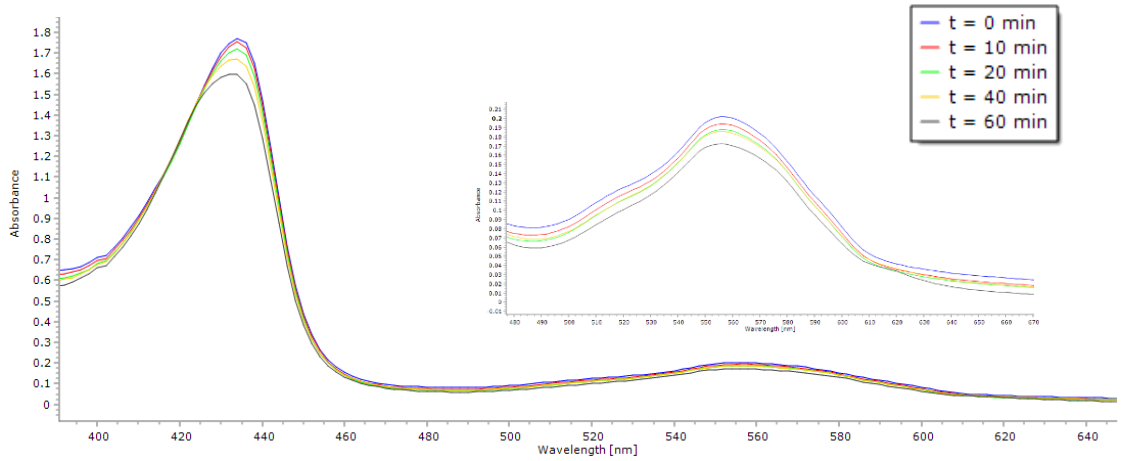

Figure 4.31: UV-visible spectra following irradiation for a total of 60 minutes of a solution containing RePPO (**4.2**) (0.01 mM) and deoxy myoglobin. Inset shows the Q-band region from 480 – 670 nm.

The same experiment was conducted with the phen-pyrido complex RePPP (**4.7**). The sample was prepared according to **Table 4.8**. The test solution containing 0.01 mM of RePPP (**4.7**) was irradiated for a total of 60 minutes and UV-vis spectra were obtained at each time point as shown in **Figure 4.32**. On first glance, the bands are characteristic of deoxy-Mb with the Soret band centred at 433 nm and the Q-band present at 555 nm. There is a decrease in both bands over time, similar to the study with RePPO (**4.2**). Again, it cannot be confirmed that the changes are due to formation of CO-myoglobin.

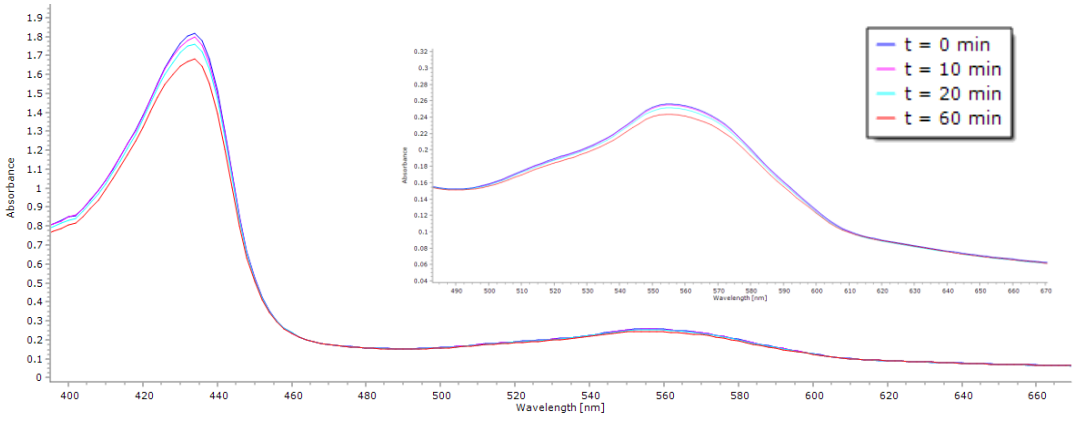

Figure 4.32: UV-visible spectra of an ACN solution containing RePPP (**4.7**) and deoxy myoglobin following irradiation for a total of 60 minutes. Inset shows the Q-band region from 480 – 670 nm.

It can be concluded that the complexes are photochemically active upon irradiation as is observed in the UV-visible spectra (**Figures 4.25 – 4.29**). The myoglobin assays could not confirm the mechanism to be CO loss. There is limited evidence for decrease in the concentration of deoxy-Mb but no definite evidence for conversion to carboxy-Mb.

4.5 Electrochemical studies of Re(I) complexes

Re(I) tricarbonyl phen complexes have well established redox activity that has seen their use in the reduction of CO_2[211], solar energy conversion[217] and as sensors.[216] Re(I) diimine complexes of general formula $[Re(CO)_3(N\text{^}N)X]$ (where X = Cl or Br) undergo at least two reductions. The first is either reversible or quasi-reversible and is associated with the diimine ligand and the second is an irreversible reduction of Re(I) to Re(O).[241] It is also common for $[Re(CO)_3(N\text{^}N)X]$ complexes to undergo an irreversible $Re^{I/II}$ oxidation at positive potentials. When a current is applied an electrochemical-chemical-electrochemical (ECE) reaction occurs. This mechanism involves a $Re^{I/II}$ oxidation (E) followed by replacement of the halide with a solvent molecule (C). This species then undergoes a second reversible oxidation of $Re^{I/II}$ (E).[242-244] A typical ECE reaction for a *fac*-$Re(CO)_3(L)Cl$ complex is shown in **Scheme 4.8**.

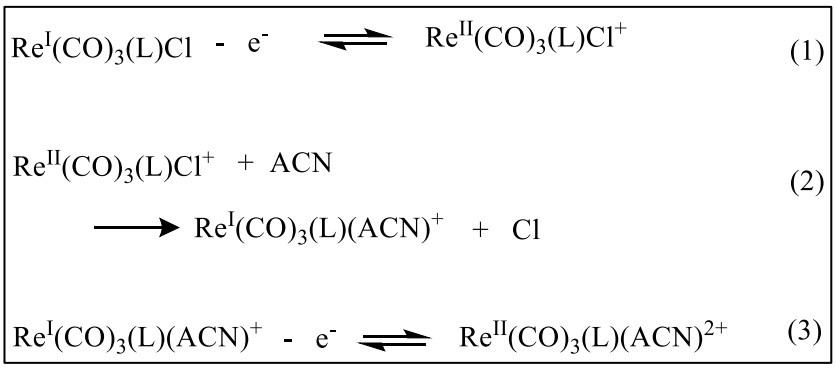

Scheme 4.8: Electrochemical and chemical processes that occur when a current is applied to $Re(CO)_3(L)Cl$[245]

The reversibility of a redox reaction is determined by the peak separation (ΔE) of E_p^{ox} and E_p^{red}. In general, when ΔE = 57 mV, the reaction is reversible. A redox couple with 57 mV > ΔE > 200 mV is quasi-reversible. An irreversible redox reaction typically has a much larger ΔE of > 200 mV.[246] The redox activity of Re(I) complexes **4.1 – 4.3** and **4.5, 4.7, 4.8** was investigated. Electrochemical studies were conducted based on the parameters used by Bao and coworkers.[247] A three-electrode cell was used for all experiments. This consisted of a glassy carbon electrode (GCE) as the working electrode, a saturated calomel electrode (SCE) as the reference electrode and platinum wire as the counter electrode. Tertbutylammonium tetrafluoroborate (TBATFB) was used as the supporting electrolyte. Non-aqueous solutions were made to contain 1 mM of the selected complex and 0.1 M of supporting electrolyte in ACN. Ferrocene was used as a control. Solutions were degassed for at least 30 minutes prior to use. A nitrogen atmosphere was maintained in the cell. Cyclic voltammetry was conducted on all complexes at a scan rate of 100 mV/s.

A standard cyclic voltammogram (CV) obtained for the ferrocene/ferrocenium couple, Fc/Fc^+ (**Figure 4.33**). Ferrocene has been well established as a standard for calibration of an electrochemical system.[247, 248] The CV shows a clear oxidation at 0.46 V vs SCE that is associated with the $Fe^{II/III}$ oxidation. The $Fe^{III/II}$ reduction is observed at 0.39 V vs SCE.

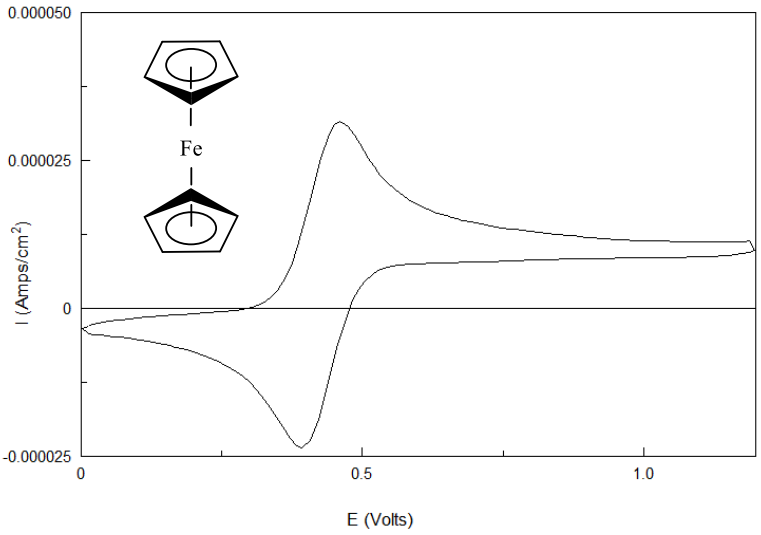

Figure 4.33: Cyclic Voltammogram of ferrocene (1 mM) in 0.1 M TBATFB/ACN; scan rate of 100 mV/s.

The simple complex Re(I) tricarbonyl phen was investigated first. However, as $[Re(CO)_3(phen)Br]$ (**4a**) was insoluble in ACN, the analogous complex $[Re(CO)_3(phen)Cl]$ was assessed. A solution was prepared as described above. The oxidation and reduction peaks are listed in **Table 4.9**. The CV of $[Re(CO)_3(phen)Cl]$ is presented in **Figure 4.34**. The oxidation peak at 1.37 V vs SCE is consistent with irreversible oxidation of $Re^{I/II}$ of Re tricarbonyl phen complexes.[241] The reduction peak at -1.37 V vs SCE is assigned to reduction of the phen ligand which is consistent with the literature.[210]

Table 4.9: Redox properties* of Re(I) complexes of phen and phendione (**2a**)

Compound	E_p^{ox} (V)	E_p^{red} (V)
$[Re(CO)_3(phen)Cl]$	-1.49, -1.27, 1.37 ($Re^{I/II}$)	-1.37 (phen)
$[Re(CO)_3(phendione)Cl]$	-1.61, -0.79, -0.09, 1.50 ($Re^{I/II}$)	-0.84, -0.17
$[Re(CO)_3(phendione)Br]$ (4b)	-0.78, -0.09, 1.49 ($Re^{I/II}$)	-0.85, -0.14

*0.1 M TBATFB in ACN, rt, vs SCE

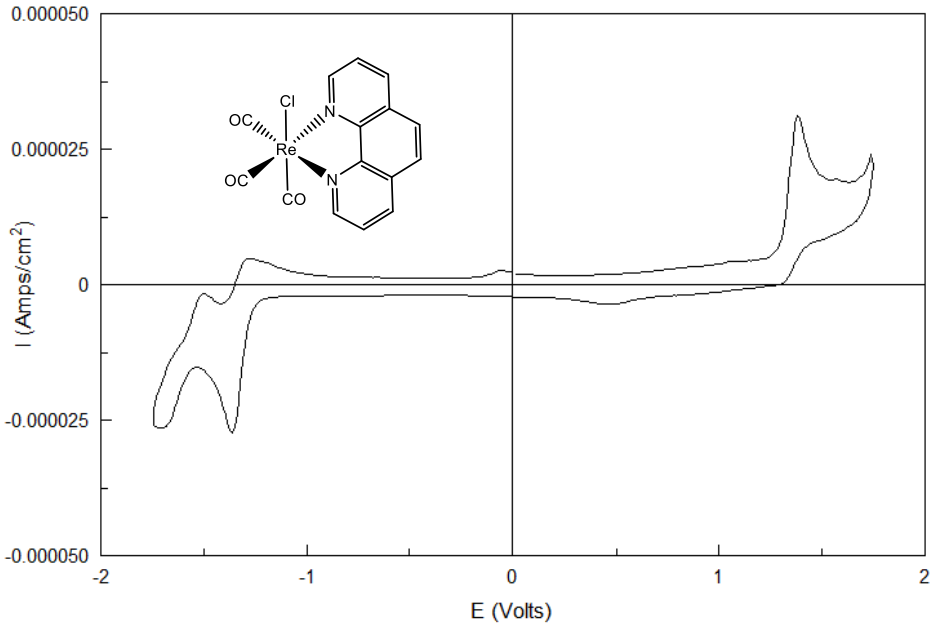

Figure 4.34: Cyclic Voltammogram of $[Re(CO)_3(phen)Cl]$ (1 mM) in 0.1 M TBATFB/ACN; scan rate of 100 mV/s.

The electrochemical properties of $[Re(CO)_3(phendione)Cl]$ were assessed in the same manner as $[Re(CO)_3(phen)Cl]$ and the CV is presented in **Figure 4.35**. As expected, there is an anodic peak at 1.50 V vs SCE that can be assigned as the irreversible $Re^{I/II}$ oxidation. Two new redox couples arise in the region -1 – 0 V compared to the CV of the simple phen complex, $[Re(CO)_3(phen)Cl]$. These redox couples are predicted to be associated with functional groups of phendione. The first redox couple (A) is observed at -0.09 V vs SCE (E_p^{ox}) and -0.17 V vs SCE (E_p^{red}) as presented in **Table 4.9**. The second redox couple (B) emerges at -0.79 V vs SCE (E_p^{ox}) and -0.84 V vs SCE (E_p^{red}). These redox couples are particularly efficient as the peak separations, ΔE are small; 0.08 and 0.05 V respectively. From these values, redox couple A can be assigned as a quasi-reversible process while B can be assigned as reversible. An additional oxidation is observed at -1.61 V vs SCE. A very similar voltammogram was recorded when the experiment was repeated for $[Re(CO)_3(phendione)Br]$, and the peaks are given in **Table 4.9.** This indicates that varying the halide ligand had little effect on the electrochemical properties of the complexes.

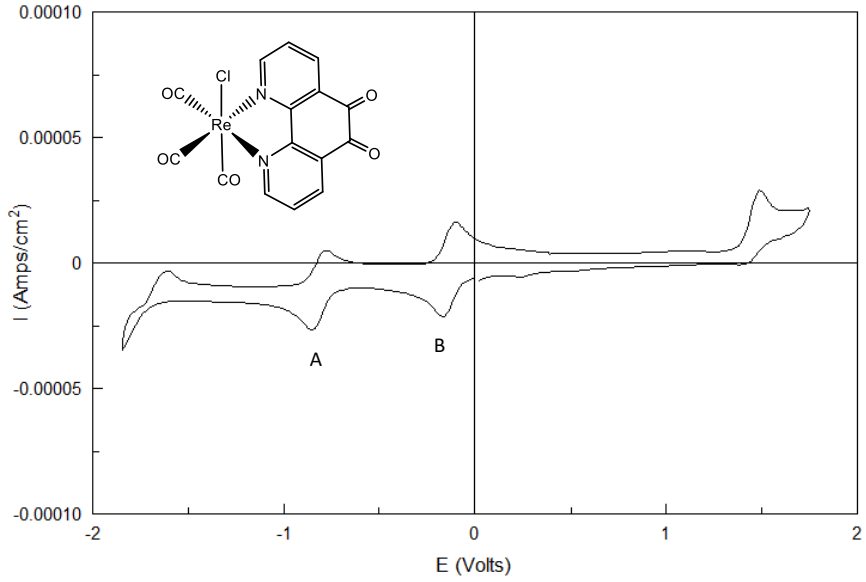

Figure 4.35: Cyclic Voltammogram of $[Re(CO)_3(phendione)Cl]$ (1 mM) in 0.1 M TBATFB/ACN; scan rate of 100 mV/s.

A series of CVs were obtained for each Re(I) phen-oxazine complexes, **4.1** – **4.3**, as described above. **Figure 4.36** shows a CV of RePPO (**4.2**). The positions of the oxidation and reduction peaks for each complex are listed in **Table 4.10**. The oxidation peaks at -0.90 and -0.05 V vs SCE and reduction peaks at -0.98 and -0.51 V vs SCE are predicted to be associated with the phen-oxazine ligand. The free phen-oxazine ligands were insoluble in ACN so electrochemical analysis could not be carried out under the same conditions as the complexes. Interestingly the irreversible $Re^{I/II}$ oxidation (ca. 1.4 V vs SCE) was little affected by the change in the alkyl chain length.

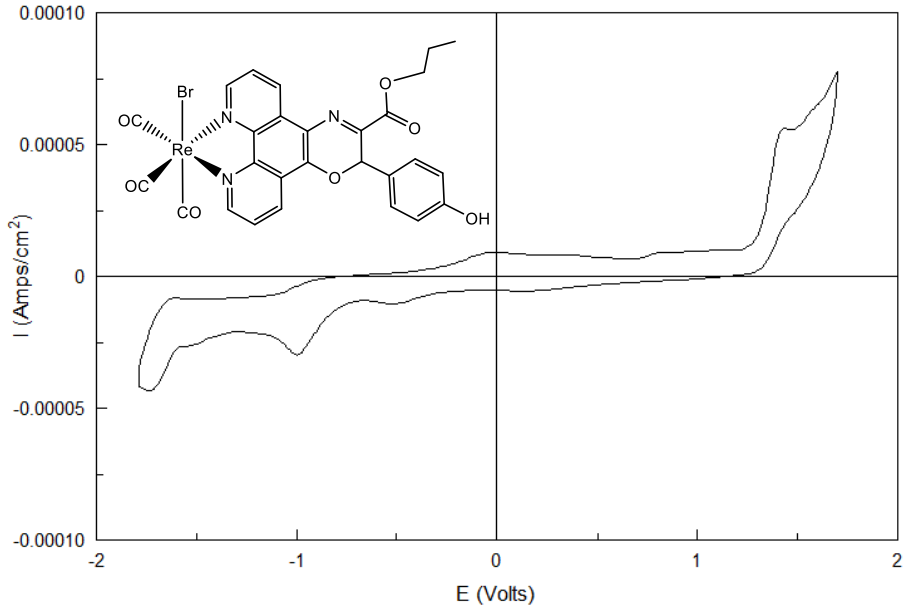

Figure 4.36: Cyclic Voltammogram of RePPO (**4.2**) (1 mM) in 0.1 M TBATFB/ACN; scan rate of 100 mV/s.

Table 4.10: Redox properties* of Re(I) complexes **4.1 – 4.3**

Compound	E_p^{ox} (V)	E_p^{red} (V)
ReMPO (4.1)	-0.79, -0.10, 0.46, 1.43 ($Re^{I/II}$)	-1.03, 0.10
RePPO (4.2)	-1.61, -0.90, -0.05, 1.42 ($Re^{I/II}$)	-0.98, -0.51
ReHPO (4.3)	-1.60, -0.96, -0.11, 1.40 ($Re^{I/II}$)	-1.01

*0.1 M TBATFB in ACN, rt, vs SCE

Cyclic voltammetry was carried out on the Re(I) phen-pyrido complexes **4.5**, **4.7** and **4.8** and the data are given in **Table 4.11**. **Figure 4.37** shows the CV of RePPP (**4.7**). When compared to the CV of RePPO (**4.2**), it is clear that the CV of RePPP (I) has three unique redox couples. These redox couples are observed in the region of -1.3 – 0 V vs SCE. The redox activity is clearly reversible in this region. Redox couple A is observed at -1.17 (E_p^{ox}) and -1.21 (E_p^{red}) V vs SCE. The second redox couple, B is observed at -0.67 (E_p^{ox}) and -0.75 (E_p^{red}) V vs SCE. The third redox couple (C) is observed at -0.08 (E_p^{ox}) and -0.16 (E_p^{red}) V vs SCE. These additional redox couples are predicted to be ligand associated. The irreversible ReI/II oxidation appears to come at a slightly higher

potential than for the phen-oxazine analogues appearing at approximately 1.5 V vs SCE.

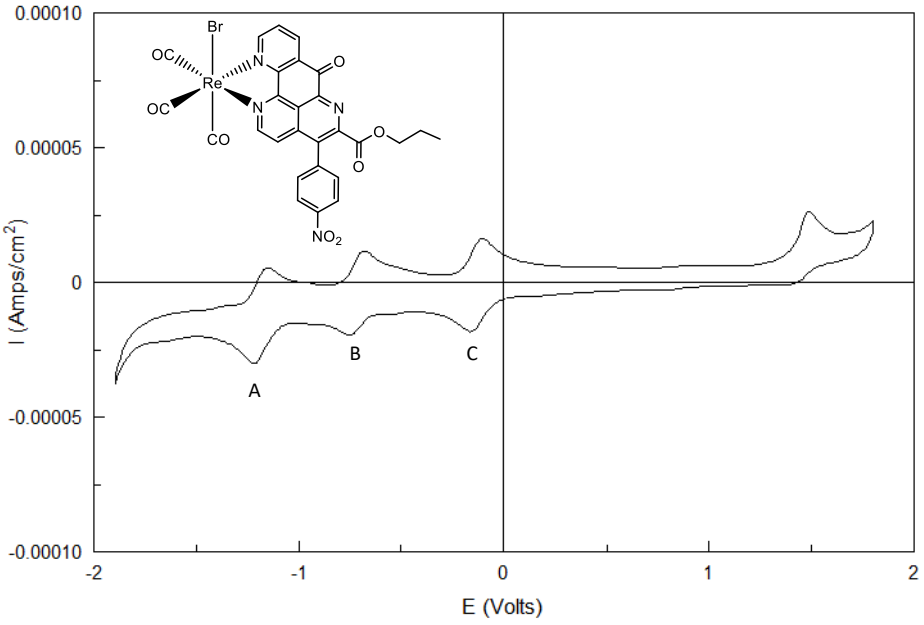

Figure 4.37: Cyclic Voltammogram of RePPP (**4.7**) (1 mM) in 0.1 M TBATFB/ACN; scan rate of 100 mV/s.

Table 4.11: Redox properties* of Re(I) complexes **4.5**, **4.7** and **4.8**

Compound	E_p^{ox} (V)	E_p^{red} (V)
ReMPP (4.5)	-1.13, -0.66, -0.11, 1.49 ($Re^{I/II}$)	-1.20, -0.15
RePPP (4.7)	-1.17, -0.67, -0.08, 1.48 ($Re^{I/II}$)	-1.21, -0.75, -0.16
ReHPP (4.8)	-1.15, -0.68, -0.11, 1.50 ($Re^{I/II}$)	-1.20, -0.74, -0.17

*0.1 M TBATFB in ACN, rt, vs SCE

The electrochemical studies of novel Re(I) phen-oxazine complexes **4.1 – 4.3** and Re(I) phen-pyrido complexes **4.5**, **4.7** and **4.8** reveal that they easily undergo $Re^{I/II}$ oxidation between 1.4 - 1.5 V vs SCE. The data demonstrates that functionalization of the phen ligand generally increases the redox activity of the complexes. The most redox active are the Re(I) phen-pyrido complexes **4.5**, **4.7** and **4.8**. The redox activity could make them good candidates for inducing reactive oxygen species (ROS). Moreover, multiple

redox couples may enable the phen-pyrido complexes to participate in redox cycling that leads to sustained ROS production. Generation of ROS can lead to oxidation of lipids, proteins and DNA and hence microbial death.[8] Redox activity may also facilitate other modes of action such as interaction with redox sensitive biological targets such as DNA or enzymes.[249]

4.6 Manganese(I) Tricarbonyl Phenanthroline Complexes

Carbonyl complexes of group 7 and 8 transition metals such as Re(I), Mn(I), Fe(II) and Ru(II) have been extensively studied for their ability to release a controlled amount of CO to biological targets.[250] This mechanism has been exploited for use as in photodynamic therapy to treat cancer.[251] This chapter has so far discussed applications of Re(I) carbonyl complexes. It was determined that the novel Re(I) complexes **4.1 – 4.8** do not readily release CO in response to a light stimulus as presented in section **4.4**. It is well known that Mn-CO bonds are weaker than Re-CO bonds and are thus likely to undergo faster ligand exchange.[252] Multiple examples of Mn(I) tricarbonyl diimine complexes have been identified as CORMs[253], electrocatalysts for reduction of CO_2[254], antimicrobial agents[255, 256] and anticancer agents.[85] It was therefore postulated that Mn(I) tricarbonyl complexes of phen-oxazine (**2.1 – 2.4**) and phen-pyrido (**2.5 – 2.8**) ligands may more readily release CO in response to UV light and still possess many of the interesting properties observed for the Re(I) complexes. To investigate the reaction of $Mn(CO)_5$ with PPO (**2.2**) and PPP (**2.7**) was attempted.

4.6.1 Synthesis of Starting Material Bromopentacarbonylmanganese(I)

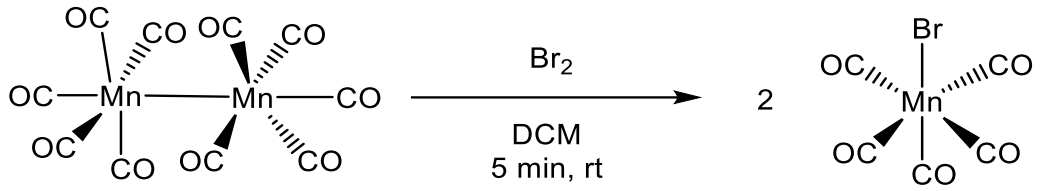

Scheme 4.9: Reaction of dimanganese decacarbonyl in the presence of bromine to produce $Mn(CO)_5Br$.

The starting material $Mn(CO)_5Br$ was synthesised following a similar methodology to that used to form $Re(CO)_5Br$ detailed in section **4.2.1** (**Scheme 4.9**). Commercially available dimanganese decacarbonyl (300 mg, 0.76 mmol) was added to DCM (5 mL) and allowed to stir at rt. Once fully dissolved, 4-5 drops of bromine were added slowly while the solution stirred. Once a deep orange colour persisted, the reaction was stirred for a further 5 minutes. After work-up a good yield of 85% was obtained. The sample was analysed using FTIR spectroscopy and the Mn-CO stretching bands at 2141, 2080, 2036 and 1982 cm^{-1} agreed with the literature.[152]

4.6.2 Attempted Synthesis of Novel Mn(I) Phenanthroline-oxazine Complex

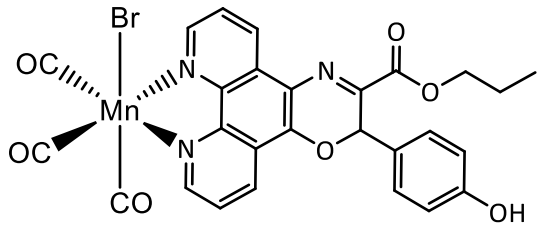

Figure 4.38: Predicted structure of $[Mn(CO)_3(\mathbf{2.2})Br]$.

The synthesis of complex $[Mn(CO)_3(\mathbf{2.2})Br]$ (**Figure 4.38**), (analogue of RePPO (**4.2**)) was attempted in the same manner as for Re(I) complexes **4.1 – 4.8**. This involved heating $Mn(CO)_5Br$ (100 mg, 0.36 mmol) and PPO (**2.2**) (148 mg, 0.36 mmol) at reflux in toluene overnight. Upon workup, the FTIR spectrum of the reaction product

revealed that no metal CO stretching bands were present. The spectrum correlated to that of the free PPO (**2.2**). It was concluded that the elevated temperature may have resulted in dissociation of the labile Mn-CO bonds. A literature protocol for the synthesis of $[Mn(CO)_3(phen)Br]$ was adopted instead.[253] This method involved adding $Mn(CO)_5Br$ (100 mg, 0.36 mmol) and PPO (**2.2**) (148 mg, 0.36 mmol) to DCM (20 mL) to create a slurry. This reaction mixture was allowed to stir at rt overnight until an orange solution developed. Upon work up, the orange product was initially analysed using IR spectroscopy. The IR spectrum shows two intense metal-carbonyl stretching bands at 2026 and 1914 cm^{-1} (**Figure 4.39**). The band at 1914 cm^{-1} has a shoulder at 1935 cm^{-1}. These data are similar to those obtained for the *fac* Re(I) complexes **4.1 – 4.8**. ^1H NMR spectrum of the product was carried out in DMSO-d6 but the spectrum was not consistent with the formation of the desired complex.

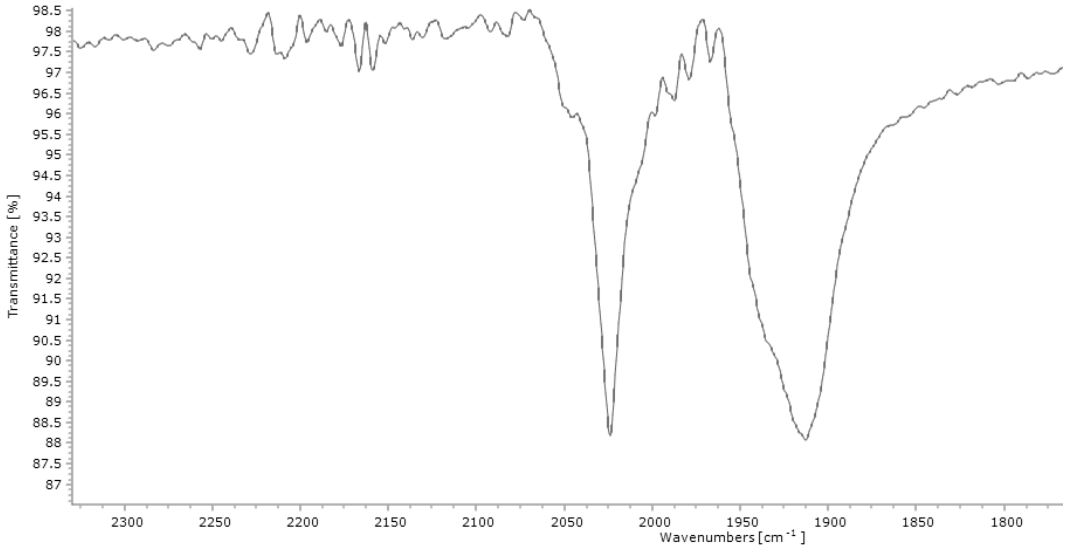

Figure 4.39: IR spectrum of the reaction product obtained from the reaction between $Mn(CO)_5$ and PPO (**2.2**) upon stirring in DCM at rt.

4.6.3 Attempted Synthesis of Novel Mn(I) Phenanthroline-pyrido Complex

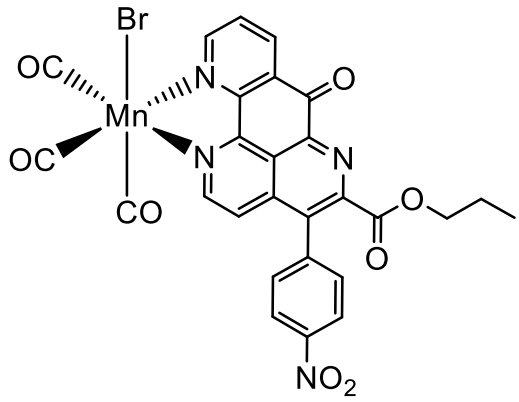

Figure 4.40: Predicted structure of [$Mn(CO)_3$(**2.7**)Br].

The protocol employed by Stanbury *et al* in the synthesis of [$Mn(CO)_3$(phendione)Br] was adopted for the attempted synthesis of [$Mn(CO)_3$(**2.7**)Br] (**Figure 4.40**).[254] $Mn(CO)_5Br$ (100 mg, 0.36 mmol) and PPP (**2.7**) (160 mg, 0.36 mmol) were added to ACN (15 mL). The reaction mixture was heated at 50 °C for 3 h. The reaction mixture was cooled to rt before evaporating to dryness. Upon workup, a deep green solid (193 mg) was collected. The solid was analysed using IR spectroscopy. Two intense Mn-carbonyl stretching bands were observed at 2024 and 1941 cm^{-1}. A band shoulder is present at 1952 cm^{-1} on the stretch at 1941 cm^{-1} as shown in **Figure 4.41**.

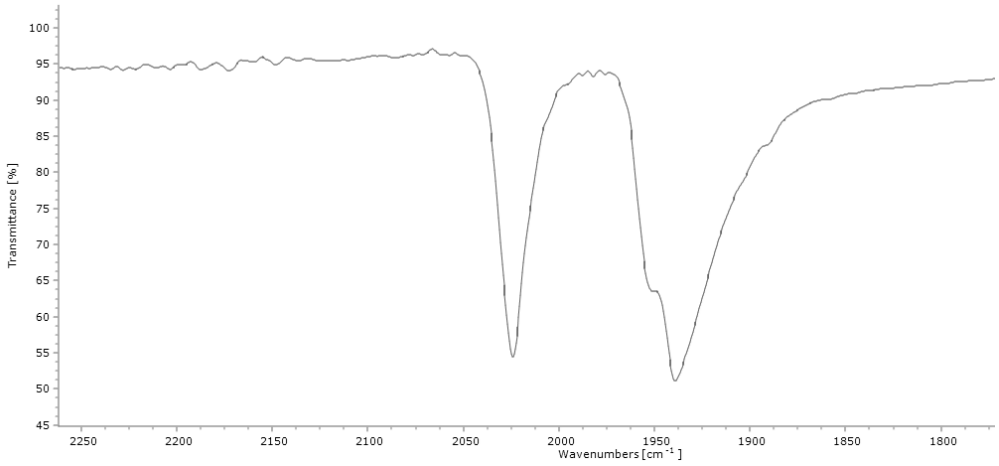

Figure 4.41: IR spectrum of the product obtained from the reaction between $Mn(CO)_5$ and PPP (**2.7**).

^{1}H NMR spectroscopy was carried out in DMSO-d6 on the product obtained from the reaction between $Mn(CO)_5$ and PPP (**2.7**) and is shown in **Figure 4.42**. Six broad singlets are observed at high chemical shifts of between 8 – 10 ppm. Broad proton signals are common for Mn complexes [257]. From the ^{1}H NMR spectrum of the free PPP (**2.7**) ligand, seven signals are expected in this region. The signals at 7.84 ppm (phenH) and 7.84 ppm (ArH) of PPP (**2.7**) are distinguishable in the free ligand but may overlap in the spectrum for the Mn complex. The signal at 8.35 ppm in the product has a relative integral of approximately 3 which aligns with this prediction. The alkyl signals present at 4.71 (OCH_2) , 2.29 (CH_2) and 1.35 (CH_3) ppm are as expected. There are some impurities present at 4.00 and 1.70 ppm that do not correlate with residual solvent. The water peak at 3.3 ppm is much broader than expected. There is a general downfield shift of resonances of the Mn(I) complex with respect to the free ligand as shown in **Figure 4.43**. There is strong evidence for the formation of [$Mn(CO)_3$(**2.7**)Br]. However, further analysis was not possible due to degradation of the product.

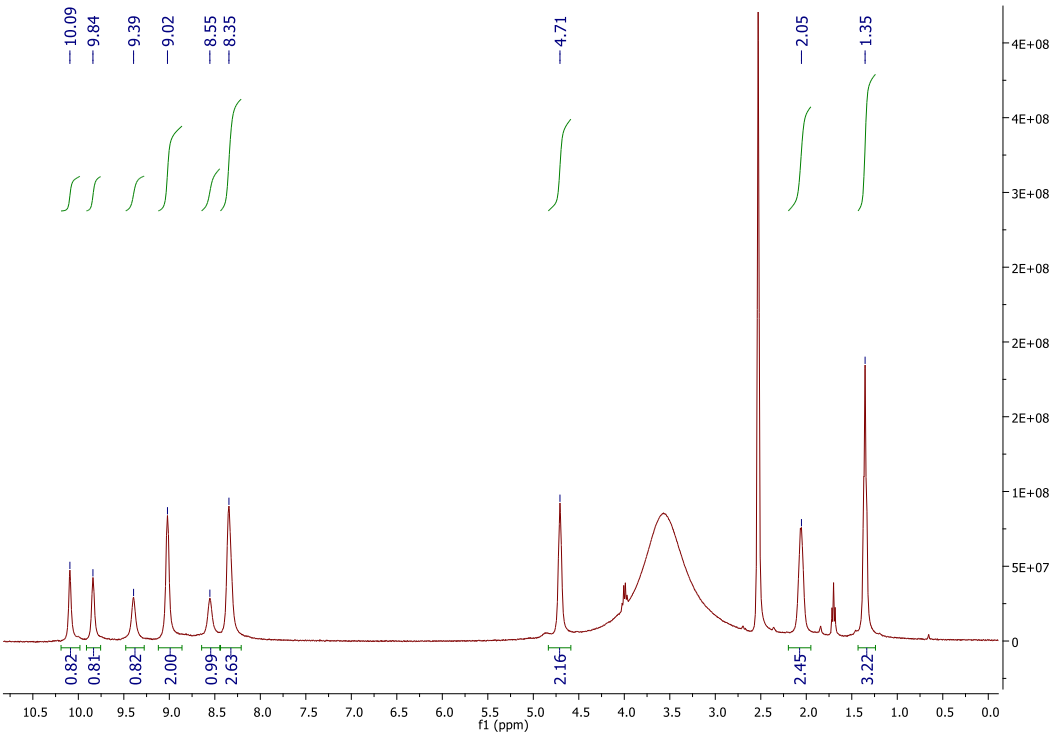

Figure 4.42: ^{1}H NMR spectrum of product obtained from the reaction between $Mn(CO)_5$ and PPP (**2.7**).

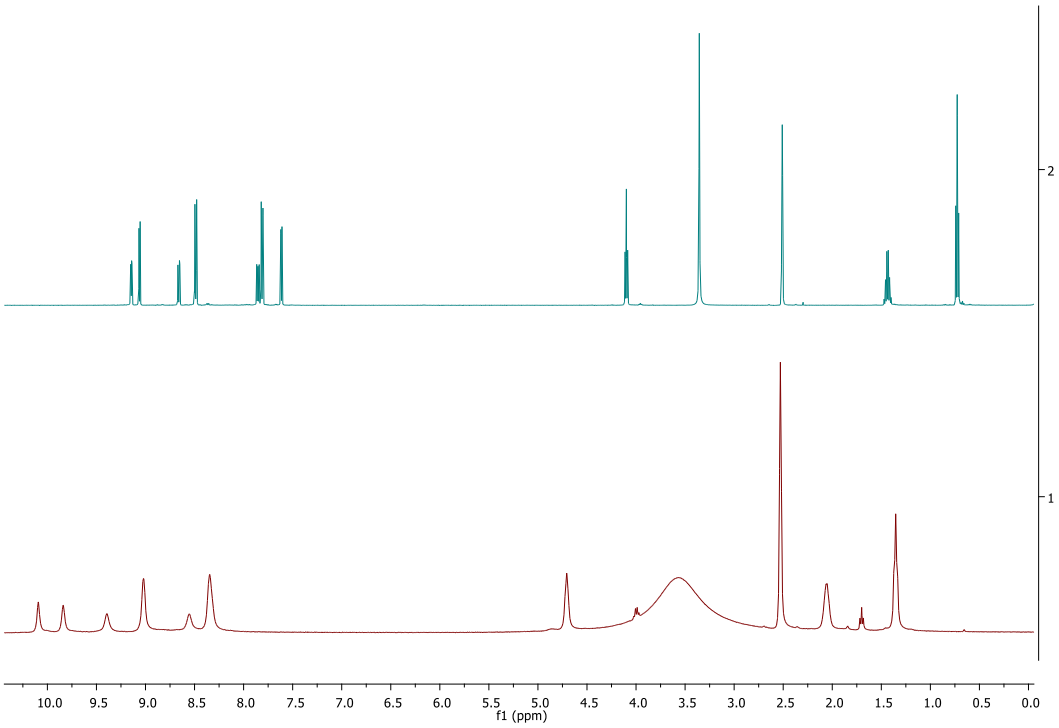

Figure 4.43: Comparison of ^{1}H NMR spectra of PPP (**2.7**) (blue) and the product obtained from the reaction between $Mn(CO)_5$ and PPP (**2.7**) (red)

IR data for [$Mn(CO)_3$(**2.2**)Br] and [$Mn(CO)_3$(**2.7**)Br] and proton NMR data for [$Mn(CO)_3$(**2.7**)Br] were consistent with the formation of the desired products. However, without full characterisation data, formation could not be confirmed. It is hoped that future work on this can refine the synthetic and purification methods to obtain samples that can be fully characterised. Appropriate handling and storage methods will need to be determined. Upon successful synthesis of products [$Mn(CO)_3$(**2.2**)Br] and [$Mn(CO)_3$(**2.7**)Br], it is hoped that their photophysical and photochemical properties can be probed. It is anticipated that the labile nature of the Mn-CO may lead to effective photo-induced CO release. Future goals include antimicrobial and anticancer testing of the targeted manganese complexes in the presence and absence of UV light.

4.7 Conclusion

This research aimed to establish a novel family of Re(I) tricarbonyl complexes of derivatised phen ligands, namely the Re(I) phen-oxazine complexes (**4.1 – 4.4**) and Re(I) phen-pyrido complexes (**4.5 – 4.8**) with potential as photoactivated CORMs. Complexes **4.1 – 4.4** were successfully synthesised and purified. Characterisation was carried out using NMR, IR and UV/vis spectroscopy, HRMS and HPLC analysis and x-ray crystallography. ^{1}H and ^{13}C NMR data revealed duplication of signals and more complex multiplicities than expected for the Re(I) phen-oxazine complexes **4.1 – 4.4** proposing they exist as a pair of diastereomers: HPLC data is consistent with this suggestion. In all cases IR data showed two intense Re-CO bands in the region of 2020 - 1800 $cm^{-1,}$ which are consistent with the formation of *fac* isomers. The UV spectra of the complexes exhibit a band with a λmax at *ca*. 390 nm in DMSO and it is proposed this band arises from a MLCT transition. Data from high resolution mass spectrometry was consistent with the formation of the desired complexes. X-ray crystallography conducted on RePPO (**4.2**) confirmed the structure. The complexes exist as the *fac* isomer in a distorted octahedral geometry.

The Re(I) phen-pyrido family **4.5 – 4.8** were successfully synthesised and purified. The complexes were characterised using NMR, IR and UV/vis spectroscopy, HRMS and x-ray crystallography. ^{1}H NMR signals of the complexes were generally shifted downfield compared to the free ligand. High chemical shift signals between 185 - 197 ppm in the ^{13}C NMR data was also consistent with formation of new complexes containing carbonyl ligands. IR data similarly presented a pair of intense metal carbonyl signals between 2010 - 1880 cm^{-1}. UV-vis spectroscopy revealed an intense absorption band centred at ca. 370 nm, assigned as a MLCT band. A second less intense MLCT band is observed at the longer wavelength of ~490 nm. Solvatochromism of this band was also evident for the phen-pyrido complexes **4.5** – **4.8**. HRMS analysis was consistent with the formation of each complex. X-ray crystallography confirmed RePPP (**4.7**) formed as the *fac* isomer.

Having successfully synthesised and characterised Re(I) complexes **4.1 – 4.8**, their photophysical and photochemical properties were investigated. The simple complex

[$Re(CO)_3$(phen)Br] (**4a**) was found to produce low intensity luminescence. However, none of the novel complexes **4.1 – 4.8** were luminescent.

Photochemical studies of a sample group of Re(I) complexes **4a**, **4b** and **4.1 – 4.8** revealed promising activity observed using UV-vis spectroscopy. Irradiation of solutions of each complex resulted in a decrease in the λ_{max} band and emergence of a new band at a longer wavelength over time. One or more isosbestic points were observed which is indicative of a straightforward photochemical reaction in which reactants are converted to products without formation of significant intermediates or side reactions. The data was initially thought to be consistent with photo-induced CO release. However, myoglobin assays revealed CO release could not be confirmed as the photochemical reaction mechanism.

Electrochemical studies by means of cyclic voltammetry were conducted on a series of the Re(I) complexes **4.1 – 4.8.** Redox behaviour was apparent for all complexes. The phen-pyrido complexes (**4.5 – 4.8**) were found to undergo more redox processes than the phen-oxazine complexes. The $Re^{I/II}$ oxidation for all complexes was found to occur between 1.30 – 1.50 V vs SCE. The various redox couples occurring between -1.30 – 0.55 V vs SCE were determined to be ligand-associated.

Synthesis of analogous Mn(I) complexes of PPO (**2.2**) and PPP (**4.7**) was attempted. Formation of [$Mn(CO)_3$(**2.2**)Br] and [$Mn(CO)_3$(**2.7**)Br] was apparent when analysed using preliminary spectroscopic analysis. However, further analytical data could not be obtained therefore, the Mn(I) complexes could not be confirmed. It is proposed that the complexes were formed but subsequently decomposed due to issues with their stability.

This chapter has presented a detailed insight into the synthesis, characterisation and properties of the novel Re(I) tricarbonyl diimine complexes **4.1 – 4.8**. The complexes exhibit promising photochemical and electrochemical behaviour. The biological activity of complexes **4.1 – 4.8** will be examined in Chapter 5.

Chapter 5

Antimicrobial and Anticancer Activity of Novel Re(I) Tricarbonyl Phenanthroline Complexes 4.1 – 4.8

Compound Structures and Codes for Chapter 5

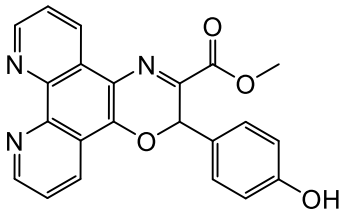

MPO (**2.1**)

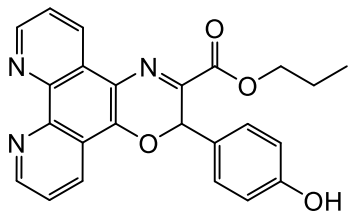

PPO (**2.2**)

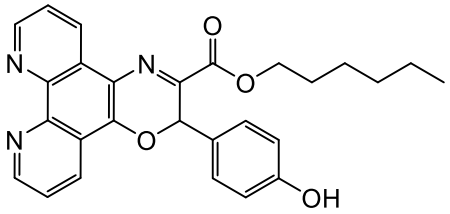

HPO (**2.3**)

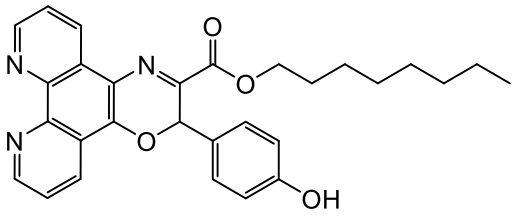

OPO (**2.4**)

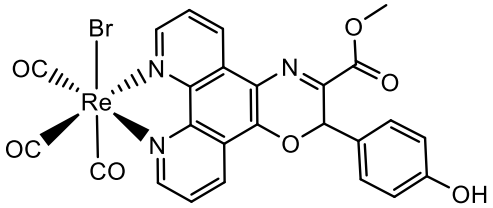

ReMPO (**4.1**)

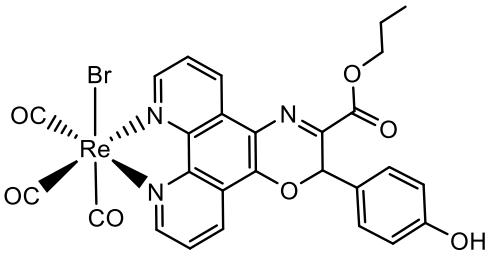

RePPO (**4.2**)

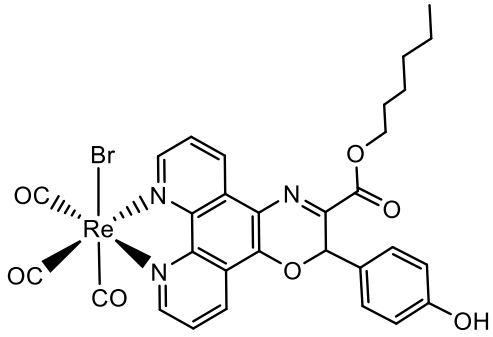

ReHPO (**4.3**)

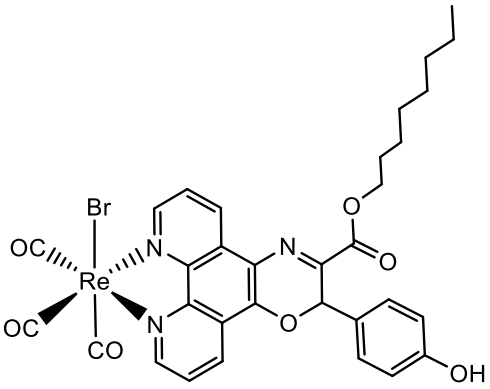

ReOPO (**4.4**)

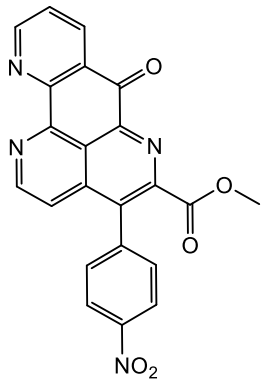

MPP (**2.5**)

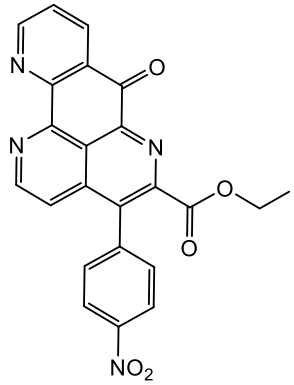

EPP (**2.6**)

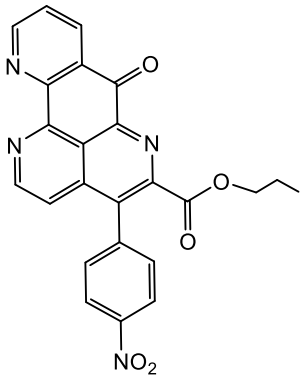

PPP (**2.7**)

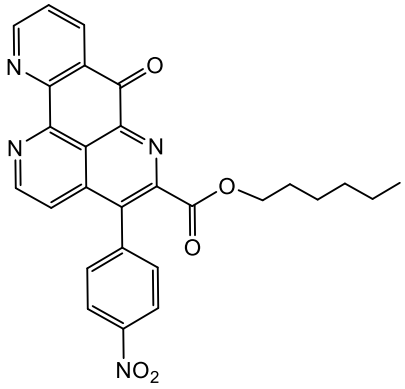

HPP (**2.8**)

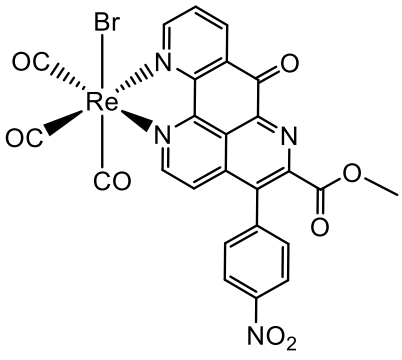

ReMPP (**4.5**)

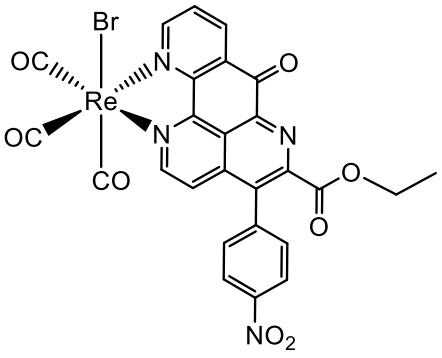

ReEPP (**4.6**)

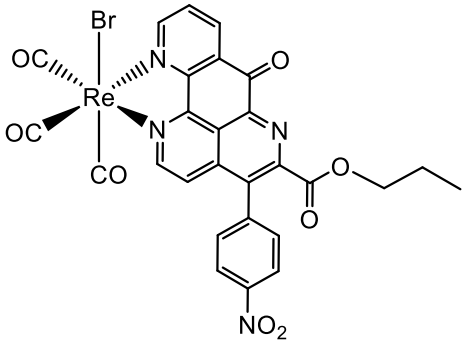

RePPP (**4.7**)

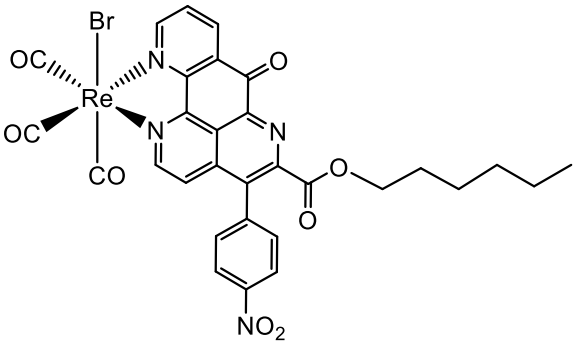

ReHPP (**4.8**)

5.1 Introduction

Antimicrobial resistance has become a leading global health threat. This is largely due to the 'antibiotic era' which has seen the exponential use and overuse of antibiotics since their discovery. Antimicrobial agents have become increasingly ineffective due to bacteria, fungi and viruses developing resistance to standard treatments. Resistance can lead to severe and even recurring infections resulting in higher rates of morbidity and mortality in patients.[8] This greatly impacts routine surgeries, c-sections, patients receiving chemotherapy and immunocompromised individuals.[97] The three main classes of antibiotics; tyrothricin, penicillin and actinomycin were discovered between 1939 - 1940. Since their discovery, there was rapid development of over 30 types of antimicrobial agents.[258] However, there has been little development of novel antimicrobial agents since the late 1980's.[96] Microbial resistance became apparent in the 1960's and 1970's with the emergence of multiple resistant microbial strains of *S. aureus* (MRSA) and *Neisseria gonorrhoeae*, *Haemophilus influenzae* and *E. coli*.[259] In 2015, the *mcr-1* gene in bacteria was discovered to contribute to high levels of resistance towards antibiotics known as polymyxins. Until 2015, polymyxins were the only class of antibiotics that had not succumbed to resistance.[260] To date, there has been little diversity in the cellular targets of known antibiotics which contributes to development of resistance.[8] There is now a critical need to develop novel, multi-modal antimicrobial agents to overcome this global crisis.

Cancer is another leading cause of death globally with over 10 million deaths recorded in 2020.[261] In Ireland, cancer accounts for 30% of deaths each year.[262] Breast, lung, colon and prostate cancers are among the most common cancers to be diagnosed.[263] Gynaecological cancers account for over 30% of cancer-related deaths amongst women.[264] Gynaecological malignancies are amongst those with the worst prognosis as they are generally detected at advanced stages which leads to high rates of drug resistance, relapse and metastasis.[265] First-line treatments include surgical resection and treatment with platinum-based therapeutics. Despite this, there is still a 70% chance of relapse for ovarian cancer patients.[266] Cancer treatment relies heavily on the use of platinum-based therapeutics. Cisplatin is the most widely used

as a first-line treatment for many cancers.[267] Although patients have an 80% response rate to cisplatin, the treatment comes with two major obstacles: toxicity and resistance.[267] Cisplatin is well known for its severe side effects which include nausea, vomiting, hair loss, urinary problems and muscle pain and weakness (as a result of peripheral neuropathy).[268] Cisplatin analogues, carboplatin and oxaliplatin were developed to reduce these toxic side effects. Chemotherapeutic treatment of ovarian cancer uses a combination of carboplatin and paclitaxel for patients at an advanced stage of disease.[269] While carboplatin and oxaliplatin have succeeded in reducing severe chemotherapy side effects, the challenge of chemo-resistance remains.

Given the significant downsides to platinum-based anticancer agents, there has been huge interest in the last few decades into finding novel therapies that incorporate other transition metals. Complexes of group 7 and 8 transition metals have come to the forefront of anticancer research in recent decades. Novel therapeutics containing iron[270], ruthenium[271], and rhenium[125] are of particular interest. There has been increasing interest in Re(I) tricarbonyl complexes due to their low *in vivo* toxicity[272], antibacterial[125] and anticancer[125, 273] properties. The Re(I) tricarbonyl core has been widely utilised in the development of agents to treat ovarian cancer *in vivo.*[131, 135, 274] We therefore sought to synthesise a family of novel Re(I) tricarbonyl phenanthroline complexes as potentially novel antimicrobial and anticancer agents with unique modes of action.

This chapter will discuss the antimicrobial screening of free phen-oxazine ligands **2.1 – 2.4**, phen-pyrido ligands **2.5 – 2.8** and Re(I) complexes **4.1 – 4.4** against *S. aureus*, MRSA, *E. coli* and *C. albicans*. Assessment of the *in vivo* toxicity of RePPO (**4.2**) and RePPP (**4.7**) against *G. mellonella* will be presented. Anticancer screening of ligands PPO (**2.2**), PPP (**2.7**) and complexes RePPO (**4.2**) and RePPP (**4.7**) against PEO1 and PEO4 ovarian cancer cell line will be discussed. The ability of these compounds to induce apoptosis against the PEO1 and PEO4 cell lines will also be presented.

5.2 *In vitro* Antimicrobial Testing of Ligands 2.1 – 2.8 and Re(I) Complexes 4.1 – 4.8

5.2.1 Antibacterial Testing of Ligands 2.1 – 2.8 and Complexes 4.1 – 4.8 against *S. aureus*, MRSA and *E. coli*

The antibacterial activity of phen-oxazine ligands **2.1 – 2.4**, phen-pyrido ligand **2.5 – 2.8** and their respective Re(I) complexes **4.1 - 4.4** and **4.5 – 4.8** was assessed. *In vitro* activity of the compounds against gram-positive bacteria, *S. aureus* and its highly resistant strain, MRSA was determined. Antibacterial testing against gram-negative bacteria, *E. coli* was also conducted. The activity of the free ligands **2.1 – 2.8** was compared to that of the Re(I) complexes.

Cultures of each bacterial strain were prepared as described in **section 2.4.2**. Briefly, a single plate colony was added to 50 mL of fresh nutrient broth media. The culture was incubated at 37 °C in an orbital shaker overnight. It was noted that MRSA required at least 24 h to culture. DMSO stock solutions of all compounds **2.1 – 2.8** and **4.1 – 4.8** were prepared at a concentration of 120 µM. *In vitro* susceptibility assays were set up as previously described in **section 2.4.3**. In initial runs, the concentration of each test compound ranged from 30 – 3.75 µM on the 96-well plates. Very active compounds were subsequently diluted down to a concentration 0.11 µM. The statistical significance was determined in relation to that observed with the control sample (5% DMSO in media). Highly significant data had a P-value of <0.0001 while moderately significant data were those with $0.0001 < P < 0.01$.[194]

5.2.1.1 *In vitro* Activity of Ligands 2.1 – 2.8 and Re(I) Complexes 4.1 – 4.8 against *S. aureus*

The results for the investigations of the ligands **2.1 - 2.8** (at concentrations of 30 – 3.75 µM) against a gram-positive bacteria, *S. aureus,* are shown in **Figure 5.1**. All of the phen-oxazine ligands had some antibacterial activity against *S. aureus*. The activity of the propyl, hexyl and octyl phen-oxazines **2.2 – 2.4** was statistically

significant at 30 µM. HPO (**2.3**) and OPO (**2.4**) were the most active members of this family; statistically significant activity was maintained even at 7.5 µM.

The data was plotted to determine MIC_{50} for the family. MPO (**2.1**) was too inactive at the concentration range tested to determine the MIC_{50}. PPO (**2.3**) and OPO (**2.4**) were determined to have MIC_{50} values of 22.9 and 4.1 µM respectively. HPO (**2.3**) was too active in the concentration range tested to determine the MIC_{50} but it is evidently less than 3.75 µM. As discussed above in **section 3.2.2.2**, the increasing lipophilicity of the ester side chain of the phen-oxazine ligands may be the structural feature that is responsible for increasing their activity. The ligands here show that changes in the length of the alkyl chain and hence the lipophilicity does have an effect on their level of activity against *S. aureus*. Activity increases in the order R = Me, to, propyl to hexyl and then drops down when R = octyl.

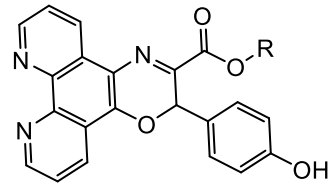

Ligand	MIC_{50} (µM)
MPO (2.1)	> 30
PPO (2.2)	22.9
HPO (2.3)	< 3.75
OPO (2.4)	4.1

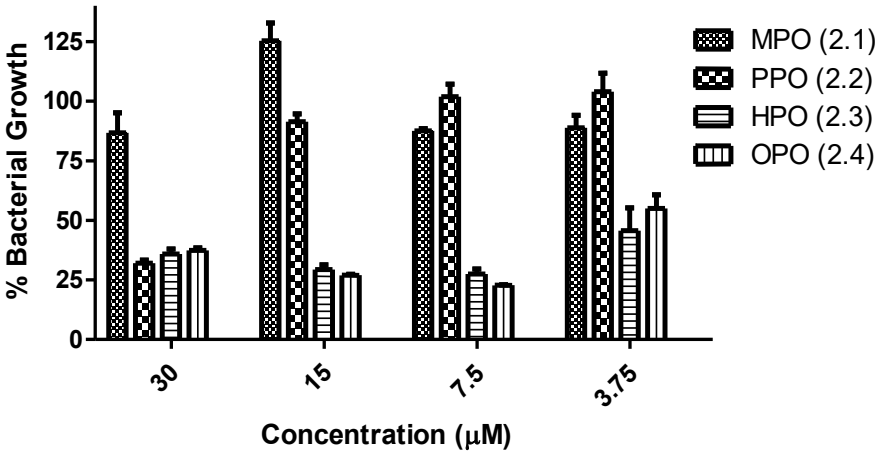

Figure 5.1: *In vitro* inhibitory effects of phen-oxazine ligands **2.1 – 2.4** across the range 30 – 3.75 µM against *S. aureus* after incubation for 24 h in nutrient broth media (where R = methyl, propyl, hexyl or octyl).

The Re(I) phen-oxazine compounds **4.1 - 4.4** (**Figure 5.2**) were moderately active against *S. aureus*. ReMPO (**4.1**) and RePPO (**4.2**) were more active than the free phen-oxazine ligands MPO (**2.1**) and PPO (**2.2**) respectively. Relative to the control, the activity of ReMPO (**4.1**) and RePPO (**4.2**) were highly statistically significant at the highest dose of 30 µM. RePPO (**4.2**) was determined to be moderately statistically significant from 15 – 3.75 µM. RePPO (**4.2**) was determined as the most active of the family with an MIC_{50} of 14.7 µM. Conversely, ReHPO (**4.3**) and ReOPO (**4.4**) were much less active their associated free ligands HPO (**2.3**) and OPO (**2.4**). It is noted that ReOPO (**4.4**) was the least active. ReOPO (**4.4**) was too inactive in the concentration range tested to determine the MIC_{50}. It is interesting to note that the most active free ligands yield the least active Re complexes.

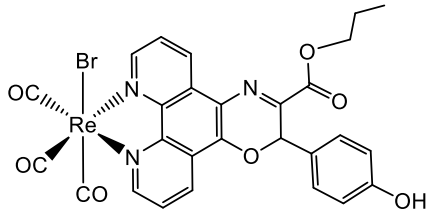

Complex	MIC_{50} (µM)
ReMPO (4.1)	28.9
RePPO (4.2)	14.7
ReHPO (4.3)	28.5
ReOPO (4.4)	> 30

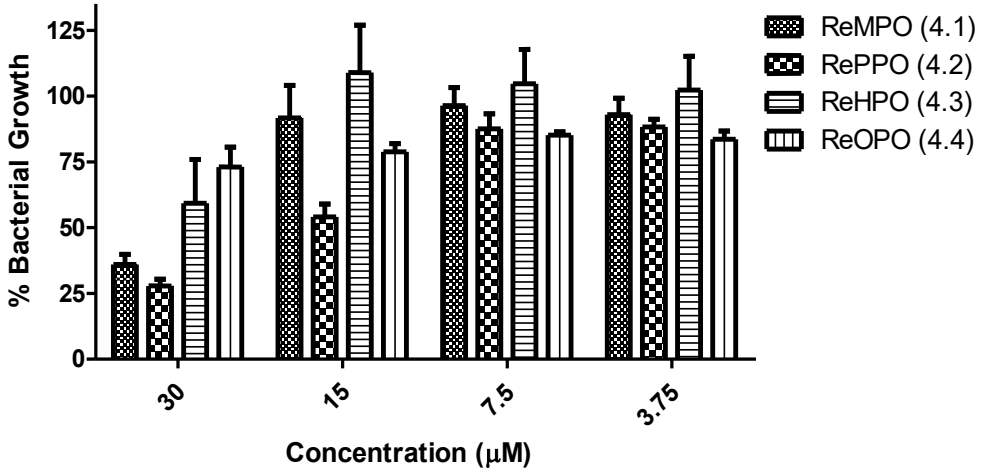

Figure 5.2: *In vitro* inhibitory effects of Re(I) phen-oxazine complexes **4.1 – 4.4** across the range 30 – 3.75 µM against *S. aureus* after incubation for 24 h in nutrient broth media (where R = methyl, propyl, hexyl or octyl).

The antibacterial activity of the free phen-pyrido ligands **2.5 – 2.8** are shown in **Figure 5.3.** The phen-pyrido ligands had a much greater ability to limit *S. aureus* growth compared to the free and coordinated phen-oxazine ligands. All ligands **2.5 – 2.8** had the ability to hold bacterial growth below 20% at concentrations as low as 0.46 µM. High statistical significance was determined for all phen-pyrido ligands at all concentrations tested relative to the control. Due to the similar activity of all the ligands at all of the concentrations studied it was not possible to determine if there was any structure activity relationship. The ligands were too active at the concentrations tested to determine the MIC_{50} values.

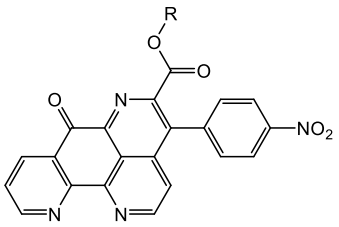

Ligand	MIC_{50} (µM)
MPP (2.5)	< 0.11
EPP (2.6)	< 0.11
PPP (2.7)	< 0.11
HPP (2.8)	< 0.11

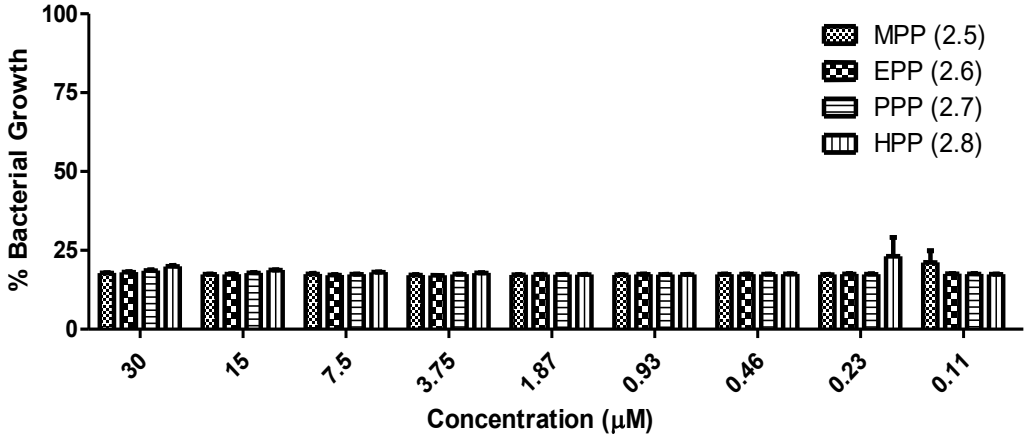

Figure 5.3: *In vitro* inhibitory effects of phen-pyrido ligands **2.5 – 2.8** across the range 30 – 0.11 µM against *S. aureus* after incubation for 24 h in nutrient broth media (where R = methyl, ethyl propyl or hexyl).

The inhibitory effects against *S. aureus* of the Re(I) phen-pyrido complexes **4.5 – 4.8** are presented in **Figure 5.4**. ReHPP (**4.8**), was the least active, and it was not studied at doses below 3.75 µM as no activity was observed at this concentration. Complexes **4.5 – 4.7** with methyl, ethyl and propyl ester side chains, maintained good activity at concentrations down to 0.46 µM with about 20% bacterial growth observed

compared to the control. MIC_{50} values were determined to be 0.38 µM (**4.5**), 0.21 µM (**4.6**), 0.17 µM (**4.7**) and 28.5 µM (**4.8**). High statistical significance was observed for **4.5 – 4.7** at doses of 30 – 0.23 µM. RePPP (**4.7**) was the most active of the family with an ability to substantially inhibit bacterial growth at concentrations as low as 0.23 µM.

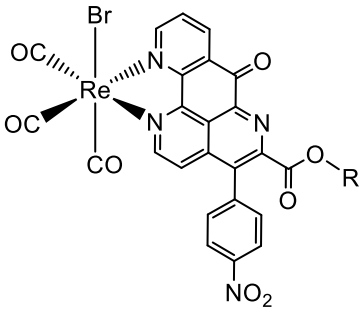

Complex	MIC_{50} (µM)
ReMPP (4.5)	0.38
ReEPP (4.6)	0.21
RePPP (4.7)	0.17
ReHPP (4.8)	28.5

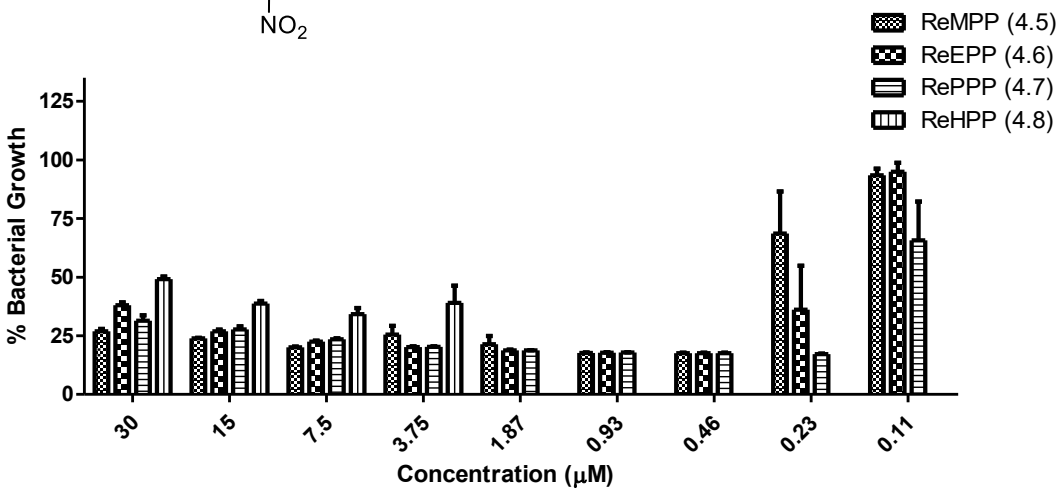

Figure 5.4: *In vitro* inhibitory effects of Re(I) phen-pyrido complexes **4.5 – 4.8** across the range 30 – 0.11 µM against *S. aureus* after incubation for 24 h in nutrient broth media (where R = methyl, ethyl propyl or hexyl).

The antibacterial screening of ligands **2.1 – 2.8** and the Re(I) complexes **4.1 – 4.8** against *S. aureus* revealed that the most active family were the uncoordinated phen-pyrido ligands **2.5 – 2.8**. This family of ligands were all equally active at the concentrations tested. Re(I) phen-pyrido complexes **4.5 – 4.7** also had good activity at does as low as 0.46 µM. It was also noteworthy that the Re(I) complexes of both ligand families were, in general, less active than the uncoordinated ligands. This was particularly evident for the ReHPO (**4.3**) and ReOPO (**4.4**). The most notable activity therefore is of the phen-pyrido ligands which produced MIC_{50} values of <0.11 µM and the Re(I) phen-pyrido complexes 4.1 – 4.3 which had MIC_{50} values between 0.17 –

0.38 μM. The most common clinical antibiotics are streptomycin, tetracycline and vancomycin which have MIC_{50} values of 10, 6 and 2 μM respectively.[176] It is evident that compounds **2.5 – 2.8** and **4.1 – 4.3** are far more potent than the standard antibacterial treatments. *S. aureus* is one of the key pathogens that contributes to AMR. It is included in the group of ESKAPE pathogens for this reason. Therefore, it is encouraging to find a novel class of compounds like the phen-pyrido ligands that have much greater ability to curtail *S. aureus* growth compared to clinical antibiotics.

5.2.1.2 *In vitro* Activity of Ligands 2.1 – 2.8 and Re(I) Complexes 4.1 – 4.8 against MRSA

Methicillin-resistant *Staphylococcus aureus* (MRSA) is a highly resistant strain of *S. aureus*. MRSA is classed as a multi-drug resistant (MDR) strain. MDR species are those which cannot be treated with three or more types of antibacterial agents.[8] MRSA is particularly prevalent in hospital and nursing home settings. Vancomycin is the current antibiotic prescribed for MRSA infections. As anticipated, there has already been cases of vancomycin-resistant *S. aureus* reported.[275]

Antibacterial testing against the multi-resistant bacterial strain MRSA was conducted in the same manner as described for *S. aureus*. Initially, all compounds were tested in the concentration range of 30 – 3.75 μM, more active compounds were subsequently tested at concentrations down to 0.11 μM to capture the MIC_{50}. The antibacterial activity of ligands **2.1 – 2.4** is presented in **Figure 5.5**. MPO (**2.1**) and had very little activity against MRSA with 88% growth observed at the highest concentration tested (30 μM). PPO (**2.2**) was also minimally active with the 30 μM dose resulting in 29% growth. The lower 15 μM dose only reduced growth to 83%. The most lipophilic members, HPO (**2.3**) and OPO (**2.4**) were the most active, with statistically significant growth control at all concentrations. Both HPO (**2.3**) and OPO (**2.4**) maintained growth below 30% down to 7.5 μM dosages. There is clearly a correlation between the lipophilicity of the ligands and the activity against MRSA. The MIC_{50} could only be

determined for PPO (**2.2**) and was 24.1 µM; for both HPO and OPO it falls below 3.75 µM.

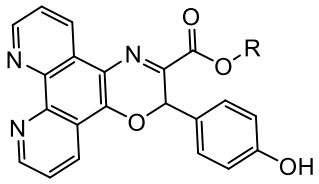

Ligand	MIC_{50} (µM)
MPO (2.1)	> 30
PPO (2.2)	24.1
HPO (2.3)	< 3.75
OPO (2.4)	< 3.75

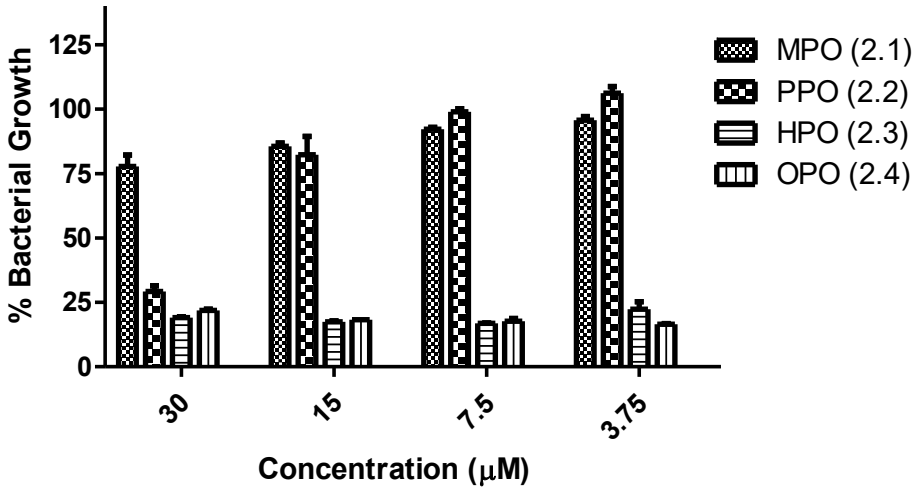

Figure 5.5: *In vitro* inhibitory effects of phen-oxazine ligands **2.1 – 2.4** across the range 30 – 3.75 µM against MRSA after incubation for 24 h in nutrient broth media (where R = methyl, propyl, hexyl, octyl).

The Re(I) phen-oxazine complexes, **4.1 – 4.4** are overall less effective against MRSA compared to the free ligands (**Figure 5.6**). Re(I) complexes **4.2 – 4.4** hold bacterial growth below 26% at the 30 µM dose which is highly statistically significant. This increases to above 50% growth at the lower dose of 15 µM. The family has limited activity at 7.5 µM and below. It is evident that the phen-oxazine complexes have much less MRSA inhibition compared to the uncoordinated ligands. MIC_{50} values were determined for RePPO (**4.2**), ReHPO (**4.3**) and ReOPO (**4.4**) as 16.5, 19.3 and 23.3 µM respectively.

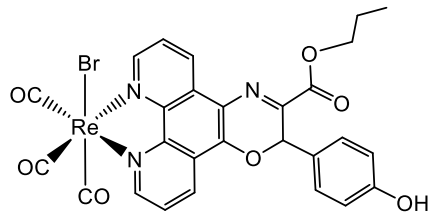

Complex	MIC_{50} (μM)
ReMPO (4.1)	> 30
RePPO (4.2)	16.5
ReHPO (4.3)	19.3
ReOPO (4.4)	23.3

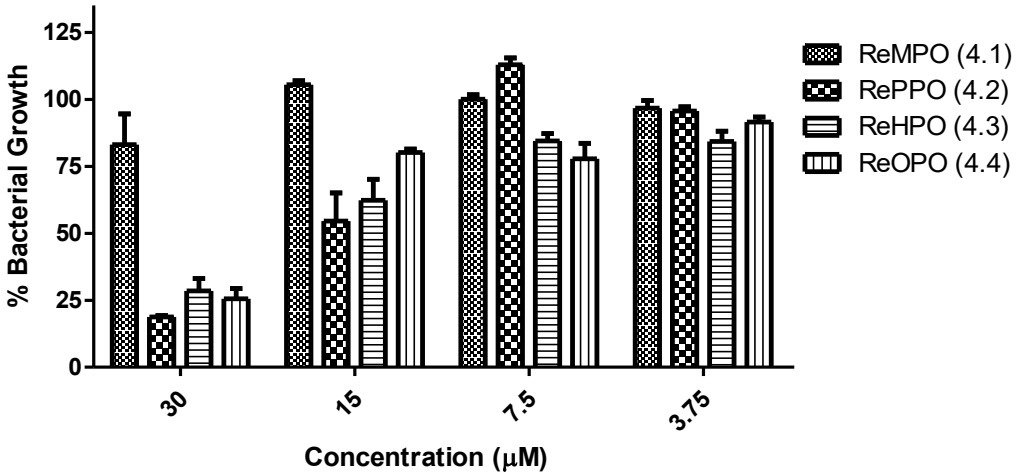

Figure 5.6: *In vitro* inhibitory effects of Re(I) phen-oxazine complexes **4.1 – 4.4** across the range 30 – 3.75 μM against MRSA after incubation for 24 h in nutrient broth media (where R = methyl, propyl, hexyl, octyl).

The phen-pyrido family **2.5 – 2.8** appear to be the most active out of the compounds tested against MRSA (**Figure 5.7**). The ligands **2.5 – 2.7** have the ability to hold bacterial growth below 25% at a dose as low as 0.93 μM. More lipophilic ligands **2.6** and **2.7** are highly active across the range of concentrations tested; they show highly statistically significant activity even at the lowest concentrations. The least lipophilic ligand, MPP (**2.5**) significantly loses activity below 0.46 μM. The MIC_{50} of MPP (**2.5**) is determined to be 0.36 μM. The other phen-pyrido ligands **2.6 – 2.8** were too active in the concentration range tested to determine their MIC_{50} but these values are below 0.11 μM in all cases.

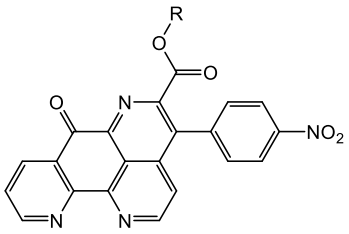

Ligand	MIC_{50} (μM)
MPP (2.5)	0.36
EPP (2.6)	< 0.11
PPP (2.7)	< 0.11
HPP (2.8)	< 0.11

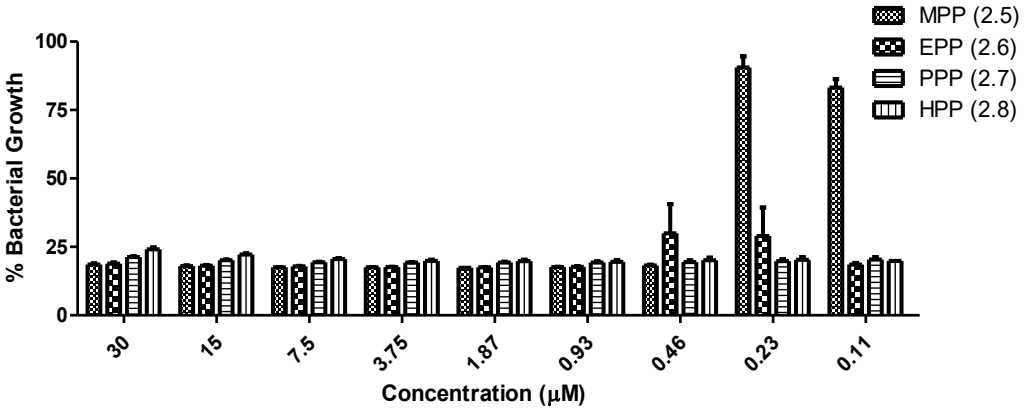

Figure 5.7: *In vitro* inhibitory effects of phen-pyrido ligands **2.5 – 2.8** across the range 30 – 0.11 μM against MRSA after incubation for 24 h in nutrient broth media (where R = methyl, ethyl, propyl, hexyl).

The antibacterial activity of complexes **4.5 – 4.8** against MRSA is shown in **Figure 5.8**. It is clear that these phen-pyrido complexes are much less active than their corresponding free ligands. Bacterial growth is held between 20 – 60% for **4.5 – 4.7** in the range 30 – 0.93 μM. All complexes have limited activity below 0.46 μM. MIC_{50} values were calculated to be 2.2 μM (**4.5**), 0.75 μM (**4.6**), 0.72 μM (**4.7**) and 7.6 μM (**4.8**). As for the results for *S. aureus* (**Figure 5.4**), there is a similar trend in the activity of the family with ReHPP (**4.8**) being the least active against MRSA.

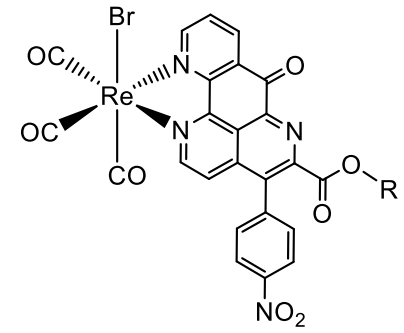

Complex	MIC_{50} (μM)
ReMPP (4.5)	ND
ReEPP (4.6)	ND
RePPP (4.7)	ND
ReHPP (4.8)	7.6

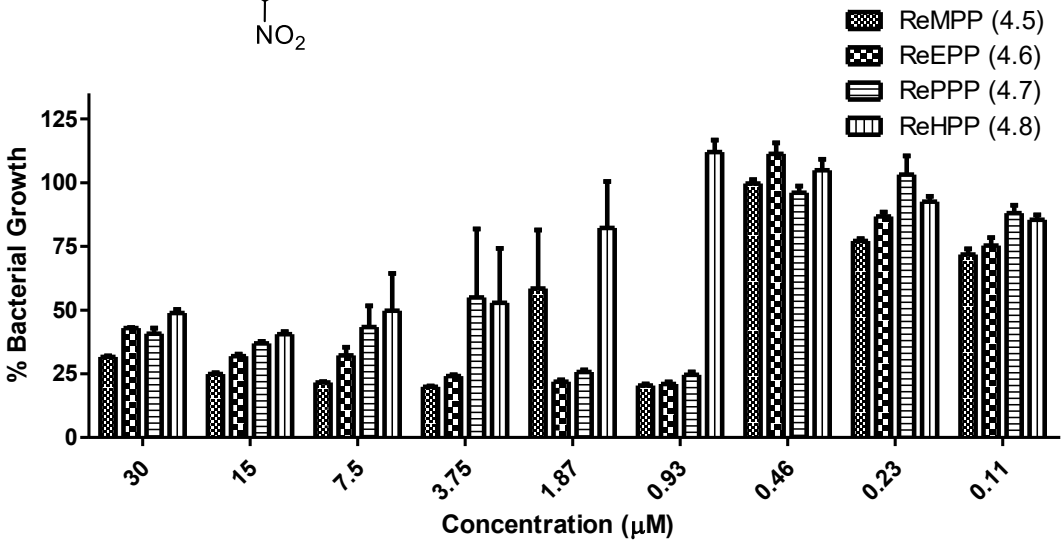

Figure 5.8: *In vitro* inhibitory effects of Re(I) phen-pyrido complexes **4.5 – 4.8** across the range 30 – 0.11 μM against MRSA after incubation for 24 h in nutrient broth media (where R = methyl, ethyl, propyl, hexyl). ND = not determined

The data presented in **Figures 5.5 – 5.8** demonstrates all compounds have some ability to inhibit the growth of MRSA. It is evident that, in general, uncoordinated phen-oxazine ligands exhibit better activity than their respective complexes. This is also the case for the uncoordinated phen-pyrido ligands **2.5 – 2.8**. The phen-pyrido ligands are clearly the most active out of all compounds tested against MRSA. Additionally, RePPP (**4.7**) holds activity to concentrations as low as 0.93 μM. Vancomycin is the antibiotic typically prescribed for MRSA infections. The MIC_{50} reported for vancomycin against MRSA is generally between 0.6 – 1.3 μM.[276] The novel phen-pyrido ligands, having MICs of <0.11 μM, appear to much more active than the standard treatment. Other treatments for MRSA infections include teicoplanin, linezolid and daptomycin which have MIC values that are much lower than vancomycin.[277] This would align the effectiveness of the phen-pyrido ligands

with these alternative treatments. These results are encouraging given the high resistance of MRSA.

Comparison of the antibacterial effects of the ligands shows that the activity against both *S. aureus* and MRSA is similar for the phen-oxazine and phen-pyrido families (**Table 5.1**). Similar values are also observed when the activity of the Re(I) complexes is compared between the two bacterial strains (**Table 5.2**).

Table 5.1: Comparison of the antibacterial activity of ligands **2.1 – 2.8** against *S. aureus* and MRSA

Ligand	**MIC_{50} (µM)**	
	S. aureus	MRSA
MPO (2.1)	> 30	> 30
PPO (2.2)	22.9	24.1
HPO (2.3)	< 3.75	< 3.75
OPO (2.4)	4.1	< 3.75
MPP (2.5)	< 0.11	0.36
EPP (2.6)	< 0.11	< 0.11
PPP (2.7)	< 0.11	< 0.11
HPP (2.8)	< 0.11	< 0.11

Table 5.2: Comparison of the antibacterial activity of Re(I) complexes **4.1 – 4.8** against *S. aureus* and MRSA

Complex	**MIC_{50} (µM)**	
	S. aureus	MRSA
ReMPO (4.1)	28.9	> 30
RePPO (4.2)	14.7	16.5
ReHPO (4.3)	28.5	19.3
ReOPO (4.4)	> 30	23.3
ReMPP (4.5)	0.38	ND
ReEPP (4.6)	0.21	ND
RePPP (4.7)	0.17	ND
ReHPP (4.8)	28.5	7.6

5.2.1.3 *In vitro* Activity of Ligands 2.1 – 2.8 and Re(I) Complexes 4.1 – 4.8 against *E. coli*

Gram-negative bacteria such as *E. coli* are usually more difficult to treat due to the presence of two cell membranes. Antibiotics therefore need to pass two lipid bilayers to enter the cell. Additionally, gram-negative bacteria often possess efflux pumps and other mechanisms that can expel antibiotics. *E. coli* is considered to have extensive drug resistance (XDR). XDR strains are those which are non-susceptible to all classes of antimicrobials. *E. coli* is a leading cause of urinary tract infections which can easily result in sepsis as a consequence of resistance to commonly prescribed drugs.[278]

Antibacterial testing against *E. coli* was carried out as described for *S. aureus* and MRSA. The phen-oxazine ligands **2.1 – 2.4** and all Re(I) complexes **4.1 – 4.8** were found to be inactive against *E. coli* at all doses tested (30 – 3.75 µM). Phen-pyrido ligands were minimally active against *E. coli* at the highest dose of 30 µM as seen in **Figure 5.9**. The inhibitory effects of **2.5 – 2.8** against *E. coli* were moderately statistically significant at 30 µM.

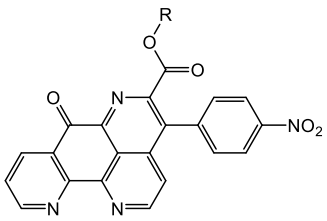

Ligand	MIC_{50} (μM)
MPP (2.5)	> 30
EPP (2.6)	> 30
PPP (2.7)	> 30
HPP (2.8)	> 30

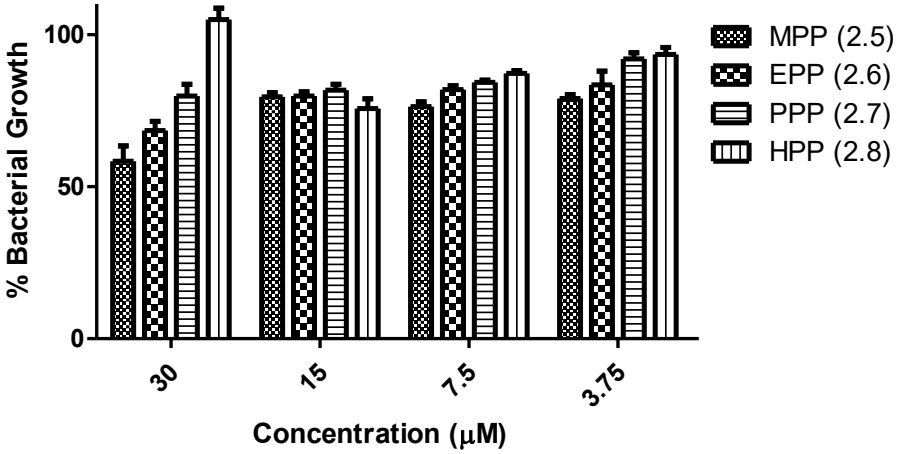

Figure 5.9: *In vitro* activity of phen-pyrido ligands **2.5 – 2.8** across the range 30 – 3.75 μM against *E. coli* after incubation for 24 h in nutrient broth media (where R = methyl, ethyl, propyl, hexyl).

These results are not surprising given that metal complexes of phen are known to be less effective against gram-negative bacteria. Cell permeability is much more difficult in gram-negative bacteria, largely due to the presence of two lipid membranes.[8, 36] *E. coli* is also capable of gaining resistant genes through horizontal gene transfer (HGT).[279] HGT involves acquiring genes from other organisms that contribute to multi-drug resistance.

5.2.2 *In vitro* Antifungal Activity of Ligands 2.1 – 2.8 and Re(I) Complexes 4.1 – 4.8 against *C. albicans*

Candida albicans is an opportunistic pathogenic yeast that can contribute to significant bloodstream infections. As discussed in Chapter 3, incidence of drug-resistant fungal infections have increased significantly in recent years. Ag(I) phen-oxazine complexes **3.1 – 3.3** exhibited significant antifungal activity against *C.*

albicans. Ligands **2.1 – 2.8** and Re(I) tricarbonyl complexes **4.1 – 4.8** were screened in a similar manner as described in **section 3.2.4**. Compounds **2.1 – 2.8** and **4.1 – 4.8** were assessed in the concentration range of 30 – 3.75 µM.

Phen-oxazine ligands **2.1 – 2.3** were previously assessed and the data are presented in **section 3.2.4**. These experiments were repeated, and antifungal assessment of these ligands is given in **Figure 5.10** and is consistent with that seen previously. Additionally, OPO (**2.4**) was tested; it was the most active of the family. This activity of OPO in the range 30 – 7.5 µM was found to be highly significant with respect to the control. An MIC_{50} of 8.1 µM was determined for OPO (**2.4**). As noted earlier, there is a clear correlation between lipophilicity and activity against *C. albicans*.

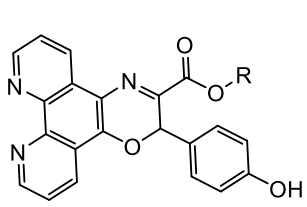

Ligand	MIC_{50} (µM)
MPO (2.1)	> 30
PPO (2.2)	23.3
HPO (2.3)	14.6
OPO (2.4)	8.2

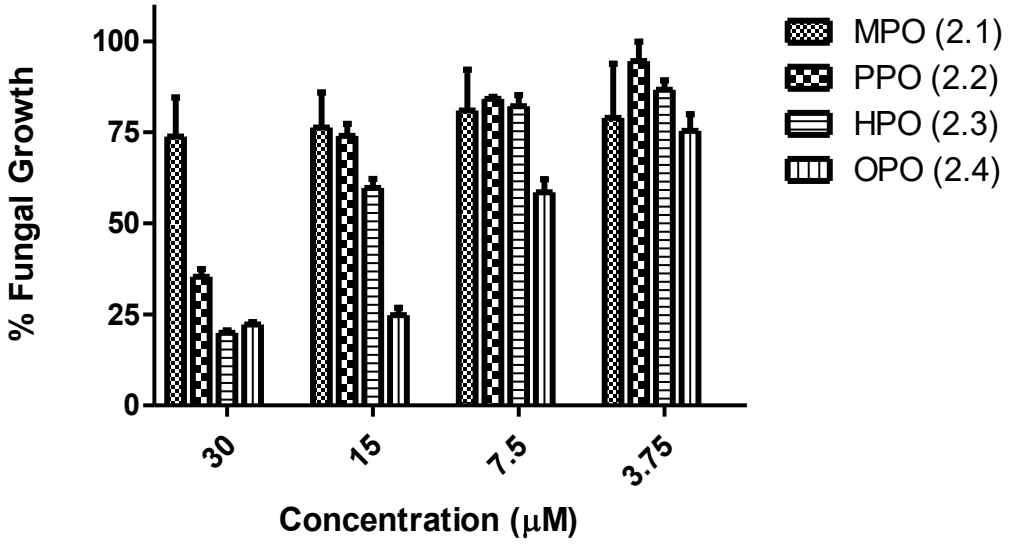

Figure 5.10: *In vitro* activity of phen-oxazine ligands **2.1 – 2.4** across the range 30 – 3.75 µM against *C. albicans* after incubation for 24 h in minimal media (where R = methyl, propyl, hexyl, octyl).

The Re(I) tricarbonyl complexes of the phen-oxazine ligands were much less active than the free ligands as seen in **Figure 5.11**. ReMPO (**4.1**) had limited activity at 30 µM. Complexes **4.2 – 4.4** displayed reasonable fungal growth inhibition at 30 µM. These data were moderately statistically significant. For all compounds, fungal growth increased to above 75% at the lower dose of 15 µM. Complexes are too inactive to allow any analysis of the impact of the length of the ester side chain. Relatively high MIC_{50} values of 24.8, 26.2 and 24.9 µM were determined for **4.2 – 4.4** respectively.

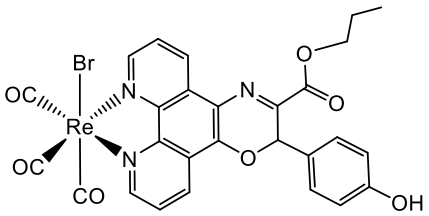

Complex	MIC_{50} (µM)
ReMPO (4.1)	> 30
RePPO (4.2)	24.8
ReHPO (4.3)	26.2
ReOPO (4.4)	24.9

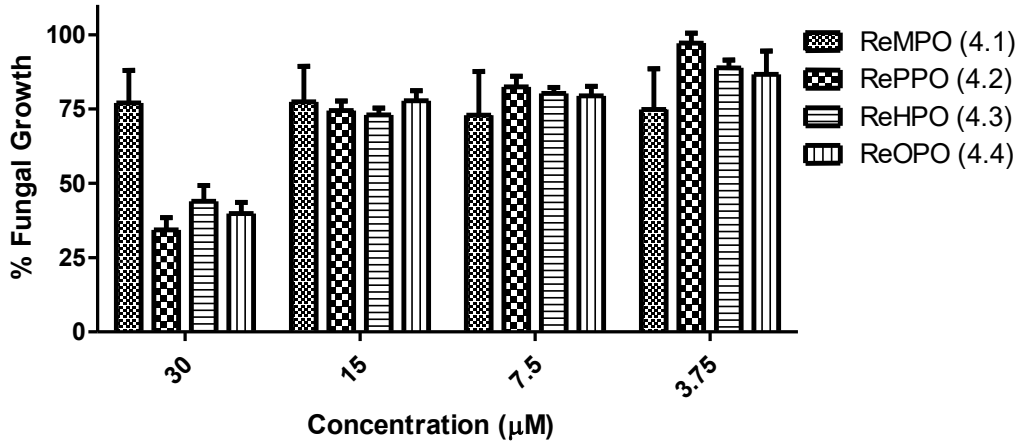

Figure 5.11: *In vitro* activity of Re(I) phen-oxazine complexes **4.1 – 4.4** across the range 30 – 3.75 µM against *C. albicans* after incubation for 24 h in minimal media (where R = methyl, propyl, hexyl, octyl).

Antifungal screening of phen-pyrido ligands **2.5 – 2.8** revealed a clear lipophilic effect on the activity against *C. albicans* as shown in **Figure 5.12**. MPP (**2.5**) and EPP (**2.6**) were moderately active with MIC_{50} values of 25.0 and 17.9 µM respectively. PPP (**2.7**) had good activity between 30 – 7.5 µM and an MIC_{50} of 6.2 µM. The most lipophilic member, HPP (**4.8**) had significant antifungal activity (an MIC_{50} could not be determined from the range of concentrations studied). Fungal growth was held below 10% down to 7.5 µM and below 20% at 3.75 µM.

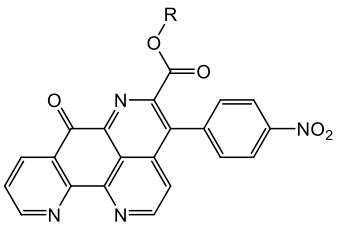

Ligand	MIC_{50} (μM)
MPP (2.5)	25.0
EPP (2.6)	17.9
PPP (2.7)	6.2
HPP (2.8)	< 3.75

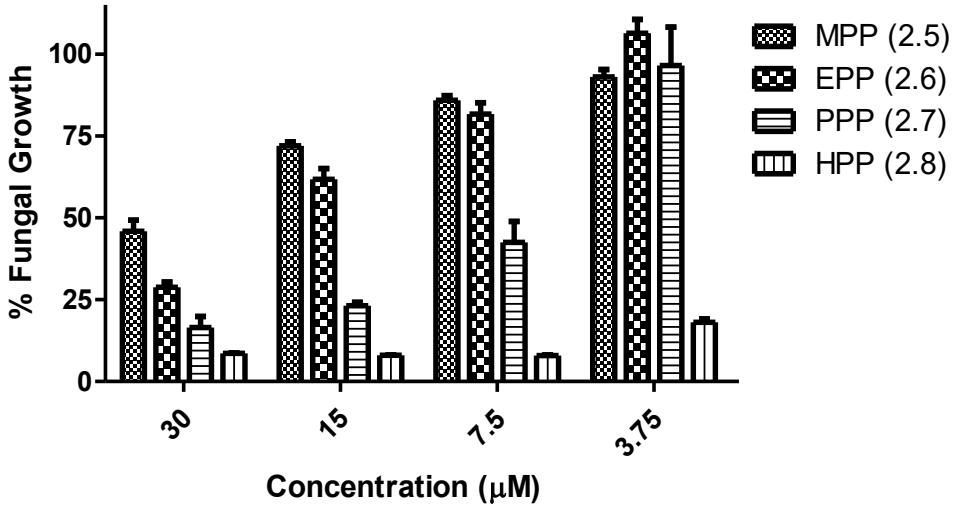

Figure 5.12: *In vitro* activity of phen-pyrido ligands **2.5 – 2.8** across the range 30 - 3.75 μM against *C. albicans* after incubation for 24 h in minimal media (where R = methyl, ethyl, propyl, hexyl).

With the exception of the methyl derivative, the Re(I) phen-pyrido complexes **4.5 – 4.8** were less active against *C. albicans* compared to the free ligands (**Figure 5.13**). ReHPP (**4.8**), the most active complex, held fungal growth at 11% at 30 μM, activity fell off rapidly and growth rose to 61% of the vehicle control for a 15 μM dose. Complexes **4.5 – 4.7** were less active than ReHPP (**4.8**) with fungal growth of between 35 – 40% at the highest dose, 30 μM. MIC_{50} values were determined to be 25.3 μM (**4.5**), 23.1 μM (**4.6**), 23.5 μM (**4.7**) and 18.0 μM (**4.8**).

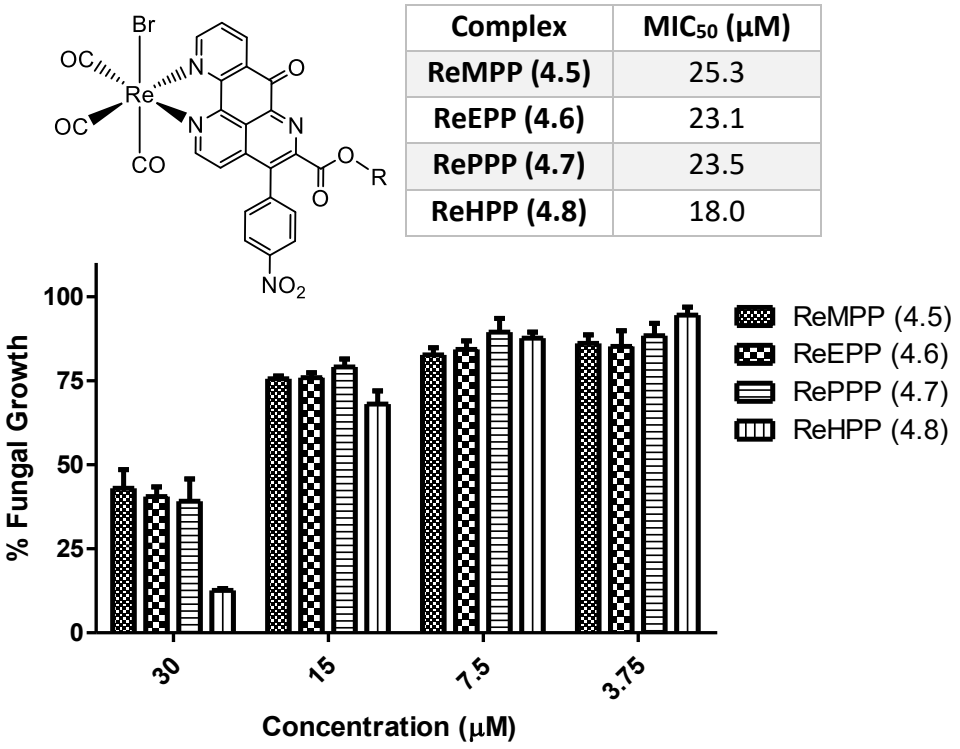

Complex	MIC_{50} (μM)
ReMPP (4.5)	25.3
ReEPP (4.6)	23.1
RePPP (4.7)	23.5
ReHPP (4.8)	18.0

Figure 5.13: *In vitro* activity of Re(I) complexes **4.5 – 4.8** across the range 30 - 3.75 μM against *C. albicans* after incubation for 24 h in minimal media (where R = methyl, ethyl, propyl, hexyl).

The antifungal activity of ligands **2.1 – 2.8** and Re(I) complexes **4.1 – 4.8** presented in **Figures 5.10 – 5.12** demonstrates, in most cases a decrease in activity upon complexation to Re(I). MPO (**2.1**) has limited activity (>75%) and PPO (**2.2**) has reasonable activity (34%) at 30 μM. HPO (**2.3**) and OPO (**2.4**) have better inhibitory effects with the latter being the most active. This decreases with complexation of phen-oxazine ligands to Re(I) where activity is only apparent at 30 μM. A similar decrease in activity upon complexation was observed for **4.6 – 4.8**. The phen-pyrido ligands PPP (**2.7**) and HPP (**2.8**) were the most active against *C. albicans* with MIC_{50} values of 6.2 μM and < 3.75 μM, their corresponding complexes **4.7** and **4.8** were found to have MIC_{50} values of 23.5 μM and 18.0 μM. Although the most active compounds PPP (**2.7**) and HPP (**2.8**) had low micromolar MIC values, they cannot compete with clinical treatment, amphotericin B which has a much lower MIC_{50} of 0.54 μM.

Biological screening of ligands **2.1 – 2.8** and their respective Re(I) complexes **4.1 – 4.8** against a variety of microbes yielded interesting results. Ligands **2.1 – 2.4** and complexes **4.1 – 4.8** were inactive against gram-negative *E. coli* growth while ligands **2.5 – 2.8** were minimally active (> 58% growth). It is evident from the data for *S. aureus*, MRSA and *C. albicans* that complexation of the phen-oxazine or phen-pyrido ligands to Re(I) generally reduces the inhibitory effects. Overall, phen-pyrido ligands **2.5 – 2.8** were found to have the greatest ability to curtail microbial growth. Ligands **2.5 - 2.8** and RePPP (**4.7**) were found to be most active against gram-positive *S. aureus* and MRSA. All phen-pyrido ligands limited *S. aureus* growth to below 20% at doses as low as 0.23 µM while RePPP (**4.7**) limited growth to below 30% from 30 – 0.23 µM. Ligands **2.5 – 2.7** had a similar ability to hold MRSA growth below 25% at doses down to 0.93 µM. The natural product, ascididemin, which is analogous to phen-pyrido (**Figure 5.14**), exhibits antimicrobial effects against *Bacillus subtilis* (gram-positive bacteria), *E. coli*, and *C. albicans* and *Cladisporinm resinae* (fungus).[280] This may explain the potent antibacterial activity observed for the phen-pyrido ligands. RePPP (**4.7**) maintained activity down to 0.93 µm, with an MIC_{50} of 0.72 µM against MRSA. A lipophilic effect was observed for the phen-pyrido ligands against *C. albicans* with HPP (**2.8**) having the greatest ability to inhibit fungal growth. It is incredibly encouraging that the phen-pyrido ligands have significant activity against bacterial and fungal strains.

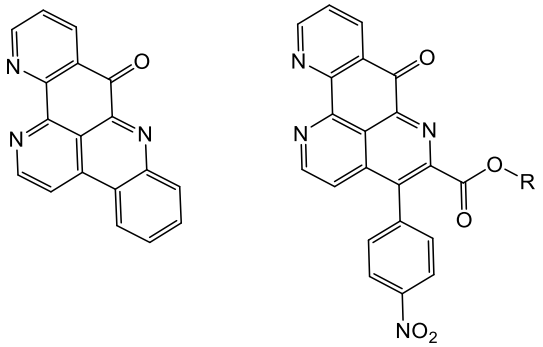

Figure 5.14: Structure of ascididemin (left) and phen-pyrido ligand (right).

5.3 *In vivo* Toxicity Towards *Galleria mellonella*

G. mellonella larvae were used to assess the *in vivo* toxicity of ligands PPO (**4.2**) and PPP (**4.7**) and Re(I) tricarbonyl complexes RePPO (**4.2**) and RePPP (**4.7**). Test solutions of each compound were prepared at 60 µM and 30 µM in 5% (v/v) DMSO in PBS. A control solution of 5% (v/v) DMSO in PBS was also prepared. Five larvae weighing between 200 – 300 mg were placed in a clean petri dish per replicate. Three replicates per test solution were conducted. Each larva was inoculated with 20 µL of test solution beside the last left proleg using a 1 mL insulin syringe. The larvae were placed in an incubator at 37 °C and monitored every 24 h up to 72 h for indications of melanisation or death. Healthy larvae appeared white in colour and had good mobility. They were gently flipped on their back and their ability to right themselves was noted. All larvae tested with the control, PPO (**2.2**), RePPO (**4.2**) and PPP (**2.7**) survived and appeared healthy after 72 h (**Table 5.3**). One larva (out of 15) tested with 60 µM of RePPP (**4.7**) melanised and died after 48 h, giving a 93% survival for the test group. It was concluded that the larvae may have been minimally affected by the 60 µM dose of RePPP (**4.7**).

Table 5.3: Percentage survival of larvae after 24, 48 and 72 h incubation following a 20 µL inoculation of test compounds PPO (**2.2**), RePPO (**4.2**), PPP (**2.7**) and RePPP (**4.7**) or control (5% v/v DMSO in PBS).

		% Survival		
Test compound	**Concentration (µM)**	**24 h**	**48 h**	**72 h**
5% (v/v) DMSO in PBS		100	100	100
PPO (2.2)	60	100	100	100
	30	100	100	100
RePPO (4.2)	60	100	100	100
	30	100	100	100
PPP (4.7)	60	100	100	100
	30	100	100	100
RePPP (4.7)	60	100	93	93
	30	100	100	100

The *in vivo* toxicity of PPO (**2.2**), PPP (**2.7**), RePPO (**4.2**) and RePPP (**4.7**) against *G. mellonella* was further assessed. This involved quantifying the number of haemocyte cells following inoculation of the compounds and comparing to the control larvae injected with 5% (v/v) DMSO in PBS. This is indicative of any potential inflammatory response. Fresh test solutions of 60 µM were prepared as before. Five larvae per test condition were injected with 20 µL of test solution. Following 3 h of incubation at 37 °C, the larvae were collected. A single larva was treated as one replicate, with 3 larvae evaluated per test condition. The lymph of the larvae was collected in a clean Eppendorf. The lymph was diluted by a factor of 5 in fresh PBS. A sample was then pipetted onto a haemocytometer and the number of cells were counted under a microscope. The control number of haemocytes was determined to be 1.23 x 10^7 cells/ml. For the test groups inoculated with 60 µM of PPO (**2.2**) and PPP (**4.7**), 1.25 x 10^7 and 1.05 x 10^7 cells/mL were calculated respectively. Similarly, the 60 µM inoculations of RePPO (**4.2**) and RePPP (**4.7**) were determined to be 1.22 x 10^7 and 1.18 x 10^7 cell/mL (**Table 5.4**). Given that the haemocyte numbers of the test compounds were similar to that of the PBS control with no significant increases, it was determined that no inflammatory response was induced by the test compounds.

Table 5.4: Haemocyte densities calculated following inoculation of 60 µM test solutions of PPO (**2.2**), PPP (**2.7**), RePPO (**4.2**) and RePPP (**4.7**)

Test Compound	Concentration (µM)	Haemocyte count (cells/mL)
5% v/v DMSO in PBS	-	1.23 x 10^7
PPO (**2.2**)	60	1.25 x 10^7
PPP (**2.7**)	60	1.05 x 10^7
RePPO (**4.2**)	60	1.22 x 10^7
RePPP (**4.7**)	60	1.18 x 10^7

5.4 *In vitro* Anticancer Testing against Ovarian Cancer Cell Lines PEO1 and PEO4

The late diagnosis and poor prognosis for patients suffering from ovarian cancer is of great concern. This is worsened by the emergence of resistance to chemotherapeutics, particularly platinum-based treatments which are one of the first lines of treatment along with surgical resection.[265, 267] The immense side effects and toxicity associated with platinum based therapies greatly impacts the patient's quality of life. There has been a huge surge in research into novel metal-based cancer treatments with minimal toxicity that can also reduce instances of chemo-resistance. Rhenium tricarbonyl phen complexes have been extensively studied for their cytotoxicity towards cancer cells.[125, 129-131, 135, 281]

The anticancer activity of PPO (**4.2**), PPP (**2.7**) and their novel Re(I) tricarbonyl complexes, RePPO (**4.2**) and RePPP (**4.7**) was assessed against the patient-derived ovarian cancer cell lines, PEO1 and PEO4. PEO1 is a cisplatin-sensitive cell line while PEO4 is a cisplatin-resistant cell line. The ability of cisplatin to reduce ovarian cancer cell viability against PEO1 and PEO4 was determined as a control. A 2D CellTitre glo 2.0 assay was set up as described in **section 2.4.5**. Test solutions of cisplatin were made to contain 1% (v/v) DMSO in complete RMPI media containing 100 – 0.78 µM of cisplatin. The test solutions were added to the wells containing cancer cells and the plates were incubated for 72 h. CellTitre glo reagent (50 µL) was added to each well. Once incubated, the fluorescent output was read on the Clariostar luminescent reader. Three replicates were obtained for each cell line. Percentage of cell viability was determined as a percentage of the Vehicle Control (VC) which consisted of 1% (v/v) DMSO in complete RPMI media (% VC Growth). The statistical significance was determined with respect to the VC. High statistical significance is defined as $P<0.0001$ while moderate statistical significance is where $0.0001 < P < 0.01$.

The 2D cell viability of PEO1 and PEO4 cells treated with chemotherapy agent, cisplatin were assessed. **Figure 5.15** shows the dose dependent decrease in cell viability in response to cisplatin in the dosage range 0.78 – 100 µM. The IC_{50} values for cisplatin were determined to be 2.82 µM (PEO1) and 15.63 µM (PEO4) as

presented in **Table 5.6**. These values are in keeping with those determined by Greenwood *et al*: 2.6 µM ± 0.85 µM (PEO1) and 14.0 µM ± 5.3 µM.[282]

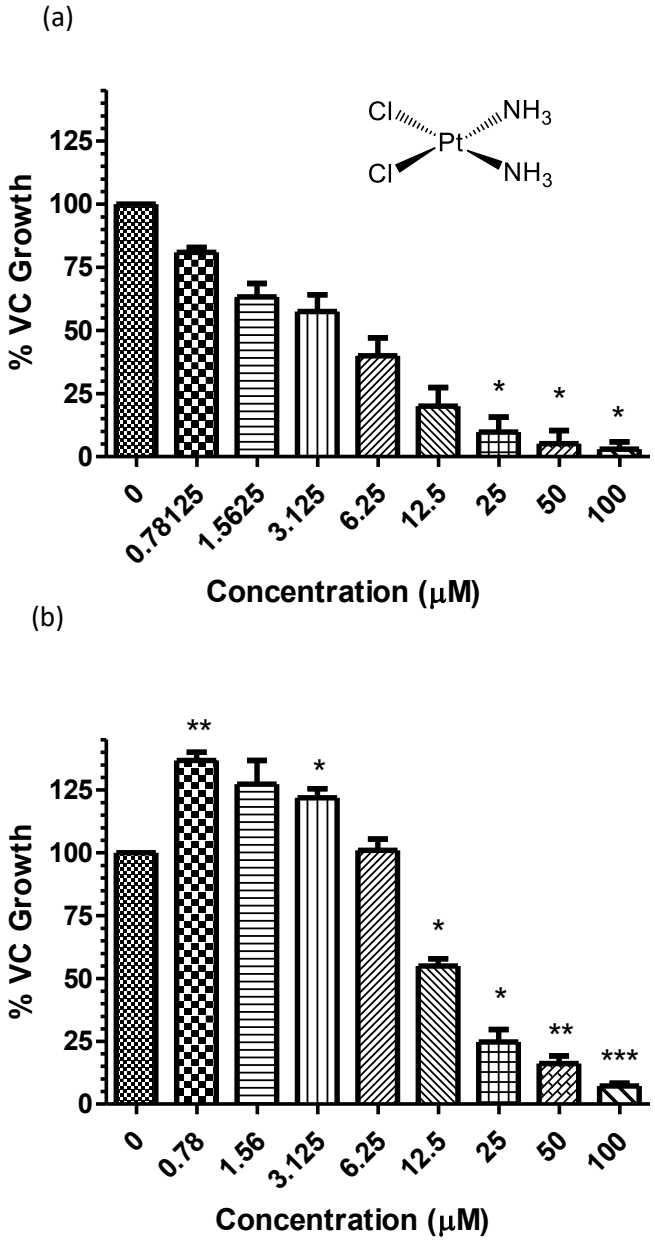

Figure 5.15: Percentage cell viability of PEO1 (a) and PEO4 (b) cells treated with cisplatin in the range 0.78 – 100 µM as compared to the VC.

The anticancer activity of test compounds PPO (**2.2**), PPP (**2.7**), RePPO (**4.2**) and RePPP (**4.7**) was determined using the same protocol as cisplatin. PPO (**2.2**) was tested in the range of 12.5 – 0.097 µM for PEO1 and PEO4 cell lines. **Figure 5.14** shows

the percentage cell viability for PPO (**2.2**) tested against PEO1 (a) and PEO4 (b). No activity was observed below 0.78 μM so the results at these concentrations have been omitted from the graph. There is significant activity observed for PPO (**2.2**) against both cell lines. High statistical significance ($P<0.0001$) was determined for 12.5 – 3.125 μM compared to the VC for PEO1. The 12.5 μM dose against PEO1 was also determined to have high statistical significance of $P<0.0001$. Doses 6.23 – 3.125 μM of PPO (**2.2**) against PEO4 had moderate significance of $0.0001 < P < 0.05$. The IC_{50} values were determined to be 3.30 μM (PEO1) and 2.79 μM (PEO4) as presented in **Table 5.6**. It is evident PPO (**2.2**) has a similar ability to inhibit cell viability of both PEO1 and PEO4. The IC_{50} of 3.30 μM against PEO1 is in a similar range to cisplatin (2.82 μM). Conversely, PPO (**2.2**) had a much greater ability to limit PEO4 viability. The IC_{50} of 2.79 μM was much lower than that of cisplatin (15.63 μM).

(a)

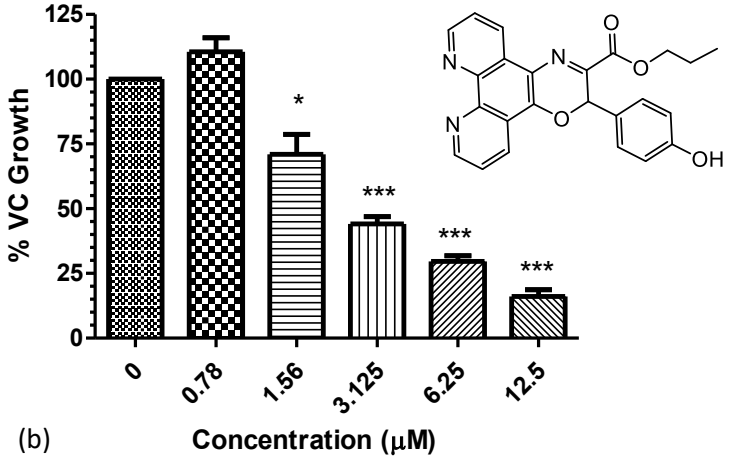

(b)

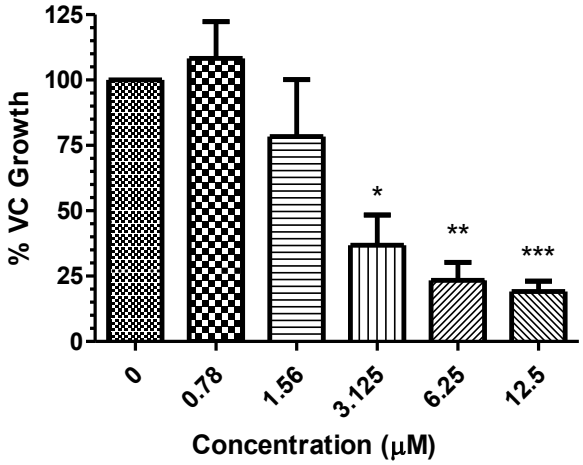

Figure 5.16: Percentage cell viability of PEO1 (a) and PEO4 (b) cells treated with PPO (**2.2**) in the range 0.78 – 12.5 μM as compared to the VC.

Re(I) tricarbonyl complex, RePPO (**4.2**) was much less active against both PEO1 and PEO4 cell lines. The complex was tested in the range 100 – 0.78 μM. Inhibition of cell viability was only observed at the highest does of 100 μM (**Figure 5.17**). It was not possible to test at higher concentrations due to precipitation of the compound at concentrations above 100 μM. The highest dose of 100 μM had significant ability to limit growth of PEO1 cells ($P<0.0001$). The same dose had a similar effect against PEO4 but this was not determined to be statistically significant. The concentration range tested did not successfully capture the IC_{50} values for this compound. It was unexpected that complexation to the Re(I) tricarbonyl core appears to significantly reduce the anticancer ability of PPO (**2.2**).

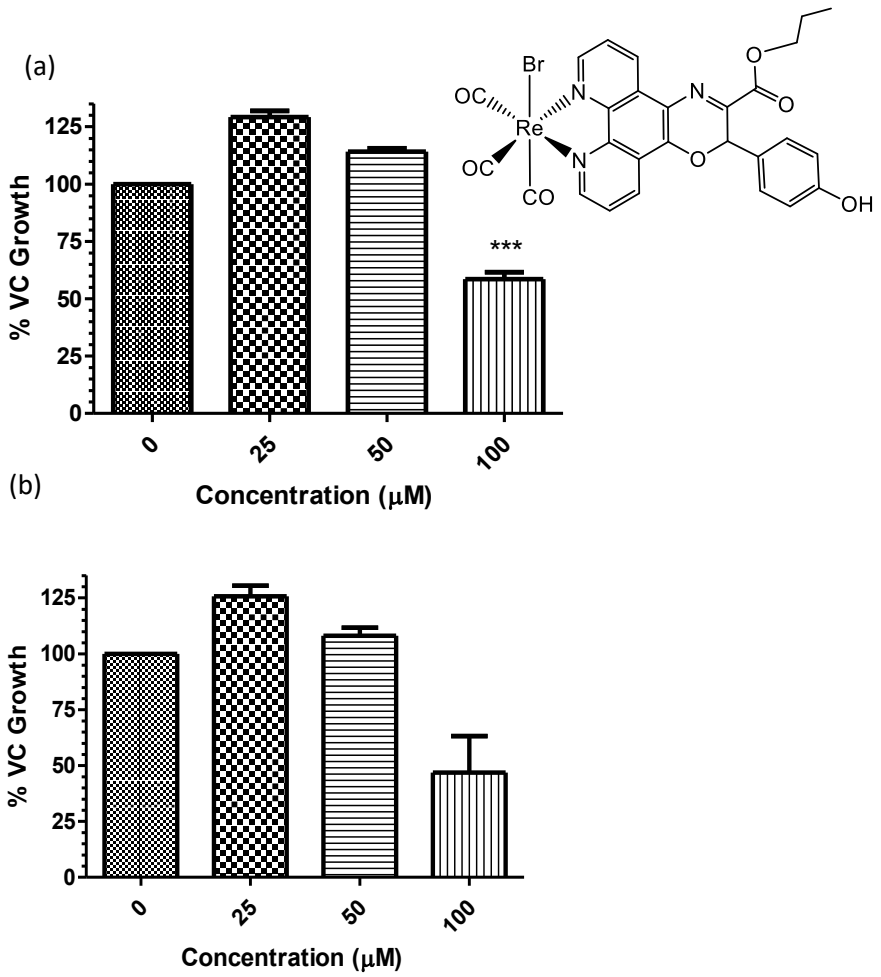

Figure 5.17: Percentage cell viability of PEO1 (a) and PEO4 (b) cells treated with RePPO (**4.2**) in the range 25 - 100 μM as compared to the VC.

The 2D cell viability of PEO1 and PEO4 cells treated with PPP (**2.7**) was assessed using concentrations from 6.10 – 0.38 nM. The ligand was extremely active showing activity in the nanomolar range against both cell lines. **Figure 5.18** shows that PPP (**2.7**) has a good ability to limit cell growth of PEO1 and PEO4 at a dose as low as 0.76 nM. The impact of PPP (**2.7**) on PEO1 at the 3.05 and 1.53 nM is reasonably significant: $0.0001 < P < 0.05$. The ability of PPP (**2.7**) to inhibit PEO4 cells is particularly evident in the range 6.10 – 0.76 nM with the inhibition at 3.05 – 0.76 nM having high statistical significance ($P<0.0001$). The IC_{50} was determined to be 1.22 nM for PEO1 and 0.78 nM for PEO4 (**Table 5.6**). PPP (**2.7**) clearly has a similar ability to limit viability of both PEO1 and PEO4 cell lines. With IC_{50} values of 1.22 and 0.78 nM,

this ligand, PPP is substantially more active than the analogous PPO and cisplatin which have IC_{50} values in the micromolar range.

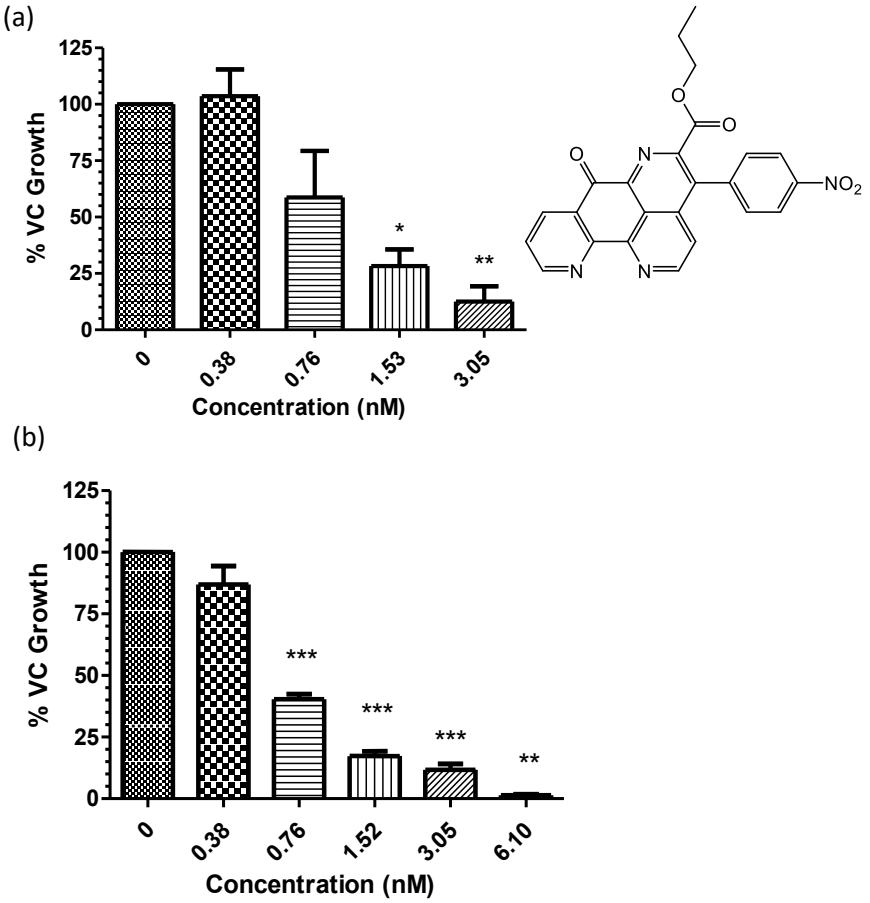

Figure 5.18: Percentage cell viability of PEO1 (a) and PEO4 (b) cells treated with PPP (**2.7**) in the range 0.38 – 3.05 nM as compared to the VC.

These results are perhaps unsurprising given that PPP (**2.7**) has structural similarity to ascididemin (**Figure 5.14**). Ascididemin has potent anticancer effects that was first reported in 1988.[283] The antimicrobial and anticancer effects are largely a result of ascididemin having a planar polycyclic structure which allows for DNA intercalation. Matsumoto and colleagues demonstrated that ascididemin can also oxidatively damage DNA in a thiol-dependent manner.[284] Ascididemin and its analogous are known to have potent anticancer activity against a variety of human cell lines. Delfourne and coworkers screened ascididemin against a host of cell lines revealing low nanomolar activity against a variety of cancers, given in **Table 5.5**.[285]

Table 5.5: *In vitro* cytotoxic effects of ascididemin reported in the literature[285]

Cell line	Cell location	IC_{50} (nM)
HCT-15	Large intestine	6
PC-3	Prostate	8
A-427	Lungs	60
MCF7	Breast	70
U-87MG	Brain	70

Anticancer testing was also conducted on RePPP (**4.7**) This complex was tested in the concentration range of 12.5 – 0.09 µM against both PEO1 and PEO4 in the same manner as the above compounds. RePPP (**4.7**) had significant ability to limit viability of both cell lines as shown in **Figure 5.19**. The inhibitory effects of RePPP (**4.7**) at doses 6.25 – 1.56 µM against PEO1 were highly significant ($P<0.0001$). The inhibitory effects of RePPP (**4.7**) against PEO4 were reasonable significant: $0.0001 < P < 0.05$. The IC_{50} values were determined to be 1.67 µM (PEO1) and 1.70 (PEO4). RePPP (**4.7**) is substantially active against both cell lines and has a greater ability than cisplatin to limit cell viability, particularly for the PEO4 cell line as seen in **Table 5.6**. The low micromolar activity of RePPP (**4.7**) shows great promise as this is the typical concentration range for standard therapeutics. This may infer lower *in vivo* toxicity than uncoordinated PPP (**2.7**) given that Re(I) tricarbonyl diimine complexes are reported to have low *in vivo* toxicity.[133, 134]

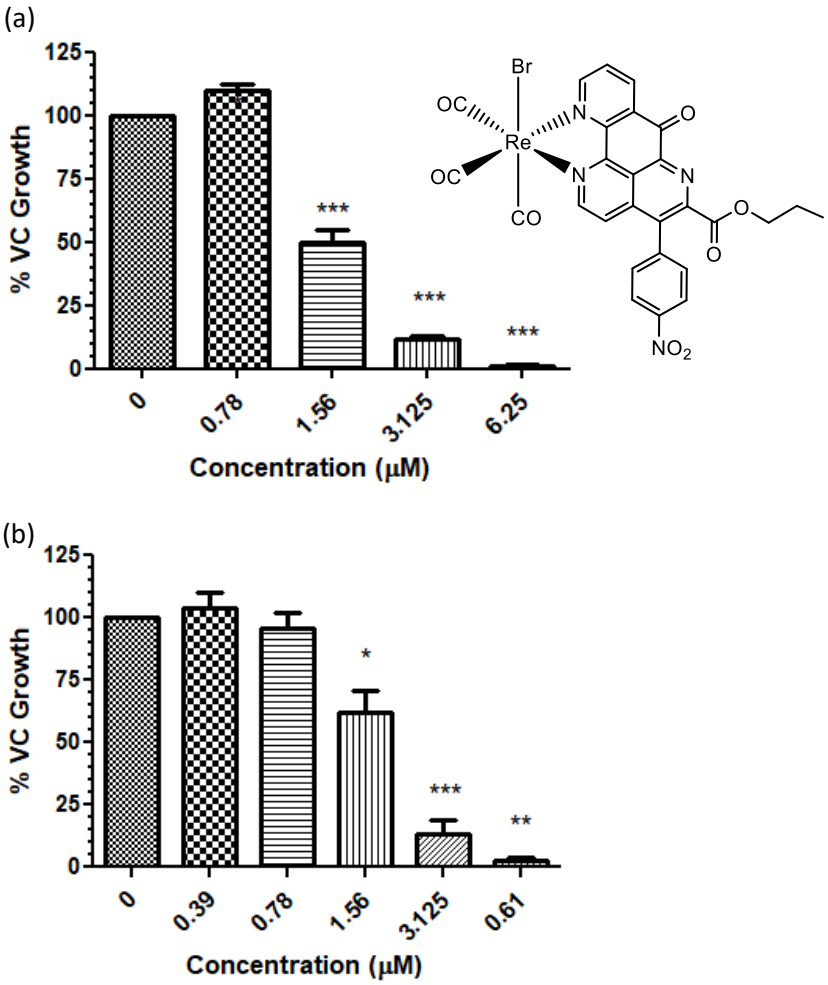

Figure 5.19: Percentage cell viability of PEO1 (a) and PEO4 (b) cells treated with RePPP (**4.7**) in the range 0.78 – 6.25 µM as compared to the VC.

Table 5.6: Compound concentrations to inhibit 50% of cell growth (IC_{50})

Compound	PEO1 IC_{50} (µM) ± SEM	PEO4 IC_{50} (µM) ± SEM
PPO (**2.2**)	3.30 ± 0.46	2.79 ± 0.67
RePPO (**4.2**)	> 100	> 100
PPP (**2.7**)	0.00122 ± 0.000287 (1.22 ± 0.28 nM)	0.000725 ± 0.000144 (0.78 ± 0.14 nM)
RePPP (**4.7**)	1.67 ± 0.11	1.70 ± 0.25
Cisplatin	2.82 ± 0.42	15.63 ± 0.48

The data presented has demonstrated the ability of PPO (**2.2**), PPP (**2.7**) and RePPP (**4.7**), but not of RePPO (**4.2**), to significantly reduce cell viability of both PEO1 and PEO4 ovarian cancer cells. It is also evident that these compounds are just as capable of limiting cisplatin-resistant PEO4 cells growth as cisplatin-sensitive PEO1 cells. This suggests that the compounds may have a mode of action unique to that of cisplatin. Although the 2D viability assay is a good indication of anticancer activity of a compound, further testing is required to determine the potential mode of action of the drugs.

5.5 Assessing the Apoptotic Ability of PPO (2.2), PPP (2.7), RePPO (4.2) and RePPP (4.7).

The results presented above are extremely encouraging in the search for novel anticancer therapeutics. There is clear evidence that PPO (**2.2**), PPP (**2.7**) and RePPP (**4.7**) have potential as novel anticancer agents. Further analysis was required to identify the potential mode of action of these compounds. A 2D caspase-3/7 apoptosis assay was conducted on each compound. This experiment involved setting up a 2D viability assay that incorporated a caspase-3/7 green dye. This protocol is described in **section 2.4.5**. The premise behind this experiment is to monitor the apoptotic markers, caspase-3/7. Caspase-3/7 are effector molecules involved in mediating cell signalling pathways leading to cell death by apoptosis. Presence of cleaved caspase (the activated form) is indicative of apoptosis[286]. The caspase-3/7 assay therefore monitors levels of cleaved caspase-3 and caspase-7 and in turn apoptosis.

The 2D apoptosis assay was set up in a similar manner to the 2D cell viability assay. The cells were treated with three concentrations of each compound. For each test sample, concentrations chosen included the IC_{50} value for both PEO1 and PEO4 cell lines. PPO (**2.2**) was tested in the range 6.25 – 1.56 μM; PPP (**2.7**) in the range 3.05 – 0.75 nM; RePPO (**4.2**) was tested at 100 μM; RePPP (**4.7**) was tested in the range 3.12 – 0.75 μM. Experiments were designed to have a VC for each test compound. Once

treated, the 96-well plates were placed in an incucyte imaging machine. Fluorescent readings and images were taken every 4 hours over 5 days. The fluorescent output (apoptosis) is measured relative to that determined at t = 0 h. The percentage of the well covered by cells (confluency) was also monitored over this time. Where apoptosis is not occurring, confluency measurements are presented to show reduced cell proliferation.

The data obtained for PPO (**2.2**) presented in **Figures 5.20** reveals gradual caspase-3/7 activation at each concentration over the course of 0 - 72 h compared to the VC (blue) for both PEO1 (a) and PEO4 (b) cell lines. This indicates that at the concentrations tested, PPO (**2.2**) has the ability to induce cell death by apoptosis against ovarian cancer cells PEO1 and PEO4.

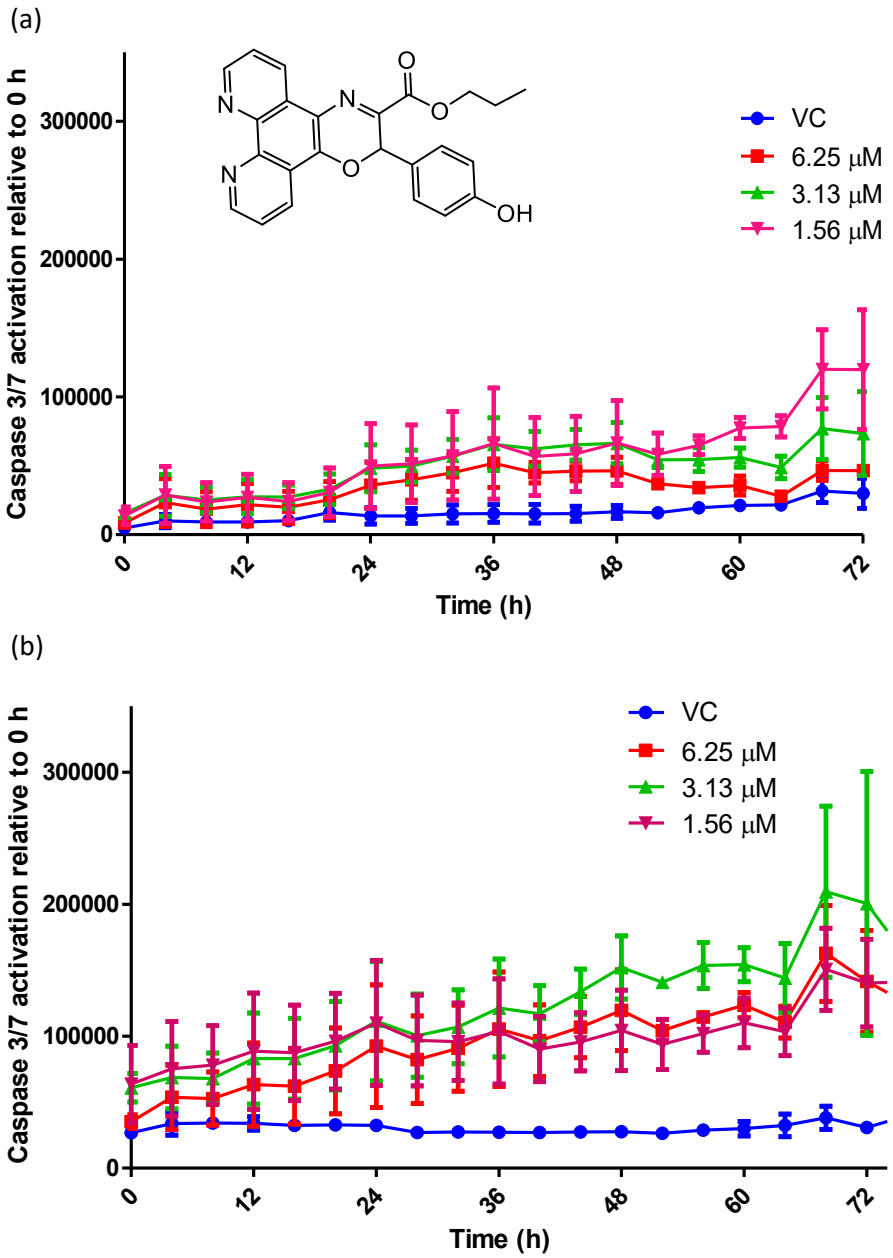

Figure 5.20: Caspase-3/7 fluorescent output over 0 – 72 h for PEO1 (a) and PEO4 (b) cells treated with PPO (**2.2**) at 6.25 – 1.56 µM

Unfortunately, the data obtained for the casapase-3/7 assay involving PPP (**2.7**) was inconclusive due to experimental errors with the VC. This assay is due to be repeated in the near future.

The Re(I) complex, RePPO (**4.2**) was shown to have a limited ability to reduce cell viability in the previous section. The active dose of 100 µM was assessed for production of cleaved caspase-3/7. **Figure 5.21** displays the fluorescent output

produced in the presence of the complex at a dose of 100 µM. The low fluorescent output observed for PEO1 suggests apoptosis was not induced. There is a greater fluorescent response for the PEO4 which is indicative of apoptosis. Anticancer activity can be a result of either cytotoxic mechanisms such as apoptosis or cytostatic mechanisms which slow or inhibit proliferation of the cancer cells without actively killing the cells [287]. Additionally, there are many mechanisms of cell death such as pyroptosis, necrosis and autophagy.[288] The confluence of RePPO (**4.2**) was also monitored during this assay. Cancer cells will continue to proliferate and increase in density (confluence) in the absence of anticancer agents until nutrients are no longer available. In contrast, cancer cells in the presence of an anticancer agent will gradually die and therefore the confluence will remain the same. **Figure 5.22** shows the confluence of the cells exposed to RePPO (**4.2**) from 0 – 72 h for PEO1 (a) and PEO4 (b). The cells in the VC have the ability to gradually increase in confluence, indicating they are unaffected by the 1% (v/v) DMSO media. The 100 µM dose of RePPO (**4.2**) appears to inhibit cell proliferation over the 72 h period for both cell lines. The complex therefore has the ability to curtail PEO1 growth by a cytostatic or cytotoxic mechanisms other than apoptosis.

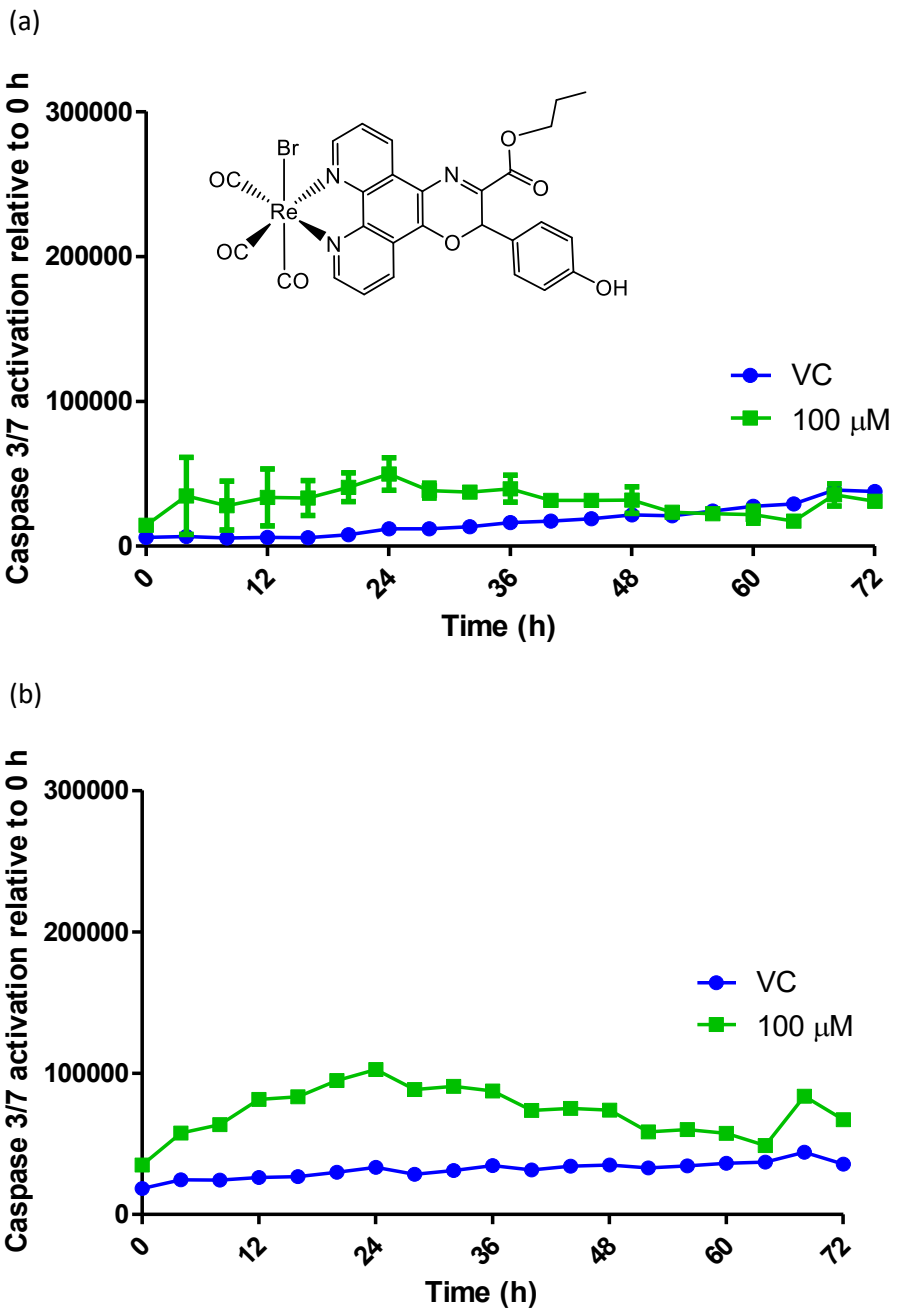

Figure 5.21: Caspase-3/7 fluorescent output over 0 – 72 h for PEO1 (a) and PEO4 (b) cells treated with RePPO (**4.2**) at 100 μM.

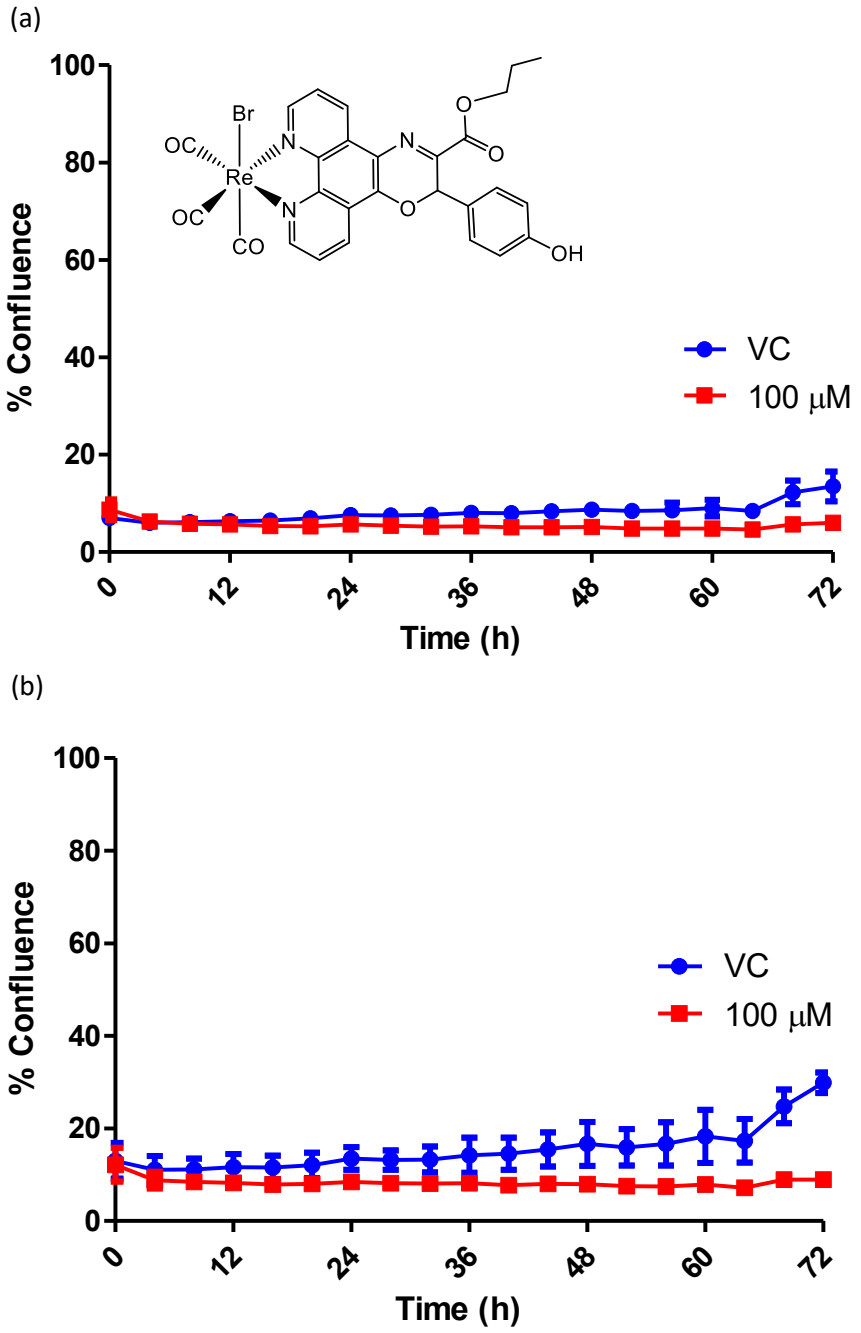

Figure 5.22: Percentage confluency of PEO1 (a) PEO4 (b) cells treated with RePPO (**4.2**) at 100 μM from 0 -72 h.

The caspase-3/7 output for RePPP (**4.7**) against PEO1 and PEO4 cell lines is presented in **Figure 5.23**. It is evident that there is little fluorescence observed for the cells treated with RePPP (**4.7**) at the doses 3.13 – 0.78 μM for both cell lines when compared to the VC. This indicates no activation of caspase-3/7 and therefore apoptosis is not induced. Interestingly, the confluency graphs shown in **Figure 5.24**

reveals that RePPP (**4.7**) does impact cell growth. It can be concluded that RePPP (**4.7**) inhibits proliferation of PEO1 and PEO4 cells by a cytostatic or alternative cytotoxic mechanism.

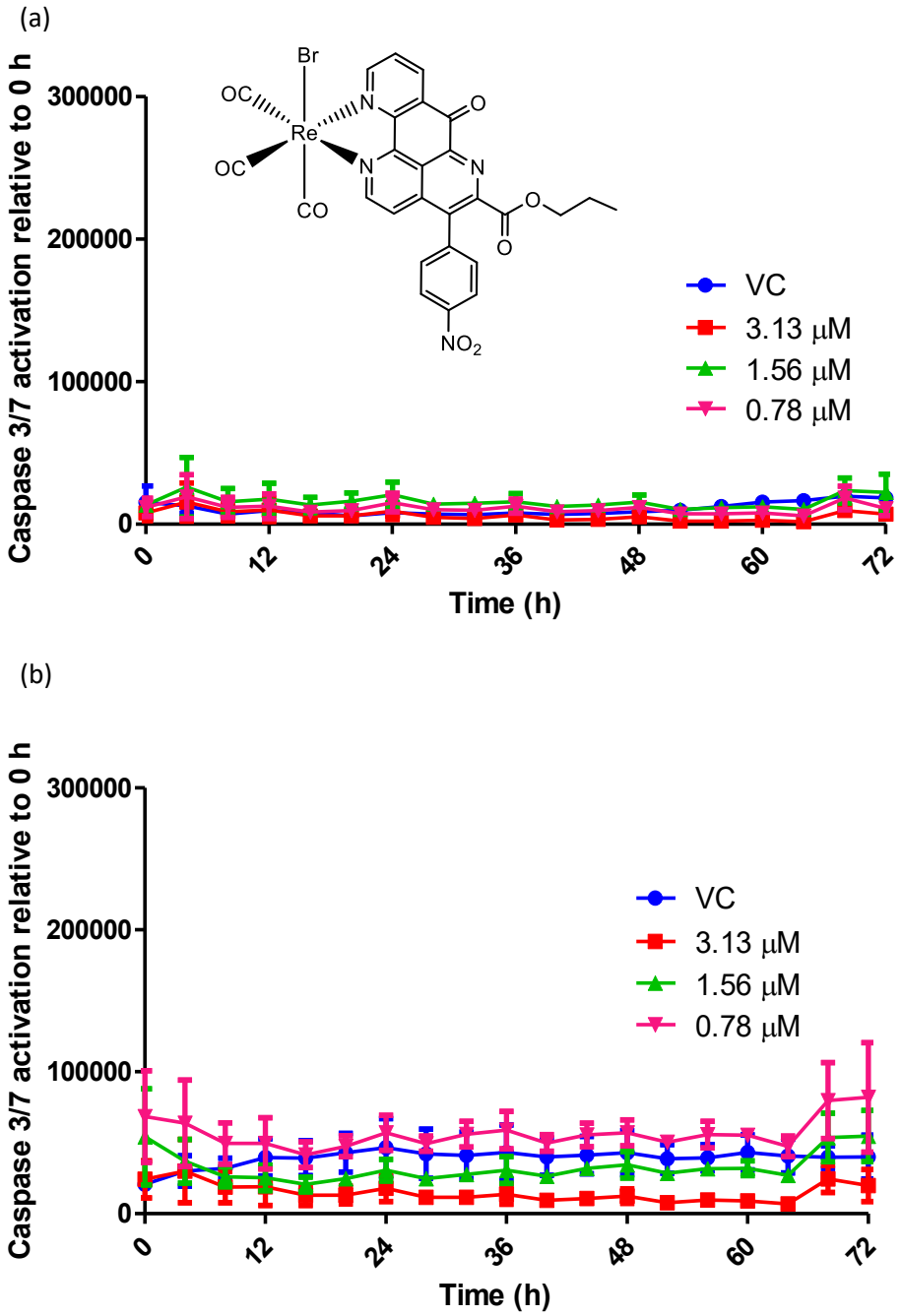

Figure 5.23: Caspase-3/7 fluorescent output over 0 – 72 h for PEO1 (a) and PEO4 (b) cells treated with RePPP (**4.7**) at 3.13 – 0.78 μM.

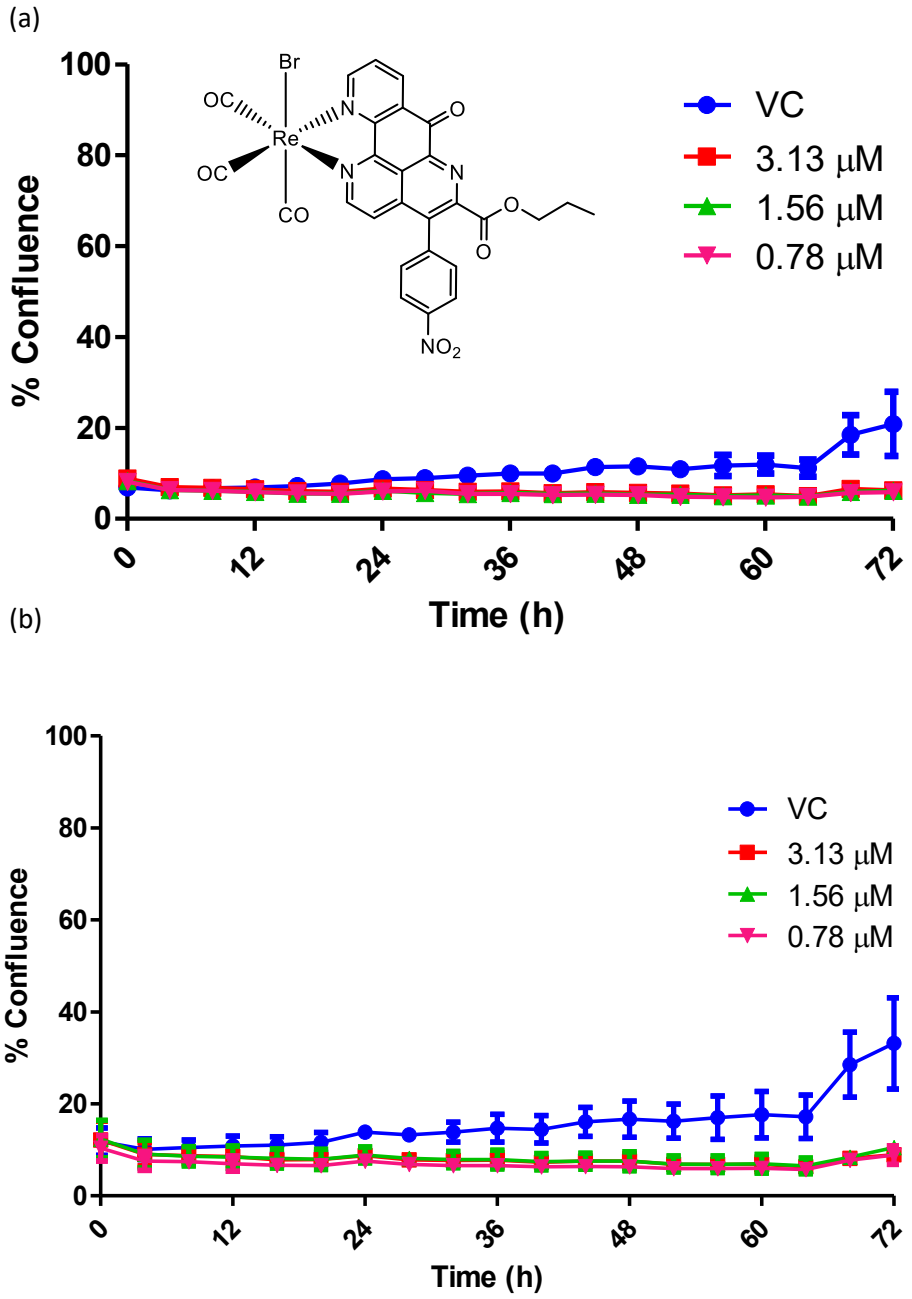

Figure 5.24: Percentage confluency of PEO1 (a) PEO4 (b) cells treated with RePPP (**4.7**) at 3.13 – 0.78 µM from 0 – 72 h .

The apoptosis assay conducted on compounds PPO (**2.2**), RePPO (**4.2**) and RePPP (**4.7**) yielded interesting results. All compounds had the ability to impact proliferation of PEO1 and PEO4 cells as observed with the 2D viability assays. It was determined that PPO (**2.2**) induced cell death by apoptosis at all concentrations tested for both cell lines. The results for PPP (**2.7**) were inconclusive given the activity observed for the VC. RePPO (**4.2**) had some ability to induce apoptosis of PEO1 cells while PEO4

cells were inhibited by an alternative manner to apoptosis is it not the case that apoptosis is evident in the case of PEO4. Finally, RePPP (**4.7**) was determined to inhibit cell growth of both PEO1 and PEO4 cells by a mechanism other than apoptosis.

5.6 Conclusion

Antimicrobial screening was conducted on phen-oxazine ligands **2.1 – 2.8**, phen-pyrido ligands **2.5 – 2.8** and their respective Re(I) tricarbonyl complexes **4.1 – 4.8** against a variety of microbes; *S. aureus*, MRSA, *E. coli* and *C. albicans*. HPO (**2.3**) and OPO (**2.4**) had good activity against *S. aureus* and MRSA. Re(I) phen-oxazines had limited activity against all species. The rhenium complexes were in general determined to be less active than the uncoordinated ligands. The phen-pyrido ligands **2.5 – 2.8** were determined to be the most potent of the compounds tested. The family had an ability to limit *S. aureus* growth to less than 25% at doses as low as 0.11 µM. Similarly, MRSA growth was limited to below 25% down to 0.93 µM. Ligands **2.5 – 2.8** were also the only compounds tested to show inhibitory effects against *E. coli*, with a 30 µM dose of MPP (**2.5**) having the greatest effect (58% growth). The more lipophilic phen-pyrido ligands PPP (**2.7**) and HPP (**2.8**) were the most active against the yeast *C. albicans*. The Re(I) phen-pyrido complexes **4.5 – 4.7** had reasonable effects against *S. aureus* and MRSA with RePPP (**4.7**) showing the greatest effect. The activity of the phen-pyrido family was shown to be more active than vancomycin and have similar activity to teicoplanin, linezolid and daptomycin. *In vivo* testing of PPO (**2.2**), PPP (**2.7**), RePPO (**4.2**) and RePPP (**4.7**) against *G. mellonella* demonstrated that the compounds are well tolerated at doses of 60 and 30 µM. Additionally, the compounds were not found to initiate an inflammatory response in the larvae. These results are incredibly encouraging in the search for novel antimicrobial agents.

In vitro anticancer testing against ovarian cancer cell lines PEO1 and PEO4 was conducted on PPO (**2.2**), PPP (**2.7**), RePPO (**4.2**) and RePPP (**4.7**). The activity was assessed using a 2D CellTitre glo viability assay. PPO (**2.2**), PPP (**2.7**) and RePPP (**4.7**) were shown to elicit a similar dose-dependent decrease in PEO1 and PEO4 cell

viability. These compounds were found have greater activity than cisplatin against the resistant PEO4 cell line. PPP (**2.7**) was extremely potent with activity in the nanomolar range. This is predicted to be due to its structure which is analogous to the potent anticancer agent, ascididemin. Low micromolar IC_{50} values of 1.67 – 3.30 μM were determined for PPO (**2.2**) and RePPP (**4.7**). RePPO (**4.2**) had a limited impact on cell viability at the highest dose of 100 μM. The potential mode of action of the four compounds was assessed by means of a 2D caspase-3/7 assay to monitor apoptosis. PPO (**2.2**) was confirmed to induce cell death by apoptosis for PEO1 and PEO4 cells. Results for PPP (**2.7**) were inconclusive due to errors with the VC. RePPO (**4.2**) had some ability to induce apoptosis in PEO1 cells but not PEO4. The mechanism for PEO4 cells is predicted to be by an alternative cytotoxic or cytostatic mechanism. This was also the case for RePPP (**4.7**). No apoptosis was identified; however, cell proliferation was greatly impacted. It is promising that there is little difference between the activity of the compounds on PEO1 and PEO4 cell lines. It is predicted that this could indicate a mechanism that is different to that of cisplatin. PPO (**2.2**), PPP (**2.7**) and RePPP (**4.7**) therefore have great potential as novel anticancer agents that can circumvent chemo-resistance mechanisms.

Chapter 6

Future Perspectives

This thesis has explored the synthesis and biological activity of derivatised phenanthroline ligands with extended conjugation, namely the phenanthroline-oxazine (**2.1 – 2.4**) and pyrido-phenanthrolinone (**2.5 – 2.8**) ligands. The first part of this research investigated the stability, solution behaviour and biological activity of Ag(I) *bis*(phenanthroline-oxazine) complexes. It was determined that the Ag(I) complexes are fluxional in solution. The solution equilibrium lies with a 1:2, Ag(I):L ratio. The phen-oxazine ligands (**2.1 – 2.3**) exhibited good antifungal activity against *C. albicans* and displayed a clear lipophilic effect; the most lipophilic variants were the most biologically active. Complexation to Ag(I) proved to greatly enhance the antifungal activity of the ligands, suggesting a synergistic effect. Phen-oxazine ligand (**2.2**) and Ag(I) phen-oxazine (**3.2**) were well tolerated by *G. mellonella* and no inflammatory response was observed in the larvae. The output of this body of work is promising and there are several avenues that can be explored going forward. The first would be to carry out proteomic analysis of *C. albicans* treated with the Ag(I) complexes. This would provide insightful information on the potential mode of action of the complexes. Additionally, the ability of the Ag(I) complexes to disrupt *Candida* adherence could be assessed. Furthermore, respiration assays could be conducted to determine if the complexes effect cellular respiration within the yeast. It would also be beneficial to determine the antifungal capabilities of the Ag(I) phen-oxazine complexes against other problematic *Candida* strains. These may include *C. parapsilosis*, *C. dubliniensis* and *C. tropicalis*. It would also be beneficial to assess their activity against other harmful species such as *Aspergillus*. Given the good activity of the Ag(I) phen-oxazine complexes, it would also be interesting to evaluate the activity of Ag(I) phen-pyrido analogues as these were not explored in this project.

This body of work has also investigated the chemical synthesis and structure characterisation as well as the photophysical, photochemical and biological properties of novel Re(I) tricarbonyl complexes (**4.1 – 4.8**). Characterisation of the Re(I) phen-oxazine family revealed they exist as a pair of diastereomers. It is hoped that future work can include separation of the diastereomeric products. The complexes were unfortunately found to be non-luminescent. Irradiation studies revealed the complexes undergo a photochemical change in response to UV light but

the nature of which was not identified. It is hoped that future work may include further investigations of this photochemical behaviour. Myoglobin assays indicated that the complexes do not readily release CO and therefore do not function as CORMs. To address this, it is hoped that the ancillary Br^- ligand could be replaced by a phosphine or tetrazolate ligand. This may enhance the CO release capabilities and provide luminescent analogues. Information on the HOMO and LUMO states were not determined during this project. DFT calculations are planned in the near future to elucidate this information for the Re(I) complexes **4.1 – 4.8**. Electrochemical studies using CV demonstrated the rich redox activity of the Re(I) phen-pyrido complexes (**4.5** – **4.8**). This behaviour may make these complexes ROS generators. It is hoped that this may be investigated using electrochemical and biological methods. The anticancer studies conducted on the lead compounds provided promising results. The 2D caspase-3/7 assay is planned to be repeated on PPP (**2.7**) in the coming months to identify its potential to induce apoptosis. It is also planned that PPO (**2.2**), PPP (**2.7**), RePPO (**4.2**) and RePPP (**4.7**) will be tested against a non-cancerous cell line. This will help to distinguish that the biological activity is specific to cancer cells rather than healthy cells.

Bibliography

1. Lemire, J. A.; Harrison, J. J.; Turner, R. J., Antimicrobial activity of metals: mechanisms, molecular targets and applications. *Nat. Rev. Microbiol.* **2013,** *11* (6), 371-384.
2. Ehrlich, P.; Bertheim, A., Über das salzsaure 3.3'-Diamino-4.4'-dioxy-arsenobenzol und seine nächsten Verwandten. *Ber. Dtsch. Chem. Ges.* **1912,** *45* (1), 756-766.
3. Ghosh, S., Cisplatin: The first metal based anticancer drug. *Bioorg. Chem.* **2019,** *88*, 102925.
4. Rosenberg, B.; Van Camp, L.; Krigas, T., Inhibition of Cell Division in Escherichia coli by Electrolysis Products from a Platinum Electrode. *Nature* **1965,** *205* (4972), 698-699.
5. Zhang, C.; Xu, C.; Gao, X.; Yao, Q., Platinum-based drugs for cancer therapy and anti-tumor strategies. *Theranostics* **2022,** *12* (5), 2115-2132.
6. Waldron, K. J.; Rutherford, J. C.; Ford, D.; Robinson, N. J., Metalloproteins and metal sensing. *Nature* **2009,** *460* (7257), 823-830.
7. Ahmed, M. H.; Ghatge, M. S.; Safo, M. K., Hemoglobin: Structure, Function and Allostery. *Subcell. Biochem.* **2020,** *94*, 345-382.
8. Viganor, L.; Howe, O.; McCarron, P.; McCann, M.; Devereux, M., The Antibacterial Activity of Metal Complexes Containing 1,10- phenanthroline: Potential as Alternative Therapeutics in the Era of Antibiotic Resistance. *Curr. Top. Med. Chem.* **2017,** *17* (11), 1280-1302.
9. Tanaka, K.; Vong, K., Unlocking the therapeutic potential of artificial metalloenzymes. *Proc. Jpn. Acad. B: Phys. Biol. Sci.* **2020,** *96* (3), 79-94.
10. Costa-Rodrigues, J.; Sá-Azevedo, R.; Balinha, J.; Ferro, G., Vegetarianism during pregnancy: Risks and benefits. *Trends Food Sci Technol.* **2018,** *79*, 28-34.
11. Bohrer, B. M., Review: Nutrient Density and Nutritional Value of Meat Products and Non-meat Foods High in Protein. *Trends Food Sci Technol.* **2017,** *65*, 103-112.

12. Da Silva Neto, J. F.; Staats, C. C.; Pontes, M. H., Editorial: Metal homeostasis in microbial physiology and virulence. *Front. cell. infect. microbiol.* **2023,** *13*.
13. Abdolmaleki, S.; Aliabadi, A.; Khaksar, S., Bridging The Gap Between Theory and Treatment: Transition Metal Complexes as Successful Candidates in Medicine. *Coord. Chem. Rev.* **2025,** *531*, 216477.
14. Gomes, R. N.; Silva, M. L.; Gomes, K. S.; Lago, J. H. G.; Cerchiaro, G., Synthesis, characterization, and cytotoxic effects of new copper complexes using Schiff-base derivatives from natural sources. *J. Inorg. Biochem.* **2024,** *250*, 112401.
15. Evans, A.; Kavanagh, K. A., Evaluation of metal-based antimicrobial compounds for the treatment of bacterial pathogens. *J. Med. Microbiol.* **2021,** *70* (5).
16. Fulgenzi, A.; Vietti, D.; Ferrero, M. E., EDTA Chelation Therapy in the Treatment of Neurodegenerative Diseases: An Update. *Biomedicines* **2020,** *8* (8), 269.
17. Casini, A.; Pöthig, A., Metals in Cancer Research: Beyond Platinum Metallodrugs. *ACS Central Science* **2024,** *10* (2), 242-250.
18. Mjos, K. D.; Orvig, C., Metallodrugs in Medicinal Inorganic Chemistry. *Chem. Rev.* **2014,** *114* (8), 4540-4563.
19. Yamashita, M., Auranofin: Past to Present, and repurposing. *Int. Immunopharmacol.* **2021,** *101*, 108272.
20. He, Z.; Han, S.; Wu, C.; Liu, L.; Zhu, H.; Liu, A.; Lu, Q.; Huang, J.; Du, X.; Li, N.; Xie, Q.; Wan, L.; Ni, J.; Chen, L.; Yang, X.; Liu, Q., Bis(ethylmaltolato)oxidovanadium(iv) inhibited the pathogenesis of Alzheimer's disease in triple transgenic model mice. *Metallomics* **2020,** *12* (4), 474-490.
21. Umumararungu, T.; Nkuranga, J. B.; Habarurema, G.; Nyandwi, J. B.; Mukazayire, M. J.; Mukiza, J.; Muganga, R.; Hahirwa, I.; Mpenda, M.; Katembezi, A. N.; Olawode, E. O.; Kayitare, E.; Kayumba, P. C., Recent developments in antimalarial drug discovery. *Bioorg. Med. Chem.* **2023,** *88-89*, 117339.

22. Zhang, S.; Wang, X.; Gao, X.; Chen, X.; Li, L.; Li, G.; Liu, C.; Miao, Y.; Wang, R.; Hu, K., Radiopharmaceuticals and their applications in medicine. *Signal Transduct. Target Ther.* **2025,** *10* (1), 1.
23. Tawhid-Islam, M.; Tsnobiladze, V., The Application, Safety, and Recent Developments of Commonly Used Gadolinium-Based Contrast Agents in MRI: A Scoping Review. *Eur. Med. J.* **2024,** *9* (3), 63-73.
24. Boschi, A.; Martini, P., Metal-Based Radiopharmaceuticals in Inorganic Chemistry. *Molecules* **2023,** *28* (5).
25. Gucký, A.; Hamuľaková, S., Targeting Biometals in Alzheimer's Disease with Metal Chelating Agents Including Coumarin Derivatives. *CNS Drugs* **2024,** *38* (7), 507-532.
26. Hašková, P.; Applová, L.; Jansová, H.; Homola, P.; Franz, K. J.; Vávrová, K.; Roh, J.; Šimůnek, T., Examination of diverse iron-chelating agents for the protection of differentiated PC12 cells against oxidative injury induced by 6-hydroxydopamine and dopamine. *Sci. Rep.* **2022,** *12* (1), 9765.
27. Hachey, A. C.; Havrylyuk, D.; Glazer, E. C., Biological activities of polypyridyl-type ligands: implications for bioinorganic chemistry and light-activated metal complexes. *Curr Opin Chem Biol* **2021,** *61*, 191-202.
28. Husseini, R.; Stretton, R. J., Studies on the antibacterial activity of phanquone: effect on metabolic activities of Escherichia coli and Staphylococcus aureus. *Microbios* **1981,** *30* (119), 7-18.
29. Masuri, S.; Vaňhara, P.; Cabiddu, M. G.; Moráň, L.; Havel, J.; Cadoni, E.; Pivetta, T., Copper(II) Phenanthroline-Based Complexes as Potential AntiCancer Drugs: A Walkthrough on the Mechanisms of Action. *Molecules* **2022,** *27* (1), 49.
30. MacLeod, R. A., The Toxicity of o-Phenanthroline for Lactic Acid Bacteria. *J. Biol. Chem.* **1952,** *197* (2), 751-761.
31. Queffélec, C.; Pati, P. B.; Pellegrin, Y., Fifty Shades of Phenanthroline: Synthesis Strategies to Functionalize 1,10-Phenanthroline in All Positions. *Chem. Rev.* **2024,** *124* (11), 6700-6902.
32. Blau, F., Die Destillation Pyridinmonocarbonsaurer Salze. *Ber. Dtsch. Chem. Ges.* **1888,** *21* (1), 1077-1078.

33. Luman, C. R.; Castellano, F. N., *Fundamentals: Ligands, Complexes, Synthesis, Purification, and Structure*. Elsevier: 2003.
34. Chelucci, G.; Addis, D.; Baldino, S., A new approach to the 1,10-phenanthroline core. *Tetrahedron Lett.* **2007,** *48* (19), 3359-3362.
35. Leiter, J.; Hartwell, J. L.; Kahler, J. S.; Kline, I.; Shear, M. J., Damage Induced in Sarcoma 37 with Chemical Agents. VI. Biphenyl, Fluorene, Phenanthrene, and Tropolone Derivatives. *J. Natl. Cancer. Inst.* **1953,** *14* (2), 365-374.
36. Dwyer, F. P.; Reid, I. K.; Shulman, A.; Laycock, G. M.; Dixson, S., The biological actions of 1,10-phenanthroline and 2,2'-bipyridine hydrochlorides, quaternary salts and metal chelates and related compounds. 1. Bacteriostatic action on selected gram-positive, gram-negative and acid-fast bacteria. *Aust. J. Exp. Biol. Med. Sci.* **1969,** *47* (2), 203-18.
37. Berger, N. A.; Johnson, E. S.; Skinner, S. A. M., Ortho-phenanthroline Inhibition of DNA Synthesis in Mammalian cells. *Exp. Cell Res.* **1975,** *96* (1), 145-155.
38. Krishnamurti, C.; Petering, D. H., Effects of Ethylenediaminetetraacetic Acid and 1,10-Phenanthroline on Cell Proliferation and DNA Synthesis of Ehrlich Ascites Cells. *Cancer Res.* **1980,** *40* (11), 4092-4099.
39. Sánchez-González, Á.; Gil, A., Elucidating the intercalation of methylated 1,10-phenanthroline with DNA: the important weight of the CH/H interactions and the selectivity of CH/π and CH/n interactions. *RSC Adv.* **2021,** *11* (3), 1553-1563.
40. Olsen, P. M.; Ruiz, C.; Lussier, D.; Le, B. K.; Angel, N.; Smith, M.; Hwang, C.; Khatib, R.; Jenkins, J.; Adams, K.; Getcher, J.; Tham, F.; Chen, Z.; Wilson, E. H.; Eichler, J. F., Synthesis, characterization, and antitumor activity of unusual pseudo five coordinate gold(III) complexes: Distinct cytotoxic mechanism or expensive ligand delivery systems? *J. Inorg. Biochem.* **2014,** *141*, 121-131.
41. Sanghvi, C. D.; Olsen, P. M.; Elix, C.; Peng, S.; Wang, D.; Chen, Z.; Shin, D. M.; Hardcastle, K. I.; MacBeth, C. E.; Eichler, J. F., Antitumor properties of five-coordinate gold(III) complexes bearing substituted polypyridyl ligands. *J. Inorg. Biochem.* **2013,** *128*, 68-76.

42. Ramírez-Silva, M. T.; Gómez-Hernández, M. n.; Pacheco-Hernández, M. d. L.; Rojas-Hernández, A.; Galicia, L., Spectroscopy study of 5-amino-1,10-phenanthroline. *Spectrochim. Acta A Mol. Biomol. Spectrosc.* **2004,** *60* (4), 781-789.
43. Neykov, M.; Nikolay, K.; Mihailova, B.; Goshev, I., Antioxidant capacity of 1,10-phenanthroline, 5-amino-1,10-phenanthroline and their Pd-Complexes. *J. Chem. Technol. Metall.* **2017,** *52*, 777-780.
44. Abel, A.; Averin, A.; Beletskaya, I.; Bessmertnykh-Lemeune, A., Transition-Metal-Catalyzed Functionalization of 1,10-Phenanthrolines and Their Complexes. *Targets Heterocycl. Syst.* **2021,** *25*.
45. Smith, G. F.; Cagle, F. W., Jr., The Improved Synthesis of 5-Nitro-1,10-Phenanthroline. *J. Org. Chem.* **1947,** *12* (6), 781-784.
46. Goss, C. A.; Abruna, H. D., Spectral, electrochemical and electrocatalytic properties of 1,10-phenanthroline-5,6-dione complexes of transition metals. *Inorg. Chem* **1985,** *24* (25), 4263-4267.
47. Wendlandt, A. E.; Stahl, S. S., Bioinspired Aerobic Oxidation of Secondary Amines and Nitrogen Heterocycles with a Bifunctional Quinone Catalyst. *J. Am. Chem. Soc.* **2014,** *136* (1), 506-512.
48. Tay, C. X.; Quah, S. Y.; Lui, J. N.; Yu, V. S.; Tan, K. S., Matrix Metalloproteinase Inhibitor as an Antimicrobial Agent to Eradicate Enterococcus faecalis Biofilm. *J. Endod.* **2015,** *41* (6), 858-63.
49. Dolan, N.; McGinley, J.; Stephens, J. C.; Kavanagh, K.; Hurley, D.; Maher, N. J., Synthesis, characterisation and antimicrobial studies of organotin(IV) complexes with 1,10-phenanthroline derivatives. *Inorganica Chim. Acta* **2014,** *409*, 276-284.
50. McCann, M.; Kellett, A.; Kavanagh, K.; Devereux, M.; Santos, A. L. S., Deciphering the Antimicrobial Activity of Phenanthroline Chelators. *Curr. Med. Chem.* **2012,** *19* (17), 2703-2714.
51. Deegan, C.; Coyle, B.; McCann, M.; Devereux, M.; Egan, D. A., In vitro anti-tumour effect of 1,10-phenanthroline-5,6-dione (phendione), [Cu(phendione)3](ClO4)2·4H2O and [Ag(phendione)2]ClO4 using human epithelial cell lines. *Chem. Biol. Interact.* **2006,** *164* (1), 115-125.

52. Lima, A. K. C.; Elias, C. G. R.; Oliveira, S. S. C.; Santos-Mallet, J. R.; McCann, M.; Devereux, M.; Branquinha, M. H.; Dutra, P. M. L.; Santos, A. L. S., Anti-Leishmania braziliensis activity of 1,10-phenanthroline-5,6-dione and its Cu(II) and Ag(I) complexes. *Parasitol. Res.* **2021,** *120* (9), 3273-3285.
53. Cirino, M. E.; Teixeira, T. R.; Silva, A. M. H.; Borges, A. C. C.; Fukui-Silva, L.; Wagner, L. G.; Fernandes, C.; McCann, M.; Santos, A. L. S.; de Moraes, J., Anthelmintic activity of 1,10-phenanthroline-5,6-dione-based metallodrugs. *Sci. Rep.* **2025,** *15* (1), 4699.
54. Shabir, G.; Forrow, N., Development and validation of a HPLC method for 4,7-phenanthroline-5,6-dione I and identification of its major impurity by HPLC-MS-APCI. *J. Chromatogr. Sci.* **2005,** *43*, 207-12.
55. Zhou, C.; Xiao, S.; Wang, M.; Jiang, W.; Liu, H.; Zhang, S.; Yang, B., Modulation of Excited State Property Based on Benzo[a, c]phenazine Acceptor: Three Typical Excited States and Electroluminescence Performance. *Front. Chem.* **2019,** *7*.
56. Batista, R. M. F.; Costa, S. P. G.; Belsley, M.; Lodeiro, C.; Raposo, M. M. M., Synthesis and Characterization of Novel (oligo)thienyl-imidazo-phenanthrolines as Versatile π-conjugated systems for Several Optical Applications. *Tetrahedron* **2008,** *64* (39), 9230-9238.
57. Singh, R. K.; Rai, D.; Yadav, D.; Bhargava, A.; Balzarini, J.; De Clercq, E., Synthesis, antibacterial and antiviral properties of curcumin bioconjugates bearing dipeptide, fatty acids and folic acid. *Eur. J. Med. Chem.* **2010,** *45* (3), 1078-1086.
58. Barrett, S.; Delaney, S.; Kavanagh, K.; Montagner, D., Evaluation of in vitro and in vivo Antibacterial Activity of Novel Cu(II)-steroid Complexes. *Inorganica Chim. Acta* **2018,** *479*, 261-265.
59. Xu, B.-B.; Jin, N.; Liu, J.-C.; Liao, A.-Q.; Lin, H.-Y.; Qin, X.-Y., Arene–Arene Coupled Disulfamethazines (or Sulfadiazine)-Phenanthroline-Metal(II) Complexes were Synthesized by In Situ Reactions and Inhibited the Growth and Development of Triple-Negative Breast Cancer through the Synergistic Effect of Antiangiogenesis, Anti-Inflammation, Pro-Apoptosis, and Cuproptosis. *J. Med. Chem.* **2024,** *67* (9), 7088-7111.

60. Sigman, D. S.; Graham, D. R.; D'Aurora, V.; Stern, A. M., Oxygen-dependent cleavage of DNA by the 1,10-phenanthroline . cuprous complex. Inhibition of Escherichia coli DNA polymerase I. *J. Biol. Chem.* **1979,** *254* (24), 12269-72.
61. Aklilu Melese, M., The Study of Antimicrobial Activities of Various Transition Metal Mixed Ligand Complexes Containing 1,10-Phenanthroline with Any Other Ligands. *Int. J. Biol. Chem.* **2022,** *7* (1), 1-10.
62. Gandra, R. M.; Pacheco, C. A.; Sangenito, L. S.; Ramos, L. S.; Souza, L. O.; McCarron, P.; McCann, M.; Devereux, M.; Branquinha, M. H.; Santos, A. L., Manganese(II), copper(II) and silver(I) complexes containing 1,10-phenanthroline/1,10-phenanthroline-5,6-dione against Candida species. *Future Microbiol.* **2024,** *19*, 385-395.
63. Dobrina Doncheva, T.; Svetozar Detelinov, M.; Ivanka Ivanova, K., Pharmacological Activity of Metal-Based Organic Complexes Against Different Viral Diseases. *Pharmacophore* **2024,** *15* (3), 1-11.
64. Abdolmaleki, S.; Aliabadi, A.; Khaksar, S., Riding The Metal Wave: A Review of the Latest Developments in Metal-based Anticancer Agents. *Coord. Chem. Rev.* **2024,** *501*, 215579.
65. Cade, G.; Cohen, M.; Shulman, A., The Action of Phenanthroline Metal Chelates and Related Substances on Erysiphelothrix rhusiopathiae and Fusiformis nodosus. *Aust. Vet. J.* **1970,** *46* (8), 387-392.
66. Butler, H. M.; Laver, J. C.; Shulman, A.; Wright, R. D., The use of phenanthroline metal chelates for the control of topical infections due to bacteria, fungi and protozoa. *Med. J. Aust.* **1970,** *2* (7), 309-14.
67. O'Shaughnessy, M.; Hurley, J.; Dillon, S. C.; Herra, C.; McCarron, P.; McCann, M.; Devereux, M.; Howe, O., Antibacterial activity of metal-phenanthroline complexes against multidrug-resistant Irish clinical isolates: a whole genome sequencing approach. *J. Biol. Inorg. Chem.* **2023,** *28* (2), 153-171.
68. Vianez Peregrino, I.; Ferreira Ventura, R.; Borghi, M.; Pinto Schuenck, R.; Devereux, M.; McCann, M.; Souza dos Santos, A. L.; FerreiraNunes, A. P., Antibacterial activity and carbapenem re-sensitizing ability of 1,10-phenanthroline-5,6-dione and its metal complexes against KPC-producing

Klebsiella pneumoniae clinical strains. *Lett. Appl. Microbiol.* **2021,** *73* (2), 139-148.

69. McCann, M.; Coyle, B.; McKay, S.; McCormack, P.; Kavanagh, K.; Devereux, M.; McKee, V.; Kinsella, P.; O'Connor, R.; Clynes, M., Synthesis and X-ray crystal structure of [Ag(phendio)2]ClO4 (phendio = 1,10-phenanthroline-5,6-dione) and its effects on fungal and mammalian cells. *BioMetals* **2004,** *17* (6), 635-645.
70. Szymański, P.; Frączek, T.; Markowicz, M.; Mikiciuk-Olasik, E., Development of copper based drugs, radiopharmaceuticals and medical materials. *BioMetals* **2012,** *25* (6), 1089-1112.
71. Ahmed, M., Transition Metal Complexes of Novel Phenanthroline Derivatives and their Antibacterial Activity. *PhD Thesis* **2019,** *Maynooth University*
72. Baker, J.; Sitthisak, S.; Sengupta, M.; Johnson, M.; Jayaswal, R. K.; Morrissey, J. A., Copper Stress Induces a Global Stress Response in Staphylococcus aureus and Represses sae and agr Expression and Biofilm Formation. *Applied and Environmental Microbiology* **2010,** *76* (1), 150-60.
73. Hindo, S. S.; Frezza, M.; Tomco, D.; Heeg, M. J.; Hryhorczuk, L.; McGarvey, B. R.; Dou, Q. P.; Verani, C. N., Metals in anticancer therapy: copper(II) complexes as inhibitors of the 20S proteasome. *Eur. J. Med. Chem.* **2009,** *44* (11), 4353-61.
74. Sigman, D. S., Nuclease activity of 1,10-phenanthroline-copper ion. *Accounts of Chemical Research* **1986,** *19* (6), 180-186.
75. Pereira, A. L.; Vasconcelos, M. A.; Andrade, A. L.; Martins, I. M.; Holanda, A. K. M.; Gondim, A. C. S.; Penha, D. P. S.; Bruno, K. L.; Silva, F. O. N.; Teixeira, E. H., Antimicrobial and Antibiofilm Activity of Copper-Based Metallic Compounds Against Bacteria Related with Healthcare-Associated Infections. *Curr. Microbiol.* **2023,** *80* (4), 133.
76. Creaven, B. S.; Egan, D. A.; Karcz, D.; Kavanagh, K.; McCann, M.; Mahon, M.; Noble, A.; Thati, B.; Walsh, M., Synthesis, characterisation and antimicrobial activity of copper(II) and manganese(II) complexes of coumarin-6,7-dioxyacetic acid (cdoaH2) and 4-methylcoumarin-6,7-dioxyacetic acid (4-MecdoaH2): X-ray crystal structures of

[Cu(cdoa)(phen)2]·8.8H2O and [Cu(4-Mecdoa)(phen)2]·13H2O (phen=1,10-phenanthroline). *J. Inorg. Biochem.* **2007,** *101* (8), 1108-1119.

77. Stănilă, A.; Braicu, C.; Stănilă, S., Antibacterial activity of copper and cobalt amino acids complexes. *Not. Bot. Horti. Agrobo.* **2011,** *39* (2), 124-129.
78. Chohan, Z. H.; Arif, M.; Sarfraz, M., Metal-based antibacterial and antifungal amino acid derived Schiff bases: their synthesis, characterization and in vitro biological activity. *Appl. Organomet. Chem.* **2007,** *21* (4), 294-302.
79. Fernandes, P.; Sousa, I.; Cunha-Silva, L.; Ferreira, M.; de Castro, B.; Pereira, E. F.; Feio, M. J.; Gameiro, P., Synthesis, characterization and antibacterial studies of a copper(II) lomefloxacin ternary complex. *J. Inorg. Biochem.* **2014,** *131*, 21-9.
80. Salomon, E.; Keren, N.; Kanteev, M.; Adir, N., Manganese in Biological Systems: Transport and Function. In *Patai's Chemistry of Functional Groups*, Wiley: 2011.
81. Kaim, W.; Schwederski, B., *Bioinorganic Chemistry: Inorganic Elements in the Chemistry of Life*. Wiley: 1994.
82. Ali, B.; Iqbal, M. A., Coordination Complexes of Manganese and Their Biomedical Applications. *ChemistrySelect* **2017,** *2* (4), 1586-1604.
83. Rosu, T.; Pahontu, E.; Maxim, C.; Georgescu, R.; Stanica, N.; Almajan, G. L.; Gulea, A., Synthesis, characterization and antibacterial activity of some new complexes of Cu(II), Ni(II), VO(II), Mn(II) with Schiff base derived from 4-amino-2,3-dimethyl-1-phenyl-3-pyrazolin-5-one. *Polyhedron* **2010,** *29* (2), 757-766.
84. Sharma, S.; Meena, R.; Satyawana, Y.; Fahmi, N., Manganese(II) complexes of biological relevance: Synthesis and spectroscopic characterization of novel manganese(II) complexes with monobasic bidentate ligands derived from halo-substituted 1H-indole-2,3-diones. *Russ. J. Gen. Chem.* **2016,** *86* (12), 2807-2816.
85. Lenis-Rojas, O. A.; Carvalho, B.; Cabral, R.; Silva, M.; Friães, S.; Roma-Rodrigues, C.; Meireles, M. S. H.; Gomes, C. S. B.; Fernández, J. A. A.; Vila, S. F.; Rubiolo, J. A.; Sanchez, L.; Baptista, P. V.; Fernandes, A. R.; Royo, B.,

Manganese(I) tricarbonyl complexes as potential anticancer agents. *J. Biol. Inorg. Chem.* **2022,** *27* (1), 49-64.

86. Roy, S.; Hagen, K. D.; Maheswari, P. U.; Lutz, M.; Spek, A. L.; Reedijk, J.; van Wezel, G. P., Phenanthroline Derivatives with Improved Selectivity as DNA-Targeting Anticancer or Antimicrobial Drugs. *ChemMedChem* **2008,** *3* (9), 1427-1434.
87. Liu, X.; Sun, B.; Kell, R. E. M.; Southam, H. M.; Butler, J. A.; Li, X.; Poole, R. K.; Keene, F. R.; Collins, J. G., The Antimicrobial Activity of Mononuclear Ruthenium(II) Complexes Containing the dppz Ligand. *ChemPlusChem* **2018,** *83* (7), 643-650.
88. Sun, D.; Zhang, W.; Yang, E.; Li, N.; Liu, H.; Wang, W., Investigation of antibacterial activity and related mechanism of a ruthenium(II) polypyridyl complex. *Inorg. Chem. Commun.* **2015,** *56*, 17-21.
89. Li, F.; Mulyana, Y.; Feterl, M.; Warner, J. M.; Collins, J. G.; Keene, F. R., The antimicrobial activity of inert oligonuclear polypyridylruthenium(ii) complexes against pathogenic bacteria, including MRSA. *Dalton Trans.* **2011,** *40* (18), 5032-5038.
90. Anbu, S.; Asaithambi, K.; Alegria, E.; Mathan, G.; Kandaswamy, M., Effect of 1,10-Phenanthroline on DNA Binding, DNA Cleavage, Cytotoxic and Lactate Dehydrogenase Inhibition Properties of Robson Type Macrocyclic Dicopper(II) Complex. *J. Coord. Chem.* **2013,** *66*, 3989–4003.
91. Tweedy, B. G., Plant extracts with metal ions as potential antimicrobial agents. *Phytopathol.* **1964,** (55), 910-914.
92. Ng, N. S.; Leverett, P.; Hibbs, D. E.; Yang, Q.; Bulanadi, J. C.; Wu, M. J.; Aldrich-Wright, J. R., The antimicrobial properties of some copper(II) and platinum(II) 1,10-phenanthroline complexes. *Dalton Trans.* **2013,** *42* (9), 3196-209.
93. Cai, X.; Pan, N.; Zou, G., Copper-1,10-phenanthroline-induced apoptosis in liver carcinoma Bel-7402 cells associates with copper overload, reactive oxygen species production, glutathione depletion and oxidative DNA damage. *Biometals* **2007,** *20* (1), 1-11.

94. Tarushi, A.; Lafazanis, K.; Kljun, J.; Turel, I.; Pantazaki, A. A.; Psomas, G.; Kessissoglou, D. P., First- and second-generation quinolone antibacterial drugs interacting with zinc(II): structure and biological perspectives. *J. Inorg. Biochem.* **2013,** *121*, 53-65.
95. Chopra, I., The increasing use of silver-based products as antimicrobial agents: a useful development or a cause for concern? *J. Antimicrob. Chemother.* **2007,** *59* (4), 587-590.
96. Hutchings, M. I.; Truman, A. W.; Wilkinson, B., Antibiotics: past, present and future. *Curr. Opin. Microbiol.* **2019,** *51*, 72-80.
97. WHO Antimicrobial Resistance: Fact Sheets. (accessed August 2024).
98. Bassetti, M.; Merelli, M.; Temperoni, C.; Astilean, A., New Antibiotics for Bad Bugs: Where are We? *Annals of Clinical Microbiology and Antimicrobials* **2013,** *12*, 22.
99. Clement, J. L.; Jarrett, P. S., Antibacterial silver. *Met. Based Drugs* **1994,** *1* (5-6), 467-82.
100. Kaštelan, S.; Anić Jurica, S.; Orešković, S.; Župić, T.; Herman, M.; Gverović Antunica, A.; Marković, I.; Bakija, I., A Survey of Current Prophylactic Treatment for Ophthalmia Neonatorum in Croatia and a Review of International Preventive Practices. *Med. Sci. Monit.* **2018,** *24*, 8042-8047.
101. Silver, S.; Phung, L. T.; Silver, G., Silver as biocides in burn and wound dressings and bacterial resistance to silver compounds. *J. Ind. Microbiol. Biotechnol.* **2006,** *33* (7), 627-634.
102. Pachaiappan, R.; Ponce, L. C.; Manavalan, K.; Awad, F.; Rajan, V. F., Chapter 10 - Nanoparticles as an exotic antibacterial, antifungal, and antiviral agents. In *Advances in Nanotechnology for Marine Antifouling*, Gupta, R. K.; Nadda, A. K.; Nguyen, T. A.; Sharma, S.; Bilal, M., Eds. Elsevier: 2023; pp 231-270.
103. Ying, N.; Liu, S.; Zhang, M.; Cheng, J.; Luo, L.; Jiang, J.; Shi, G.; Wu, S.; Ji, J.; Su, H.; Pan, H.; Zeng, D., Nano delivery system for paclitaxel: Recent advances in cancer theranostics. *Colloids Surf. B Biointerfaces* **2023,** *228*, 113419.

104. Lansdown, A. B., Silver in health care: antimicrobial effects and safety in use. *Curr. Probl. Dermatol.* **2006,** *33*, 17-34.

105. Azzopardi, E. A.; Ferguson, E. L.; Thomas, D. W., The Enhanced Permeability Retention Effect: A New Paradigm for Drug Targeting in Infection. *J. Antimicrob. Chemother.* **2013,** *68* (2), 257-74.

106. Nikaido, H.; Pagès, J. M., Broad-specificity efflux pumps and their role in multidrug resistance of Gram-negative bacteria. *FEMS Microbiol. Rev.* **2012,** *36* (2), 340-63.

107. Morones-Ramirez, J. R.; Winkler, J. A.; Spina, C. S.; Collins, J. J., Silver enhances antibiotic activity against gram-negative bacteria. *Sci. Transl. Med.* **2013,** *5* (190), 190ra81.

108. Yang, H.-C.; Pon, L. A., Toxicity of Metal Ions Used in Dental Alloys: A Study in the Yeast Saccharomyces cerevisiae. *Drug Chem. Toxicol.* **2003,** *26* (2), 75-85.

109. Viganor, L.; Galdino, A. C.; Nunes, A. P.; Santos, K. R.; Branquinha, M. H.; Devereux, M.; Kellett, A.; McCann, M.; Santos, A. L., Anti-Pseudomonas aeruginosa activity of 1,10-phenanthroline-based drugs against both planktonic- and biofilm-growing cells. *J. Antimicrob. Chemother.* **2016,** *71* (1), 128-34.

110. O'Shaughnessy, M.; McCarron, P.; Viganor, L.; McCann, M.; Devereux, M.; Howe, O. The Antibacterial and Anti-Biofilm Activity of Metal Complexes Incorporating 3,6,9-Trioxaundecanedioate and 1,10-Phenanthroline Ligands in Clinical Isolates of Pseudomonas aeruginosa from Irish Cystic Fibrosis Patients *Antibiotics,* **2020**, *9* (10).

111. Ahmed, M.; Rooney, D.; McCann, M.; Devereux, M.; Twamley, B.; Galdino, A. C. M.; Sangenito, L. S.; Souza, L. O. P.; Lourenço, M. C.; Gomes, K.; dos Santos, A. L. S., Synthesis and Antimicrobial Activity of a Phenanthroline-Isoniazid Hybrid Ligand and its Ag+ and Mn2+ Complexes. *BioMetals* **2019,** *32* (4), 671-682.

112. Thornton, L.; Dixit, V.; Assad, L. O. N.; Ribeiro, T. P.; Queiroz, D. D.; Kellett, A.; Casey, A.; Colleran, J.; Pereira, M. D.; Rochford, G.; McCann, M.; O'Shea, D.; Dempsey, R.; McClean, S.; Kia, A. F.-A.; Walsh, M.;

Creaven, B.; Howe, O.; Devereux, M., Water-soluble and photo-stable silver(I) dicarboxylate complexes containing 1,10-phenanthroline ligands: Antimicrobial and anticancer chemotherapeutic potential, DNA interactions and antioxidant activity. *J. Inorg. Biochem.* **2016,** *159*, 120-132.

113. Niu, Z. L.; Zhou, S. H.; Wu, Y. Y.; Wu, T. T.; Liu, Q. S.; Zhao, Q. H.; Ji, H.; Ren, X.; Xie, M. J., Multifunctional O-phenanthroline silver(I) complexes for antitumor activity against colorectal adenocarcinoma cells and antimicrobial properties by multiple mechanisms. *J. Inorg. Biochem.* **2023,** *246*, 112293.

114. Siegesmund, A.; Köckerling, M., Hexanuclear Chalcogenide-Supported Rhenium Cluster Compounds: Structures, Properties, and Applications. In *Ref. Mod. Chem. Mol. Sci Chem Eng*, Elsevier: 2016.

115. King, A., This is not new. A short history of materials criticality and supply-chain challenges. In *Crit. Mat.*, King, A., Ed. Elsevier: 2021; pp 19-51.

116. Shegani, A.; Triantis, C.; Nock, B. A.; Maina, T.; Kiritsis, C.; Psycharis, V.; Raptopoulou, C.; Pirmettis, I.; Tisato, F.; Papadopoulos, M. S., Rhenium(I) Tricarbonyl Complexes with (2-Hydroxyphenyl)diphenylphosphine as PO Bidentate Ligand. *Inorg. Chem* **2017,** *56* (14), 8175-8186.

117. Enslin, L. E.; Purkait, K.; Pozza, M. D.; Saubamea, B.; Mesdom, P.; Visser, H. G.; Gasser, G.; Schutte-Smith, M., Rhenium(I) Tricarbonyl Complexes of 1,10-Phenanthroline Derivatives with Unexpectedly High Cytotoxicity. *Inorg. Chem* **2023,** *62* (31), 12237-12251.

118. Maisuls, I.; Wolcan, E.; Piro, O. E.; Castellano, E. E.; Petroselli, G.; Erra-Balsells, R.; Cabrerizo, F. M.; Ruiz, G. T., Synthesis, Structural Characterization and Biological Evaluation of Rhenium(I) Tricarbonyl Complexes with β-Carboline Ligands. *ChemistrySelect* **2017,** *2* (27), 8666-8672.

119. Ramamurthy, V.; Schanze, K. S., *Semiconductor Photochemistry And Photophysics*. Taylor & Francis INC International Concepts: 2003; Vol. 10.

120. Dinjus, E., Electrochemical and Electrocatalytic Reactions of Carbon Dioxide. *Z. Phys. Chem.* **1995,** *189* (2), 278-279.

121. Grätzel, M., Solar Energy Conversion by Dye-Sensitized Photovoltaic Cells. *Inorg. Chem* **2005,** *44* (20), 6841-6851.

122. Arakawa, H.; Aresta, M.; Armor, J. N.; Barteau, M. A.; Beckman, E. J.; Bell, A. T.; Bercaw, J. E.; Creutz, C.; Dinjus, E.; Dixon, D. A.; Domen, K.; DuBois, D. L.; Eckert, J.; Fujita, E.; Gibson, D. H.; Goddard, W. A.; Goodman, D. W.; Keller, J.; Kubas, G. J.; Kung, H. H.; Lyons, J. E.; Manzer, L. E.; Marks, T. J.; Morokuma, K.; Nicholas, K. M.; Periana, R.; Que, L.; Rostrup-Nielson, J.; Sachtler, W. M. H.; Schmidt, L. D.; Sen, A.; Somorjai, G. A.; Stair, P. C.; Stults, B. R.; Tumas, W., Catalysis Research of Relevance to Carbon Management: Progress, Challenges, and Opportunities. *Chem. Rev.* **2001,** *101* (4), 953-996.

123. Zhao, G.-W.; Zhao, J.-H.; Hu, Y.-X.; Zhang, D.-Y.; Li, X., Recent advances of neutral rhenium(I) tricarbonyl complexes for application in organic light-emitting diodes. *Synth. Met.* **2016,** *212*, 131-141.

124. Kam-Wing Lo, K.; Chun-Ming Ng, D.; Hui, W.-K.; Cheung, K.-K., Luminescent rhenium(i) polypyridine complexes with an isothiocyanate moiety–versatile labelling reagents for biomolecules. *Dalton Trans.* **2001,** (18), 2634-2640.

125. Schindler, K.; Zobi, F., Anticancer and Antibiotic Rhenium Tri- and Dicarbonyl Complexes: Current Research and Future Perspectives. *Molecules* **2022,** *27* (2).

126. Siegmund, D.; Lorenz, N.; Gothe, Y.; Spies, C.; Geissler, B.; Prochnow, P.; Nuernberger, P.; Bandow, J. E.; Metzler-Nolte, N., Benzannulated Re(i)–NHC complexes: synthesis, photophysical properties and antimicrobial activity. *Dalton Trans.* **2017,** *46* (44), 15269-15279.

127. Sovari, S. N.; Radakovic, N.; Roch, P.; Crochet, A.; Pavic, A.; Zobi, F., Combatting AMR: A molecular approach to the discovery of potent and non-toxic rhenium complexes active against C. albicans-MRSA co-infection. *Eur. J. Med. Chem.* **2021,** *226*, 113858.

128. Wu, L.; Cai, X.; Zhu, H.; Li, J.; Shi, D.; Su, D.; Yue, D.; Gu, Z., PDT-Driven Highly Efficient Intracellular Delivery and Controlled Release of CO in

Combination with Sufficient Singlet Oxygen Production for Synergistic Anticancer Therapy. *Advanced Functional Materials* **2018,** *28* (41), 1804324.

129. Chakraborty, I.; Jimenez, J.; Sameera, W. M. C.; Kato, M.; Mascharak, P. K., Luminescent Re(I) Carbonyl Complexes as Trackable PhotoCORMs for CO delivery to Cellular Targets. *Inorg. Chem* **2017,** *56* (5), 2863-2873.

130. Knopf, K. M.; Murphy, B. L.; MacMillan, S. N.; Baskin, J. M.; Barr, M. P.; Boros, E.; Wilson, J. J., In Vitro Anticancer Activity and in Vivo Biodistribution of Rhenium(I) Tricarbonyl Aqua Complexes. *J. Am. Chem. Soc.* **2017,** *139* (40), 14302-14314.

131. Marker, S. C.; MacMillan, S. N.; Zipfel, W. R.; Li, Z.; Ford, P. C.; Wilson, J. J., Photoactivated in Vitro Anticancer Activity of Rhenium(I) Tricarbonyl Complexes Bearing Water-Soluble Phosphines. *Inorg. Chem* **2018,** *57* (3), 1311-1331.

132. Ramos, C.; Prado, F.; Gomes do Carmo, M.; Farias, G.; Souza, B.; Da Hora Machado, A. E.; Otavio, A.; Patrocinio, A. O., Temperature Dependent Emission Properties of Re I Tricarbonyl Complexes with Dipyrido-Quinoxaline and Phenazine Ligands. *J. Braz. Chem. Soc.* **2021,** *33*.

133. Schindler, K.; Cortat, Y.; Nedyalkova, M.; Crochet, A.; Lattuada, M.; Pavic, A.; Zobi, F., Antimicrobial Activity of Rhenium Di- and Tricarbonyl Diimine Complexes: Insights on Membrane-Bound S. aureus Protein Binding. *Pharmaceuticals (Basel)* **2022,** *15* (9).

134. Delasoie, J.; Pavic, A.; Voutier, N.; Vojnovic, S.; Crochet, A.; Nikodinovic-Runic, J.; Zobi, F., Identification of novel potent and non-toxic anticancer, anti-angiogenic and antimetastatic rhenium complexes against colorectal carcinoma. *Eur. J. Med. Chem.* **2020,** *204*, 112583.

135. Konkankit, C. C.; King, A. P.; Knopf, K. M.; Southard, T. L.; Wilson, J. J., In Vivo Anticancer Activity of a Rhenium(I) Tricarbonyl Complex. *ACS Medicinal Chemistry Letters* **2019,** *10* (5), 822-827.

136. Davidge, K. S.; Motterlini, R.; Mann, B. E.; Wilson, J. L.; Poole, R. K., Carbon monoxide in biology and microbiology: surprising roles for the "Detroit perfume". *Adv Microb Physiol* **2009,** *56*, 85-167.

137. Ryter, S. W.; Otterbein, L. E., Carbon monoxide in biology and medicine. *Bioessays* **2004,** *26* (3), 270-80.

138. Leffler, C. W.; Parfenova, H.; Jaggar, J. H., Carbon monoxide as an endogenous vascular modulator. *Am J Physiol Heart Circ Physiol* **2011,** *301* (1), H1-h11.

139. Khan, H.; Faizan, M.; Niazi, S. U. K.; Madiha; Muhammad, N.; Zhang, W., Water-Soluble Carbon Monoxide-Releasing Molecules (CORMs). *Topics in Current Chemistry* **2022,** *381* (1), 3.

140. Balakrishna, M. S.; Ghosh, P. Metal Carbonyls. (accessed 07 2025).

141. Ismailova, A.; Kuter, D.; Bohle, D. S.; Butler, I. S., An Overview of the Potential Therapeutic Applications of CO-Releasing Molecules. *Bioinorganic Chemistry and Applications* **2018,** *2018* (1), 8547364.

142. Cheng, J.; Hu, J., Recent Advances on Carbon Monoxide Releasing Molecules for Antibacterial Applications. *ChemMedChem* **2021,** *16* (24), 3628-3634.

143. Ling, K.; Men, F.; Wang, W.-C.; Zhou, Y.-Q.; Zhang, H.-W.; Ye, D.-W., Carbon Monoxide and Its Controlled Release: Therapeutic Application, Detection, and Development of Carbon Monoxide Releasing Molecules (CORMs). *Journal of Medicinal Chemistry* **2018,** *61* (7), 2611-2635.

144. Tien Vo, T. T.; Vo, Q. C.; Tuan, V. P.; Wee, Y.; Cheng, H.-C.; Lee, I. T., The potentials of carbon monoxide-releasing molecules in cancer treatment: An outlook from ROS biology and medicine. *Redox Biology* **2021,** *46*, 102124.

145. Choi, H.-I.; Zeb, A.; Kim, M.-S.; Rana, I.; Khan, N.; Qureshi, O. S.; Lim, C.-W.; Park, J.-S.; Gao, Z.; Maeng, H.-J.; Kim, J.-K., Controlled therapeutic delivery of CO from carbon monoxide-releasing molecules (CORMs). *Journal of Controlled Release* **2022,** *350*, 652-667.

146. Zheng, R. H.; Guo, H. C.; Jiang, H. J.; Xu, K. H.; Liu, B. B.; Sun, W. L.; Shen, Z. Q., A new and convenient synthesis of phendiones oxidated by $KBrO_3/H_2SO_4$ at room temperature. *Chin. Chem. Lett.* **2010,** *21* (11), 1270-1272.

147. Stein, G.; Nudelman, A.; Rephaeli, A.; Gil-Ad, I.; Weizman, A. Conjugates for Treating Neurodegenerative Diseases and Disorders. 2012.

148. Ndinguri, M. W.; Black, C. A.; Gosser, A. L.; Reitz, S.; Sutphin, C.; Fronczek, F. R.; Cormier, L. E., Exploring the synthesis and characterization of fac-Re(CO)3L complexes using diethylenetriamine derivative functionalized at the central nitrogen. *Inorganica Chim. Acta* **2021,** *520*, 120291.

149. Fantini, G.; Dallerba, E.; Massi, M.; Lowe, A. B., Luminescent copolymer-rhenium(I) hybrid materials via picolylamine-modified poly(pentafluorophenyl acrylate). *Macromol. Chem. Phys.* **2020,** *221* (15), 2000135.

150. Souza, B. L.; Faustino, L. A.; Prado, F. S.; Sampaio, R. N.; Maia, P. I. S.; Machado, A. E. H.; Patrocinio, A. O. T., Spectroscopic characterization of a new Re(i) tricarbonyl complex with a thiosemicarbazone derivative: towards sensing and electrocatalytic applications. *Dalton Trans.* **2020,** *49* (45), 16368-16379.

151. Kaplanis, M.; Stamatakis, G.; Papakonstantinou, V. D.; Paravatou-Petsotas, M.; Demopoulos, C. A.; Mitsopoulou, C. A., Re(I) tricarbonyl complex of 1,10-phenanthroline-5,6-dione: DNA binding, cytotoxicity, anti-inflammatory and anti-coagulant effects towards platelet activating factor. *J. Inorg. Biochem.* **2014,** *135*, 1-9.

152. Vielhaber, T.; Topf, C., Manganese-catalyzed homogeneous hydrogenation of ketones and conjugate reduction of α,β-unsaturated carboxylic acid derivatives: A chemoselective, robust, and phosphine-free in situ-protocol. *Applied Catalysis A: General* **2021,** *623*, 118280.

153. Berkow Elizabeth, L.; Lockhart Shawn, R.; Ostrosky-Zeichner, L., Antifungal Susceptibility Testing: Current Approaches. *Clin. Microbiol. Rev.* **2020,** *33* (3), 10.1128/cmr.00069-19.

154. Promega CellTiter-Glo 2.0 Assay. (accessed October 2024).

155. Collaborators, A. R., Global burden of bacterial antimicrobial resistance in 2019:a systematic analysis. *Lancet* **2022,** *399* (10325), 629-655.

156. Ruekit, S.; Srijan, A.; Serichantalergs, O.; Margulieux, K. R.; Mc Gann, P.; Mills, E. G.; Stribling, W. C.; Pimsawat, T.; Kormanee, R.; Nakornchai, S.; Sakdinava, C.; Sukhchat, P.; Wojnarski, M.; Demons, S. T.;

Crawford, J. M.; Lertsethtakarn, P.; Swierczewski, B. E., Molecular characterization of multidrug-resistant ESKAPEE pathogens from clinical samples in Chonburi, Thailand (2017–2018). *BMC Infect. Dis.* **2022,** *22* (1), 695.

157. WHO *Global antimicrobial resistance and use surveillance system (GLASS) report*; 2022.

158. Kainz, K.; Bauer, M. A.; Madeo, F.; Carmona-Gutierrez, D., Fungal Infections in Humans: The Silent Crisis. *Microb. Cell.* **2020,** *7* (6), 143-145.

159. Casalini, G.; Giacomelli, A.; Antinori, S., The WHO fungal priority pathogens list: a crucial reappraisal to review the prioritisation. *Lancet Microbe* **2024,** *5* (7), 717-724.

160. Möhler, J. S.; Sim, W.; Blaskovich, M. A. T.; Cooper, M. A.; Ziora, Z. M., Silver bullets: A new lustre on an old antimicrobial agent. *Biotechnol. Adv.* **2018,** *36* (5), 1391-1411.

161. Shahzad, M. N.; Ahmed, N., Effectiveness of Aloe Vera gel compared with 1% silver sulphadiazine cream as burn wound dressing in second degree burns. *J. Pak. Med. Assoc.* **2013,** *63* (2), 225-30.

162. Boateng, J.; Catanzano, O., Silver and Silver Nanoparticle-Based Antimicrobial Dressings. In *Therapeutic Dressings and Wound Healing Applications*, 2020; pp 157-184.

163. Vagabov, V. M.; Ivanov, A. Y.; Kulakovskaya, T. V.; Kulakovskaya, E. V.; Petrov, V. V.; Kulaev, I. S., Efflux of potassium ions from cells and spheroplasts of Saccharomyces cerevisiae yeast treated with silver and copper ions. *Biochemistry (Mosc)* **2008,** *73* (11), 1224-1227.

164. Hecel, A.; Kolkowska, P.; Krzywoszynska, K.; Szebesczyk, A.; Rowinska-Zyrek, M.; Kozlowski, H., Ag+ Complexes as Potential Therapeutic Agents in Medicine and Pharmacy. *Curr. Med. Chem.* **2019,** *26* (4), 624-647.

165. Gandra, R. M.; McCarron, P.; Viganor, L.; Fernandes, M. F.; Kavanagh, K.; McCann, M.; Branquinha, M. H.; Santos, A. L. S.; Howe, O.; Devereux, M., In vivo Activity of Copper(II), Manganese(II), and Silver(I) 1,10-Phenanthroline Chelates Against Candida haemulonii Using the Galleria mellonella Model. *Front. microbiol.* **2020,** *11*.

166. Aslam, S.; Isab, A. A.; Alotaibi, M. A.; Saleem, M.; Monim-ul-Mehboob, M.; Ahmad, S.; Georgieva, I.; Trendafilova, N., Synthesis, Spectroscopic Characterization, DFT Calculations and Antimicrobial Properties of Silver(I) Complexes of 2,2'-Bipyridine and 1,10-Phenanthroline. *Polyhedron* **2016,** *115*, 212-218.

167. Coyle, B.; McCann, M.; McKee, V.; Devereux, M., Synthesis and X-ray crystal structure of a tetracyclic gem-cis-bis(aminal) formed from N,N'-bis(2-aminophenyl)ethylenediamine and 1,10-phenanthroline-5,6-dione. *ARKIVOC* **2003,** *2003* (7), 59-66.

168. Ritter, K.; Pehlken, C.; Sorsche, D.; Rau, S., Optimized synthesis of a tert-butyl-phenyl-substituted tetrapyridophenazine ligand and its Ru(ii) complexes and determination of dimerization behaviour of the complexes through supramolecular "Fingerhakel". *Dalton Trans.* **2015,** *44* (19), 8889-8905.

169. Kumar, R.; Mathur, P., Aerobic oxidation of 1,10-phenanthroline to phen-dione catalyzed by copper(ii) complexes of a benzimidazolyl Schiff base. *RSC Adv.* **2014,** *4* (63), 33190-33193.

170. Buckley, B. R.; Neary, S. P.; Elsegood, M. R. J., The First Enantiomerically Pure Thiadiazol-3-one 1-oxide and Thiatriaza-indene 3-oxide Systems Chiral at the Sulfur Atom. *Tetrahedron: Asymmetry* **2010,** *21* (16), 1959-1962.

171. Capilato, J. N.; Philippi, S. V.; Reardon, T.; McConnell, A.; Oliver, D. C.; Warren, A.; Adams, J. S.; Wu, C.; Perez, L. J., Development of a novel series of non-natural triaryl agonists and antagonists of the Pseudomonas aeruginosa LasR quorum sensing receptor. *Bioorg. Med. Chem.* **2017,** *25* (1), 153-165.

172. Ahmed, M.; Rooney, D.; McCann, M.; Casey, J.; O'Shea, K.; Twamley, B., Tuning the Reaction Pathways of Phenanthroline-Schiff Bases: Routes to Novel Phenanthroline Ligands. *Dalton Trans.* **2019,** *48* (40), 15283-15289.

173. Raja, P. M. V.; Barron, A. R. NMR Spectroscopy. (accessed September 2024).

174. Liu, X. IR Spectrum and Characteristic Absorption Bands. (accessed September 2024).

175. McCann, M.; McGinley, J.; Ni, K.; O'Connor, M.; Kavanagh, K.; McKee, V.; Colleran, J.; Devereux, M.; Gathergood, N.; Barron, N.; Prisecaru, A.; Kellett, A., A New Phenanthroline–oxazine Ligand: Synthesis, Coordination Chemistry and Aypical DNA Bnding Iteraction. *Chem. Commun.* **2013,** *49* (23), 2341-2343.

176. Ahmed, M.; Ward, S.; McCann, M.; Kavanagh, K.; Heaney, F.; Devereux, M.; Twamley, B.; Rooney, D., Synthesis and Characterisation of Phenanthroline-oxazine Ligands and their Ag(I), Mn(II) and Cu(II) Complexes and their Evaluation as Antibacterial Agents. *BioMetals* **2022,** *35* (1), 173-185.

177. Valkó, K. L., Chapter 13 - Application of HPLC measurements for the determination of physicochemical and biomimetic properties to model in vivo drug distribution in support of early drug discovery. In *Handb. Anal. Sep.*, Valkó, K. l., Ed. Elsevier Science B.V.: 2020; Vol. 8, pp 667-758.

178. Lau, E., 5 - Preformulation Studies. In *Separation Science and Technology*, Ahuja, S.; Scypinski, S., Eds. Academic Press: 2001; Vol. 3, pp 173-233.

179. LCGC, Understanding Gradient HPLC. *LCGC* **2013,** *31* (7), 578.

180. Li, P. G.; Wang, Q. L.; Li, D. S.; Fu, F.; Qi, G. C., Crystal structure of bis(1,10-phenanthroline-N,N')silver(I) mononitrate, [Ag(C12H8N2)2][NO3]. *Z. Kristallog.* **2006,** *221* (3), 391-392.

181. Kalinowska-Lis, U.; Felczak, A.; Chęcińska, L.; Zawadzka, K.; Patyna, E.; Lisowska, K.; Ochocki, J., Synthesis, characterization and antimicrobial activity of water-soluble silver(i) complexes of metronidazole drug and selected counter-ions. *Dalton Trans.* **2015,** *44* (17), 8178-8189.

182. Savić, N. D.; Vojnovic, S.; Glišić, B. Đ.; Crochet, A.; Pavic, A.; Janjić, G. V.; Pekmezović, M.; Opsenica, I. M.; Fromm, K. M.; Nikodinovic-Runic, J.; Djuran, M. I., Mononuclear silver(I) complexes with 1,7-phenanthroline as potent inhibitors of Candida growth. *Eur. J. Med. Chem.* **2018,** *156*, 760-773.

183. Lewis, D. L.; Estes, E. D.; Hodgson, D. J., The infrared spectra of coordinated perchlorates. *J. Mol. Struct.* **1975,** *5* (1), 67-74.

184. Schilt, A. A.; Taylor, R. C., Infra-red spectra of 1:10-phenanthroline metal complexes in the rock salt region below 2000 cm−1. *J. Inorg. Nucl. Chem.* **1959,** *9* (3), 211-221.

185. Krishnamurthy, S. S.; Soundararajan, S., O-Phenanthroline Complexes of rare-earth perchlorates. *Z. fur Anorg. Allg. Chem.* **1966,** *348* (5-6), 309-312.

186. Shahabadi, N.; Kashanian, S.; Ahmadipour, Z., DNA Binding and Gel Electrophoresis Studies of a New Silver(I) Complex Containing 2,9-Dimethyl-1,10-Phenanthroline Ligands. *DNA Cell Biol.* **2010,** *30* (3), 187-194.

187. Gil, V. M. S.; Oliveira, N. C., On the use of the method of continuous variations. *J. Chem. Educ.* **1990,** *67* (6), 473.

188. Huang, M.; Corbin, J. R.; Dolan, N. S.; Fry, C. G.; Vinokur, A. I.; Guzei, I. A.; Schomaker, J. M., Synthesis, Characterization, and Variable-Temperature NMR Studies of Silver(I) Complexes for Selective Nitrene Transfer. *Inorg. Chem* **2017,** *56* (11), 6725-6733.

189. Awan, A.; Truong, H.; Lancashire, R. J. Crystal Field Theory. (accessed September 2024).

190. Sidambaram, P.; Colleran, J., Evaluating the anticancer properties and real-time electrochemical extracellular bio-speciation of bis (1,10-phenanthroline) silver (I) acetate monohydrate in the presence of A549 lung cancer cells. *Biosens Bioelectron* **2021,** *175*, 112876.

191. Graham, K. Dynamic NMR. (accessed September 2024).

192. Schaller, C. Chelation. (accessed September 2024).

193. Prabhu, D. D.; Kumar, N. S. S.; Sivadas, A. P.; Varghese, S.; Das, S., Trigonal 1,3,4-Oxadiazole-Based Blue Emitting Liquid Crystals and Gels. *J. Phys. Chem. B* **2012,** *116* (43), 13071-13080.

194. Rodríguez-Arias, R. J.; Guachi-Álvarez, B. O.; Montalvo-Vivero, D. E.; Machado, A., Lactobacilli displacement and Candida albicans inhibition on initial adhesion assays: a probiotic analysis. *BMC Res. Notes* **2022,** *15* (1), 239.

195. Klepser, M. E.; Ernst, E. J.; Ernst, M. E.; Pfaller, M. A., Growth medium effect on the antifungal activity of LY 303366. *Diagn Microbiol Infect Dis* **1997,** *29* (4), 227-31.

196. Müller, F. M. C.; Kurzai, O.; Hacker, J.; Frosch, M.; Mühlschlegel, F., Effect of the growth medium on the in vitro antifungal activity of micafungin (FK-463) against clinical isolates of Candida dubliniensis. *J. Antimicrob. Chemother.* **2001,** *48* (5), 713-715.

197. Hoeprich, P. D.; Huston, A. C., Effect of culture media on the antifungal activity of miconazole and amphotericin B methyl ester. *J. Infect. Dis.* **1976,** *134* (4), 336-41.

198. Weerasekera, M. M.; Wijesinghe, G. K.; Jayarathna, T. A.; Gunasekara, C. P.; Fernando, N.; Kottegoda, N.; Samaranayake, L. P., Culture media profoundly affect Candida albicans and Candida tropicalis growth, adhesion and biofilm development. *Mem. Inst. Oswaldo. Cruz.* **2016,** *111* (11), 697-702.

199. Nguyen, M. H.; Yu Christine, Y., Influence of Incubation Time, Inoculum Size, and Glucose Concentrations on Spectrophotometric Endpoint Determinations for Amphotericin B, Fluconazole, and Itraconazole. *J. Clin. Microbiol.* **1999,** *37* (1), 141-145.

200. Combes, J.; Imatoukene, N.; Couvreur, J.; Godon, B.; Fojcik, C.; Allais, F.; Lopez, M., An optimized semi-defined medium for p-coumaric acid production in extractive fermentation. *Process Biochem.* **2022,** *122*, 357-362.

201. Hitkova, H. Y.; Georgieva, D. S.; Hristova, P. M.; Sredkova, M. P., Antifungal Susceptibility of Candida albicans Isolates at a Tertiary Care Hospital in Bulgaria. *Jundishapur J. Microbiol* **2019,** *12* (7).

202. Jacobsen, I. D., Galleria mellonella as a model host to study virulence of Candida. *Virulence* **2014,** *5* (2), 237-9.

203. Li, D.-D.; Deng, L.; Hu, G.-H.; Zhao, L.-X.; Hu, D.-D.; Jiang, Y.-Y.; Wang, Y., Using Galleria mellonella-Candida albicans Infection Model to Evaluate Antifungal Agents. *Biol. Pharm. Bull.* **2013,** *36* (9), 1482-1487.

204. Tsai, C. J.-Y.; Loh, J. M. S.; Proft, T., Galleria mellonella infection models for the study of bacterial diseases and for antimicrobial drug testing. *Virulence* **2016,** *7* (3), 214-229.

205. Kavanagh, K.; Sheehan, G. The Use of Galleria mellonella Larvae to Identify Novel Antimicrobial Agents against Fungal Species of Medical Interest *J. Fungi* [Online], 2018.

206. Senior, N. J.; Titball, R. W., Isolation and primary culture of Galleria mellonella hemocytes for infection studies. *F1000Res.* **2020,** *9*, 1392.

207. Vertyporokh, L.; Wojda, I., Immune response of Galleria mellonella after injection with non-lethal and lethal dosages of Candida albicans. *J. Invertebr. Pathol.* **2020,** *170*, 107327.

208. Yang, H.-F.; Pan, A.-J.; Hu, L.-F.; Liu, Y.-Y.; Cheng, J.; Ye, Y.; Li, J.-B., Galleria mellonella as an in vivo model for assessing the efficacy of antimicrobial agents against Enterobacter cloacae infection. *J. Microbiol. Immunol. Infect.* **2017,** *50* (1), 55-61.

209. Lee, L. C.-C.; Leung, K.-K.; Lo, K. K.-W., Recent development of luminescent rhenium(i) tricarbonyl polypyridine complexes as cellular imaging reagents, anticancer drugs, and antibacterial agents. *Dalton Trans.* **2017,** *46* (47), 16357-16380.

210. Komreddy, V.; Ensz, K.; Nguyen, H.; Rillema, D. P.; Moore, C. E., Design, synthesis, and photophysical properties of Re(I) tricarbonyl 1,10-phenanthroline complexes. *J. Mol. Struct.* **2021,** *1223*, 128739.

211. Shakeri, J.; Farrokhpour, H.; Hadadzadeh, H.; Joshaghani, M., Photoreduction of CO2 to CO by a mononuclear Re(i) complex and DFT evaluation of the photocatalytic mechanism. *RSC Adv.* **2015,** *5* (51), 41125-41134.

212. Ranasinghe, K.; Handunnetti, S.; Perera, I. C.; Perera, T., Synthesis and characterization of novel rhenium(I) complexes towards potential biological imaging applications. *Chem. Cent. J.* **2016,** *10* (1), 71.

213. Hernández Mejías, Á. D.; Poirot, A.; Rmili, M.; Leygue, N.; Wolff, M.; Saffon-Merceron, N.; Benoist, E.; Fery-Forgues, S., Efficient photorelease of carbon monoxide from a luminescent tricarbonyl rhenium(i) complex

incorporating pyridyl-1,2,4-triazole and phosphine ligands. *Dalton Trans.* **2021,** *50* (4), 1313-1323.

214. Liew, H. S.; Mai, C. W.; Zulkefeli, M.; Madheswaran, T.; Kiew, L. V.; Delsuc, N.; Low, M. L., Recent Emergence of Rhenium(I) Tricarbonyl Complexes as Photosensitisers for Cancer Therapy. *Molecules* **2020,** *25* (18).

215. Anonymous Electronic Transitions and Luminescence. (accessed November 2024).

216. Higgins, B.; DeGraff, B. A.; Demas, J. N., Luminescent Transition Metal Complexes as Sensors: Structural Effects on pH Response. *Inorg. Chem* **2005,** *44* (19), 6662-6669.

217. Komreddy, V.; Ensz, K.; Nguyen, H.; Paul Rillema, D., Synthesis and characterization of rhenium(I) 4,4'-dicarboxy-2,2'-bipyridine tricarbonyl complexes for solar energy conversion. *Inorganica Chim. Acta* **2020,** *511*, 119815.

218. Wright, M. A.; Wright, J. A., PhotoCORMs: CO release moves into the visible. *Dalton Trans.* **2016,** *45* (16), 6801-6811.

219. Evans, C.; Ahmed, M.; Beirne, D. F.; McCann, M.; Kavanagh, K.; Devereux, M.; Rooney, D.; Heaney, F., Synthesis, characterisation, and solution behaviour of Ag(I) bis(phenanthroline-oxazine) complexes and the evaluation of their biological activity against the pathogenic yeast Candida albicans. *BioMetals* **2023**.

220. Delfourne, E.; Kiss, R.; Le Corre, L.; Dujols, F.; Bastide, J.; Collignon, F.; Lesur, B.; Frydman, A.; Darro, F., Synthesis and in vitro antitumor activity of ring C and D-substituted phenanthrolin-7-one derivatives, analogues of the marine pyridoacridine alkaloids ascididemin and meridine. *Bioorg. Med. Chem.* **2004,** *12* (15), 3987-3994.

221. Frayne, L.; Das, N.; Paul, A.; Amirjalayer, S.; Buma, W. J.; Woutersen, S.; Long, C.; Vos, J. G.; Pryce, M. T., Photo- and Electrochemical Properties of a CO2 Reducing Ruthenium–Rhenium Quaterpyridine-Based Catalyst. *ChemPhotoChem* **2018,** *2* (3), 323-331.

222. Herrick, R.; Wrona, I.; McMicken, N.; Jones, G.; Ziegler, C.; Shaw, J., Preparation and characterization of rhenium(I) compounds with amino ester

derivatized diimine ligands. Investigations of luminescence. Crystal structures of Re(CO)(3)Cl(pyca-beta-AlA-OEt) and Re(CO)(3)Cl(pyca-L-Asp(OMe)-OMe). *J. Organomet. Chem.* **2004,** *689*, 4848-4855.

223. Suárez-Ortiz, G. A.; Hernández-Correa, R.; Morales-Moreno, M. D.; Toscano, R. A.; Ramirez-Apan, M. T.; Hernandez-Garcia, A.; Amézquita-Valencia, M.; Araiza-Olivera, D., Diastereomeric Separation of Chiral fac-Tricarbonyl(iminopyridine) Rhenium(I) Complexes and Their Cytotoxicity Studies: Approach toward an Action Mechanism against Glioblastoma. *J. Med. Chem.* **2022,** *65* (13), 9281-9294.

224. Kalyanasundaram, K., Luminescence and redox reactions of the metal-to-ligand charge-transfer excited state of tricarbonylchloro-(polypyridyl)rhenium(I) complexes. *J. Chem. Soc., Faraday Trans. 2* **1986,** *82* (12), 2401-2415.

225. Ng, C.-O.; Lai, S.-W.; Feng, H.; Yiu, S.-M.; Ko, C.-C., Luminescent rhenium(i) complexes with acetylamino- and trifluoroacetylamino-containing phenanthroline ligands: Anion-sensing study. *Dalton Trans.* **2011,** *40* (39), 10020-10028.

226. Yam, V. W. W.; Wong, K. M. C.; Chong, S. H. F.; Lau, V. C. Y.; Lam, S. C. F.; Zhang, L.; Cheung, K. K., Synthesis, electrochemistry and structural characterization of luminescent rhenium(I) monoynyl complexes and their homo- and hetero-metallic binuclear complexes. *J. Organomet. Chem.* **2003,** *670* (1-2), 205-220.

227. Marini, A.; Muñoz-Losa, A.; Biancardi, A.; Mennucci, B., What is Solvatochromism? *J. Phys. Chem. B* **2010,** *114* (51), 17128-17135.

228. Dodsworth, E. S.; Hasegawa, M.; Bridge, M.; Linert, W., 2.27 - Solvatochromism. In *Comp. Coord. Chem. II*, McCleverty, J. A.; Meyer, T. J., Eds. Pergamon: Oxford, 2003; pp 351-365.

229. Manuta, D. M.; Lees, A. J., Solvatochromism of the metal to ligand charge-transfer transitions of zerovalent tungsten carbonyl complexes. *Inorg. Chem* **1986,** *25* (18), 3212-3218.

230. Peng, Y.-X.; Xu, D.; Wang, N.; Tao, T.; Hu, B.; Huang, W., Comparisons on isomeric 1,10-phenanthroline aromatic heterocyclic

derivatives with triphenylamine and thiophene donors before and after rhenium(I) carbonyl complexation. *Tetrahedron* **2016,** *72* (24), 3443-3453.

231. Palion-Gazda, J.; Choroba, K.; Penkala, M.; Rawicka, P.; Machura, B., Further Insights into the Impact of Ligand-Localized Excited States on the Photophysics of Phenanthroline-Based Rhenium(I) Tricarbonyl Complexes. *Inorg. Chem* **2024,** *63* (2), 1356-1366.

232. Gonçalves, M. R.; Frin, K. P. M., Synthesis, characterization, photophysical and electrochemical properties of rhenium(I) tricarbonyl diimine complexes with triphenylphosphine ligand. *Polyhedron* **2017,** *132*, 20-27.

233. Orsa, D. K.; Haynes, G. K.; Pramanik, S. K.; Iwunze, M. O.; Greco, G. E.; Ho, D. M.; Krause, J. A.; Hill, D. A.; Williams, R. J.; Mandal, S. K., The one-pot synthesis and the fluorescence and cytotoxicity studies of chlorotricarbonyl(α-diimine)rhenium(I), fac-(CO)3(α-diimine)ReCl, complexes. *Inorg. Chem. Commun.* **2008,** *11* (9), 1054-1056.

234. Collery, P.; Desmaele, D.; Vijaykumar, V., Design of Rhenium Compounds in Targeted Anticancer Therapeutics. *Curr. Pharm. Des.* **2019,** *25* (31), 3306-3322.

235. Lakowicz, J. R., *Principles of Fluorescence Spectroscopy*. 3rd edition ed.; Springer: 2006.

236. Ng, C.-O.; Lo, L. T.-L.; Ng, S.-M.; Ko, C.-C.; Zhu, N., A New Class of Isocyanide-Containing Rhenium(I) Bipyridyl Luminophore with Readily Tunable and Highly Environmentally Sensitive Excited-State Properties. *Inorg. Chem* **2008,** *47* (17), 7447-7449.

237. Wallace, L.; Rillema, D. P., Photophysical properties of rhenium(I) tricarbonyl complexes containing alkyl- and aryl-substituted phenanthrolines as ligands. *Inorg. Chem* **1993,** *32* (18), 3836-3843.

238. Vanek, T.; Kohli, A. Biochemistry, Myoglobin (accessed October 2024).

239. Atkin, A. J.; Lynam, J. M.; Moulton, B. E.; Sawle, P.; Motterlini, R.; Boyle, N. M.; Pryce, M. T.; Fairlamb, I. J. S., Modification of the deoxy-myoglobin/carbonmonoxy-myoglobin UV-vis Assay for Reliable

Determination of CO-release Rates from Organometallic Carbonyl Complexes. *Dalton Trans.* **2011,** *40* (21), 5755-5761.

240. Carlsson, M. L. R.; Kanagarajan, S.; Bülow, L.; Zhu, L.-H., Plant based production of myoglobin - a novel source of the muscle heme-protein. *Sci. Rep.* **2020,** *10* (1), 920.

241. Artem'ev, A. V.; Petyuk, M. Y.; Berezin, A. S.; Gushchin, A. L.; Sokolov, M. N.; Bagryanskaya, I. Y., Synthesis and Study of Re(I) tricarbonyl Complexes Based on Octachloro-1,10-phenanthroline: Towards Deep Red-to-NIR Emitters. *Polyhedron* **2021,** *209*, 115484.

242. Carreño, A.; Solís-Céspedes, E.; Zúñiga, C.; Nevermann, J.; Rivera-Zaldívar, M. M.; Gacitúa, M.; Ramírez-Osorio, A.; Páez-Hernández, D.; Arratia-Pérez, R.; Fuentes, J. A., Cyclic voltammetry, relativistic DFT calculations and biological test of cytotoxicity in walled-cell models of two classical rhenium (I) tricarbonyl complexes with 5-amine-1,10-phenanthroline. *Chem. Phys. Lett.* **2019,** *715*, 231-238.

243. Paolucci, F.; Marcaccio, M.; Paradisi, C.; Roffia, S.; Bignozzi, C. A.; Amatore, C., Dynamics of the electrochemical behavior of diimine tricarbonyl rhenium(I) complexes in strictly aprotic media. *J. Phys. Chem. B* **1998,** *102* (24), 4759-4769.

244. Czerwieniec, R.; Kapturkiewicz, A.; Lipkowski, J.; Nowacki, J., Re(I)(tricarbonyl)+ complexes with the 2-(2-pyridyl)-N-methyl-benzimidazole, 2-(2-pyridyl)benzoxazole and 2-(2-pyridyl)benzothiazole ligands - Syntheses, structures, electrochemical and spectroscopic studies. *Inorganica Chimica Acta* **2005,** *358* (9), 2701-2710.

245. Czerwieniec, R.; Kapturkiewicz, A.; Lipkowski, J.; Nowacki, J., Re(I)(tricarbonyl)+ complexes with the 2-(2-pyridyl)-N-methyl-benzimidazole, 2-(2-pyridyl)benzoxazole and 2-(2-pyridyl)benzothiazole ligands – syntheses, structures, electrochemical and spectroscopic studies. *Inorganica Chim. Acta* **2005,** *358* (9), 2701-2710.

246. Wang, H.; Sayed, S. Y.; Luber, E. J.; Olsen, B. C.; Shirurkar, S. M.; Venkatakrishnan, S.; Tefashe, U. M.; Farquhar, A. K.; Smotkin, E. S.;

McCreery, R. L.; Buriak, J. M., Redox Flow Batteries: How to Determine Electrochemical Kinetic Parameters. *ACS Nano* **2020,** *14* (3), 2575-2584.

247. Bao, D.; Millare, B.; Xia, W.; Steyer, B. G.; Gerasimenko, A. A.; Ferreira, A.; Contreras, A.; Vullev, V. I., Electrochemical Oxidation of Ferrocene: A Strong Dependence on the Concentration of the Supporting Electrolyte for Nonpolar Solvents. *J. Phys. Chem. A* **2009,** *113* (7), 1259-1267.

248. Bond, A. M.; Henderson, T. L. E.; Mann, D. R.; Mann, T. F.; Thormann, W.; Zoski, C. G., A Fast Electron Transfer Rate for the Oxidation of Ferrocene in Acetonitrile or Dichloromethane at Platinum Disk Ultramicroelectrodes. *Analytical Chemistry* **1988,** *60* (18), 1878-1882.

249. Jungwirth, U.; Kowol, C. R.; Keppler, B. K.; Hartinger, C. G.; Berger, W.; Heffeter, P., Anticancer activity of metal complexes: involvement of redox processes. *Antioxid Redox Signal* **2011,** *15* (4), 1085-127.

250. Mansour, A. M.; Khaled, R. M.; Ferraro, G.; Shehab, O. R.; Merlino, A., Metal-based carbon monoxide releasing molecules with promising cytotoxic properties. *Dalton Trans.* **2024,** *53* (23), 9612-9656.

251. Monro, S.; Colón, K. L.; Yin, H.; Roque, J., 3rd; Konda, P.; Gujar, S.; Thummel, R. P.; Lilge, L.; Cameron, C. G.; McFarland, S. A., Transition Metal Complexes and Photodynamic Therapy from a Tumor-Centered Approach: Challenges, Opportunities, and Highlights from the Development of TLD1433. *Chem. Rev.* **2019,** *119* (2), 797-828.

252. Mavrodiev, V. K.; Furlei, I. I.; Sultanov, S.; Nekrasov, Y. S.; Belousov, Y. A., Resonance capture of electrons by cyclopentadienyltricarbonylmanganese and -rhenium derivatives. *Russ. Chem. Bull.* **1997,** *46* (6), 1113-1115.

253. Jimenez, J.; Chakraborty, I.; Mascharak, P. K., Synthesis and Assessment of CO-Release Capacity of Manganese Carbonyl Complexes Derived from Rigid α-Diimine -Ligands of Varied Complexity. *Eur. J. Inorg. Chem.* **2015,** *2015* (30), 5021-5026.

254. Stanbury, M.; Compain, J.-D.; Trejo, M.; Smith, P.; Gouré, E.; Chardon-Noblat, S., Mn-carbonyl molecular catalysts containing a redox-

active phenanthroline-5,6-dione for selective electro- and photoreduction of CO2 to CO or HCOOH. *Electrochim. Acta* **2017,** *240*, 288-299.

255. Toscani, A.; Hind, C.; Clifford, M.; Kim, S.-H.; Gucic, A.; Woolley, C.; Saeed, N.; Rahman, K. M.; Sutton, J. M.; Castagnolo, D., Development of photoactivable phenanthroline-based manganese(I) CO-Releasing molecules (PhotoCORMs) active against ESKAPE bacteria and bacterial biofilms. *Eur. J. Med. Chem.* **2021,** *213*, 113172.

256. Friães, S.; Trigueiros, C.; Gomes, C. S. B.; Fernandes, A. R.; Lenis-Rojas, O. A.; Martins, M.; Royo, B., Antimicrobial Activity of Manganese(I) Tricarbonyl Complexes Bearing 1,2,3-Triazole Ligands. *Molecules* **2023,** *28* (21), 7453.

257. Wang, Z.; Ma, N.; Lu, X.; Liu, M.; Liu, T.; Liu, Q.; Solan, G. A.; Sun, W.-H., Robust and efficient transfer hydrogenation of carbonyl compounds catalyzed by NN-Mn(i) complexes. *Dalton Trans.* **2023,** *52* (30), 10574-10583.

258. Swartz, M. N., Impact of antimicrobial agents and chemotherapy from 1972 to 1998. *Antimicrob Agents Chemother* **2000,** *44* (8), 2009-16.

259. Hakenbeck, R.; Tarpay, M.; Tomasz, A., Multiple changes of penicillin-binding proteins in penicillin-resistant clinical isolates of Streptococcus pneumoniae. *Antimicrob Agents Chemother* **1980,** *17* (3), 364-71.

260. Liu, Y. Y.; Wang, Y.; Walsh, T. R.; Yi, L. X.; Zhang, R.; Spencer, J.; Doi, Y.; Tian, G.; Dong, B.; Huang, X.; Yu, L. F.; Gu, D.; Ren, H.; Chen, X.; Lv, L.; He, D.; Zhou, H.; Liang, Z.; Liu, J. H.; Shen, J., Emergence of plasmid-mediated colistin resistance mechanism MCR-1 in animals and human beings in China: a microbiological and molecular biological study. *Lancet Infect Dis* **2016,** *16* (2), 161-8.

261. Ferlay, J.; Ervik, M.; Lam, F.; M, C.; Mery, L.; Pineros, M. Global Cancer Observatory: Cancer Today. (accessed October 2024).

262. NCRI *Cancer in Ireland 1994-2021: Annual statistical report of the National Cancer Registry*; National Cancer Registry Ireland: 2023.

263. WHO, Cancer. (accessed October 2024).

264. Priyadarshini, S.; Swain, P. K.; Agarwal, K.; Jena, D.; Padhee, S., Trends in gynecological cancer incidence, mortality, and survival among elderly women: A SEER study. *Aging Medicine* **2024,** *7* (2), 179-188.

265. Akter, S.; Rahman, M. A.; Hasan, M. N.; Akhter, H.; Noor, P.; Islam, R.; Shin, Y.; Rahman, M. H.; Gazi, M. S.; Huda, M. N.; Nam, N. M.; Chung, J.; Han, S.; Kim, B.; Kang, I.; Ha, J.; Choe, W.; Choi, T. G.; Kim, S. S. Recent Advances in Ovarian Cancer: Therapeutic Strategies, Potential Biomarkers, and Technological Improvements *Cells,* **2022**, *11* (4).

266. Bachmann, C. New Achievements from Molecular Biology and Treatment Options for Refractory/Relapsed Ovarian Cancer—A Systematic Review *Cancers*, **2023**, *15* (22).

267. Amable, L., Cisplatin Resistance and Opportunities for Precision Medicine. *Pharmacol. Res.* **2016,** *106*, 27-36.

268. Gold, J. M.; Raja, A. Cisplatin. (accessed October 2024).

269. Havasi, A.; Cainap, S. S.; Havasi, A. T.; Cainap, C. Ovarian Cancer—Insights into Platinum Resistance and Overcoming It. *Med* **2023**, *59* (3).

270. Wani, W. A.; Baig, U.; Shreaz, S.; Shiekh, R. A.; Iqbal, P. F.; Jameel, E.; Ahmad, A.; Mohd-Setapar, S. H.; Mushtaque, M.; Ting Hun, L., Recent advances in iron complexes as potential anticancer agents. *New J. Chem.* **2016,** *40* (2), 1063-1090.

271. Lee, S. Y.; Kim, C. Y.; Nam, T. G., Ruthenium Complexes as Anticancer Agents: A Brief History and Perspectives. *Drug Des Devel Ther* **2020,** *14*, 5375-5392.

272. Huang, Z.; Wilson, J. J., Therapeutic and Diagnostic Applications of Multimetallic Rhenium(I) Tricarbonyl Complexes. *Eur. J. Inorg. Chem.* **2021,** *2021* (14), 1312-1324.

273. Neuditschko, B.; King, A. P.; Huang, Z.; Janker, L.; Bileck, A.; Borutzki, Y.; Marker, S. C.; Gerner, C.; Wilson, J. J.; Meier-Menches, S. M., An Anticancer Rhenium Tricarbonyl Targets Fe–S Cluster Biogenesis in Ovarian Cancer Cells. *Angewandte Chemie International Edition* **2022,** *61* (43), e202209136.

274. Marker, S. C.; King, A. P.; Granja, S.; Vaughn, B.; Woods, J. J.; Boros, E.; Wilson, J. J., Exploring the In Vivo and In Vitro Anticancer Activity of Rhenium Isonitrile Complexes. *Inorg. Chem* **2020,** *59* (14), 10285-10303.

275. Loomba, P. S.; Taneja, J.; Mishra, B., Methicillin and Vancomycin Resistant S. aureus in Hospitalized Patients. *J. Glob. Infect. Dis.* **2010,** *2* (3).

276. Niveditha, N.; Sujatha, S., Worrisome trends in rising minimum inhibitory concentration values of antibiotics against methicillin resistant Staphylococcus aureus – Insights from a tertiary care center, South India. *The Brazilian Journal of Infectious Diseases* **2015,** *19* (6), 585-589.

277. Bawankar, N. S.; Agrawal, G. N.; Zodpey, S. S., Unmasking a looming crisis: Escalating MIC of last resort drugs against MRSA isolates from a tertiary care hospital in Central India. *Indian Journal of Medical Microbiology* **2024,** *51*, 100707.

278. De Oliveira, D. M. P.; Forde, B. M.; Kidd, T. J.; Harris, P. N. A.; Schembri, M. A.; Beatson, S. A.; Paterson, D. L.; Walker, M. J., Antimicrobial Resistance in ESKAPE Pathogens. *Clin. Microbiol. Rev.* **2020,** *33* (3).

279. Chen, C.-W.; Hsu, C.-Y.; Lai, S.-M.; Syu, W.-J.; Wang, T.-Y.; Lai, P.-S., Metal nanobullets for multidrug resistant bacteria and biofilms. *Advanced Drug Delivery Reviews* **2014,** *78*, 88-104.

280. Lindsay, B. S.; Barrows, L. R.; Copp, B. R., Structural requirements for biological activity of the marine alkaloid ascididemin. *Bioorg. Med Chem Lett.* **1995,** *5* (7), 739-742.

281. King, A. P.; Marker, S. C.; Swanda, R. V.; Woods, J. J.; Qian, S.-B.; Wilson, J. J., A Rhenium Isonitrile Complex Induces Unfolded Protein Response-Mediated Apoptosis in Cancer Cells. *Chem. Eur. J.* **2019,** *25* (39), 9206-9210.

282. Greenwood, H. E.; McCormick, P. N.; Gendron, T.; Glaser, M.; Pereira, R.; Maddocks, O. D. K.; Sander, K.; Zhang, T.; Koglin, N.; Lythgoe, M. F.; Årstad, E.; Hochhauser, D.; Witney, T. H., Measurement of Tumor Antioxidant Capacity and Prediction of Chemotherapy Resistance in Preclinical Models of Ovarian Cancer by Positron Emission Tomography. *Clin. Cancer. Res.* **2019,** *25* (8), 2471-2482.

283. Kobayash, J. i.; Cheng, J.-f.; Nakamura, H.; Ohizumi, Y.; Hirata, Y.; Sasaki, T.; Ohta, T.; Nozoe, S., Ascididemin, a novel pentacyclic aromatic alkaloid with potent antileukemic activity from the okinawan tunicate didemnum sp. *Tetrahedron Lett.* **1988,** *29* (10), 1177-1180.

284. Matsumoto, S. S.; Sidford, M. H.; Holden, J. A.; Barrows, L. R.; Copp, B. R., Mechanism of action studies of cytotoxic marine alkaloids: ascididemin exhibits thiol-dependent oxidative DNA cleavage. *Tetrahedron Lett.* **2000,** *41* (10), 1667-1670.

285. Delfourne, E.; Darro, F.; Portefaix, P.; Galaup, C.; Bayssade, S.; Bouteillé, A.; Le Corre, L.; Bastide, J.; Collignon, F.; Lesur, B.; Frydman, A.; Kiss, R., Synthesis and In Vitro Antitumor Activity of Novel Ring D Analogues of the Marine Pyridoacridine Ascididemin: Structure−Activity Relationship. *J. Med. Chem.* **2002,** *45* (17), 3765-3771.

286. Shi, Y., Caspase activation, inhibition, and reactivation: a mechanistic view. *Protein Sci.* **2004,** *13* (8), 1979-87.

287. Anttila, J. V.; Shubin, M.; Cairns, J.; Borse, F.; Guo, Q.; Mononen, T.; Vázquez-García, I.; Pulkkinen, O.; Mustonen, V., Contrasting the Impact of Cytotoxic and Cytostatic Drug Therapies on Tumour Progression. *PLoS Comput. Biol.* **2019,** *15* (11), e1007493.

288. Green, D. R.; Llambi, F., Cell Death Signaling. *Cold Spring Harb Perspect Biol* **2015,** *7* (12).

Appendix

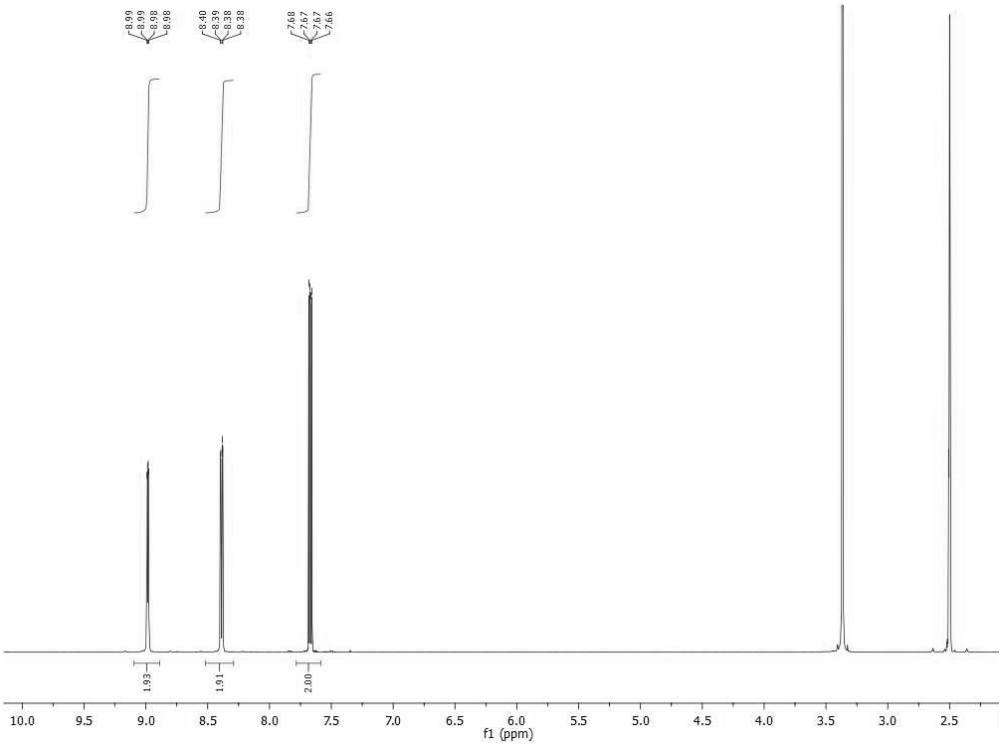

^{1}H NMR spectrum of phendione (**2a**) in DMSO-d6

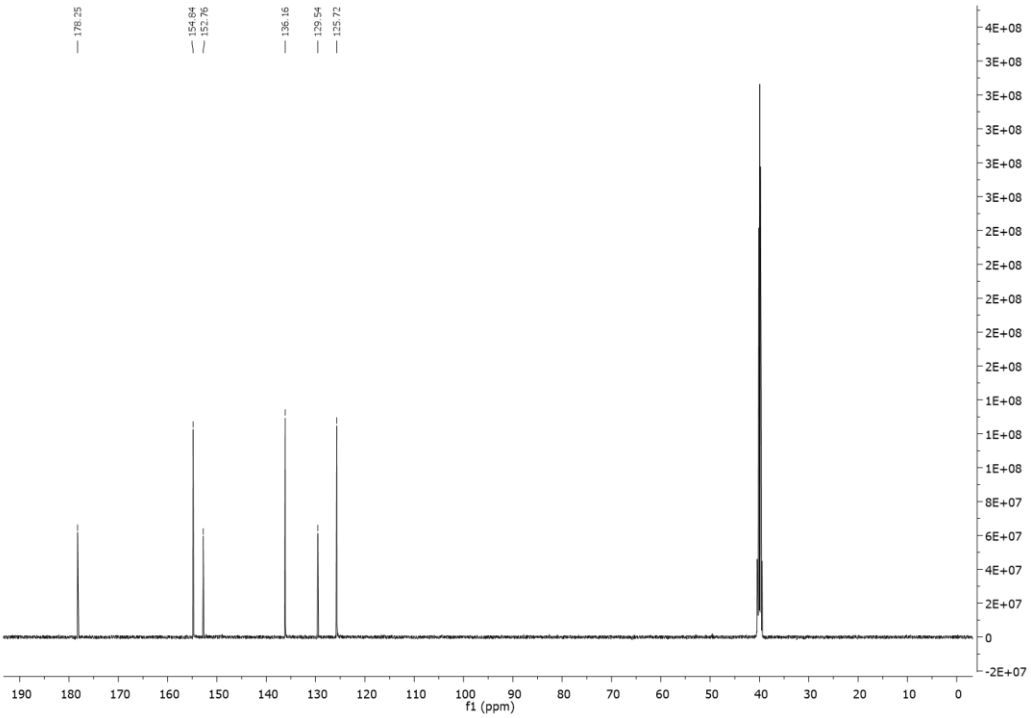

^{13}C NMR spectrum of phendione (**2a**) in DMSO-d6

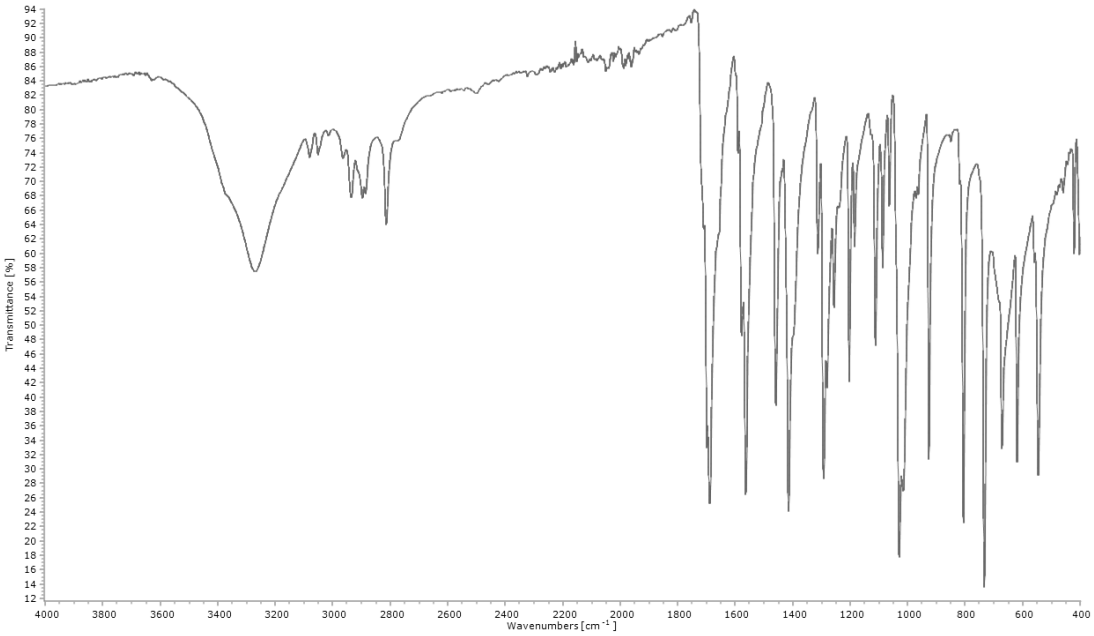

FTIR (ATR, cm^{-1}) spectrum of phendione (**2a**)

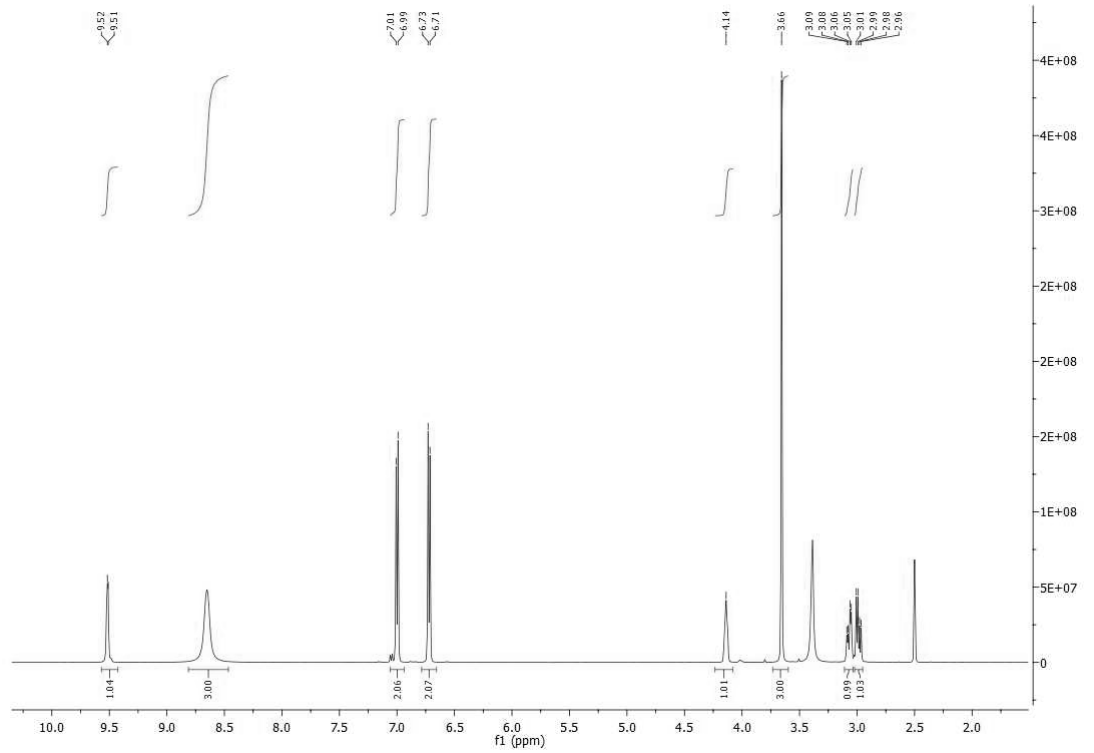

^{1}H NMR spectrum of LTME (**1.1**) in DMSO-d6

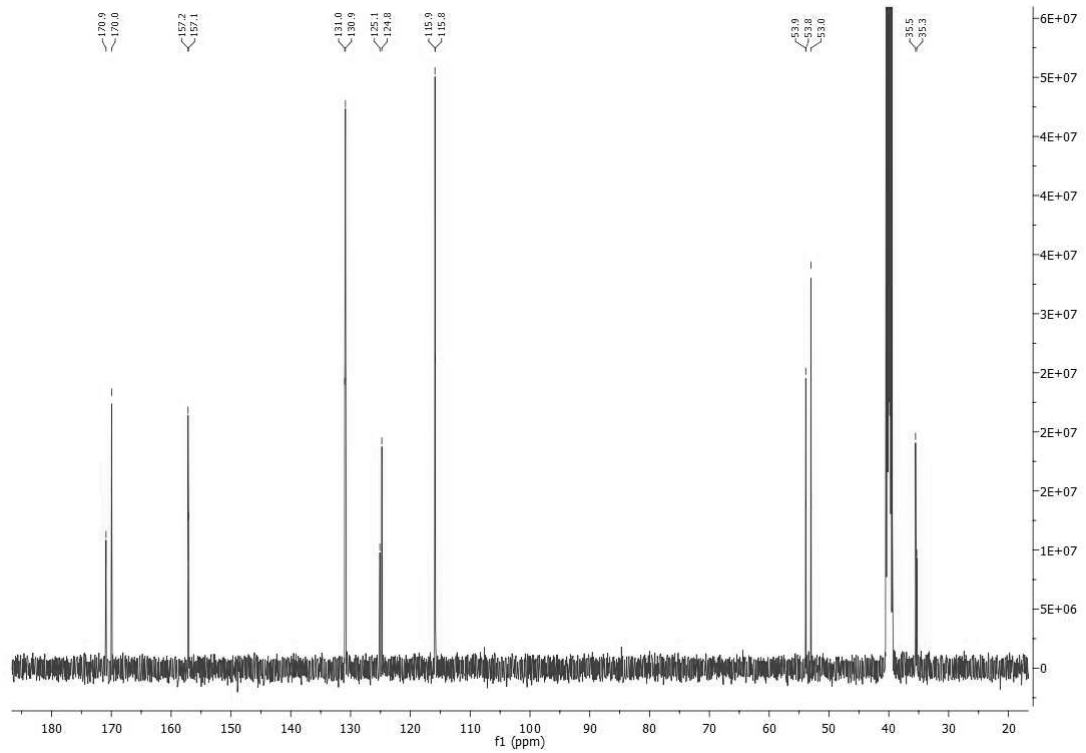

^{13}C NMR spectrum of LTME (**1.1**) in DMSO-d6

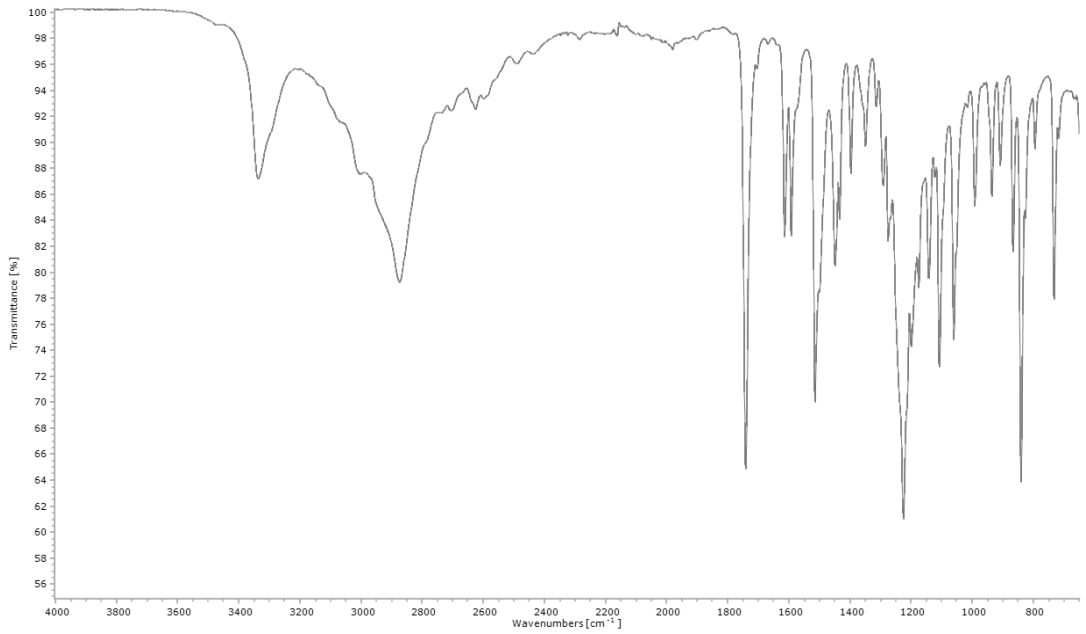

FTIR (ATR, cm^{-1}) spectrum of LTME (**1.1**)

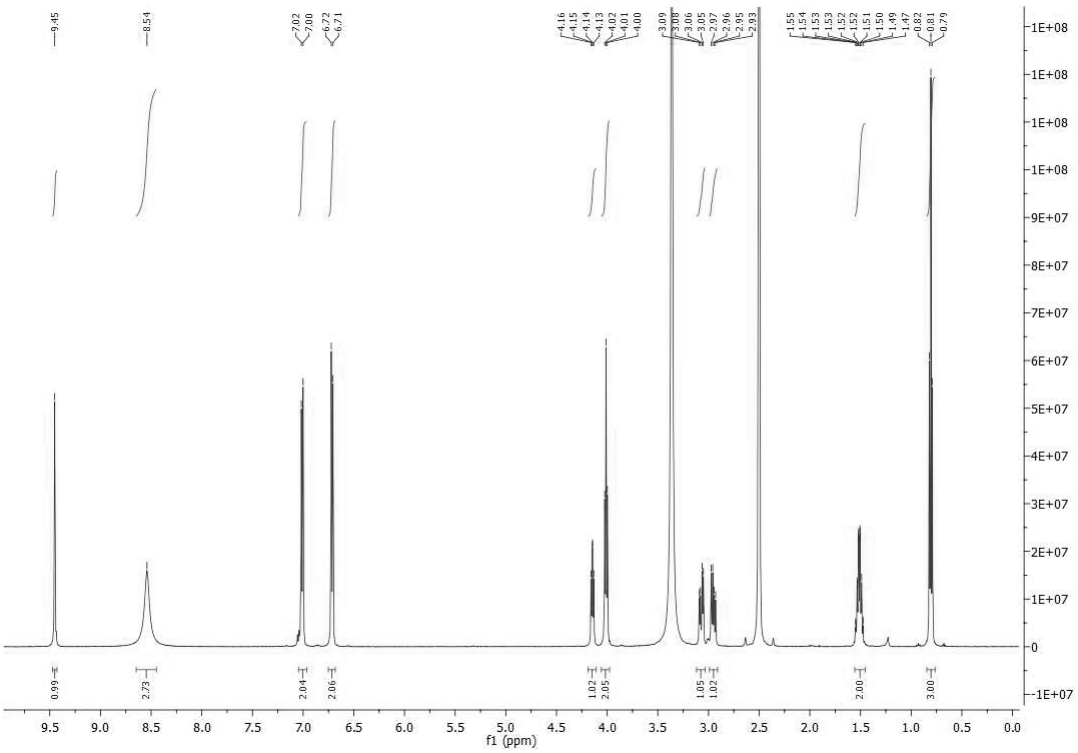

^{1}H NMR spectrum of LTPE (**1.2**) in DMSO-d6

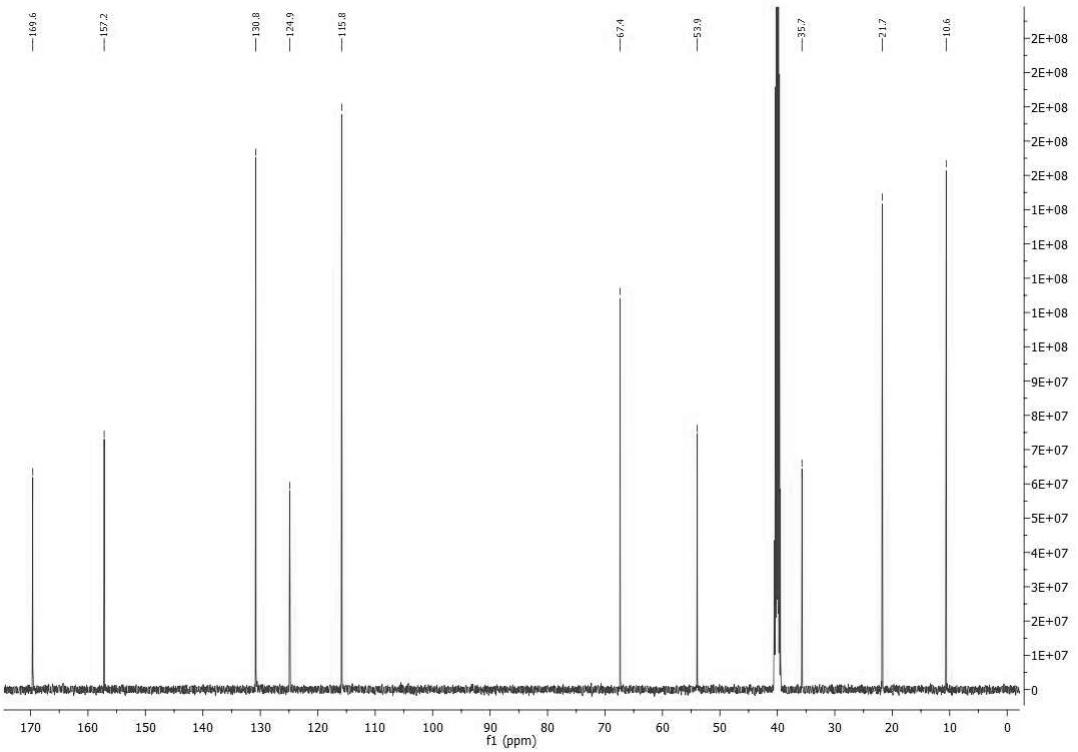

^{13}C NMR spectrum of LTPE (**1.2**) in DMSO-d6

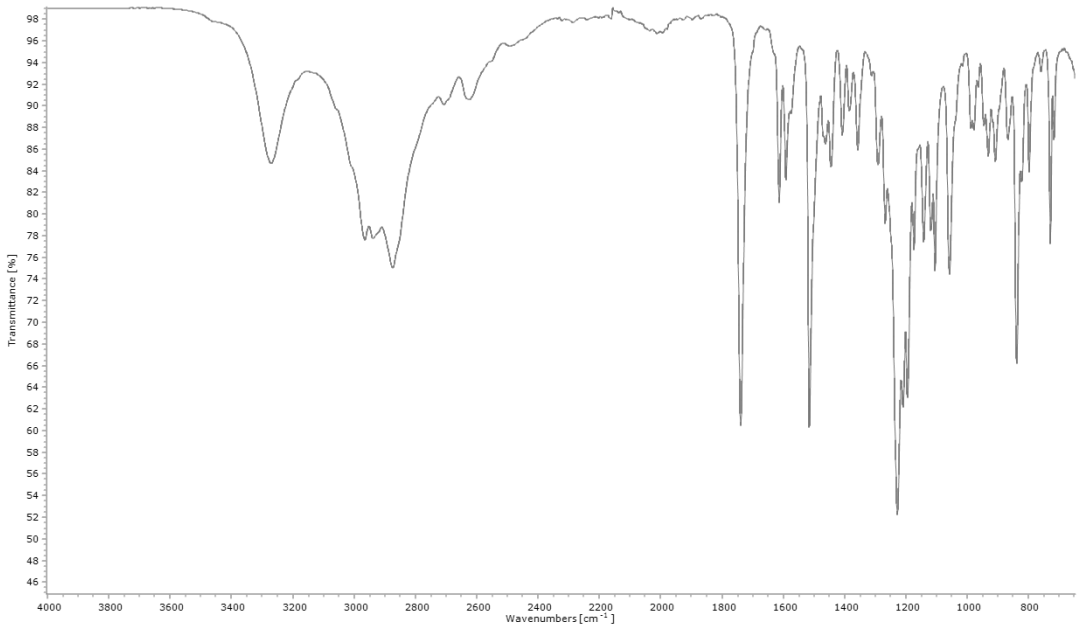

FTIR (ATR, cm^{-1}) spectrum of LTPE (**1.2**)

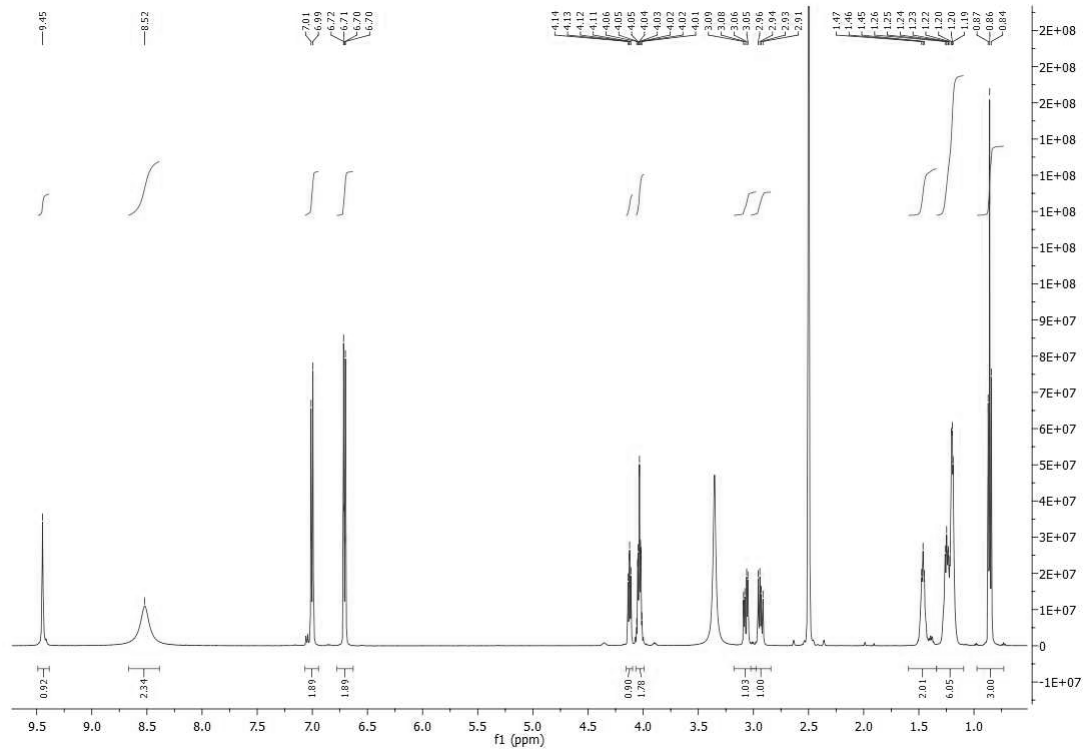

^{1}H NMR spectrum of LTHE (**1.3**) in DMSO-d6

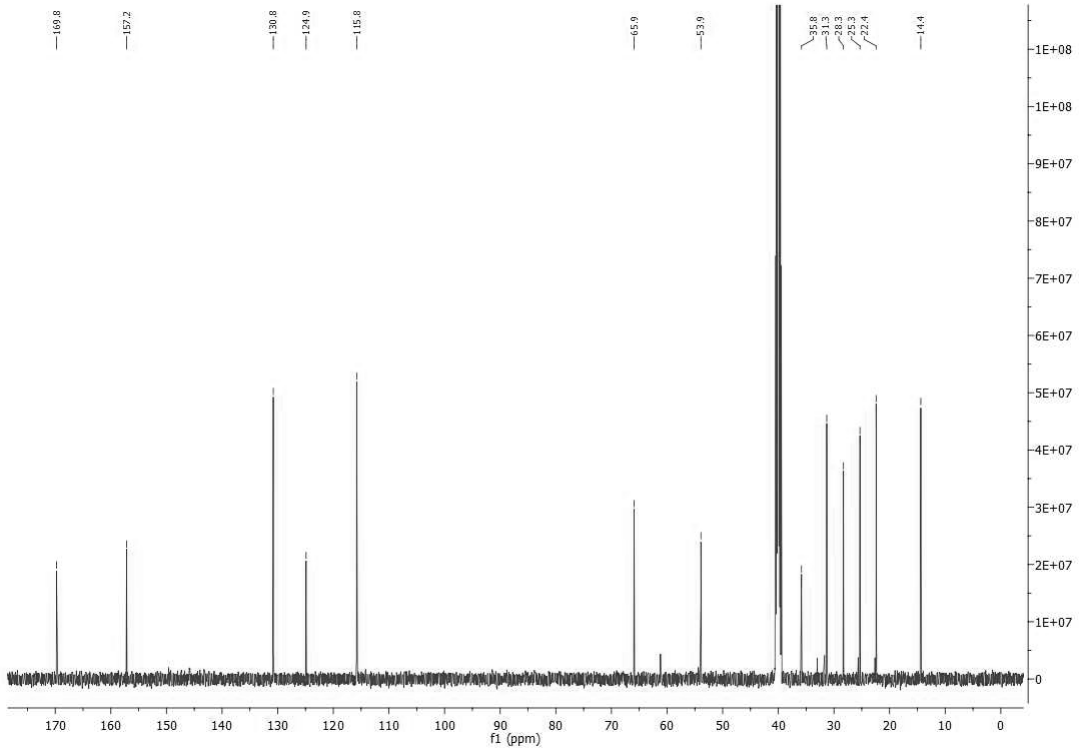

^{13}C NMR spectrum of LTHE (**1.3**) in DMSO-d6

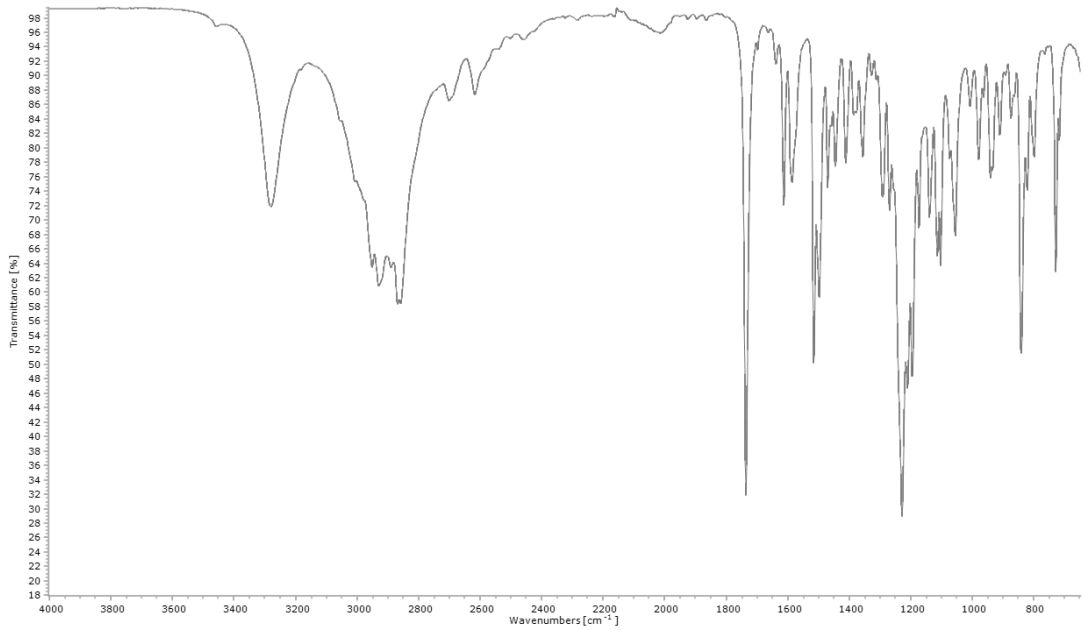

FTIR (ATR, cm^{-1}) spectrum of LTHE (**1.3**)

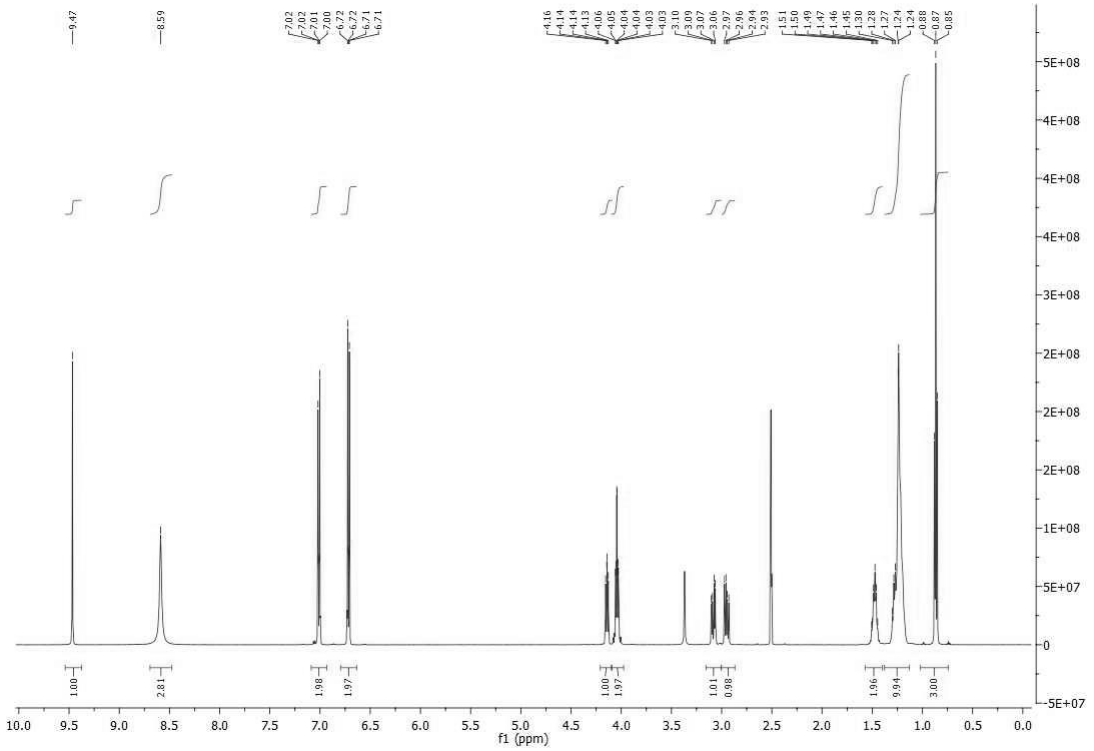

^{1}H NMR spectrum of LTOE (**1.4**) in DMSO-d6

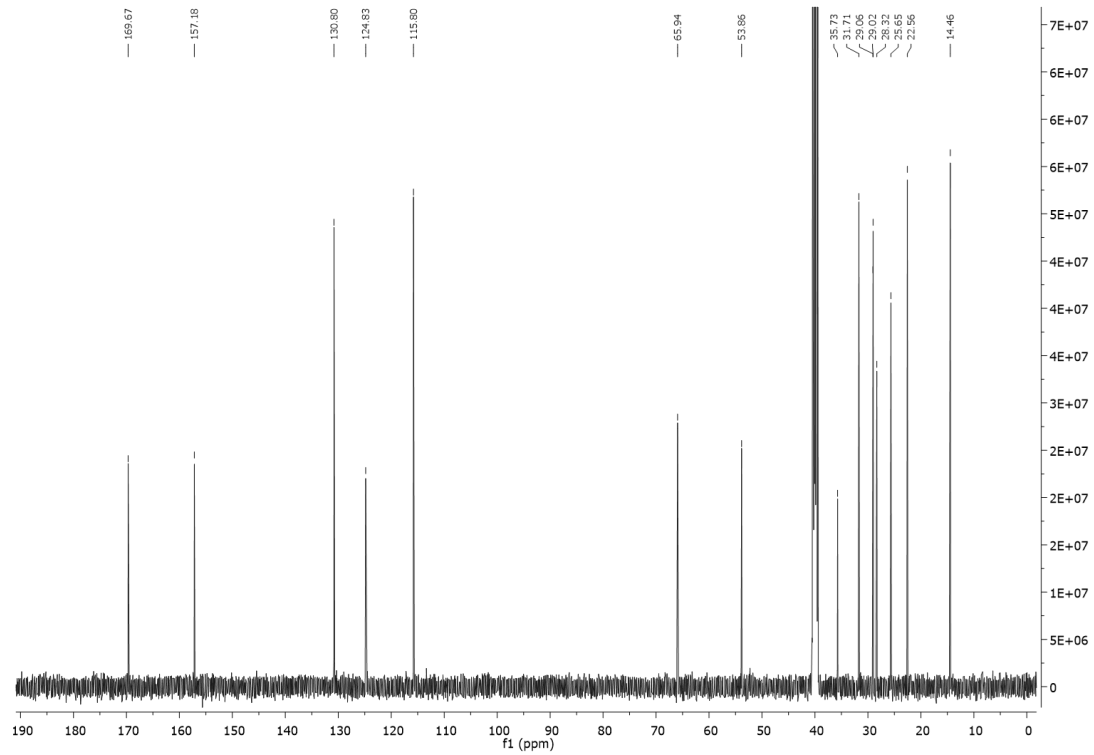

^{13}C NMR spectrum of LTOE (**1.4**) in DMSO-d6

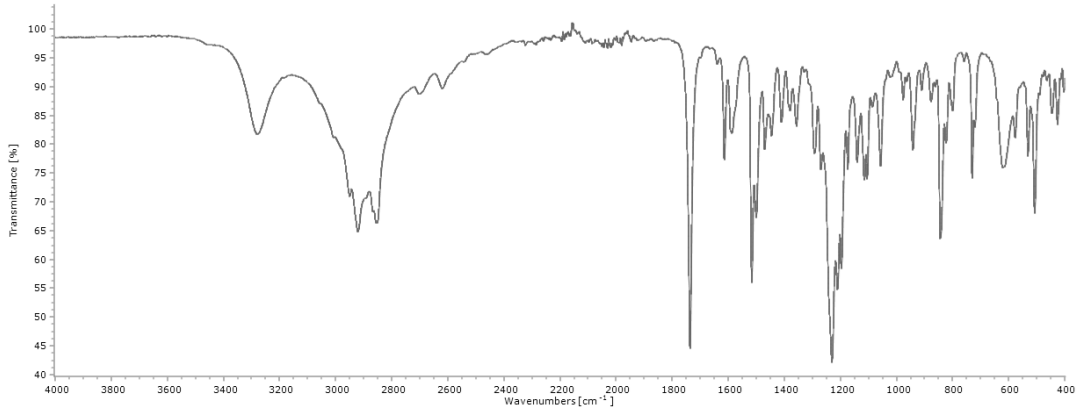

FTIR (ATR, cm^{-1}) spectrum of LTOE (**1.4**)

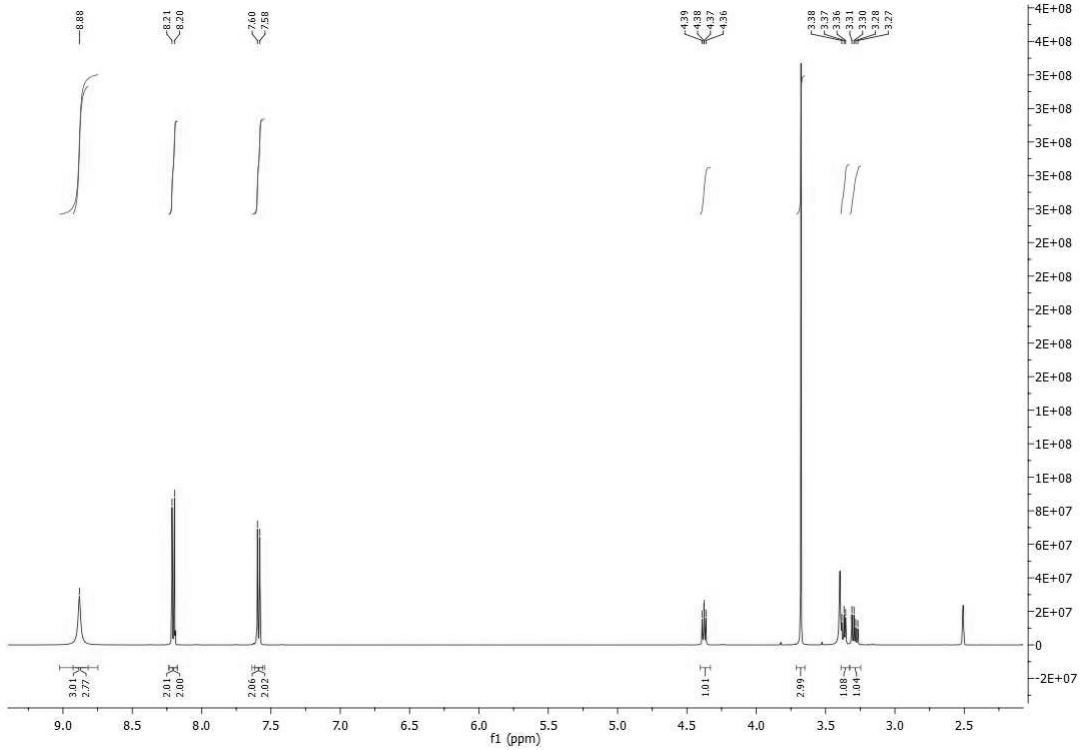

^{1}H NMR spectrum of NPME (**1.5**) in DMSO-d6

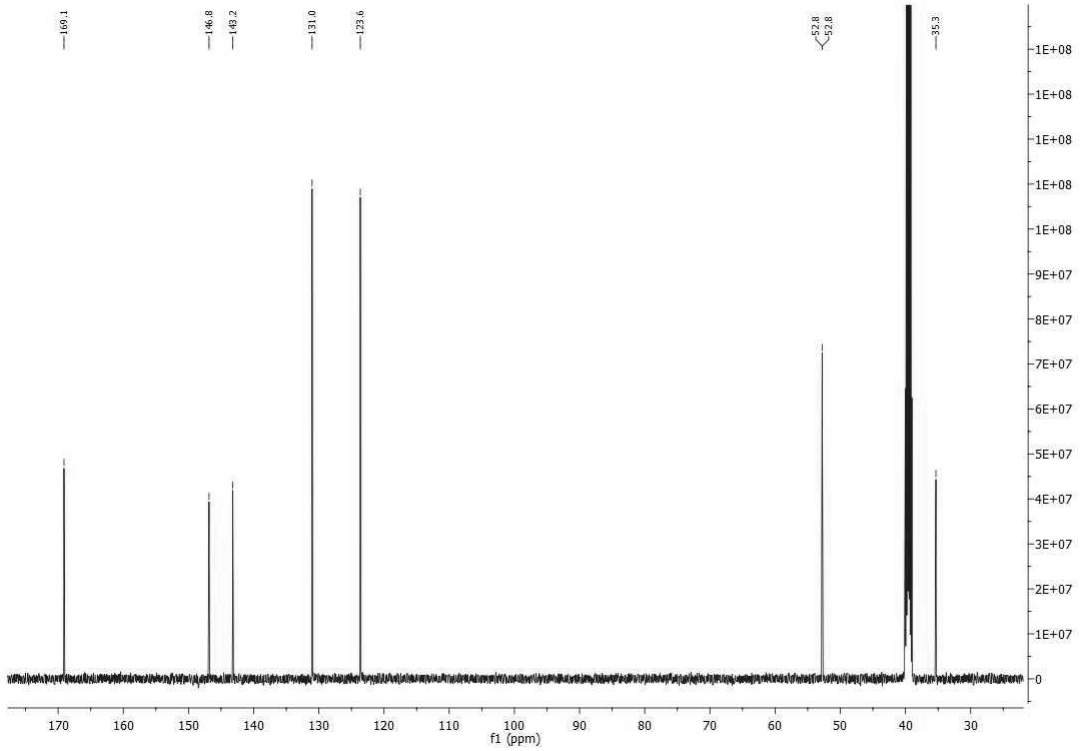

^{13}C NMR spectrum of NPME (**1.5**) in DMSO-d6

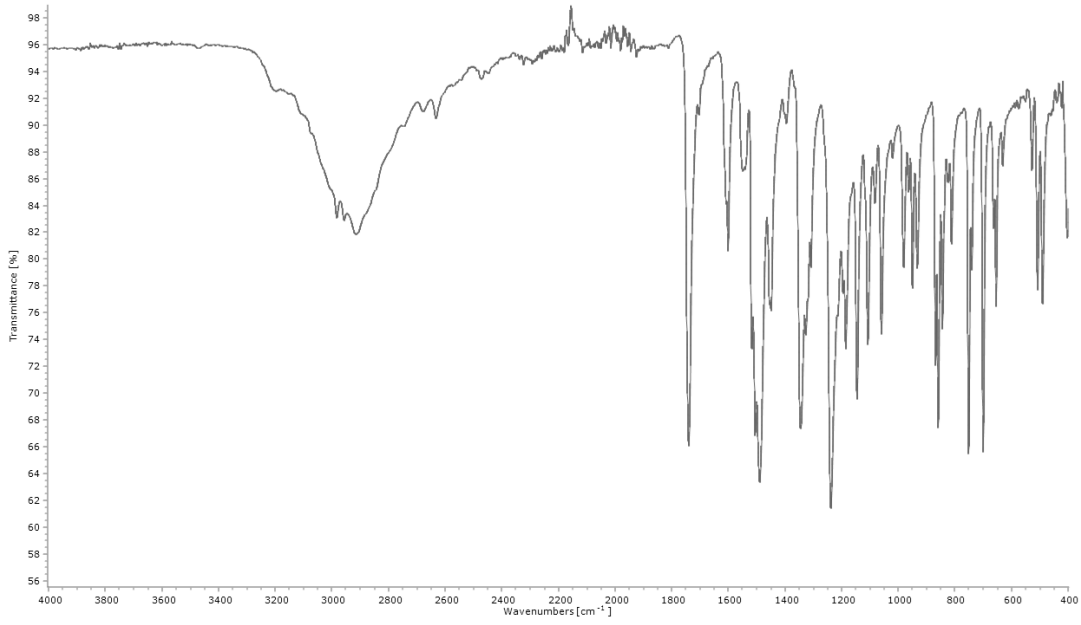

FTIR (ATR, cm^{-1}) spectrum of NPME (**1.5**)

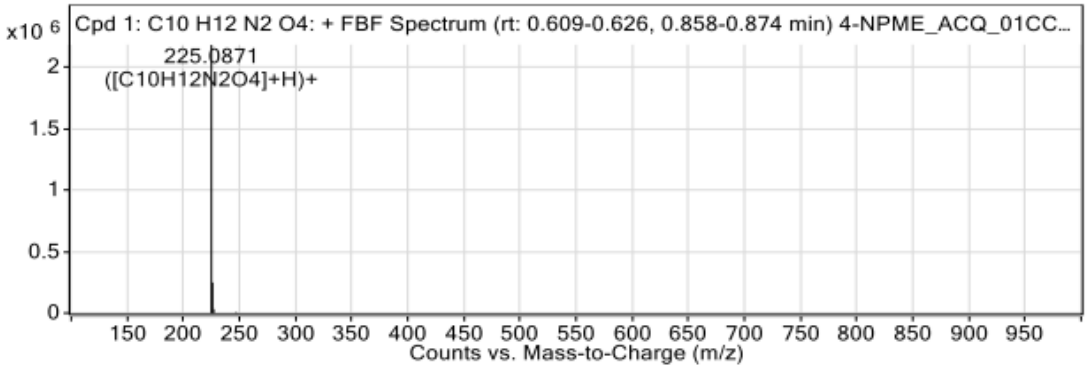

ESI Mass spectrum recorded in positive ionisation mode showing the isotopic pattern for NPME (**1.5**)

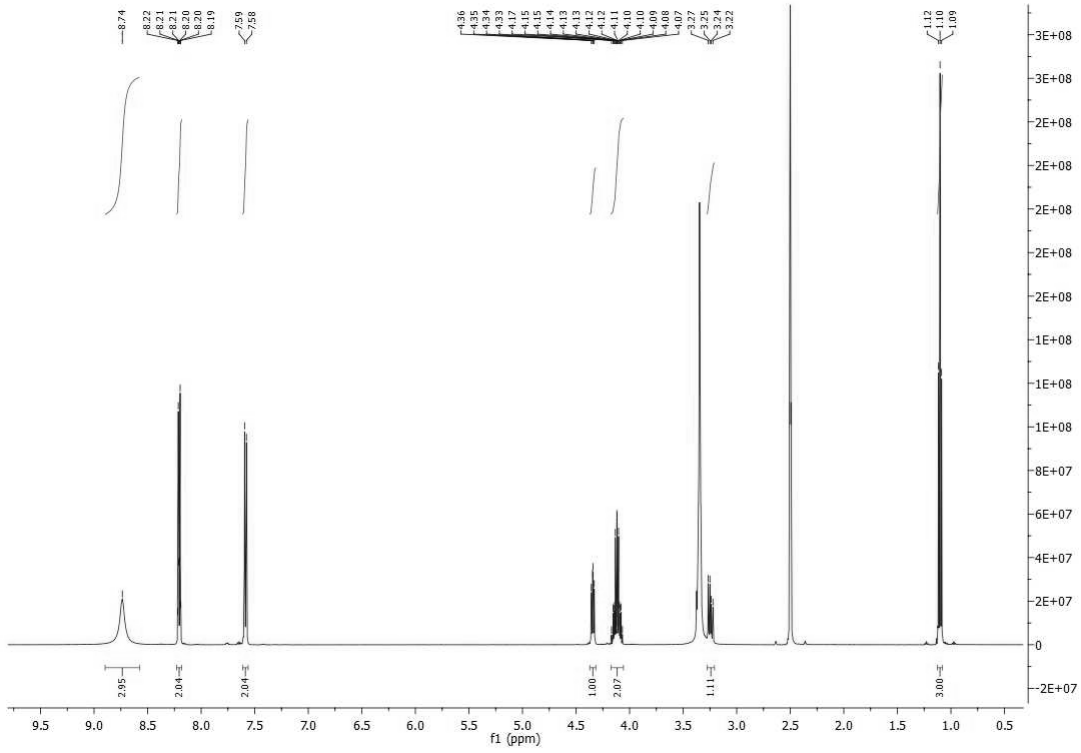

^{1}H NMR spectrum of NPEE (**1.6**) in DMSO-d6

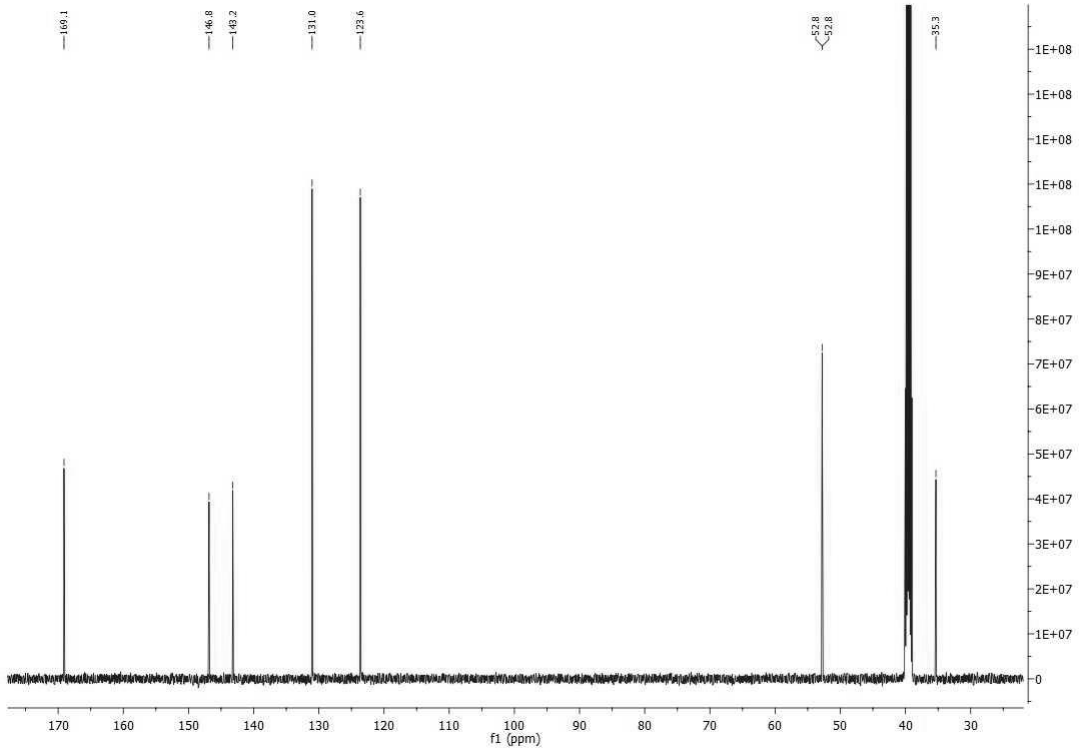

^{13}C NMR spectrum of NPEE (**1.6**) in DMSO-d6

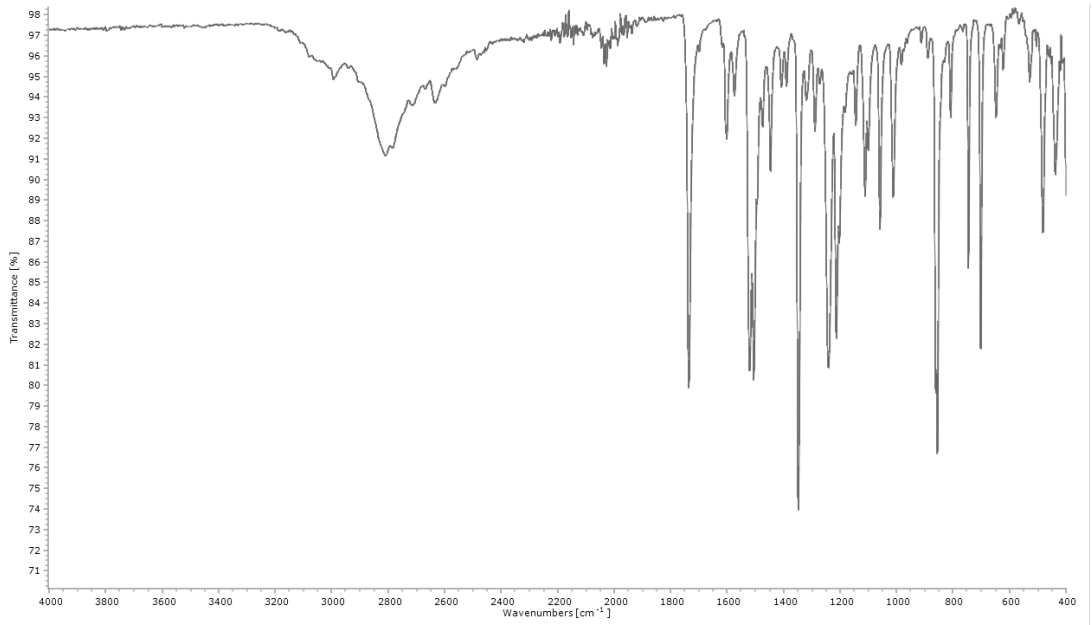

FTIR (ATR, cm^{-1}) spectrum of NPEE (**1.6**)

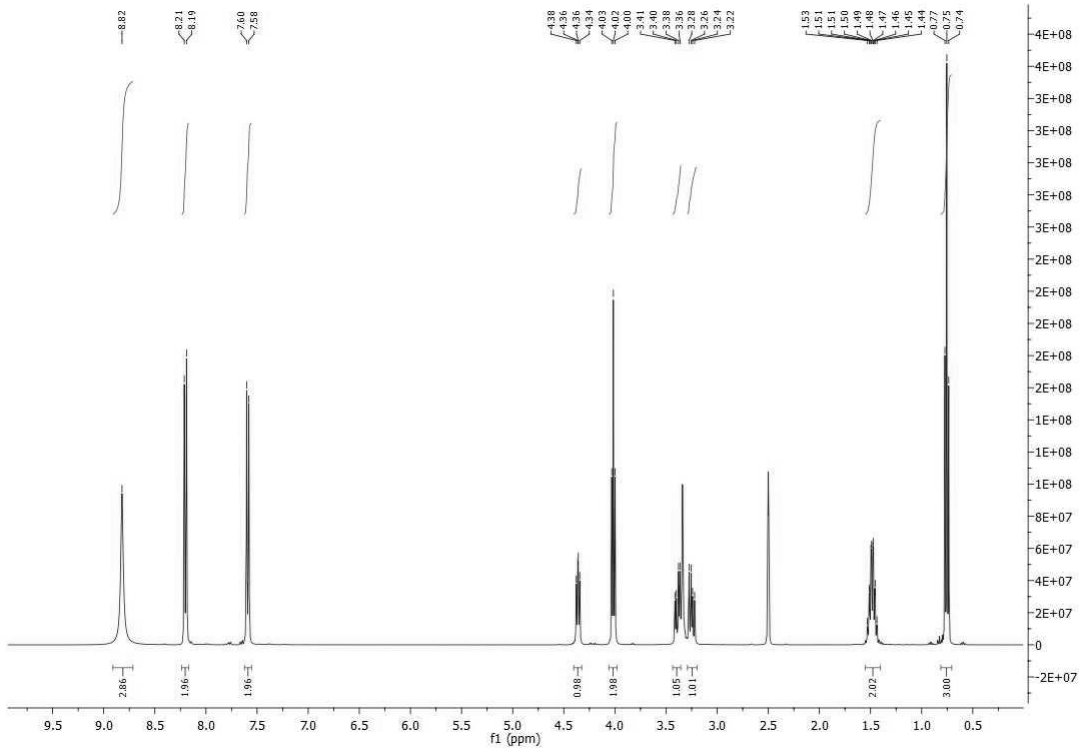

^{1}H NMR spectrum of NPPE (**1.7**) in DMSO-d6

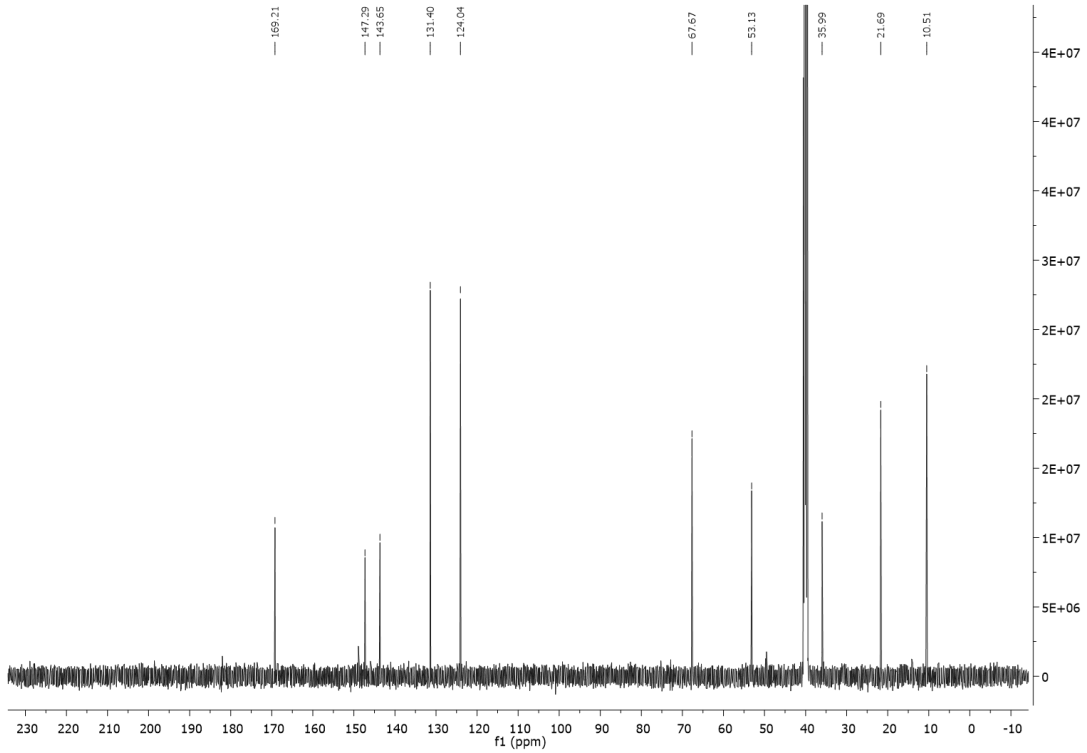

^{13}C NMR spectrum of NPPE (**1.7**) in DMSO-d6

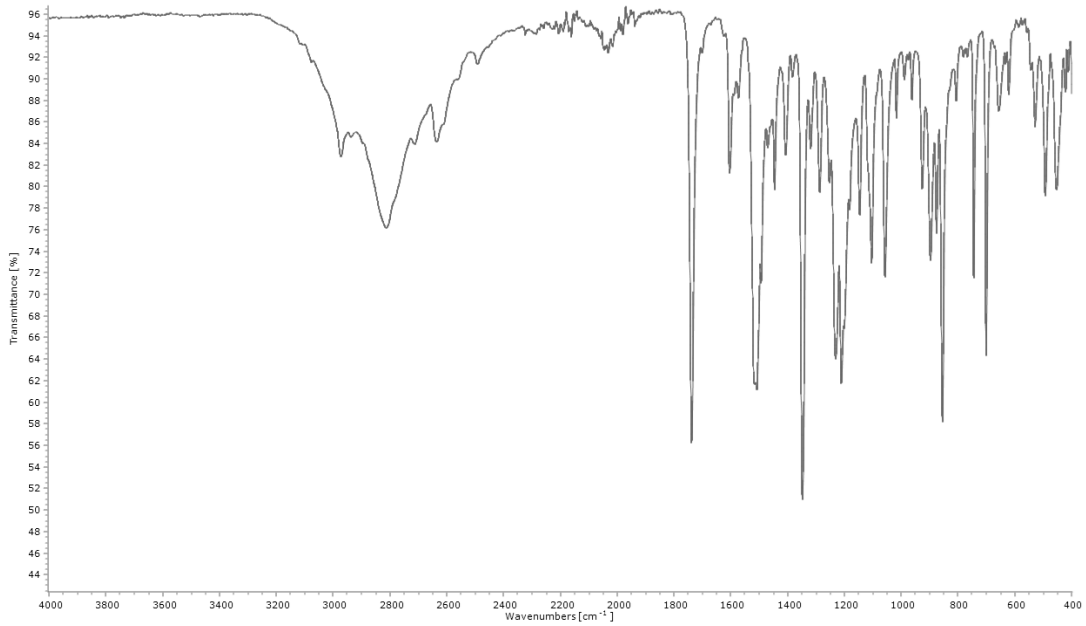

FTIR (ATR, cm^{-1}) spectrum of NPPE (**1.7**)

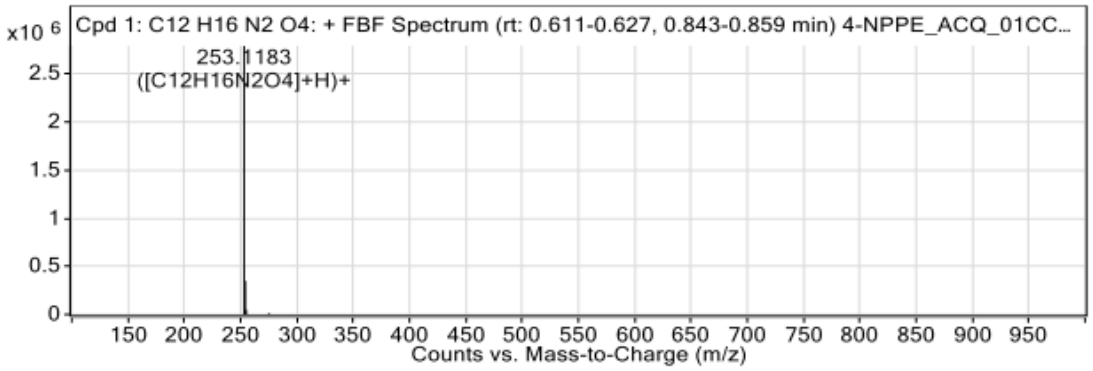

ESI Mass spectrum recorded in positive ionisation mode showing the isotopic pattern for NPPE (**1.7**)

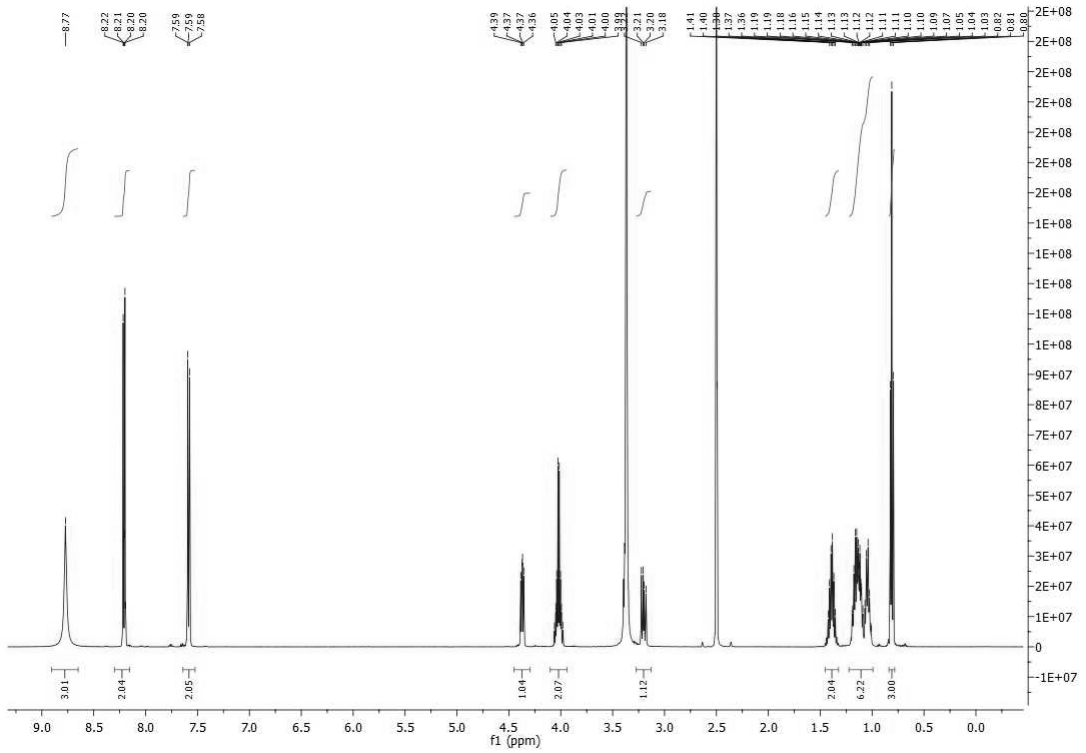

^{1}H NMR spectrum of NPHE (**1.8**) in DMSO-d6

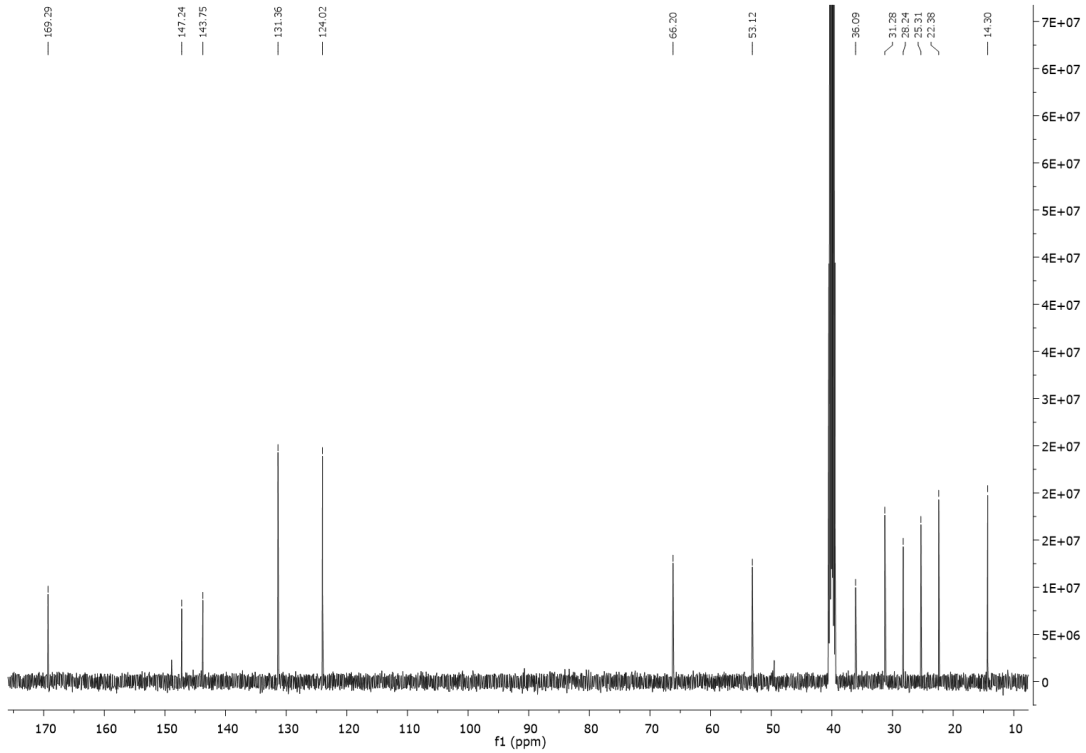

^{13}C NMR spectrum of NPHE (**1.8**) in DMSO-d6

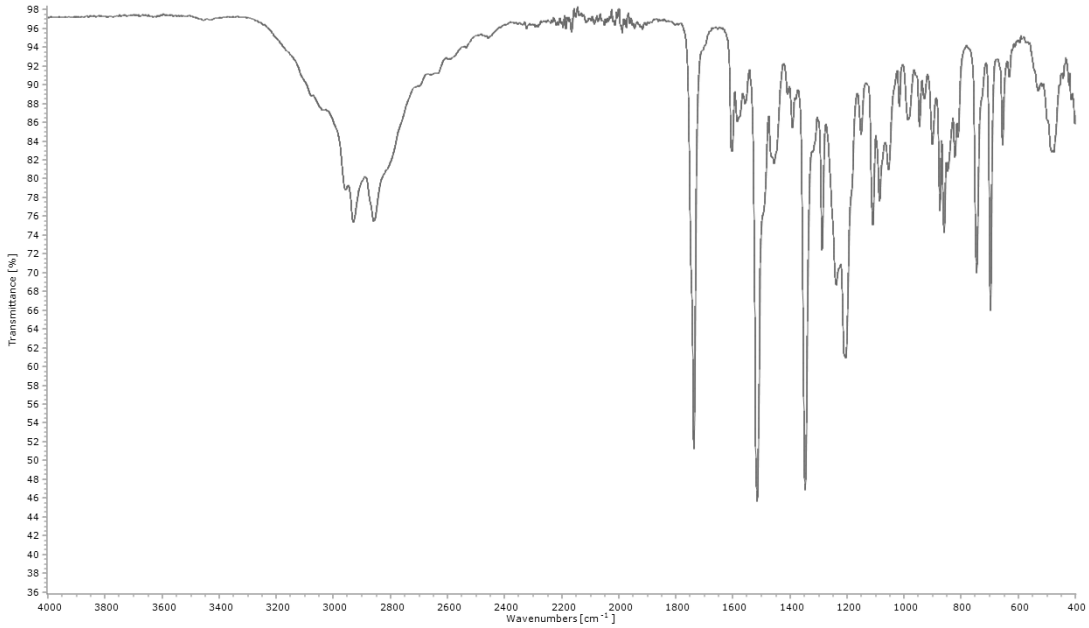

FTIR (ATR, cm^{-1}) spectrum of NPHE (**1.8**)

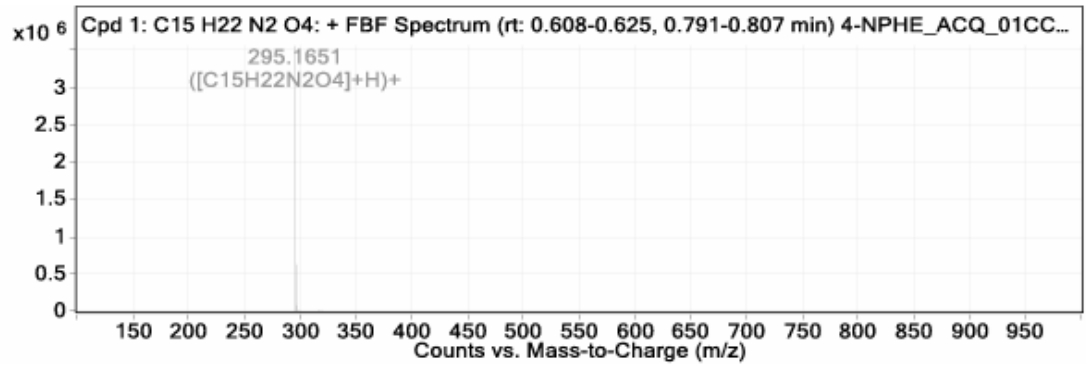

ESI Mass spectrum recorded in positive ionisation mode showing the isotopic pattern for NPHE (**1.8**)

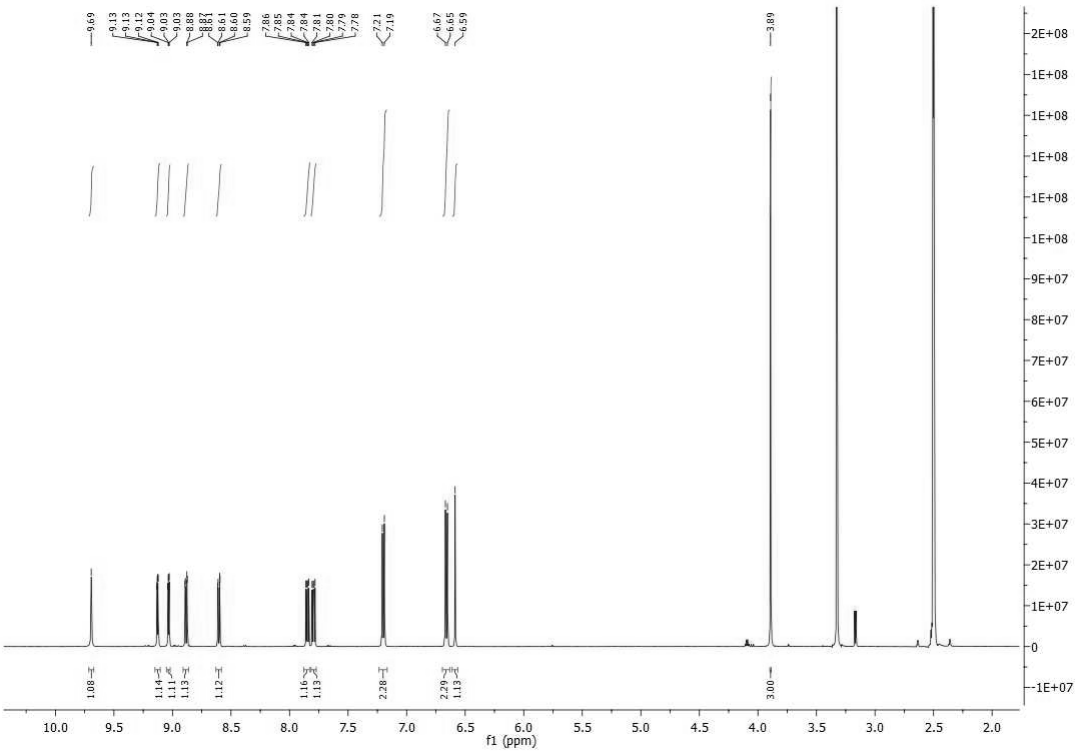

^{1}H NMR spectrum of MPO (**2.1**) in DMSO-d6

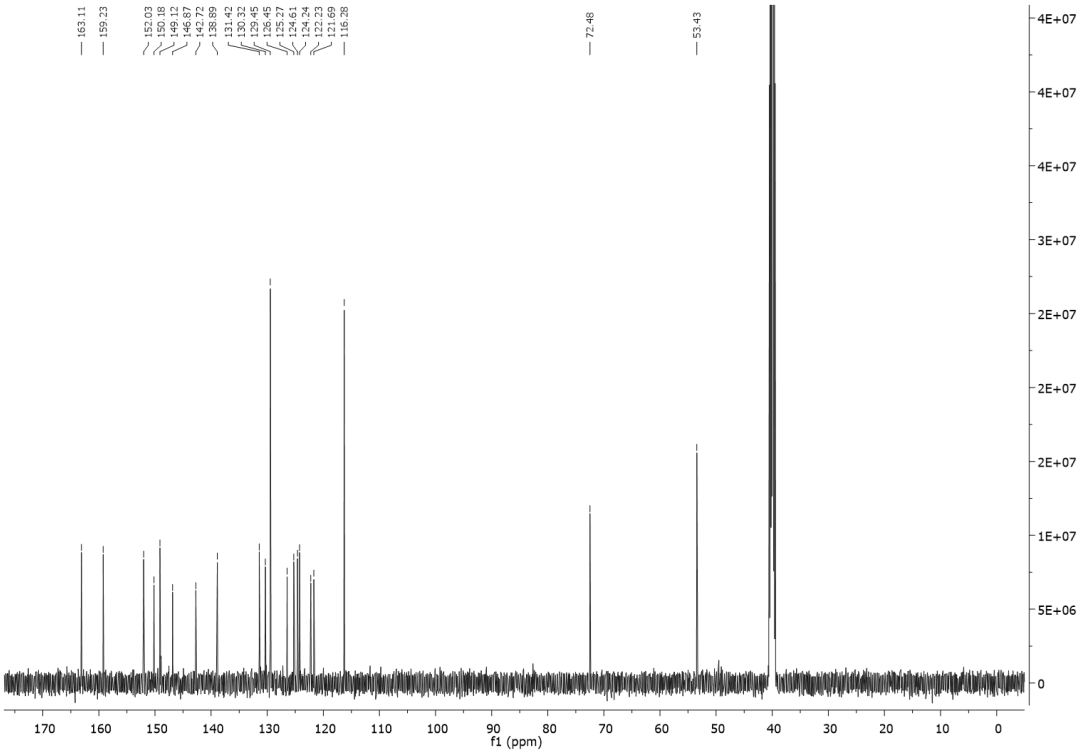

^{13}C NMR spectrum of MPO (**2.1**) in DMSO-d6

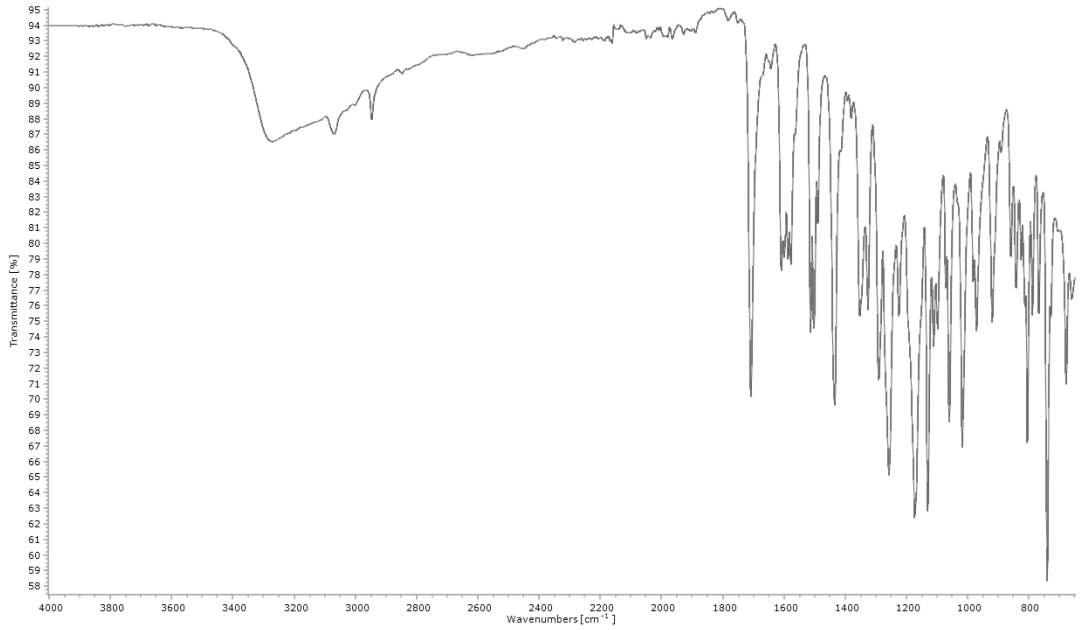

FTIR (ATR, cm^{-1}) spectrum of MPO (**2.1**)

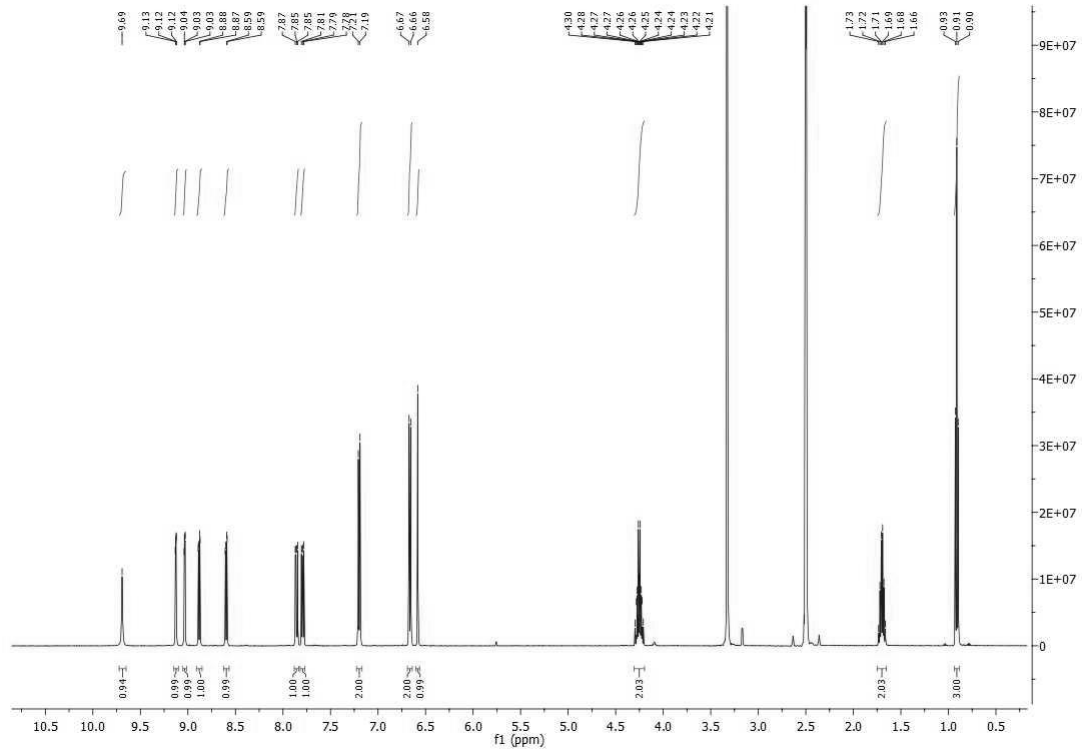

^{1}H NMR spectrum of PPO (**2.2**) in DMSO-d6

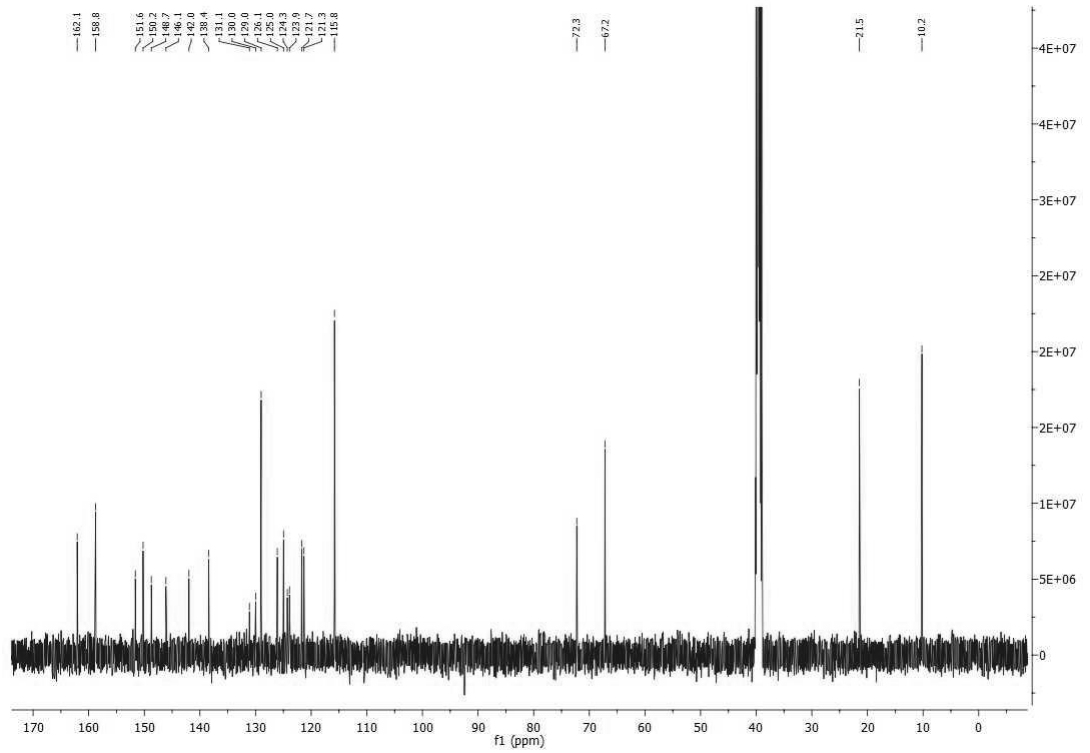

^{13}C NMR spectrum of PPO (**2.2**) in DMSO-d6

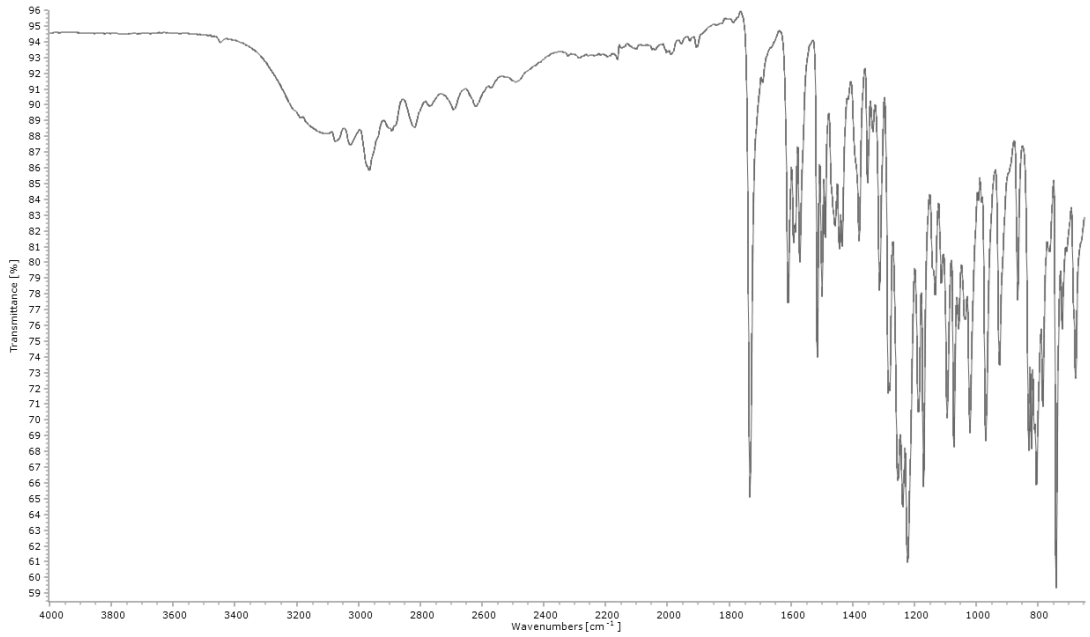

FTIR (ATR, cm^{-1}) spectrum of PPO (**2.2**)

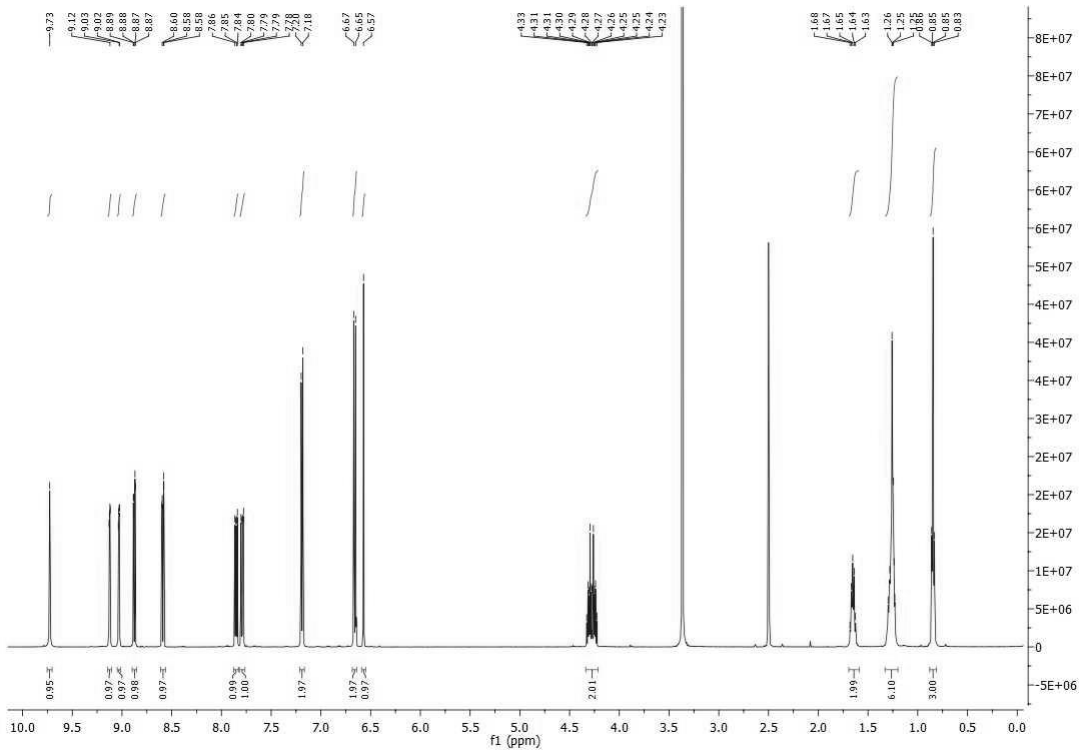

^{1}H NMR spectrum of HPO (**2.3**) in DMSO-d6

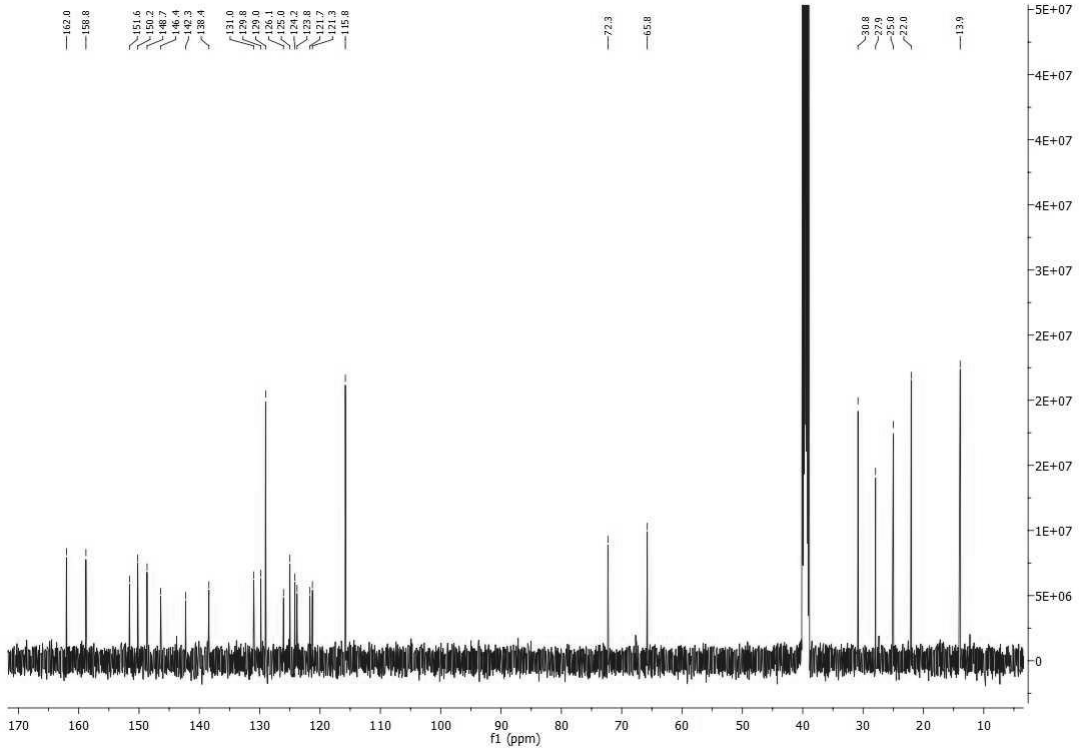

^{13}C NMR spectrum of HPO (**2.3**) in DMSO-d6

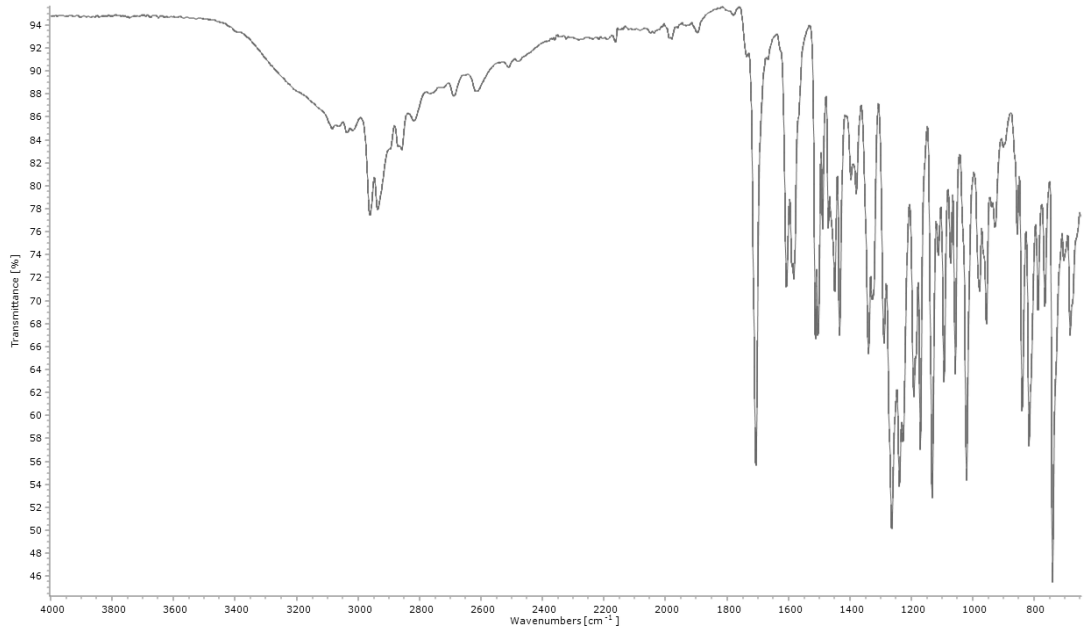

FTIR (ATR, cm^{-1}) spectrum of HPO (**2.3**)

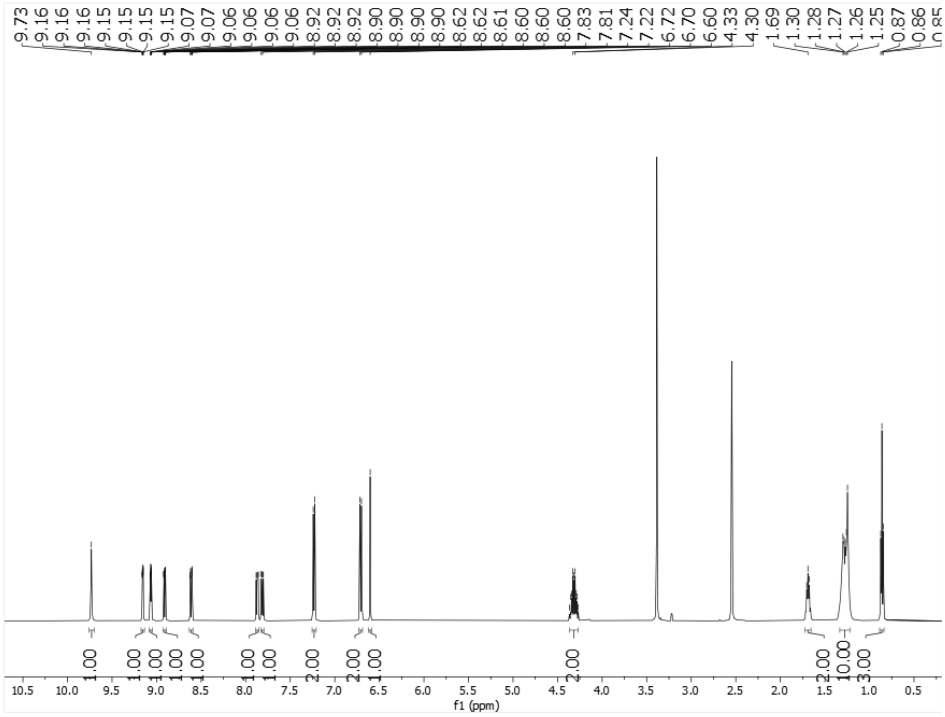

^{1}H NMR spectrum of OPO (**2.4**) in DMSO-d6

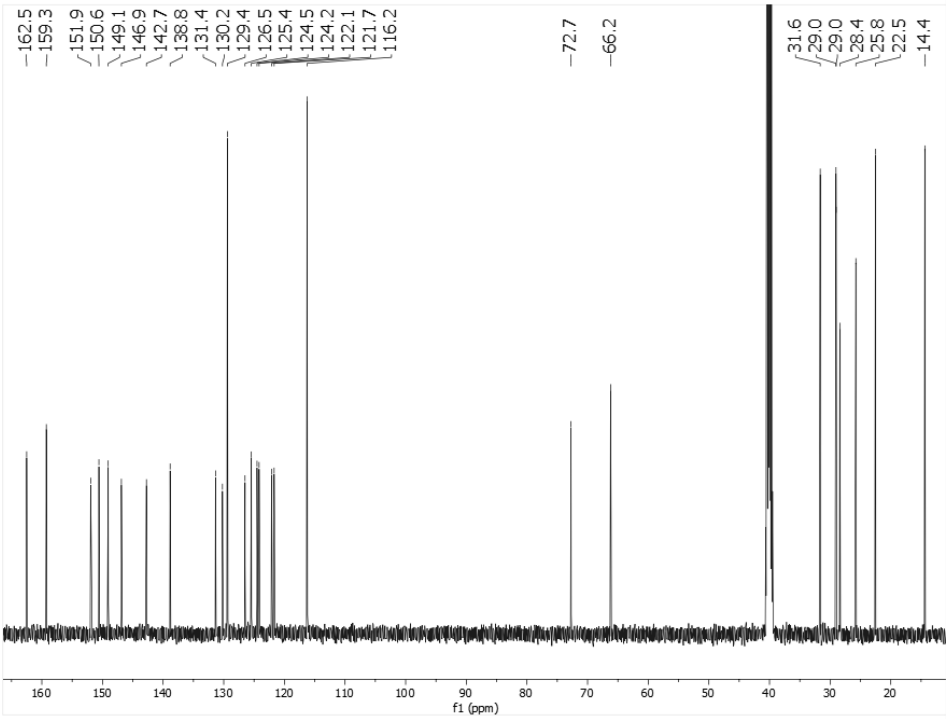

^{13}C NMR spectrum of OPO (**2.4**) in DMSO-d6

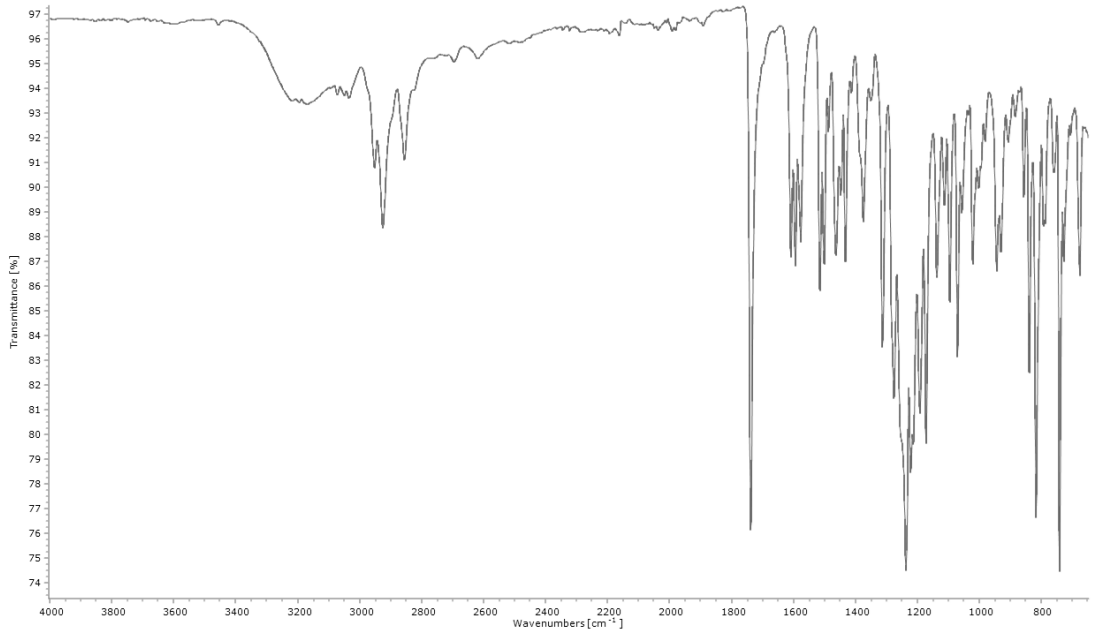

FTIR (ATR, cm^{-1}) spectrum of OPO (**2.4**)

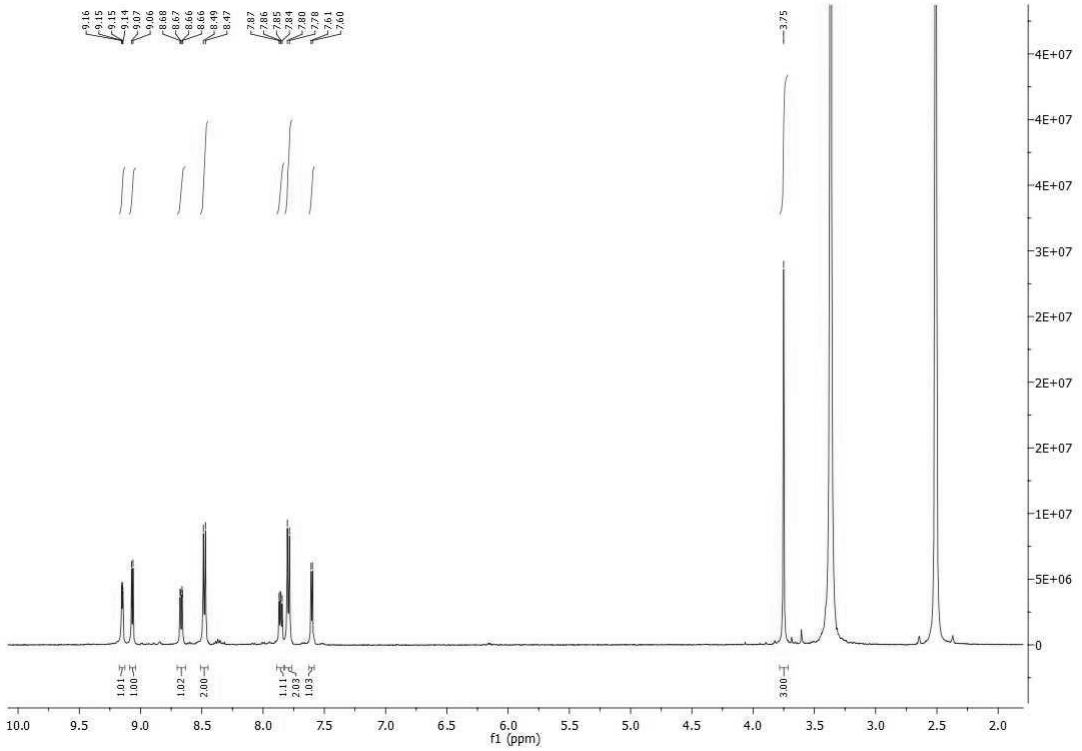

^{1}H NMR spectrum of MPP (**2.5**) in DMSO-d6

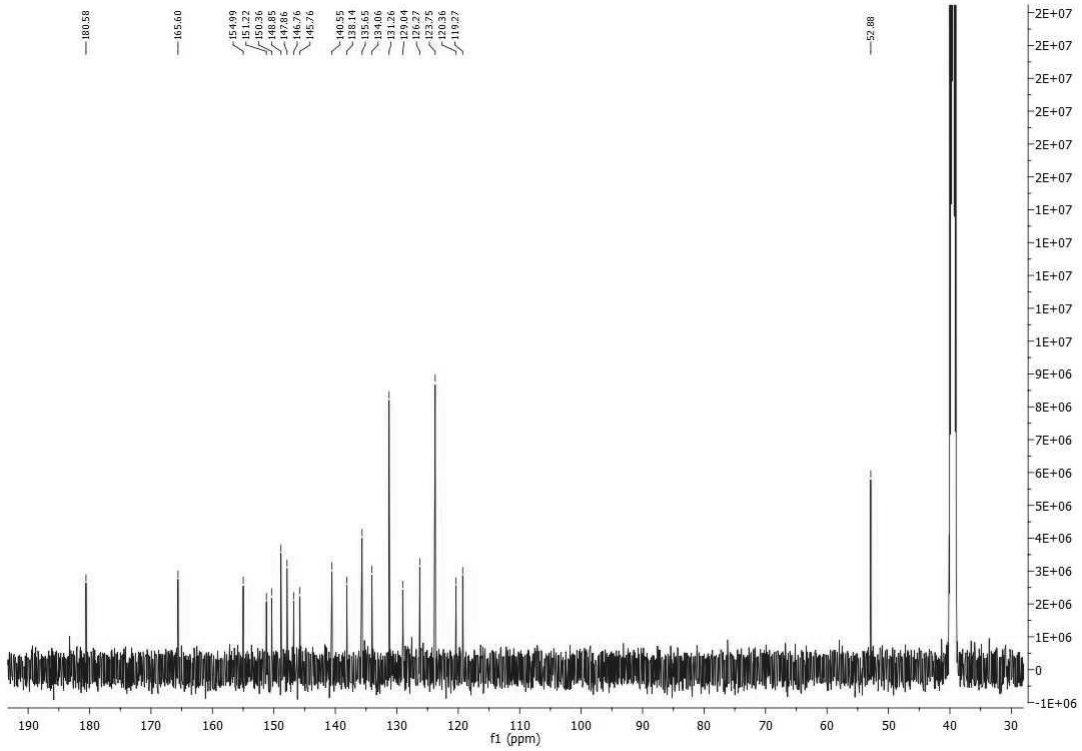

^{13}C NMR spectrum of MPP (**2.5**) in DMSO-d6

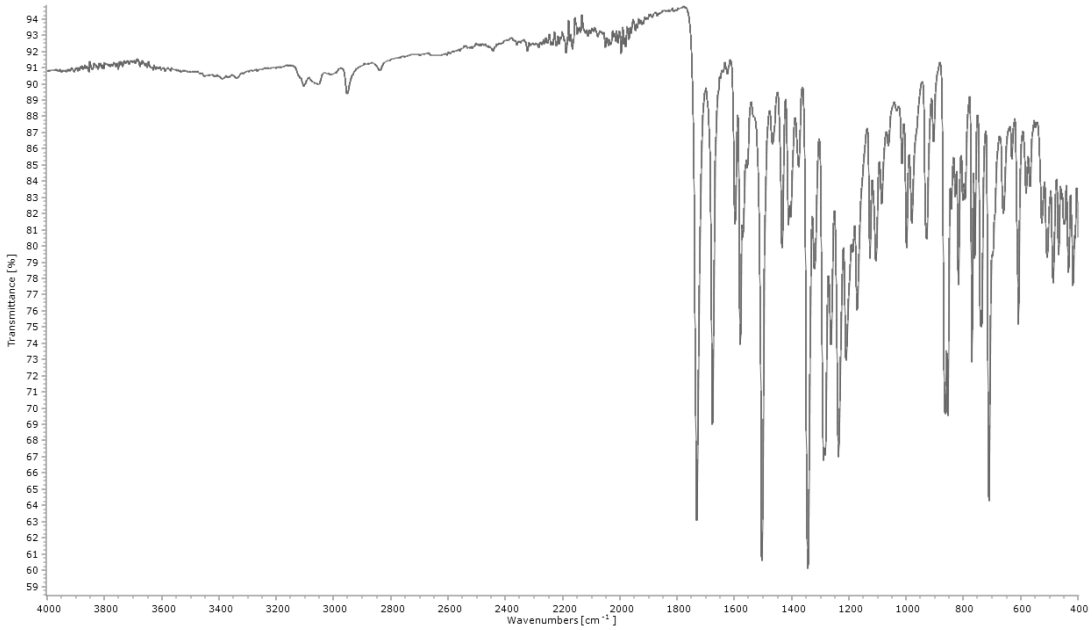

FTIR (ATR, cm^{-1}) spectrum of MPP (**2.5**)

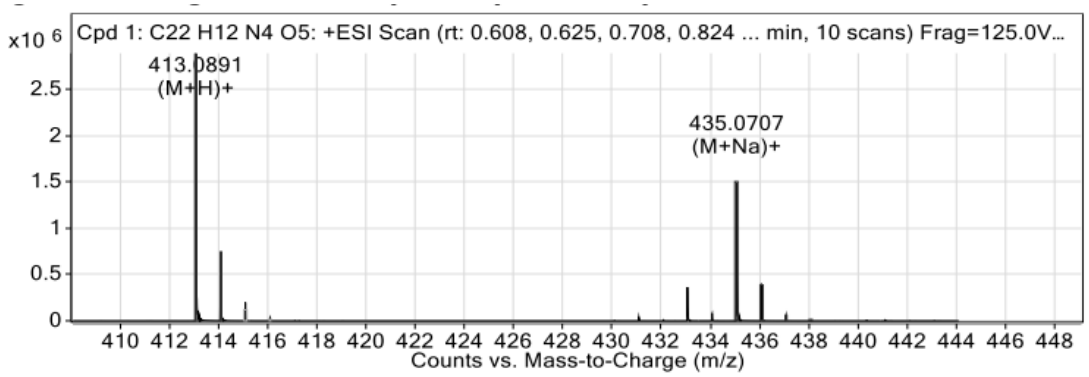

ESI Mass spectrum recorded in positive ionisation mode showing the isotopic pattern for MPP (**2.5**)

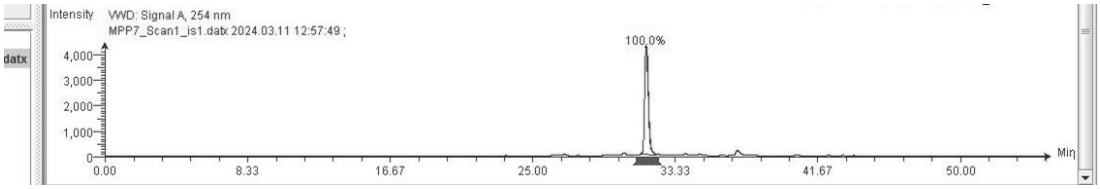

HPLC trace of MPP (**2.5**)

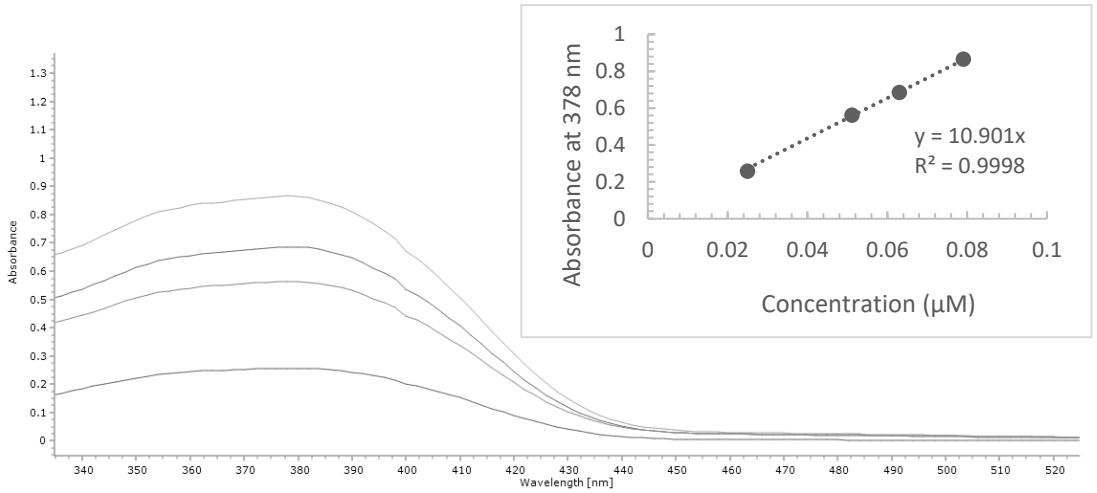

UV-visible spectra of MPP (**2.5**) in DMSO at concentrations of 2.50 x 10^{-5} – 7.99 x 10^{-5} M in DMSO used to determine the extinction coefficient (ε). ε = 10,901 M^{-1} cm^{-1}

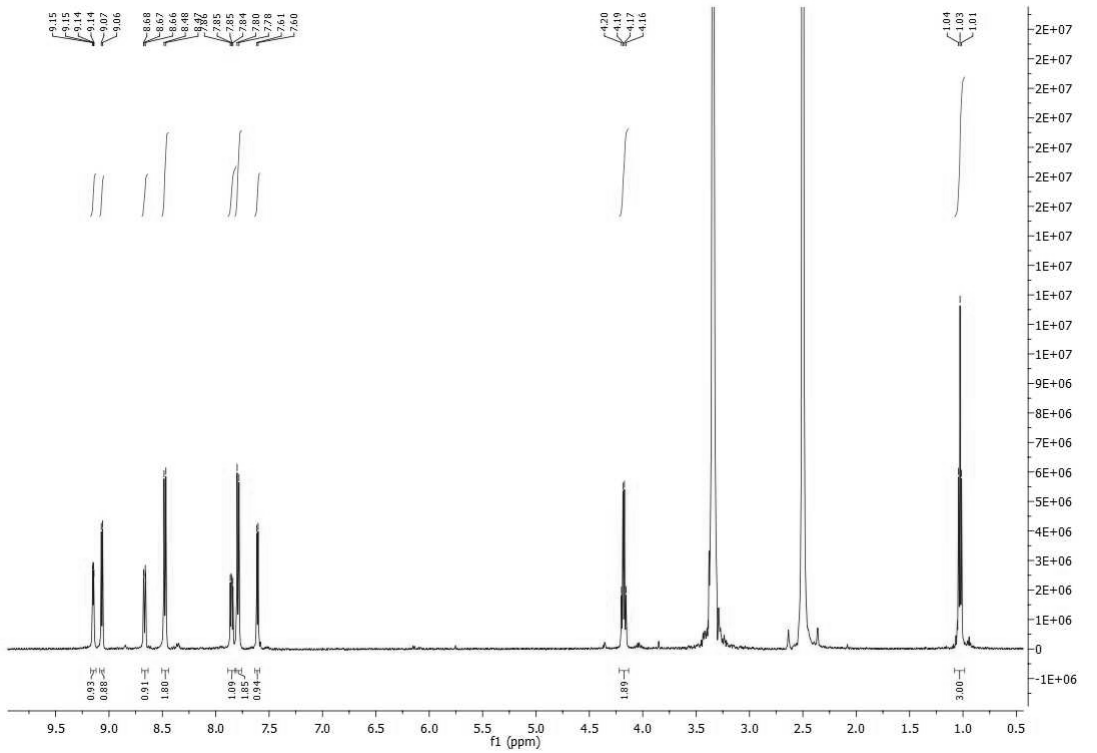

^{1}H NMR spectrum of EPP (**2.6**) in DMSO-d6

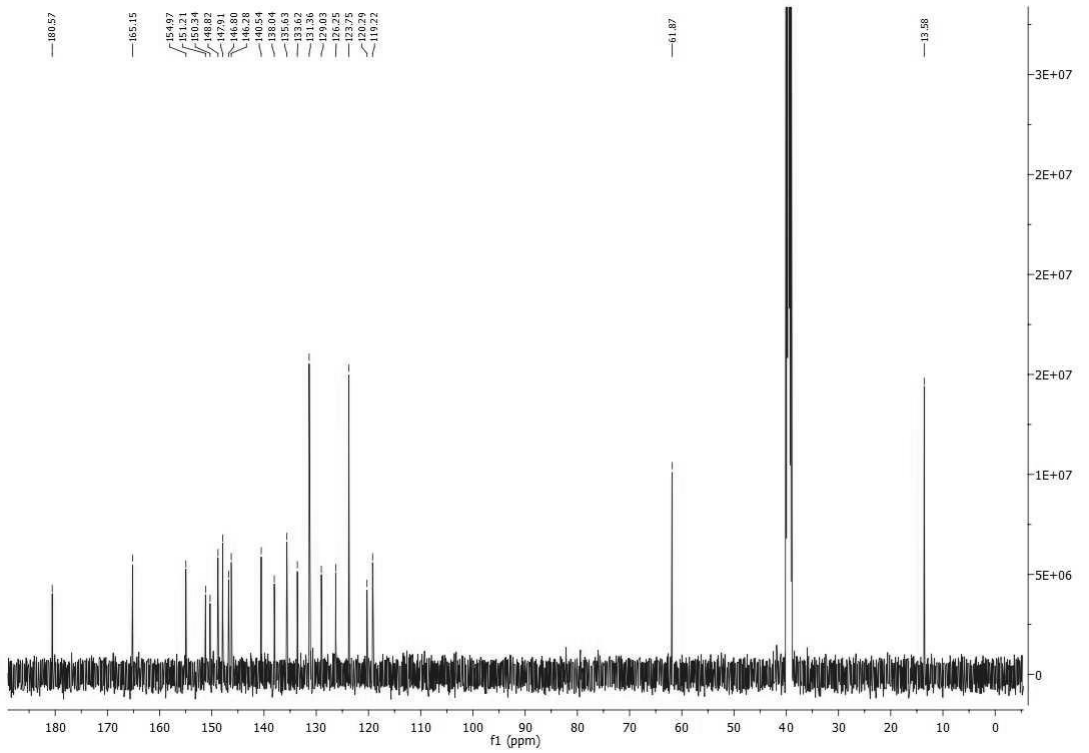

^{13}C NMR spectrum of EPP (**2.6**) in DMSO-d6

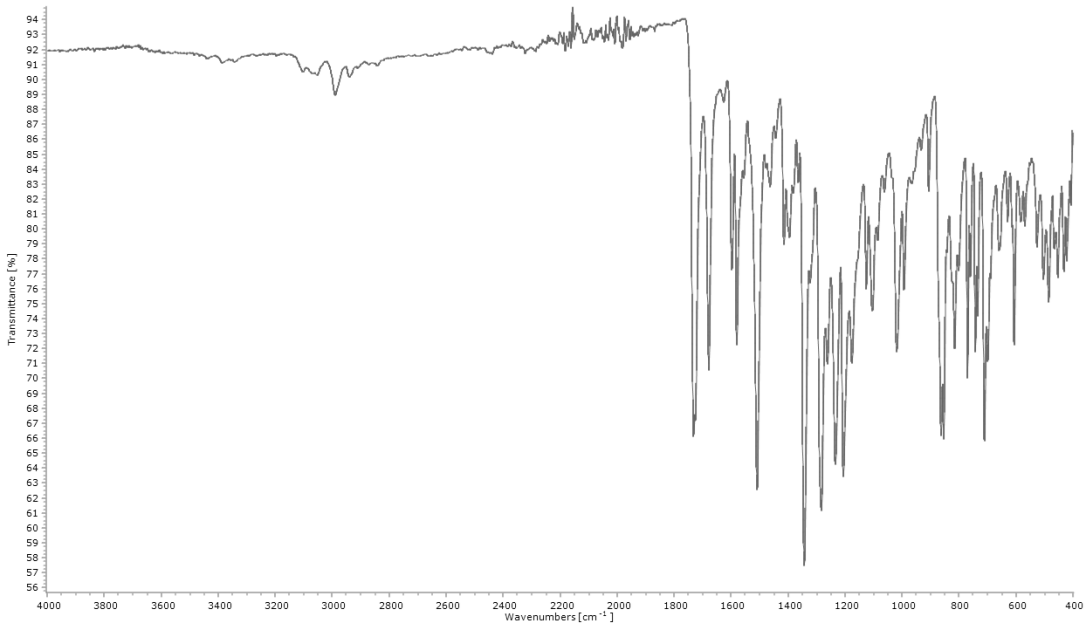

FTIR (ATR, cm^{-1}) spectrum of EPP (**2.6**) in ATR mode

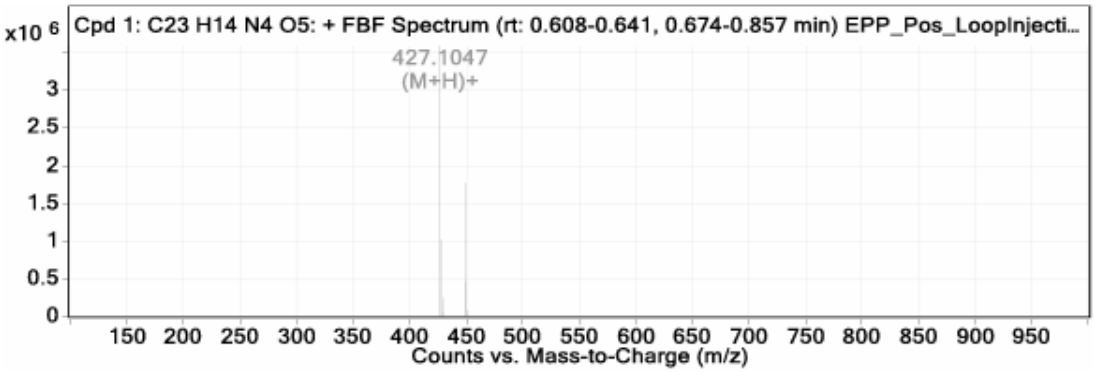

ESI Mass spectrum recorded in positive ionisation mode showing the isotopic pattern for EPP (**2.6**)

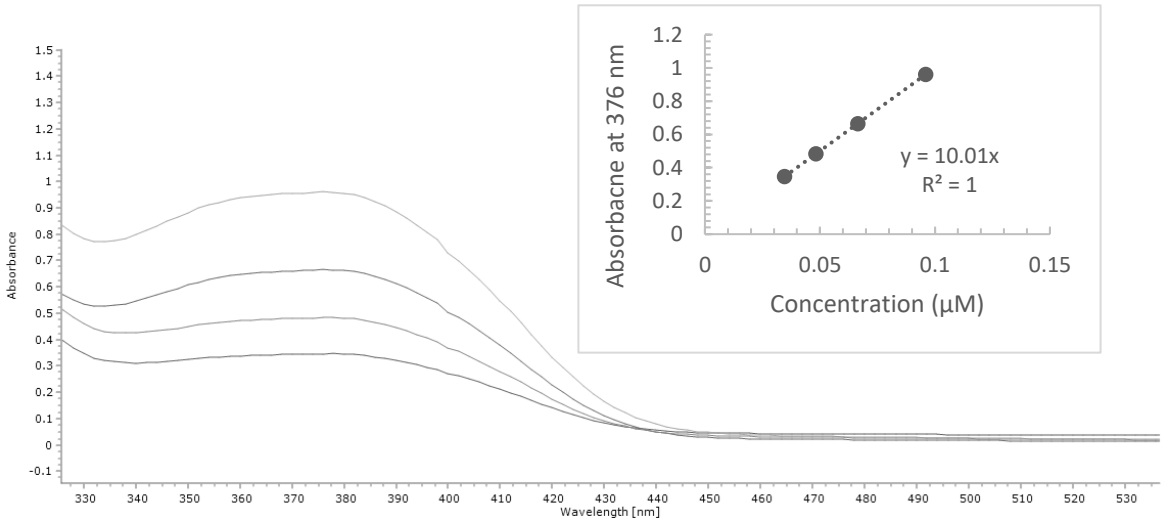

UV-visible spectra of EPP (**2.6**) in DMSO at concentrations of 3.46 x 10^{-5} – 9.60 x 10^{-5} M in DMSO used to determine the extinction coefficient (ε). ε = 10,010 M^{-1} cm^{-1}.

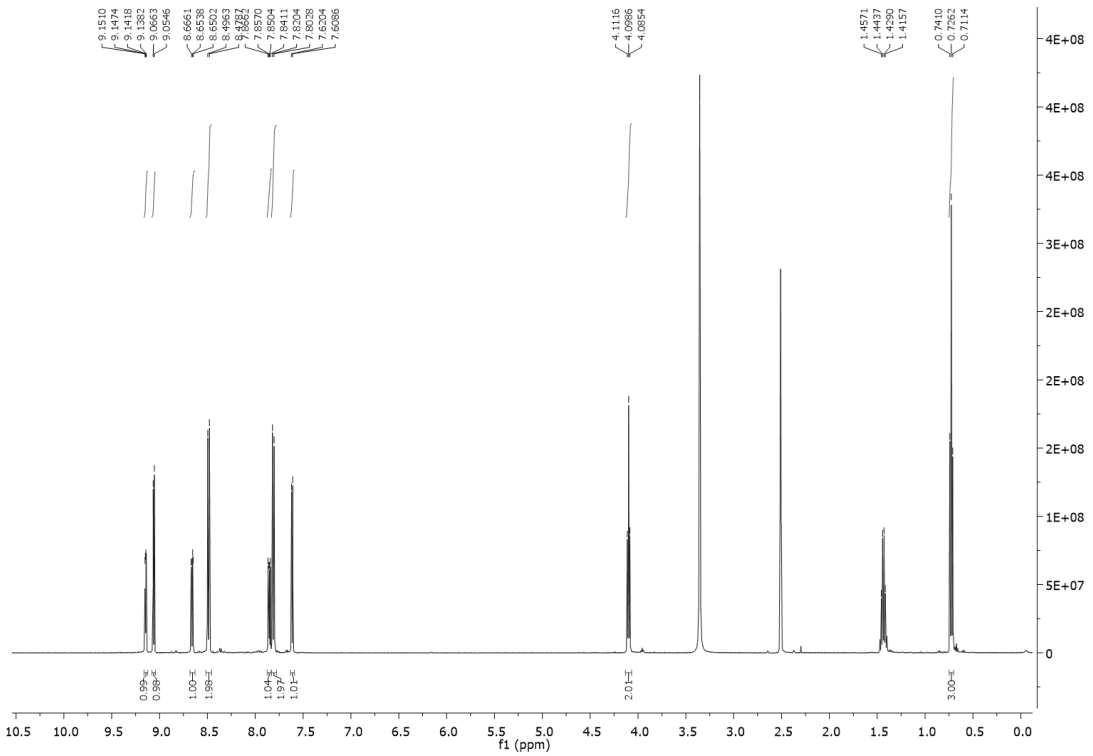

^{1}H NMR spectrum of PPP (**2.7**) in DMSO-d6

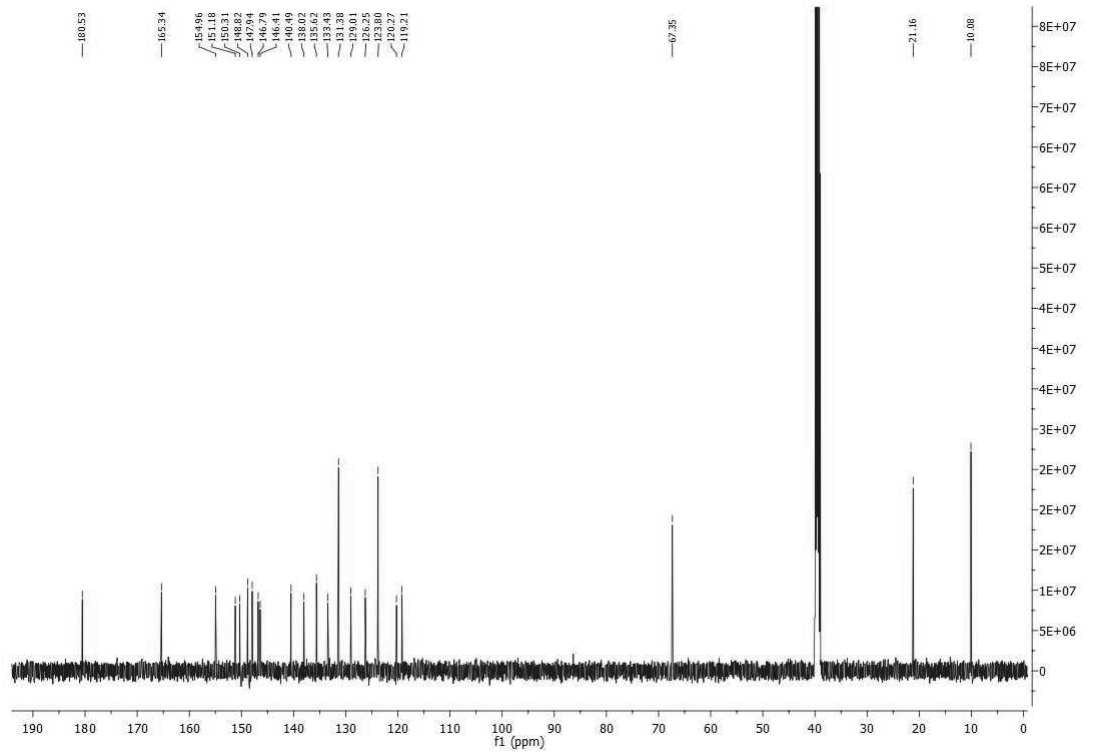

^{13}C NMR spectrum of PPP (**2.7**) in DMSO-d6

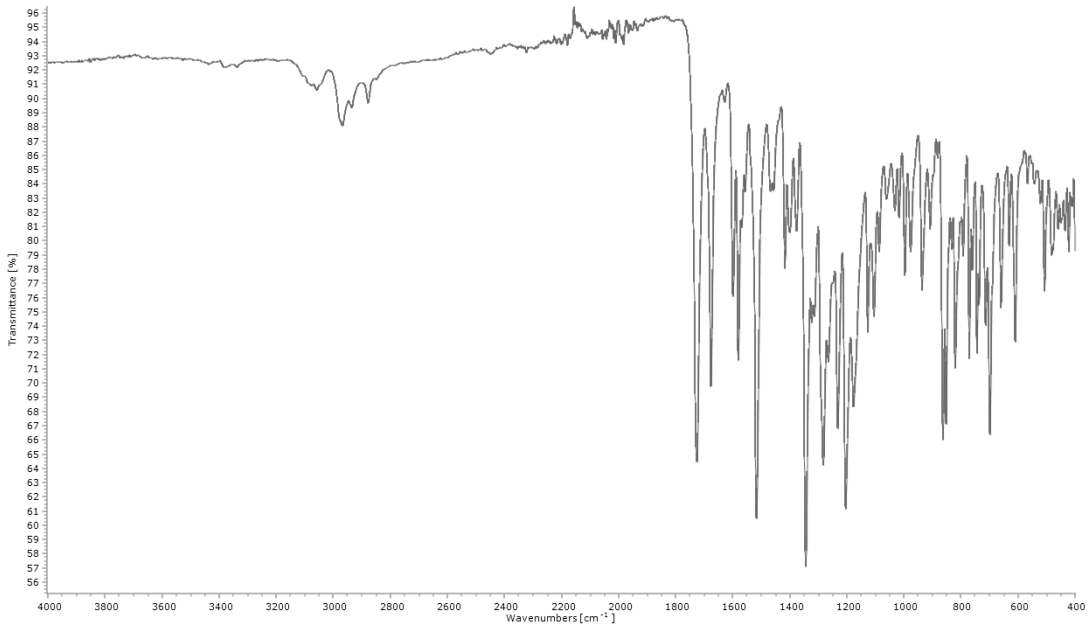

FTIR (ATR, cm^{-1}) spectrum of PPP (**2.7**)

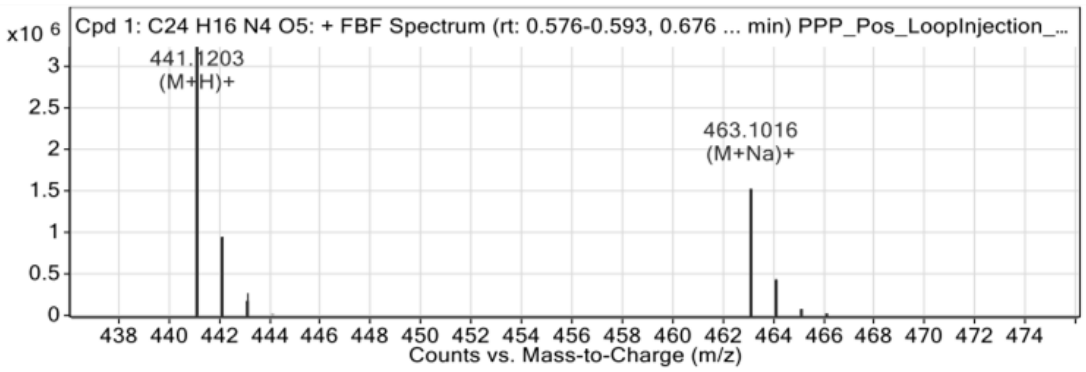

ESI Mass spectrum recorded in positive ionisation mode showing the isotopic pattern for PPP (**2.7**)

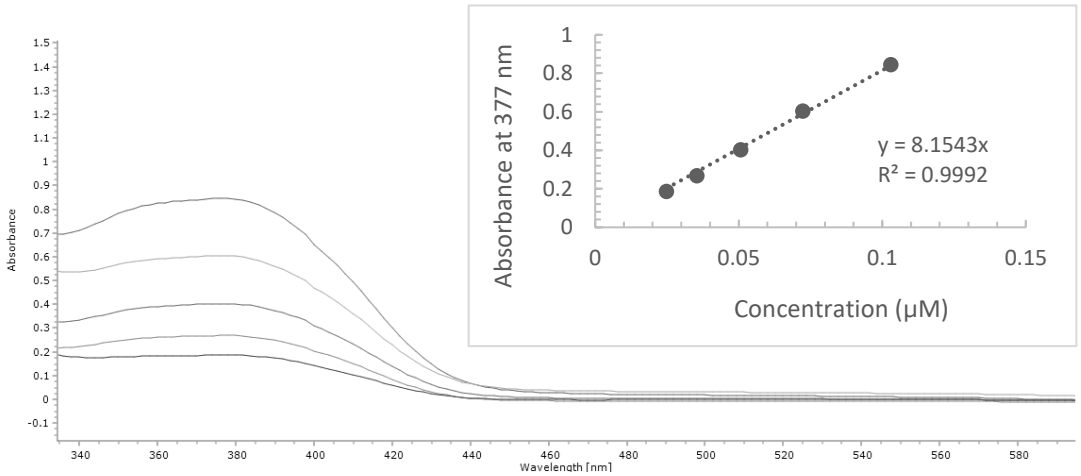

UV-visible spectra of PPP (**2.7**) in DMSO at concentrations of 2.48 x 10^{-5} – 1.03 x 10^{-4} M in DMSO used to determine the extinction coefficient (ε). ε = 8,154.3 M^{-1} cm^{-1}

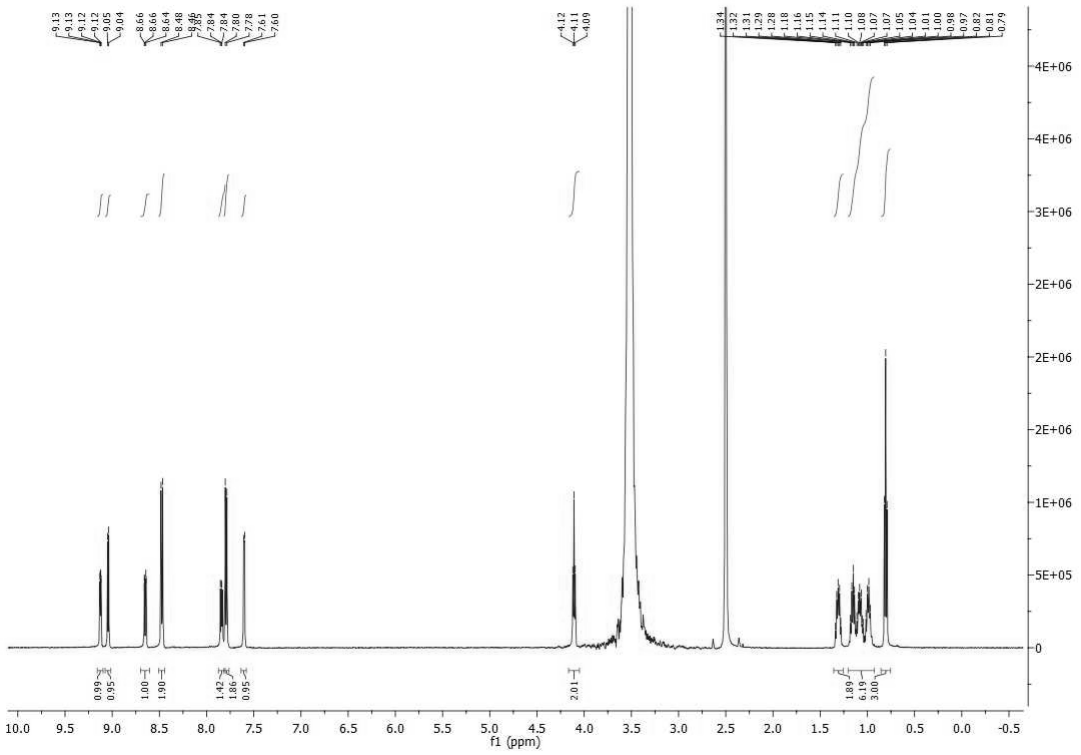

^{1}H NMR spectrum of HPP (**2.8**) in DMSO-d6

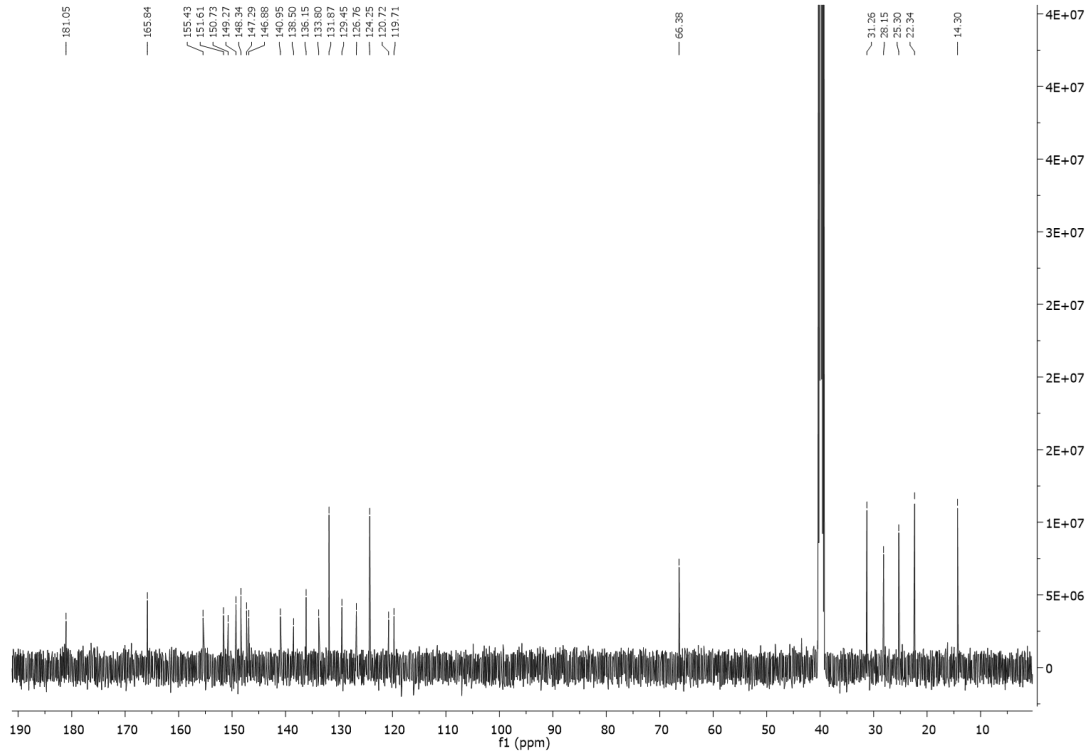

^{13}C NMR spectrum of HPP (**2.8**) in DMSO-d6

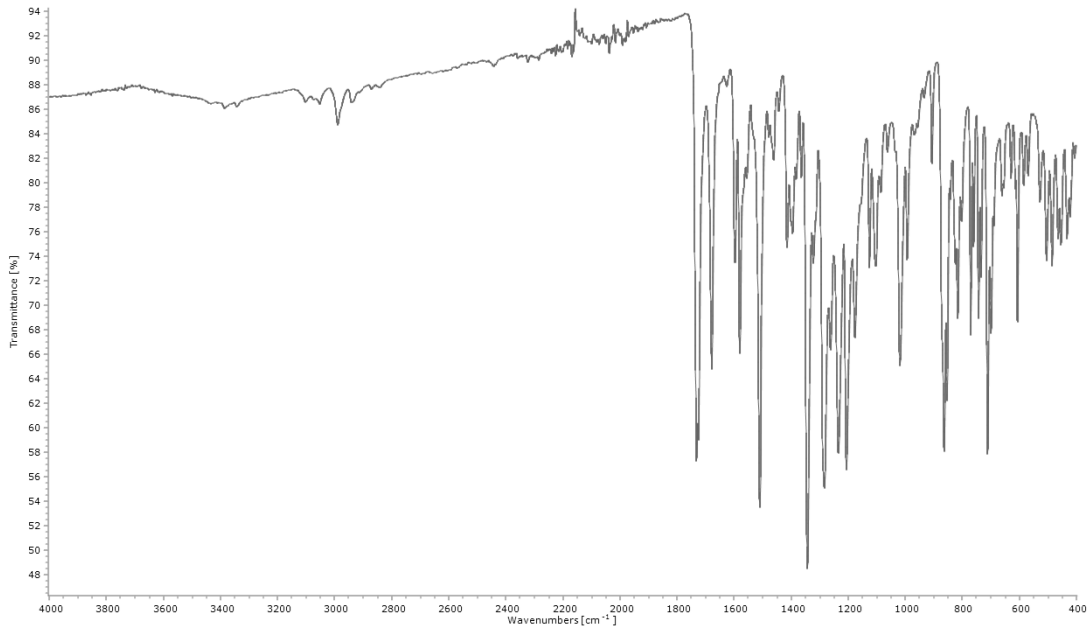

FTIR (ATR, cm^{-1}) spectrum of HPP (**2.8**)

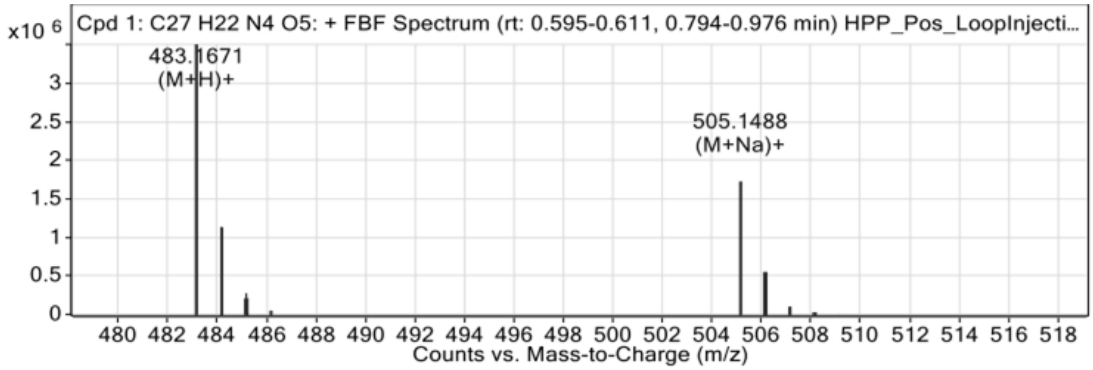

ESI Mass spectrum recorded in positive ionisation mode showing the isotopic pattern for HPP (**2.8**)

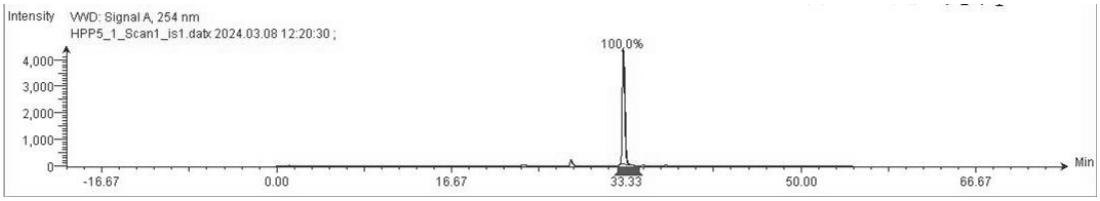

HPLC trace of HPP (**2.8**)

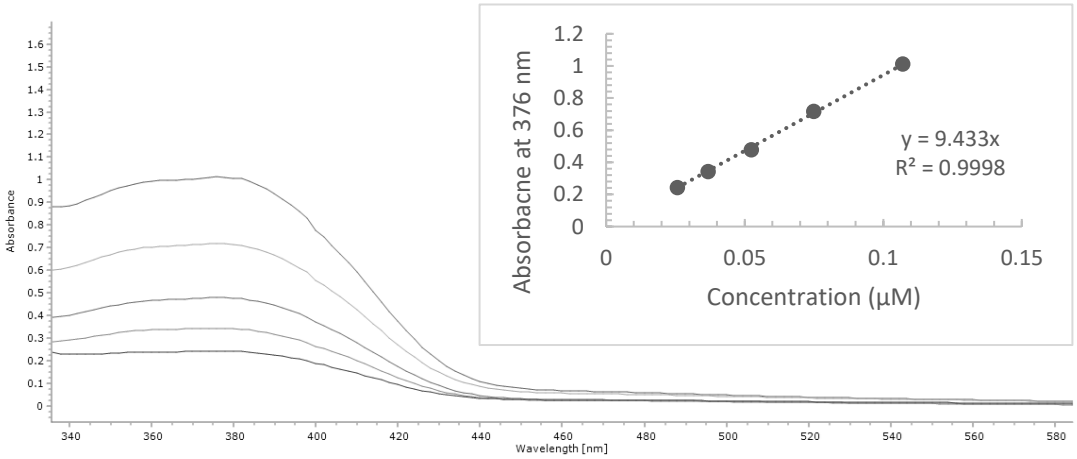

UV-visible spectra of HPP (**2.8**) in DMSO at concentrations of 2.57 x 10^{-5} – 1.07 x 10^{-5} M in DMSO used to determine the extinction coefficient (ε). ε = 9,433 M^{-1} cm^{-1}.

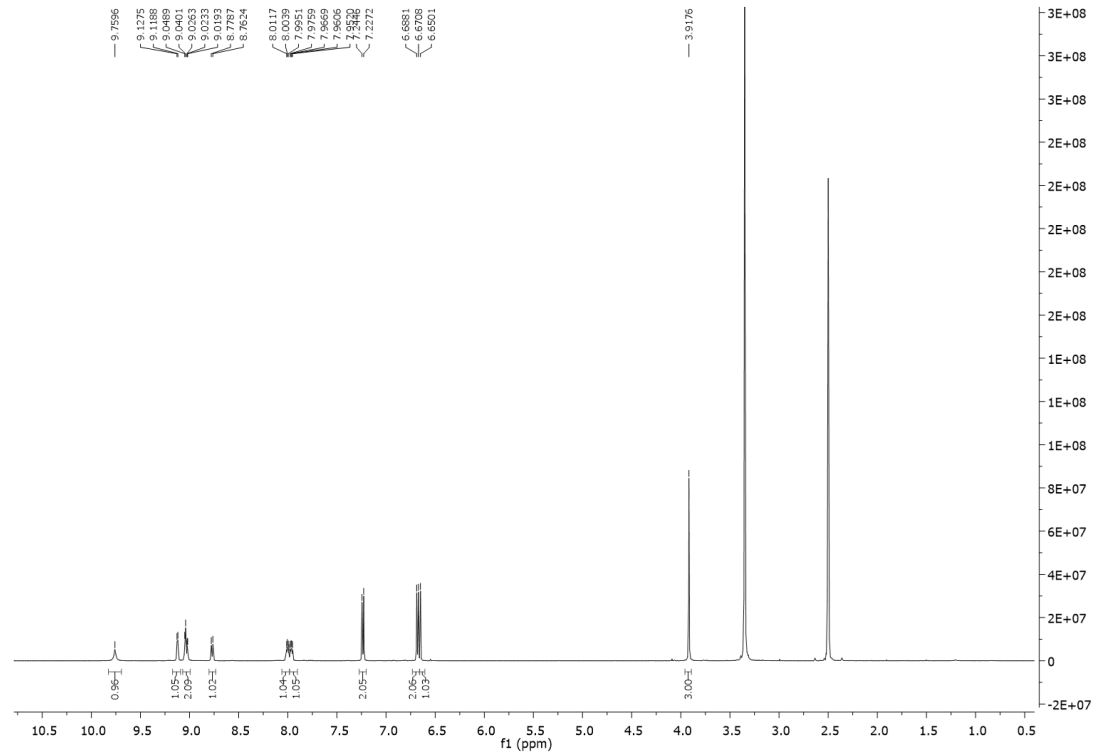

^{1}H NMR spectrum of Ag(MPO)$_2$ (**3.1**) in DMSO-d6

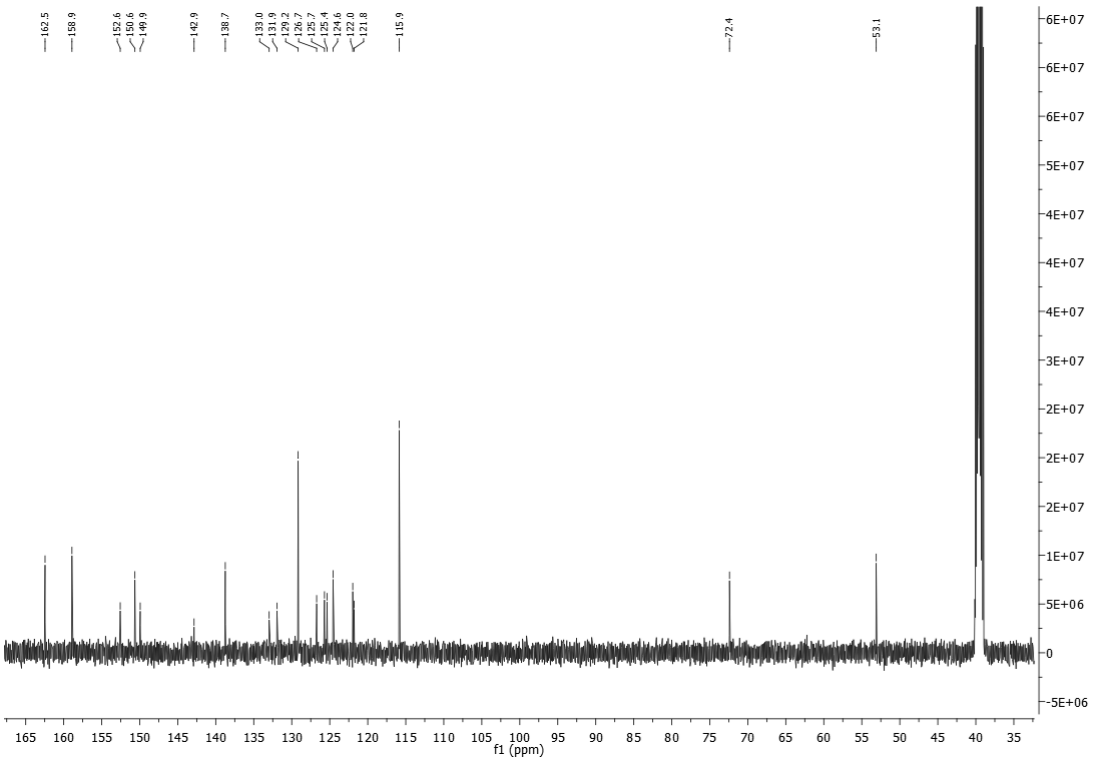

^{13}C NMR spectrum of Ag(MPO)$_2$ (**3.1**) in DMSO-d6

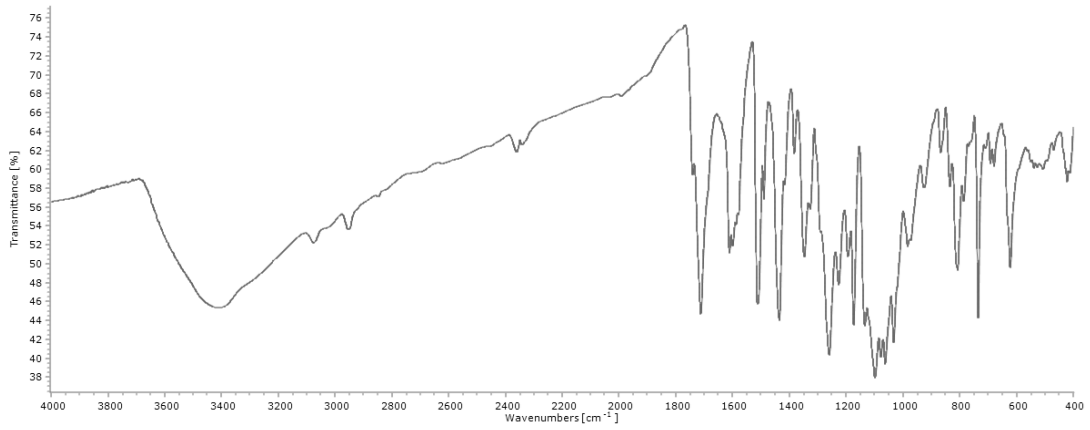

FTIR (KBr, cm^{-1}) spectrum of $Ag(MPO)_2$ (**3.1**)

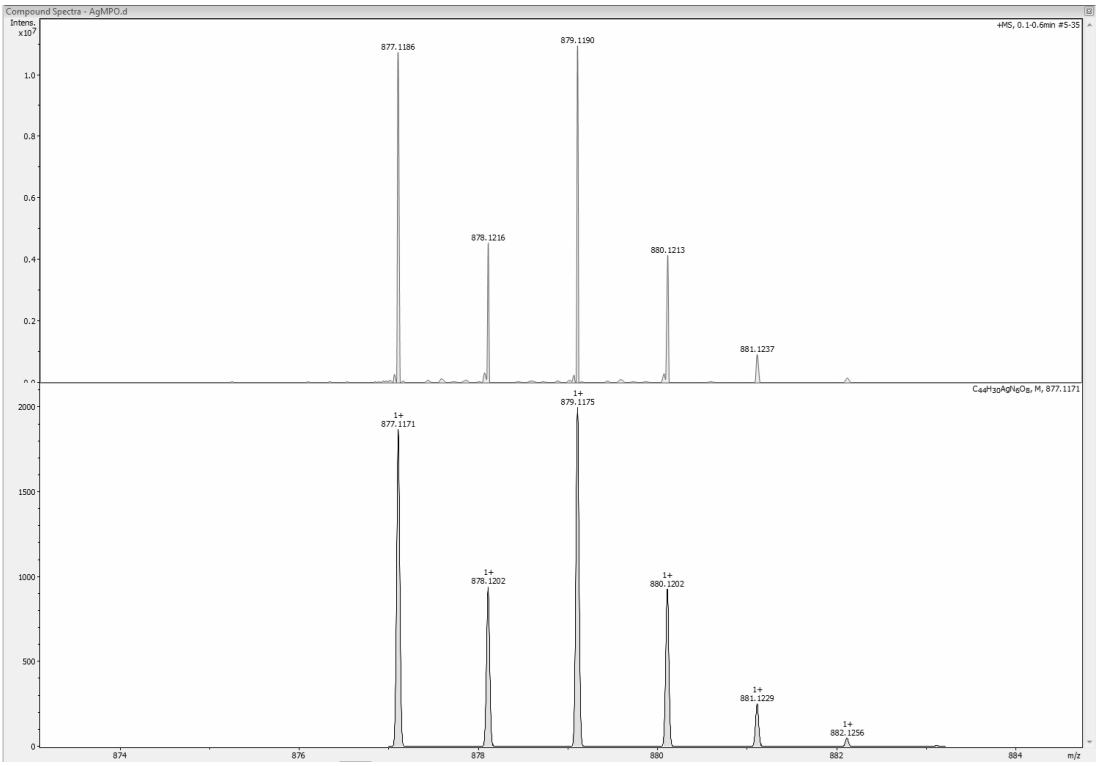

ESI Mass spectrum recorded in positive ionisation mode showing the isotopic pattern (top) and simulation of isotopic pattern (bottom) for $Ag(MPO)_2$ (**3.1**)

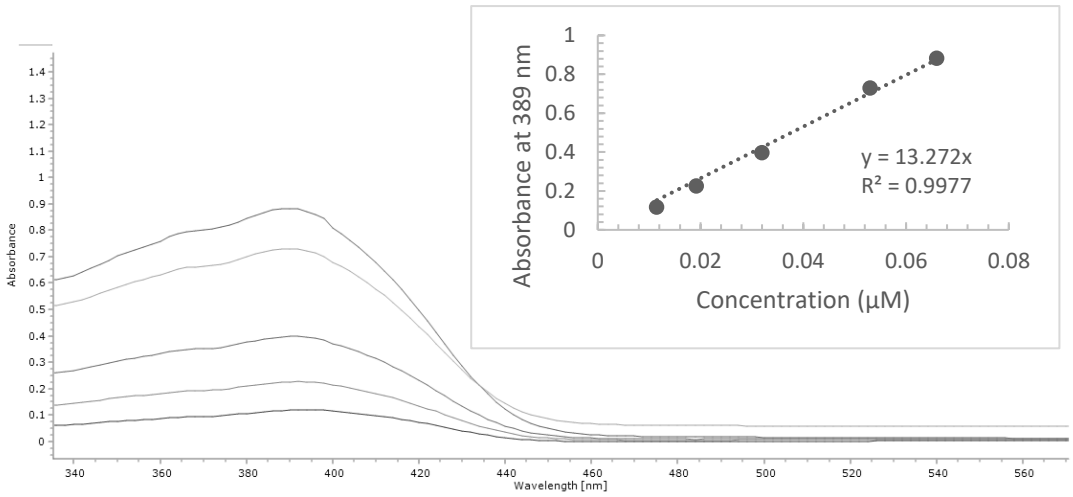

UV-visible spectra of $Ag(MPO)_2$ (**3.1**) in DMSO at concentrations of 1.15 x 10^{-5} – 6.67 x 10^{-5} M in DMSO used to determine the extinction coefficient (ε). ε = 13,172 M^{-1} cm^{-1}

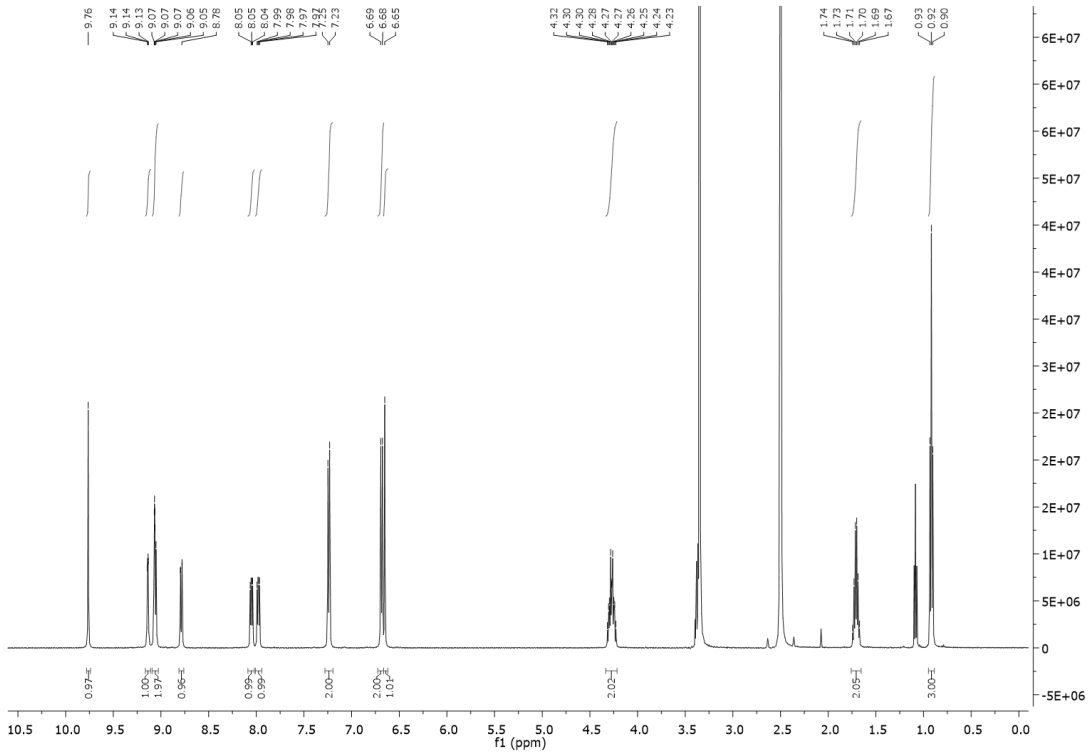

^{1}H NMR spectrum of $Ag(PPO)_2$ (**3.2**) in DMSO-d6

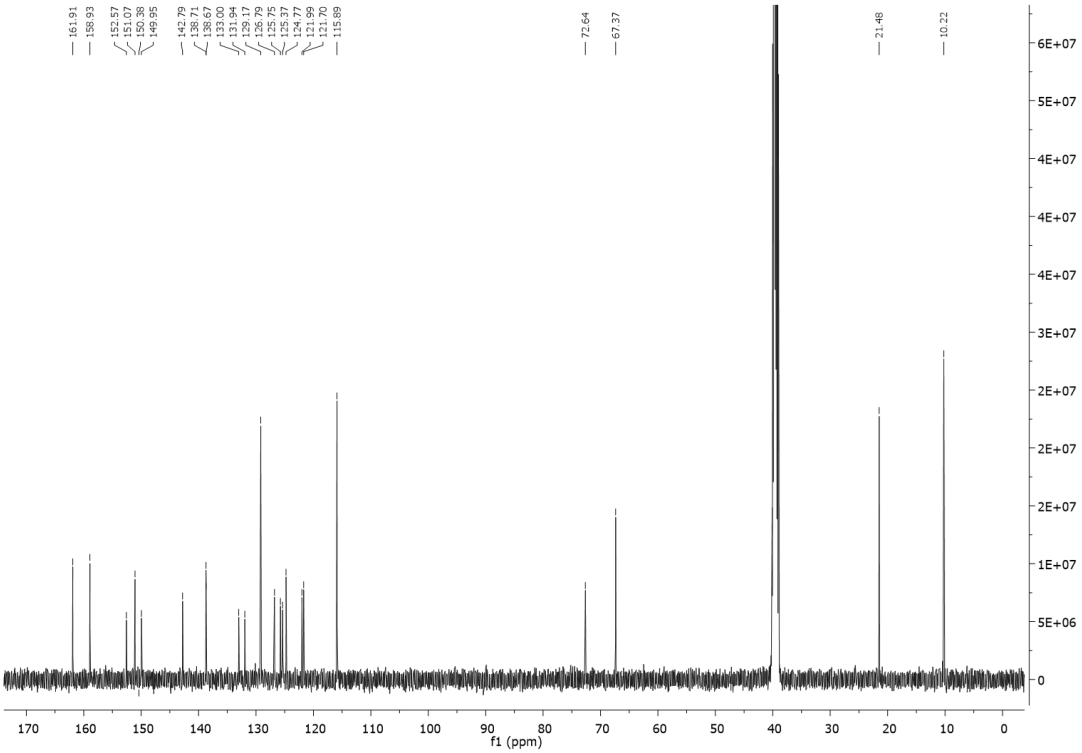

^{13}C NMR spectrum of $Ag(PPO)_2$ (**3.2**) in DMSO-d6

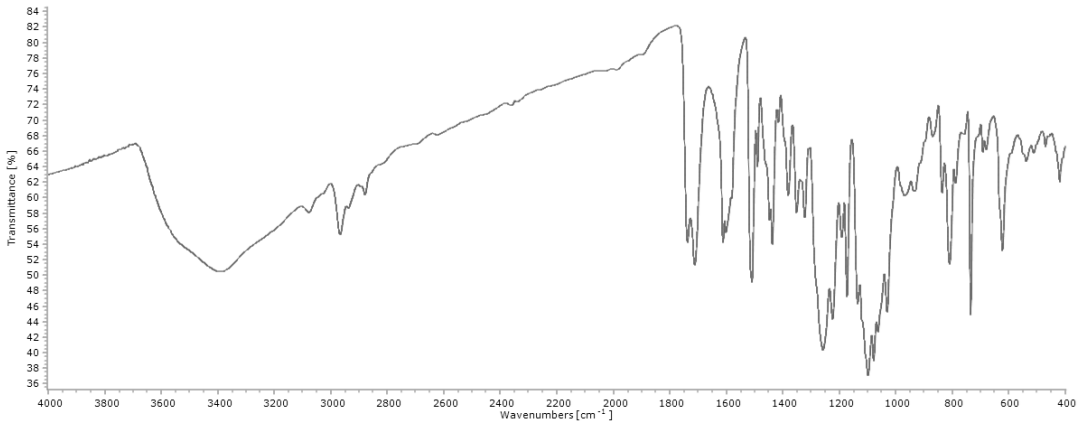

FTIR (KBr, cm^{-1}) spectrum of $Ag(PPO)_2$ (**3.2**)

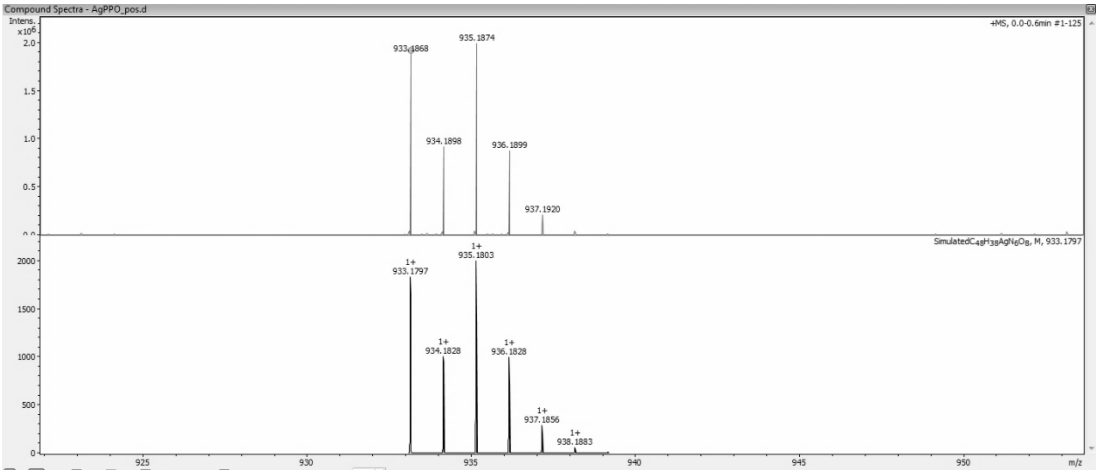

ESI Mass spectrum recorded in positive ionisation mode showing the isotopic pattern (top) and simulation of isotopic pattern (bottom) for $Ag(PPO)_2$ (**3.2**)

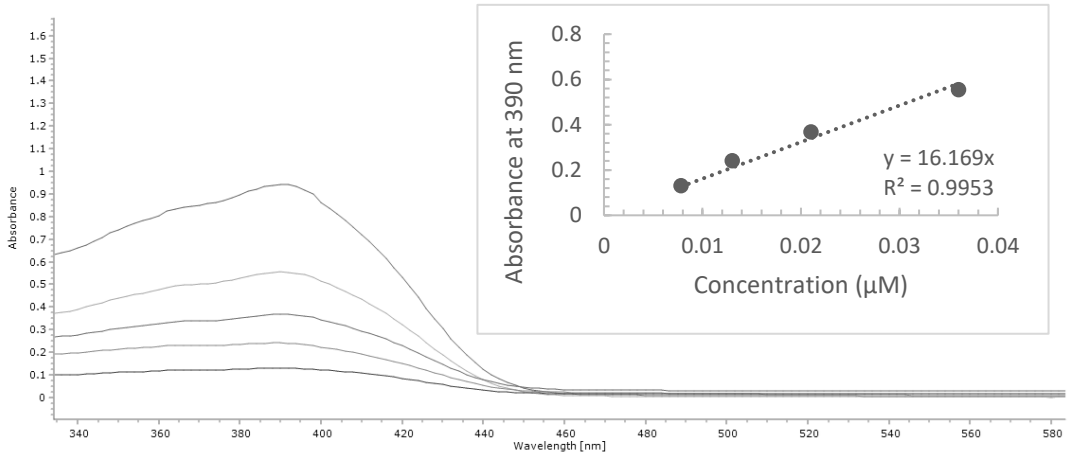

UV-visible spectra of $Ag(PPO)_2$ (**3.2**) in DMSO at concentrations of 7.85 x 10^{-6} – 3.64 x 10^{-5} M in DMSO used to determine the extinction coefficient (ε). ε = 15,629 $M^{-1}cm^{-1}$

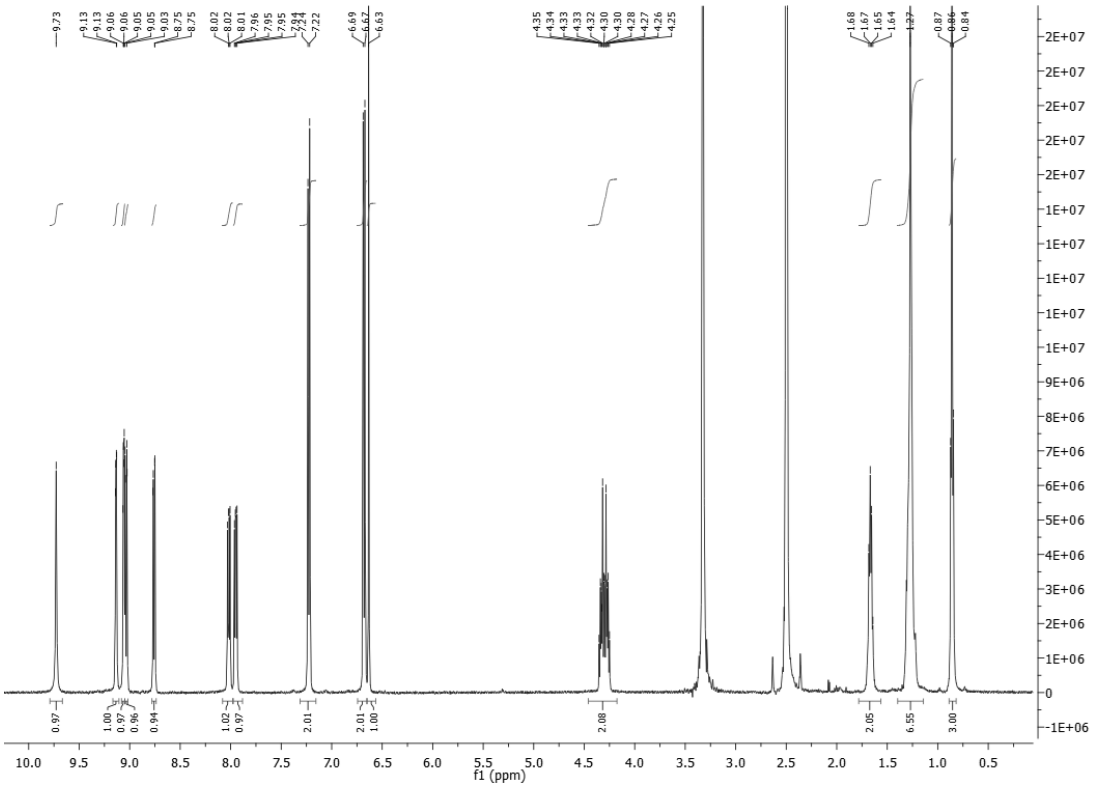

^{1}H NMR spectrum of $Ag(HPO)_2$ (**3.3**) in DMSO-d6

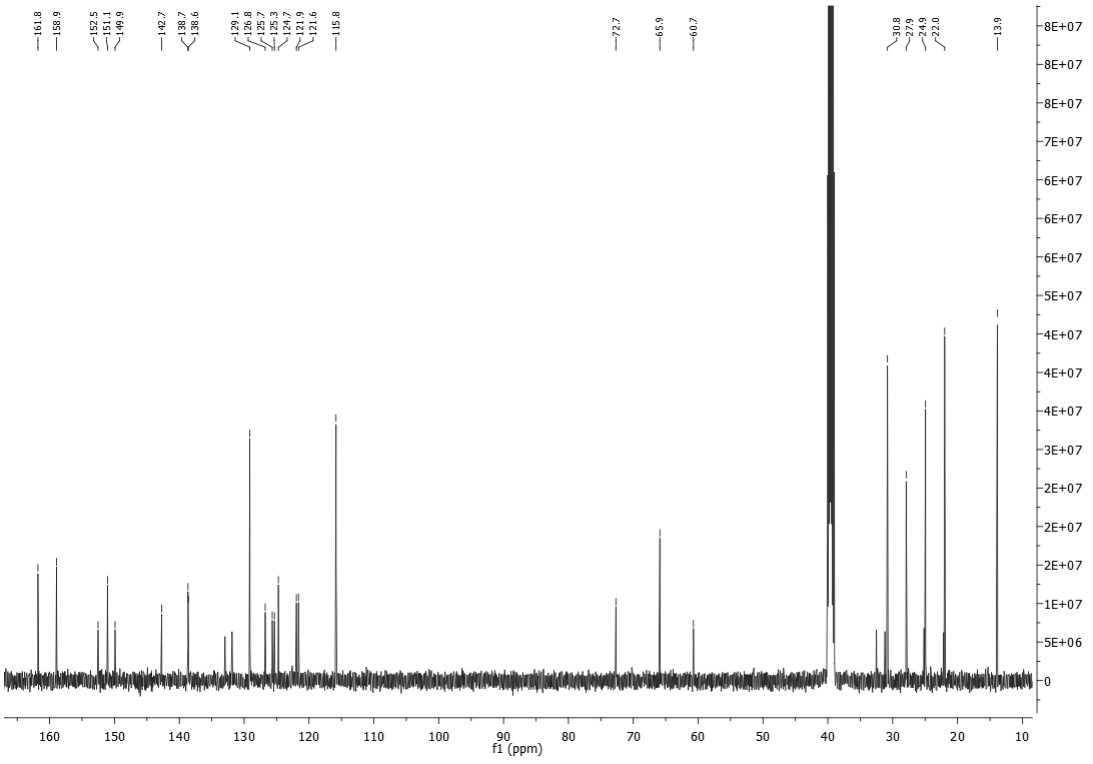

^{13}C NMR spectrum of $Ag(HPO)_2$ (**3.3**) in DMSO-d6

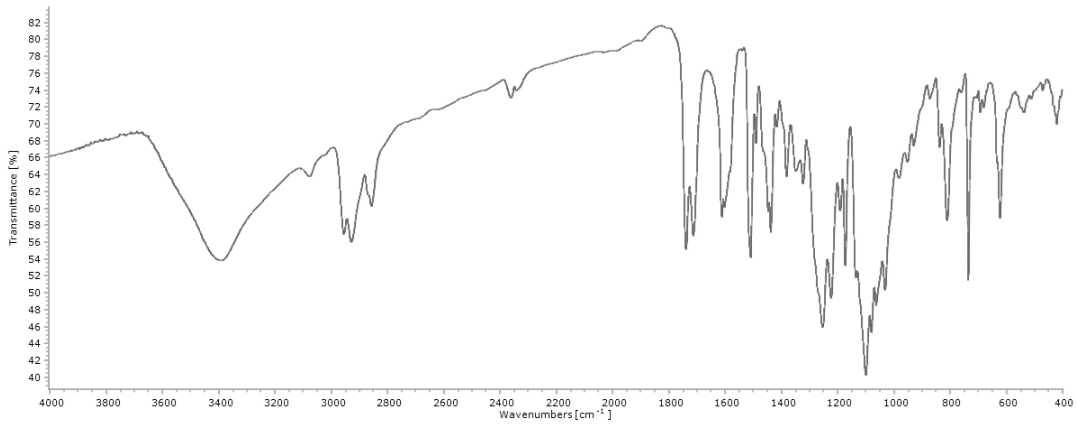

FTIR (KBr, cm^{-1}) spectrum of $Ag(HPO)_2$ (**3.3**)

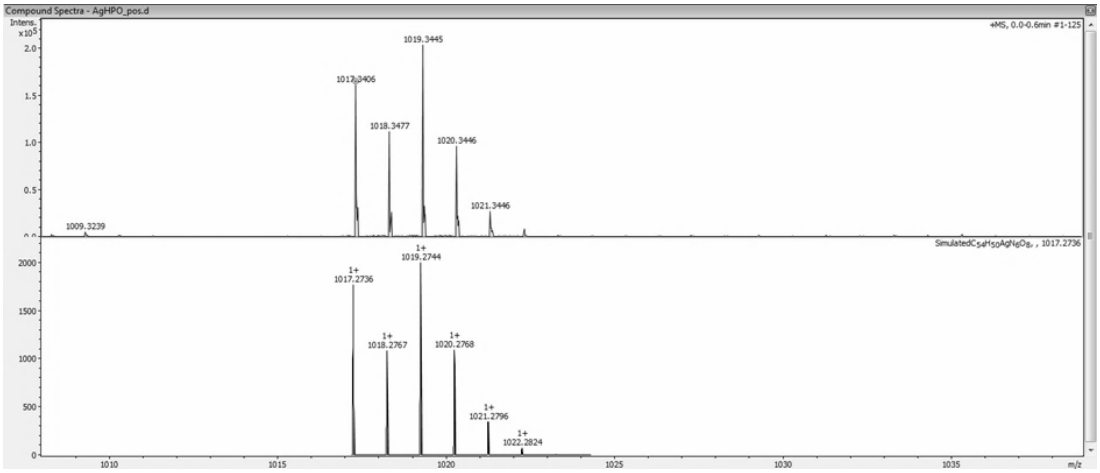

ESI Mass spectrum recorded in positive ionisation mode showing the isotopic pattern (top) and simulation of isotopic pattern (bottom) for $Ag(HPO)_2$ (**3.3**)

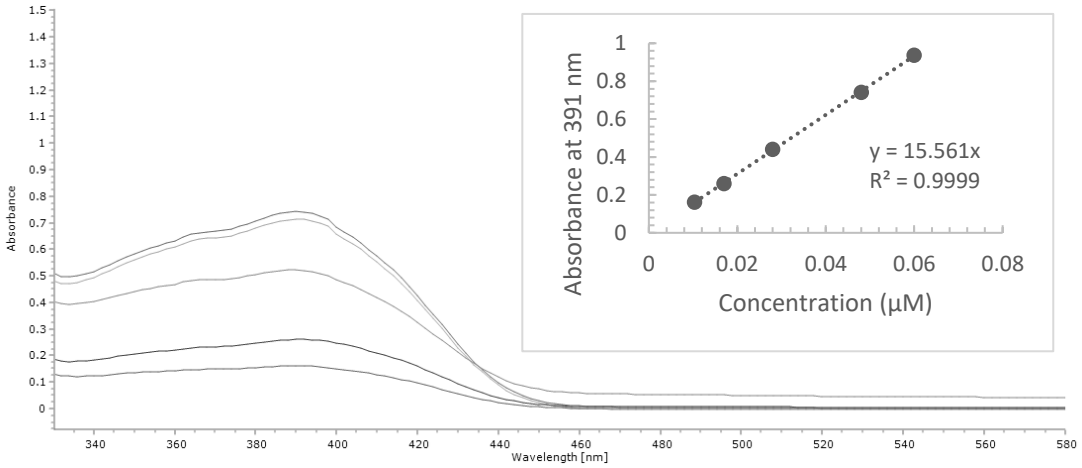

UV-visible spectra of $Ag(HPO)_2$ (**3.3**) in DMSO at concentrations of 1.03 x 10^{-5} – 6.00 x 10^{-5} M in DMSO used to determine the extinction coefficient (ε). ε = 15,877 $M^{-1}cm^{-1}$

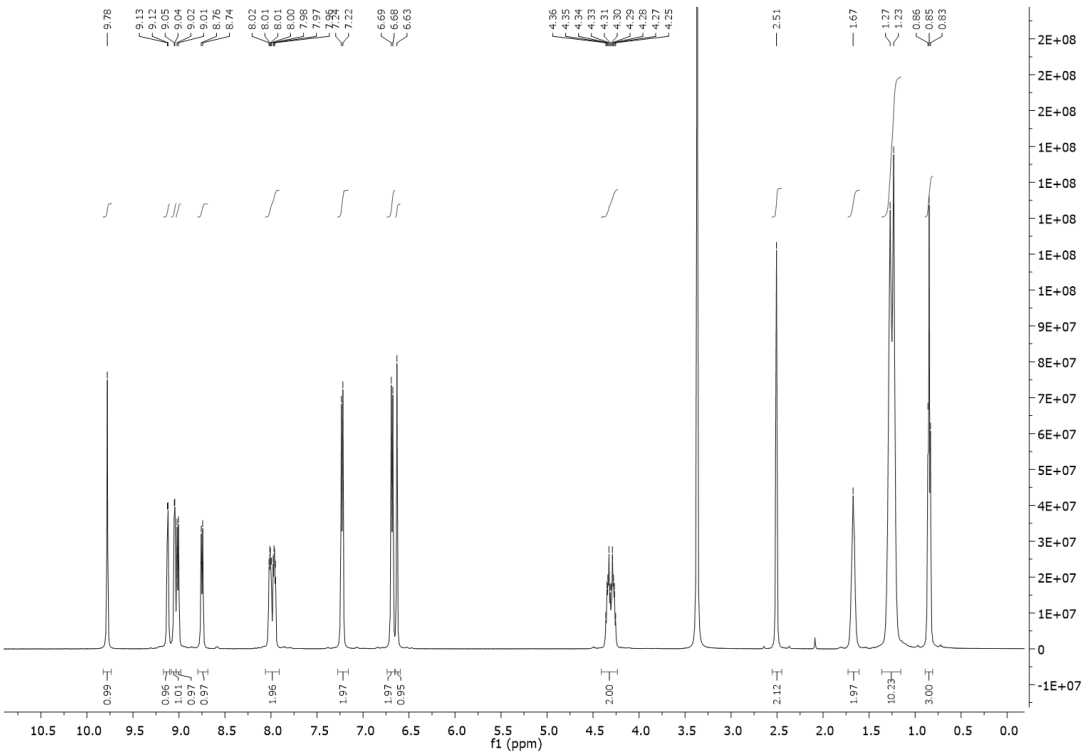

^{1}H NMR spectrum of $Ag(OPO)_2$ (**3.4**) in DMSO-d6

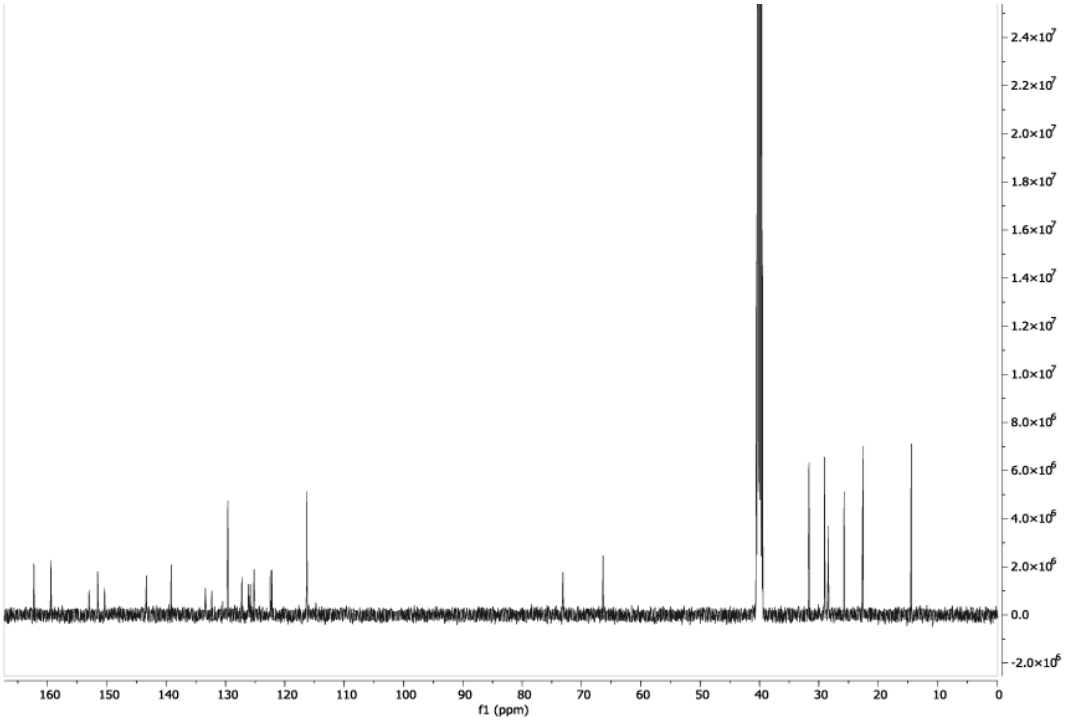

^{13}C NMR spectrum of $Ag(OPO)_2$ (**3.4**) in DMSO-d6

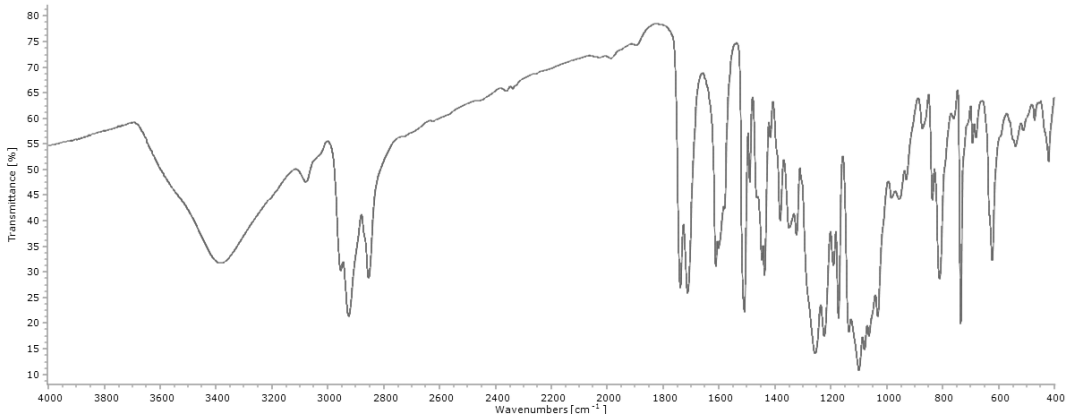

FTIR (KBr, cm^{-1}) spectrum of $Ag(OPO)_2$ (**3.4**)

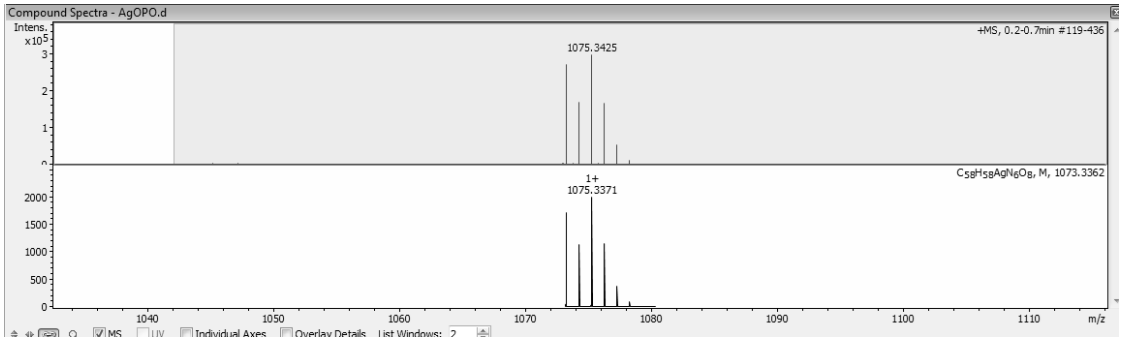

ESI Mass spectrum recorded in positive ionisation mode showing the isotopic pattern (top) and simulation of isotopic pattern (bottom) for $Ag(OPO)_2$ (**3.4**)

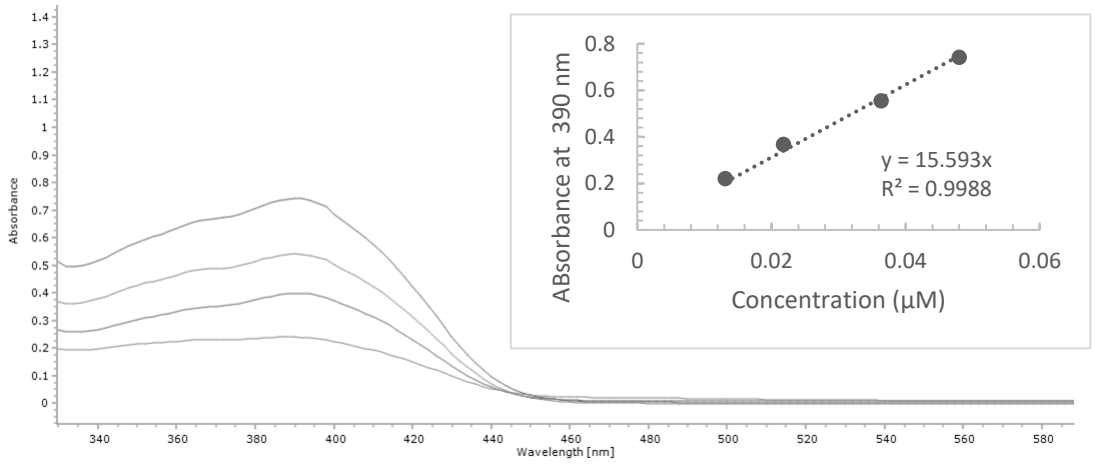

UV-visible spectra of $Ag(OPO)_2$ (**3.4**) in DMSO at concentrations of 1.31×10^{-5} – 3.64×10^{-5} M in DMSO used to determine the extinction coefficient (ε). ε = 15,656 M^{-1} cm^{-1}

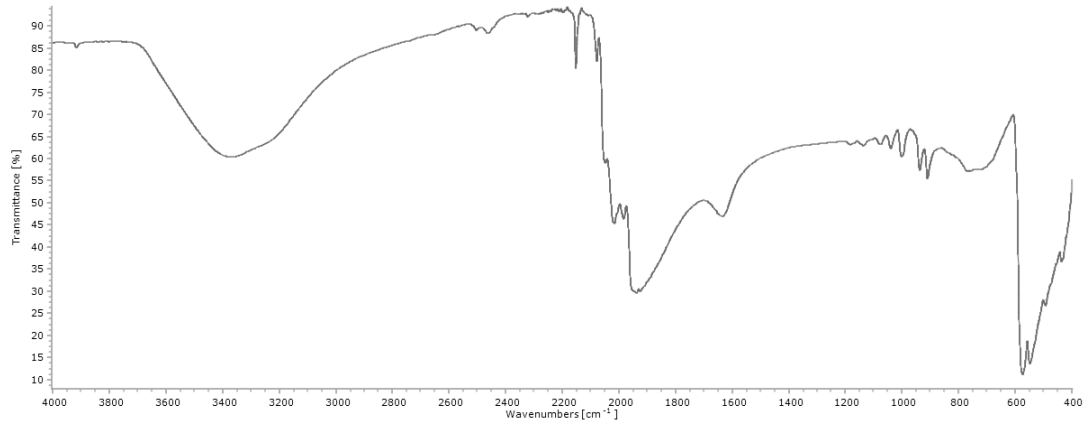

FTIR (ATR, cm^{-1}) spectrum of $Re(CO)_5Br$

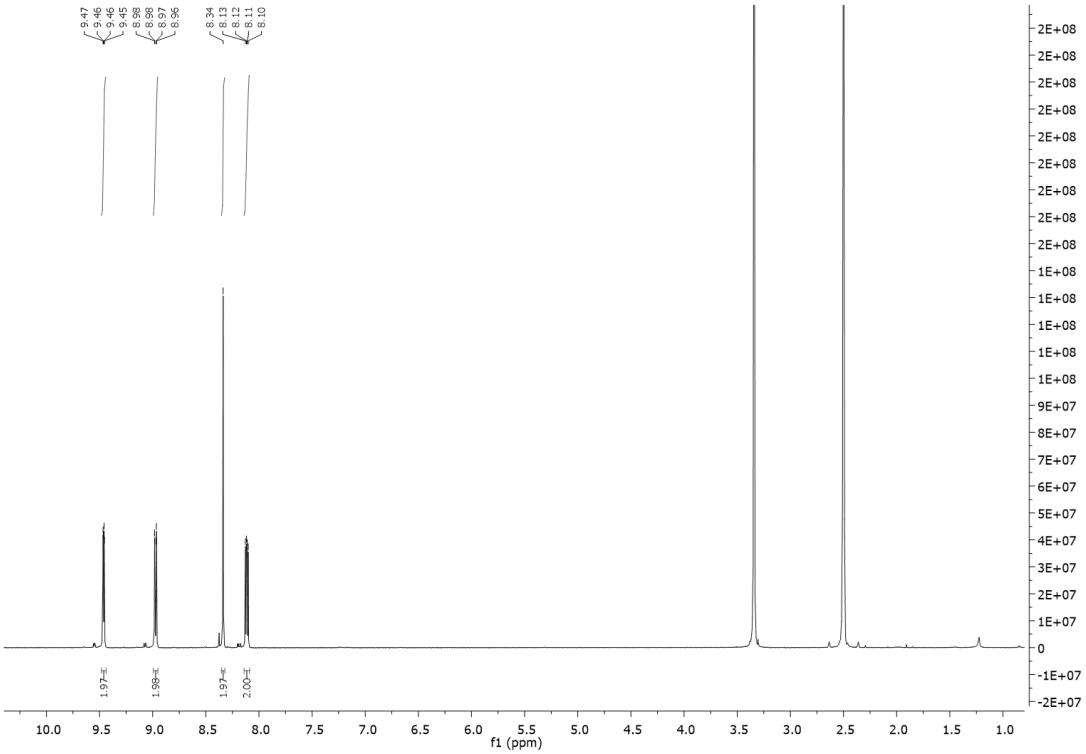

^{1}H NMR spectrum of [Re(CO)$_3$(phen)Br] (**4a**) in DMSO-d6

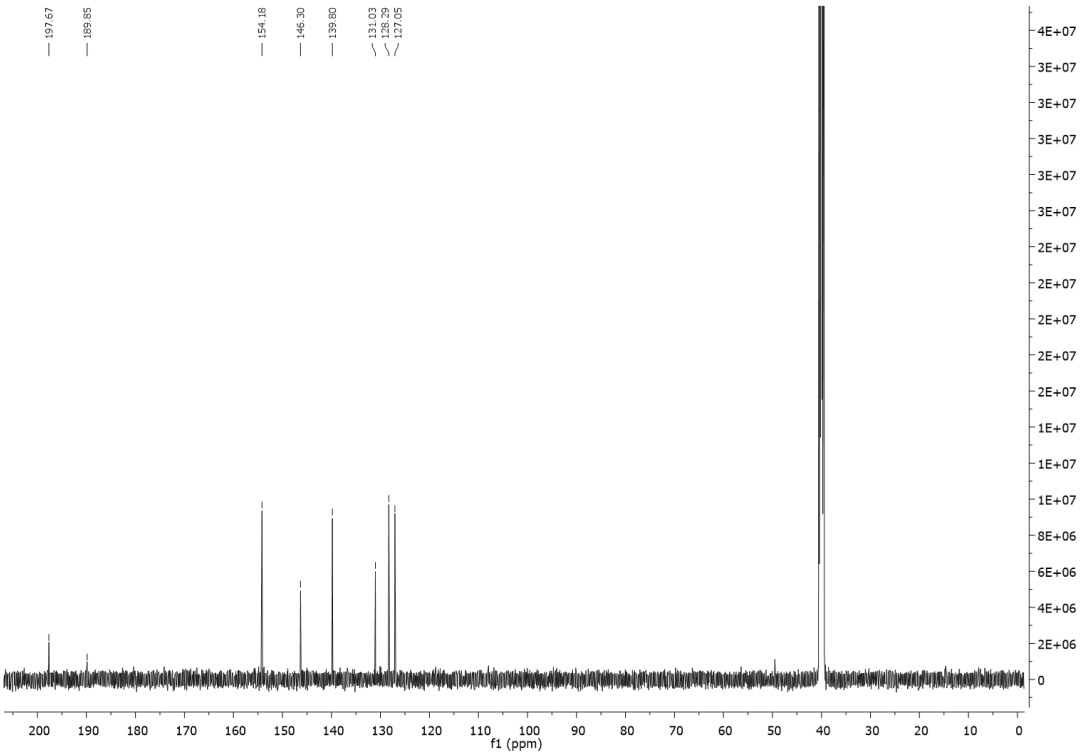

^{13}C NMR spectrum of [Re(CO)$_3$(phen)Br] (**4a**) in DMSO-d6

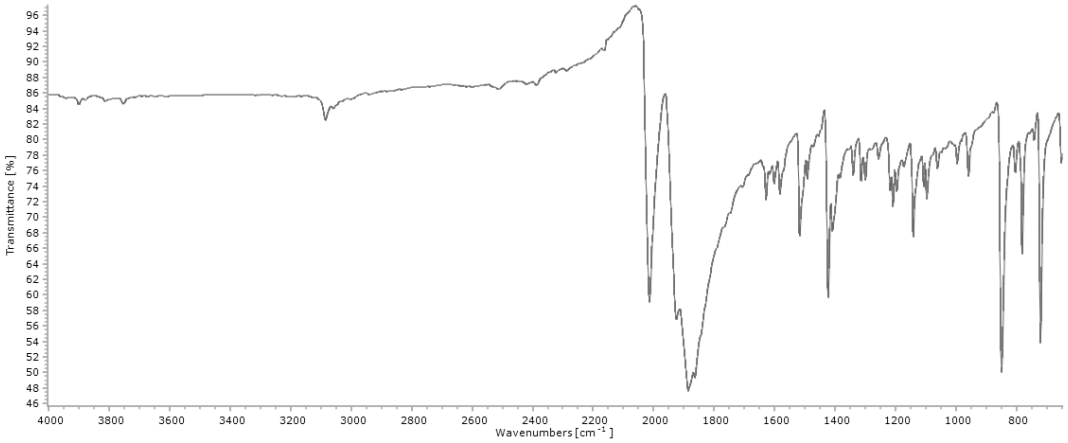

FTIR (ATR, cm^{-1}) spectrum of $[Re(CO)_3(phen)Br]$ (**4a**)

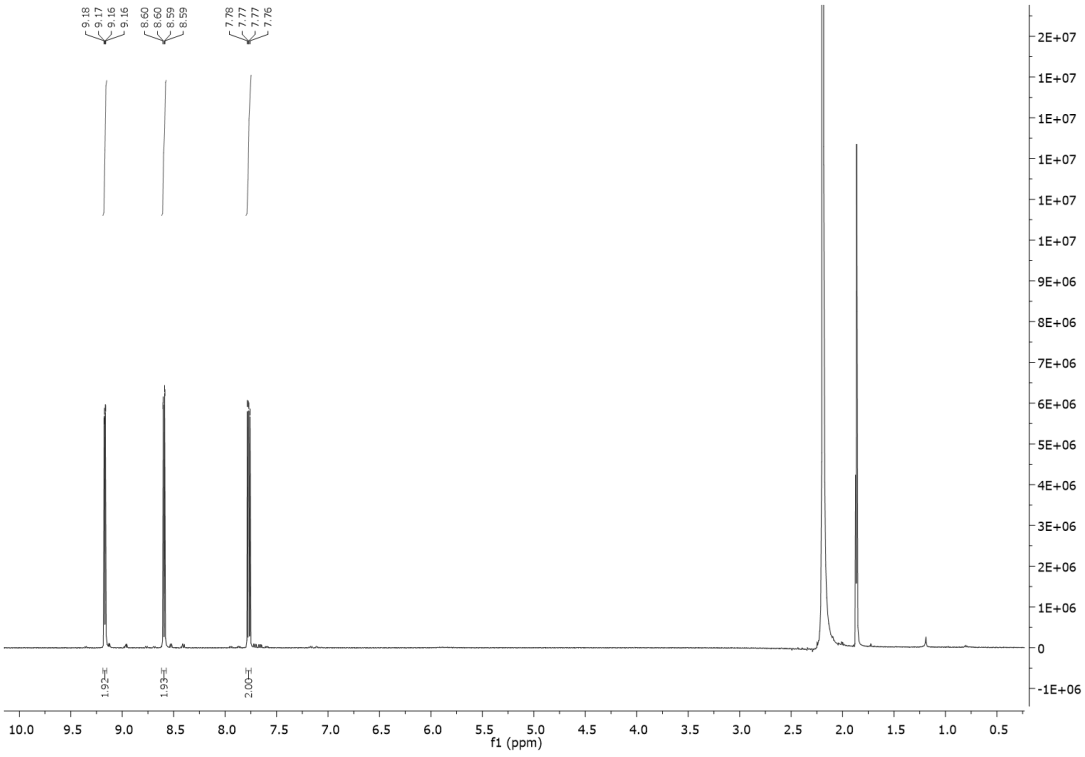

^1H NMR spectrum of $[Re(CO)_3(phendione)Br]$ (**4b**) in CD_3CN

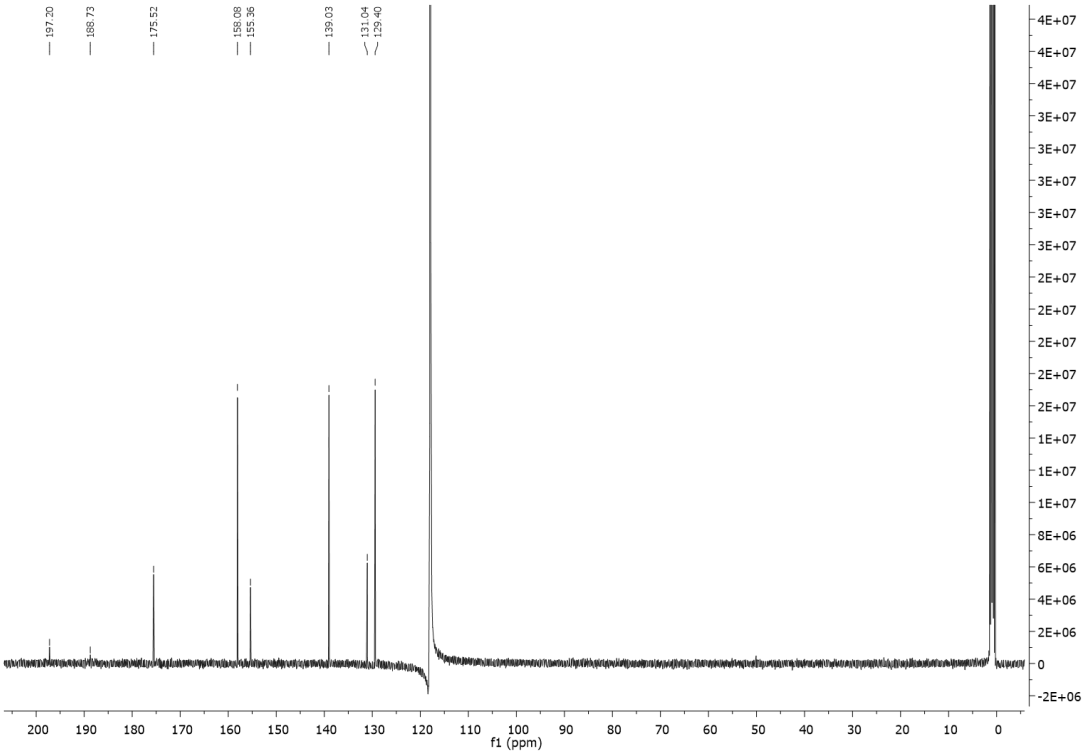

^{13}C NMR of $[Re(CO)_3(phendione)Br]$ (**4b**) in CD_3CN

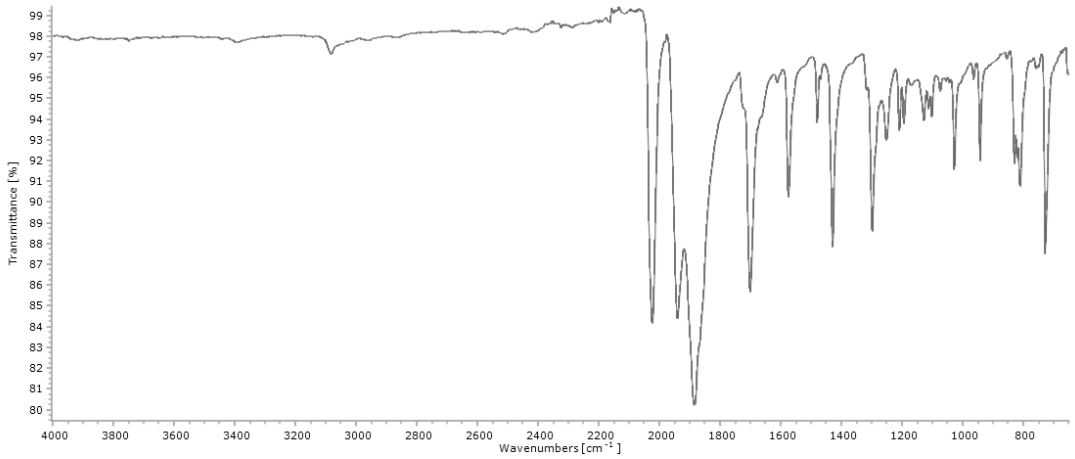

FTIR (ATR, cm^{-1}) spectrum of $[Re(CO)_3(phendione)Br]$ (**4b**)

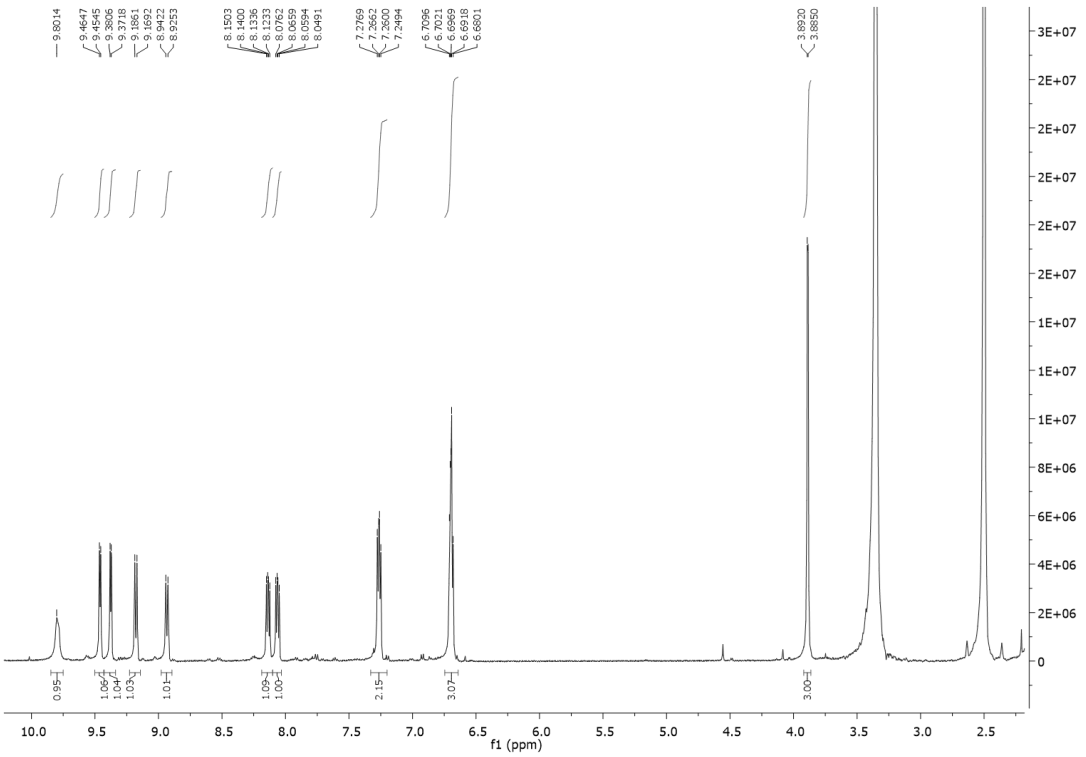

^{1}H NMR spectrum of ReMPO (**4.1**) in DMSO-d6

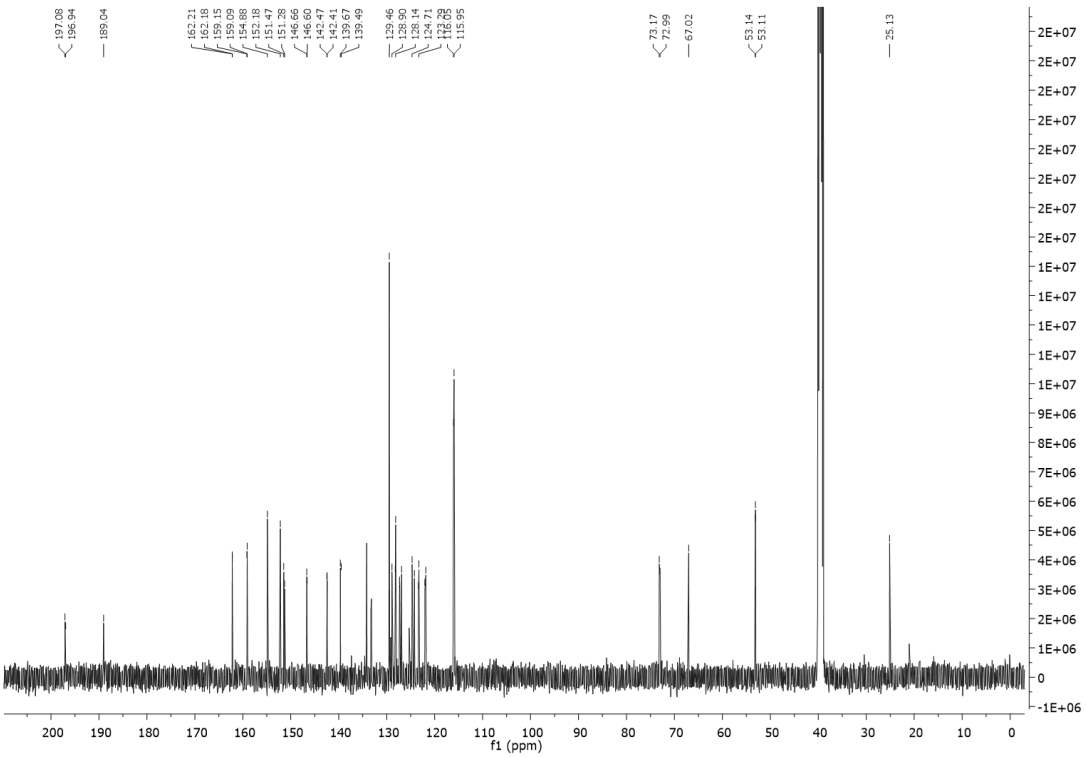

^{13}C NMR spectrum of ReMPO (**4.1**) in DMSO-d6

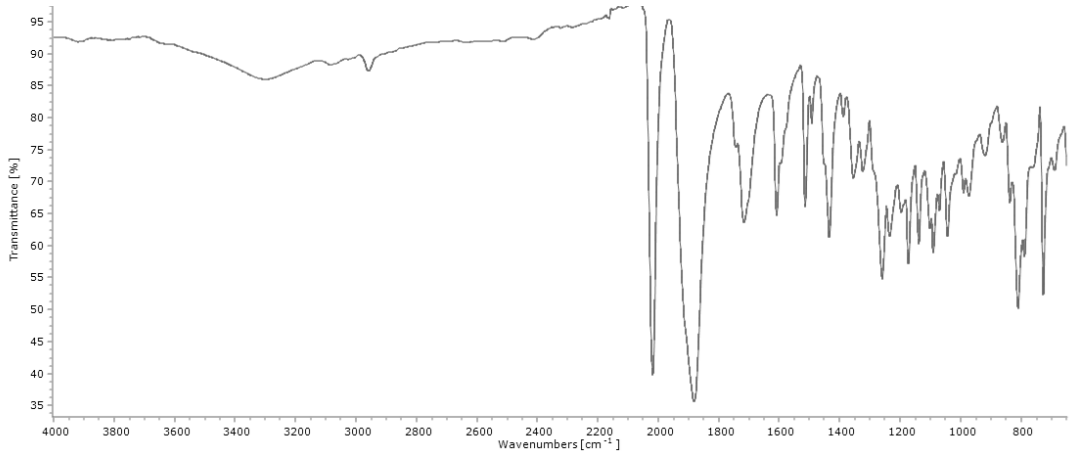

FTIR (ATR, cm^{-1}) spectrum of ReMPO (**4.1**)

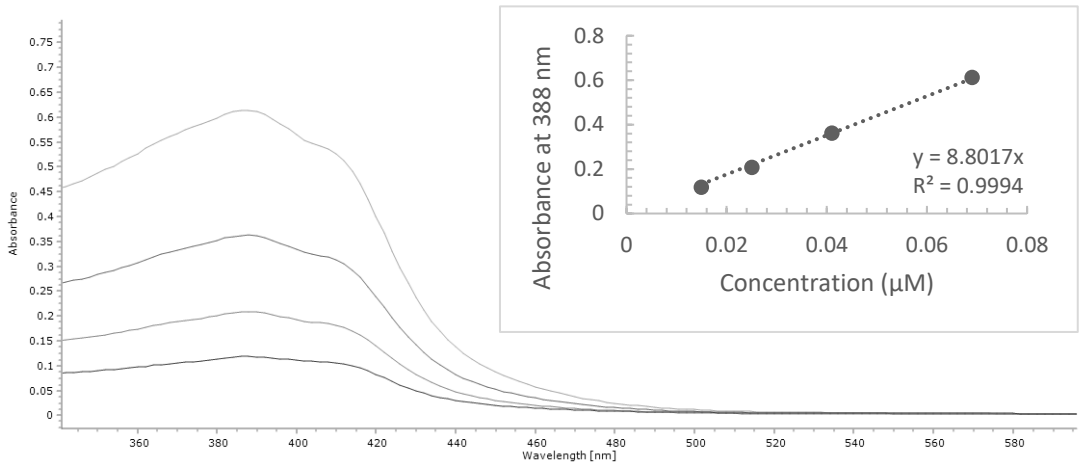

UV-visible spectra of ReMPO (**4.1**) in DMSO at concentrations of 1.49 x 10^{-5} – 6.93 x 10^{-5} M in DMSO used to determine the extinction coefficient (ε). ε = 8,801 $M^{-1}cm^{-1}$

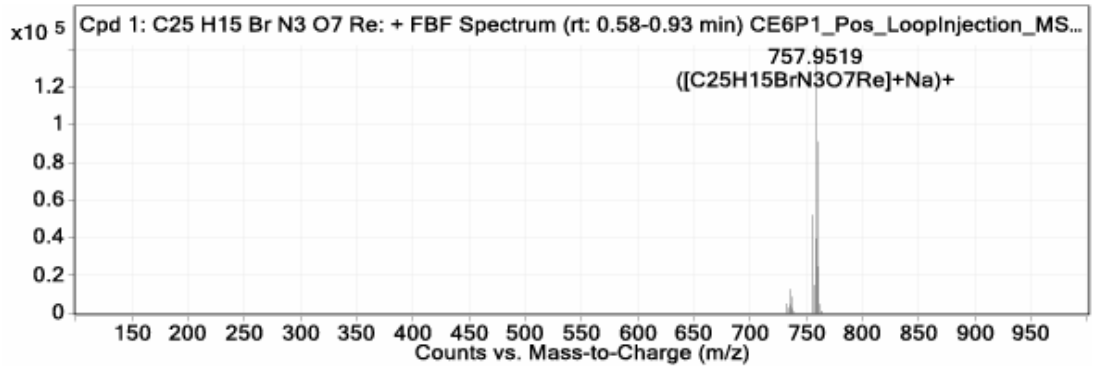

ESI Mass spectrum recorded in positive ionisation mode showing the isotopic pattern for ReMPO (**4.1**)

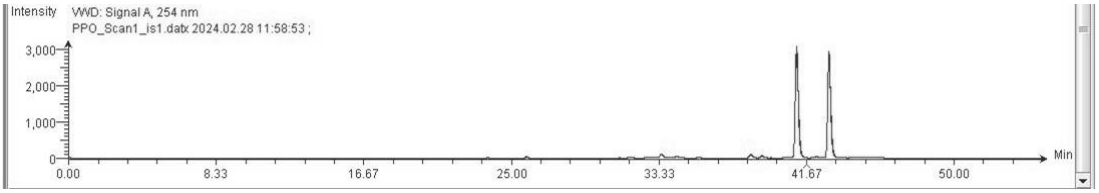

HPLC trace of ReMPO (**4.1**)

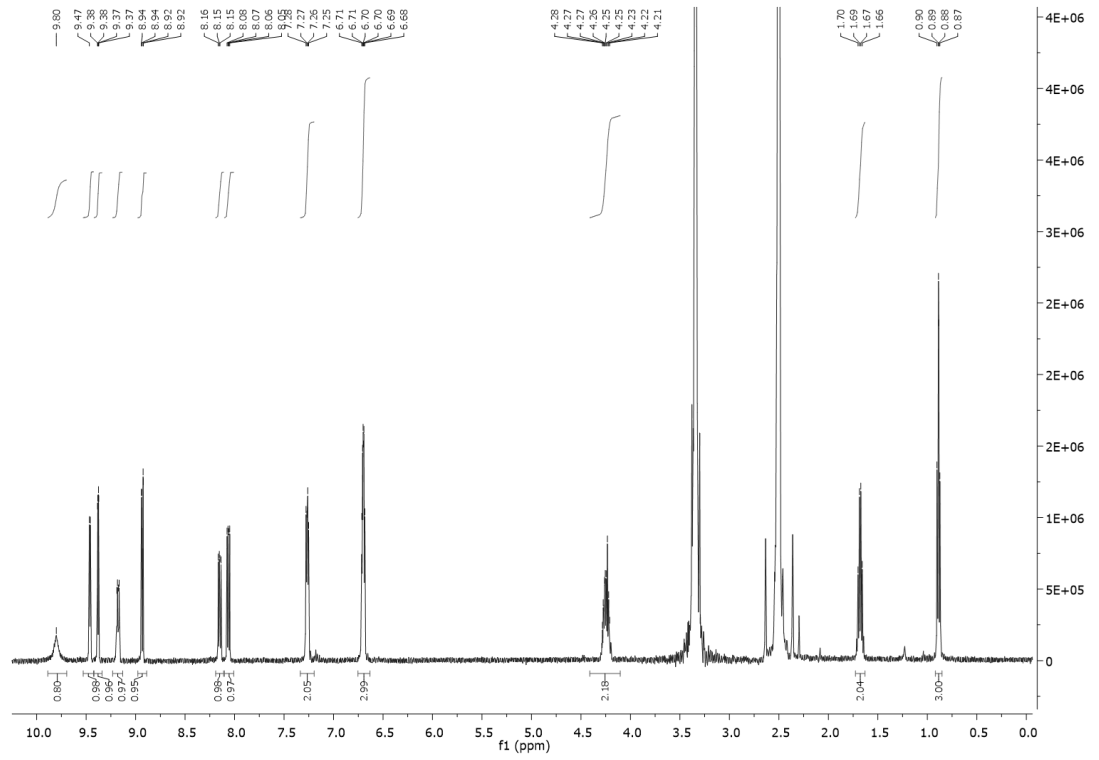

^{1}H NMR spectrum of RePPO (**4.2**) in DMSO-d6

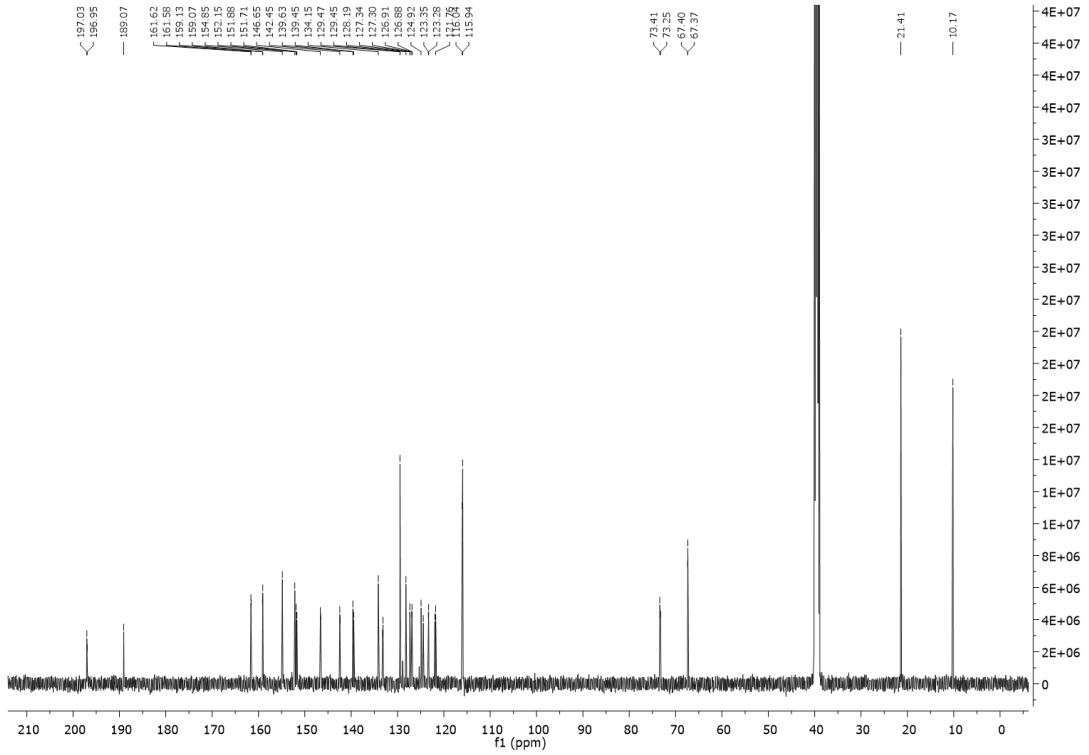

^{13}C NMR spectrum of RePPO (**4.2**) in DMSO-d6

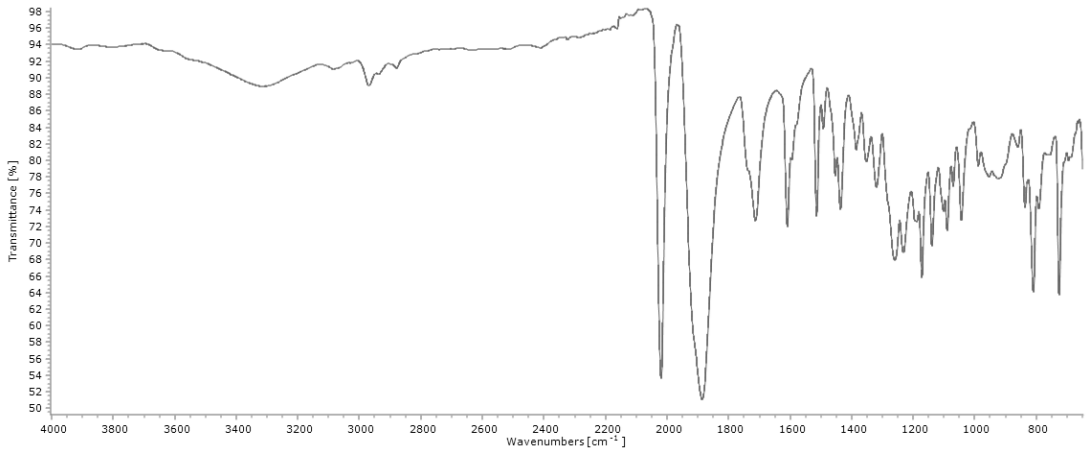

FTIR (ATR, cm^{-1}) spectrum of RePPO (**4.2**)

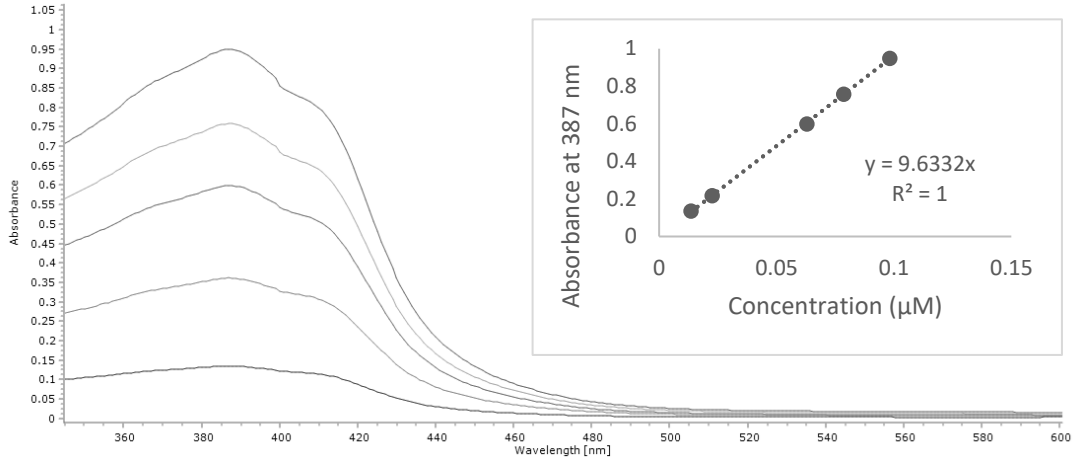

UV-visible spectra of RePPO (**4.2**) in DMSO at concentrations of 1.35 x 10^{-5} – 9.82 x 10^{-5} M in DMSO used to determine the extinction coefficient (ε). ε = 9,633 $M^{-1}cm^{-1}$

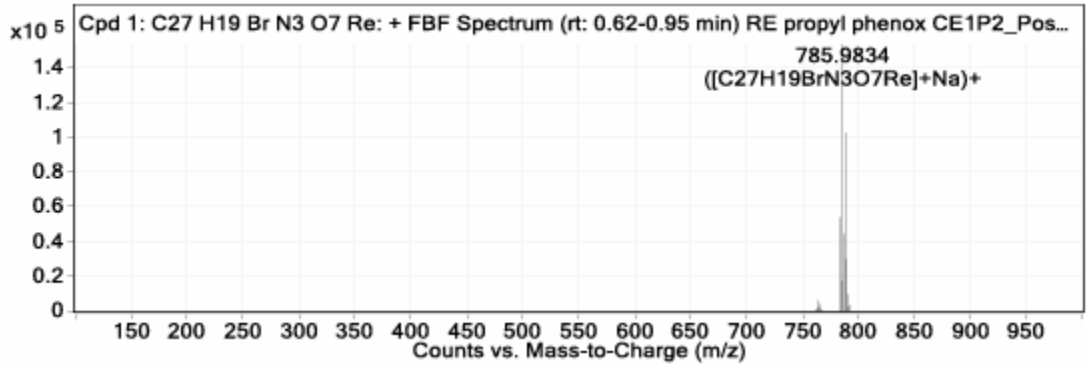

ESI Mass spectrum recorded in positive ionisation mode showing the isotopic pattern for RePPO (**4.2**)

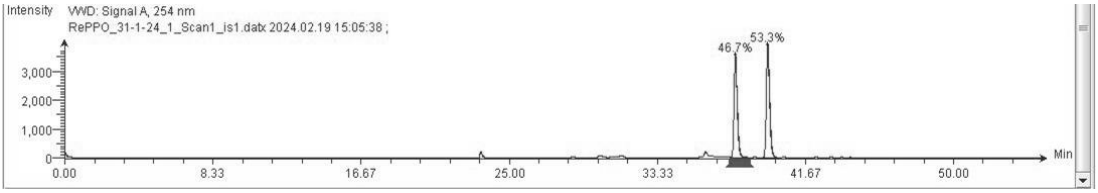

HPLC trace of RePPO (**4.2**)

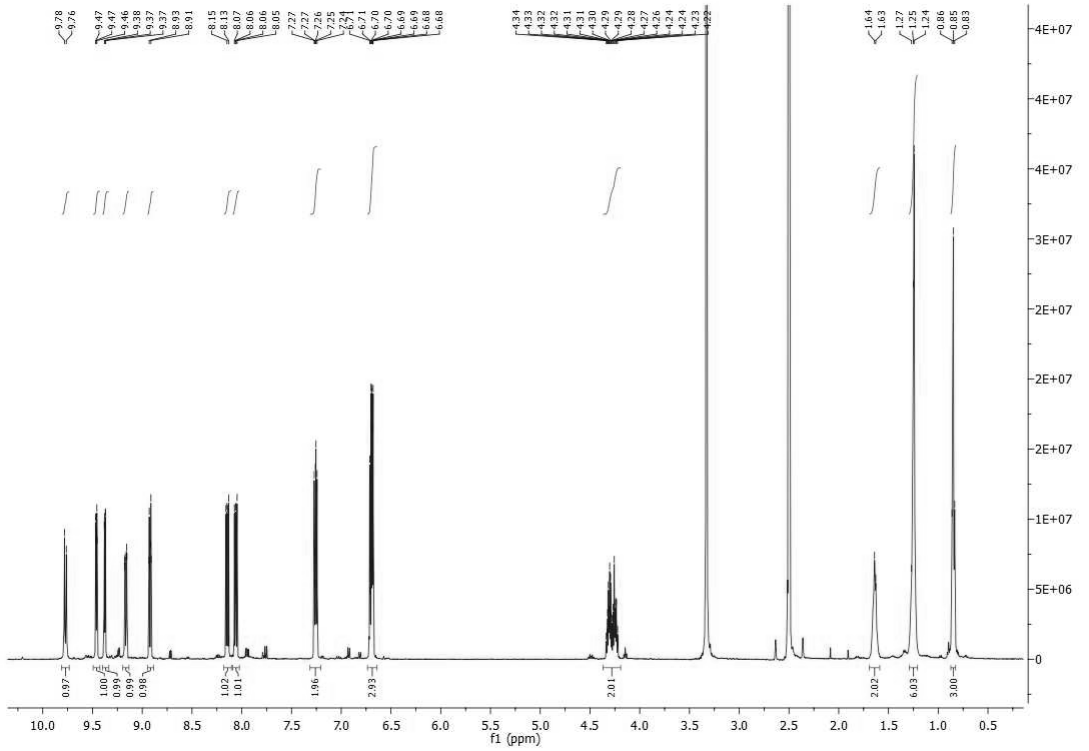

^{1}H NMR spectrum of ReHPO (**4.3**) in DMSO-d6

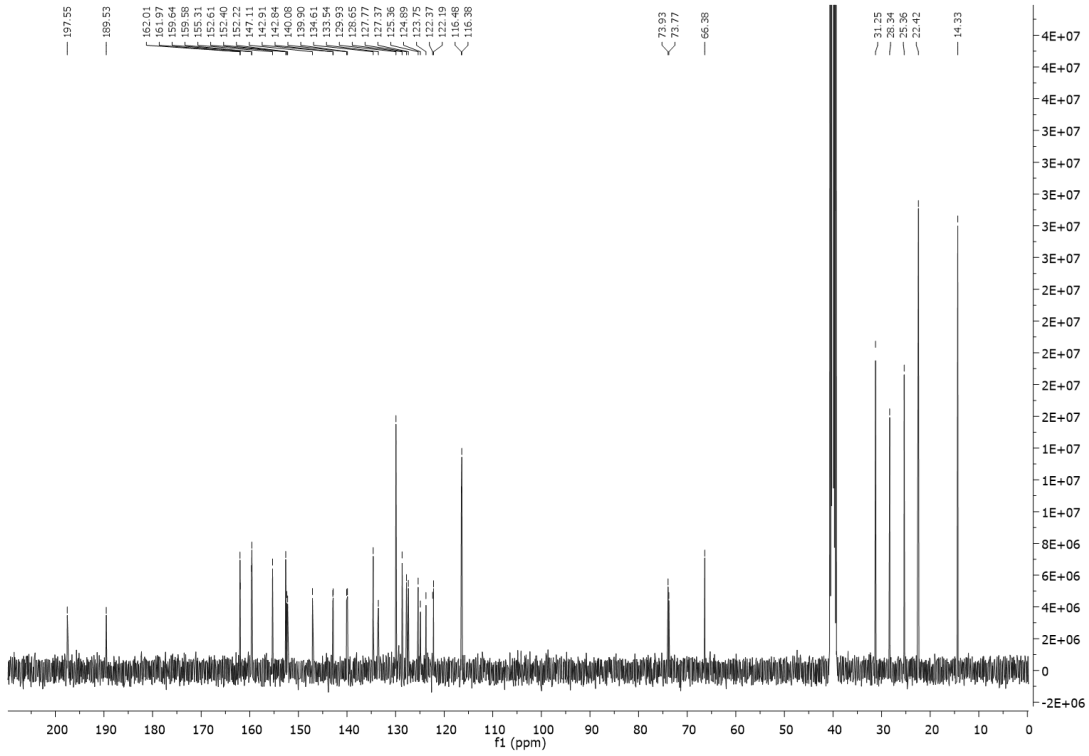

^{13}C NMR spectrum of ReHPO (**4.3**) in DMSO-d6

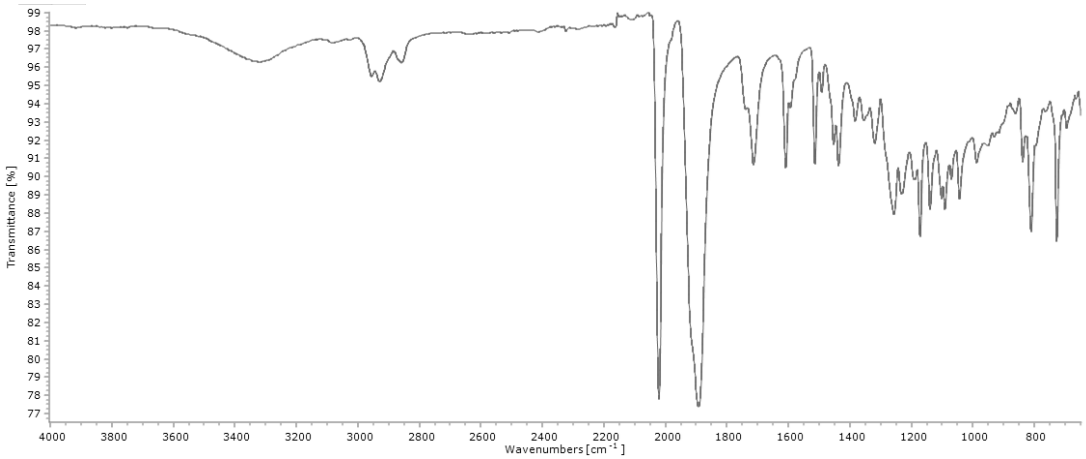

FTIR (ATR, cm^{-1}) spectrum of ReHPO (**4.3**) in ATR mode

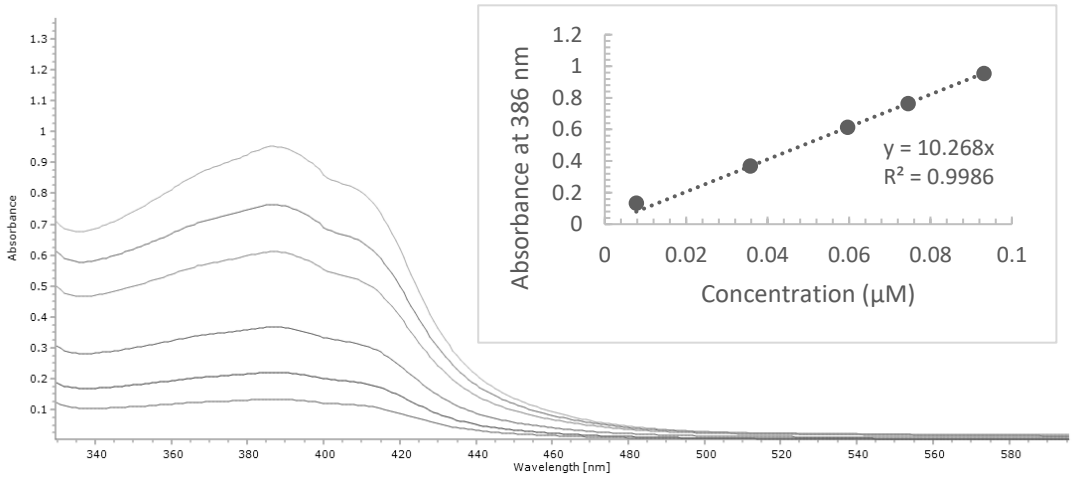

UV-visible spectra of ReHPO (**4.3**) in DMSO at concentrations of 7.67 x 10^{-6} – 9.31 x 10^{-5} M in DMSO used to determine the extinction coefficient (ε). ε = 10,268 $M^{-1}cm^{-1}$

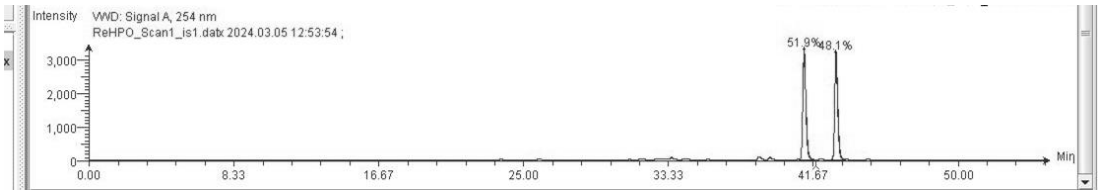

HPLC trace of ReHPO (**4.3**)

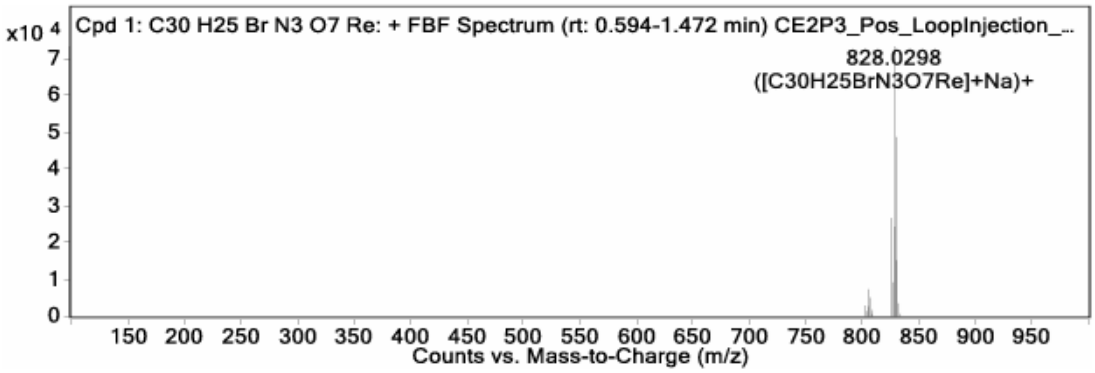

ESI Mass spectrum recorded in positive ionisation mode showing the isotopic pattern for ReHPO (**4.3**)

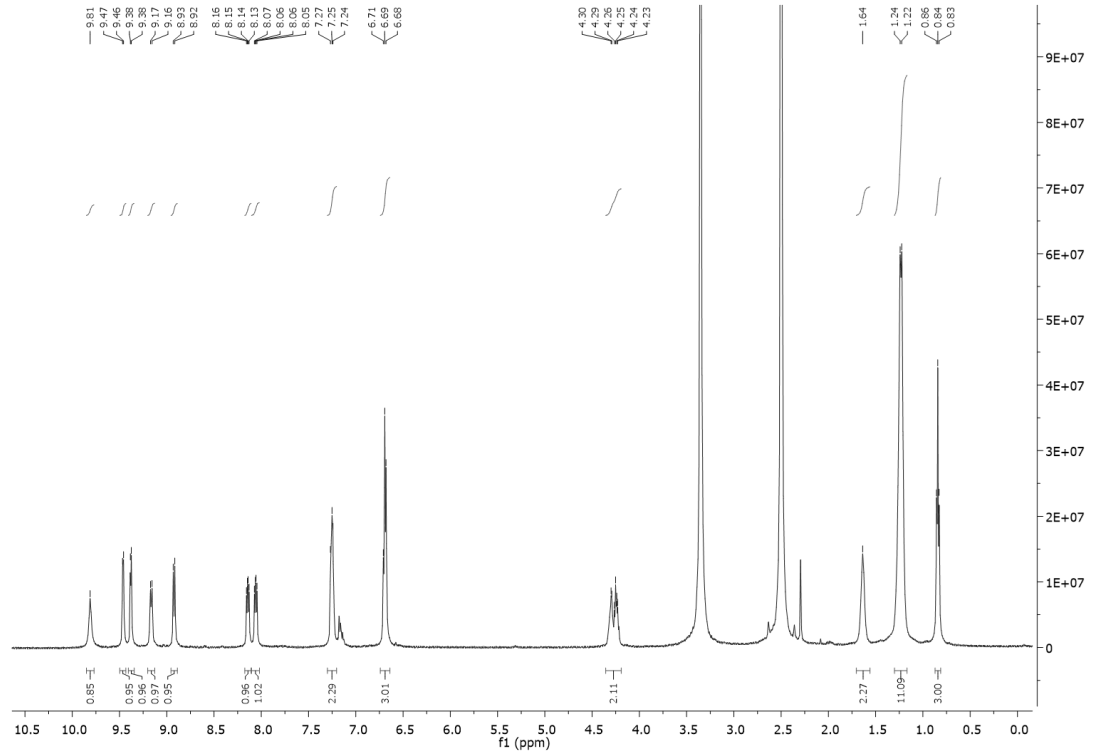

^{1}H NMR spectrum of ReOPO (**4.4**) in DMSO-d6

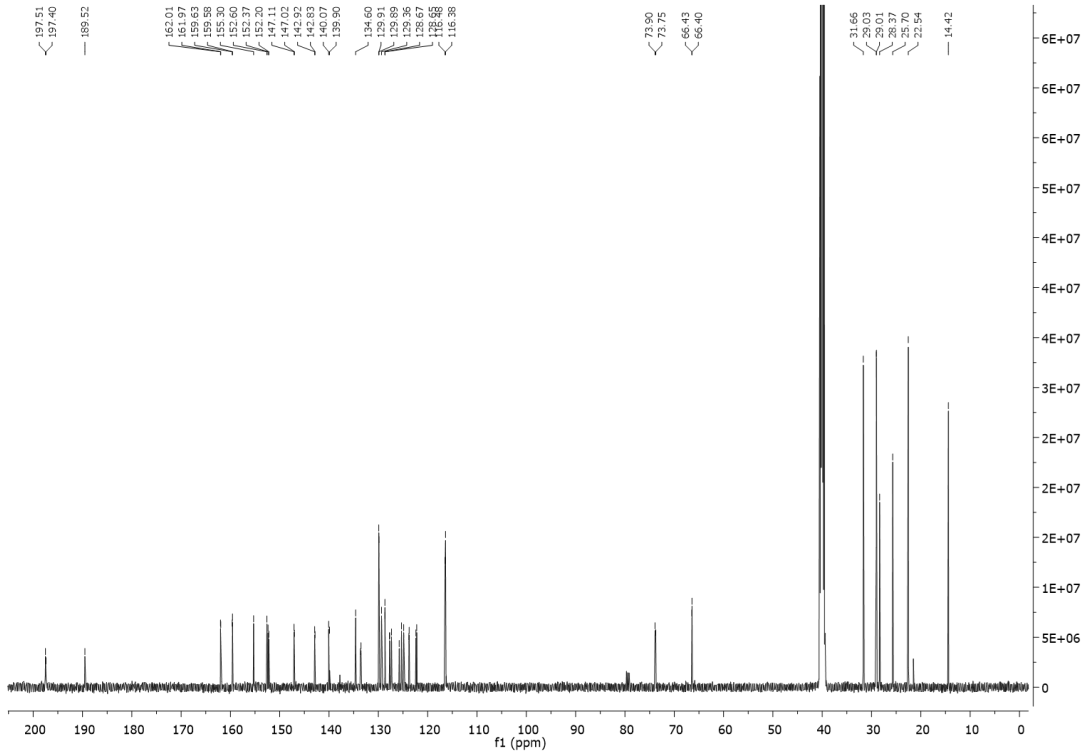

^{13}C NMR spectrum of ReOPO (**4.4**) in DMSO-d6

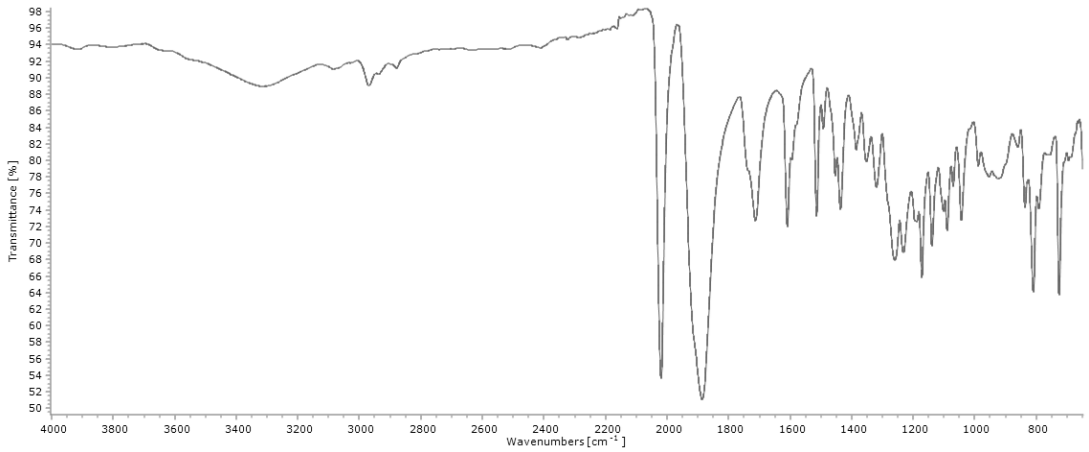

FTIR (ATR, cm^{-1}) spectrum of ReOPO (**4.4**)

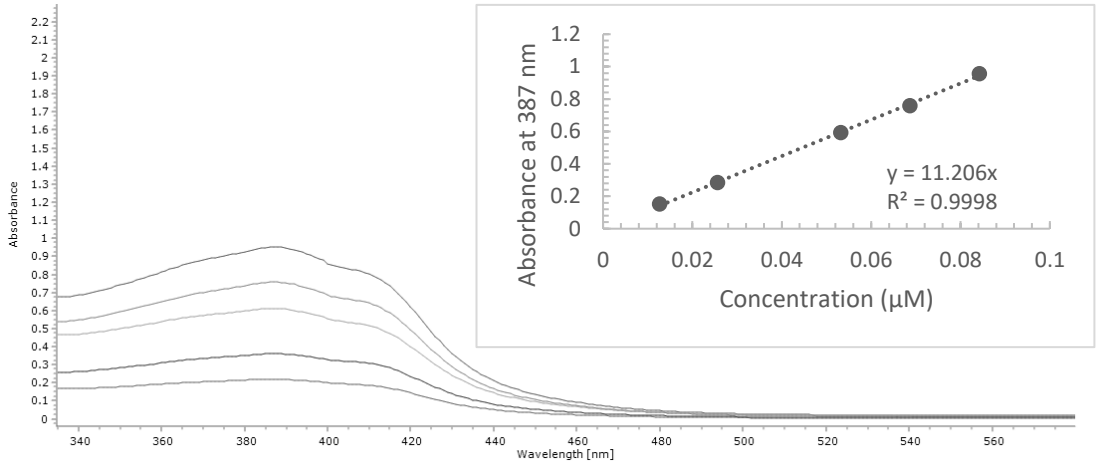

UV-visible spectra of ReOPO (**4.4**) in DMSO at concentrations of 1.27 x 10^{-5} – 8.42 x 10^{-5} M in DMSO used to determine the extinction coefficient (ε). ε = 11,206 $M^{-1}cm^{-1}$

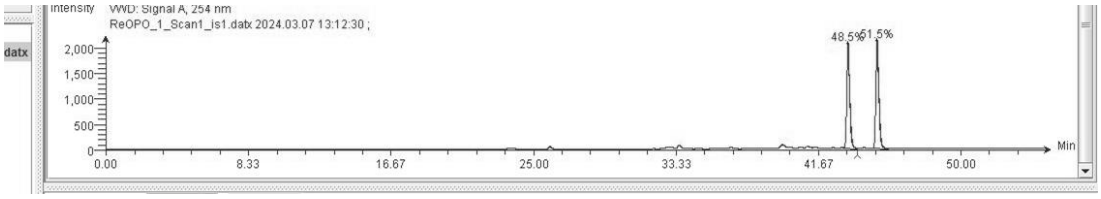

HPLC trace of ReOPO (**4.4**)

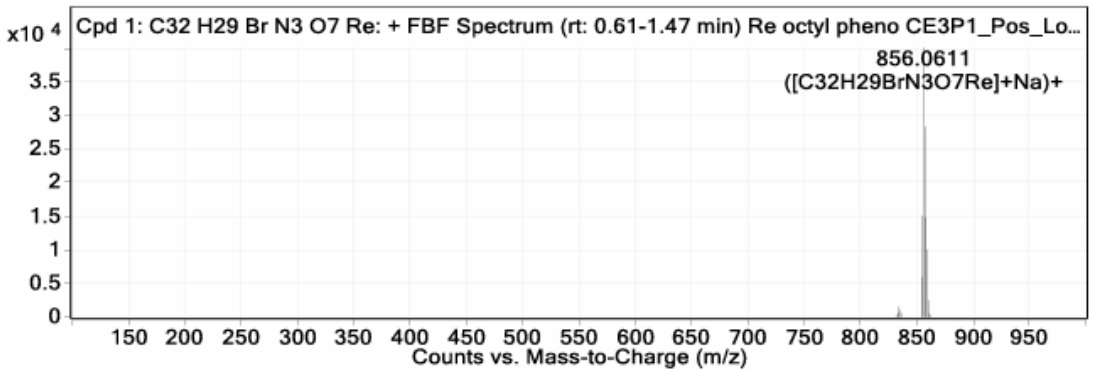

ESI Mass spectrum recorded in positive ionisation mode showing the isotopic pattern for ReOPO (**4.4**)

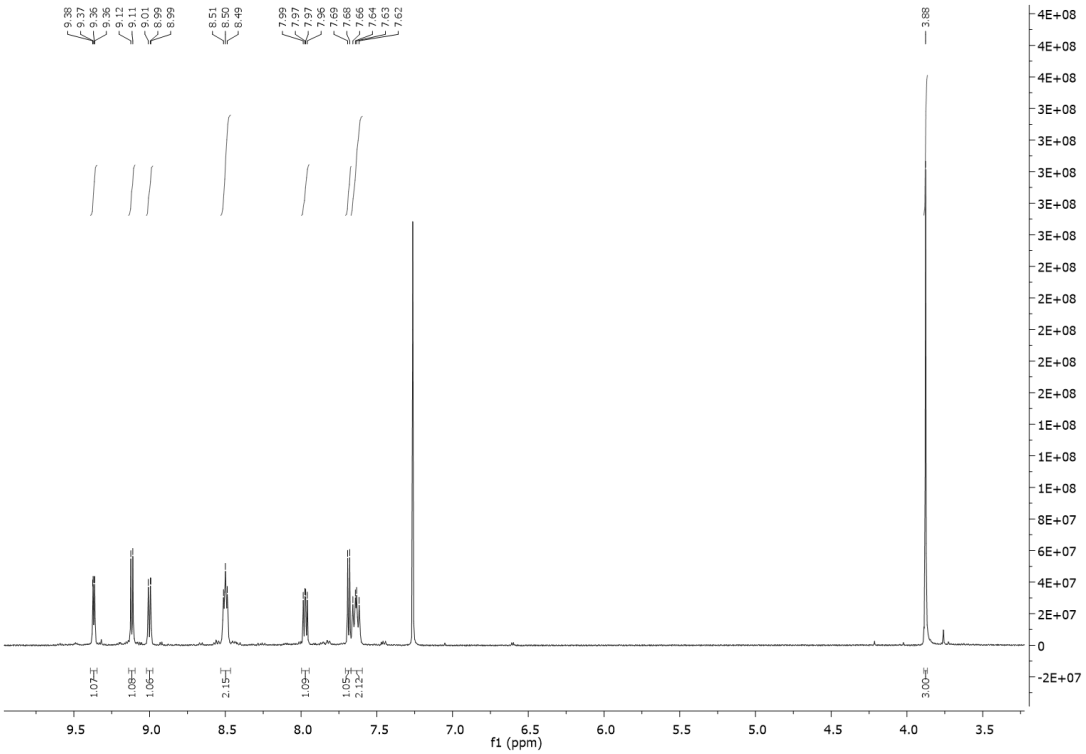

^{1}H NMR spectrum of ReMPP (**4.5**) in DMSO-d6

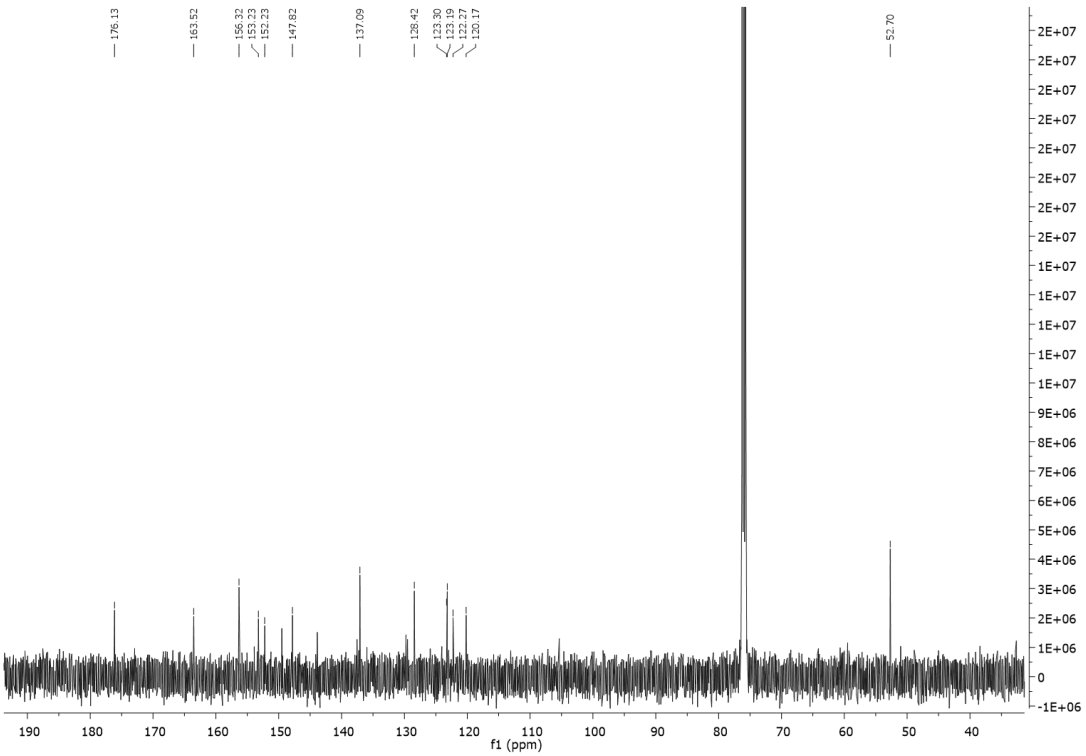

^{13}C NMR spectrum of ReMPP (**4.5**) in DMSO-d6

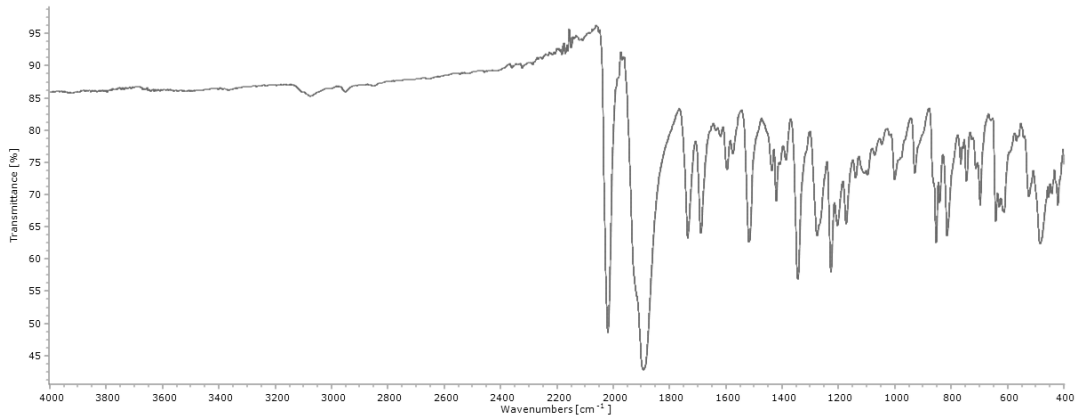

FTIR (ATR, cm^{-1}) spectrum of ReMPP (**4.5**)

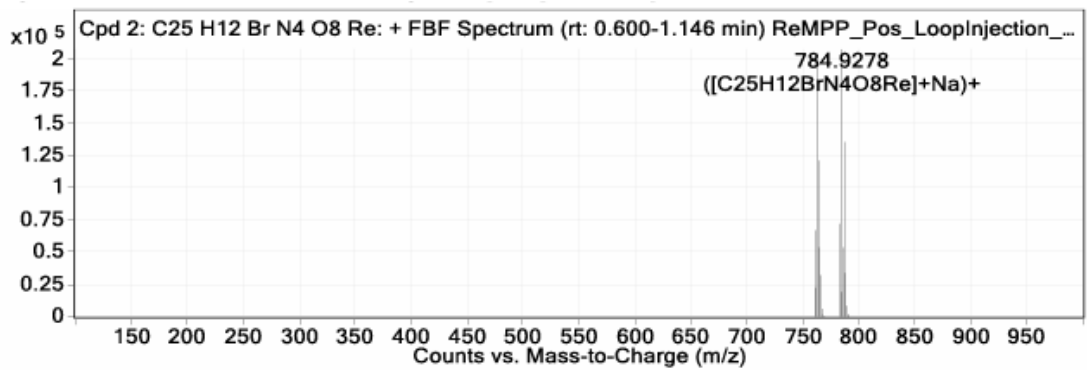

ESI Mass spectrum recorded in positive ionisation mode showing the isotopic pattern for ReMPP (**4.5**)

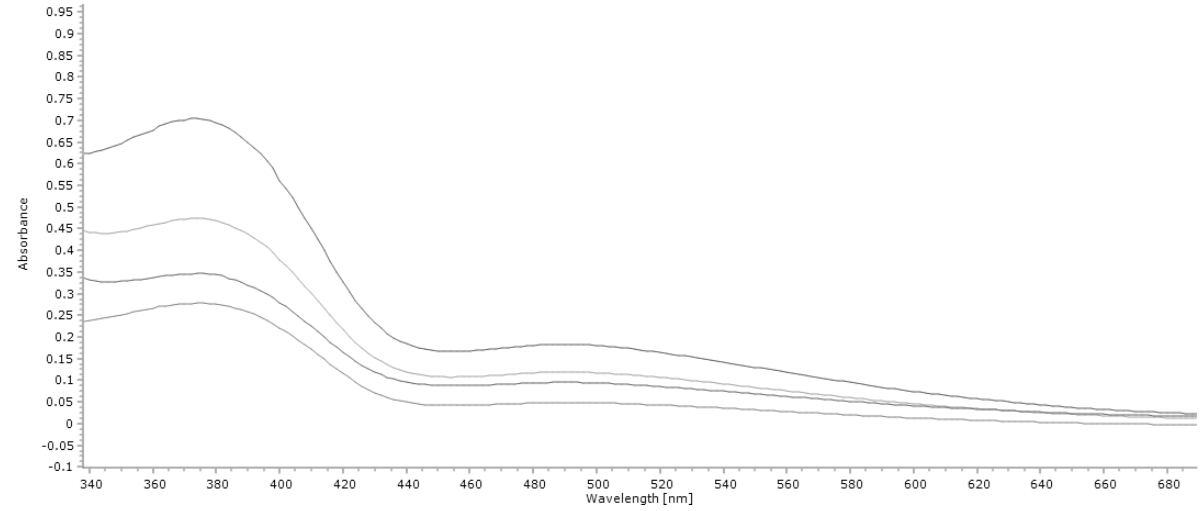

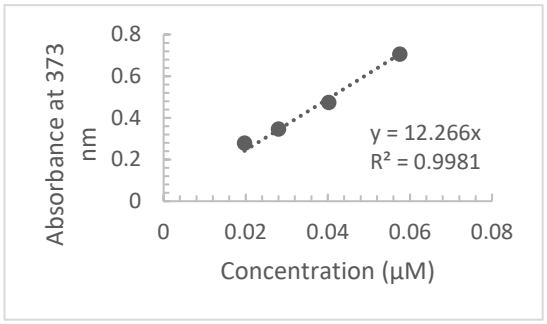

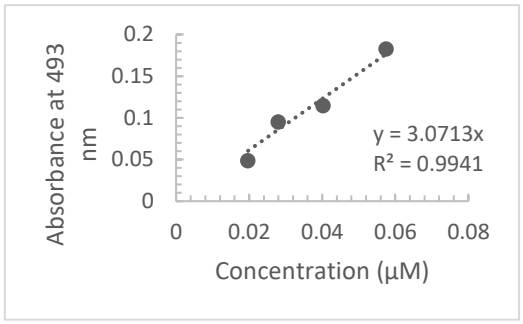

UV-visible spectra of ReMPP (**4.5**) in DMSO at concentrations of 1.97 x 10^{-5} – 5.75 x 10^{-5} M in DMSO used to determine the extinction coefficient (ε). ε1 = 12,266 M^{-1} cm^{-1} (λ_{max1} = 375 nm), ε2 = 3,071 $M^{-1}cm^{-1}$ (λ_{max2} = 493 nm).

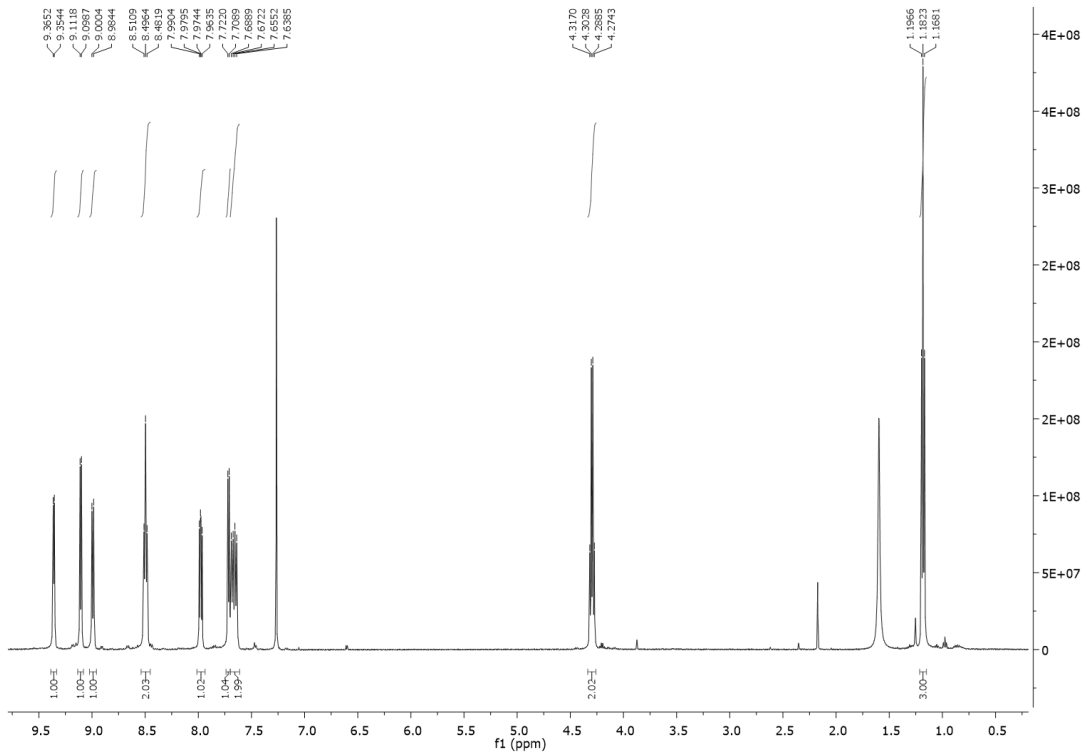

^{1}H NMR spectrum of ReEPP (**4.6**) in CD_3Cl

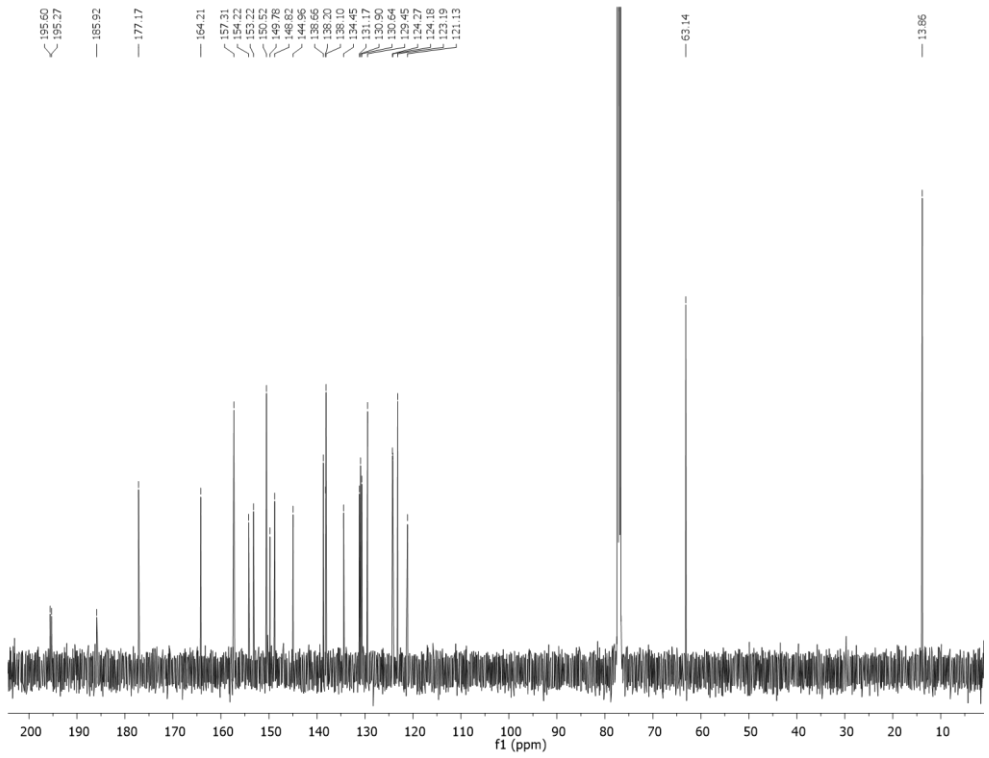

^{13}C NMR of ReEPP (**4.1**) in CD_3Cl

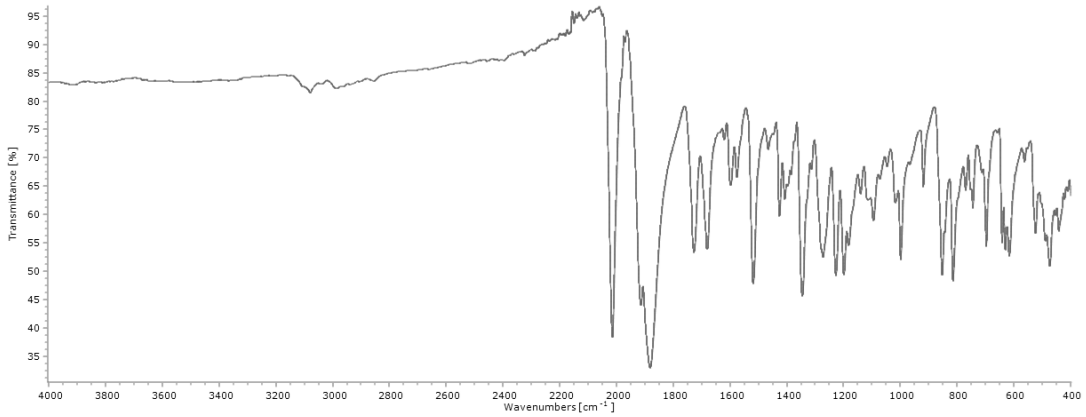

FTIR (ATR, cm^{-1}) spectrum of ReEPP (**4.6**)

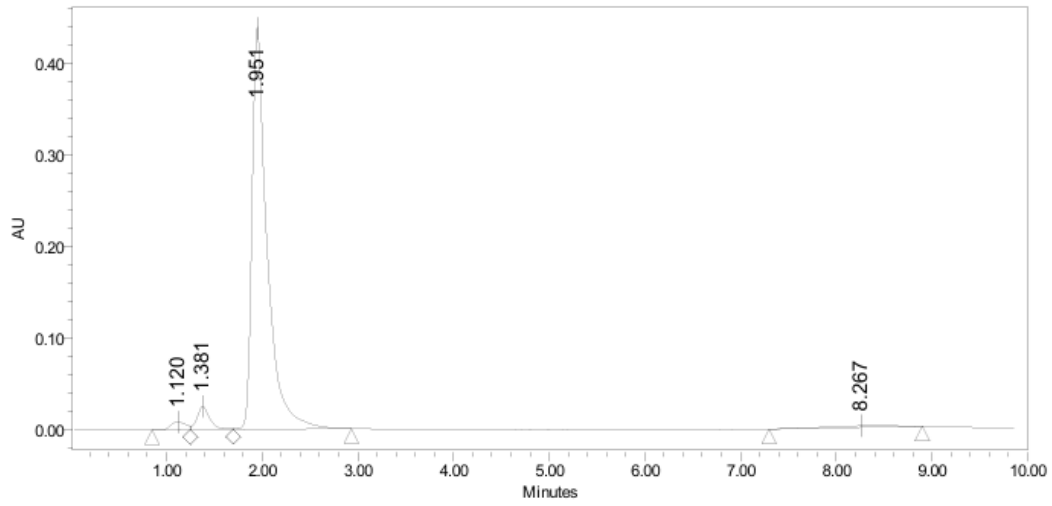

HPLC trace of ReEPP (**4.6**)

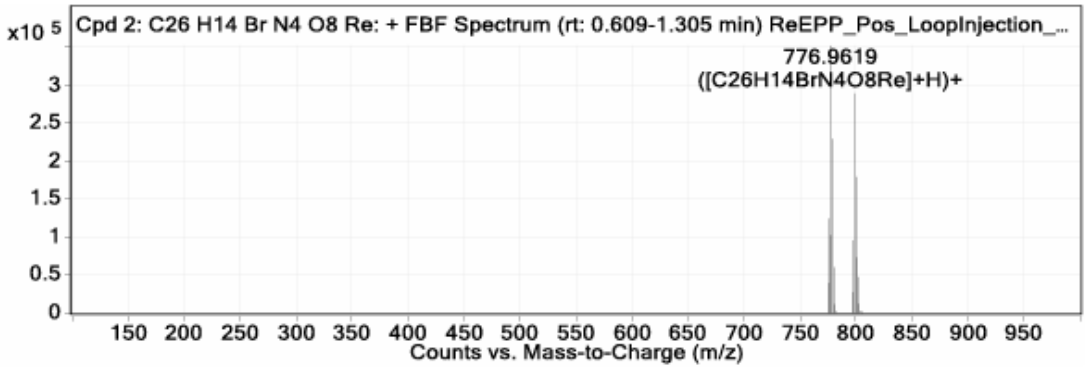

ESI Mass spectrum recorded in positive ionisation mode showing the isotopic pattern for ReEPP (**4.6**)

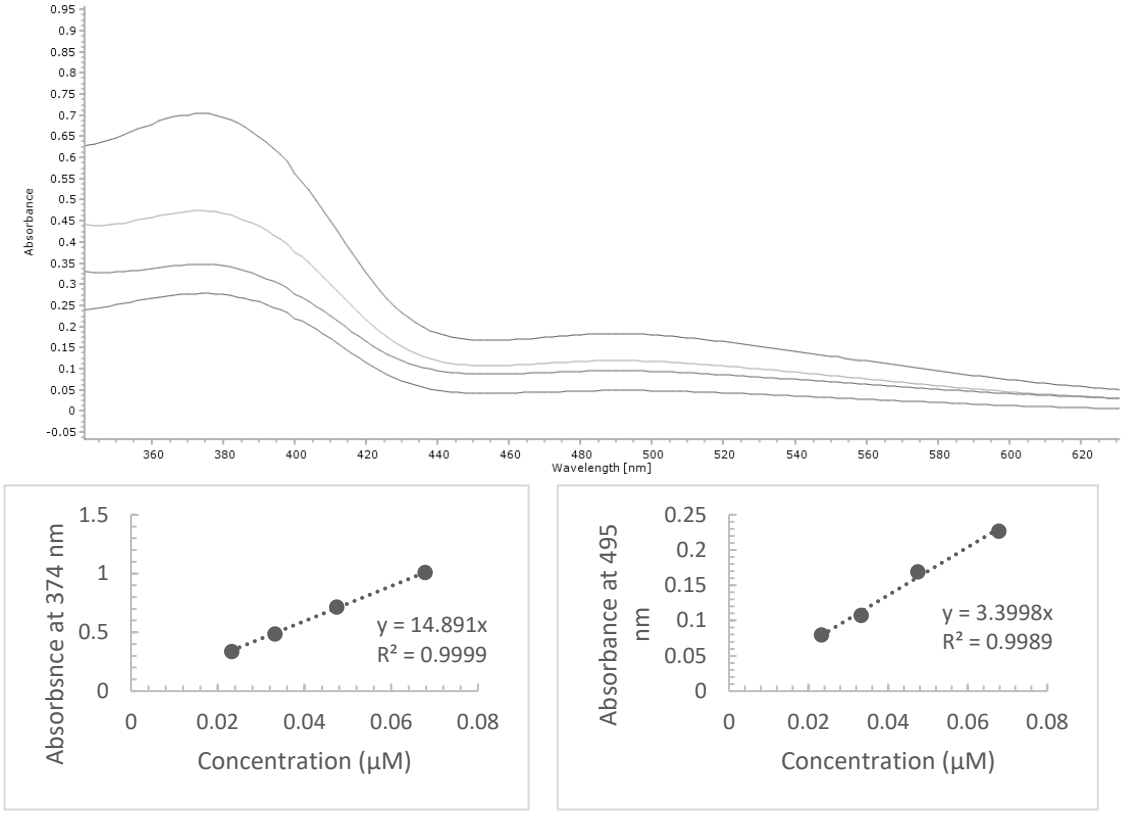

UV-visible spectra of ReEPP (**4.6**) in DMSO at concentrations of 1.62 x 10^{-5} – 6.78 x 10^{-5} M in DMSO used to determine the extinction coefficient (ε). ε1 = 14,907 M^{-1} cm^{-1} (λ_{max1} = 374 nm), ε2 = 3,426. $M^{-1}cm^{-1}$ (λ_{max2} = 495 nm).

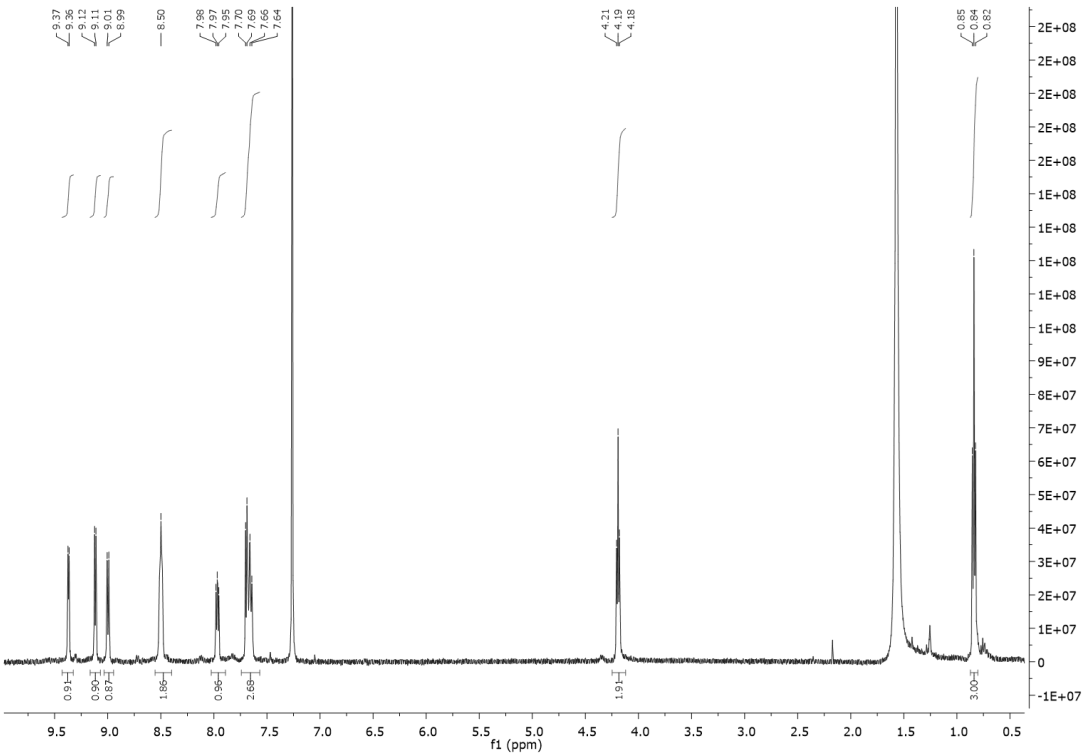

^{1}H NMR spectrum of RePPP (**4.7**) in CD_3Cl

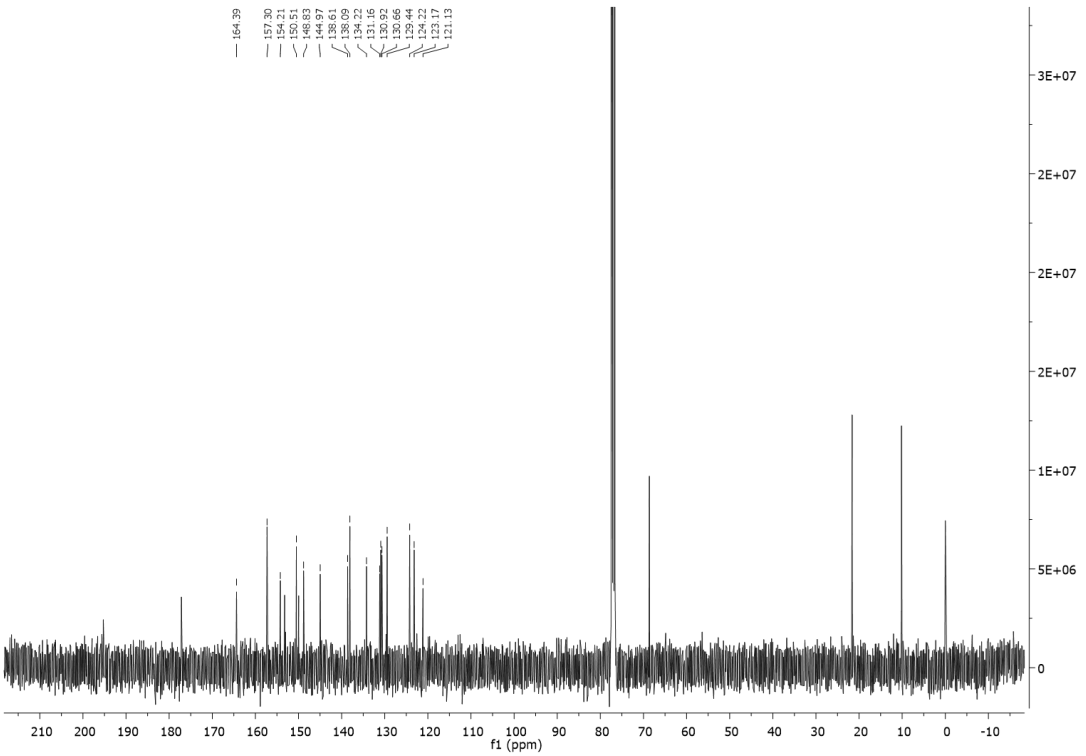

^{13}C NMR spectrum of RePPP (**4.7**) in CD_3Cl

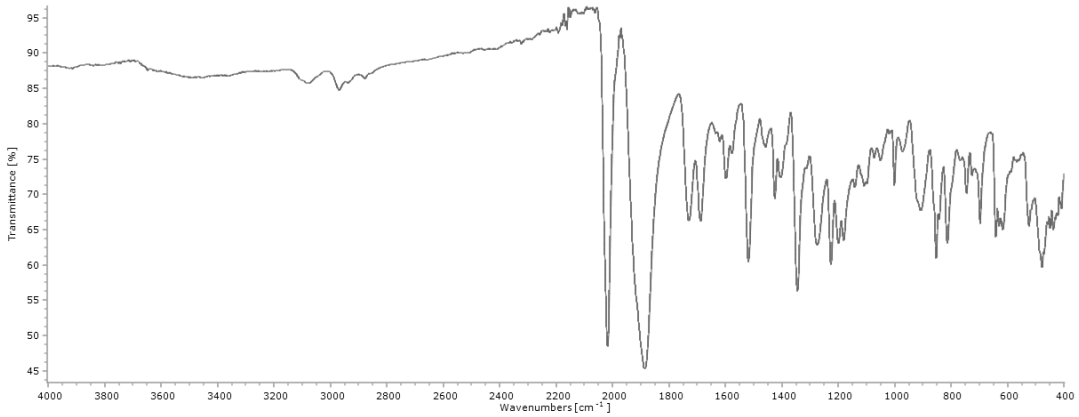

FTIR (ATR, cm^{-1}) spectrum of RePPP (**4.7**)

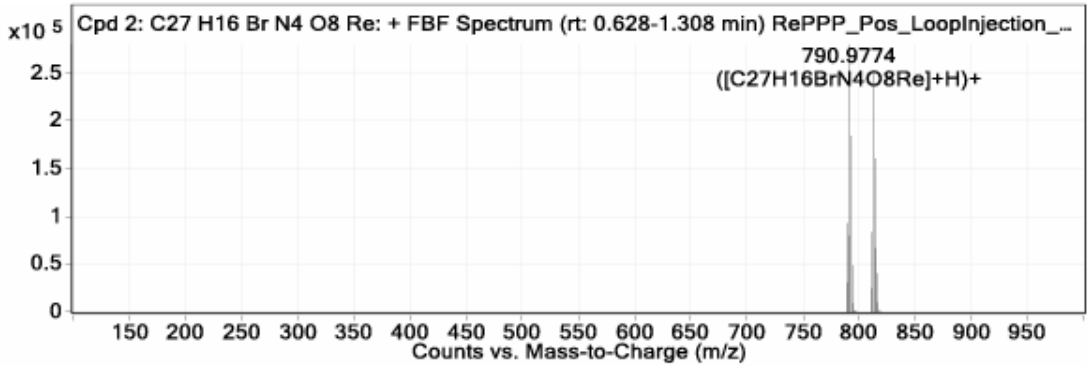

ESI Mass spectrum recorded in positive ionisation mode showing the isotopic pattern for RePPP (**4.7**)

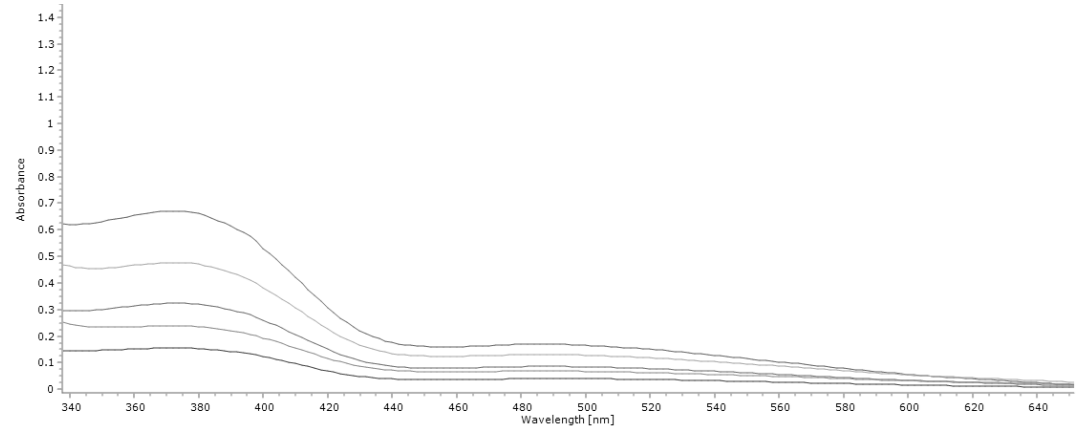

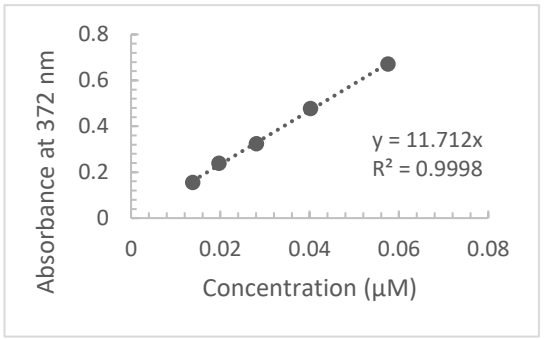

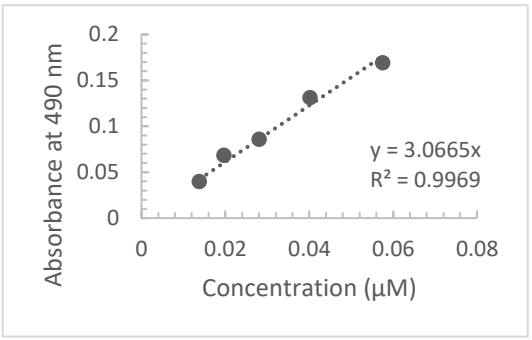

UV-visible spectra of RePPP (**4.7**) in DMSO at concentrations between 1.38 x 10^{-5} – 5.75 x 10^{-5} M in DMSO used to determine the extinction coefficient (ε). ε1 = 11,712 $M^{-1}cm^{-1}$ (λ_{max1} = 372 nm), ε2 = 3,066 M^{-1} cm^{-1} (λ_{max2} = 490 nm).

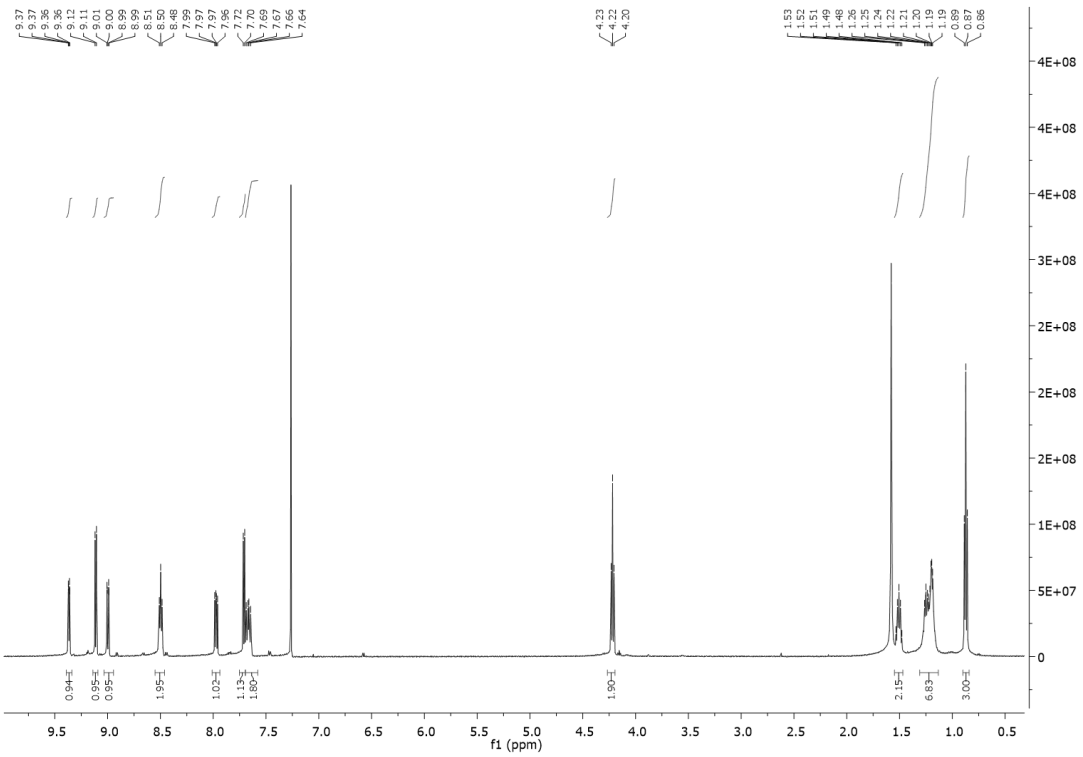

^{1}H NMR spectrum of ReHPP (**4.8**) in CD_3Cl

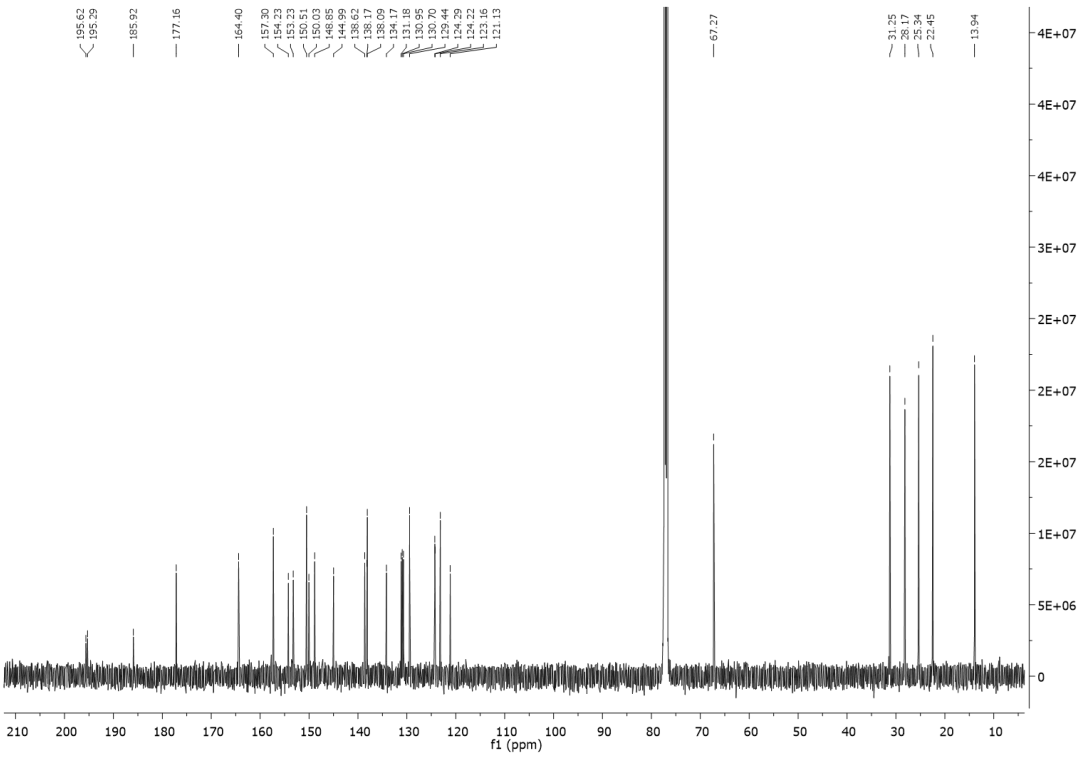

^{13}C NMR spectrum of ReHPP (**4.8**) in CD_3Cl

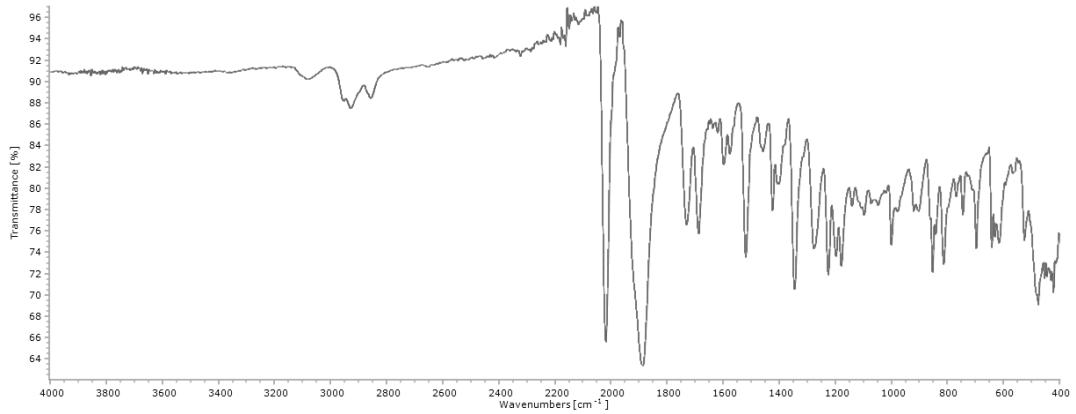

FTIR (ATR, cm^{-1}) spectrum of ReHPP (**4.7**)

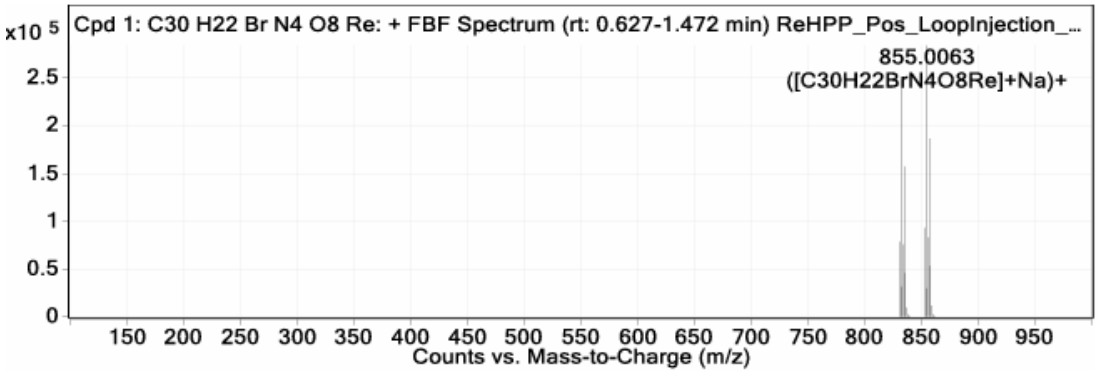

ESI Mass spectrum recorded in positive ionisation mode showing the isotopic pattern for ReHPP (**4.8**)

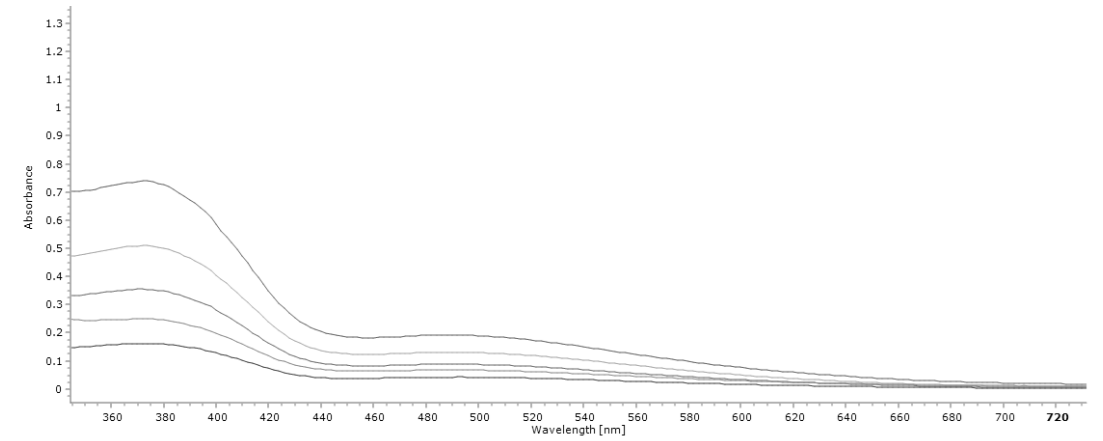

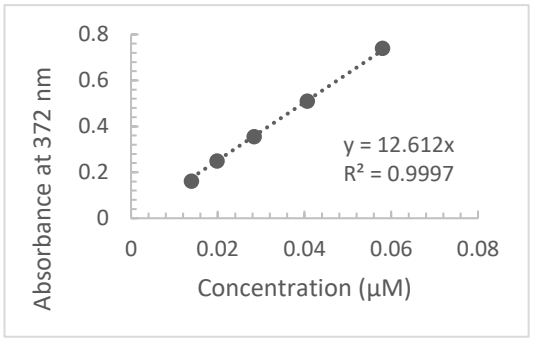

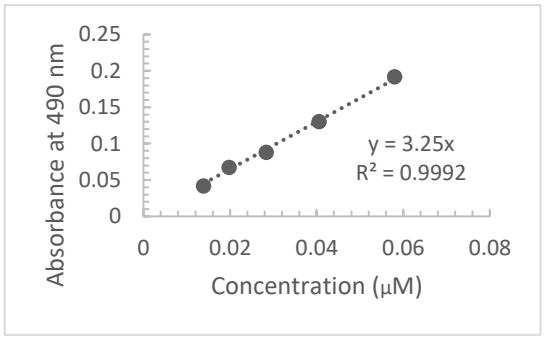

UV-visible spectra of ReHPP (**4.8**) in DMSO at concentrations of 1.39 x 10^{-5} – 5.80 x 10^{-5} M in DMSO used to determine the extinction coefficient (ε). ε1 = 12,612 M^{-1} cm^{-1} (λ_{max1} = 375 nm), ε2 = 3,250 $M^{-1}cm^{-1}$ (λ_{max2} = 493 nm).

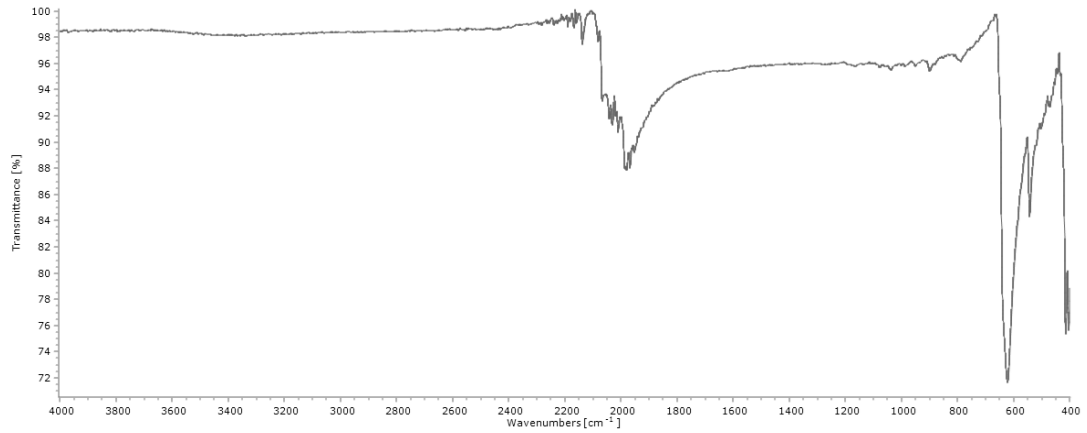

FTIR (ATR, cm^{-1}) spectrum of $Mn(CO)_5Br$

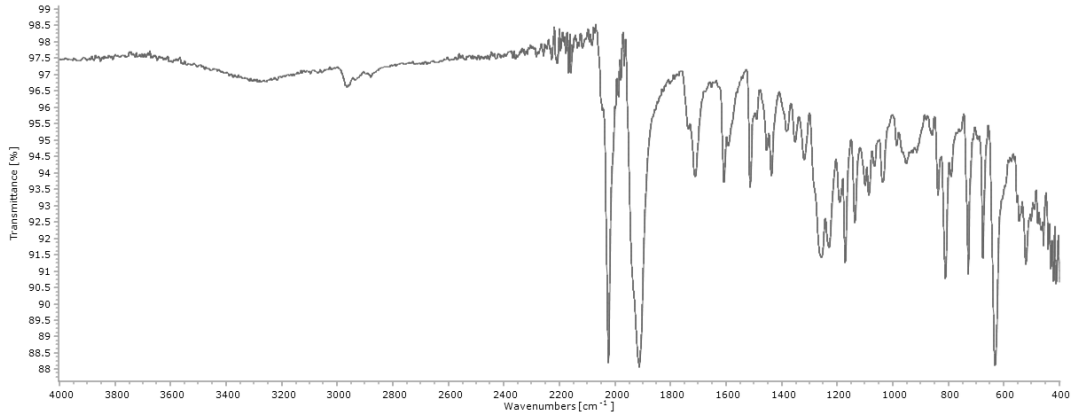

FTIR (ATR, cm^{-1}) spectrum of the product of the reaction between $Mn(CO)_5Br$ and PPO (**2.2**)

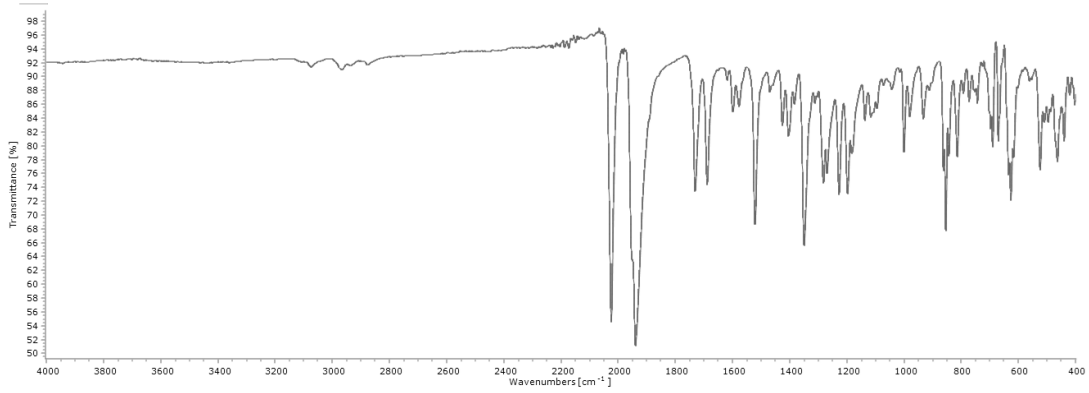

FTIR (ATR, cm^{-1}) spectrum of the product of the reaction between $Mn(CO)_5Br$ and PPP (**2.7**)

Crystallography Data

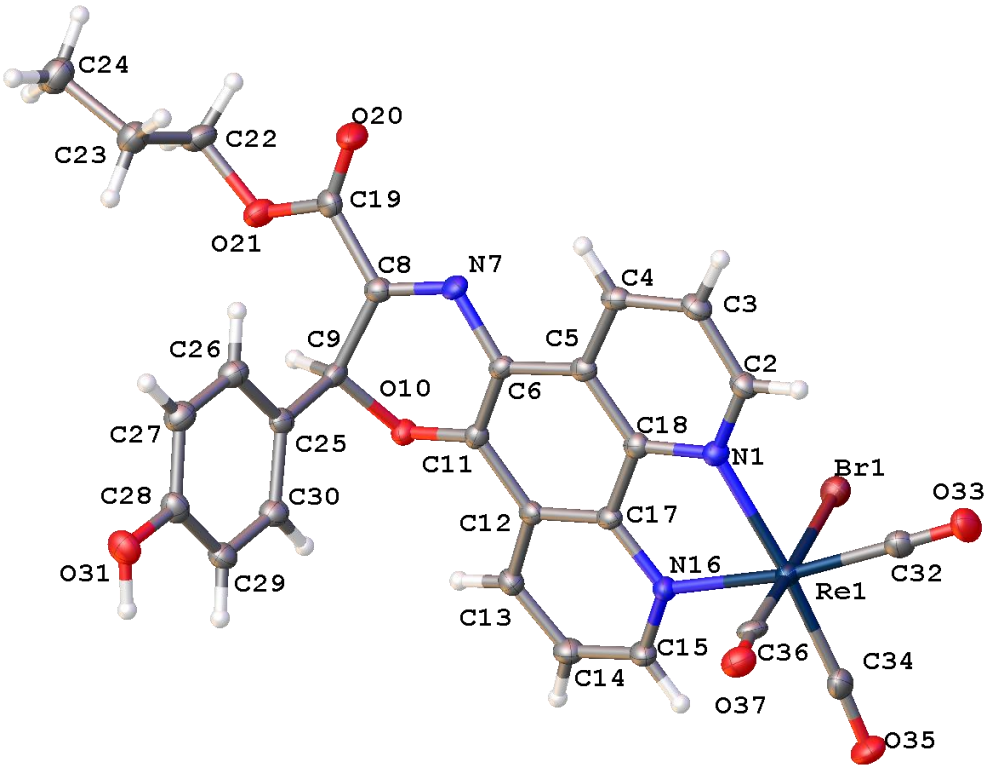

Molecular structure of RePPO (**4.2**) showing the Re complex. Displacement parameters shown at 50% probability.

Crystal data and structure refinement for RePPO (**4.2**)

Empirical formula	$C_{27}H_{19}BrN_3O_7Re$
Formula weight	763.56
Temperature [K]	100(2)
Crystal system	orthorhombic
Space group (number)	$Pbca$ (61)
a [Å]	23.2478(5)
b [Å]	8.8797(2)
c [Å]	23.9340(6)
α [°]	90
β [°]	90
γ [°]	90
Volume [Å^3]	4940.8(2)
Z	8
ρ_{calc} [gcm^{-3}]	2.053
μ [mm^{-1}]	11.996
F(000)	2944
Crystal size [mm^3]	0.091×0.057×0.018
Crystal colour	clear yellow
Crystal shape	plate
Radiation	Cu K_α (λ=1.54178 Å)
2θ range [°]	7.61 to 139.92 (0.82 Å)
Index ranges	−28 ≤ h ≤ 26 −10 ≤ k ≤ 10 −28 ≤ l ≤ 29
Reflections collected	45619
Independent reflections	4664 R_{int} = 0.0575 R_{sigma} = 0.0281

Completeness to θ = 67.679°	100.0 %
Data / Restraints / Parameters	4664/1/357
Absorption correction T_{min}/T_{max} (method)	0.5858/0.7533 (multi-scan)
Goodness-of-fit on F^2	1.036
Final *R* indexes [$I \geq 2\sigma(I)$]	R_1 = 0.0280 wR_2 = 0.0697
Final *R* indexes [all data]	R_1 = 0.0329 wR_2 = 0.0725
Largest peak/hole [eÅ^{-3}]	1.82/−0.75

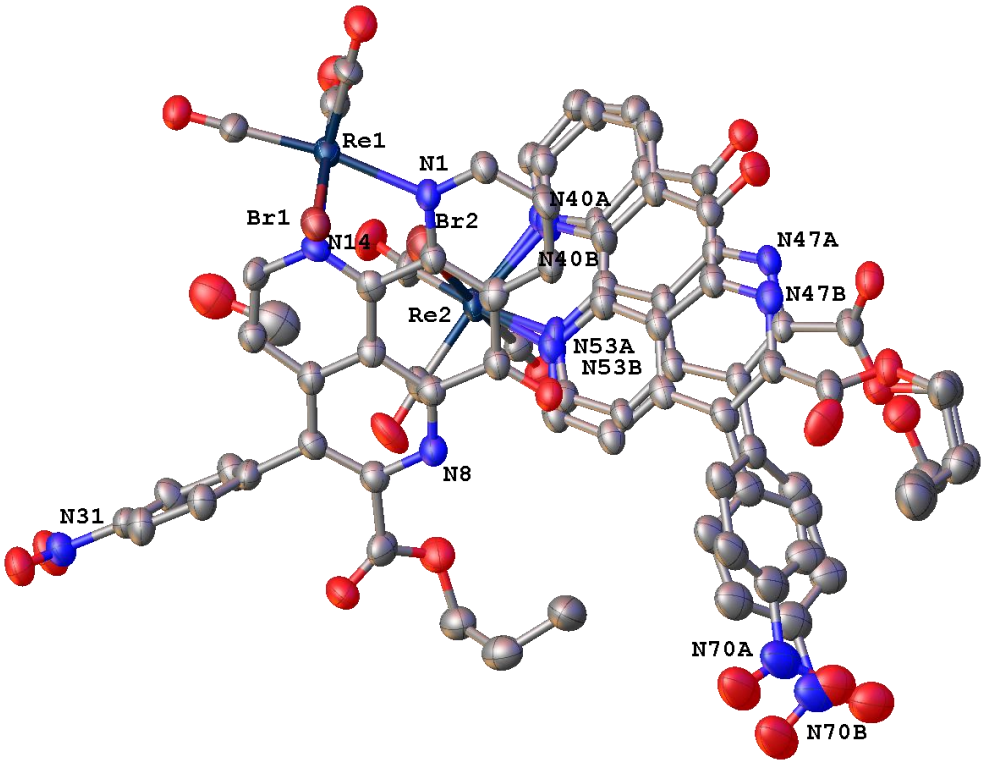

Disordered molecular structure of RePPP (**4.7**) showing both independent complexes in the asymmetric unit as well as two partially occupied MeOH solvent molecules. One ligand is disordered. Displacement parameters shown at 50% probability and hydrogen atoms omitted for clarity.

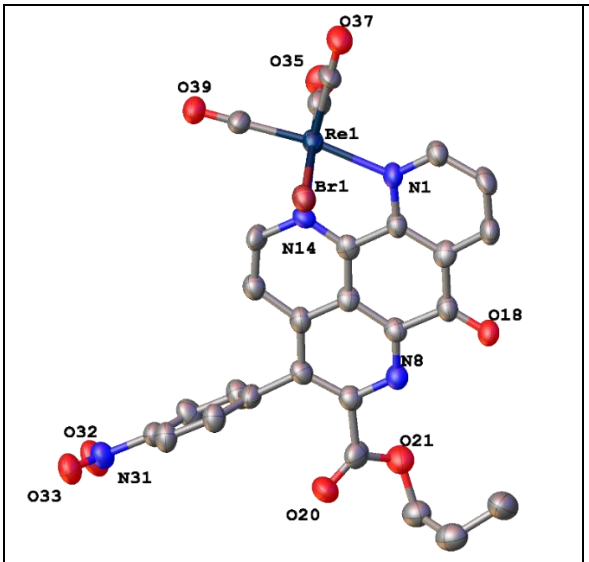

A

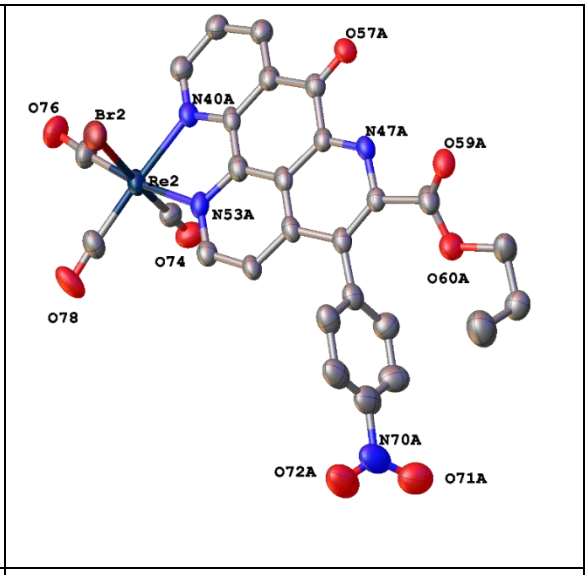

B

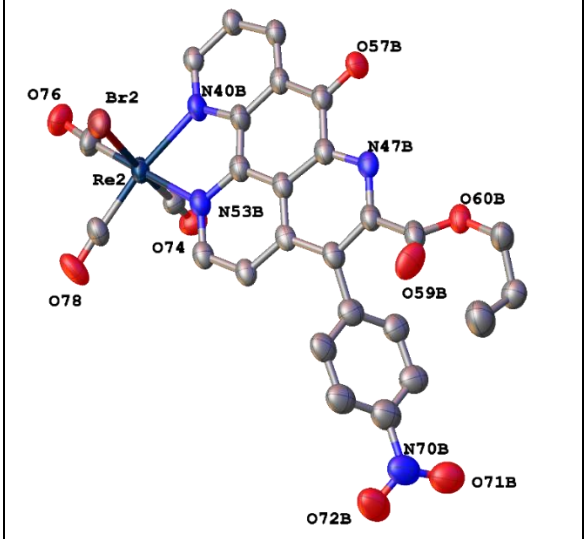

C

Individual representations of the complexes in RePPP (**4.7**) with (A) not disordered, (B) majority occupied moiety disordered ligand in complex2, 78% occupied and (C) minority occupied disordered ligand in complex2 at 22% occupied.

Crystal data and structure refinement for RePPP (**4.7**).

Empirical formula	$C_{27.70}H_{18.80}BrN_4O_{8.70}Re$
Formula weight	812.98
Temperature [K]	100(2)
Crystal system	triclinic
Space group (number)	$P\overline{1}$ (2)
a [Å]	12.6692(3)
b [Å]	13.5756(4)
c [Å]	16.3975(4)
α [°]	96.5844(18)
β [°]	100.1983(17)
γ [°]	97.355(2)
Volume [Å^3]	2725.46(12)
Z	4
ρ_{calc} [gcm^{-3}]	1.981
μ [mm^{-1}]	10.984
F(000)	1570
Crystal size [mm^3]	0.139×0.038×0.023
Crystal colour	red
Crystal shape	plate
Radiation	Cu K_α (λ=1.54178 Å)
2θ range [°]	5.53 to 137.29 (0.83 Å)
Index ranges	−15 ≤ h ≤ 15 −16 ≤ k ≤ 16 −19 ≤ l ≤ 19
Reflections collected	34304

Independent reflections	9970 R_{int} = 0.0679 R_{sigma} = 0.0706
Completeness to θ = 67.679°	99.7 %
Data / Restraints / Parameters	9970/1524/996
Absorption correction T_{min}/T_{max} (method)	0.6007/0.7531 (multi-scan)
Goodness-of-fit on F^2	1.020
Final *R* indexes [$I \geq 2\sigma(I)$]	R_1 = 0.0537 wR_2 = 0.1346
Final *R* indexes [all data]	R_1 = 0.0757 wR_2 = 0.1499
Largest peak/hole [eÅ^{-3}]	2.07/−1.24